The ascent and emplacement of granitic magma: The northern Arran granite

England, Richard. W

THE ASCENT AND EMPLACEMENT OF GRANITIC MAGMA: THE NORTHERN ARRAN GRANITE

by

Richard W. England.

A thesis submitted for the degree of Doctor of Philosophy
at the Department of Geological Sciences, University of Durham.

September 1988.

COPYRIGHT

No part of this thesis has been previously submitted for a degree at this university or any other university. The work described in this thesis is entirely that of the author, except where reference is made to previous published or unpublished work.

ABSTRACT

This thesis is a study of the mechanisms by which granitic magmas rise through the crust to be emplaced at a level above their source, with particular reference to diapirism, and how these mechanisms may be analysed by combined structural and petrological studies. The Northern Arran granite is used as an example of how this problem may be approached.

The Northern Arran granite is a two component granite of Tertiary age intruded into structurally heterogeneous upper crustal rocks under regional tension. A synform concentric to the granite, synchronous with the development of a narrow thermal aureole, records the vertical ascent of a single body of magma with a hemispherical upper surface. Post ascent, radial expansion of this body, indicated by flattening strains parallel to its surface and superimposed on the concentric synform records a change in shape of the pluton. This was permitted by the reactivation of an existing fault which the pluton intersected during its ascent.

Petrological studies of the outer coarse unit of the northern granite indicate that it is a single body of magma derived by differentiation of a crustally contaminated basaltic source. Theoretical modelling of the crystallisation of the coarse granite shows that textural and chemical variations, are consistent with solidification by sidewall crystallisation (liquid fractionation) but not fractional crystallisation. The inner (younger) fine granite is also a single body of magma derived from the same or a similar source as the coarse granite. The sharp undeformed contacts between the coarse and fine granites and the presence of internal sheets in the fine granite parallel to its contacts with the coarse granite are consistent with emplacement of the fine granite as a series of pulses which filled a propagating ring dyke fracture within the coarse granite.

Theoretical modelling of the ascent of the coarse granite using the Hot Stokes equation indicates that bouyancy driven ascent aided by a reduction in wall rock viscosity controlled by the rate of heat loss of from the granite is a viable ascent mechanism.

The patterns of strain in the aureole of the Northern Arran granite result from the ascent and emplacement of a single diapiric body. They provide examples of the types of structure which may be used to recognise and distinguish between diapiric ascent and radial expansion. This has important implications for the study of ballooning diapirs. The reactivation of an existing fault system during emplacement suggests that existing crustal structure can influence the final geometry of an intrusive body.

It is shown that the complete evolution of the Northern Arran granite can be determined using a combination of structural and petrological data. Structural data provides constraints on the later stages of ascent and the emplacement of granitic plutons. Petrological data can be used to constrain the origin, early stages of ascent and the crystallisation of a magma body.

PREFACE

This thesis would not have been completed without the help of many friends and colleagues from Durham and other universities during the last three years.

In particular I wish to thank my supervisors, Donny Hutton and Henry Emeleus, on whose initiative this research was instigated, both of whom have considerably influenced my ideas and thoughts through stimulating discussion and criticism throughout the last three years.

I am also grateful to Ian Meighan (Queen's University, Belfast) for supplying me with additional samples of the northern granite and for useful discussions on the geochemistry of British Tertiary granites. Thanks also to John Hudson (University of Leicester) for the communication of stable isotope data (not used in this thesis) and for discussions on various aspects of the geology of Arran. Special thanks must also go to Ron Hardy, without whose help and patience the geochemical data used in this thesis would not have materialised, and to Nick Pearce for allowing me to use his trace element analysis programs for processing the data. Analytical facilities were provided by the Durham Geological Sciences department and the computation was carried out in the university computer centre. This research was funded by Natural Environment Research Council grant no. GT4/85/GS/27.

I should also like to thank Ron Lambert and George Randall for making the thin sections. Carole Blair typed numerous letters and abstracts, Karen Gittins assisted in the drafting of many diagrams and Gerry Dresser and Alan Carr took numerous photographs for me. Dave Asberry provided additional assistance on numerous occasions.

Many friends on the Isle of Arran made my fieldwork very enjoyable. In particular I wish to thank the Wilkinsons of Corrie and the Mosses of Brodick for their hospitality.

I have thoroughly enjoyed working alongside many of the postgraduate students at Durham. In particular I wish to thank Chris Jones, Ken McCaffrey and Steve Jolley with whom I have shared a room and many discussions and practical jokes with over the last two years. Simon Day and Nick Smith have discussed numerous aspects of Tertiary igneous geology for which I am grateful. My apologies to anyone who feels they should have been mentioned. Had I tried to thank everyone I would never have completed this thesis!

CONTENTS

A geological map of Northern Arran is included at the back of this thesis which is intended for use with chapters 2 to 5 and chapter 7.

CHAPTER 1

THE ASCENT AND EMPLACEMENT OF GRANITIC MAGMA

> A review of the literature, in general makes it obvious that we do not yet have dependable criteria that are acceptable to geologists as a whole to distinguish between the products of the different mechanisms of emplacement. There would also probably be little dissent from the view that such geological problems will not be solved by field geology alone, but by retention of what seems good in old ideas with constant rethinking and co-ordination of new hypotheses, of data from new experiments and new laboratory studies, and of new results of field geology aided by the rare "flash of insight" new idea.
>
> A. F. Buddington, 1959.

The majority of granitic bodies are intrusive. At the present surface they are found in rocks from which they cannot have been directly derived. The exceptions to this are the the migmatite complexes and those granites produced by fractionation of basaltic magma within a closed chamber. The object of this thesis is to investigate the mechanisms by which granitic magmas rise through the crust to be emplaced at a level above that at which they originated, and how these mechanisms may be resolved by integrated structural and petrological studies. The Northern Arran granite is used as an example of how this problem may be approached.

It is possible, from exposed granitic intrusions to collect a great deal of data which may be used to elucidate the final stages of their ascent and their emplacement. However these data may not immediately reveal much about the evolution of the granite as it rose through the crust. It is possible to envisage the evolution of a granitic magma during ascent from its source to its level of emplacement as a kinematic process involving constant physical and chemical modification as it interacts with the crust. The crystallised magma exposed at the surface records

the cumulative effect of these modifications, but may not directly record the processes which produced them. Similarly studies of aureole deformation and fabrics within a granite can reveal much about its mechanism of emplacement and crystallisation, but little about its actual ascent.

Major questions facing researchers working on granitic magmas are: What is the nature of the processes effecting the magmas during ascent? How significant are their effects? and how can they be recognised? Once these questions have been resolved it may be possible to understand the origin of granitic magmas.

1.1 The Granite Problem: Implications for the Ascent of Granitic Magma.

A great deal of previous and current work, largely on the petrology of granites is devoted to finding a solution to what is commonly referred to as 'the granite problem': Are granites of igneous, metamorphic or metasomatic origin? The study of this problem is largely beyond the scope of this thesis, although it is clear that much of our current understanding of the ascent and emplacement of granitic magmas is derived from the investigation of this problem.

Early evidence for an igneous origin of granitic magmas was drawn from field studies which showed that granitic bodies were clearly intrusive and that large intrusive bodies have dicordant contacts with the country rocks into which they were emplaced (Cloos, 1923; Daly, 1933; Balk, 1937). However it was recognised that the volume occupied by intrusive bodies was larger than that which could be explained by dilation of the country rock, and that a 'space problem' existed. Cloos (1923) attempted to resolve this problem by envisaging large batholiths as sheets, the emplacement of which present less of a space problem, although vertical or horizontal extension of the crust was still required to accommodate them. Opponents of a magmatic origin of granite favoured a metamorphic or metasomatic origin which did not constitute a space problem since this theory envisaged

production of granite by transformation of pre-existing rocks and did not require an increase in the volume of the crust. An early proponent of this theory (Sederholm, 1907) invoked the term migmatites to describe granites produced by partial melting (or anatexis) of crustal rocks.

It is clear at this early stage of the study of granitic rocks that the origin of granitic magma favoured by particular researchers was strongly influenced by their own field observations. From these observations it was recognised that granites occur in a variety of settings which were generally related to what are now referred to as orogenic belts. Eskola (1932), who regarded all granites as magmatic, classified them as syn-, late-, or post-tectonic according to their association with phases of regional metamorphism and deformation. This classification (in various forms) remains in use, and has clearly influenced current approaches to the study of the ascent and emplacement of granitic magma.

Eskola (1932) regarded syn-tectonic granites as those which were gneissose, concordent with the country rock (having gradational contacts) and containing abundant inclusions of basic material. Late-tectonic granites were defined as discordant (or only partially concordant), even grained and rarely gneissose. Post tectonic granites lacked a gneissic fabric and hence were considered to have been intruded after the last phases of deformation. While Eskola's (1932) classification was intended to be objective later classifications of this type, particularly those of Read (1957) 'The Granite Series', and of Buddington (1959) contained genetic connotations. Read (1957) modified the classification of Eskola (1932) to include a relationship between granite type and crustal level. Read (1957) saw migmatites (autochthonous granite) as forming at the deepest levels of orogenic belts during the peak of tectonic activity. Discordant or partially discordant (parautochthonous) foliated granites were intruded at higher levels during the latter stages of orogeny and true magmatic intrusive, unfoliated, granites were emplaced at the highest levels of the crust after deformation had ceased. Read (1957) suggested that the

parautochthonous granites had detached from migmatite complexes to rise higher in the crust. This view, that granites emplaced at high levels in the crust were derived by segregation and ascent of magma from lower levels was expanded by Buddington (1959), who rejected the time dependant nature of the classifications of Eskola (1932) and Read (1957). Instead, Buddington (1959) classified granites according to characteristics observed at three different levels or emplacement zones within the crust. The autochthonous granites of Read (1957) were assigned to the 'Catazone' (7 - 12 miles beneath the surface), parautochthonous granites to the 'Mesozone' (5 - 9 miles beneath the surface) and magmatic intrusive granites to the 'Epizone' (0 - 5 miles beneath the surface). However Buddington (1959), in his review of the styles of emplacement of North American granites, recognised that there was a clear transition between the three types and that granites were intruded at all levels during orogenesis. Buddington (1959) regarded the three zones of emplacement as being primarily depth related but also noted that they could be interpreted as zones of intensity which were depth (pressure) and temperature dependant. This view also accommodated the variations in the rheological properties of the country rock into which the granites were emplaced. Field evidence supporting this observation, which is now regarded as of critical importance in influencing mechanisms of igneous emplacement, had been previously described by Balk (1937, after Cloos) in a description of the structural features of igneous rocks.

It is clear these early approaches to solving the granite problem were consistently based on the assumption that granite occurring at progressively higher levels in the crust had risen from lower levels. A clear difference in style of emplacement was also noted at different levels in the crust which reflected the change in its rheological properties with depth.

1.2 The Ascent of Granitic Magma.

Recent reviews of the ascent and emplacement of granitic magmas (Pitcher, 1979; Bateman, 1984) have noted that there are two schools of thought on their mechanism of ascent. The first is that of ductile flow, synonymous with diapirism, which involves the rise of discrete bodies of magma driven by bouyancy forces. The second is that of brittle fracture which involves the ascent of magma along pre-existing or magma driven fractures under pressure. These mechanisms will be discussed separately.

1.2.1 Ductile Flow.

The ascent of magma driven by bouyancy forces is a physically efficient process requiring no external stresses on the magma other than gravity. Consequently this process may occur in any region of the crust undergoing horizontal extension, contraction or zero finite longitudinal strain. The formulation of the Hot Stokes equation for diapiric ascent of a magma body through the crust by an extension of the Stokes Equation (Marsh, 1982; Daly & Raefsky, 1985) indicates that it is possible for a body of granitic magma to rise diapirically for a short distance through the crust. The equation predicts that subsequent bodies of magma following the same path as the first would rise further and more rapidly because heat loss from the first body would have reduced the viscosity of the crustal rocks which would reduce the drag forces on the second body, providing it rose before the thermal perterbation caused by heating during the rise of the first body had decayed. This theoretical approach also indicates that granites will rise by bouyancy driven mechanisms irrespective of their own viscosity, but that the effective viscosity of the wall rocks is a critical factor in controlling ascent.

Good analogues between the ascent mechanism and geometry of salt diapirs (Braunstein & O'Brien, 1968; Jackson & Talbot, 1986 and Talbot & Jackson, 1987) and granitic bodies can be drawn from experimental studies (Grout, 1945;

Ramberg, 1967; Dixon, 1975 and Soula, 1982). The centrifuged models of Ramberg (1967) and Soula (1982) showed that the bouyancy driven ascent of fluids in a viscous medium could produce structures analogous to gneissic and plutonic domes. Pitcher (1979) cites many examples of forcefully emplaced plutons which could be interpreted as diapirs on the basis that they possess shapes comparable to those generated in centrifuge experiments designed to model diapiric ascent. However a major problem lies in the interpretation of evidence for diapiric ascent. Few intrusions show actual evidence of having risen through the crust, in the form of structures in their wall rocks which can be clearly assigned to deformation that accommodated vertical ascent of the pluton. This will be discussed further below. The stem or root of a diapiric body, the existence of which is implied by experimental studies and analogues with salt and mud diapirs, has not been identified. This also requires explanation if diapirism is to be invoked as a major mechanism of transport of granitic magmas in the crust.

Essentially diapirism is a forceful mechanism of ascent. The experimental, theoretical and observed analogues all record the rise of bouyant material which is accommodated by deformation of the medium (the crust) through which the body is ascending. The patterns of strain induced in the medium have been examined experimentally by Dixon (1975) and more recently by Schmeling et al. (1988). Both these studies indicate that diapirism causes dilation of the crust and high strains to develop parallel to the surface of the rising body. These strains are continually modified as the body ascends through the medium, suggesting that crustal rocks adjacent to diapirs may exhibit complex, multiphase deformation histories.

Criteria for the recognition of diapiric bodies, based on their structure, have been outlined by Coward (1981) and Bateman (1984). These are summarised below:

a. Less dense material should occupy circular to oval shaped complexes enclosed

by denser material.

b. Structures such as foliation, cleavage and lineations should be developed parallel to the surface of the less dense material and should be parallel to any foliation developed within the less dense material. The foliation should intensify toward the contact between the dense and less dense material.

c. Strain distributions should involve sub-horizontal extension in the crestal region of the less dense material. The long axis of the strain ellipsoid should be tangential to the crestal region. In the trunk of diapiric complexes (by analogy to salt diapirs (Talbot & Jackson, 1987)) the long axes of the strain ellipsoid should be vertical and possibly associated with synchronous folds with radial axial planes.

These criteria, derived from field observations of diapiric structures are consistent with the strain patterns predicted by the analogue models of Dixon (1975) and Schmeling et al. (1988). It is clear that many intrusive bodies display these features. However, as noted above, it should be recognised that in order to identify a diapir it is necessary to prove that it has actually risen to its present level as a diapir, i.e. that it is a piercement structure.

Consequently it can be seen that there is a great deal of largely unsubstantiated evidence for the diapiric ascent of granitic magma which is largely based upon theoretical and experimental models and field observations of analogous salt structures.

1.2.2 Brittle Fracture.

There are numerous examples of basic magma of low viscosity rising great distances through the crust in dykes. These vertical fractures either follow existing faults or weaknesses in the crust or they form immediately ahead of the rising sheet of magma (in the plane containing the maximum and intermediate principal stresses) by magmafracting. The ascent of the magma is driven by the magmatic

pressure which is approximately equal to the weight of the rocks overlying the source of the magma. It has been suggested by Bateman (1984) and demonstrated by Le Fort et al. 1987 that granitic magmas of low viscosity may also rise in this mannner. Clough et al. (1909) and Anderson (1936) suggested that cauldron subsidence could also permit the ascent of granitic magma in the crust. Both these mechanisms involve brittle fracture of the crust. Ascent of magma through dykes does not constitute a significant space problem since the crust is extended across the dyke and the resulting space is filled with magma. However the accumulation of magma in an expanding chamber fed by a dyke as envisaged by Bateman (1984) does require an excess extension of the crust (in excess of that resulting from formation of the dyke) to accommodate the developing intrusive body. Dilation of the crust is also required to accommodate a magma body accumulating below a developing ring fracture, but providing collapse of the unsupported block of crustal rocks is balanced by upward flow of magma the volume of the crust is conserved while the magma is redistributed at a higher level in the crust. Hence it is clear that while ascent of the magma through the crust by mechanisms involving fracturing of the crust may initially appear an attractive solution to the space problem it cannot account for the development of magma bodies with substantial horizontal and vertical dimensions.

The brittle fracture hypothesis conflicts with many of the current ideas on the rheology of granites. While Wickham (1987) concluded that one of the most effective ways of extracting magma from a partially molten source region was by fracturing the source region and tapping partial melt along the fracture it is clear that this process would only occur if the source region was capable of sustaining a deviatoric stress. Applying a stress to a partially molten zone ($\approx$ 30% melt) would cause it to flow and prevent segregation of felsic from mafic components. The developing magma body would be enriched in'restite' to such a degree that it would be too viscous for it to move any great distance in a dyke.

Hence brittle fracturing would not be an effective mechanism for accumulating and redistributing large quantities of partially melted crust. The restite hypothesis (Chappell et al., 1987) invoked to explain the wide variety of xenolithic material commonly found in granitic rocks implies that some granitic magmas carried a significant proportion of solid or partially solidified material derived from their source. This would cause an increase in the effective viscosity of the magma. The magnitude of this increase would depend largely on the proportion of solid in the magma. Providing this did not exceed 50% the effect would not be significant. Arzi (1978), van der Molen & Patterson (1979) and McBirney & Murase (1984) showed that the viscosity of magma increases rapidly once it contains more than 50% solid material, which would severely inhibit the ability of a magma to flow along a dyke.

Bateman (1984) considered that many diapiric plutons were ballooning diapirs; bodies of magma which expanded in-situ following ascent through a dyke. Bateman (1984) suggested crystallisation of the magma during ascent (as a result of heat loss to the wall rocks) caused its viscosity to increase to such an extent that it was no longer capable of ascent in a dyke, and hence it became immobilised. Magma ascending through the dyke would dilate the existing immobilised material, causing lateral expansion of the dyke and the formation of an expanding or ballooning pluton. The wall rocks and the magma body would record strain patterns identical to those defined as criteria for the identification of diapiric bodies but would show no evidence of vertical ascent.

This example emphasises the close relationship between the ascent and emplacement of granitic magmas, and that the two processes cannot be considered as entirely independant. In the case of ductile flow (section 1.2.1) the ascent of a rising diapiric body could result in the emplacement of a pluton at the level at which it came to rest, possessing many of the characteristics of a diapiric body. However, as will be demonstrated in the following section, it is clear that this is

not always the case.

It is apparent from the work on ascent processes that mechanisms for ascent by ductile flow (which have attracted the most attention) present the most significant conceptual problems. The ascent of magma by brittle fracture of the crust presents fewer problems but the transition from a feeder dyke to a forcefully emplaced body is more difficult to envisage.

Both mechanisms can explain many of the geochemical features of granitic intrusions. Many plutons are zoned either as a result of crystal fractionation processes (Bateman & Chappell, 1979; Atherton, 1981) or by the emplacement of multiple pulses of magma into the same chamber, as envisaged by Harry & Richey (1963). In the first case zonation may be controlled by in-situ crystallisation processes generating evolved liquids in the core of the intrusion. This evolved liquid may subsequently rise through the crystal liquid mush precipitated from it to produce sharply defined zones of chemically contrasting, yet chemically related, magma (Bateman & Chappell, 1979; Tindale et al., 1988). This process is different from the emplacement of multiple pulses of magma to produce compositionally zoned plutons e.g. Ardara (Holder, 1979) which requires injection of more than one pulse of magma into the magma chamber. These pulses could be injected into the chamber via dykes or may result from the emplacement of a diapiric body into the existing magma chamber. The first case offers the possibility of inflation of a magma body by a continuous flux of magma or pulsatory expansion. The second case could only cause pulsatory expansion of the magma chamber. Multiple injection of magma into the same pluton does not exclude zonation as a result of crystal fractionation. Consequently zonation in granitic intrusions should be interpreted carefully and the origins of the zonation investigated on the basis of careful geochemical studies designed to test a multipulse vs fractional crystallisation hypothesis.

1.3 The Emplacement of Granitic Magma.

Pitcher (1979) emphasised the point made by Leake (1978) that there may be a contrast in the geometry of an ascending body of magma and its emplacement geometry. A critical question facing investigators of emplacement mechanisms is: How does the process of emplacement affect the final shape of the granitic intrusion? Once this has been resolved it may be possible to deduce how the magma body reached the level at which it was emplaced. As noted above the final geometry of an intrusive body may be a function of its ascent mechanism, but this need not be the case. Essentially mechanisms of emplacement can be divided into forceful and passive.

1.3.1 Forceful Emplacement of Granitic Magma.

Forceful emplacement of granitic magma involves the displacement of crustal rocks to create a volume for the magma to fill by essentially ductile deformation. This could be interpreted as a natural extension of ascent by ductile flow, but the two processes are not always associated. There are numerous examples of forcefully emplaced plutons, which share the common feature of a strongly deformed aureole e. g. Flamanville (Martin, 1953); Rogart (Soper, 1963); Ploumanac'h (Barriere, 1977); Papoose Flat (Sylvester et al., 1978); Ardara (Holder, 1979) and Cannibal Creek (Bateman, 1984). Balk (1937, after Cloos) observed that many plutons showed evidence of in-situ expansion to produce strong flattening strains parallel to the surface of the pluton, both within the pluton and outside it. Such intrusions may show obvious evidence of multiple injection of magma e.g. Ploumanac'h and Ardara, which could have contributed to the expansion and deformation of their envelopes or they may lack such evidence e.g. Flamanville, Cannibal Creek. Evidence of forceful emplacement is not an indicator of ascent by ductile flow. Bateman (1984) modelled the inflation of the Cannibal creek pluton as a ballooning diapir fed by a dyke. (section 1.2.2). Pitcher (1979) used

the examples of Ploumanac'h and Bidwell Bar (Compton, 1955) to illustrate that initial intrusion of forcefully emplaced plutons may have occurred by mechanisms associated with passive emplacement i.e. brittle faulting and cauldron subsidence respectively. These examples indicate that emplacement of magmas is an evolving process which reflects changes in the way magma and crust interact which does not necessarily follow the early depth related classifications of Read and Buddington.

1.3.2 Passive Emplacement of Granitic magma.

Passive emplacement of granitic magma involves the displacement of crustal rocks to create a volume for the magma to fill by brittle deformation. As discussed above (section 1.3.1) and by analogy to mechanisms of forceful emplacement, mechanisms of passive emplcement are not necessarily associated with those of ascent by brittle fracture. The process of passive emplacement is typified by the formation of ring dykes (Clough et al., 1909). In a recent review of ring complex granites Bonin (1986) indicated that such structures may form above diapiric bodies as a result of extension of crustal rocks in the roof of a diapir as it rose into higher and progressively more brittle crust. Walker (1975) proposed a similar model for the evolution of the British Tertiary central complexes, in which early diapirism led to the formation of ring dykes and cone sheets. This is a clear example of how one style of emplacement may influence the style of emplacement of subsequent intrusions.

1.3.3 The Role of Tectonics.

It is clear from the discussion above that the association of forceful and passive mechanisms of emplacement and the transition between them which may occur during emplacement of the same plutonic complex at the same crustal level contravenes the classifications of Read and Buddington which related mechanisms of emplacement to depth.

Consequently there is the need for a unifying theory or approach which can accommodate both 'forceful' and 'passive' emplacement mechanisms at any level in the crust. A general concensus of opinion is emerging that the answer lies in an increased understanding of the role of tectonics in influencing the ascent and emplacement of granitic magmas. An approach which has its roots in the chronological – tectonomagmatic classifications of Read and Buddington.

The stimulus for investigations into the role of tectonics in the emplacement of granitic magmas has come from the study of the Donegal Batholith (Pitcher & Berger, 1972). This granitic complex comprises eight intrusive granites of similar age which show a range of styles of emplacement e.g. stoping (Thorr), passive (ring dyke) (Rosses, Barnesmore), ballooning (Ardara) and diapiric wedging in an evolving shear zone (Main Donegal granite), all at the same crustal level. According to the classification of Read (1957) the Thorr, Rosses and Barnesmore plutons would have been intruded at higher crustal levels than the Ardara and Main Donegal plutons, which infers vertical movement of the crust during emplacement. The work of Pitcher (in Pitcher & Berger, 1972) clearly indicated that emplacement of the plutons was synchronous with deformation of the Caledonian rocks and it was concluded that 'the character of the granitic pluton, and of its relationship with its present envelope, need bear little relationship to its position in the crust'. The synchronous association of different styles of emplacement at the same level in the crust clearly indicated that the theory of Read was incorrect, and that emplacement of the granites was clearly related to the structural evo-

lution of the region. Further work resulted in the development of a model which related emplacement of the granites to the sinistral shear zone which dominates the structure of Donegal (Hutton, 1982). Hutton (1982) demonstrated that the distribution of stresses within the shear zone could produce local zones of tension or compression into which magma was emplaced. The resulting geometry of the individual plutons were controlled by the stresses acting on the rising magma e.g. the passively emplaced Rosses pluton was intruded into a zone of tension developed in a convex (releasing) bend in the shear zone surrounding the Main Donegal granite while the forcefully emplaced Ardara pluton was intruded into a zone of compression at the tip of the shear zone. This interpretation implied that forcefully emplaced plutons are intruded in zones of tectonic contraction and passively emplaced plutons are intruded in zones of tectonic extension. There exists a good deal of evidence to support this interpretation. In particular, cauldron subsidence is a consistent feature of granites emplaced in regions of tectonic extension.

Davies (1982) described the geology of the Ajjaj shear zone in northern Saudi Arabia into which a series of Pan African granites were emplaced. A detailed study of the strains within the shear zone indicated a volume increase during deformation which Davies (1982) attributed to the emplacement of diapiric granites. This example illustrates that the emplacement of granitic magma into high crustal levels need not constitute a space problem if the necessary volume/void is created by tectonic processes.

Brun & Pons (1981) and Soula (1982) also considered the interaction between emplacement and tectonic stress through the study of forcefully emplaced magma bodies in regions of tectonic contraction. They showed that the patterns of strain recorded by the deformation of the plutons and their aureoles reflected the interaction between the bouyancy forces driving the ascent of the plutons and the tectonic forces deforming the rocks into which they were emplaced. The resulting

fabrics which record the evolving strain patterns around a pluton during ascent reflect the relative magnitudes of the two stress systems. Strong regional fabrics only slighly deflected around the intruding granite indicate a dominance of the regional tectonic stress field. Regional fabrics deflected around the intruding body reflect the dominance of emplacement related stresses.

The recognition that the emplacement of granitic magmas and their final geometry is the result of a complex interplay between magmatic stresses and tectonic stresses clearly indicates that granites should be studied in the context of their tectonic environment rather than as discrete bodies independent of their surroundings.

This approach has been stressed in a recent review by Hutton (1988a) who viewed the variety of mechanisms of emplacement of granitic magmas as 'a function of the interaction between the natural magma bouyancy forces and ambient tectonic forces'.

This succinct theory allows for a great deal of flexibility in interpreting the ascent and emplacement of granitic magmas in different tectonic environments and in its flexibility provides a tool for interpreting granites without the need to return to a more rigid classification of the type devised by Read (1957) and Buddington (1959).

1.4 The Northern Arran Granite.

The introductory sections have briefly considered the evolution of the principal theories and current trends in the study of the ascent and emplacement of granitic magmas. It is clear that many questions remain unanswered. Some assumptions remain critically untested, yet form the basis of generally accepted viewpoints. There is clearly the need to fill gaps in our knowledge before these assumptions are found to be incorrect and any theories based upon them become unsubstantiated. This thesis deals with the following aspects of the ascent and emplacement of

granitic magma:

Is it possible for magmas to ascend as diapirs? and if so can the vertical ascent of a diapiric body be identified from structures observed in the field?

What is the relationship between the shape of a magma body during ascent and its final shape after emplacement? Is it possible to image these changes by structural studies?

While the effect of tectonic stress is becoming clear are there other factors which influence emplacement geometry, e.g. existing crustal structure, and what are their effects? This requires the study of magma bodies emplaced in areas of minimal tectonic activity.

While the structural approach to the investigation of ascent and emplacement mechanisms advocates detailed study of both the granite and its aureole few studies of granites have been made which attempt a comprehensive integrated investigation of the interrelationship between the structure and petrology of a granite and the implications this may have for constraining ascent and emplacement mechanisms.

The Northern Arran Granite provides a suitable testing ground for examining these problems. This granite is one of a number of intrusive centres of Early Tertiary age which together with an extensive suite of extrusive basaltic rocks collectively form the British Tertiary Volcanic Province. It was emplaced into structurally inhomogeneous upper crustal rocks. A synchronous suite of Tertiary basalt dykes indicates the crust was extended by approximately 5% during the emplacement of the granite, which makes the pluton suitable for a study to investigate the effects of pre-existing structure on emplacement geometry.

The granite dominates the geology of the north of the Isle of Arran. Existing work (Gunn, 1903; Tyrrell, 1928) shows that it is a large sub-circular boss approximately 13 km in diameter. It is composed of two units. An outer coarse grained granite which completely surrounds a younger fine granite of irregular form.

The granite is surrounded for 300° of its circumference by strongly deformed rocks of Dalradian (Upper Cambrian to ?Lower Ordovician) age. On its eastern side the granite is faulted against rocks of Lower Devonian (ORS) age. The Dalradian rocks are separated from the ORS rocks by a fault to the NE of the granite and by an unconformity to the south and east of the granite. To the north and east of the granite and between 1 and 2 km from its contact with the Dalradian and ORS rocks a major NE – SW striking fault system downthrows rocks of Carboniferous and Permian age against the Dalradian and ORS.

Much of the coarse granite and certain areas of the fine granite are well exposed which provides an opportunity for a comprehensive study of geochemical variations within the granite. Preliminary geochemical work had been carried out by Dickin et al. (1981) as part of a contribution to the study of the geochemical affinities of the granitic rocks (crustal melt or basaltic differentiate?) of the British Tertiary Volcanic Province which has occupied petrologists for much of this century (Thompson, 1982). However the major and trace element geochemistry has never been studied in detail. An investigation was begun, but not completed (Johnson & Meighan, 1975).

The original aims of this research were to record the sequence of deformation in the Dalradian rocks at the margin of the granite and to correlate them with structures within the granite and determine how the aureole structure may be related to the injection of pulses of magma identified by variations in chemistry within the pluton. As with most research projects these aims were frequently modified as work progressed and results were obtained. The following chapters describe and discuss these results and their implications for the study of the ascent and emplacement of granitic magmas.

CHAPTER 2

PRE–TERTIARY GEOLOGY

Before describing the detailed geology of the Northern Arran Granite and the features associated with its intrusion this chapter discusses the evolution of the geology of the upper Clyde area and the underlying crustal structure prior to intrusion of the granite.

2.1 Dalradian Structure and Stratigraphy.

The Dalradian rocks of Northern Arran (Fig. 2.1) can be divided into five lithological units (Figs. 2.2 & 2.3), repeated by Caledonian (480–500 Ma) folding (Anderson, 1944), which are clearly exposed to the north of the granite between Lochranza and Corloch. To the west and south of the Northern Granite identification of these units is more difficult because most of the exposed rocks have been strongly deformed by the emplacement of the granite. The oldest Dalradian rocks occur in the core of the Aberfoyle synform, a downward facing Caledonian anticline exposed between Lochranza and Corloch (Fig. 2.3). These are black/purple pelites (mudstones) with thin bands of quartzose volcanic ash and chert (Fig. 2.2). These pelites are overlain by a series of normally graded grits and psammites (siltstones and sandstones) with occasional pelites. The graded beds are typically 0.5 m to 1 m thick. The third unit, composed of green psammitic pelites and pelites, grades upward into a second sequence of normally graded psammitic units which show an overall coarsening upward on the east side of the fold axis from psammites to pebbly grits. The grits at the top of this sequence have a sharp junction against a band of graphitic pelite, which has an arcuate outcrop to the west of the Northern Granite as well as being exposed to the east of the fold axis, to the

Figure 2.1. Geological map of Arran and the surrounding North Clyde area, showing the general features of the onshore and offshore geology (after McLean & Deegan, 1978).

Fig. 2.1

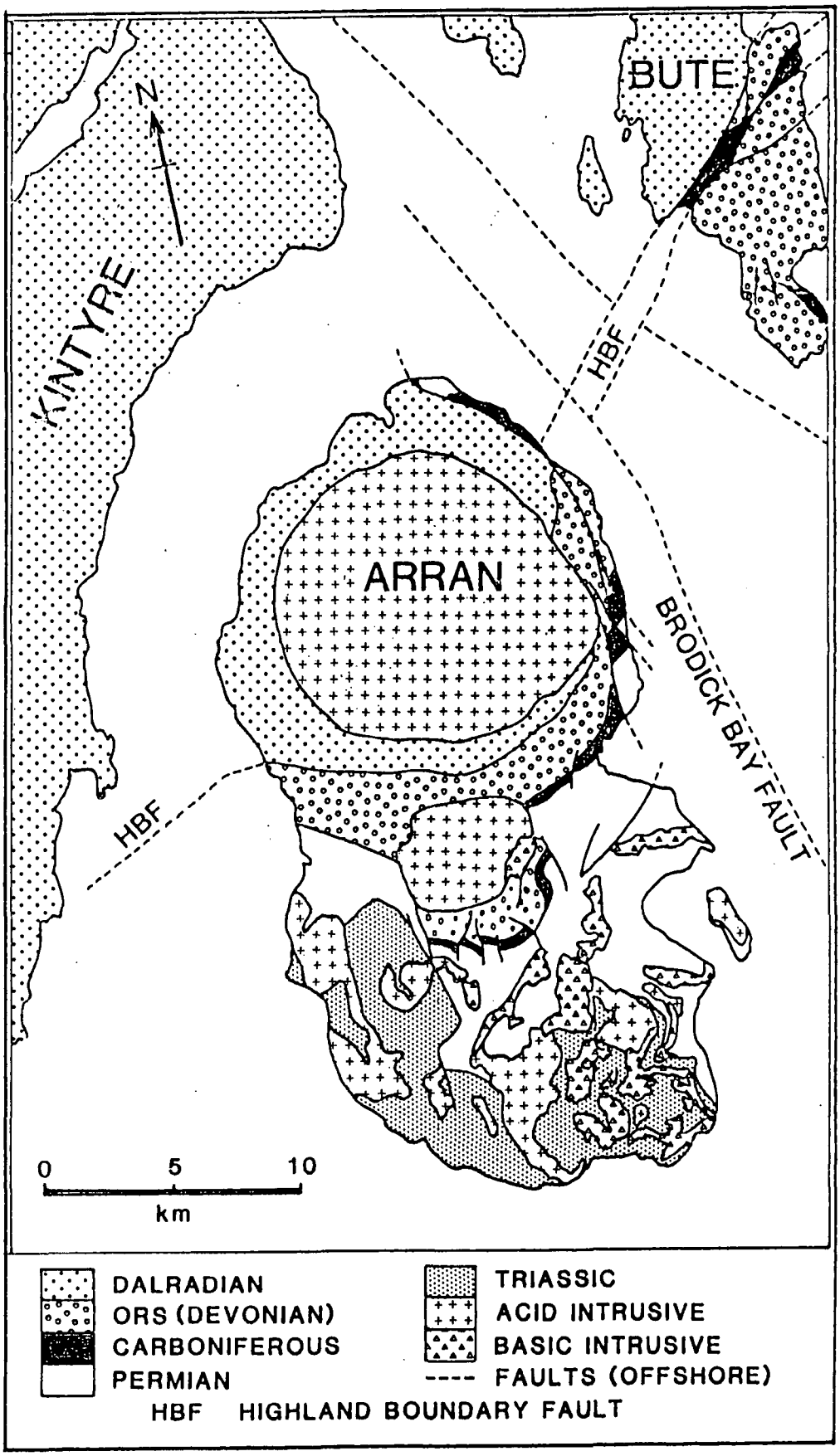
BUTE
N
KINTYRE
HBF
ARRAN
BRODICK BAY FAULT
HBF
0
5
10
km
DALRADIAN
ORS (DEVONIAN)
CARBONIFEROUS
PERMIAN
TRIASSIC
ACID INTRUSIVE
BASIC INTRUSIVE
---- FAULTS (OFFSHORE)
HBF HIGHLAND BOUNDARY FAULT

Figure 2.2. Summary of the stratigraphy of the Dalradian (Southern Highland Group) rocks exposed on Arran. Inset map shows extent of outcrop of Dalradian and location of section A-B; Top right: Cross section A-B from Lochranza to Corloch showing gross structure and distribution of stratigraphic units (arrows indicate younging direction, HBC Highland Border Complex); Bottom left: Generalized sedimentary log of Dalradian succession; Bottom right: A correlation between the thickness of stratigraphic units exposed on SE and NW limbs of Aberfoyle Synform. (Note: sequence is given 'right way up' to emphasise that units now exposed in SE limb were originally deposited to NW of the sequence now exposed in the NW limb.)

Fig. 2.2

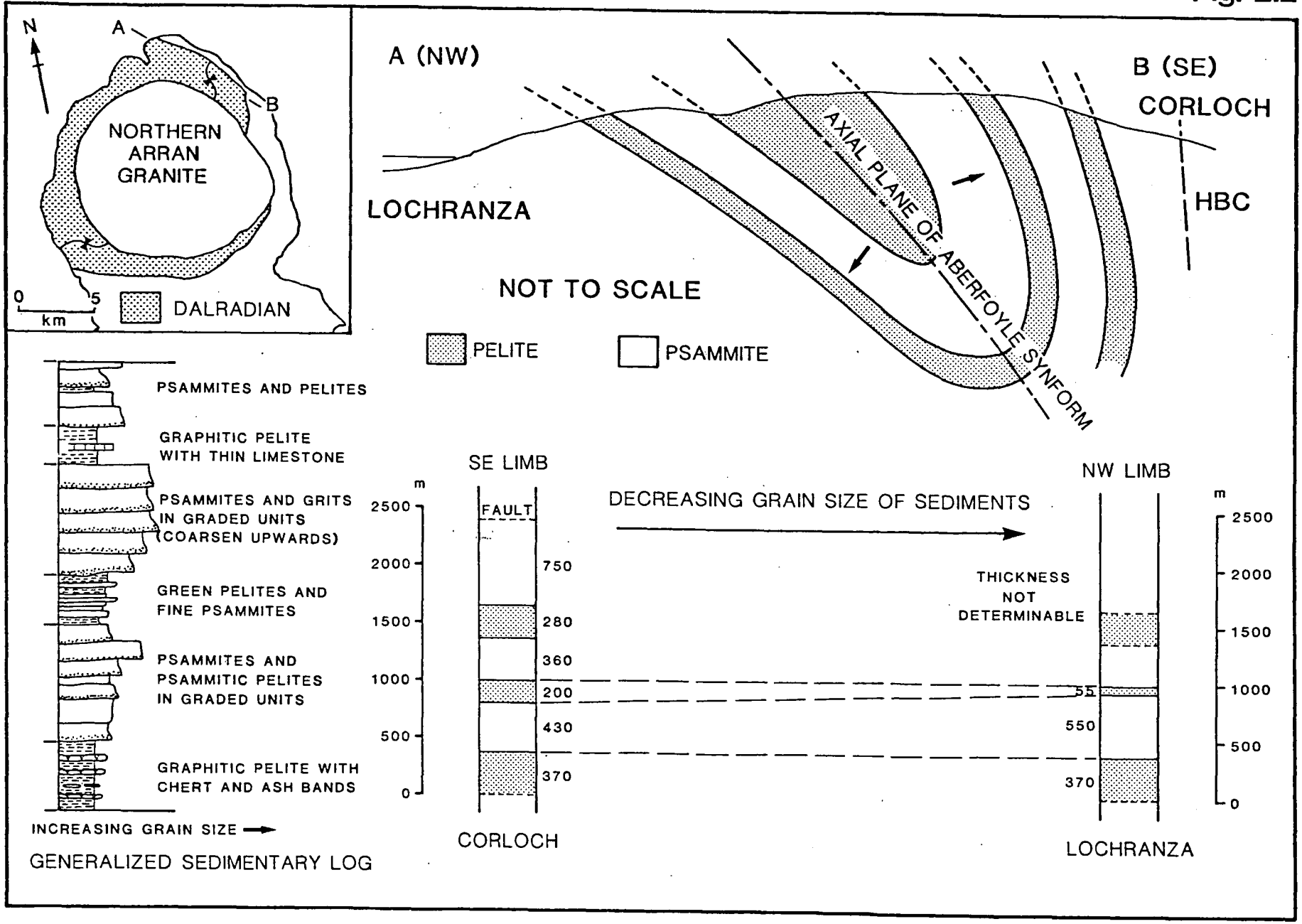
N
A
B
NORTHERN ARRAN GRANITE
0
5
km
DALRADIAN
A (NW)
B (SE)
CORLOCH
HBC
LOCHRANZA
AXIAL PLANE OF ABERFOYLE SYNFORM
NOT TO SCALE
PELITE
PSAMMITE
PSAMMITES AND PELITES
GRAPHITIC PELITE WITH THIN LIMESTONE
PSAMMITES AND GRITS IN GRADED UNITS (COARSEN UPWARDS)
GREEN PELITES AND FINE PSAMMITES
PSAMMITES AND PSAMMITIC PELITES IN GRADED UNITS
GRAPHITIC PELITE WITH CHERT AND ASH BANDS
INCREASING GRAIN SIZE
m
2500
2000
1500
1000
500
0
GENERALIZED SEDIMENTARY LOG
SE LIMB
NW LIMB
DECREASING GRAIN SIZE OF SEDIMENTS
FAULT
750
280
360
200
430
370
THICKNESS NOT DETERMINABLE
55
550
370
CORLOCH
LOCHRANZA

Figure 2.3. Geological map of the Dalradian rocks of North Arran. The figure shows the distribution of the major lithological types mapped around the granite together with the orientation of bedding and the S_s/S_1 intersection lineation.

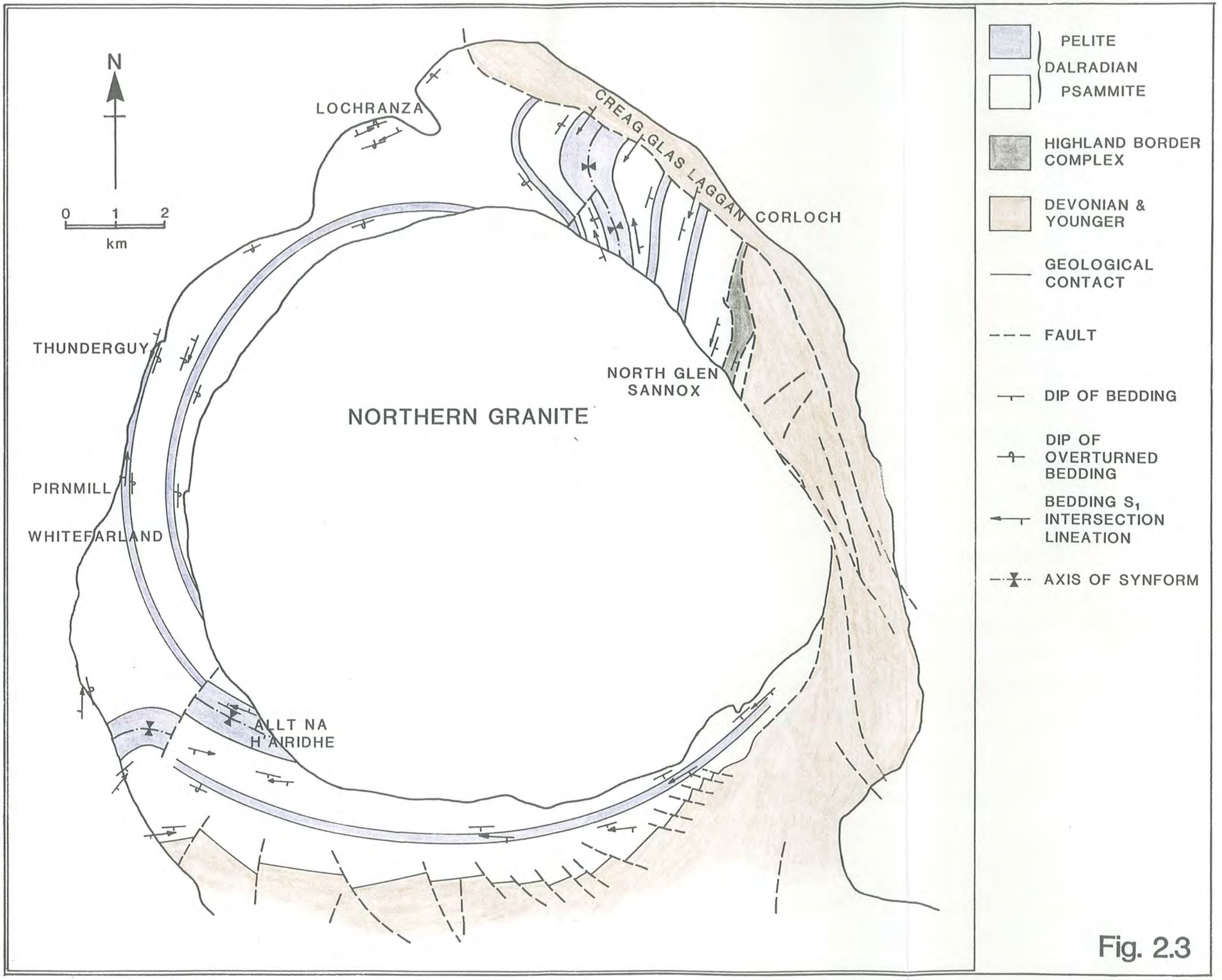
N
0 1 2
km
LOCHRANZA
CREAG GLAS
LAGGAN
CORLOCH
THUNDERGUY
NORTH GLEN SANNOX
NORTHERN GRANITE
PIRNMILL
WHITEFARLAND
ALLT NA H'AIRIDHE
PELITE
DALRADIAN
PSAMMITE
HIGHLAND BORDER COMPLEX
DEVONIAN & YOUNGER
GEOLOGICAL CONTACT
FAULT
DIP OF BEDDING
DIP OF OVERTURNED BEDDING
BEDDING S_1 INTERSECTION LINEATION
AXIS OF SYNFORM

Fig. 2.3

north of the granite. This unit, which is finely laminated, is recorded as containing a thin limestone in the Pirnmill and Thunderguy area (Gunn, 1903), which has been correlated with the Leny Limestone exposed at Callander. The latter has yielded specimens of the Lower Cambrian trilobite genus Pagetes (Pringle, 1940) This age would place the succession of Dalradian rocks in Arran within the Southern Highland Group, the youngest unit of the Dalradian Supergroup, (Harris et al., 1975). However Henderson & Robertson (1982, pp 439) noted that structural interpretations have placed the Leny limestone within the Highland Border Complex. Such an interpretation would appear to be invalidated by the data of Curry et al. (1984) who have demonstrated that the Highland Border Complex is of Arenig age.

The sequences exposed on either side of the fold axis can be correlated on the basis of comparable lithology and thickness (Figs. 2.2 & 2.3). Black shales are always found in the core of the synform, but the pelite bands higher in the sequence may not be so laterally persistent. In particular the green psammitic pelite and pelite band is frequently difficult to distinguish in the field and to the west of the granite at Pirnmill and Whitefarland it appears to be replaced by a band of graphitic pelite. The graphitic pelite at the top of the sequence can be followed clearly from Glen Catacol to Pirnmill but elsewhere it is poorly exposed. To the south of the granite a graphitic pelite occurs sub-parallel to the Dalradian-northern granite intrusive contact. This could be correlated with the middle pelite band. The upper graphitic pelite is not seen to the south of the granite (Fig. 2.3).

As noted above the Dalradian rocks of Arran are folded in the Aberfoyle Synform, which is of Caledonian age. The existence of a fold within the Dalradian of Arran was first noted by Anderson (1944), on the basis of the repeated sequence of sediments in the Lochranza to Corloch area described above. Anderson (1944) used the graded beds as evidence of younging to show the presence of an anticline. This interpretation was corrected by Shackleton (1958) who showed on the basis of

younging directions along the cleavage planes (facing direction) that the structure is a downward facing anticline. The data presented here are consistent with this generally accepted interpretation.

Throughout the Dalradian rocks of Arran the earliest fabric considered to be the result of regional deformation of the sedimentary sequence described above is a penetrative cleavage (S_1) parallel to the axial planes of minor (F_1) folds. This cleavage is overprinted by a spaced extensional cleavage (S_2) which cuts the axial planes of the F_1 folds at a shallow angle. The deformation events producing these foliations will be referred to as D_1 and D_2 respectively. The hinge of the major F_1 fold was then refolded (indicated by an increasing dip of S_2 in an easterly direction) by D_3 which also resulted in folding of the D_1 and D_2 minor structures (Fig. 2.4).

The S_1 cleavage and F_1 minor folds are best developed in the pelitic bands exposed throughout the sequence, particularly on the Pirnmill and Lochranza shores on the western limb of the Aberfoyle Synform. On this easterly dipping limb the S_1 cleavage dips steeper than bedding so minor structural vergence is to the west, indicating the existence of an antiform to the west and a synform to the east. Combining this with evidence of younging direction, (e.g. graded bedding and rip-up clasts) which indicate the sediments are overturned and young to the west shows that facing is downward to the east on S_1 and confirms that the synform is a downward facing anticline. This interpretation is supported by evidence from minor D_1 structures on the eastern limb of the fold. Here cleavage dips shallower than bedding so that D_1 minor structures verge east. The rocks are the right way up (younging east) and hence the facing direction on S_1 remains downward and to the east (Fig. 2.4).

Changes in vergence mapped from cleavage and minor fold geometries confirms the way up evidence which indicates that the axial plane of the Aberfoyle synform lies within the lowest pelitic unit. This is best displayed in the cliffs of Creag Glas

Figure 2.4. A diagramatic summary of the structural evolution of the Dalradian rocks during Caledonian deformation. The three figures show the progressive stages of folding, cleavage development and bedding cleavage orientations from D_1 through to D_3.

Fig. 2.4

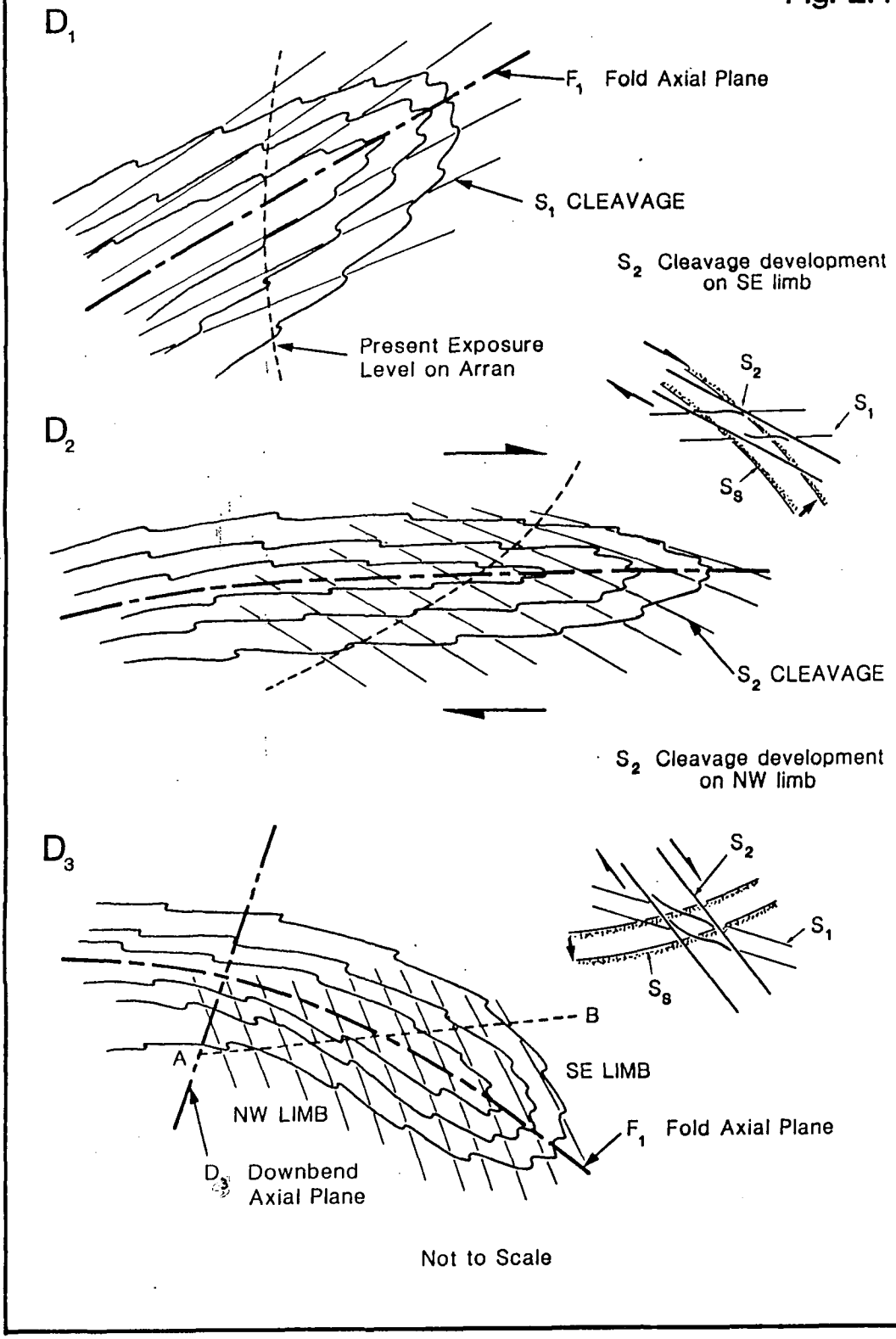
D1
F1 Fold Axial Plane
S1 CLEAVAGE
S2 Cleavage development on SE limb
Present Exposure Level on Arran
S2
S1
S8
D2
S2 CLEAVAGE
S2 Cleavage development on NW limb
D3
S2
S1
S8
B
A
SE LIMB
NW LIMB
F1 Fold Axial Plane
D3 Downbend Axial Plane
Not to Scale

Laggan (GR 972503), but can also be determined from exposures in the Allt na h'Airidhe (GR 818398), to the south of the granite.

The S_2 cleavage is pervasive, and is responsible for the marked coarse foliation of the Dalradian rocks. Again it is best seen on the shores between Lochranza and Dougrie where it is well developed in all but the coarsest psammitic rocks. S_2 is an extensional spaced cleavage which clearly overprints the D_1 minor structures. The spacing varies with grain size. To the west of the Aberfoyle synform it is generally steeper than bedding and to the east it is sub-parallel. The geometry of the S_2 cleavage suggests it formed as a result of flattening and shearing of the D_1 anticline toward the SE. This would be consistent with emplacement of the D_1 fold as a nappe structure to form a recumbent antiform by simple shear, as suggested by Harris et al. (1976). However no strong SE plunging stretching lineation was noted in the field which might support this model.

Mapping across the fold core from Lochranza to Corloch shows a general increase in dip of the S_2 cleavage from 50^o to 70^o, interpreted as the result of D_3 folding around a NW dipping axial plane probably associated with the down-bending of the Aberfoyle Synform to form the steep belt described by Shackleton (1958) (Fig. 2.4).

Following the Caledonian deformation the Dalradian rocks appear to have been largely involved in faulting prior to the emplacement of the Tertiary Northern Granite. In particular early movements along the Highland Boundary Fault resulted in emplacement of a slice of the Highland Border Complex within the Dalradian exposed in North Glen Sannox. The contacts between the two groups of rocks are not well exposed but Henderson & Robertson (1982) have suggested they are thrusts, on the basis of structural data (Fig. 2.5). Dalradian rocks were also affected by movements on the Laggan/Brodick Bay Fault system which originated during the Carboniferous.

Figure 2.5. The structure and stratigraphy of the Highland Border Complex rocks exposed in North Glen Sannox (after Henderson & Robertson, 1982).

Fig. 2.5

NORTH GLEN SANNOX

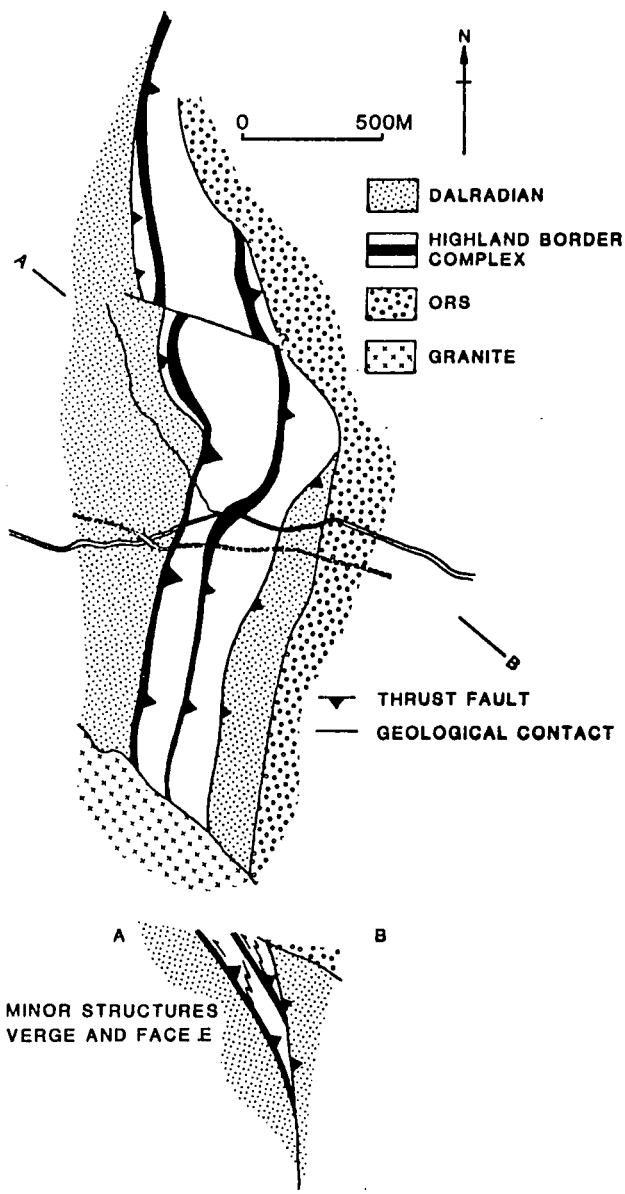

2.2 Petrography of the Dalradian Rocks.

In thin section the pelites, psammites and grits grade into each other in terms of increasing grain size and decreasing clay mineral content. The pelites have a clay content between 40% and 70%. The remainder of this rock type is composed of quartz, chlorite, lithic (quartzite) fragments, albite, opaques and occasional biotite. The S_1 and S_2 cleavages are variably developed. When apparent, S_1 is a penetrative shape and grain alignment cleavage. S_2 which is a spaced pressure solution cleavage is most commonly developed. Where both cleavages are well developed, and intersect at a low angle, the quartz and albite grains are deformed into lensoid 'fish'. Quartz commonly shows undulose extinction and the albite has deformation bands crossing the twin lamellae. Micas mantle the more resistant grains accentuating the S_1 cleavage. Opaques concentrate along the solution planes of the S_2 cleavage. Chlorite can be observed growing along S_1 cleavage planes bent into alignment with S_2 and porphyroblasts of chlorite are cut by S_2. Unaligned grains suggest that post S_2 growth also occurred. Retrogressive metamorphism is indicated by late growth of white mica along the S_2 cleavage planes (Plate 2.1).

The psammites contain a considerably lower fraction of clay minerals (10% to 15%). They are composed dominantly of quartz, large grains of which show clear effects of grain reduction during deformation of the rocks in the form of grain boundary recrystallisation, subgrain growth and undulose extinction. Some grains have associated pressure shadows of granular quartz developed during rotation into the S_1 cleavage plane (Plate 2.2). The smaller quartz grains show a polygonal texture characteristic of dynamic recrystallisation. More resistant grains of albite show deformed twin lamellae, boudinage and well developed syn-S_2 pressure shadows. The general shape of the larger grains suggest they were originally sub-angular to sub-rounded. The S_1 cleavage is generally poorly developed, S_2 being dominant. When the latter is well developed the quartz shows a

Plate 2.1. Typical pelitic Dalradian rock composed of fine grained quartz and micas. S_1 and S_2 are penetrative pressure solution cleavages. S_2 is the dominant cleavage (orientated E - W) which cuts the S_1 cleavage (orientated ENE - WSW) to form an anastomosing fabric. Dalradian pelite, No. 302, Glen Charmadale, GR 948805. Width of field = 3.5 mm, Plane polarised light.

Plate 2.2. Typical Dalradian psammite composed of quartz, minor amounts of alkali feldspar, lithic fragments and micas. Photomicrograph shows well developed S_1 and S_2 cleavages formed by grain alignment. Undeformed porphyroblasts of metamorphic chlorite are developed along cleavage planes. S_1 runs from the top left of the field to the bottom right. Syn - S_1 grain rotation is indicated by rotated porphyroblasts of quartz with pressure shadows cut by the S_2 extensional crenulation cleavage (orientated E - W). Dalradian psammite, No. 601, Catacol shore, GR 915506. Width of field = 3.5 mm, Plane polarised light.

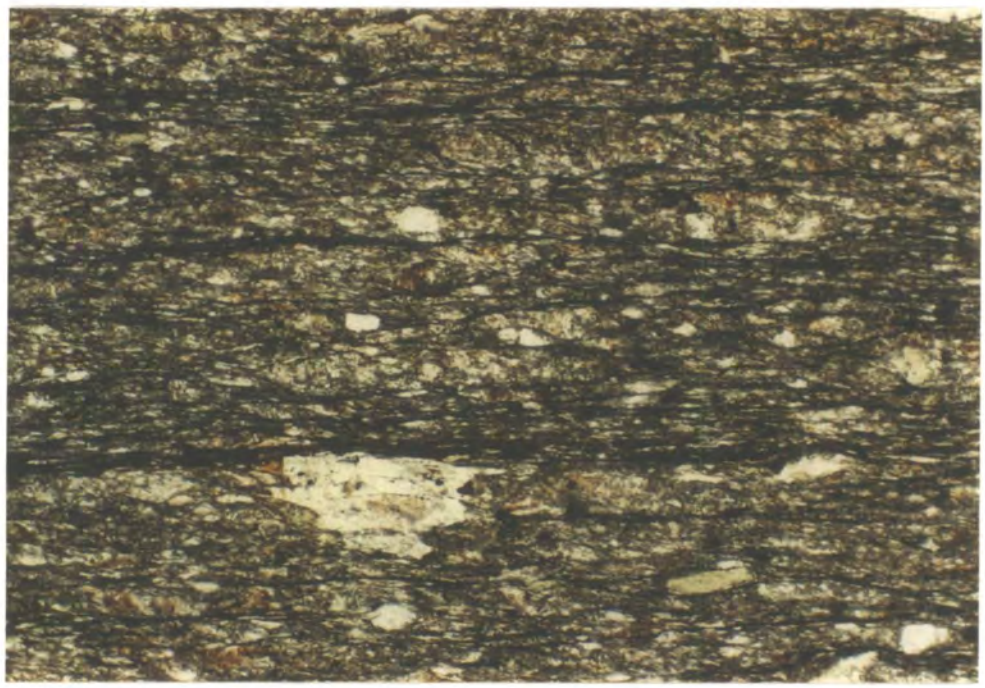

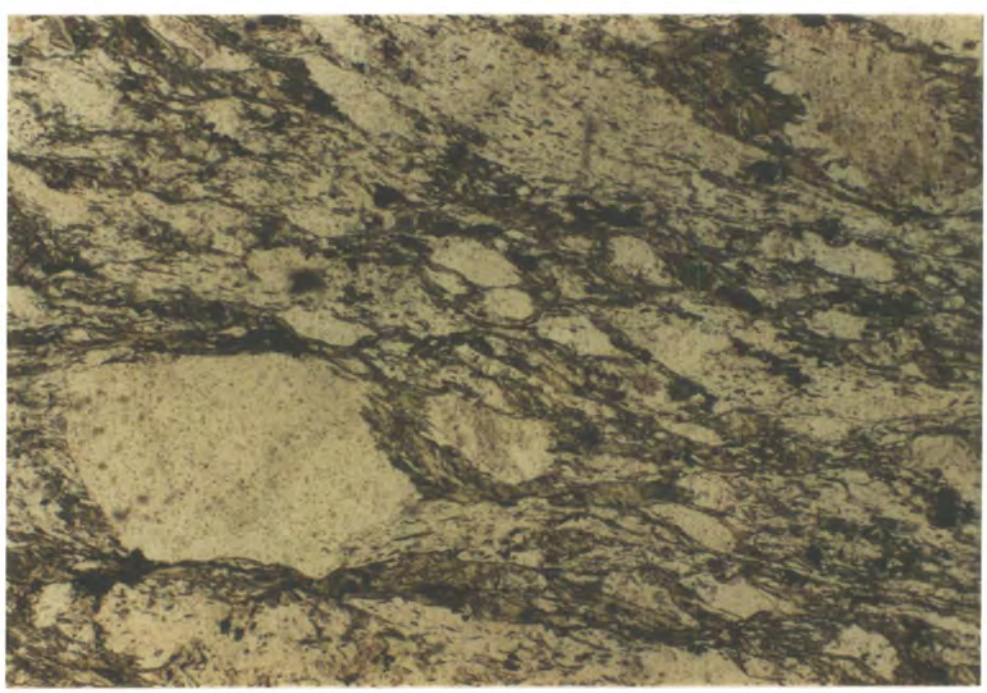

very strong alignment fabric with the development of ribbons of subgrains in the foliation plane. Both cleavages are usually defined by an alignment of mica grains. Chlorite growth is again pre to post S_2. Some post S_2 fractures/joints are filled with chlorite but their actual age cannot be determined. Epidote also occurs in these rocks and is thought to have grown from the breakdown of albite or a more calcic plagioclase. The samples described here were collected well away from the granite aureole to avoid the effects of hydrothermal alteration, although such an origin for the epidote cannot be ruled out. The grits show similar features to the psammites (Plate 2.2).

In conclusion, examination of the rocks indicates they are both texturally and mineralogically immature sediments derived from a proximal low grade metamorphic terrane. The fabric of the rocks clearly records the development of the two distinct cleavages seen in the field. The presence of porphyroblasts of chlorite and the growth of chlorite along S_2 cleavage planes indicates the rocks were subjected to greenschist facies pressures and temperatures during deformation. Since the chlorite pre and post-dates the development of the S_2 cleavage it appears that the peak of metamorphism is of syn-D_2 age. Later (post D_2) retrogressive metamorphism is represented by grain recrystallisation and growth of white mica along S_2 cleavage planes.

2.3 Upper Crustal Structure.

The southeast margin of the Dalradian rocks in Scotland is taken to be the NE–SW striking Highland Boundary Fault (HBF). Within the fault zone lie fragments of black shale and spilites belonging to the Ordovician Highland Border Complex (HBC), Curry et. al. (1984) (Fig. 2.5). To the south of this fault, and locally overlapping to the north, lie conglomerates, sandstones and volcanics of Lower Devonian (Lower ORS) age, within the Midland Valley of Scotland.

Bamford et al. (1977 & 1978) published a seismic refraction profile across the

Midland Valley which revealed the main features of the velocity structure of its northern margin (Fig. 2.6). This profile revealed that there was no geophysical discontinuity across the Highland Boundary Fault zone. Instead the northern margin of the Midland Valley was marked by the abrupt thinning of the uppermost layer of a three layered velocity structure (Fig. 2.6). This is also indicated by a gravity profile across the HBF, McLean & Deegan (1978). Both these profiles indicate that there is no appreciable difference in the density of the rocks to the north and south of the fault beneath the upper layer.

From the surface geology it is known that the upper layer represents the Devonian and Carboniferous sediments infilling the Midland Valley graben, which have a maximum thickness of 2.5 km adjacent to the HBF in the region of the geophysical profiles described above. The middle velocity layer which lies between 2.5 and 8 km in the region of the HBF, and has a P-wave velocity of 5.8 to 6.0 kms^{-1} is known to be the Dalradian to the north of the HBF. To the south of the HBF the layer does not outcrop at the surface and hence the rock type it represents is not known. It is possible that it is an extension of the Dalradian as suggested by McLean & Deegan (1978) and indicated by the presence of Dalradian clasts in agglomerates within the Tertiary central complex, which lies to the South of the Dalradian/ORS unconformity on Arran. However these clasts could be derived from fragments of Dalradian in the ORS (Friend et al., 1963). Bluck (1984) interpreted the Midland valley as an Ordovician – Devonian volcanic – plutonic arc massif floored by a metamorphic terrane of uncertain affinities.

The lower crustal layer which lies below a depth of between 6 and 8 km and has P-wave velocities in excess of 6.4 kms^{-1} clearly extends north of the HBF in the profile of Bamford et al. (1977) (Fig. 2.6). The nature of this layer appears to have been resolved by studies of xenoliths collected from Carboniferous volcanic vents in the Midland Valley. Graham & Upton (1978) and Hunter et al. (1984) have described acid, intermediate and basic xenoliths of granulite facies paragneiss

Figure 2.6. A cross section of the deep structure of the Midland Valley of Scotland and adjacent areas, determined from the LISPB siesmic refraction profile (Bamford, 1978). Velocity values are in kms^{-1}.

Fig. 2.6.

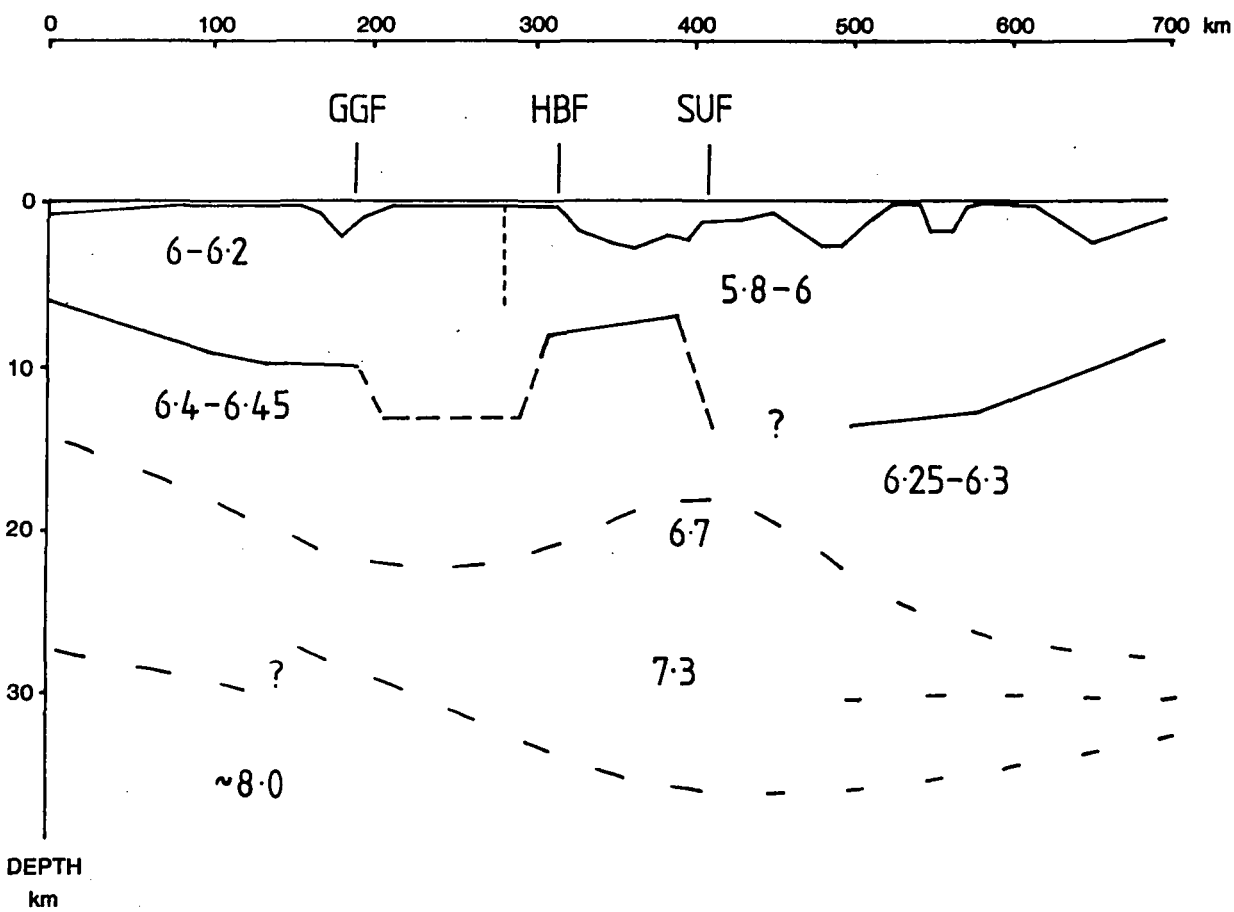
0
100
200
300
400
500
600
700 km
GGF
HBF
SUF
0
10
20
30
6-6·2
5·8-6
6·4-6·45
?
6·25-6·3
6·7
?
7·3
~8·0
DEPTH
km

which equilibrated at 11 kbar and 850°C. Van Breeman & Hawksworth (1980) obtained a $^{147}Sm/^{144}Nd$ age of 1180 ± 55 Ma for one of these xenoliths. This suggests the lower crust in this region was formed during the Grenvillian orogeny. Densities for the xenoliths of between 2.8 and 3.2 gcm^{-3} imply P-wave velocities of the range 6.5 to 7.5 kms^{-1} (Hunter et al., 1984) which are consistent with the velocities determined by Bamford et al. (1977) for the lower crust.

2.4 The Highland Boundary Fault

In mainland Scotland the HBF can be clearly followed from Stonehaven in the NE to the Isle of Bute in the SW. However the position of the fault on the Isle of Arran has been the subject of some discussion (Gunn, 1903; Bailey, 1926; Anderson, 1944; Friend et al., 1963 & 1970). Between Bute and North Arran McLean & Deegan (1978) record a change in structural style along strike from the fault where it outcrops on Bute. Projection of this geophysical discontinuity indicates that the HBF should outcrop at Corloch on the NE coast of Arran. However, later movement on the Laggan fault has downthrown a succession of Upper Palaeozoic rocks in this area which transgress and obscure the fault. Inland of the Laggan fault Lower ORS rocks are apparently faulted against rocks of the HBC and the Dalradian in North Glen Sannox. To the south of the northern granite the Dalradian–ORS contact is clearly an unconformity, first recognised by Friend et al., (1963). The unconformity can be traced to Dougrie on the west coast of Arran. Further along strike geophysical data from Kilbrannan Sound indicates the HBF continues in a Southwesterly direction toward Kintyre (McLean & Deegan, 1978).

The unconformity can be interpreted as an onlap of ORS sediments onto Dalradian to the NW of the actual fault, with the ORS being rotated into its present steep orientation by emplacement of the northern granite. However this does not explain why the fault apparently outcrops in North Sannox at the same topo-

graphic height in a position that prior to the intrusion of the granite was directly along strike from the unconformity now exposed to the south. This problem may be resolved by interpreting the proposed fault marking the western limit of the ORS in North Sannox area as a later normal fault of Tertiary age (accommodating updoming around the intruding granite), as suggested by Friend et al., (1963, pp 419), which propagated up through the ORS from the true HBF, displacing the Dalradian rocks downwards. The ORS rocks onlapping the Dalradian to the NW of this fault could then have been eroded away leaving only the faulted contact exposed (Fig. 2.7).

This hypothesis implies that the HBF is not exposed at the surface in Arran and that it was both cut and deflected to the SE by the intrusion of the Northern Granite. This interpretation will be discussed later in the context of the emplacement of the Northern Granite.

2.5 Post Devonian Geology.

Offshore reflection and refraction siesmic data (McLean & Deegan, 1978) indicates the presence of a number of NW–SE trending faults bounding the NE Arran trough and cutting the strike of the HBF. Hall (1978) noted that the Carboniferous and Permian successions thicken across these faults from the E and NE shores of Arran into the trough, indicating syn-sedimentary fault movement, and that the faults are of Carboniferous age. The Laggan fault has been linked by Hall (1978) with the largest of the offshore faults (the Brodick Bay Fault) bounding the West side of the trough. The age of the Laggan and associated onshore faults is not known since there are few features within the preserved Carboniferous and Permian successions which suggest they were active during sedimentation (Astin & MacDonald, 1983). Gunn (1903) proposed that all the onshore faults were of Tertiary age and that they formed during forceful emplacement of the northern granite. There is a concensus of opinion with Gunn that the faults were active

Figure 2.7. An interpretation of the exposures of the Dalradian-ORS contact on Arran. Map shows the distribution of Dalradian and ORS rocks in the Firth of Clyde area and the position of the Highland Boundary Fault as inferred from geophysical data (McLean & Deegan, 1978). Sections A-B (North Sannox) and C-D (Dougrie) summarize the structural evolution of the contact before (left) and after (right) emplacement of the Tertiary Northern Granite. HBC Highland Border Complex, HBF Highland Boundary Fault.

Fig. 2.7

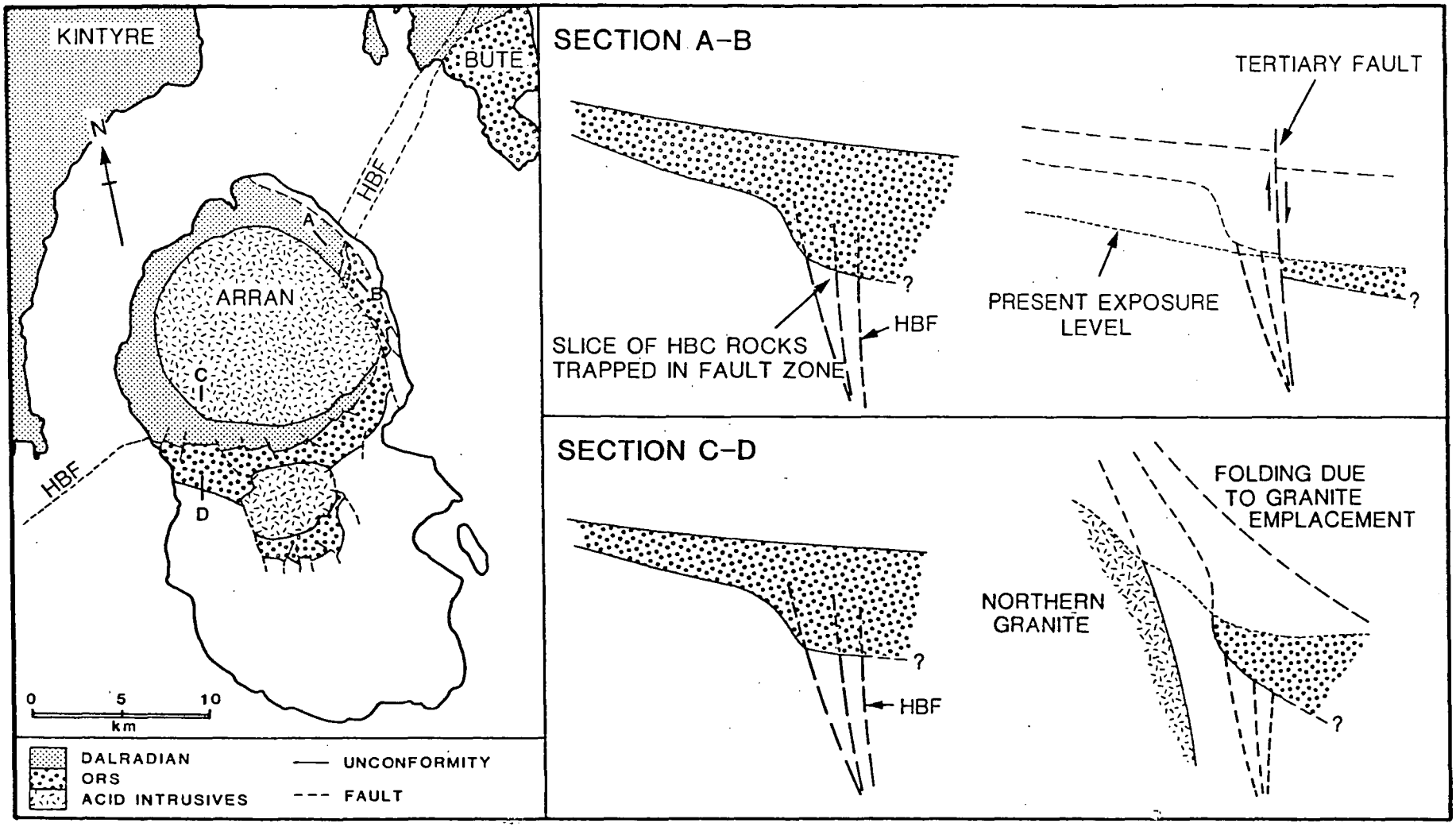
KINTYRE
BUTE
N
HBF
A
B
ARRAN
C
D
HBF
0
5
10
km
DALRADIAN
ORS
ACID INTRUSIVES
UNCONFORMITY
FAULT
SECTION A–B
TERTIARY FAULT
SLICE OF HBC ROCKS
TRAPPED IN FAULT ZONE
HBF
PRESENT EXPOSURE
LEVEL
SECTION C–D
HBF
FOLDING DUE
TO GRANITE
EMPLACEMENT
NORTHERN
GRANITE

during the emplacement of the granite (Bailey, 1926; Tyrrell, 1928; Friend et al., 1963; Woodcock & Underhill, 1987) but Tyrrell (1928) and Woodcock & Underhill (1987) considered them to be reactivated older faults.

The Permian aeolian sandstones and fluvial sandstones and breccias are conformably overlain by Triassic marine and lacustrine muds and silts with occasional sandstones. Rhaetic and younger Mesozoic rocks are confined to remanee masses within the Tertiary central volcanic complex, which lies to the south of the northern granite. An estimate of the amount of subsidence in the central complex was obtained by King (1955) using these masses. At Dereneneach (GR 930331) Permian rocks lie unconformably on Upper ORS, adjacent to the complex. 300m to the NE, within agglomerates of the central complex, lies a large xenolith of Upper Triassic and Rhaetic which indicates subsidence of approximately 900m, (the approximate thickness of the exposed Permian and Triassic rocks on Arran). George (1966) used this subsidence to determine an estimate for the thickness of rock overlying the northern granite, while it was being emplaced, of 2600 m, (neglecting the effects of erosion due to uplift). Using the estimated thicknesses of the Permian and Mesozoic rocks and overlying Tertiary basalts from King (1955) an estimate of 1065m of rock overlying the Carboniferous can be obtained assuming these units maintain constant thickness across the north of the island. It is known from surface exposure that the Carboniferous rocks increase in thickness from zero at Dereneneach, W of the central complex, to 800m on the Laggan shore, NE of the Northern Granite. This suggests about 400m of Carboniferous may have overlain the granite.

The thickness of Dalradian and ORS rocks above the granite is difficult to determine. It is clear that the granite penetrated its carapace of Dalradian along its eastern margin, but the thickness of Dalradian in the roof of the intrusion is impossible to determine. It is apparent that the ORS thinned rapidly across the postulated position of the HBF. Friend et al., (1963) showed that the Lower and

Upper ORS to the South and East of the fault have a cumulative thickness of between 1800 and 1900m. However only a few metres of Upper ORS cornstones and conglomerates are present at Hutton's Unconformity on the North Newton shore (GR 934518) and the ORS may be absent at Catacol where boulders of Carboniferous and Dalradian *but no ORS* form a rocky shoal exposed at low water, (GR 910500), Friend et al. (1970). This suggests that there was only a thin layer of ORS rocks above the northern granite.

From the evidence described above an approximate minimum thickness for the roof of the granite of 2000m can be determined. In any estimate of this type there exists a large margin of error, particularly in this case as none of the estimated thicknesses for the strata involved can be verified accurately due to subsequent erosion of the roof of the northern granite. However this review of the postulated structure of the roof of the intrusion emphasises the point made by Woodcock & Underhill (1987) that the Northern Arran Granite was not intruded into a simple 'layer cake' stratigraphy (Fig. 2.8).

2.6 Summary.

The Northern Arran Granite was intruded into an area of complex geology. Two major normal faults, the early Highland Boundary Fault cut by the later Carboniferous Brodick Bay Fault, form margins to ORS and Permo-Carboniferous sedimentary basins. The sediments within these basins thinned rapidly to the NW and W across these faults and over Dalradian basement rocks folded by Caledonian deformation into a downward facing anticline with a NW–SE strike, parallel to the HBF. The Permian is overlain by Mesozoic and early Tertiary rocks of unknown thickness. The intrusion of an early Palaeocene NNW–SSE trending alkaline Olivine and Tholeiitic Dolerite dyke swarm immediately prior to and during the intrusion of the northern granite, Tyrrell (1928) and Dagley et al. (1978), indicates the regional stress system was dominantly tensional in a

ENE–WSW direction during intrusion.

CHAPTER 3

CONTACT METAMORPHISM

The Northern Arran Granite is surrounded by a narrow concentric zone of thermally altered rocks (Fig. 3.1). This thermal alteration is attributed to intrusion of the coarse granite because it parallels the granite contact, and the stable mineral assemblages developed within the thermal aureole indicate temperatures in excess of those reached during greenschist facies Caledonian metamorphism. Turner (1981) noted that the degree of thermal metamorphism experienced by the rocks surrounding an intruding body of magma depends upon the maximum temperature to which they are heated. This essentially depends upon the following factors: the size, temperature and solidus temperature of the intruding magma body; the specific heat capacities, latent heat and thermal conductivities of the magma and the surrounding rocks, and the initial temperature and water content of the surrounding rocks. All these factors can be determined from experimental data, (e.g. Lovering, 1936; Heuze, 1983), but the process of thermal metamorphism is complicated by less well constrained parameters such as the rate of intrusion, multiple magma injection, syn- and post-intrusion convection of the magma and syn and post intrusion convection of vapour (water/CO_2) within the surrounding rocks, and between the surrounding rocks and the magma (Turner, 1981). Many of these factors will be discussed later in the context of the mechanism of emplacement of the granite. This present section deals with estimating the temperature of the thermal aureole from the mineral assemblages developed in the rocks within it and determining the relative age of the thermal metamorphism to the fabrics developed during deformation of the aureole.

Figure 3.1. A map of the thermal aureole of the Northern Arran Granite showing the extent and distribution of the two metamorphic facies indentified from the petrography of the rocks collected at the locations indicated by their respective sample numbers as given in the text.

Fig. 3.1.

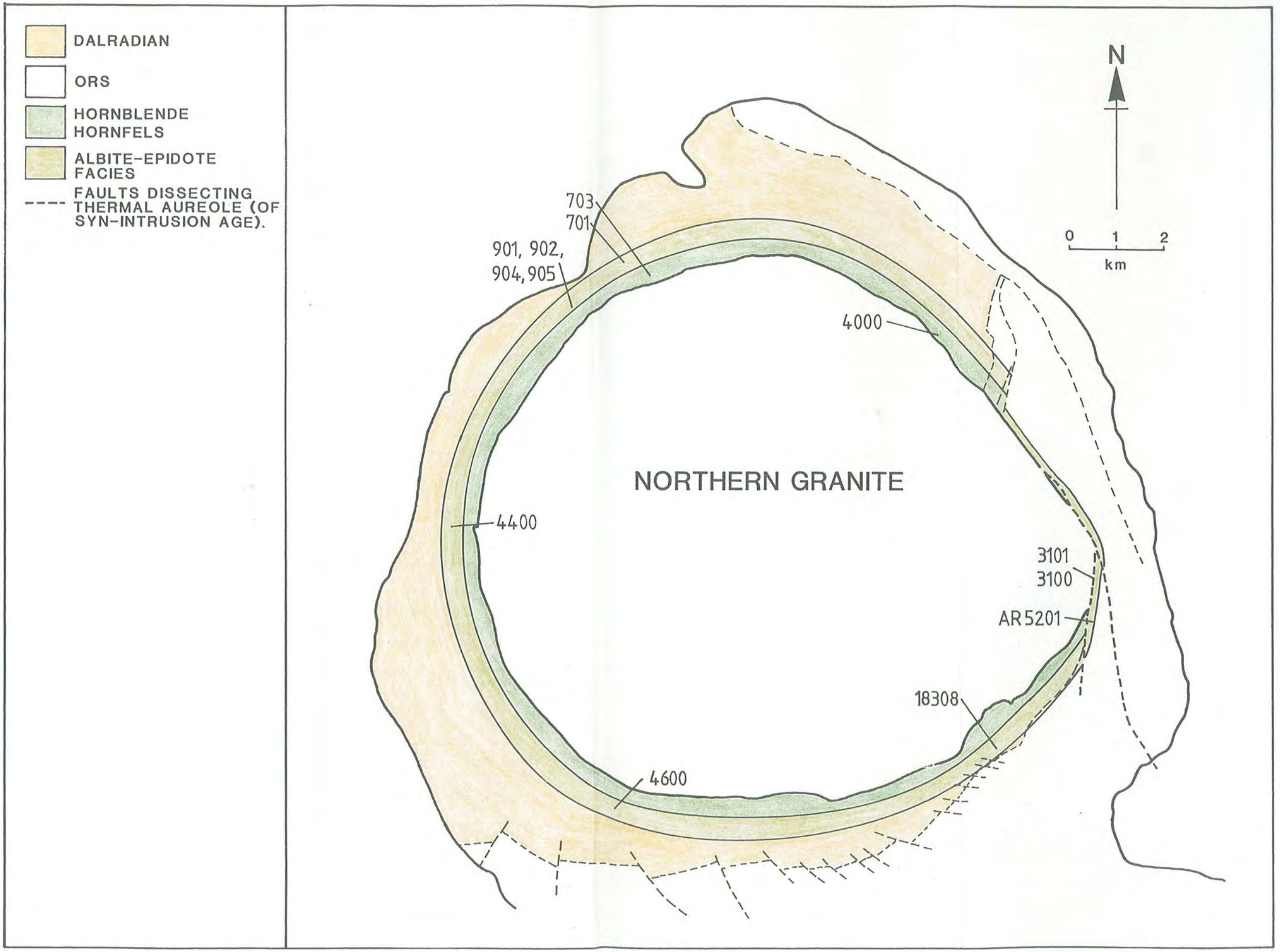
DALRADIAN
ORS
HORNBLENDE HORNFELS
ALBITE-EPIDOTE FACIES
FAULTS DISSECTING THERMAL AUREOLE (OF SYN-INTRUSION AGE).
N
0 1 2
km
703
701
901, 902,
904, 905
4000
NORTHERN GRANITE
4400
3101
3100
AR5201
18308
4600

3.1 The Contact Metamorphic Aureole.

The development of thermal metamorphic mineral assemblages within the aureole of the Northern Arran Granite, previously described by Gunn (1903) and Tyrrell (1928), is strongly dependent upon the distribution of the different lithologies present. As noted in chapter 2, the granite is almost completely surrounded by Dalradian greenschist facies pelites, psammites and grits, except along its eastern margin where it is in contact with ORS sandstones and pillow basalts and shales of the HBC.

The first effects of thermal metamorphism can be detected in pelitic lithologies between 400 and 500 m from the Dalradian/granite contact. In rocks collected from Glen Iorsa (No. 4600, GR 910379, 450 m from the contact) (Fig. 3.1 and Plate 3.1) and the Allt Gobhlach (No. 4400, GR 882441, 425 m from the contact) fine granular biotite begins to replace chlorite, and in the latter, small (1–2 mm) rounded porphyroblasts of cordierite appear. In certain rocks chlorite appears to be stable closer to the contact with the granite. A semipelite collected from the Allt nan Eireannach (No. 901, GR 910486, 250 m from the contact) retains lensoid fish of chlorite of syn–S_2 age while new chlorite, epidote and actinolite have developed as fine grained granular aggregates along and across the pre-existing S_2 cleavage planes. Muscovite, chlorite and graphitic pelites collected from the same locality (Nos. 902, 904, 905) (Plate 3.2) show development of porphyroblasts of prismatic andalusite which cut the S_2 cleavage. A similar graphitic pelite (No. 701) belonging to the same stratigraphic horizon and at the same distance from the contact, collected 500 m along strike in the Abhainn Bheag (GR 918489) showed no evidence of the development of andalusite.

Pelitic rocks less than 200 m from the granite show increasingly pervasive development of granular biotite, porphyroblastic cordierite and recrystallisation of quartz to form equidimensional, granular, strain free aggregates typical of hornfels rocks. The sporadic occurrence of andalusite (Tyrrell, 1928) is probably controlled

Plate 3.1. This pelitic rock shows the growth of granular biotite over the pre-existing Caledonian fabric. The biotite is then distorted during the development of the S_3 pressure solution cleavage. The granular biotite is interpreted as indicative of thermal metamorphism. Dalradian pelite, No. 4600, Glen Iorsa, GR 910379. Width of field = 1.5 mm, plane polarised light.

Plate 3.2. This pelitic rock shows well developed prismatic andalusite cutting the S_2 cleavage (orientated E - W). These porphyroblasts have been rotated during syn-intrusion deformation and development of the S_3 cleavage. Pressure shadows developed during rotation of the porphyroblasts show no consistent sense of shear, which suggest pure flattening strains. A weak S_3 conjugate cleavage is developed in this rock, which can be detected from the folding of S_2. Thin section cut in a vertical plane normal to the granite, with S_2 sub-parallel to the granite contact. Dalradian pelite No. 902a, Allt an Eireannach, GR 910486. Width of field = 3.5 mm, plane polarised light.

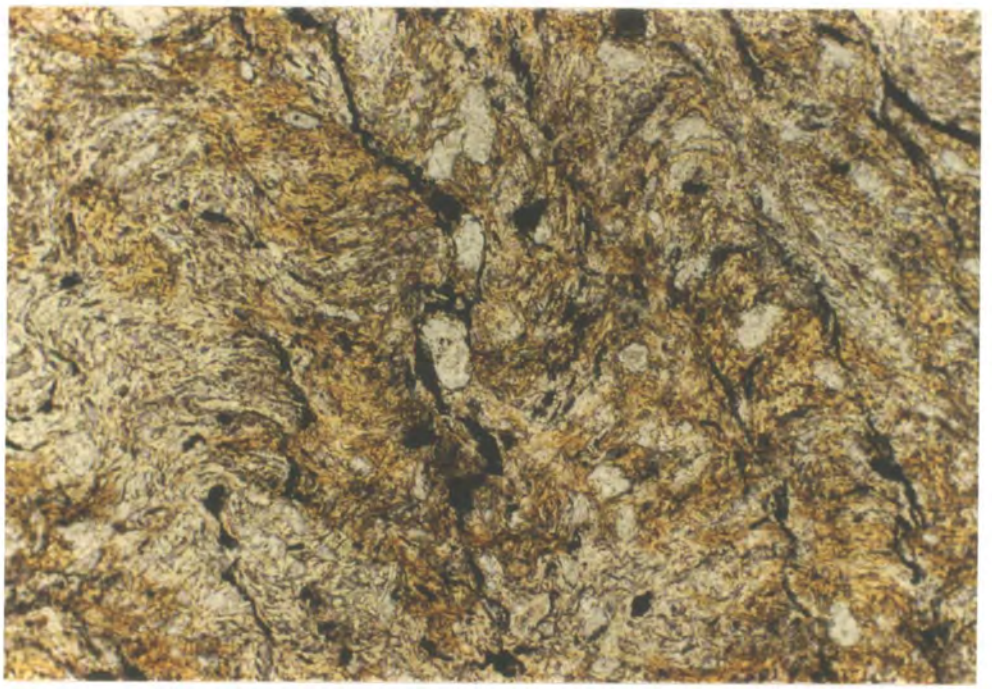

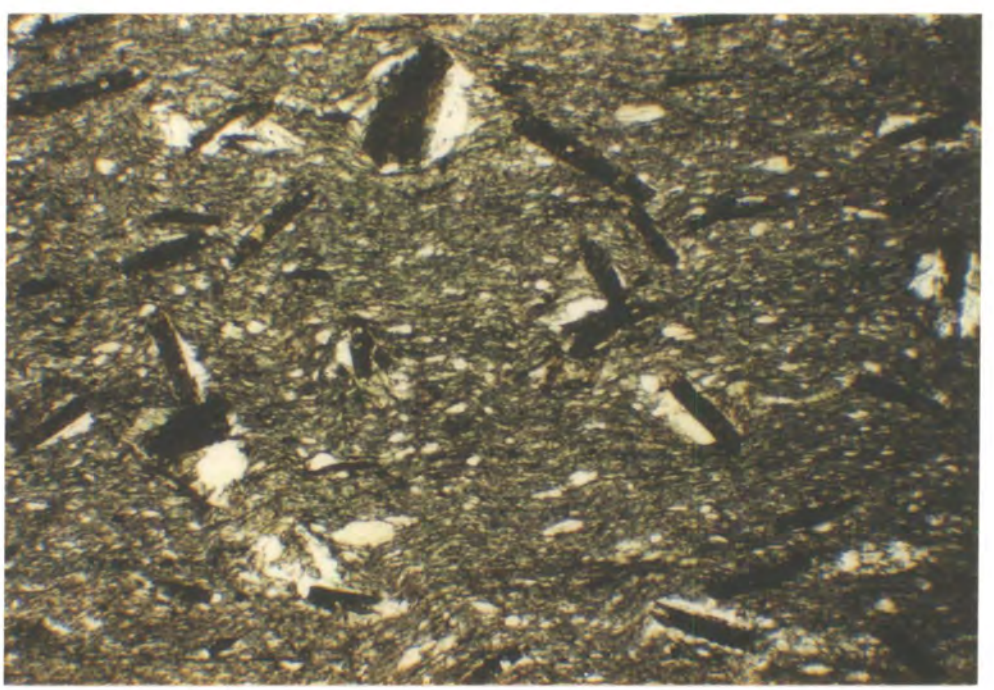

by variations in the aluminium content of the rocks. A hornfels collected from an unnamed tributary to North Sannox Burn (No. 4000, GR 985469, 40 m from the contact) (Plate 3.3) has fine (0.1–0.5 mm) granular aggregates of biotite, cordierite and andalusite developed along the S_2 cleavage planes. The rest of the rock is composed of equidimensional, recrystallised biotite, muscovite, strain free quartz and opaques which overprint the existing Caledonian fabric.

The psammitic rocks show the first signs of alteration at distances less than 200 m from the granite contact. The original quartz grains have recrystallised to equigranular mosaics of strain free crystals, producing tough flinty hornfels. In rocks with a high clay content (e.g. No. 703, collected from the Abhainn Bheag) the existing cleavage planes are preserved by a secondary growth of granular aggregates of biotite and opaques. These quartz rich rocks do not have the high magnesium, iron and aluminium contents necessary to crystallise cordierite or andalusite.

The ORS rocks within the aureole also show evidence of thermal alteration during emplacement of the granite. In Glen Rosa (GR 986381, 500 m from the contact) ORS rocks are bleached to a pale grey colour by reduction of their haematite cement. These rocks also contain small (1 mm) crystals of granular epidote. They are separated from the granite by Dalradian rocks which become increasingly hornfelsed toward the granite. Immediately below the ORS unconformity the Dalradian rocks contain granular epidote, actinolite and biotite (e.g. No. 18308, Univ. of Durham collection). These pass into rocks which show extensive recrystallisation to tough cordierite-bearing hornfels with equigranular textures. Andalusite has also been recorded in these rocks (Tyrrell, 1928).

Tyrrell (1928) recorded bleaching and epidotisation of the ORS within a 50 m wide zone adjacent to the eastern margin of the granite. At the contact between the ORS rocks and the granite the sandstones are brecciated and contain epidote, chlorite and actinolite. Two rocks, one collected from the Uisge nam Fear (No.

Plate 3.3. This photomicrograph shows an intergrowth of granular biotite and andalusite (circled) together with cordierite (forming grey felted masses) developed along a foliation plane in a Dalradian pelite. Biotite, cordierite, andalusite hornfels, No. 4000b, North Glen Sannox, GR 985469. Width of field = 3.5 mm, plane polarised light.

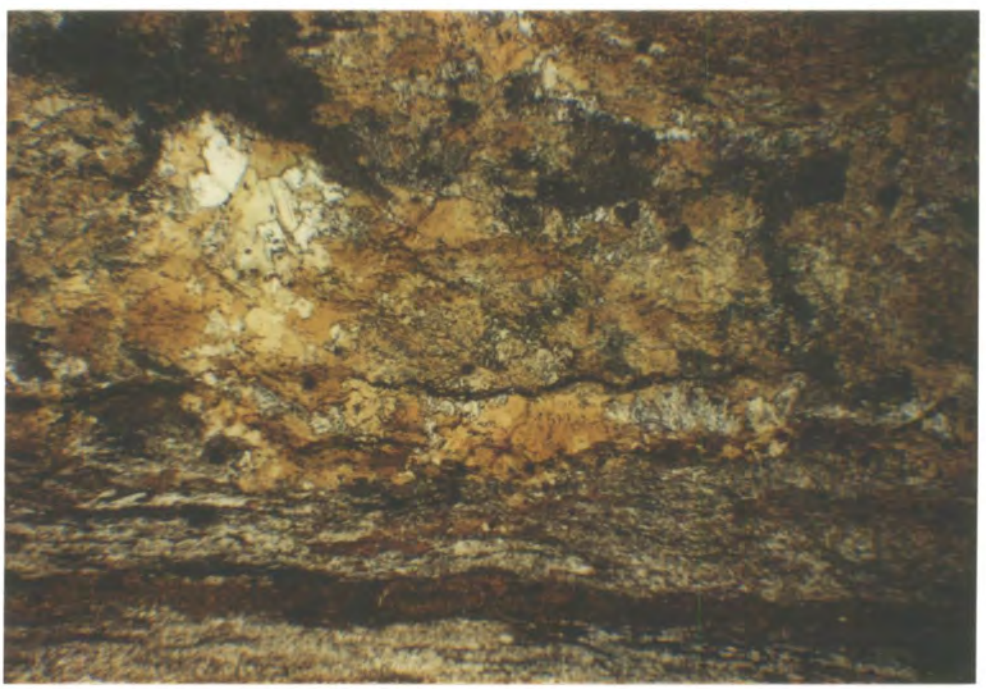

AR5201, GR 012413, 60 m from the contact) and the other from Corrie Burn (No. 3100, Plate 3.4, GR 012417, 4 m from the contact) are composed of bleached, unrecrystallised sandstone containing granular aggregates of epidote, chlorite and actinolite. This rock has been crushed to form a cataclastic fault breccia, composed of angular clasts of altered sandstone in a matrix of finely ground quartz, sandstone clasts and epidote. The sample from Corrie Burn shows further growth of undeformed chlorite and actinolite between the sandstone clasts, after initial brecciation of the rock. Undeformed sheaths of chlorite are also seen in the rock from the Uisge nam Fear. A second rock (No. 3101) (Plate 3.5) collected at the ORS/granite contact in Corrie Burn shows that brecciation of these later bands of chlorite and actinolite is synchronous with brittle deformation of the granite along the contact.

3.2 Interpretation of Aureole Temperatures.

The thermally metamorphosed rocks in the aureole of the Northern Arran Granite can be divided into two groups on the basis of the mineral assemblages developed within them. This new mineral growth clearly overprints the Caledonian fabrics described in chapter 2. The strongly recrystallised hornfels rocks containing the mineral assemblage biotite–cordierite–(andalusite)–muscovite–quartz–opaques form one group. The ORS adjacent to the eastern margin of the granite and the Dalradian rocks outside the hornfels zone (i.e. over 200 m from the granite contact) form the second group. These are characterised by the mineral assemblage epidote–actinolite–biotite–chlorite–muscovite–quartz, and do not show recrystallisation to an equigranular hornfels. These mineral assemblages can be assigned to the hornblende–hornfels facies and the albite–epidote facies respectively.

Turner (1981) defined the upper limit of the albite–epidote facies (the lower limit of the hornblende–hornfels facies) by the breakdown of epidote and the

Plate 3.4. Photomicrograph of a breccia collected 4 m from the contact between the ORS and the coarse granite in Corrie burn. The rock has previously been described as a mylonite. Angular grains of quartz and sandstone in a matrix of finely ground quartz is indicative of brittle, cataclastic deformation at low temperatures and/or high strain rates. Acicular actinolite is developed along a fracture. Granular epidote is visible in the groundmass. Cataclasite, No. 3100, Corrie burn, GR 012417. Width of field = 3.5 mm, crossed polars.

Plate 3.5. Cataclastic rock collected from the contact between the coarse granite (left side of view) and ORS (right side of view). This rock is similar to No. 3100 (Plate 3.4) but shows further deformation which results in the brecciation of the actinolite veins noted in 3100. Cataclasite, No. 3101, Corrie burn, GR 012417. Width of field = 3.5 mm, crossed polars.

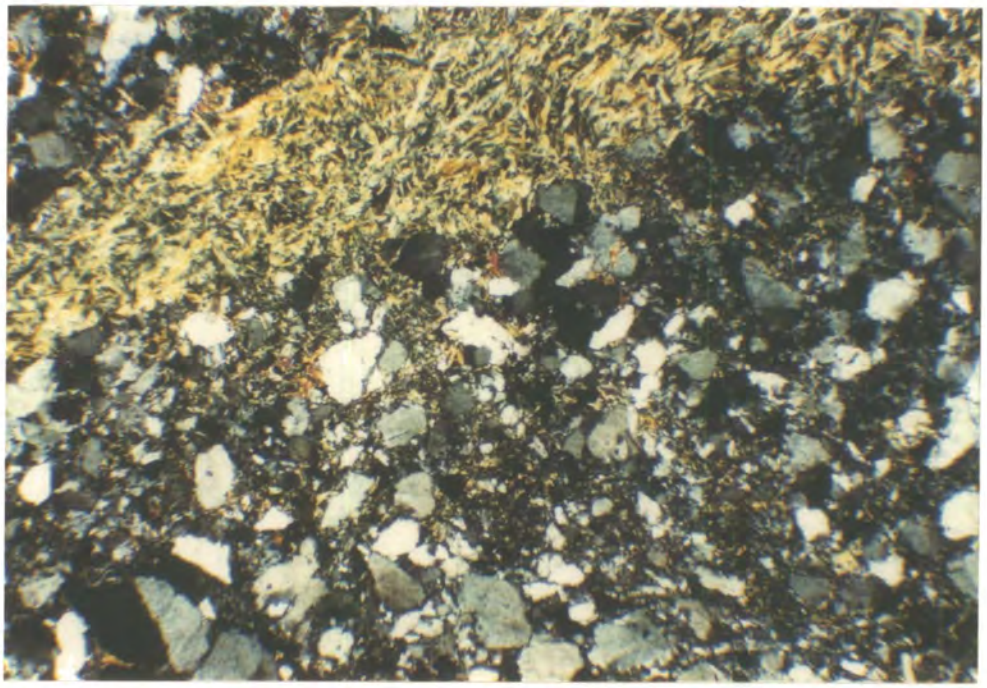

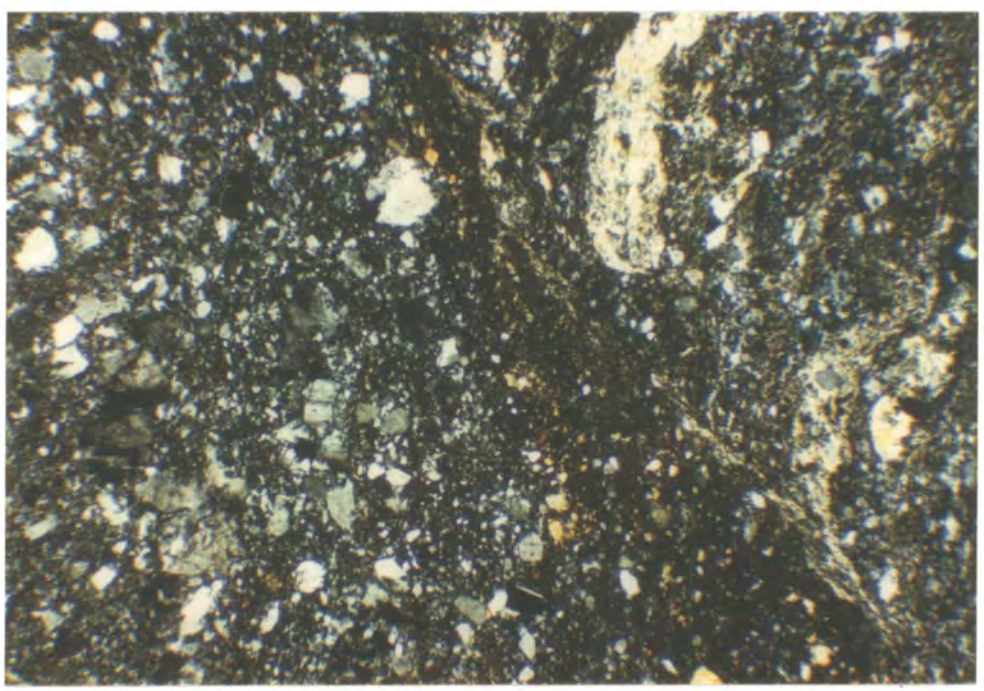

transformation of actinolite to aluminous hornblende, and the upper limit of the hornblende–hornfels facies as lying in the region of the muscovite breakdown reaction:-

$$\text{muscovite} = \text{corundum} + \text{alkali feldspar} \qquad 3.1$$

A crystallisation pressure of between 0.5 and 1.0 kbar can be assumed if the thickness of the roof of the granite is taken to be between 2 and 3 km (chapter 2). At these pressures, reaction 3.1 occurs at approximately 600°C using the pressure–temperature grid for quartz-saturated pelitic rocks published by Pattison & Harte (1985). Turner (1981) suggested the lower limit of the hornblende–hornfels facies occurred at approximately 350°C, and the lower limit of the albite–epidote facies at 300°C 1 kbar $_pH_2O$. Since all the rocks described from the aureole of the Northern Arran granite are quartz- saturated and contain the assemblage quartz + muscovite, neither of which are being consumed at the expense of the growth of alkali feldspar or sillimanite/andalusite, an upper limit can be placed on the temperature of the metamorphic aureole. The reaction:-

$$\text{muscovite} + \text{quartz} = \text{sillimanite} + \text{alkali feldspar} + H_2O \qquad 3.2$$

occurs at approximately 550°C at 1kbar, $_pH_2O$ (Pattison & Harte, 1985), indicating a maximum aureole temperature of 550°C. This temperature is greatly in excess of the temperature range of greenschist facies regional metamorphism (250 to 350°C) previously experienced by the Dalradian rocks.

3.3 The Structure of the Metamorphic Aureole.

The Dalradian the rocks metamorphosed in the hornblende–hornfels facies are always found within 200 m of the granite, inside the zone of albite–epidote facies rocks. The two zones are clearly concentric (Fig. 3.1) and of approximately constant width suggesting that a uniform temperature gradient existed normal to the margin of the granite. This indicates that thermal alteration of the Dalradian

rocks is clearly associated with the rise of the hot granitic magma. It also supports field mapping which indicates that the granite has a uniform steeply dipping contact with the Dalradian.

The ORS rocks along the eastern margin of the granite have developed an albite–epidote facies mineral assemblage indicating they equilibrated at between 300 and 350°C. The only rocks containing hornblende–hornfels facies mineral assemblages along the eastern contact are Dalradian hornfelsed semi-pelites which form a narrow inlier exposed in the Allt a' Chapuill (GR 004442), which are intruded by the granite, and separated by a fault from ~~unmetamorphosed~~ albite-epidote facies ORS. There is good evidence that this fault continues along the contact between the granite and the ORS for some distance to the south. In Coire nan Larach burn (GR 012430) a 2 m wide zone of recrystallised breccia separates the ORS from the granite. The rocks from Corrie burn (described above) clearly indicate fault movement along the contact during development of the thermal aureole (and by implication during emplacement of the granite). A similar fault rock (AR 5201) was also described from the ORS outcropping against a sheared Dalradian hornfels in the Usige nam Fear. These fault breccias have previously been described as 'a narrow zone of compact sheared material' by Bailey (1926), and as a mylonite by Tyrrell (1928). Both these authors clearly mapped a fault - the Goat Fell Fault - along the Eastern margin of the granite.

A complete sequence of ORS and Dalradian rocks metamorphosed in the albite–epidote facies through to hornblende–hornfels facies Dalradian rocks occurs in Glen Rosa (see above). Along the eastern margin of the granite this sequence is not observed and the width of the thermal aureole is considerably truncated, from approximately 500 m to 50m, by faulting which appears to have cut out albite–epidote facies Dalradian rocks in the Usige nam Fear and the Allt a' Chappuil (Fig. 3.2). The truncation of the thermal aureole appears to have been caused by this faulting. The reduction in width of the thermal aureole may

Figure 3.2. Detailed map of the eastern margin of the Northern Granite showing the truncation of the thermal aureole of the granite by postulated syn-intrusion movement on the Goat Fell Fault. (A cross section through the contact at Allt a' Chapuill is given in Fig. 4.36.)

Fig. 3.2.

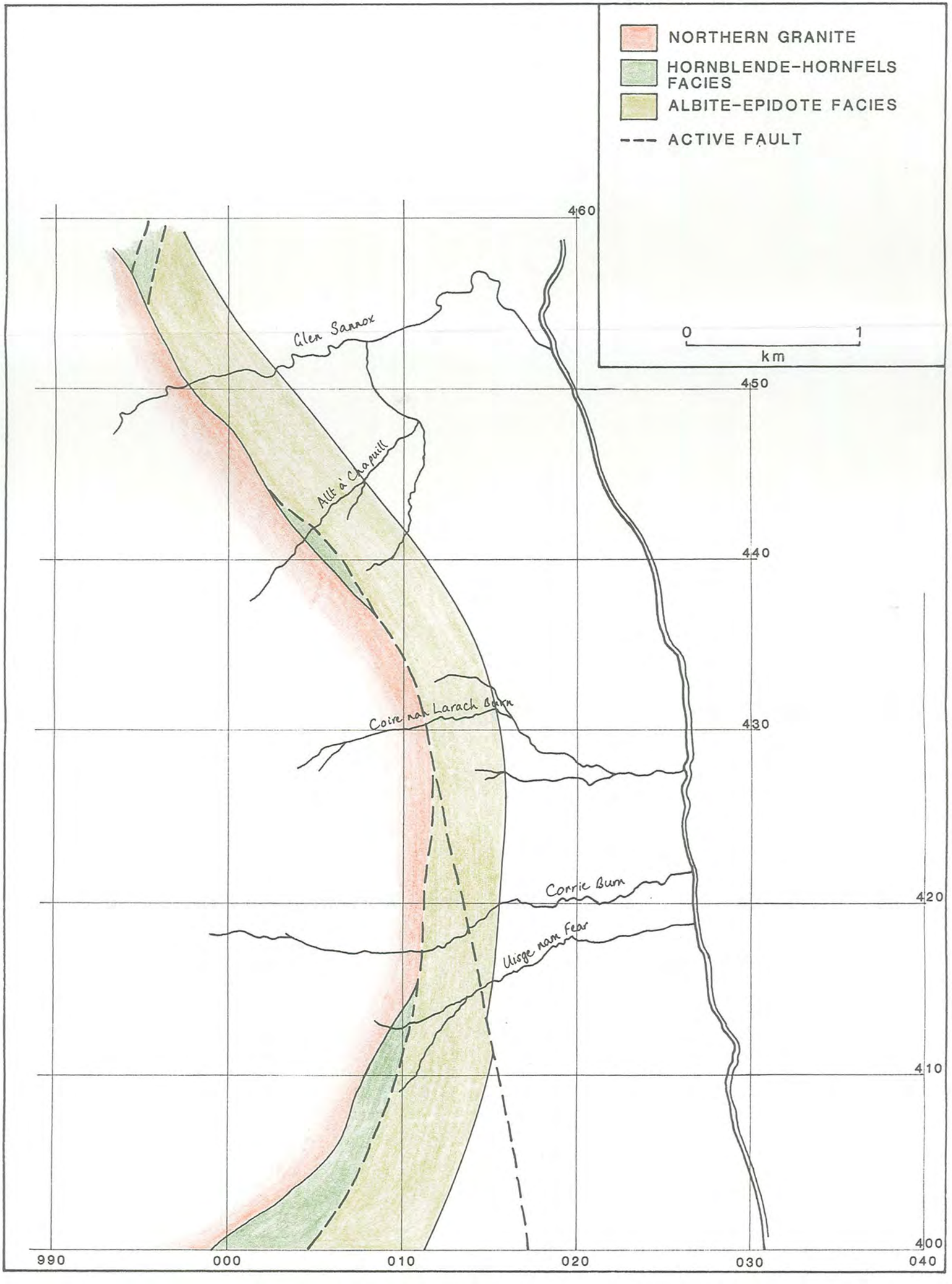
NORTHERN GRANITE
HORNBLENDE-HORNFELS FACIES
ALBITE-EPIDOTE FACIES
ACTIVE FAULT
0
1
km
Glen Sannox
Allt a' Chapuill
Coire nan Larach Burn
Corrie Burn
Uisge nam Fear
460
450
440
430
420
410
400
990
000
010
020
030
040

also have been enhanced by a decrease in the thermal gradient. This could have been caused by water circulating through the fault breccias developed along the contact conducting away heat. Alternatively the granite may have partly cooled before the ORS was faulted against it, and hence it would have heated the latter to a lower maximum temperature.

3.4 Fabric Development.

A number of thin sections taken from Dalradian pelites collected at Glenshant Hill (GR 989395) and North Glen Sannox (GR 985472) show porphyroblasts of cordierite, (2–4 mm in dia.), cut by, and flattened in the plane of a pressure solution cleavage (Plate 3.6). Other samples from the Allt an Eireannach (GR 910486) (Plate 3.2) show a conjugate crenulation cleavage distorted around porphyroblasts of andalusite which have overgrown the S_2 cleavage. These samples indicate that deformation of the rocks occurred after the peak of thermal metamorphism. In these samples, the flattening indicated by the cleavage is sub-parallel to the granite margin. At Glenshant Hill it can be clearly demonstrated that this cleavage is axial planar to a set of minor folds, which deform the S_2 cleavage. The axial planes of these folds and the cleavage dip steeply northward, while bedding dips steeply to the south. This relationship indicates northward vergence, toward the granite. The development of this cleavage and its age relative to the emplacement of the granite will be discussed in the next chapter.

3.5 Summary.

The Northern Arran Granite has a narrow thermal aureole which is approximately 500 m in width. The Dalradian rocks record increasing metamorphic grade toward the granite. Actinolite, chlorite, epidote bearing rocks of albite–epidote facies paragenesis (300 to 350°C at 1 kbar) grade into biotite, cordierite, andalusite

Plate 3.6. Well developed cordierite cut by a pressure solution cleavage (S_3) in a hornfelsed pelite. Cordierite hornfels, No. 4900, Glenshant Hill, GR 989394. Width of field = 3.5 mm, crossed polars.

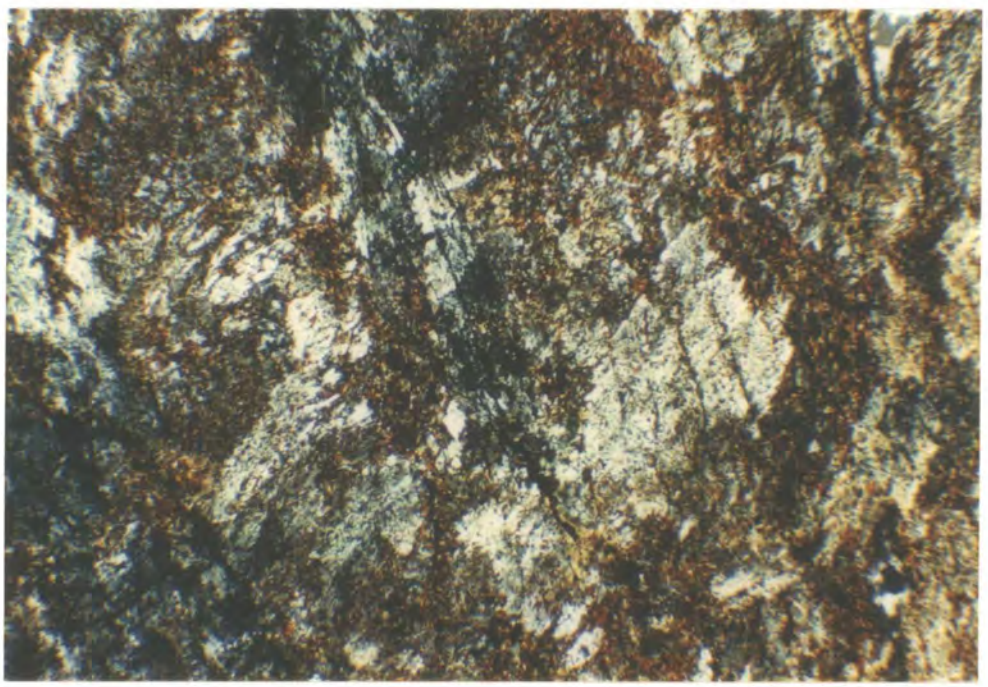

bearing hornfels of hornblende hornfels facies paragenesis (350 to 600°C at 1 kbar). A maximum aureole temperature of 550°C can be implied from the absence of any evidence that the muscovite, quartz dehydration reaction (reaction 3.2) occurred in any of the Dalradian rocks. South of the granite, in Glen Rosa, rocks metamorphosed at albite–epidote facies temperatures are found on both sides of the ORS/Dalradian unconformity. The Dalradian rocks then pass into hornblende–hornfels facies rocks indicating the aureole is completely developed in this area. On the eastern margin of the granite the Dalradian rocks are largely absent. Here the aureole is truncated to a width of 50 m by faulting which displaced albite–epidote facies ORS rocks against the granite during its emplacement. The otherwise regular, concentric, geometry of the aureole indicates that the granite has smooth steeply dipping contacts with its wall rocks.

Porphyroblasts developed in the pelitic Dalradian rocks pre-date a spaced cleavage which is axial planar to a set of folds which deform the S_2 cleavage. These folds and associated cleavage verge toward the contact with the granite.

CHAPTER 4

INTRUSION RELATED STRUCTURES AROUND THE NORTHERN ARRAN GRANITE

Since the earliest recorded geological fieldwork in Arran, by Hutton (1795), it has been recognised that the Northern Arran Granite is surrounded by rocks strongly deformed by its emplacement. Gunn (1903), and subsequently Bailey (1926) and Tyrrell (1928), regarded the granite as being forcefully emplaced. This view of the outer granite is generally accepted. Most of the post–Permian movement in the Laggan/Brodick Bay fault system has always been attributed to intrusion of the granite (Tyrrell, 1928; Woodcock & Underhill, 1987), but the deformation of the Dalradian rocks during intrusion of the granite has never been the subject of detailed work. However it is clear that the deformation of the Dalradian rocks may provide more information about the ascent and emplacement of the granite than the faulted ORS–Carboniferous rocks.

This chapter will describe the deformation of the Dalradian rocks and how the resulting structures may be interpreted. This is followed by a description and discussion of the faulting associated with the emplacement of the granite. Finally the interpretation of the gross structure of the aureole will be discussed and a model for the ascent and emplacement of the granite based on the structural data will be derived.

4.1 The Contact between the Dalradian rocks and the Northern Granite.

For much of its circumference the contact between the outer coarse granite and its aureole is poorly exposed. The sub-circular contact shown on geological maps (Fig. 4.1) is largely established on the basis of an increase in slope as the contact

Figure 4.1. The geology of North Arran, showing the structure of the Dalradian rocks and the position of the Granite/Dalradian contact.

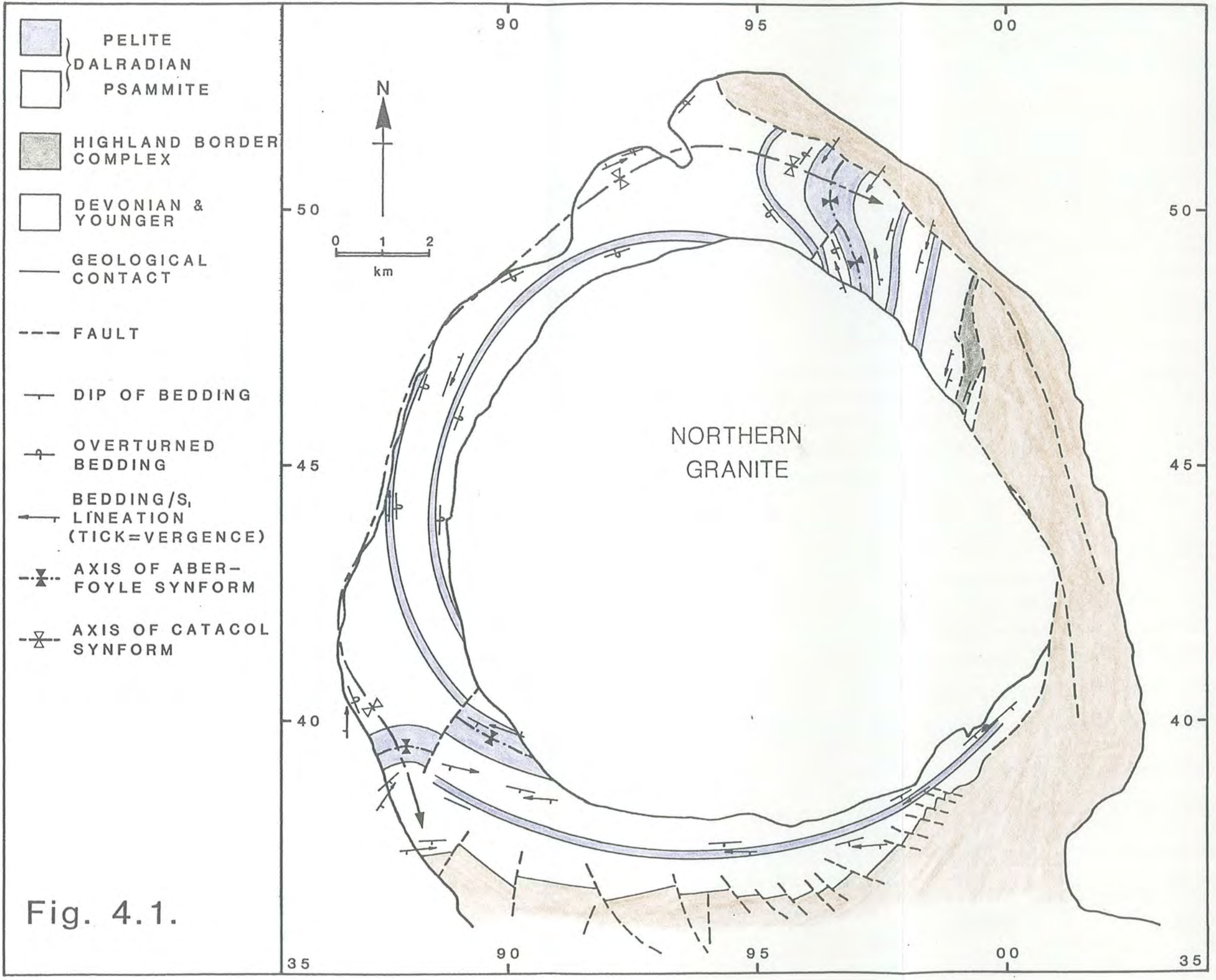
PELITE
DALRADIAN
PSAMMITE
HIGHLAND BORDER COMPLEX
DEVONIAN & YOUNGER
GEOLOGICAL CONTACT
FAULT
DIP OF BEDDING
OVERTURNED BEDDING
BEDDING/S1 LINEATION (TICK=VERGENCE)
AXIS OF ABER-FOYLE SYNFORM
AXIS OF CATACOL SYNFORM
N
0 1 2
km
NORTHERN GRANITE
90
95
00
50
45
40
35

Fig. 4.1.

is crossed from the aureole into the granite. However there are some exposures of the contact with good vertical relief which give an indication of its orientation. On the northern margin of the granite the contact is well exposed in the cliffs of Tor Nead an Eoin (GR 950491), and the hills of Madadh Lounie (GR 921487) and Creagan nan Gobhar (GR 911487) on either side of the mouth of Glen Catacol. On its western margin the contact is exposed in the Allt Goblach (GR 884439) and to the south of the granite on Glenshant Hill (GR 986394). At Tor Nead an Eoin and in Glen Catacol the contact dips steeply outward at about 80^o near sea level; shallowing to 70^o at 300 m. In the Allt Goblach it is vertical. The contact can be traced from Glenshant Hill to the Garbh Allt across Glen Rosa where it extends to the southeast, indicating a steep dip in this direction.

The contact is generally smooth and very sharp. The Dalradian rocks always dip away from the margin of the granite or are parallel to it on a gross scale. In detail the contact is slightly irregular. For example, at Madadh Lounie, Creagan nan Gobhar and Glenshant Hill a limited number of sub-horizontal and irregular veins of granite cut the Dalradian. Xenoliths of Dalradian in the granite are rare, even at the contact, where they are found only within the chilled margins of the intrusion. Along the west and south sides of the intrusion the strike of the Dalradian rocks is parallel to the edge of the granite. To the northeast and southwest the Dalradian rocks in the core of the Aberfoyle synform strike at an angle to the contact. Between Torr Nead an Eoin and Cnocan Donna (GR 995460) the Dalradian and Highland Border Complex rocks strike approximately North–South. Hence they must be cut by the NW–SE trending margin of the granite. This relationship can be demonstrated in a small tributary to North Sannox Burn at GR 980473. However in North Sannox burn a well exposed contact at GR 985468 indicates that the Dalradian rocks are locally deformed so that their strike is parallel to the contact. Southwest of the granite the contact is not exposed and hence it is impossible to determine whether the Dalradian rocks are deflected

from their general East–West strike within the core of the Aberfoyle synform.

Within the 200 m wide zone of hornfels rocks (chapter 3) the Dalradian rocks dip very steeply outward from the granite at between 70^o and 80^o. Outside the hornfels zone the dip shallows sharply to around 60^o. On the western side of the granite graded bedding in grits exposed to the east of Thunderguy at GR 884464, and along the west coast of the island, consistently indicate that these rocks are overturned and that they young toward the granite. South of the granite similar graded units indicate the rocks are the right way up and young toward the South. The S_1 cleavage in these rocks always dips at a shallower angle than bedding, confirming that all the Dalradian rocks exposed to the south of the granite lie in the SE limb of the Aberfoyle Synform (chapter 2).

The strike of the pelitic units in the core of the Aberfoyle Synform is clearly distorted from the NE–SW regional trend of this structure. To the northeast and southwest of the granite its strike is deflected eastwards, sub-parallel to the granite margin. In both areas the rocks retain their original steep dip.

Hence it appears from the stratigraphy of the Dalradian rocks and their contact with the granite that the Aberfoyle Synform has been partly cut and partly deformed by the intrusion of the pluton. The granite clearly cuts the axial plane and core of the fold, but deflects its northwest and southeast limbs upwards and outwards ~~respectively~~. This has resulted in the development of a zone of steeply outward dipping rocks around the granite.

4.2 Geometry of the Catacol Synform and Associated Minor Structures.

Exposures of SE dipping Dalradian rocks which young to the NW can be found along the coast between Catacol (GR 910496) and North Newton (GR 941522). These rocks, and others exposed on the coast further south (chapter 2), lie in the NW limb of the Aberfoyle synform. The S_1 cleavage in these rocks dips more steeply than bedding, so they are downward facing. The northwest and westerly

dipping rocks adjacent to the granite and lying to the northwest of the axial plane of the Aberfoyle synform also belong to the NW limb of this structure (Fig. 4.1). However the S_1 cleavage in these rocks dips at a shallower angle than bedding. This is due to the refolding of the NW limb of the Aberfoyle synform about the axial plane of a later synform parallel to the granite/Dalradian contact. This structure was first noted by Gunn (1903). Bailey (1926) observed that its axial plane was concentric to the granite and hence attributed its formation to forceful intrusion of the pluton into the Dalradian. This fold is referred to as the Catacol Synform.

The hinge of the synform can be traced as a zone of neutrally verging folds in pelitic and psammitic Dalradian rocks which outcrop on the western shores of the island (approximately 1.5 km from the granite). To the north of Catacol and to the south of Whitefarland point (GR 867427) the fold runs inland, crossing the axial plane of the Aberfoyle synform to the northeast and southwest of the granite at approximately 90^o before fading out (Fig. 4.1). Hence the fold is largely confined to the NW limb of the Aberfoyle synform.

As noted above, uplift of the Dalradian rocks has occurred to the south of the granite, but no fold appears in this area. The dip of the Dalradian rocks decreases as they pass beneath the ORS unconformity. Similarly dips in the ORS rocks decrease southwards away from the granite. Shallow southward regional dips can be measured in Permian rocks approximately 5 km to the south of the granite at Machrie (GR 897330). This suggests uplift due to the intrusion of the northern granite diminished within a radius of 5 km from its margin.

The Catacol synform refolds the Aberfoyle synform and the S_1 and S_2 cleavages developed during the Caledonian deformation (chapter 2). The scale and geometry of this refolding has been examined using the bedding (S_s), and the bedding/S_1 cleavage intersection lineation (S_s/S_1). There is no evidence that the geometry of this lineation has been strongly disturbed by post D_1 Caledonian

deformation. The lithostratigraphy and the S_2 cleavage geometry are unsuitable for analysing the structure of the Catacol synform because the lithostratigraphy around the granite is not uniform and the S_2 cleavage cross cuts the axial plane of the Aberfoyle synform so that it does not have a constant vergence relationship to bedding on either side of the axial plane of this structure.

Immediately south of the Laggan Fault between North Newton and Creag Glas Laggan (GR 972503) a narrow strip of Dalradian rocks have the NE–SW regional strike of the Dalradian on the Scottish mainland. On this basis these rocks are taken to be largely unaffected by syn-intrusion deformation. Hence they could be used as a reference orientation in determining the geometry of the Catacol synform and the deformation associated with its formation. Inland of these localities the strike and axial plane of the Aberfoyle synform swings toward a NW–SE strike about the axial plane of the Catacol synform.

Figure 4.2 shows that the 'undeformed' rocks of the Aberfoyle synform, immediately south of the Laggan Fault, dip at between 20^o and 80^o toward the East and have a NNE–SSW to NE–SW strike. This strike variation suggests they have been slightly deflected from the NE–SW strike measureable across the Isle of Bute. The S_s/S_1 intersection lineation is sub-horizontal and parallel to the strike of bedding.

Across the axial plane of the Catacol synform bedding shows a wide variation in dip and dip direction from 70^o toward the E, to 30^o toward the NNE (Fig. 4.3). The steeply eastward dipping rocks lie on the SE limb of the Aberfoyle synform in the North Sannox area. These rocks show little evidence of having been refolded. The shallowly dipping NW–SE striking rocks from Glen Charmadale lie in the NW limb of the Aberfoyle synform. Their rotation is clearly the result of folding around the axial plane of the Catacol synform. The S_s/S_1 intersection lineation south of the Catacol synform is rotated into a N–S orientation, but remains sub-horizontal. Figures 4.2 and 4.3 do show some variation in the orientation of this

Figure 4.2. Equal area stereogram showing the orientation of bedding (solid circles) and the S_3/S_1 intersection lineation (crosses) measured from the Dalradian rocks between North Newton and Creag Glas Laggan, north of the axial plane of the Catacol synform. The great circle shows the average dip of bedding in the northern limb of the Catacol synform.

Figure 4.3. Equal area stereogram showing the orientation of bedding (solid circles) and the S_3/S_1 intersection lineation (crosses) measured from the Dalradian rocks in Glen Charmadale and North Glen Sannox, south of the axial plane of the Catacol synform. Great circle shows the average dip of bedding in the southern limb of the Catacol synform.

Fig. 4.2.

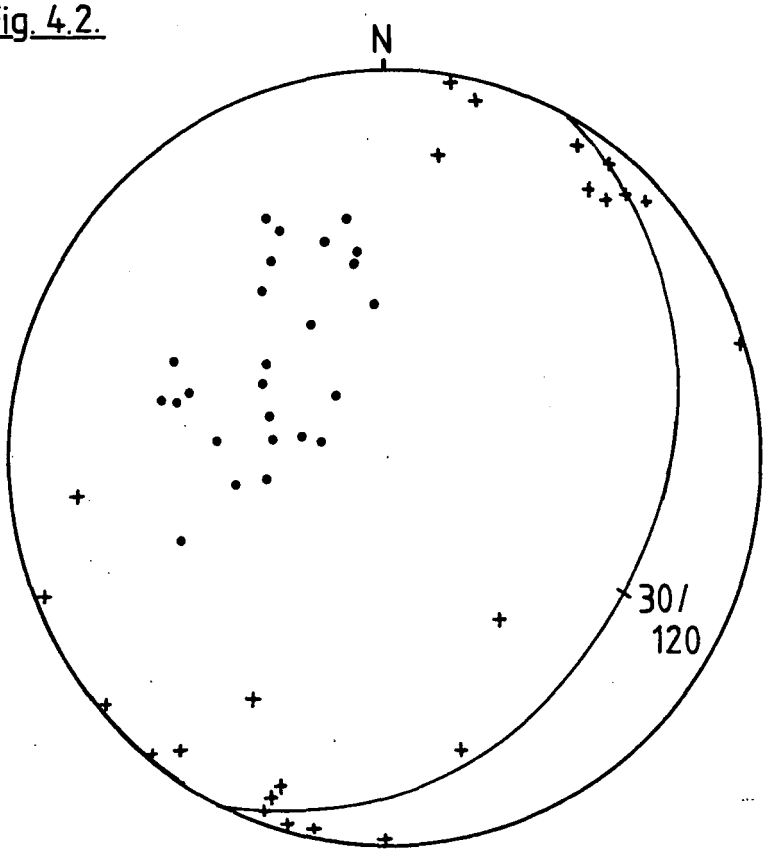

Fig. 4.3.

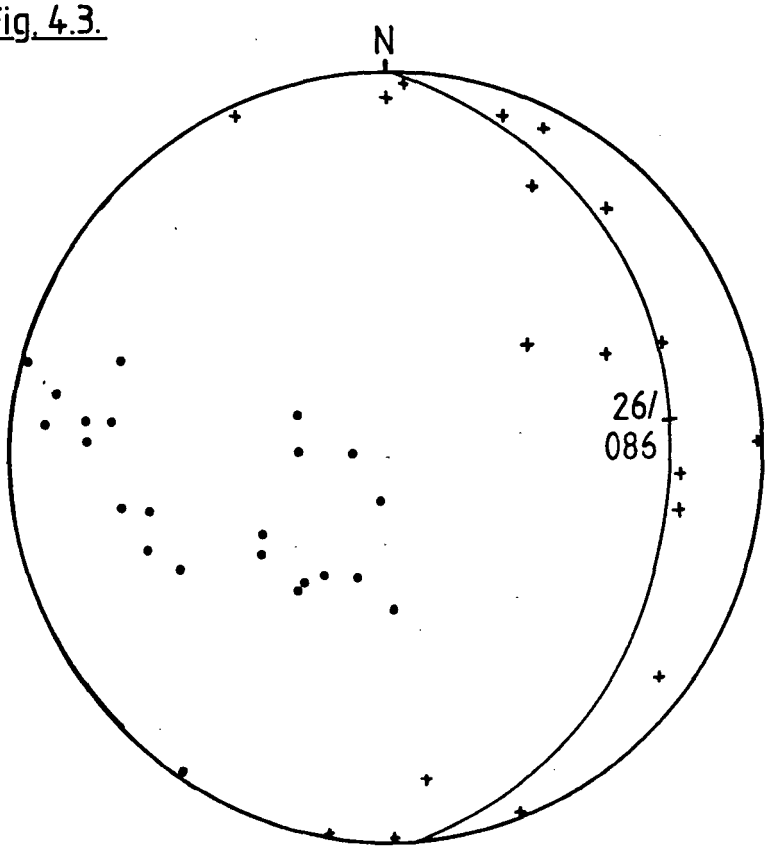

lineation. In particular the more steeply dipping lineations are due to the non-parallel strike of S_s and S_1 measured at some localities.

The geometry of the Catacol Synform to the north of the granite can be deduced by combining figures 4.2 and 4.3 (Fig. 4.4). From this it can be seen that the S_s/S_1 intersection lineations lie on a poorly defined great circle, suggesting that the fold is of 'similar' type (Ramsay, 1960). There is considerable spread in bedding orientation, but reference to figs 4.2 and 4.3 allow the two limbs of the Catacol synform to be defined. An average orientation of the undeformed limb of 30^o toward 120^o (dip and dip direction) was determined from figure 4.2 by obtaining the best fit great circle to the S_s/S_1 intesection lineations. Each measurement of a lineation is taken as the plunge of that lineation on the bedding plane at outcrop. Hence the lineation must lie on a bedding plane when plotted on the stereonet. Fitting the lineations to a great circle gives an average orientation for bedding in a particular limb of the fold. This technique was used to determine an orientation of 26^o toward 086^o for the deformed limb of the fold from figure 4.3. This estimation is poor due to the wide range of orientations shown by bedding in this limb, as it is not a planar feature. This is particularly clear from figure 4.1 which shows that it swings into an orientation which is sub-parallel to the margin of the granite. The angle of dip of bedding remains almost constant along strike around the axial plane of the Catacol synform. The deformed limb is not upturned against the granite, except close to its margin.

The intersection of the two great circles repesenting the fold limbs indicates the Catacol synform plunges at 29^o toward 084^o. By constructing the profile plane and determining the position of the hinge of the fold the approximate orientation of axial plane of the Catacol synform can be determined (Fig. 4.4).

The refolded core of the Aberfoyle synform is poorly exposed to the south-west of the Northern Granite. Figure 4.5 shows the S_s and S_s/S_1 intersection lineation for the Dalradian rocks in the western limb of the Catacol synform be-

Figure 4.4. Equal area stereogram compiled from Figs. 4.2 & 4.3, showing the geometry of the Catacol synform to the north of the northern granite.

Fig. 4.4.

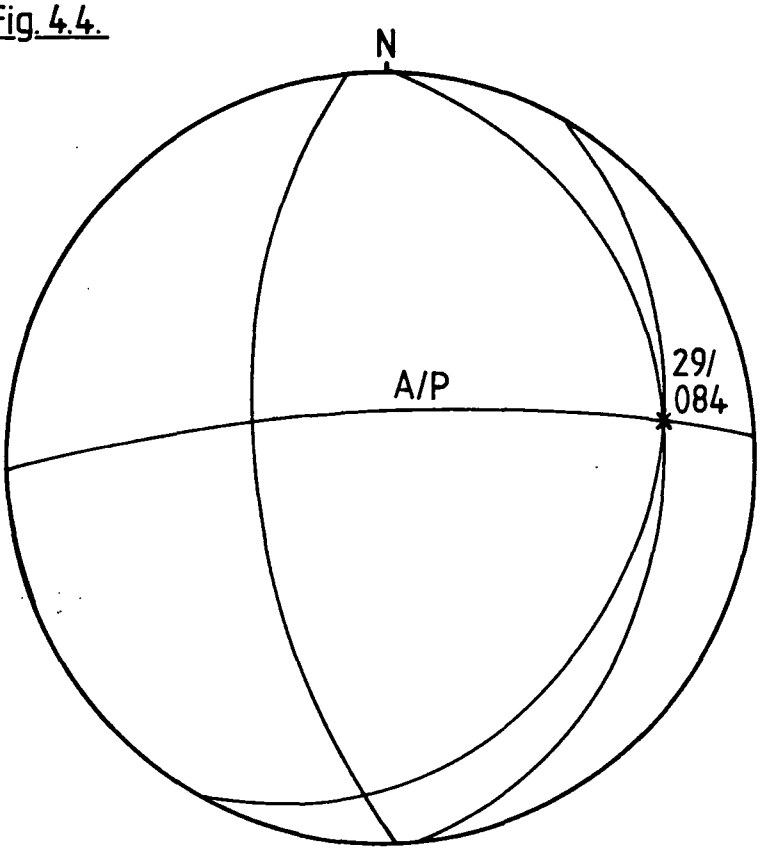

tween Whitefarland and Dougrie (GR 877374). The only feature notable from this set of data is the NW–SE strike of bedding parallel to the granite margin. This suggests intrusion of the granite has distorted the Dalradian rocks from the regional NE–SW trend. Figure 4.6 shows the orientation of bedding and the S_s/S_1 intersection lineation taken from two stream sections (Glen Scaftigill and the Allt na'h Airidhe) which expose rocks in the SE limb of the Aberfoyle synform. These rocks are overturned and dip steeply ($60^o - 80^o$) toward the NW. This suggests these rocks have not been strongly affected by the intrusion of the granite.

Further east, between Glen Iorsa and Glenshant Hill, the strike of bedding in the SE limb of the Aberfoyle Synform is parallel to the southern margin of the granite (Fig. 4.1). This is the result of open folding of the rocks about a steeply SE plunging axis parallel to the margin of the granite, which is reflected in the spread of the S_s/S_1 intersection lineation data from its original sub-horizontal orientation (Fig. 4.7).

As noted above, the Dalradian rocks in the NW limb of the Aberfoyle synform, on the western side of the island, dip away from the granite. The axis of the Catacol synform runs along the coast in this area. As with the Dalradian south of the granite, the strike of bedding in these rocks is parallel to the edge of the intrusion (Fig. 4.1). Figure 4.8 shows data collected from the Thunderguy (GR 880467) and Pirnmill (GR 871441) area, where the granite/Dalradain contact has a NNE–SSW strike. The plot shows that the S_s/S_1 intersection lineation has remained approximately horizontal, suggesting that folding in this area took place around an axis parallel to the strike of bedding. The range of dip shown by bedding reflects the steepening of the eastern limb of the Catacol synform against the granite.

Figures 4.9 and 4.10 show data collected from sections through Lochranza and Catacol, normal to the axis of the Catacol synform. Both figures indicate a variation in the dip of bedding either side of the fold axis (the poles to bedding

Figure 4.5. Equal area stereogram showing the orientation of bedding (solid circles) and the S_3/S_1 intersection lineation (crosses) measured from the Dalradian rocks in the western limb of the Catacol synform between Whitefarland and Dougrie.

Figure 4.6. Equal area stereogram showing the orientation of bedding (solid circles) and the S_3/S_1 intersection lineation (crosses) measured from the Dalradian rocks in the SE limb of the Aberfoyle synform to the east of the axial plane of the Catacol synform, SW of the northern granite.

Fig. 4.5.

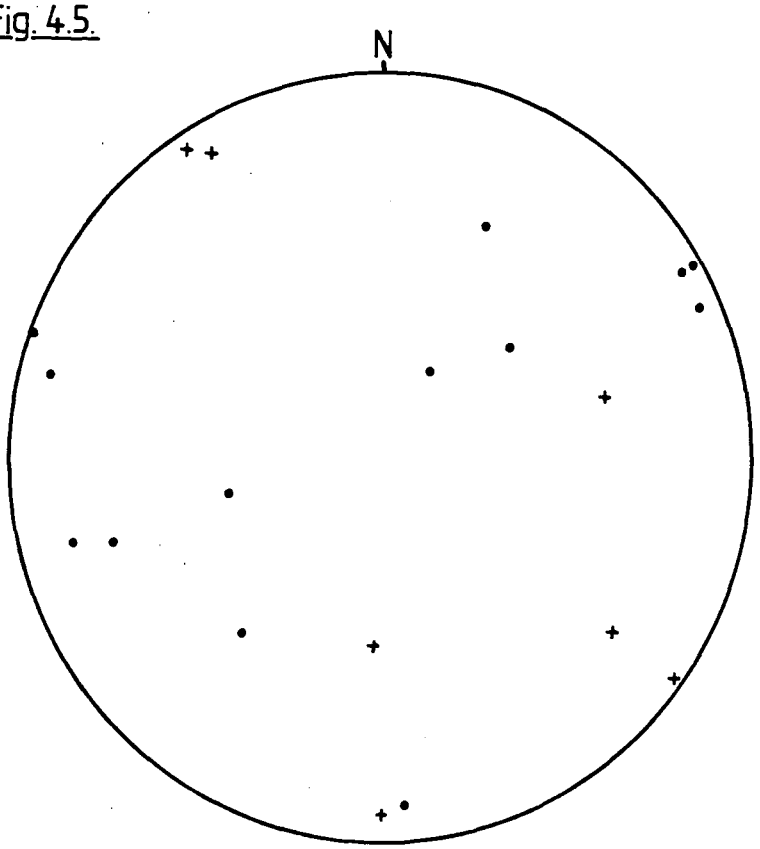

Fig. 4.6.

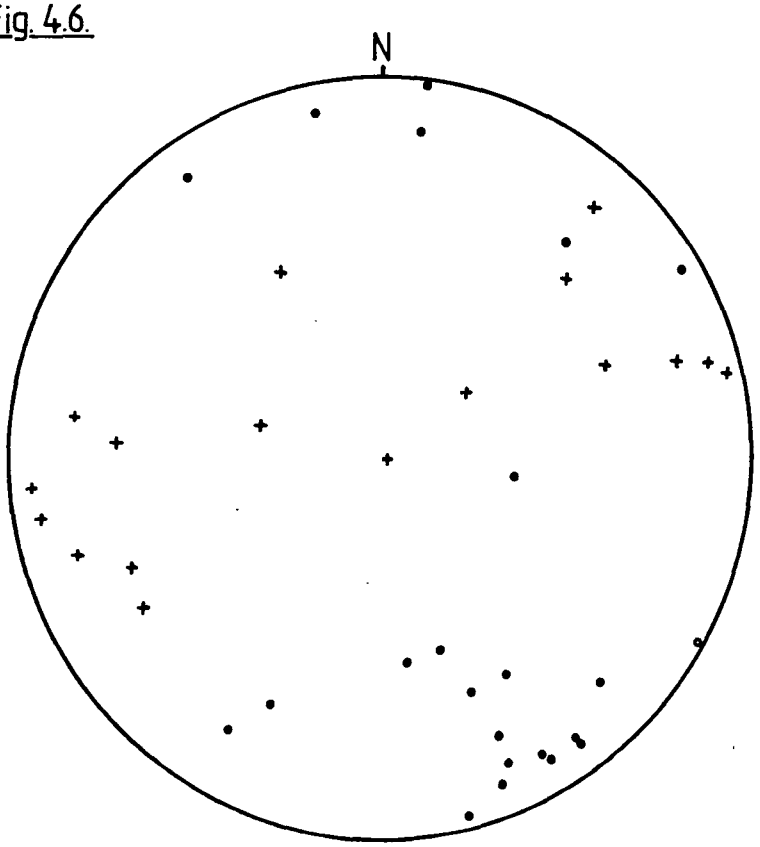

Figure 4.7. Equal area stereogram showing the orientation of bedding (solid circles) and the S_3/S_1 intersection lineation (crosses) measured from the Dalradian rocks to the south of the northern granite, between Glen Iorsa and Glenshant Hill.

Fig. 4.7.

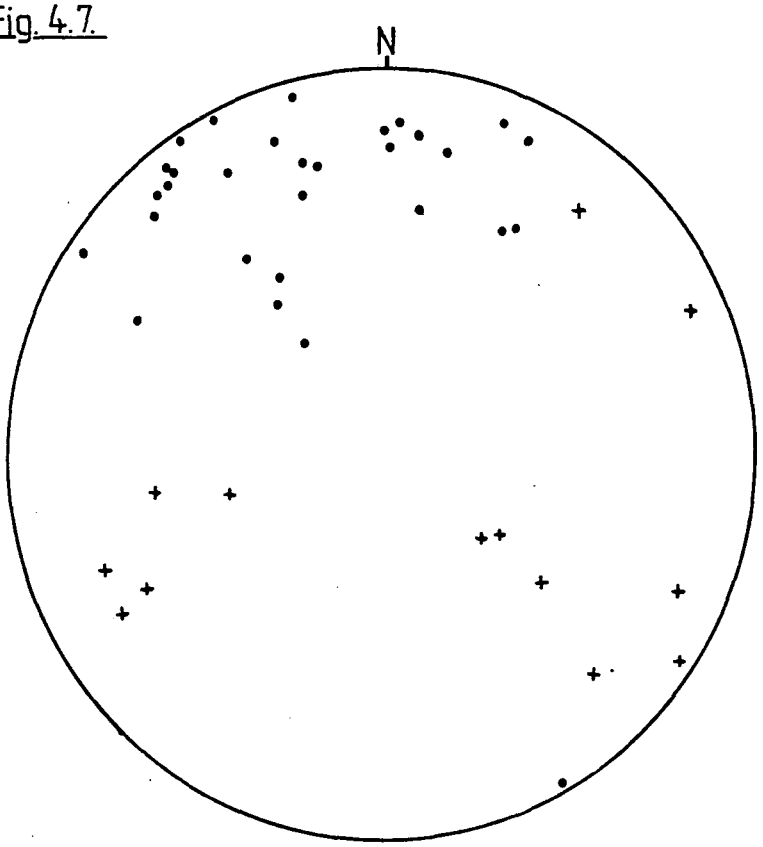

Figure 4.8. Equal area stereogram showing the orientation of bedding (solid circles) and the S_3/S_1 intersection lineation (crosses) measured from the Dalradian rocks to the west of the northern granite.

Fig. 4.8.

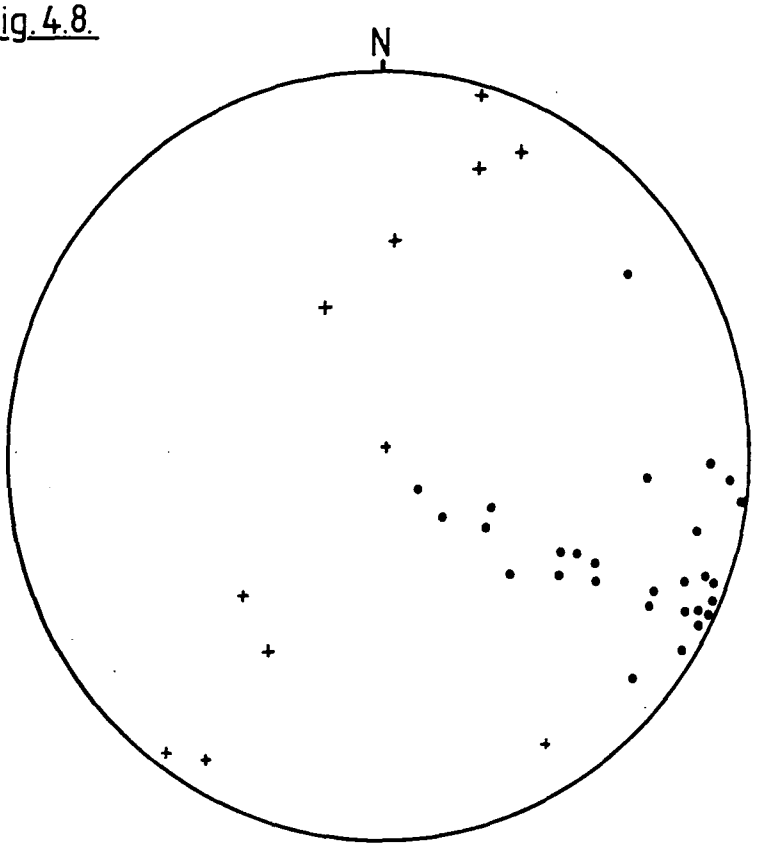

Figure 4.9. Equal area stereogram showing the orientation of bedding (solid circles) and the S_3/S_1 intersection lineation (crosses) measured from a cross section, normal to the axis of the Catacol synform, through Lochranza. The axial plane of the Catacol synform is marked A/P.

Figure 4.10. Equal area stereogram showing the orientation of bedding (solid circles) and the S_3/S_1 intersection lineation (crosses) measured from a cross section, normal to the axis of the Catacol synform, through Catacol. The axial plane of the Catacol synform is marked A/P.

Fig. 4.9.

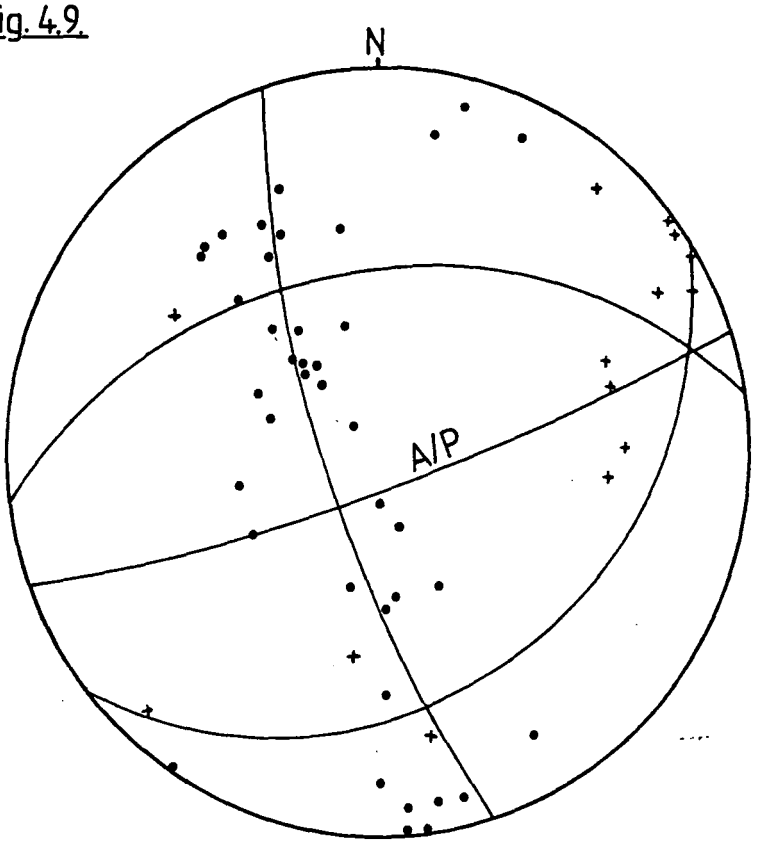

Fig. 4.10.

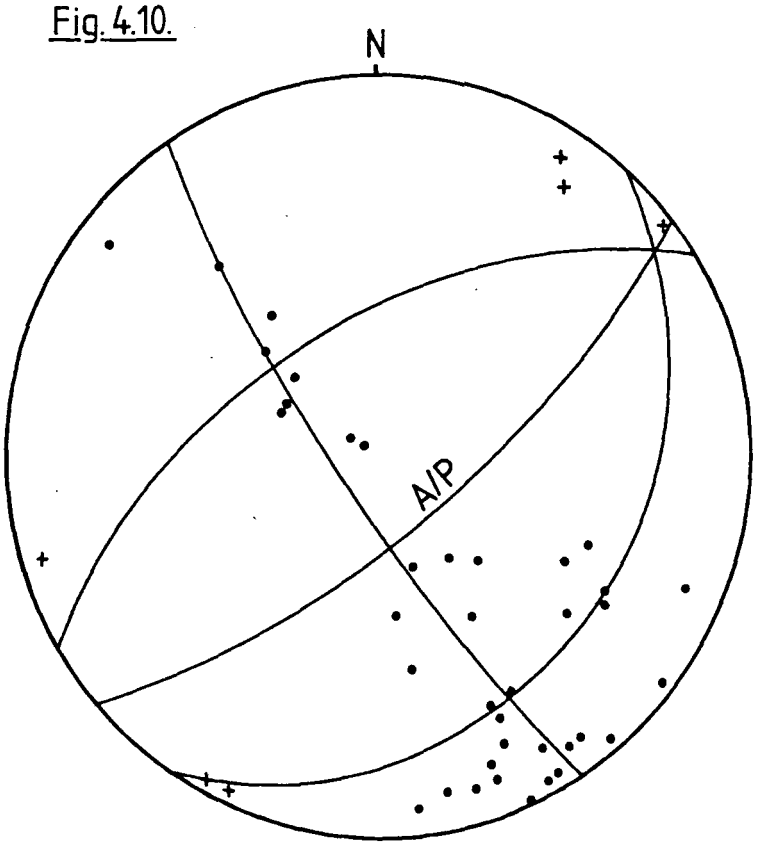

planes lie along the profile plane of the fold) indicating that the Catacol synform has a cylindrical geometry in these areas. This differs from the more angular geometry of the fold in Glen Charmadale, indicated in figures 4.2 and 4.3. The spread in orientation data for the NW dipping limb of the fold in figure 4.10 is due to plotting data from a number of localities adjacent to the granite margin. The S_s/S_1 intersection lineation data, although poor, suggests the lineation remains approximately horizontal in the Catacol area (Fig. 4.10) but steeper plunges measured in the Lochranza section indicates folding across the strike of bedding (Fig. 4.9). Comparison of these figures with figure 4.4 indicates a decrease in the angle of plunge of the hinge of the Catacol synform. The rotation of the hinge direction toward a more northerly azimuth in Figs. 4.9 and 4.10 reflects the change in strike of the axial plane of the fold so that it remains parallel to the edge of the granite. A change in dip direction of the axial plane of the fold from ~~toward~~ away from the granite in Glen Charmadale, to ~~away from~~ towards the granite in Lochranza and Catacol is also indicated. The increasing plunge of the Catacol synform (Figs. 4.4, 4.9 & 4.10) toward the axial plane of the Aberfoyle synform is a consequence of the increasing dip of the Dalradian rocks in the axial plane of the former.

The stereonets do not clearly show the actual profile of the fold in the Lochranza and Catacol areas. These are shown in figure 4.11 (Plate 4.1). The main feature of interest is the zone of steeply dipping rocks which extends to about 200m from the granite, outside which the dip begins to shallow toward the fold hinge. This zone corresponds to the hornfels zone described in chapter 3. These rocks have been strongly recrystallised and are segregated into quartzose and mafic rich bands along the original S_2 cleavage planes. Bedding and the S_1 cleavage are often completely overprinted by this recrystallisation. Recrystallisation of these rocks at elevated temperatures would have softened them and hence they would be more deformable. This would have allowed a zone of enhanced strain to develop parallel and adjacent to the margin of the granite during its intrusion. The

Figure 4.11. Cross sections through a) Lochranza, and b) Catacol, showing the profile of the Catacol synform between the coast and the granite/Dalradian contact. The fold is slightly asymmetric; its axial plane dips steeply toward the granite. A zone of steeply dipping rocks occurs against the granite. The width of this zone corresponds closely to that of the hornblende-hornfels zone; the outer edge of which is marked by a dashed line.

Fig. 4.11.

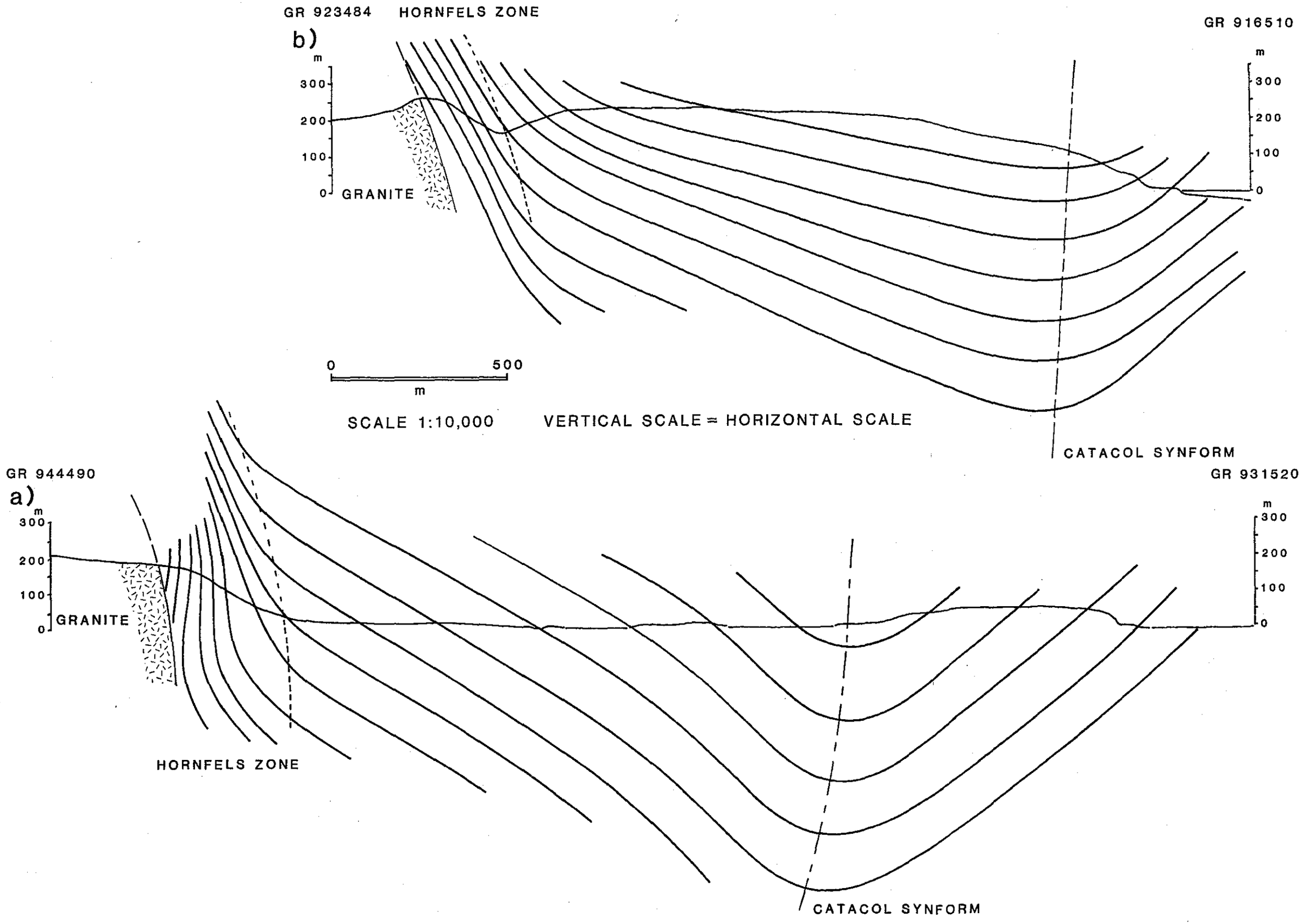
GR 923484
HORNFELS ZONE
b)
m
300
200
100
0
GRANITE
GR 916510
m
300
200
100
0
0
500
m
SCALE 1:10,000
VERTICAL SCALE = HORIZONTAL SCALE
CATACOL SYNFORM
GR 944490
a)
m
300
200
100
0
GRANITE
GR 931520
m
300
200
100
0
HORNFELS ZONE
CATACOL SYNFORM

Plate 4.1. View of the north side of Glen Catacol. The granite (right side of view, white outcrop) can be seen in contact with Dalradian psammites (left side of view, grey outcrop) on Madadh Lounie. The Dalradian dips vertically at its contact with the granite, but shallows rapidly toward the west, as indicated by the ridges in the topography (cf Fig. 4.11b).

granular hornfels texture of these rocks is probably the result of annealing, or secondary recrystallisation, following deformation (Hobbs et. al., 1976). This zone of steepened rocks is not confined to the inner limb of the Catacol synform but is developed wherever hornblende-hornfels facies Dalradian rocks are in contact with the granite.

A post S_2 age for the Catacol synform can be established from the vergence of axial planar minor folds (F_3) which deform the S_2 cleavage (Fig. 4.12). Between the hinge of the synform and the margin of the granite these minor folds verge away from the hinge, toward the granite. This is consistent with their formation being the result of the development of the synform. This limb of the Catacol synform will be referred to as the 'inner limb' in the following sections. Between the axial plane of the synform and the coast the post S_2 folds verge away from the granite (i.e. opposite vergence to the folds on the inner limb). This limb of the fold will be referred to as the 'outer limb'. The core of the fold can be traced from a zone of these strongly developed post S_2 folds which show neutral vergence, as noted above.

Minor post S_2 folds are also developed in the southeast limb of the Aberfoyle synform to the south of the granite, where they verge toward the intrusion. Hence it is clear that their formation is not directly related to development of the Catacol synform, but perhaps more closely to folding of the Dalradian rocks over the Northern Granite to form an antiformal dome structure.

A third cleavage (S_3) occurs in the pelitic lithologies of the Dalradian. This cleavage is generally weak and is rarely found in the semi-pelitic or psammitic rocks. It is developed parallel to the axial planes of the post-S_2 folds. When the orientation of this cleavage is studied in detail it is clear that it is not always parallel to the strike of bedding or the axial plane of the Catacol synform. Figure 4.13 shows that this cleavage cross cuts, or transects, the fold axis. The presence of a transecting cleavage suggests a component of shear across the fold during its

Figure 4.12. Equal area stereogram showing the orientation of post S_2 folds (F_3) (open circles) taken from the cross section through the Catacol synform at Catacol (Fig. 4.10 & 4.11 b)). The data show a broad distribution which is bisected by the axial plane of the synform (solid line).

Fig. 4.12.

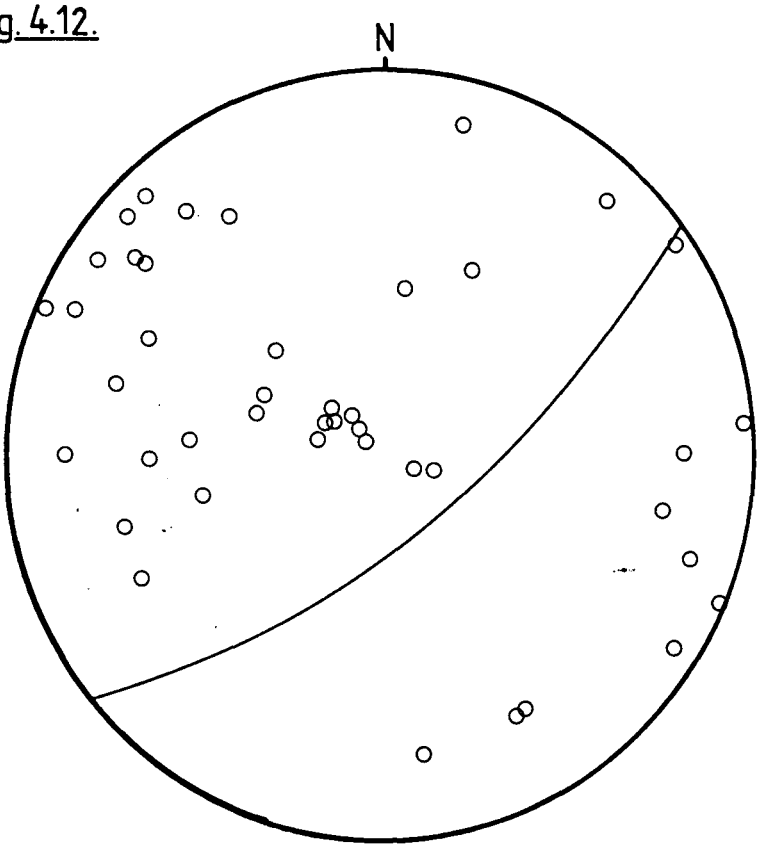

development. The cleavage would have formed slightly later than the fold. The fold axis would have been rotated out of the X–Y plane of the strain ellipsoid before the necessary strain ($\approx$ 10%) developed in these rocks to produce the cleavage (Soper, 1986). Alternatively the stress field may have rotated relative to the pre-existing axial plane causing the cleavage to form in a different orientation.

The S_3 foliation is commonly developed as a pressure solution cleavage, particularly in the hornfels zone (Chapter 3). It is always aligned sub-parallel to the granite margin and hence it represents flattening in this plane. The cleavage is not folded or rotated into a shallower orientation within the steepened inner limb of the synform adjacent to the granite. The cleavage cuts porphyroblasts of cordierite developed in the Hornfels zone (section 3.4 and Plate 3.6). Therefore the S_3 cleavage developed during or after thermal metamorphism. This implies a syn thermal aureole age for the Catacol synform, which confirms Bailey's (1926) assumption that it was related to the emplacement of the granite. Outside the hornfels zone (e.g. in the Allt an Eireannach, GR 910486) orientated thin sections show that the S_3 cleavage develops a conjugate set (Plate 3.2). Both cleavages are distorted around porphyroblasts of andalusite, which have associated quartz filled pressure shadows. The geometry of the pressure shadows suggest they formed during rotation of the porphyroblasts into the flattening plane indicated by the cleavage. The rotated porphyroblasts do not show a consistent shear sense in thin sections cut in vertical and horizontal planes normal to the margin of the granite. This suggests the S_3 cleavage developed by pure shear and that it represents a flattening strain ($k \approx 0$) normal to the granite contact. ($k = \frac{X}{Y}/\frac{Y}{Z}$ and X, Y and Z are the major intermediate and minor axes of the strain ellipsoid.) The porphyroblasts developed in the hornfels zone which are cut by the pressure solution cleavage show no clear distortion which would suggest simple shear deformation. Hence it has also been assumed that the cleavage in the inner part of the aureole also represents a flattening strain as a result of pure shear. A pure shear model for

formation of the cleavage is clearly not compatible with the hypothesis that it is a transecting cleavage recording a component of shear (Fig. 4.13) but supports the idea that the stress field rotated between the formation of the Catacol synform and the cleavage.

It has been established from structural data that the Catacol synform is an arcuate structure, concentric to the margin of the Northern Arran Outer granite, which refolds the NW limb and axial plane of the Caledonian Aberfoyle synform. A cleavage (S_3) cross cutting the axial plane of the Catacol synform and cutting porphyroblasts in the metamorphic aureole of the granite indicate the fold is of syn-intrusion age. The granite clearly cuts the axial plane of the Aberfoyle synform so that the SW limb of this structure now lies to the south of the granite. The inner limb of the Catacol synform now dipping steeply away from the granite was formed by the refolding of the NW limb of the Aberfoyle synform. Adjacent to the granite is a zone of rocks which have a near vertical dip parallel to the granite contact. The width of this zone corresponds closely to the width of the hornblende–hornfels zone of the thermal aureole. The S_3 cleavage developed sub-parallel to the margin of the granite and post dating the growth of contact metamorphic mineral assemblages indicates flattening strains developed around the intrusion in the plane of its contact with the Dalradian as temperatures began to fall.

4.3 The Formation of the Catacol Synform: Evidence for the Vertical Ascent of a Magma Body.

The general geometry and present orientation of the Aberfoyle and Catacol synforms is shown in figure 4.14. As noted above the outer limb of the Catacol synform is formed from the relatively undeformed SE dipping NW limb of the Aberfoyle synform. This limb dipped toward the SE prior to intrusion of the granite. Therefore the inner limb of the Catacol synform was formed by upturning

Figure 4.13. Map of North Arran showing the geometry of the S_3 cleavage with respect to the margin of the northern granite, and the axial plane of the Catacol synform.

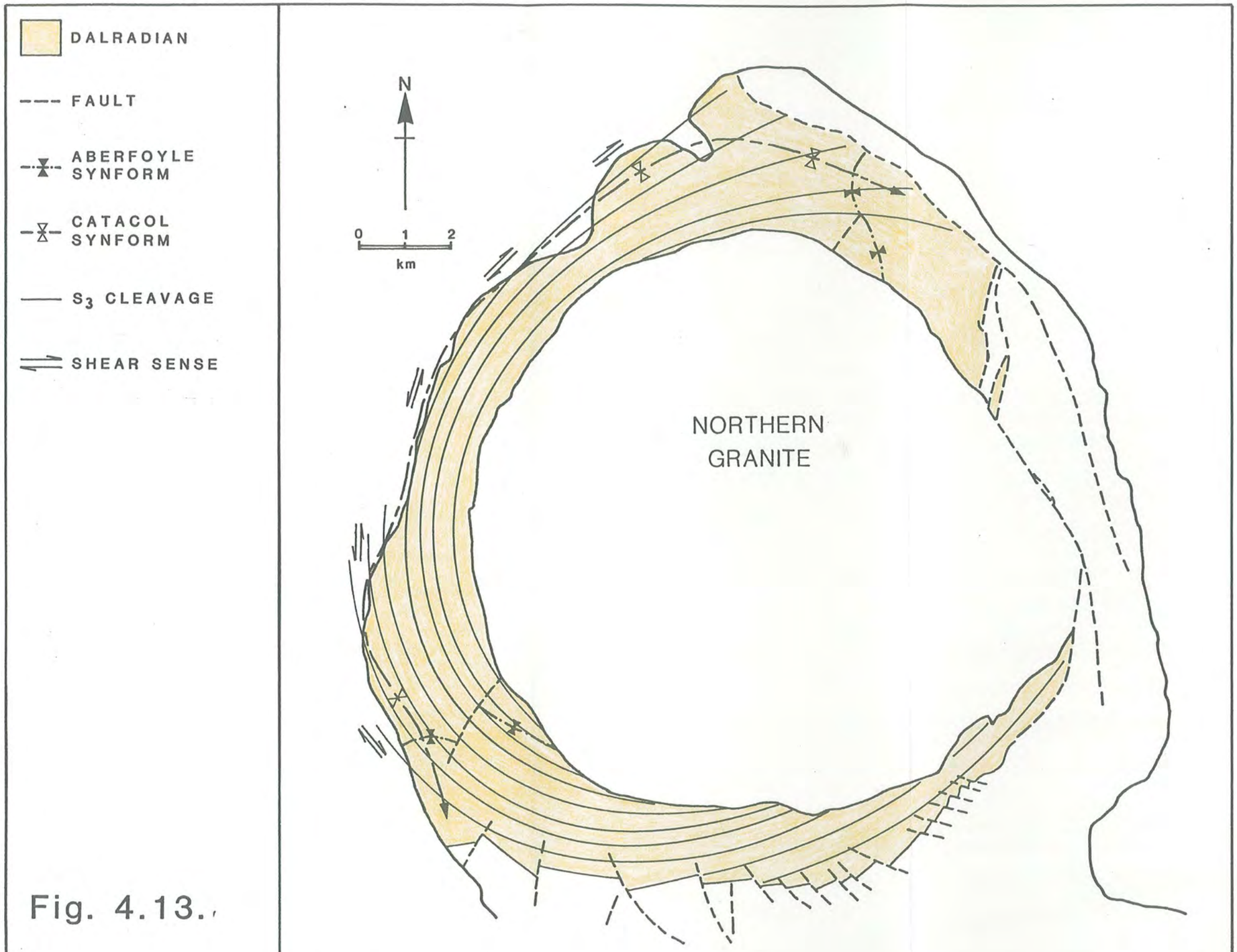
DALRADIAN
FAULT
ABERFOYLE SYNFORM
CATACOL SYNFORM
S_3 CLEAVAGE
SHEAR SENSE
N
0 1 2
km
NORTHERN GRANITE

Fig. 4.13..

Figure 4.14. A three dimensional drawing of the interpreted structure of the Dalradian rocks around the Northern Arran Granite as viewed from the west. The granite (unshaded) is shown as a sub-spherical body with a hemispherical upper surface. The bedding planes of the Aberfoyle synform and the axial plane of this structure (shaded) are shown deformed around the intrusion. The axial plane of the Catacol synform runs parallel to the margin of the granite across the NW limb of the Aberfoyle synform shown in the foreground

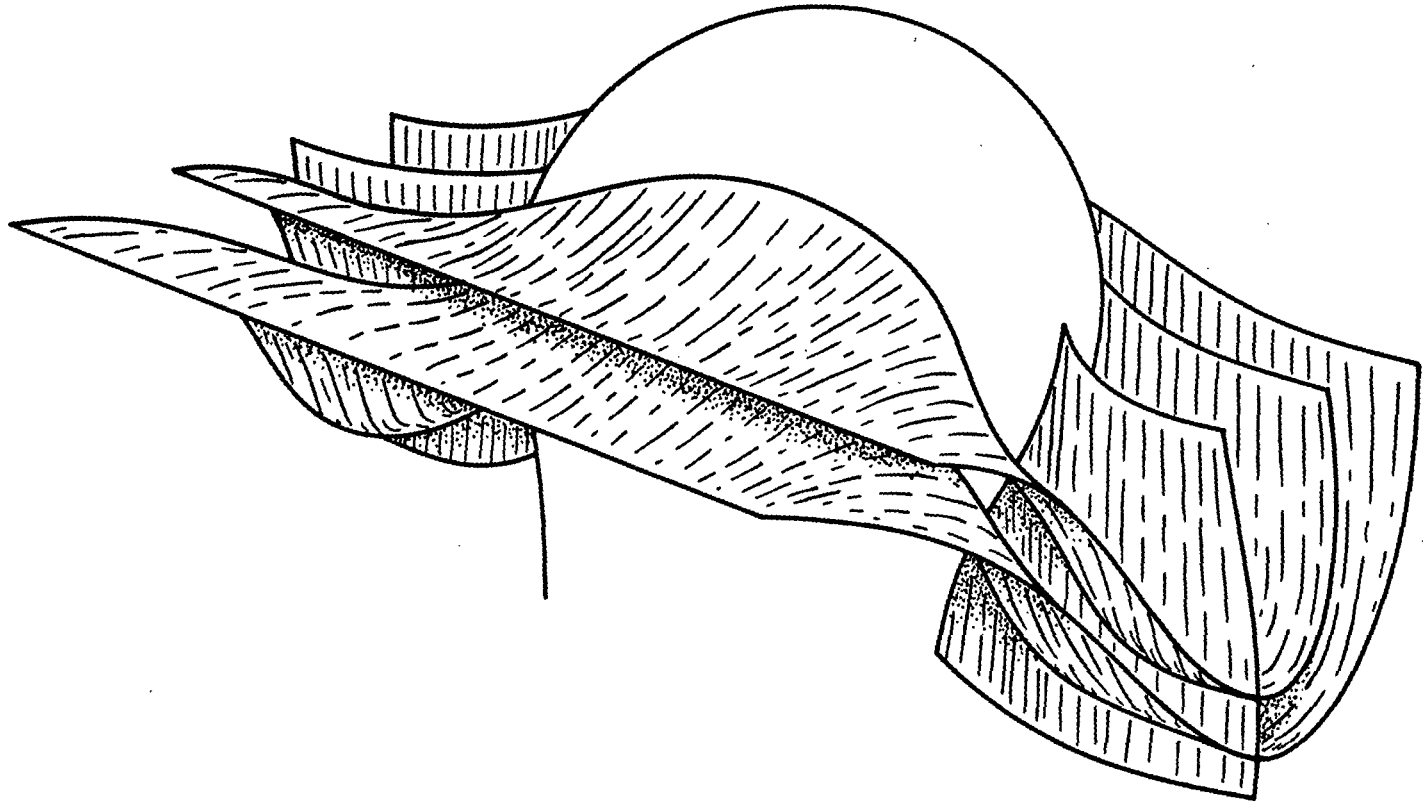

Fig. 4.14.

part of the NW limb of the Caledonian fold along a hinge parallel to the margin of the granite. Hence the Catacol synform is strictly a monoform structure since it formed by shear of one limb only. The SE limb of the Aberfoyle synform is not folded by the Catacol synform. Rocks belonging to this limb are exposed to the south of the granite where they appear to have been deflected upwards and outwards ~~in a horizontal plane~~ during emplacement of the granite.

The granite has clearly cut the axial plane of the Aberfoyle synform. In doing so it appears to have cut this fold structure into two so that it rose between the NE and SW limbs of the fold. The present geometry of the NW and SE limbs of the Aberfoyle synform appear to be controlled by their geometry prior to the intrusion of the granite. If the granite rose vertically up the axial plane of the fold the SE limb would have been sub-parallel to the surface of the body and could simply have been pushed aside. The NW limb would have intersected the surface of the body at a high angle and hence would have to be deflected upward (or downward) to permit ascent of the granite. Consequently the Catacol synform would have developed as the rising granite intersected rocks dipping at a high angle to its surface. Hence the development of the Catacol synform is largely confined to the NW limb of the Aberfoyle synform.

The axial plane of the Aberfoyle synform is folded into a NW–SE orientation around the axial plane of the Catacol synform both to the NE and SW of the granite. Hence the margin of the granite cuts the axial plane of the former at a shallow angle (Fig. 4.1). The S_s/S_1 intersection lineation remains sub-horizontal (Figs. 4.2 & 4.3) around this fold structure indicating that folding was achieved with very little deflection of the F_1 fold hinge in a vertical plane. Thus it appears that the folding resulted from sideways movement of the Dalradian. This indicates that formation of the Catacol synform involved both upward and outward displacement of the aureole rocks.

Where vertical exposure is good (e.g. Glen Catacol, Torr Nead an Eoin) it

is clear that the zone of hornblende-hornfels facies rocks maintains a constant thickness parallel to the granite contact. Although these rocks are more steeply dipping than the adjacent albite-epidote facies rocks they do not obviously record higher strains. No feature such as strongly stretched pebbles, suggesting high strain ductile deformation was noted. It is possible that such features were obliterated by the secondary recrystallisation but relict fabrics might still be expected in some of the rocks. However it is clear from the quartz-mafic segregation and the development of the S_3 cleavage in the pelitic units that these rocks were strongly flattened parallel to the contact with the granite. High strains may be absent because in detail the granite cuts the Dalradian bedding and foliation at the contact (section 4.1) which would represent an infinite strain since originally continuous bedding has been completely attenuated (Fig. 4.15).

Figure 4.16 shows schematically the distribution of an originally horizontal lineation following vertical intrusion of a hemispherical body. In the case of North Arran the granite only updomes one limb of the Aberfoyle synform. Hence only one half of the dome structure is of interest in interpreting the structure of the aureole of the granite in this case. Where the lineation is parallel to the margin of the rising body it will retain its sub-horizontal orientation. At increasingly high initial angles to the margin of the intruding body the stretching lineation is steepened and also rotated in a horizontal plane. As a hemispherical body rises it induces a strain over its surface which would potentially develop a stretching lineation in a vertical plane with a trajectory as indicated by the arrows in figure 4.16 (b). With increasing strains the pre-existing lineation intersecting the body at a high angle becomes further steepened. However lineations at shallow angles to the margin of the intrusive body will retain a near horizontal orientation but will be rotated parallel to the margin of the body. This is because for any single horizontal plane the radius of the concentric synform will increase as the hemisphere rises and rotates its roof rocks outward and upward (Fig. 4.17).

Figure 4.15. The geometry of the Dalradian rocks adjacent to the northern granite (cf Fig. 4.11). Bedding is upturned within the hornfels zone and then cut by the granite. The graph shows qualitatively the distribution of strain (η) across the inner limb of the Catacol synform, into the hornfels zone. Maximum strains occur at the contact where bedding is truncated by the granite.

Fig. 4.15.

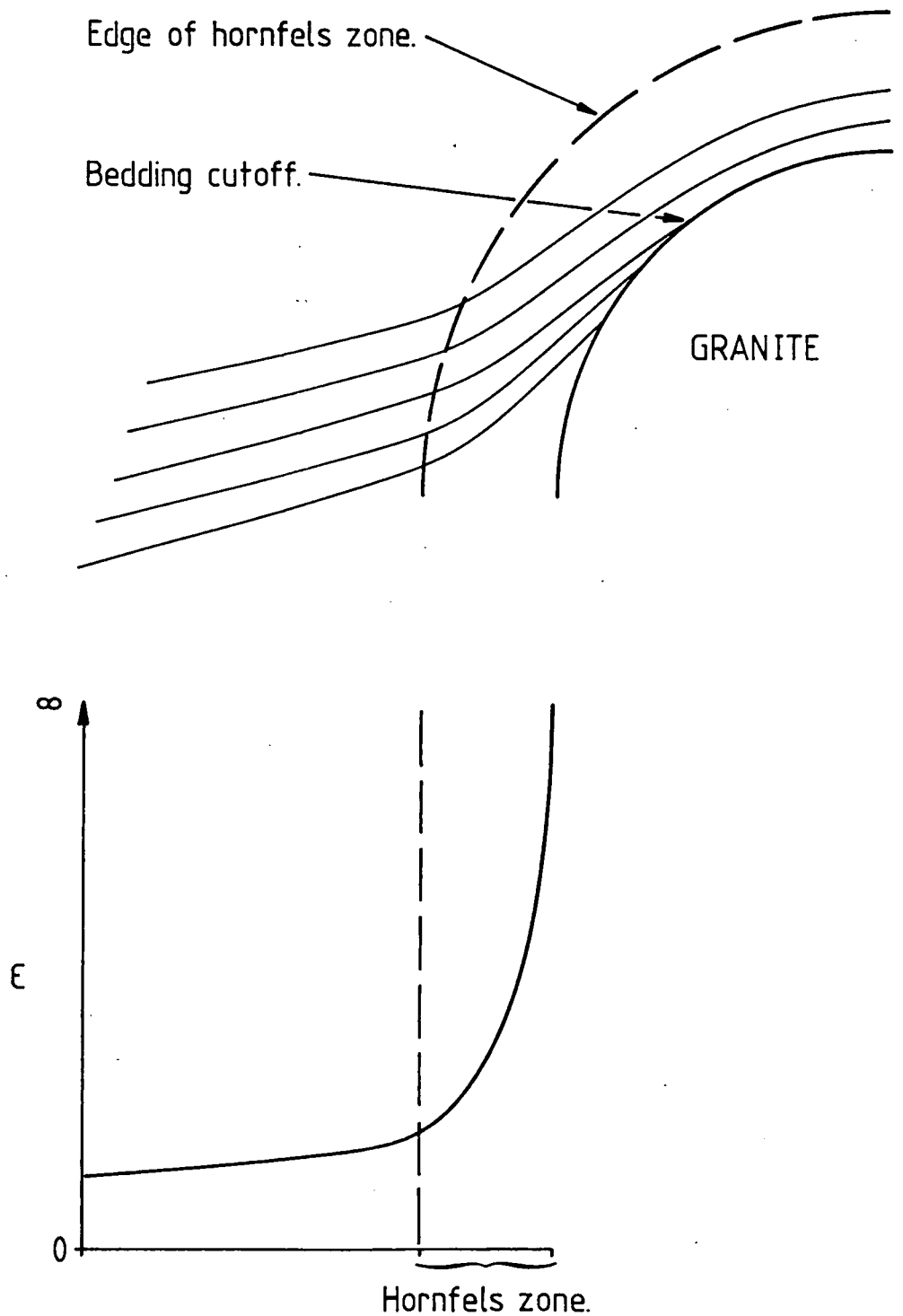
Edge of hornfels zone.
Bedding cutoff.
GRANITE
∞
ε
0
Hornfels zone.

Figure 4.16. The reorientation of an originally horizontal lineation over an intruding hemispherical body, in plan b), and as plotted on a stereogram c).

Fig. 4.16.

a.

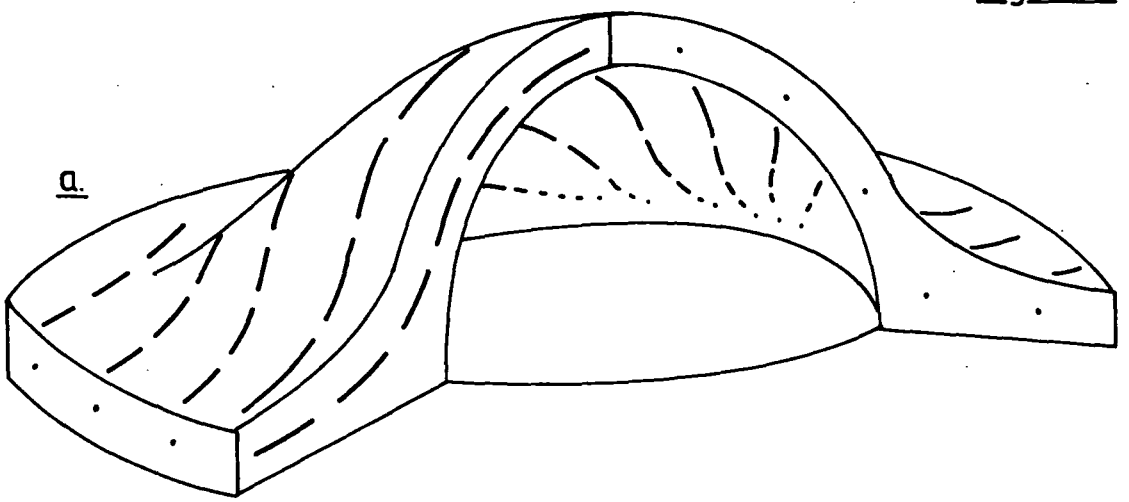

b.

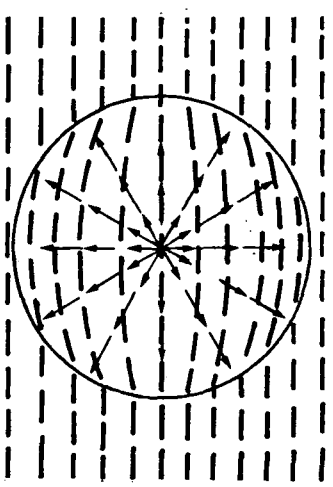

c.

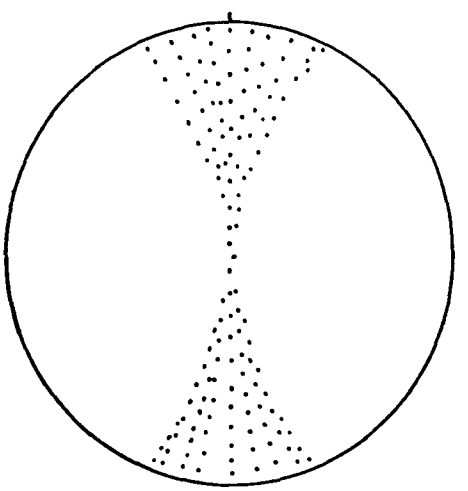

Figure 4.17. The rise of a hemispherical body of constant radius (r) into a fixed initially horizontal surface (A-A) produces a fold of gradually increasing wavelength (2d). The radius of the axial plane of the concentric synform (d) increases parabolically (thin line).

Fig. 4.17.

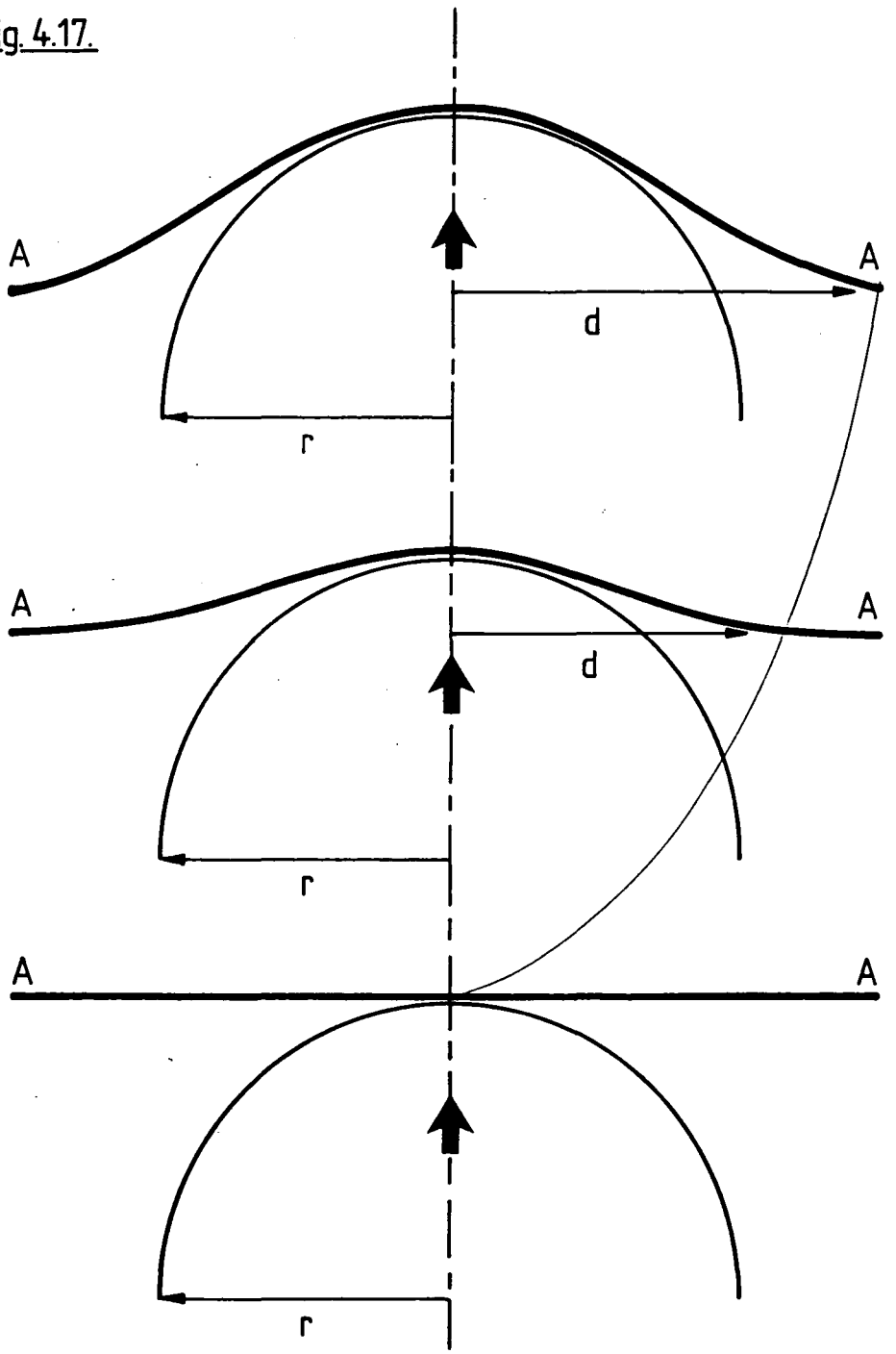

At its present level of exposure the Arran Granite has steeply outward dipping or vertical contacts with the Dalradian, implying that the maximum diameter of the granite is presently exposed, if it has a spherical shape. Consequently the S_s/S_1 intersection lineation (which had an originally sub-horizontal orientation, section 2.1) around the margin of the granite should be generally horizontal and tangential to the contact. This is confirmed by figs. 4.18 (a) & 4.18 (b). If more of the roof of the granite had been preserved a wider variation in plunge of the lineation would have been observed. Hence the data at the present level of exposure are consistent with the vertical ascent of a magma body with a hemispherical upper contact against the country rock having been intruded into the Dalradian.

If the Catacol synform developed by upward and continual folding of the NW limb of the Aberfoyle synform during the vertical ascent of a hemispherical body in the manner described above, the axial plane of the Catacol synform should dip away from the granite (Fig. 4.19a), if the radius of folding increases around the magma body as it rises. Hence there should be evidence of outward migration of the fold hinge. The axial plane of the fold is only known to dip away from the granite in the Glen Charmadale area (Fig. 4.4), and there is no good evidence that the hinge migrated outwards in the manner suggested. The S_3 cleavage is not folded in any way and there are very few F_3 folds on the inner limb of the synform which show vergence away from the granite.

This discrepancy is probably because the Dalradian rocks would not have shown spatially uniform rheological behavior around the rising granite. Cold rocks outside the thermal aureole and above the granite (i.e. close to the surface) would fold more slowly and with a longer initial wavelength, because of their high viscosity (Ramsay & Huber, 1987). Hence the hinge of the developing concentric synform in these rocks may be some distance from the axis of ascent of the magma body. However rocks close to the granite, in the softened hornfelsed zone described above, would deform rapidly around the rising magma body, before it cut through

Figure 4.18. Equal area stereogram showing the measurements of the S_3/S_1 intersection lineation taken around the margin of the northern granite (103 points). The data are contoured in Fig. 4.18 b). This emphasises the near horizontal orientation of the majority of these data. Compare with Fig. 4.16 c).

Fig. 4.18.

a.

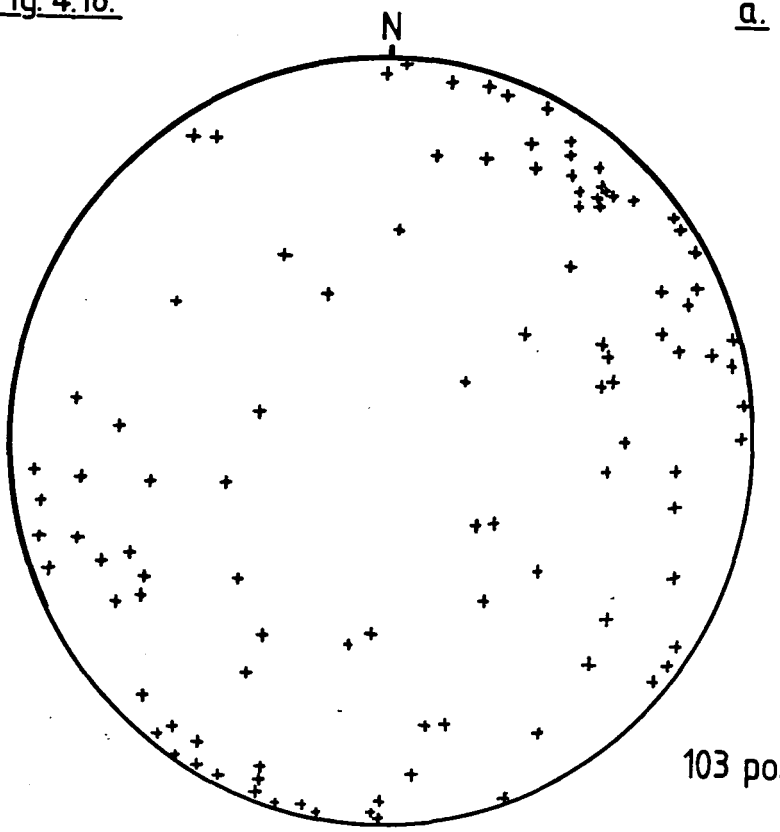

103 points.

b.

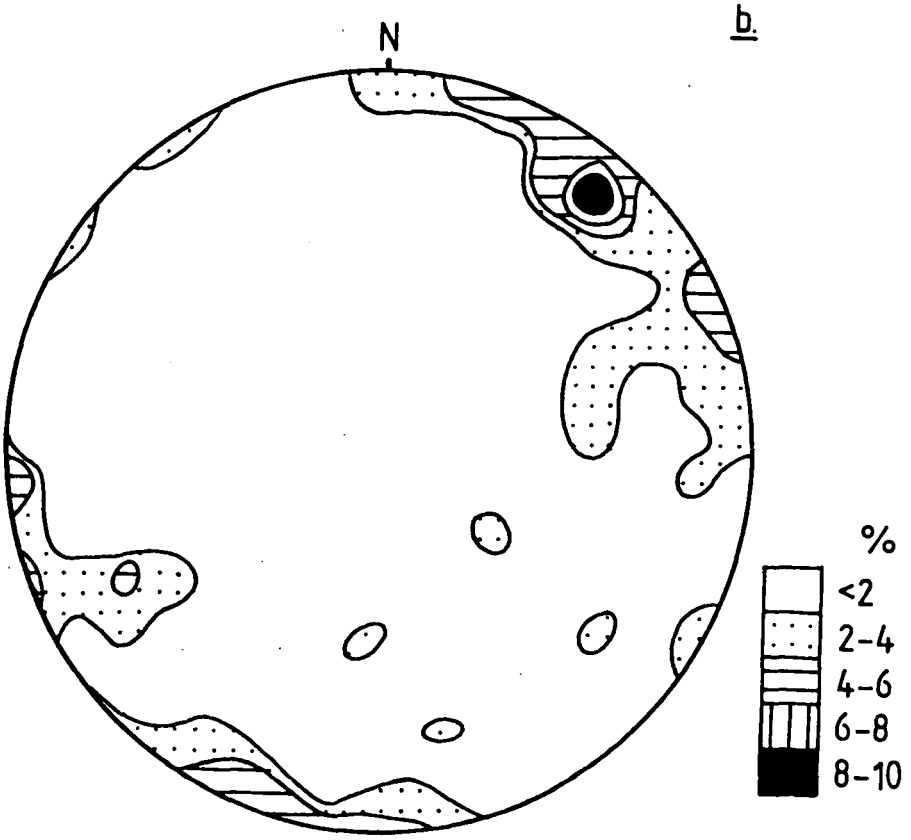

Figure 4.19. The development of a concentric synform around a rising hemispherical body for, a) rocks of spatially uniform viscosity, and b) of spatially non-uniform viscosity. Fig. 4.19 b) shows an outward migrating softened zone in which the inner limb of the concentric synform is further deformed by the rising granite (cf. Fig. 4.15).

Fig. 4.19.

a.

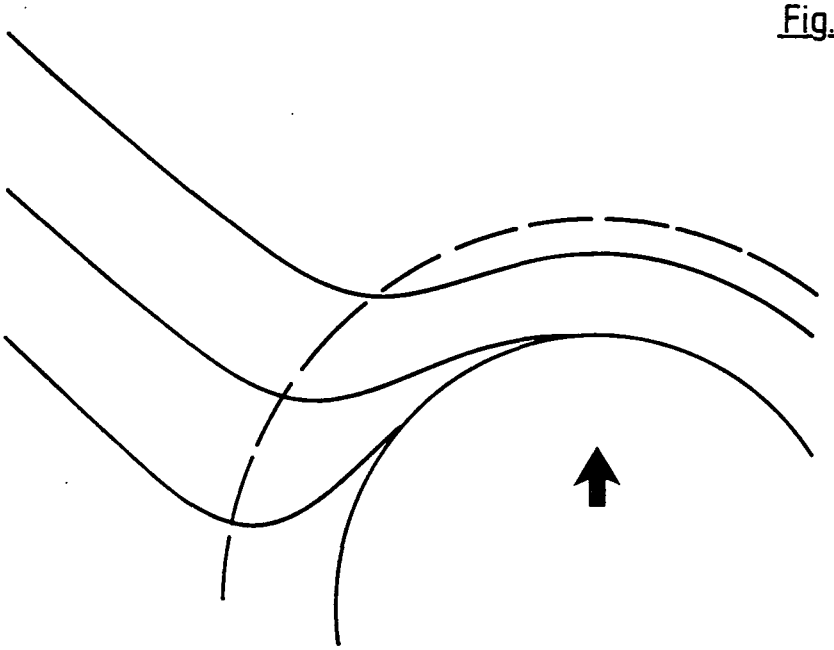

b.

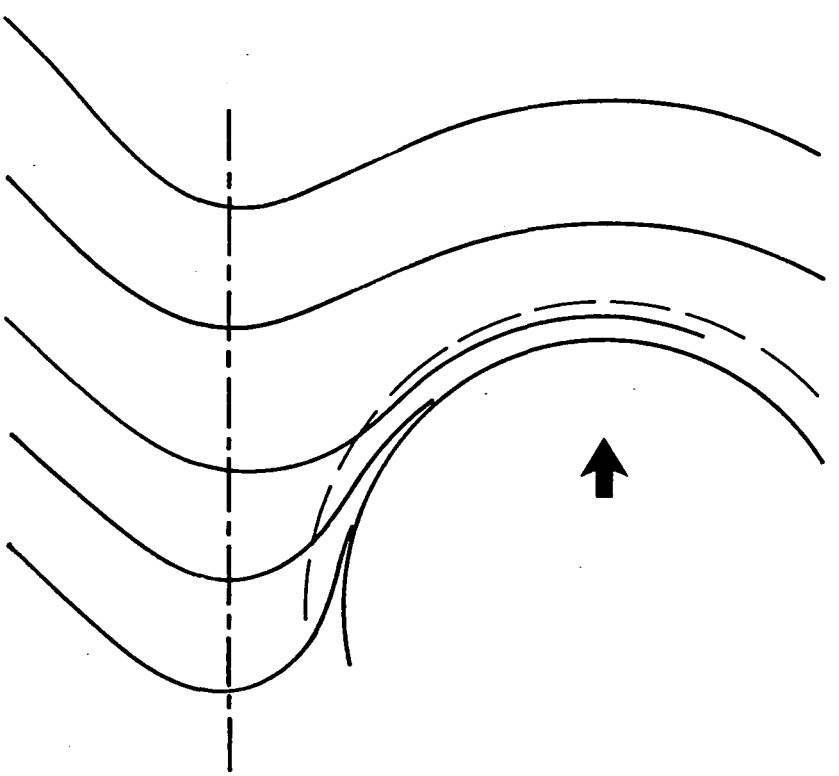

them (Fig. 4.19 (b)), because of their diminished viscosity, due to recrystallisation (White, 1977). In this case only the softened zone would migrate outwards. This would not involve refolding of the fold limb. Since outward movement of the softened zone would encompass a component of radial compression it may have been responsible for the development of the S_3 cleavage.

The structural evolution of the Catacol synform is consistent with such a model. The development of the S_3 cleavage reflects the changing radius of the Northern Granite during its ascent. Compression around the granite would have caused the cleavage to develop parallel to its margin (Fig. 4.20). Since the Catacol synform would no longer be parallel to the reorientated margin of the granite it is cut by the cleavage. Figure 4.13 shows that the cleavage is cut by the granite. This indicates that the granite must have continued to change shape following the formation of the cleavage, and after the formation of the Catacol Synform. These changes in the shape of the northern granite are recorded by the progressive structural development of its aureole during its ascent from the depth at which its rise caused the Catacol synform to develop, at the present level of exposure, to the level at which it came to rest.

This section indicates that the structures developed in the aureole of the Northern Granite described in sections 4.1 and 4.2 can be ascribed to the vertical ascent of a hemispherical body of magma. The sequential development of a concentric synform, an outward migrating zone of thermally softened rock and a cleavage transecting the early synform records an increasing radius of deformation as would be observed at a single level through which a hemispherical body was rising. In addition to producing a foliation concentric to its axis of ascent the granite has also clearly cut the Dalradian rocks through which it rose. These features of the aureole of the Northern Arran Granite are consistent with the ascent of a diapiric body (Coward, 1981; Bateman, 1984) (Chapter 1).

Figure 4.20. The development of the S_3 cleavage and its present geometry with respect to the margin of the intrusion reflects the changing shape of the northern granite during its ascent and emplacement. The upper figure indicates the initial geometry of the Catacol synform which is then cut by the S_3 cleavage as the radius of the pluton increases during the final stages of ascent (section C–D). Further changes in the shape of the granite cause it to cut the cleavage (centre figure).

Fig. 4.20.

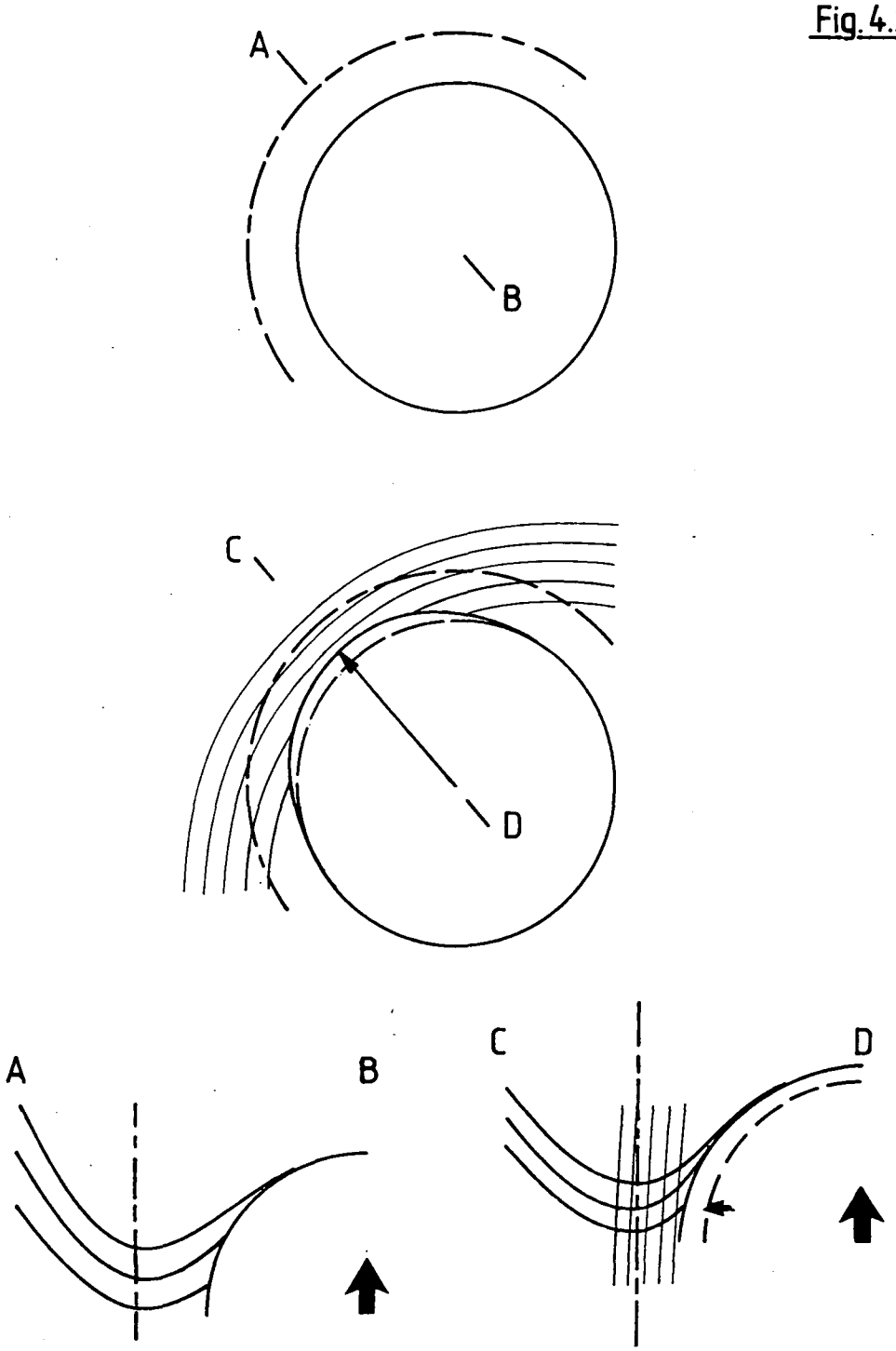

4.4 Structures Adjacent to the Granite.

The preceeding sections have dicussed the broad structure of the aureole of the Northern Arran outer granite and how it relates to the ascent of the intrusion. This section describes the structures in the Dalradian rocks immediately adjacent to the granite.

The steeply dipping Dalradian rocks next to the granite have been strongly recrystallised to a granular hornfels (chapter 3). The recrystallisation has destroyed much of the Caledonian fabric of the rocks. In most cases only the prominent S_2 cleavage is preserved as a segregation of quartz and mafic phases. The S_1 cleavage and bedding are locally preserved but can rarely be traced from outside the hornfels zone to the granite margin. In addition to the hornfelsing the rocks close to the granite margin are veined with quartz and occasional undeformed sheets of fine grained granite.

Angular F_3 minor folds verging toward the granite are strongly developed within the hornfels zone (Plate 4.2). These folds are cut by single and conjugate shear planes (Plate 4.3). Displacement of the foliation across these planes is consistent with extension parallel to the contact and compression normal to the contact. These shears were recorded in all the exposed Dalradian rocks within approximately 100 m of the contact. Their density varies from isolated shears or conjugate sets to well developed intersecting conjugate sets immediately adjacent to the granite. Planes with different orientations showed no consistent cross cutting relationships. The amount of displacement across each shear was difficult to determine due to a lack of matching foliation planes which could clearly be indentified on either side of the shear planes. In addition the variable intensity of development of these shears has made estimates of the strains they represent impossible.

Figures 4.21, 4.22 & 4.23 show contoured plots of shear plane orientations taken from Glenshant Hill and Glen Rosa, Creagan nan Caorach and Creag a

Plate 4.2. Angular folding of the S_2 cleavage in hornfelsed psammites at Creagan nan Caorach. These folds developed on the inner limb of the Catacol synform verge toward the granite contact which lies 10 m to the right of this photograph.

Plate 4.3. Conjugate shearing of hornfelsed Dalradian rocks adjacent to the granite contact at Creag a' Chaise. In this view movement on a shear plane is indicated by the displacement of a pair of folds so that their hinges coincide.

Figure 4.21. Equal area stereonet of extensional shear plane data from Glenshant Hill and Glen Rosa. a). Contoured plot of data. b). Orientation of mean shear planes (solid lines) taken from a), and the principal stress orientations. Large open circle indicates approximate orientation of granite – Dalradian contact.

Fig. 4.21.

a.

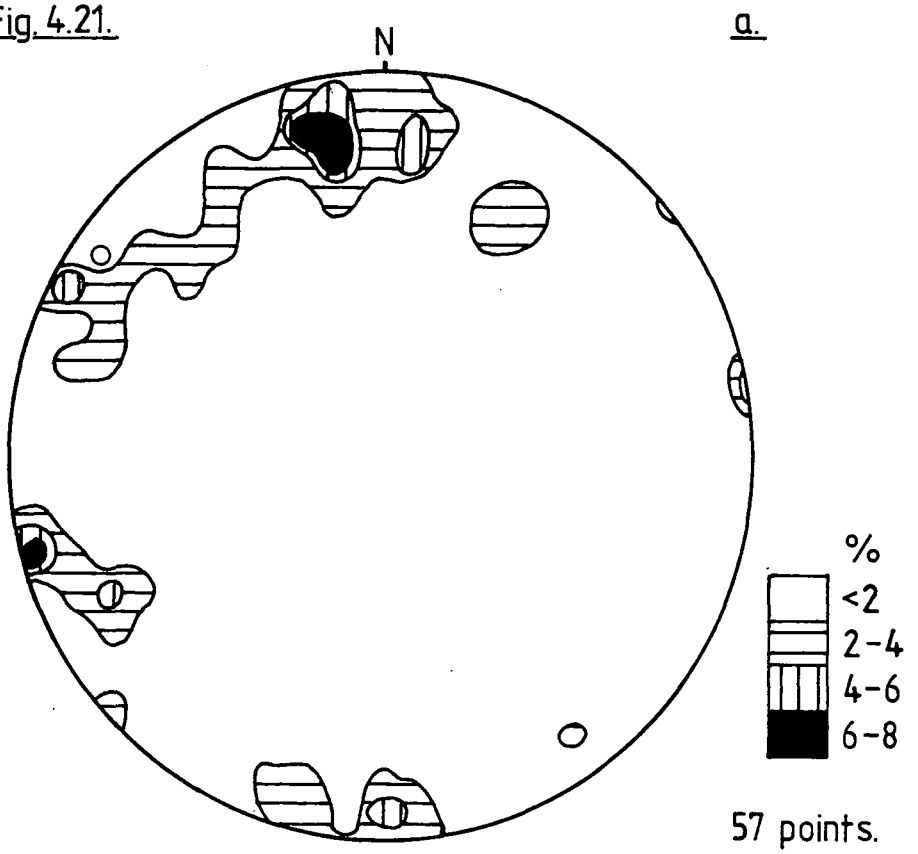

b.

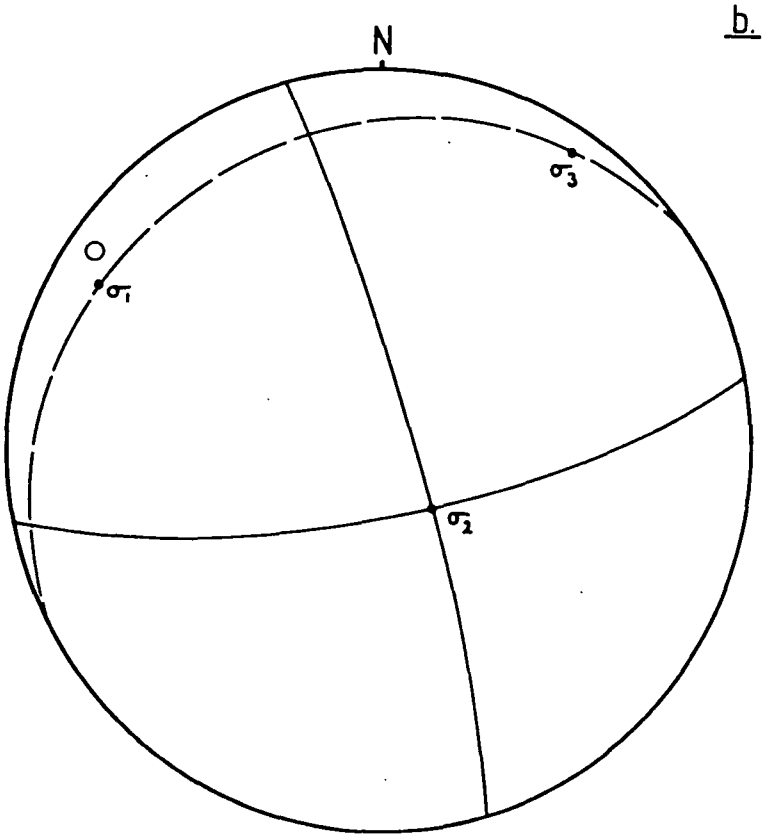

Figure 4.22. Equal area stereonet of extensional shear plane data from Creagan nan Caorach and Creag a Chaise. a). Contoured plot of data. b). Orientation of mean shear planes (solid lines) taken from a), and the principal stress orientations. Large open circle indicates approximate orientation of granite – Dalradian contact.

Fig. 4.22.

a.

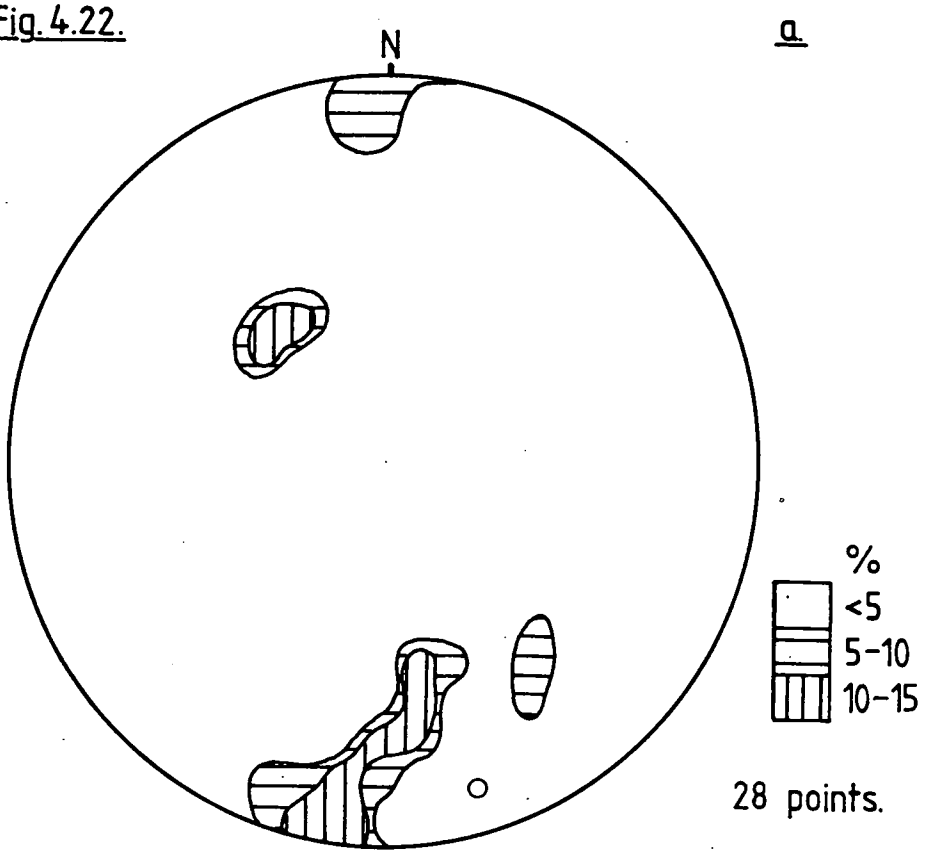

b.

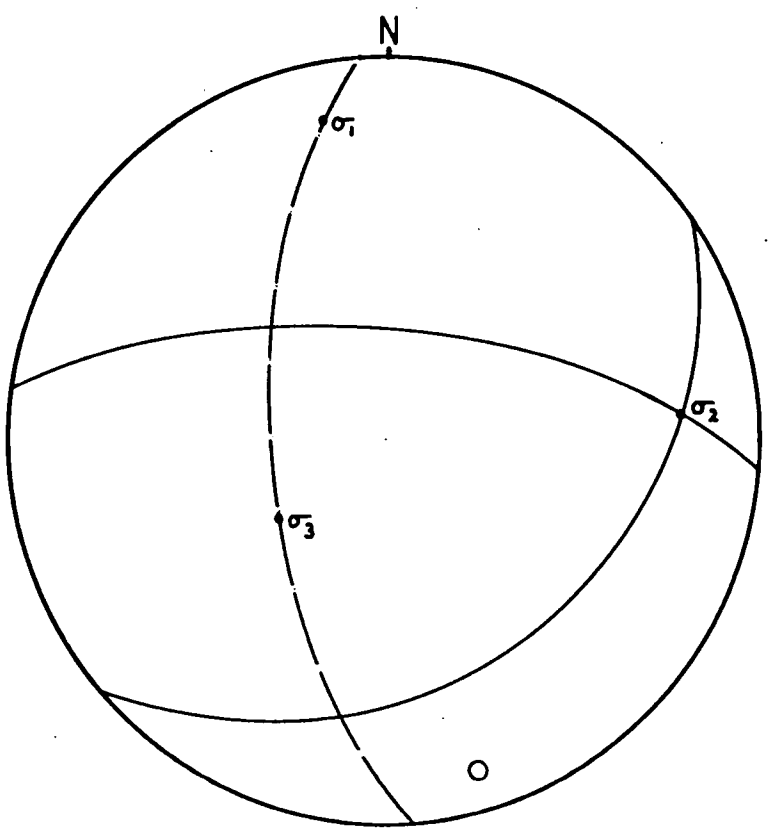

Figure 4.23. Equal area stereonet of extensional shear plane data from Glen Catacol and Corein Lochain. a). Contoured plot of data. b). Orientation of mean shear planes (solid lines) taken from a), and the principal stress orientations. Large open circle indicates approximate orientation of granite – Dalradian contact.

Fig. 4.23.

a

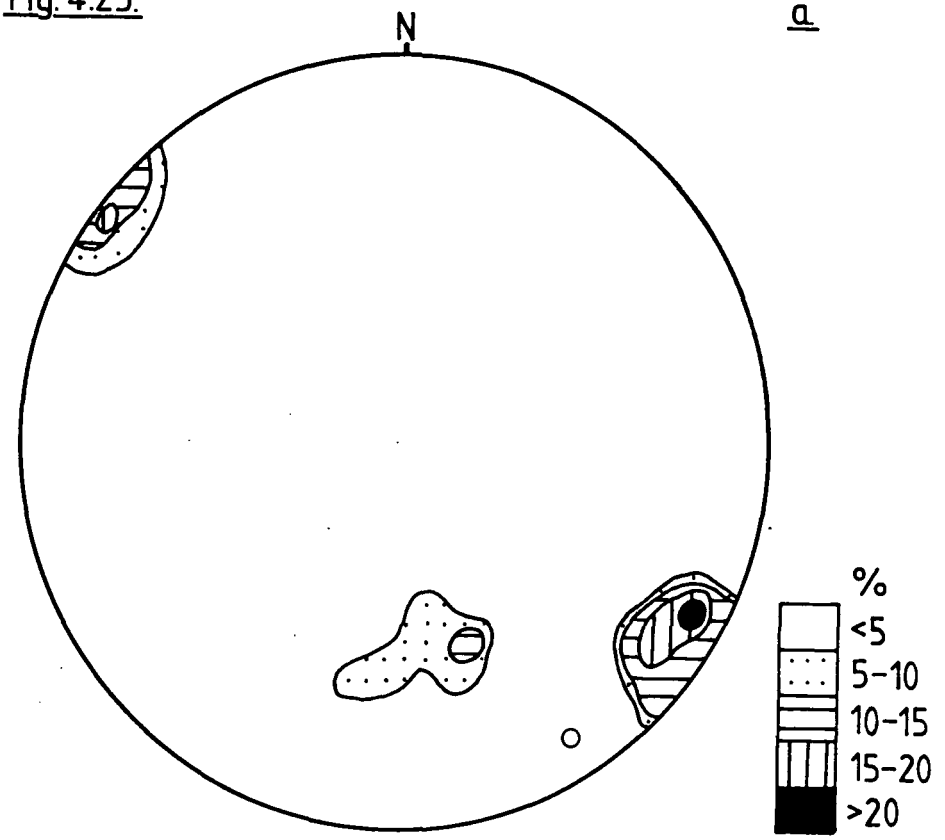

27 points.

b.

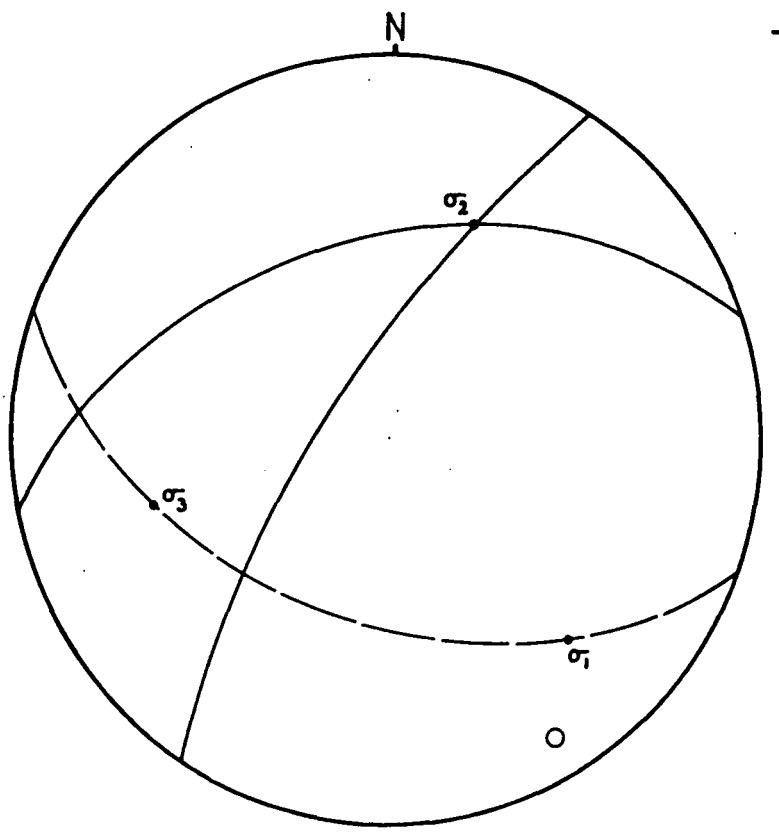

Chaise, and Glen Catacol and Corein Lochain respectively. The orientation of the mean shear planes in Figs. 4.21b, 4.22b & 4.23b are taken from the maxima defined in the contoured plots. The orientation of the σ_1 direction was determined from the shear sense across the planes measured in the field. The stereograms show that σ_1 is consistently normal to the margin of the granite. The σ_2 direction is taken to lie in the intersection of the shear planes. The stereograms also indicate that the plane containing σ_1 and σ_2 bisects the acute angle between the shear planes in Glenshant Hill and Glen Rosa and the obtuse angles in Glen Catacol and at Creagan nan Caorach. This may reflect a variation in the magnitude of strain across these fractures since greater extension would be possible across planes at an angle of $> 45^o$ to σ_1 than would be possible across planes at an angle of $< 45^o$ to σ_1. Hence a greater extensional strain parallel to the contact is implied in the Glen Catacol and Creagan nan Caorach areas.

The flattening plane defined by σ_2 and σ_3 is sub-parallel to the contact. A lack of data on the the magnitude of the strain across individual shear planes or sets of planes prevented determination of the relative length of the axes of the strain ellipse. In particular it was not possible to determine the amount of strain parallel to σ_2. Consequently while it appears that the strain was non-plane (k=1), but oblate ($0 < k < 1$), it was not possible to demonstrate this.

In the Glenshant Hill and Glen Rosa area the shear planes intersect along steeply dipping axes. This implies that the maximum extension must have occurred in a sub-horizontal plane. In Glen Catacol and at Creagan nan Caorach the planes intersect at a shallow angle suggesting that maximum extension occurred in a sub-vertical direction.

A further set of data was collected from North Glen Sannox (Figure 4.24) In this area bedding and the S_2 foliation strike at a steep angle to to the edge of the granite in contrast to the areas described above where S_S and S_2 are parallel to the contact. This has resulted in the development of shears and minor folds with

Figure 4.24. Equal area stereonet of extensional shear plane data from North Glen Sannox. a). Contoured plot of data. b). Orientation of mean shear planes (solid lines) taken from a), and the principal stress orientations. Large open circle indicates approximate orientation of granite – Dalradian contact; closed circles, bedding and crosses the plunge of F_3 folds.

Fig. 4.24.

a.

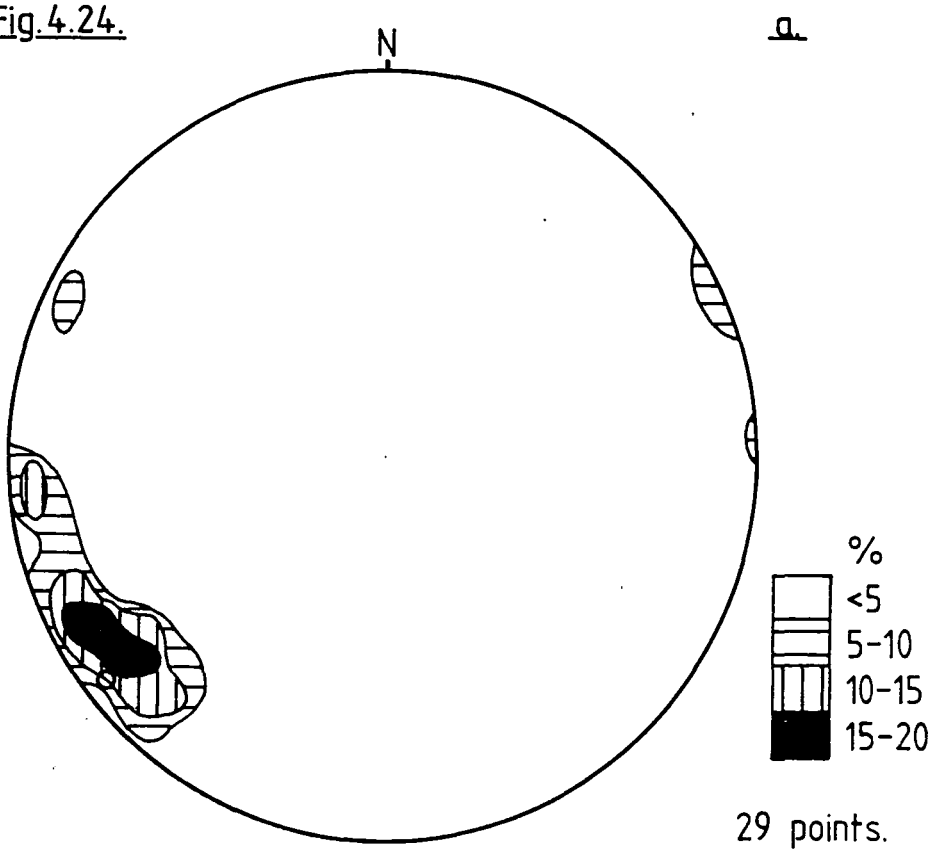

b.

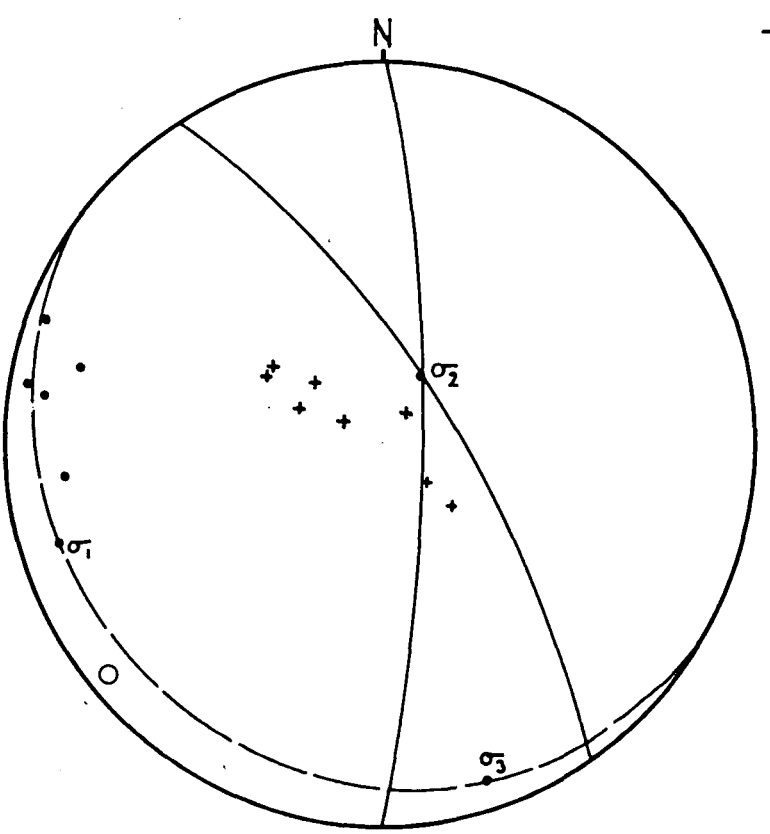

contractional geometries sub-parallel to the margin of the granite. The shear sense across the shear planes indicates that σ_1 is approximately normal to the contact. Figure 4.24a shows one dominant set of shear planes parallel to the granite contact and a second set with an approximately N-S strike oblique to the contact. The two groups of shears intersect on a steeply plunging axis which is sub-parallel to the plunge of the minor folds in the area (Fig. 4.24). Again the relative magnitudes of the X, Y and Z axes of the strain ellipsoid cannot be determined. The vertical intersection of the planes indicates strong extension in a horizontal plane sub-parallel to the margin of the granite.

The shear planes described above are cut by a well developed set of horizontal joints which are particularly well developed in the Glen Catacol and Creagan nan Caorach areas. These joints are the last structures to form in the aureole where they are restricted to between 50 and 100 m of the contact. Small offsets across these joints indicate that they post date the shear planes. The sense of movement across the joints indicates a small component of overshear to the north and west at the above localities. Where measurable, displacements on these joints were of the order of a few mm. At a number of localities the joints have been exploited by horizontal sheets of fine granite, which also cut the coarse granite in the vicinity of the contact (Plate 4.4). These intrusions are interpreted as evolved aplitic intrusions on the basis of their chemistry (chapter 5). The formation of these horizontal joints and the emplacement of the aplites along them is compatible with the observation that the maximum extension direction within the deforming rocks adjacent to the granite in Glen Catacol and at Creagan nan Caorach was vertical. It is thought that the joints formed during the cooling of the aureole rocks. Contraction of the rock occurred as a result of the release of elastic strains induced in the rocks during extension.

4.5 Interpretation of Flattening Strains.

Plate 4.4. Horizontal joints developed in hornfelsed Dalradian adjacent to the granite at Creag a' Chaise. Dilation across these joints in a vertical plane is indicated by the injection of veins of aplitic granite (white sheet above hammer handle).

Evidence for flattening parallel to the margin of the granite during a late stage of the development of the Catacol synform has been discussed in section 4.3. It has been assumed that the cleavage (S_3) developed at this stage represents a minimum 10% flattening strain (Soper, 1986), formed by pure shear, normal to the margin of the granite. Flattening would have resulted in an increase in the surface area of the contact between the granite and the Dalradian rocks. This could only be achieved by an increase in volume of the magma body, or a change in its shape. Hence the development of the cleavage and the extensional shears record a transition from uplift and foldings, to accommodate the rise of the magma body, to radial expansion at its present level. Alternatively it could be argued that the increase in surface area of the contact could be the result of the rise of a hemispherical body through a single horizon (Fig. 4.17). If this was the case the cleavage and the shears would have been rotated into a steeper angle within the softened hornfels zone as the intrusion moved upwards. As noted above (section 4.3) there is no evidence for this. Since the flattening planes defined by the cleavage and the extensional shears are sub-parallel to the granite margin both features are interpreted as having formed as a result of approximately coaxial deformation. Field evidence indicates they represent the final increments in the deformation of the aureole by the intruding magma body. Since the granite cuts the S_3 cleavage at a number of localities (Fig. 4.13), but not the flattening planes defined by the extensional shears, it appears the cleavage pre-dates the shears. This implies a change in the stress field in the aureole of the granite which is controlled by the geometry of the ascending magma body. The maximum compressive stress would act normal to its surface. Hence a change in the strain field in the aureole would reflect a shape change in the surface of the pluton. Therefore it appears that the Northern Arran granite changed shape between the formation of the S_3 cleavage and the extensional shears.

Late coaxial deformation of the aureole of the Northern Arran granite is

recorded by the widespread development of kink bands within the core of the Catacol synform (Plate 4.5). Kink bands form during shortening of rocks with a strong pre-existing foliation or anisotropy (Donath, 1969; Dewey, 1965 & 1969; Anderson, 1974 and Cosgrove, 1976). The geometry of the kink bands depends upon the orientation of the σ_1 direction relative to the foliation (Donath, 1969 and Figure 4.25). Dewey (1965) showed that kink bands formed when the angle between σ_1 and the foliation was approximately 25^o. This relationship was used to constrain the orientation of the σ_1 direction during the formation of kink bands which occur within the core of the Catacol synform at Catacol and Lochranza. The geometry of conjugate sets of kink bands developed in the outer and inner limbs of the synform were measured and mean values were plotted on stereonets (Figs. 4.26 & 4.27 and Plate 4.6), from which the orientation of the principal stress axes were determined. This indicated that the compressive stress (σ_1) responsible for the formation of the kink bands lies in an approximately horizontal plane in both limbs of the fold. The σ_1 axes are not coincident (cf. Figs. 4.26 & 4.27). This is interpreted as the result of compression across a plunging fold axis (section 4.2) so that the strike of the S_2 foliation was not normal to the axis of compression. The flattening plane indicated by the conjugate kink bands would have formed perpendicular to the maximum compressive stress resolved normal to the pre-existing foliation and hence it may not accurately record the actual σ_1 direction. However it remains clear that σ_1 was directed away from the granite contact.

The kink bands have a different geometry on either side of the fold axis. Consequently the S_2 cleavage must have been at a different angle to σ_1 on either side of the fold axis. Hence the kink bands must post-date the formation of Catacol Synform (Fig. 4.28). This can be confirmed from a few exposures at Lochranza and Catacol where the kink bands can be seen folding the S_3 cleavage (Plate 4.5). This suggests the kink bands may be the same age as the extensional

Plate 4.5. Well developed kink bands in Dalradian pelites on the North Newton shore. These kink bands fold the S_3 cleavage which is visible below the tape measure.

Plate 4.6. Conjugate kink bands in Dalradian psammites from North Newton. Analysis of the orientation and the geometry of these kink bands was used to deduce the geometry of the stress field in the core of the Catacol synform.


RABTOCK

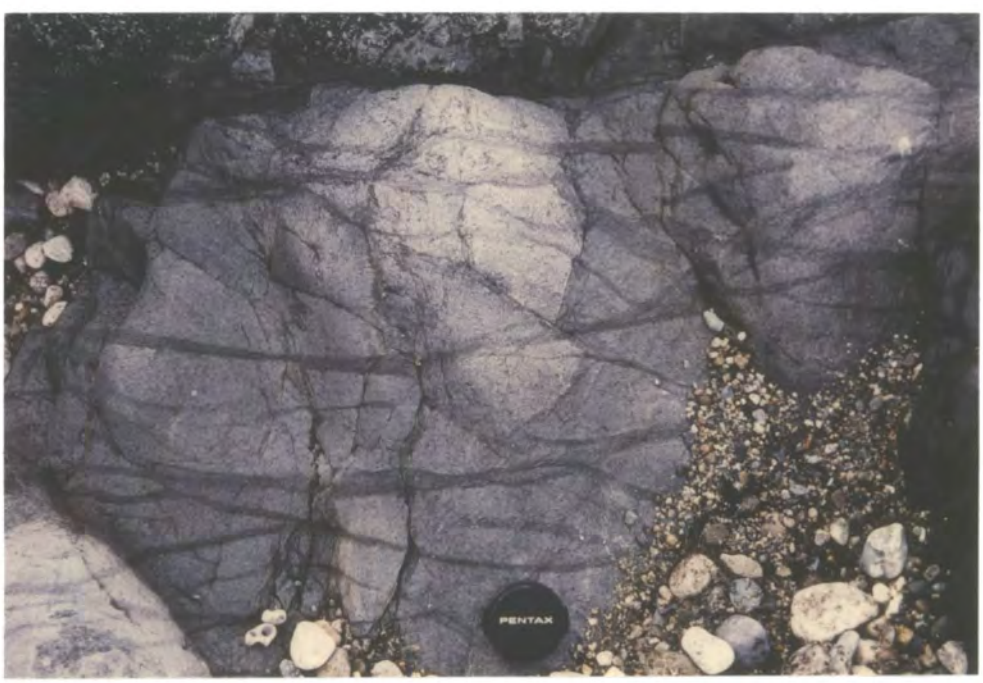
PENTAX

Figure 4.25. Schematic diagram showing the geometry of kink bands. α, β and γ are the interlimb angles and S the width of the kink band. The range of possible orientations of σ_1 to the pre-existing foliation is also shown.

Fig. 4.25.

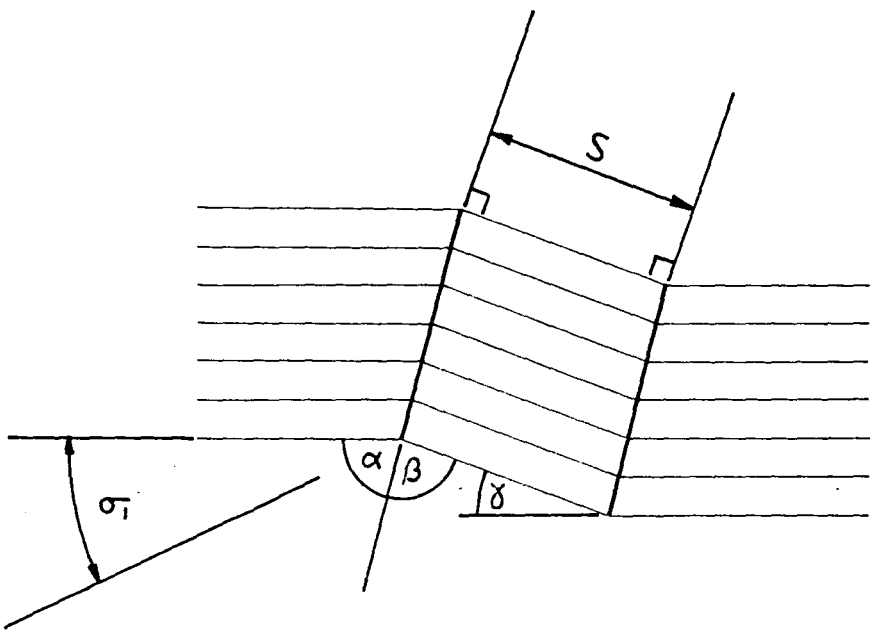

Figure 4.26. Equal area stereonet showing the orientation of the principal stresses determined from the conjugate sets of kink bands (solid lines) developed in the inner limb of the Catacol Synform at Lochranza.

Figure 4.27. Equal area stereonet showing the orientation of the principal stresses determined from the conjugate sets of kink bands (solid lines) developed in the outer limb of the Catacol Synform at Lochranza.

Fig. 4.26.

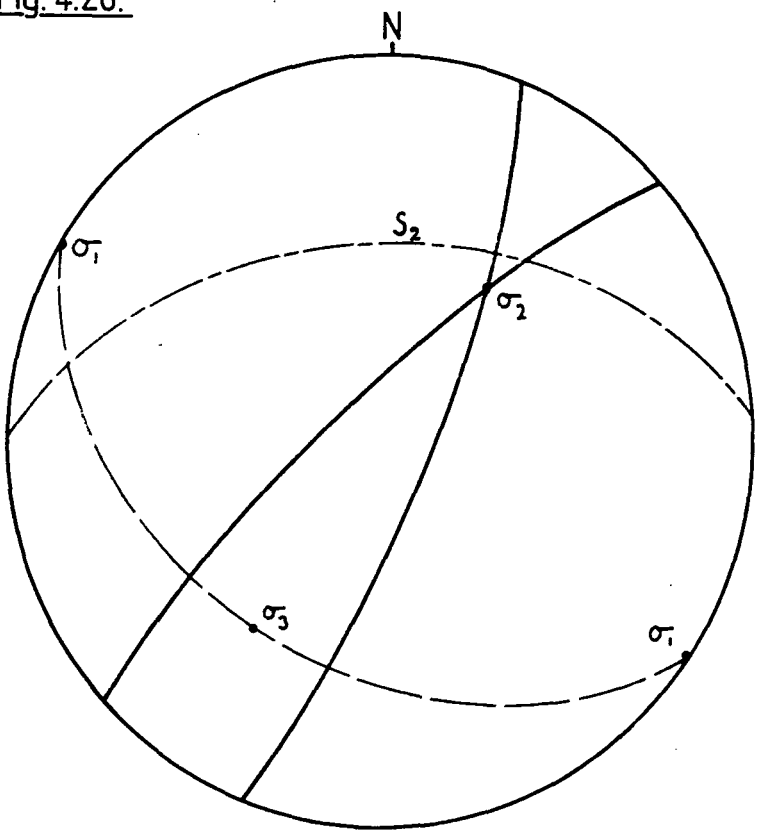

Fig. 4.27.

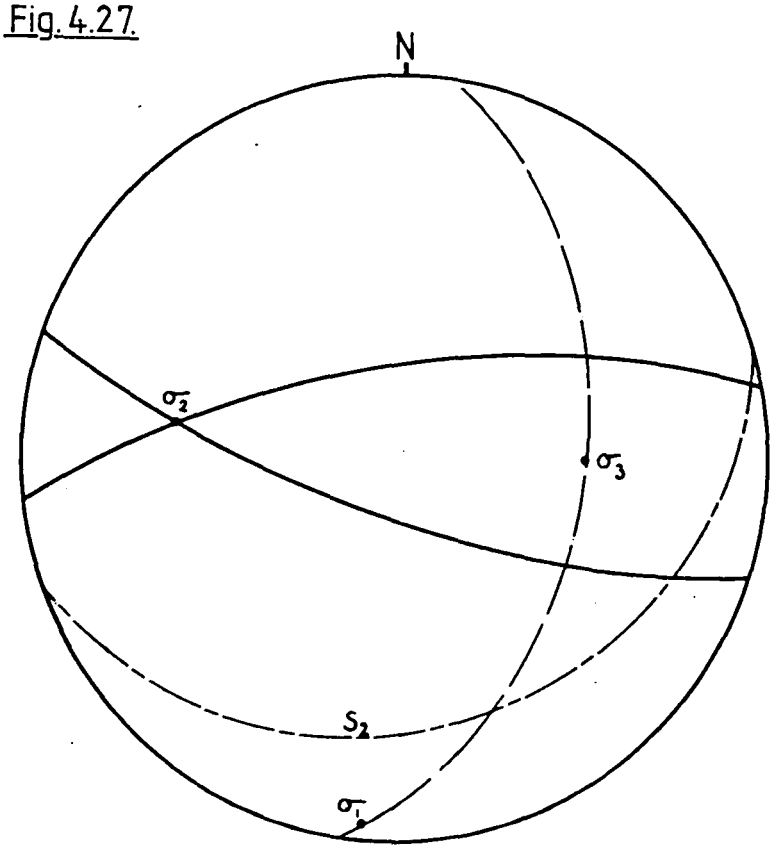

Figure 4.28. Upper figure: A schematic cross section normal to the axial plane of the Catacol Synform showing the orientation of the σ_1 direction on either side of the fold axis constructed from Figs. 4.26 & 4.27. σ_1 is approximately horizontal on both sides of the fold axis which excludes folding following kink band formation. It should be noted that σ_1 forms a larger angle with the foliation than that predicted ($\approx 25^o$) by Dewey (1969). Lower figure shows the geometry of the kink bands in the inner and outer limbs of the synform. The sense of vergence is opposite to that of the minor (F_3) folds.

Fig. 4.28.

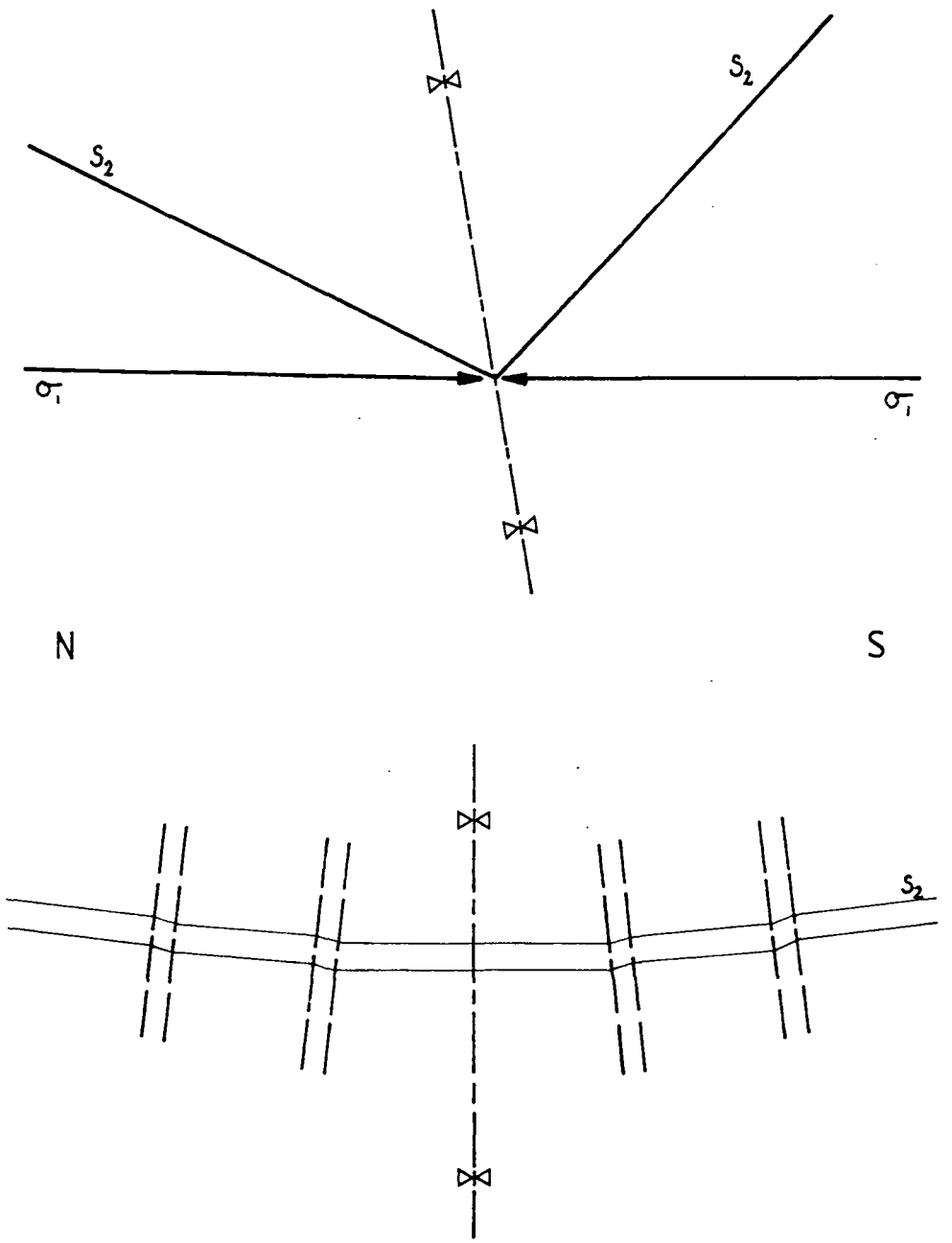

shears described in section 4.4. This is also indicated by the similar orientation of the σ_1 direction indicated by the kink bands and the extensional shears developed to the south of Lochranza, at Creagan nan Caorach and Creag a Chaise (cf Figs. 4.22 and 4.26 & 4.27).

The fact that the σ_1 direction indicated by the kink bands in both limbs of the Catacol Synform, is horizontal indicates that there has been no further folding around the axis of the synform following the development of the kink bands. Hence it appears that the later structures formed in the aureole of the northern granite record a change in deformation from simple shear, producing the inner limb of the Catacol Synfom during ascent of the granite to coaxial pure shear generating flattening strains as a result of in-situ shape changes of the pluton.

It is important to note that kink bands are not developed to the south of the granite in the SE limb of the Aberfoyle Synform. Since the formation of kink bands is critically dependent upon the orientation of a pre-existing foliation it must be concluded that at the time of kink band formation (i.e. syn-extensional shear formation) the S_2 foliation was already steepened against the intrusion in this area. Therefore the conditions for kink band formation would not have been satisfied. This observation also explains why kink bands are not found within the steeply dipping softened zone adjacent to the pluton in the Lochranza and Catacol areas. It also provides further evidence that the steepened zone formed before the development of the extensional shears.

Estimations of the spacing between individual kink bands in the Lochranza and Catacol areas, together with measurements of the width of the kink bands (S) and the angle (γ) (Fig. 4.25) were used to determine an approximate value of 8% for the flattening strains produced by kink band formation. This value is considered to be a maximum value for bulk shortening of the aureole by kink band formation since it represents shortening normal to the stike of the foliation and because the kink bands are not pervasive. A more accurate value could

be in the order of 4%. This shortening estimate should be added to the 10% value for shortening due to cleavage formation. As noted above no estimate of shortening due to extensional shearing was possible. In order to accommodate this the estimate of shortening due to kink band formation has been retained at 8% and homogeneous strain during the late coaxial deformation of the aureole has been assumed.

4.6 Faulting.

4.6.1 Faults within the Catacol Synform.

Detailed mapping within the core of the Catacol Synform (Figs. 4.29 & 4.30) revealed a number of shallow to steep faults parallel to the strike of bedding and the axial plane of the fold (Plate 4.7). These faults can be traced into a set of vertical faults radial to the margin of the granite. The faults clearly cut the F_3 folds and in places fault breccias developed along the faults contain angular clasts of pelite with a well developed crenulation cleavage, which is identified as S_3. Hence these faults post-date the development of the Catacol synform. Where there is good stratigraphic control (e.g. at North Newton, Fig. 4.29 and North Thunderguy, Fig 4.30) the steep faults parallel to the fold axis can be seen to cut up section and duplicate the stratigraphy. Hence they are reverse or thrust faults. Where the stratigraphic control was poor shear sense indicators (displacement across minor faults, displaced fold cores) confirmed that the faults were consistently of reverse type (Plate 4.8). Growth fibres in quartz veins developed in the fault planes indicated that the transport direction was normal to the fold axis. Reverse faults occur in both the outer and inner limbs of the Catacol synform where they always dip toward the fold axis. The angle of dip shallows toward the fold axis. Hence it appears that the reverse faults root in the core of the synform. Poor vertical exposure meant that it was not possible to trace a fault across the core of the synform or to identify the root of one of the reverse faults.

Figure 4.29. Detailed sketch map of post S_3 faulting within the core of the Catacol synform at North Newton.

Fig. 4.29.

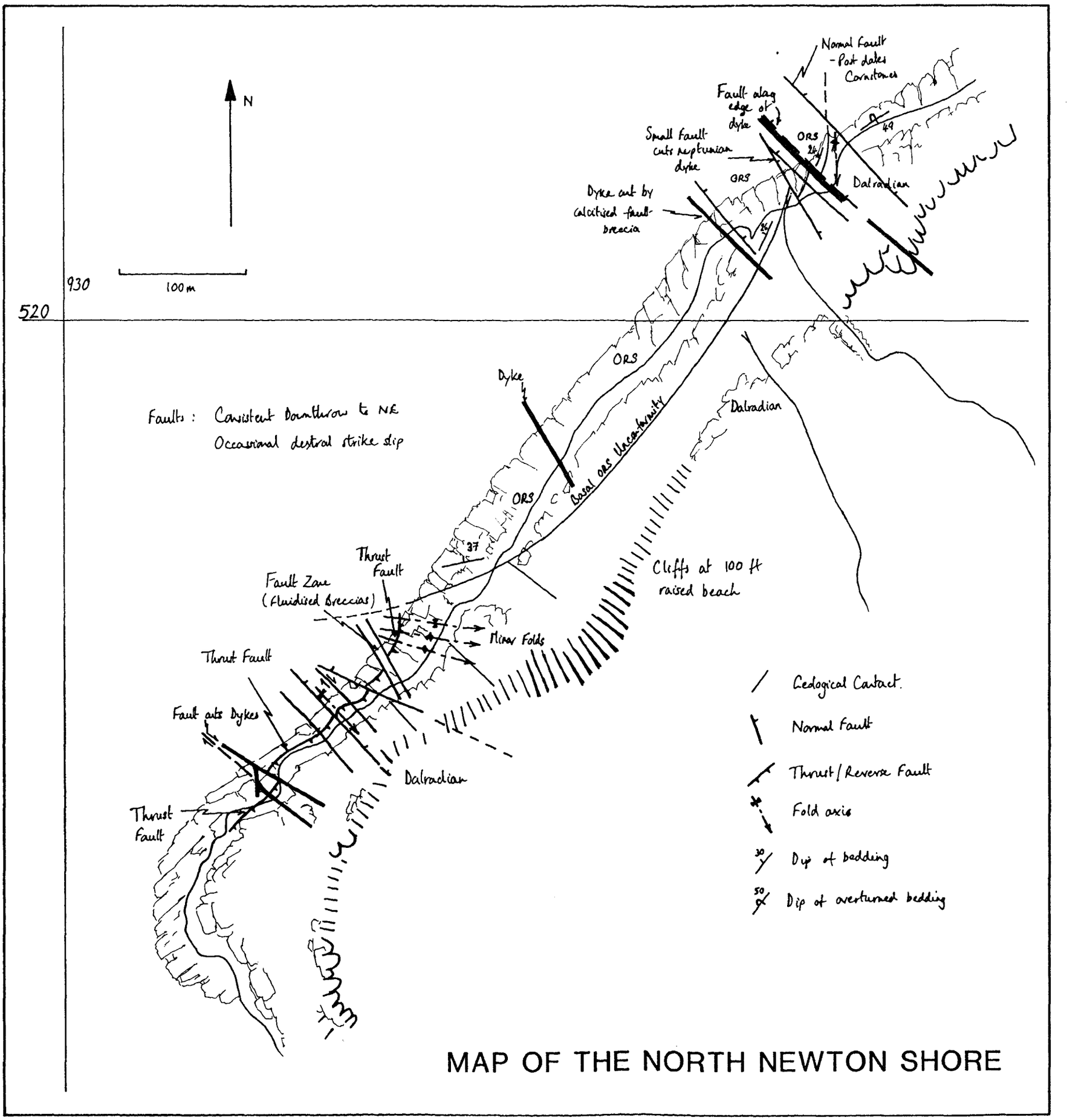

MAP OF THE NORTH NEWTON SHORE

Figure 4.30. Detailed sketch map of post S_3 faulting within the core of the Catacol synform at North Thunderguy.

SKETCH MAP OF SHORE AT NORTH THUNDERGUY – Drawn from original field map.

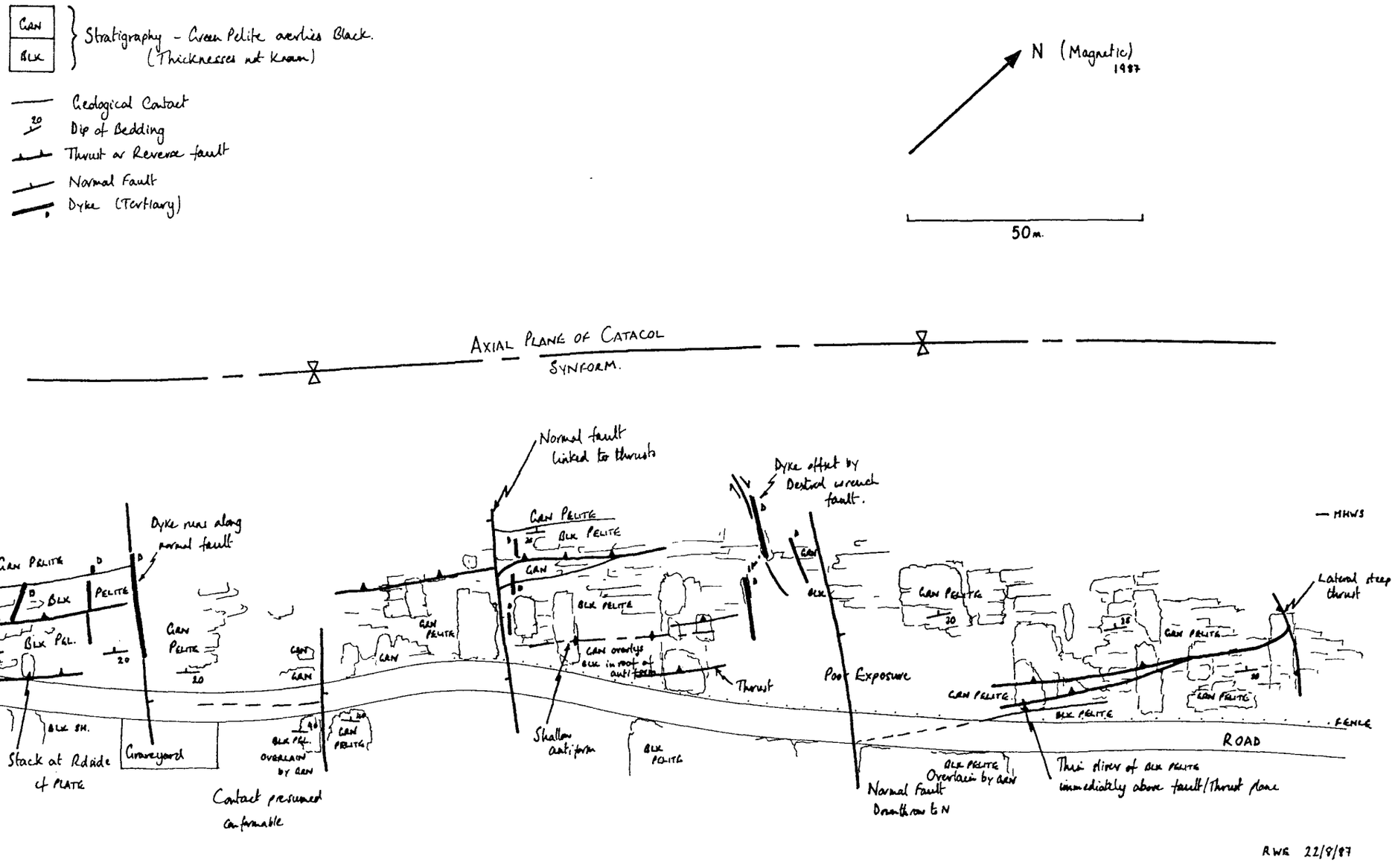

Plate 4.7. A westward dipping reverse fault cutting Dalradian pelites at North Thunderguy (Fig. 4.30).

Plate 4.8. A detail of Plate 4.7. This photograph shows the plane of the reverse fault and the imbrication of minor folds in the footwall indicating reverse displacement.

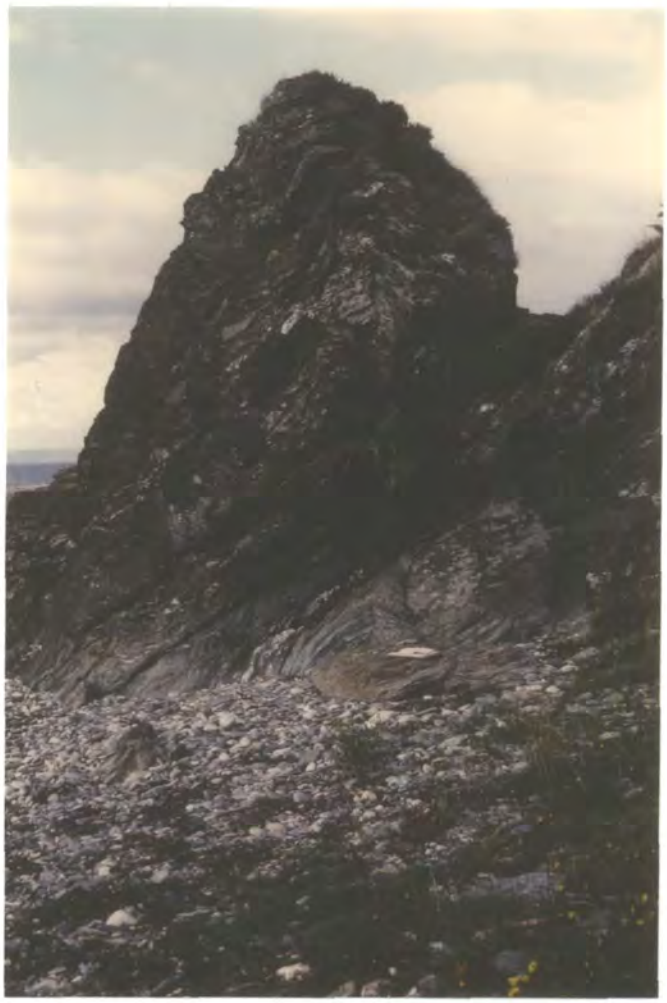

If the reverse faults do root in the core of the Catacol synform they may be regarded as 'out of synform thrusts' (Fig. 4.31). Thrust faults with this geometry accommodate compression in the core of a synform by acting as slip planes along which material is transported from the core of the fold to its limbs. This results in flattening normal to the fold axis and extension in the plane of the fold axis (Fig. 4.31) which is compatible with the displacements observed in the core of the Catacol synform. The geometry of this strain pattern is indentical to that recorded by the extensional shears at the margin of the granite and the kink bands within the limbs of the Catacol synform. Using this observation and the established relative age of the faults it is inferred that all these structures are synchronous and result from the same late flattening of the aureole of the granite.

Rooting of reverse faults below the synform is difficult to reconcile with the field evidence. Given that they post date the Catacol synform and record flattening parallel to the outer surface of the granite they would have to steepen toward the fold axis if they were to root below it, or against the side of the rising granite.

Reverse faults in both the inner and outer limbs of the Catacol synform can be traced into the vertical faults radial to the granite. The vertical faults are known to be the same age as the reverse faults on the basis of the criteria defined above. Radial dykes cutting the Dalradian rocks may have exploited the radial faults while others are cut by the faults or have faults running along their margins or centres. This confirms that the faults are of Tertiary age. The age relationship of the reverse and vertical faults indicate that they must form a linked fault system which appears to have accommodated both the flattening strains resulting from compression of the fold core and the circumferential extension which would have resulted from flattening of the aureole normal to the surface of the intrusion. In accommodating the circumferential extension the vertical faults would have permitted the reverse faults to remain normal to the fold axis. Had all the reverse faults propagated at the same stratigraphic level the tip lines of the faults would

Figure 4.31. A cross section through the Catacol synform showing the interpreted geometry of the reverse faults. Displacements on the faults record vertical extension and horizontal shortening consistent with compression of the fold core normal to the margin of the granite.

Fig. 4.31.

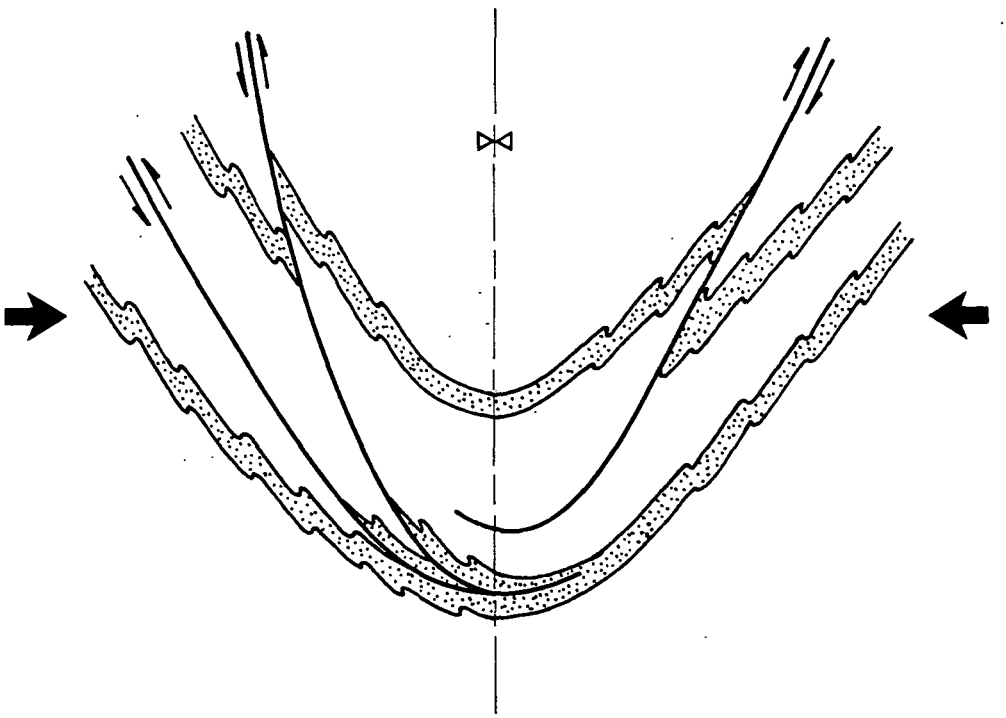

have either been convergent (on the inner limb of the synform) or divergent (on the outer limb of the synform). This would produce zones of compression or tension respectively. These would have been released by the faults stepping up or down in the stratigraphy across the vertical faults. Displacements across the normal faults are difficult to determine due to a lack of piercing points. Locally displacements of dykes and quartz viens indicate both sinistral and dextral strike slip movement, and others indicate vertical (normal) displacements. In either case measured displacements rarely exceed a few metres. Displacements across the reverse faults are of similar magnitude, suggesting that shortening across the aureole is limited. However the cumulative effect of reverse faulting over a vertical section greater than that exposed may have resulted in considerable shortening within the core of the synform (Fig. 4.31).

The faults contain breccias composed of Dalradian derived from the rocks marginal to the faults partially supported in a hematite stained matrix of finely ground Dalradian psammite and pelite. These breccias were also found in the hinges of F_3 folds within the psammitic units. They strongly resemble fluidised breccias in strongly deformed Silurian psammites and pelites in the Balbriggan inlier (E Ireland) described by Murphy (1984) (Plate 4.9). An increase in pore fluid pressure (e.g. by increasing the stress on a fluid filled crack) is known to reduce the normal stress across the fracture which results in a decrease in the resistance to shear failure of the rock (Sibson et al. (1975). Once fracturing occurs flow of the pore fluid under high pressure contributes to the deformation of the rock producing a fault breccia (Sibson et al. 1975; Murphy, 1984). The larger clasts within the breccia remain largely undisturbed, but are surrounded by fluidised material carried by the escaping pore waters (Murphy, 1984). In this case it appears that water became trapped in the psammitic rocks during the formation of the Catacol Synform. As the strain increased across the core of the synform, particularly as flattening strains were imposed on the structure, the fluid

Plate 4.9. An example of a well developed fluidised breccia from Catacol shore. Clasts of semi-pelite are surrounded by a matrix of fluidised, brecciated semi-pelite. The larger clasts show a well developed preferred orientation and only limited displacement of the original bedding.


PENTAX

pressure rose to the point at which the shear strength of the rocks was exceeded and faulting occurred. Had the fluid not been present it is probable that the faulting would have occurred at higher strains and that brittle deformation may have been supressed, allowing further folding to occur.

The origin of these fluids is not entirely clear but the red hematite staining of some of the breccias point to the overlying Carboniferous or Permian rocks (chapter 2) as a possible source. These successions contain considerable volumes of iron cemented porous sandstones and conglomerates. Friend et al. (1970) discussed the weathering of the Dalradian rocks below the Caledonian unconformity. Their conclusions suggest that hematite bearing solutions may have penetrated the Dalradian rocks to some depth along 'neptunian dykes' and fractures. The hematite concentrated in the fault breccias was probably filtered out and redeposited during flow of the fluids following faulting.

4.6.2 Faults to the south of the Granite.

Friend et al. (1963) mapped a group of parallel NW–SE striking dextral strike slip faults on the west side of Glen Rosa. These authors proved that the contact between the ORS and the Dalradian to the south of the northern granite was a steeply southward dipping unconformity rather than a fault (Gunn, 1903; Tyrrell, 1928). In the Glen Rosa area the ORS rocks directly above the unconformity are overturned. Where the unconformity can be mapped further to the west it is always seen to dip steeply southward. The steep dips of the ORS rocks decrease toward the south indicating a radius of updoming, around the south of the granite, of approximately 5 km (section 4.2). By extrapolating the measured orientation of the unconformity where it is exposed Friend et al. (1963) showed that the contact is stepped. In order to accommodate this stepping Friend et al. (1963) invoked a series of strike slip faults normal to bedding in the ORS (Fig. 4.32). Some of these faults can be found in the field, notably in the Garbh Allt (GR

Figure 4.32. Geological map showing the location and orientation of strike slip faults to the south of the granite (after Friend et al. 1963).

Fig. 4.32

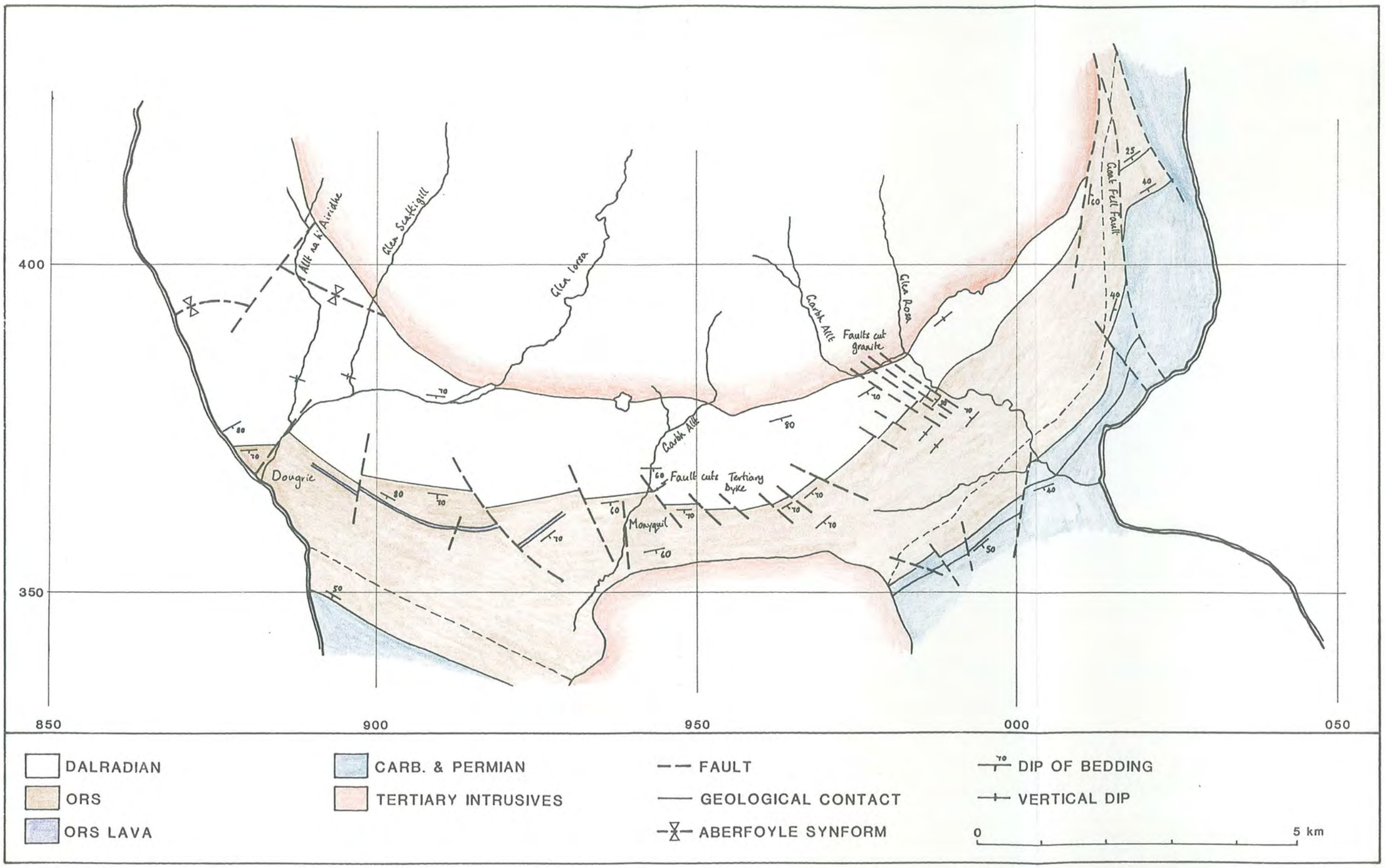
400
350
850
900
950
000
050
Allt na h'Airidhe
Glen Sladdaigill
Glen Iorsa
Glen Rosa
Garbh Allt
Faults cut granite
Goat Fell Fault
Dougrie
Garbh Allt
Fault cuts Tertiary dyke
Monyquil
DALRADIAN
ORS
ORS LAVA
CARB. & PERMIAN
TERTIARY INTRUSIVES
FAULT
GEOLOGICAL CONTACT
ABERFOYLE SYNFORM
DIP OF BEDDING
VERTICAL DIP
0
5 km

943366) where Dalradian pelites are brecciated by a fault which cuts a Tertiary dolerite dyke and offsets the Dalradian rocks to the south on its northern side. A thin basalt lava flow, of ORS age, exposed between Monyquil (GR 937354) and Dougrie is also offset by faults which have a strike which cuts the ORS/Dalradian unconformity.

Sub-horizontal slickensides noted in a number of localities on the west side of Glen Rosa (Friend et al., 1963) indicate strike slip movement on the faults. At one locality on the south bank of the Garbh Allt (GR 980385) shallowly southward plunging slickensides were found on joint surfaces within the granite approximately 4 m from its contact with the Dalradian. The marginal granite exposed in the stream bed is cut by a series of zones of intense jointing along strike from the faults which cut the ORS/Dalradian unconformity. These observations indicate that strike slip movement must have occurred on the faults after the margins of the granite had solidified.

With the exception of two faults near Dougrie all the faults south of the granite show dextral strike slip movement. Since the faults cut steeply dipping ORS and Dalradian it appears that the Dalradian rocks in the Glen Rosa area have been displaced some distance to the SW after updoming. The sequential development of F_3 folds followed by extensional shears in the rocks to the south of the granite (as noted above) is interpreted as the result of updoming over the rising granite, followed by radial flattening of the aureole. The stress field indicated by the geometry of the shear planes is consistent with the stress field indicated by the dextral strike slip faults, which are oblique to the margin of the granite. On this basis these structures are interpreted as being broadly contemporaneous. However the shears and the normal faults record different patterns of strain. The extensional shears indicate flattening normal to the margins of the granite (described above). The dextral strike slip faults indicate that this flattening was produced during expansion of the granite toward the SE, which is accommodated by movement on

the Goat Fell fault which forms the eastern margin of the granite.

4.6.3. Faulting on the eastern side of the Granite.

It has already been established from the truncation of the thermal aureole that the eastern margin of the northern granite is bounded by a fault which was active during emplacement (chapter 3). This fault (the Goat Fell Fault) is sub parallel to a NNW–SSE striking set of normal faults which form part of the Laggan fault system (Fig. 4.33). As noted in chapter 2 seismic data from the Firth of Clyde (McLean & Deegan, 1978) indicate the Laggan–Brodick Bay fault system was active during the Carboniferous and Permian. It is not clear whether the Goat Fell Fault was active during this period of time. It may be linked to a N–S trending fault which runs southward to Brodick Bay. There is no evidence that it continues for any significant distance north of the Allt a' Chapuill or Glen Sannox. It clearly does not cut the Dalradian on the north side of Lochranza as suggested by Bailey (1926). There is no evidence exposed at the surface of any offset in the Dalradian stratigraphy or the axial plane of the Catacol Synform in the area. Hence the fault appears to be isolated from the main part of the Laggan Fault system. It is possible that it pre-existed the granite as a footwall collapse structure to the Laggan Fault (Fig. 4.34).

These faults and particularly their expression in the Permian sandstones have been the subject of a recent study by Underhill & Woodcock (1987) and Woodcock & Underhill (1987). These authors showed that numerous slip hardening faults developed in the high porosity Permian aeolian sandstones (Plate 4.10) by upward diffusion of syn-intrusion displacements on the pre-existing faults of the Laggan Fault system (Underhill & Woodcock, 1987). They showed that the density of the faults decreased with increasing distance from the northern granite and hence related their formation to deformation during intrusion of the pluton. Woodcock & Underhill (1987) subdivided the slip hardening faults into three distinct

Figure 4.33. Geological map showing the geometry of the Laggan fault system between North Glen Sannox and Corrie, east of the granite. (Contours at 50 m intervals.)

Fig. 4.33

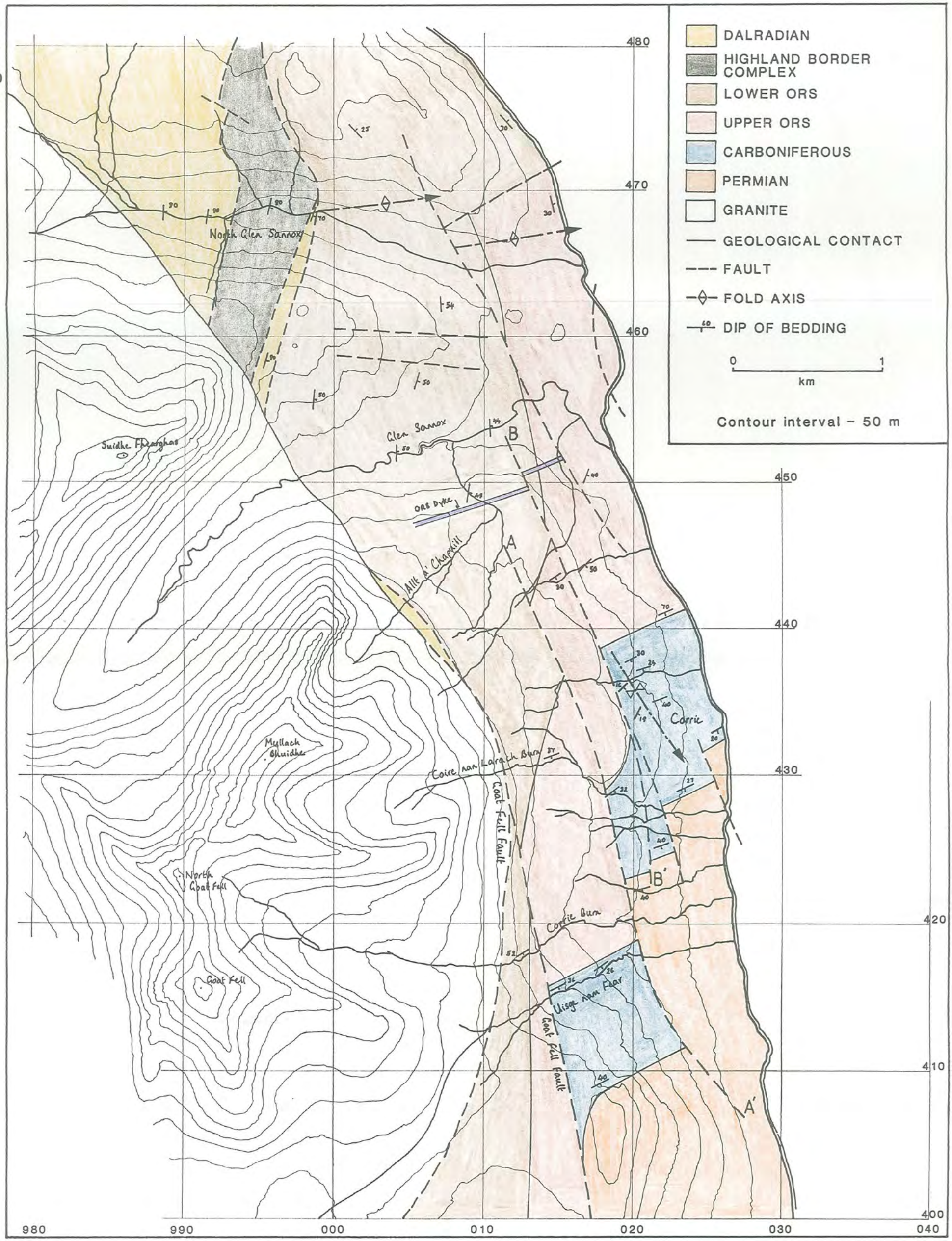
DALRADIAN
HIGHLAND BORDER COMPLEX
LOWER ORS
UPPER ORS
CARBONIFEROUS
PERMIAN
GRANITE
GEOLOGICAL CONTACT
FAULT
FOLD AXIS
DIP OF BEDDING
0
1
km
Contour interval – 50 m
North Glen Sannox
Glen Sannox
Suidhe Fhearghas
ORS Dyke
Allt a' Chaptuill
Corrie
Coire nan Laraich Burn
Coat Fell Fault
Mullach Bhuidhe
North Goat Fell
Goat Fell
Corrie Burn
Uisge nam Fear
A
A'
B
B'
480
470
460
450
440
430
420
410
400
980
990
000
010
020
030
040

Figure 4.34. Cross section through the Laggan Fault System west of Corrie prior to the intrusion of the granite.

Fig. 4.34.

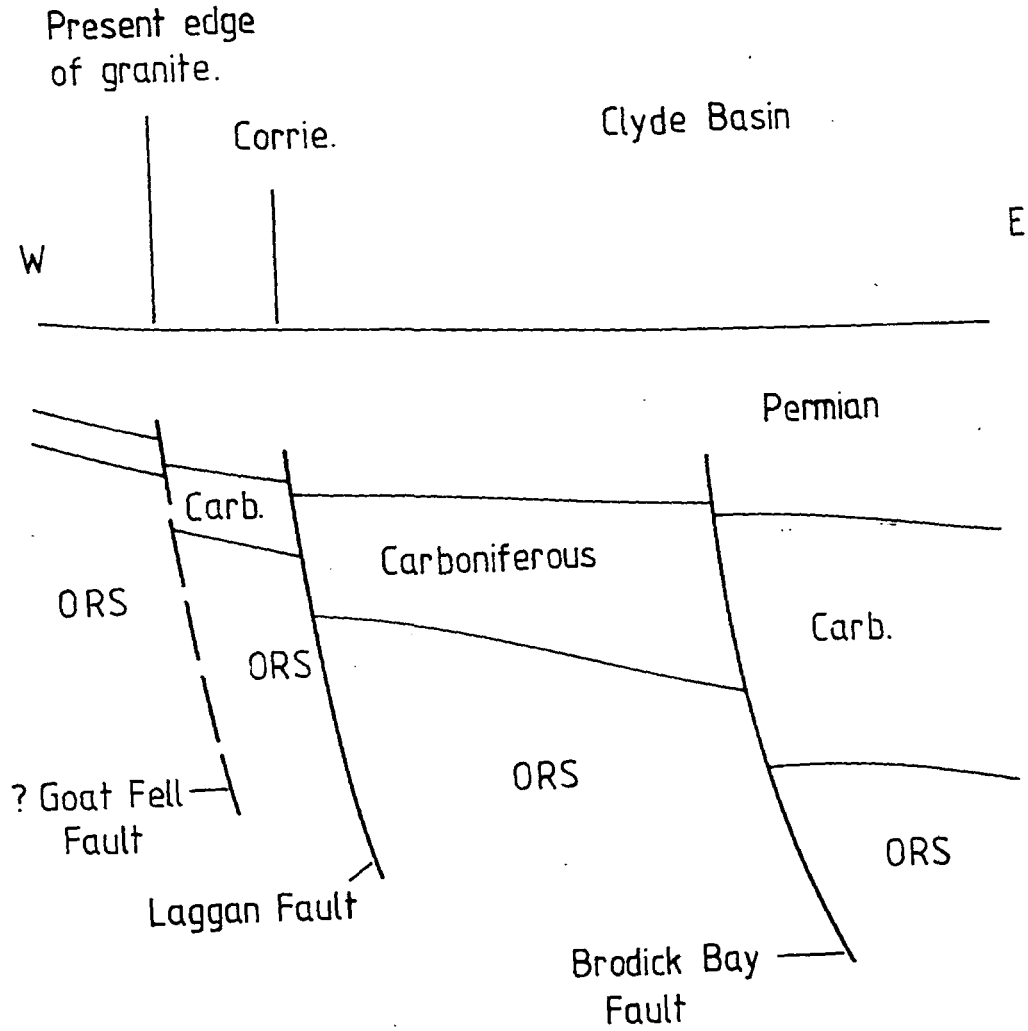
Present edge
of granite.
Corrie.
Clyde Basin
W
E
Permian
Carb.
Carboniferous
ORS
ORS
Carb.
ORS
ORS
? Goat Fell
Fault
Laggan Fault
Brodick Bay
Fault

Plate 4.10. Slip hardening faults developed in the Permian sandstone at Corrie. This photograph shows a well developed conjugate set of these anastomosing faults or granulation seams.

systems on the basis of the orientation of conjugate faults of similar geometries. Two of these fault systems, system N (faults with a NW–SE strike intersecting to form conjugate sets with vertical or NW–SE striking intersections) and system E (faults with an E–W strike intersecting to form conjugate sets with vertical or sub-horizontal E–W striking intersection lineations) were shown to define strains which indicate a complex stress field existed during their formation. Woodcock & Underhill (1987) attributed this to modification of the stress field around the granite by the complex pre-intrusion structure of the area. A third system of faults, system L (conjugate faults with shallow dips and which intersect to give sub-horizontal intersections radial to the Northern Granite) were developed some distance from known pre-existing faults. The strain represented by this fault system was considered to have resulted from a stress field relatively unmodified by any pre-existing basement structures and hence give a more accurate representation of the stress field around the granite during its emplacement.

The strain axes deduced from the three systems, and in particular the system L faults, indicate a vertical z axis (sub-horizontal stretching) and a horizontal x axis radial to the granite, within a radius of approximately 15 km of the centre of the intrusion and a vertical y axis outside this radius (Fig. 4.35). This pattern records doming over the granite over a wider area than is detectable from the dip of bedding (section 4.2).

This updoming appears to have preceeded dip slip faulting on the Laggan Fault system. Radial extension over the granite of the Permian rocks recorded by the slip hardening fault systems could only have continued while the Permian formed a continuous layer over the granite. Once this layer became discontinuous (i.e. as a result of being cut by faulting) then new slip hardening faults would only form as a result of the dissipation of local stresses. Woodcock & Underhill (1987) suggest this process is indicated by the development of strong system N faults in the Permian rocks along strike from the Laggan fault system west of

Figure 4.35. The strain pattern around the northern granite deduced from the geometry of slip hardening fault systems (after Woodcock & Underhill, 1987). The figure indicates updoming and associated radial stretching of the roof of the granite occurred within a 15 km radius of the centre of the intrusion.

Fig. 4.35

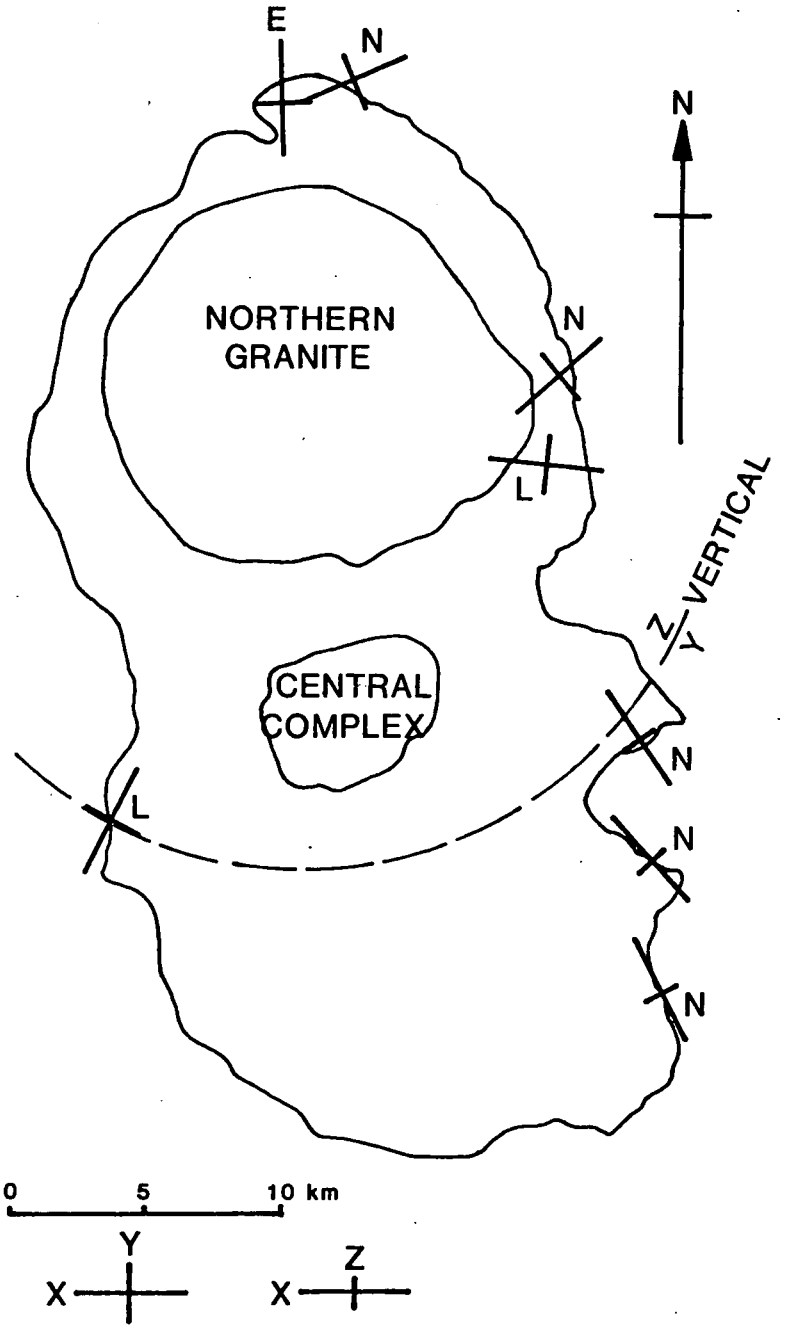

Axes of the Strain Ellipse
from Slip Hardening Faults

Corrie, and a strong set of system E faults east of the Glen Rosa strike slip faults in response to movement on the sub-Permian faults caused by the ascent of the granite. The strain pattern indicated by these faults is not consistent with displacements on the sub-Permian faults, indicating the continued influence of the stress field associated with the granite (Woodcock & Underhill, 1987). The overall strain pattern indicated by the Laggan Fault system is of normal faulting with a downthrow away from the granite. A feature consistent with the forceful ascent of an intrusive body.

Where the position of the Brodick Bay Fault can be determined offshore it has an approximately straight NW–SE strike. This differs from the Laggan Fault system which shows a curvature parallel to the strike of the granite (Fig 4.33). This curvature of the fault system appears to be restricted to the area immediately adjacent to the granite, which suggests that it is related to the intrusion. A certain amount of updoming is associated with the normal faulting and outward bending of the fault system. Woodcock & Underhill (1987) showed that the North Sannox anticline (Gunn, 1903; Tyrrell, 1928; Friend et al., 1963) has a conical geometry, with the axis of the cone plunging away from the granite. A number of radial faults were also mapped in this area (Fig. 4.33). These appear to have developed to accommodate stretching parallel to the margin of the granite which resulted from the outward bending of the rocks. This may have resulted in the reactivation of the Highland Boundary Fault, which has a present orientation radial to the granite in the North Sannox area (chapter 2) (Fig. 4.33).

It is clear that the SW limb of the Aberfoyle synform does not form a continuous arc to the south of the granite. The boundary between the Dalradian and ORS rocks and the projected strike of bedding within the Dalradian is clearly truncated and displaced sinistrally across the Goat Fell Fault. At Allt a' Chapuill the fault runs between the ORS and a thin sliver of Dalradian. The contact between this Dalradian and the granite is very irregular, being extensively veined

by sheets of chilled granite, but shows no evidence of significant faulting. At this locality and at a similar contact exposed in the Uisge nam Fear the granite has locally developed a foliation. Thin sections of the foliated rocks indicate they are foliated cataclasites (Chester et al., 1985) (Plate 4.11). This records brittle deformation of solid granite at low temperatures or high strain rates.

There is no strong evidence for the sense of movement along the Goat Fell Fault. Shear sense from the foliated cataclasites indicate dip slip movement. The fault breccias in Corrie burn and between the ORS and Dalradian in Allt a' Chapuill and the Uisge nam Fear give no indication of shear sense. Truncation of the thermal aureole is most easily explained by dominantly normal faulting. This would also account for the presence of the hornblende–hornfels facies Dalradian rocks at Allt a Chapuill which are juxtaposed against epidote–albite facies ORS by faulting (Fig. 4.36). A major component of strike slip movement is recorded on the continuation of the fault to the south where Carboniferous strata are upturned through 40^{o} and displaced 2 km sinistrally along the fault.

While this displacement can be accounted for by the intrusion of the granite it is not clear whether all the dislpacement is of Tertiary age or if some of it is Permo–Carboniferous. The seismic data from the Firth of Clyde (McLean & Deegan, 1978) suggests that the fault system was active during the Permian, which implies that the Carboniferous rocks may have been displaced by normal faulting in the same direction as would result from the ascent of the granite. The slip hardening faults record the upward dissipation of Tertiary movements, on the Laggan fault system which cut into the Permian. The development of the slip hardening faults indicates that the Permian was not cut by major faults before the Tertiary (Underhill & Woodcock, 1987) (Fig. 4.34). However Astin & MacDonald (1983) have described evidence for syn-depositional faulting from the Permian of Arran. Hence the best indicator of Tertiary fault displacements is the top of the Permian but this is not exposed in the vicinity of the granite.

Plate 4.11. Crushing during movement along the Goat Fell fault resulted in deformation of the margin of the coarse granite. Fracturing of grains and grain reduction has produced a cataclastic rock. Bands of fine grained brecciated rock separating less deformed regions have produced a foliation. The granular texture of the matrix is the result of post defoarmation annealing, indicating that the intrusion was still warm at the time of deformation. Crushed marginal fine grained facies of coarse granite, No. AR 5202, Uisge nam Fear, GR 011413. Width of field = 3.5 mm, crossed polars.

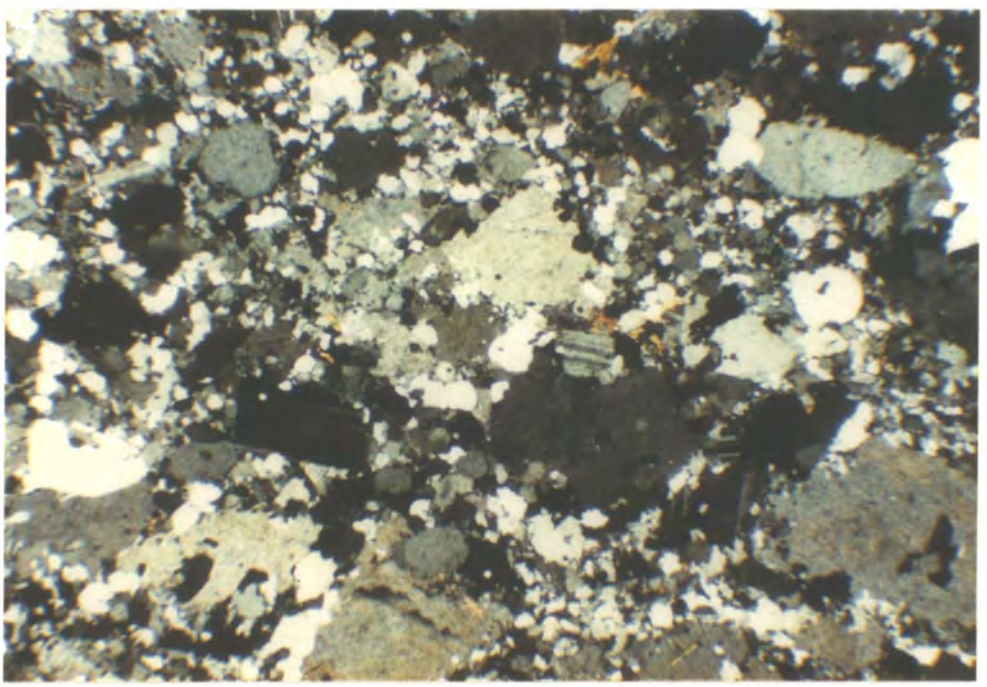

Figure 4.36. Schematic diagram showing the postulated syn-intrusion displacement on the Goat Fell Fault which resulted in truncation of the thermal aureole and uplift of Dalradian rocks at Allt a' Chapuill.

Fig. 4.36.

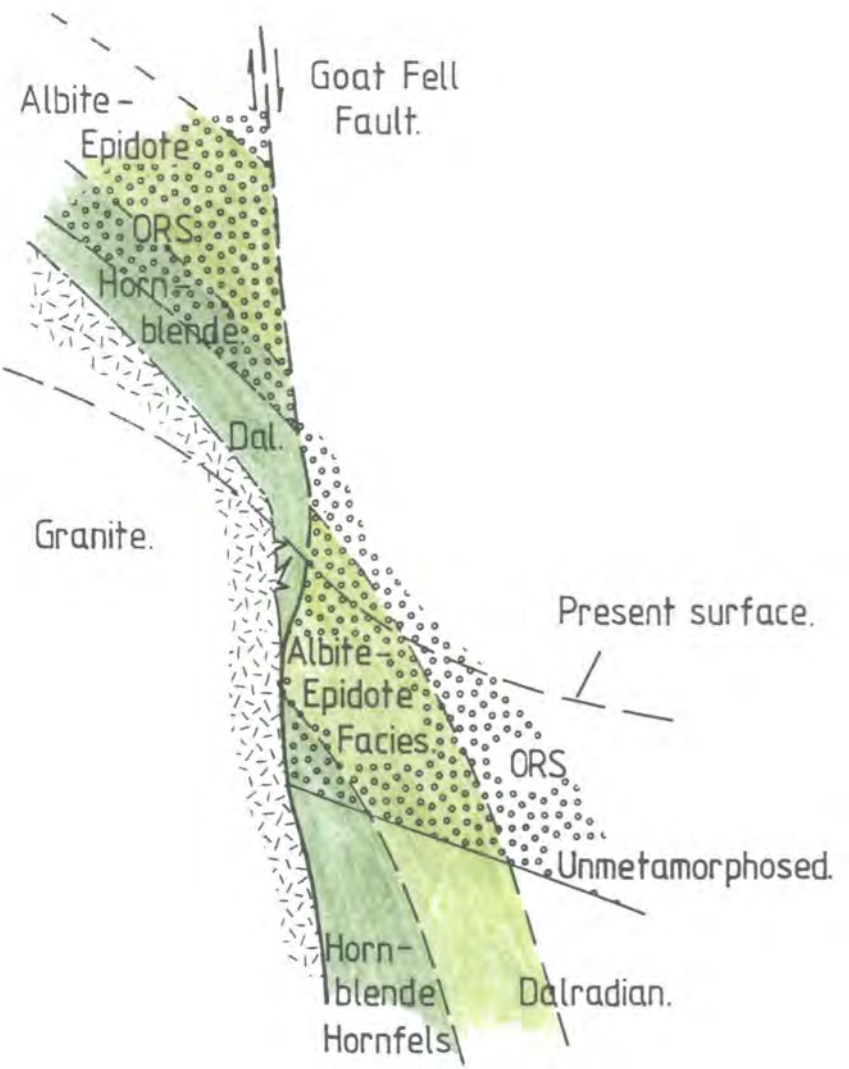
W.
E.
Albite-
Epidote
ORS.
Horn-
blende.
Dal.
Granite.
Goat Fell
Fault.
Present surface.
Albite-
Epidote
Facies.
ORS.
Unmetamorphosed.
Horn-
blende
Hornfels
Dalradian.

Consequently the base of the Permian is used as an indicator of displacements and Permian syn-sedimentary faulting is neglected as there is no evidence for it in the sections discussed below. It is apparent from the map that both normal and sinistral strike slip displacements on the faults to the west of Corrie village could produce the observed outcrop pattern. Mapping of these faults and the changes in dip on either side of them confirmed that the Carboniferous sequence thins toward the south (Gunn, 1903; Tyrrell, 1928; Chapter 2).

Outcrop width in the direction of dip remains approximately constant between the faults. Hence the displacement on the faults was restored by projecting the dip orientations along the fault planes and matching outcrop widths within the Carboniferous (Fig. 4.37). On one fault restoration was initially attempted by constructing the displacement from a piercing point formed by the intersection of a middle to upper ORS dyke (outcropping to the south of Sannox Burn) with the top of the lower ORS. Restoring the apparent movement of this point does not restore the base of the Permian across the fault. This may be due to Permian syn-sedimentary faulting. However a solution can be obtained by restoring the base of the Permian as described above by projecting the dips of the Carboniferous. The remaining offset on the dyke was then equal to the displacement of the top of the lower ORS. This indicates movement on the fault of upper ORS age, which is consistent with a change in thickness of the Upper ORS across the fault. Hence there is evidence that the Laggan fault was active before the Carboniferous. The net Tertiary displacements indicated by the restoration of the base of the Permian (Fig. 4.37) indicate oblique slip (containing normal and sinistral strike slip components) on the faults. Since it was not possible to determine the actual movement on all the faults it is not possible to give absolute displacements across the fault system.

The history of faulting on the eastern side of the Northern Arran Granite indicates that it intersected a set of NW–SE trending faults of Carboniferous age

Figure 4.37. Cross sections (1:10,000 scale) along the fault planes to the west of Corrie showing the thinning of the Carboniferous sequence to the south. The sections were restored to the base of the Permian by matching the width of outcrops of the Carboniferous strata (see overlay for displacement on faults, indicated by red lines. Section B-B' indicates Upper ORS fault movement.

Fig. 4.37 A

Section to west of Fault A-A'.

Section to east of Fault A-A'

(Scale 1:10,000)

Top Carboniferous

Base Carboniferous

A

400
300
200
100
0

A

400
300
200
100
0

Base Carboniferous

Top Carboniferous.

A'

400
300
200
100
0 m

A'

400
300
200
100
0 m

Section to west of Fault B-B'

Section to east of Fault B-B'

(Scale 1:10,000)

Top Lwr ORS

Top Lwr ORS

ORS Dyke

ORS Dyke

Top Carboniferous

B

400
300
200
100
0

B

400
300
200
100
0

Base Carboniferous

Top Carboniferous

Top Carboniferous

B'

400
300
200
100
0 m

B'

400
300
200
100
0 m

Fig. 4.37.

A-A'.

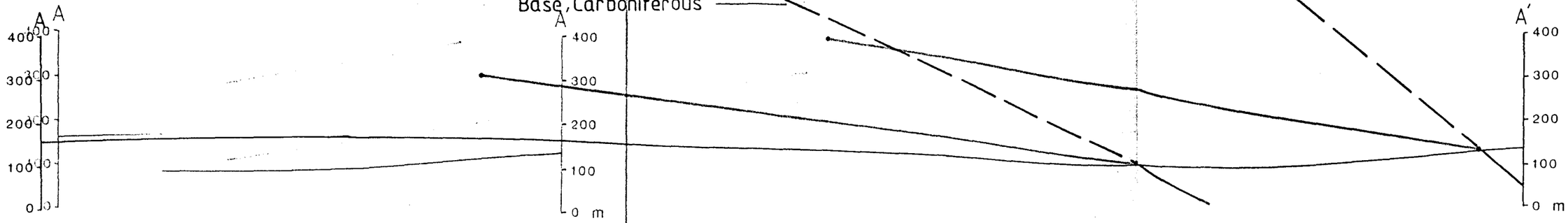
Section to west of Fault A-A'.
Base Carboniferous
Top Carboniferous
A
A'
400
300
200
100
0 m

B-B'

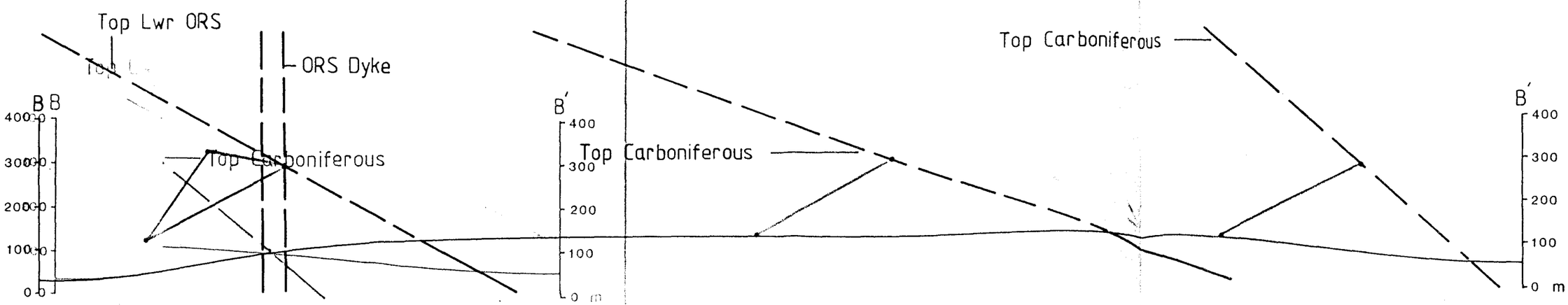
Section to west of Fault B-B'
Top Lwr ORS
ORS Dyke
Top Carboniferous
B
B'
400
300
200
100
0 m

during its ascent. Subsequent movements on this fault system strongly influenced the emplacement of the granite on its eastern side. This is in contrast to the north, west and south margins of the intrusion where the structure of the aureole is dominated by the intrusion of the pluton rather than by the existing structure. Early normal displacements on the Laggan Fault system, following stretching of the cover is indicated by the geometry of slip hardening faults developed in the Permian (Woodcock & Underhill, 1987). Syn-intrusion vertical movement is recorded on the Goat Fell Fault by the truncation of the thermal aureole (chapter 3 & Fig. 4.36). The vertical movement on this fault along the granite-ORS contact appears to have been translated into sinistral strike slip in the country rocks where the fault continues to the south of the granite. This would have accommodated the increased radius of the granite body during its ascent. Some radial expansion and concentric extension of the granite is indicated by the outward bending of the Laggan Fault system, updoming in the Sannox and North Sannox area to produce the conical North Sannox antiform, and strike slip movement on the faults to the west of Corrie.

4.7 Interpretation of the Syn–emplacement Faulting: A Summary.

Within the Dalradian rocks a system of linked normal and reverse faults in the core of the Catacol synform, and a set of dextral strike slip faults to the south of the granite indicate horizontal radially directed stresses acted on the aureole. Such a stress field is also recorded by conjugate extensional shears developed along the margin of the granite and kink bands in the limbs of the Catacol synform. Formation of these structures is the last deformation event recorded by the aureole rocks. Contemporaneous faults, shears and kink bands clearly cut the minor folds associated with the early updoming around the granite (section 4.3). Hence they represent the last increment in the strain history of the aureole. All these structures define flattening strains ($k \approx 0$) parallel to the margin of the granite.

The shortening of the aureole indicated by these strains is therefore a direct record of radial expansion of the granite during the final stages of its emplacement.

The dextral strike slip faults within the Dalradian and ORS rocks to the south of the granite indicate increasing southward displacement toward the Goat Fell fault along this section of the contact. Sinistral strike slip movement on the Goat Fell Fault appears to have accommodated this deformation of the contact. The SE directed expansion of the pluton in this area appears to have been permitted by movements on these faults.

Movements of Tertiary age on the pre–existing Laggan Fault system on the east side of the granite record a strain history of early updoming followed by normal faulting with a component of strike slip in respose to ascent and outward expansion of the granite. This sequence is broadly compatible with the deformation sequence recorded in the Dalradian rocks. However it is apparent that reactivation of the Laggan Fault system clearly influenced the deformation history in this area by localising displacements necessary to accommodate the intruding pluton.

The Goat Fell Fault appears to have acted as a lateral wall to the granite, which prevented strong radial expansion of the pluton along its eastern margin. There is no evidence for radially directed stresses (as are recorded in the Dalradian rocks), along this section of the contact. These appear to have been dissipated by expansion of the granite parallel to the fault plane, either by uplift of the roof or by strike slip movement along its southerly extension into the country rock, as is indicated by field evidence.

4.8. The Structural Evolution of the Aureole of the Northern Arran Granite.

The aureole of the Northern Arran Granite shows contrasting styles of deformation. To the north, west and south of the granite the early deformation history is dominated by ductile mechanisms of folding and cleavage development, which

accommodated updoming of the Dalradian above a rising hemispherical magma body. Later deformation is dominated by synchronous semi-brittle (adjacent to the granite) to brittle mechanisms of extensional shearing and faulting, which record radial flattening of the aureole. To the east of the granite, aureole deformation is dominated by faulting throughout emplacement. This contrast in style of deformation reflects the complex structure of North Arran prior to the intrusion of the granite (chapter 2). It should be emphasised that the contrast does not reflect a different style of emplacement on the eastern margin of the intrusion. The aureole of the Northern Granite records the interaction between a rising body of magma and complex upper crustal structures.

Overprinting of strain patterns within the aureole record a continuous sequence of deformation. These strains reflect progressive intrusion of the granite and changes in the geometry of the pluton in response to inhomogeneous aureole deformation. The evolution of the aureole indicates that its geometry following early phases of deformation subsequently influenced later patterns of strain development.

The transition from ductile to brittle deformation can be explained in terms of progressive deformation of a cooling thermal aureole. As the granite rose it would have gradually lost heat to the country rocks by conduction or convection. This would result in a gradually diminishing heat content within the magma and a tendency toward equal temperatures in the granite and its wall rocks. Secondly ascent of the granite would have resulted in displacement of the aureole rocks toward the surface causing them to cool (assuming the associated uplift at the surface resulted in erosion). Once brittle deformation occurred fluid pathways would develop which could further enhance heat transfer from the aureole. This latter process may have dominated on the eastern side of the granite where the thermal aureole is truncated by the Goat Fell Fault.

The early structural development of the aureole of the granite discussed in

section 4.3 clearly indicates the ascent of a bouyancy driven piercement structure or diapir. An alternative interpretation would be that the intrusion was a laccolith. The structure of the aureole of the Northern Arran Granite is similar to the structure of the aureoles of laccolithic bodies. In particular the concentric folding and overburden failure due to faulting (Gilbert, 1877; Johnson & Pollard, 1973; Pollard & Johnson, 1973; Dixon & Simpson, 1987; Jackson & Pollard, 1988). However the aureole of the Northern Arran Granite records strong flattening strains along the margin of the intrusion. Also the pre-existing structure of North Arran does not provide a suitable floor structure upon which the laccolith would have initiated as a sill. These features were used by Jackson & Pollard (1988) to make distinctions between laccoliths and stocks.

The flattening strains developed in the aureole record a late phase of radial shortening in response to an increase in the radius of the magma body at its present exposure level. This feature of aureole deformation has been attributed to inflation or ballooning of the intrusive body (Holder, 1979; Bateman, 1985). In its strictest sense ballooning implies expansion of the pluton by an increase in the volume of magma. This point will be examined in chapter 5. The flattening strains within the aureole of the Arran granite may subsequently be found to reflect ballooning *sensu-stricto* or they may represent a change in the shape of the pluton, with no change in volume, during the latter stages of its emplacement. A distinction between these processes cannot be made on the basis of the aureole deformation alone.

A restoration of the aureole of the Northern Granite using the strain estimates discussed in section 4.5 was performed as an aid to modelling the intrusion of the pluton. In addition to the estimates for late coaxial shortening (8%) and formation of the S_3 cleavage (10% shortening) measurements of the F_3 fold geometries gave an estimate of 25% shortening (Folded length / Original length) normal to the limbs of the Catacol synform. A further 32% shortening was indicated by a

comparison of the width of the inner limb of the synform to its actual length measured from sheet dip (Fig. 4.11). The latter is a minimum value since it ignores any shortening in the outer limb. These strains are summarized in table 4.1:-

Table 4.1.

Structure	Estimation of Shortening
Catacol Synform	32%
Minor Folds	25%
Total Shortening due to folding	51%
S_3 cleavage	10%
Flattening Strains (e.g. Kink Bands)	8%
Total Shortening due to radial expansion	17%
Total shortening	62%

These calculations, although representing very general estimates, are thought to be a reasonable approximation to the strains imposed during the early folding and later flattening. It is apparent from the table that the bulk of the aureole strain necessary to accommodate the emplacement of the Northern Arran Granite occurred during the early folding phase, while the magma was still rising.

In restoring the aureole these strain increments were successively removed in reverse order to the list in Table 4.1. (Fig. 4.38). Restoration of the strike slip faults to the south of the granite clearly indicates that the last increment of aureole strain involved expansion of the granite toward the SE, producing the notable bulge in the margin of what is an otherwise almost circular intrusion. This caused clockwise rotation of the SW limb of the Aberfoyle synform as it was displaced sinistrally along the Goat Fell Fault. The fact that the restored Dalradian is no longer in contact with the Goat Fell Fault is thought to reflect synchronous clockwise rotation within the Dalradian rocks to the west of the granite, and outward bending of the Laggan Fault system in response to an increase in the circumference of the magma body. The restoration of this has not been attempted

Figure 4.38. A sequential restoration of the aureole of the Northern Arran Granite. Progressive increments of deformation have been removed assumming homogeneous pure shear in the order 1 - 2 - 3. Strain increments removed at each stage are taken from Table 4.1. Inset shows the idealised plan of a planar surface intersecting a spherical body, cf. stage 3 of the restoration of the NW limb of the Aberfoyle synform. The inset shows the geometry of a planar surface intersecting a shere in cross section and plan view.

Fig. 4.38

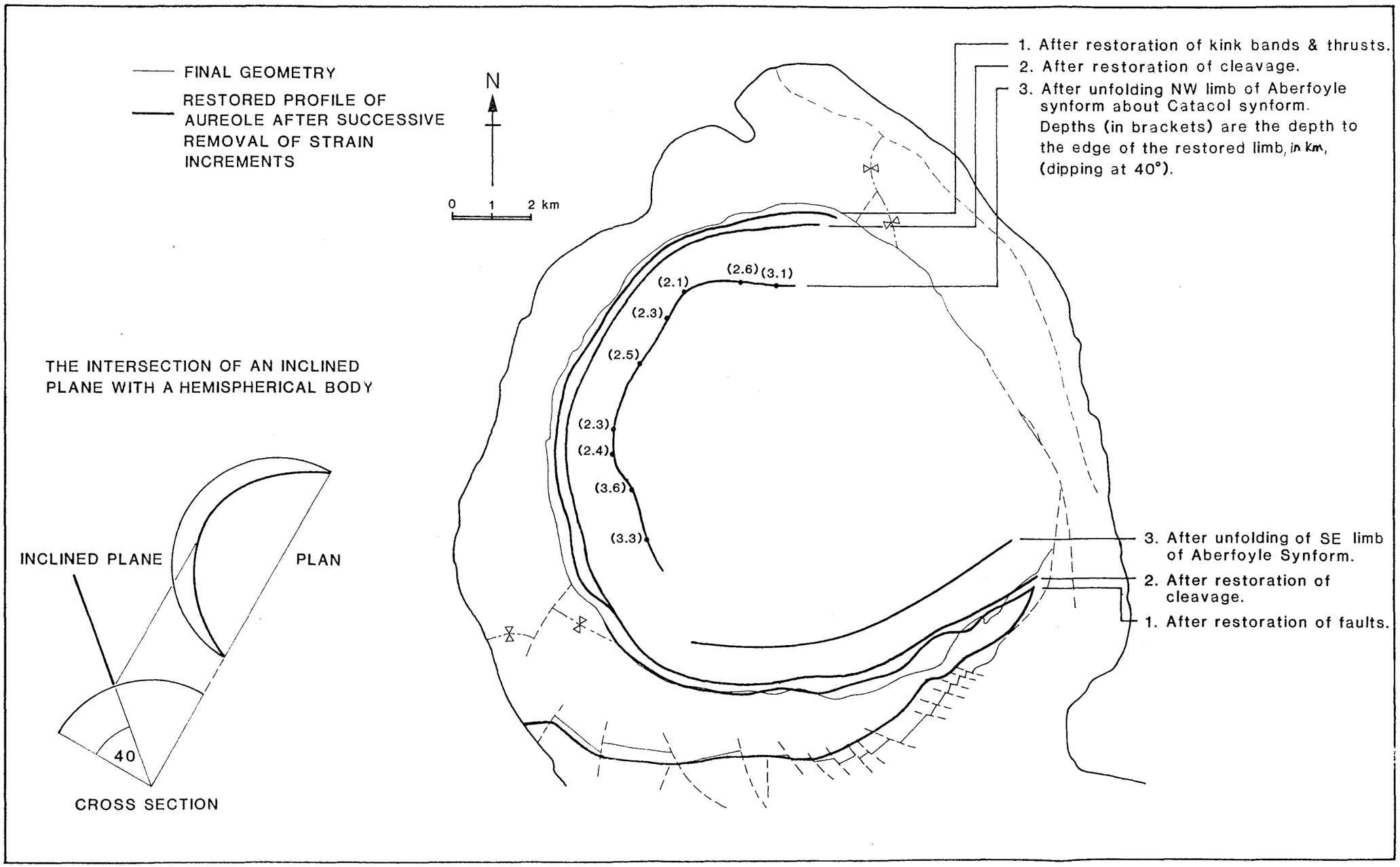
FINAL GEOMETRY
RESTORED PROFILE OF AUREOLE AFTER SUCCESSIVE REMOVAL OF STRAIN INCREMENTS
N
0 1 2 km
1. After restoration of kink bands & thrusts.
2. After restoration of cleavage.
3. After unfolding NW limb of Aberfoyle synform about Catacol synform.
Depths (in brackets) are the depth to the edge of the restored limb, in km, (dipping at 40°).
(2.1)
(2.6)
(3.1)
(2.3)
(2.5)
(2.3)
(2.4)
(3.6)
(3.3)
3. After unfolding of SE limb of Aberfoyle Synform.
2. After restoration of cleavage.
1. After restoration of faults.
THE INTERSECTION OF AN INCLINED PLANE WITH A HEMISPHERICAL BODY
INCLINED PLANE
PLAN
40
CROSS SECTION

due to a lack of knowledge of the strains involved.

Restoration of the strains due to the late coaxial deformation around the west and north sides of the granite indicate the radius of the granite must have increased during this phase of deformation. Removal of these increments indicates that the S_3 cleavage originally had an elliptical geometry, with the major axis lying in a WSW–ENE orientation. The cleavage has been interpreted as forming during flattening parallel to the granite contact during the final stages of folding. Since the granite now cuts the cleavage, particularly along its SE margin it appears that the pluton changed shape during the later stages of emplacement rather than expanding uniformly.

Since the S_3 cleavage cross cuts the axial plane of the Catacol synform it is also clear that the granite also changed shape during the later stages of folding. The apparent shear across the synform, indicated by the cross cutting geometry of the cleavage, is interpreted as the result of a change in the geometry of the stress field (rotation of σ_1 relative to the fold axis) as the pluton changed shape, by deforming the inner limb of the synform, rather than actual simple shear deformation of the aureole.

Removal of the 10% strain estimated for formation of the crenulation cleavage indicates that the granite occupied a roughly circular space at this stage, confirming the interpretation that the granite was initially circular in plan, and probably hemispherical. The initial increment in the deformation sequence is considered to be the formation of the Catacol synform. There is no evidence of earlier intrusion related deformation. The synform was unfolded to restore the NW limb of the Aberfoyle synform to its original geometry (determined from the undeformed outer limb). The effect of limb parallel shortening during F_3 fold development was also removed at this stage. After the fold had been restored to its original SW dipping orientation the depth to the present cutoff of the limb against the granite was determined at a number of points along the lower edge of the restored limb.

This indicated that the restored edge of the NW limb of the Aberfoyle synform is elliptical in plan and broadly circular in the plane of the limb. Such a geometry would be expected for the intersection of an inclined planar surface with a sphere (Fig. 4.38). The SE limb of the Aberfoyle synform was restored to its original orientation by back rotating it by 10^o (from 80^o to 70^o). The unfolded portion of this limb exposed to the NE of the granite dips at 70^o.

The field evidence indicates that the folding is entirely due to the ascent of the pluton. The folding is then overprinted by flattening strains caused by radial expansion of the pluton. An estimate of the original diameter of the pluton as it came to rest can be determined from figure 4.38 (asumming it was spherical), by measuring the diameter of the pluton after removing the strain produced during the development of the S_3 cleavage. This indicates the original radius of the pluton (during ascent) was 6 km, compared with a final radius of approximately 6.5 km.

Hence the radius of the granite increased by 8.3% of its original radius during emplacement. This is in strong contrast to the Ardara pluton which Holder (1979) showed to have created at least 72% of its volume by radial expansion. This corresponds to a 52% increase in the radius of the pluton with respect to its original radius during emplacement. Bateman (1985) suggested that the Cannibal Creek pluton (Queensland, Australia) created approximately 70% of its volume by in-situ expansion following ascent of the magma through a dyke (Chapter 1).

The reason for this apparent discrepancy in the figures for radial extension of the Arran granite when compared with other plutons which record radial flattening of their wall rocks will be discussed further after the chemical evolution of the granite has been considered.

Following restoration a large volume of Dalradian rock remains unaccounted for. Much of this space could be closed by backrotating the SE limb of the Aberfoyle synform to its original position. Further space could be closed by straight-

ening the Laggan Fault system. The remaining volume of the Dalradian rocks, which must have formed part of the NW limb and the core of the Aberfoyle synform must be assumed to have formed the now eroded roof of the granite, where it would have been displaced during the early stages of ascent of the pluton.

The restoration of the aureole indicates that the granite ascended through the NW limb of the Aberfoyle synform and bisected the axial plane of the fold. The present strike of the fold axial trace indicates that the axial plane was folded around a steeply SE plunging fold axis. The structural relationship between the granite and the Aberfoyle synform demonstrates that the granite could not have risen up the Highland Boundary Fault (HBF) as suggested by Richey (1939). Since the granite rose vertically through the NW limb of the Aberfoyle synform it must clearly have risen to the north of the fault. The southeastward deflection of the Aberfoyle synform can be used to invoke a similar displacement of the HBF, partly by folding and partly by strike slip movement along the Goat Fell Fault, as suggested in chapter 2.

Restoration of the aureole of the Northern Arran Granite indicates that the deformation sequence deduced from the structure of the aureole is viable. Early updoming due to diapiric ascent of a broadly spherical or hemispherical body of magma resulted in the formation of the Catacol synform, updoming across the Laggan Fault system and folding of the SE limb of the Aberfoyle synform around a steeply SE plunging axis. Flattening strains are interpreted as recording an initial increase in the radius of deformation during continued ascent of the magma body which is overprinted by coaxial flattening in a plane parallel to the margin of the intrusion. These strains suggest either ballooning or a change in shape of the pluton which involve in-situ radial and concentric extension of the magma body. These strains are expressed as extensional shears at the contact with the granite and the development of a linked thrust and normal fault system in the contracting core of the Catacol synform. The final strain increment involved extension of the

pluton in a SE direction. This was accommodated by strike slip movement on the Goat Fell Fault and a set of faults developed to the south of the granite.

This model describes an idealised sequence of events in the deformation of the aureole of the Northern Arran Granite. From this model it is inferred that the granite rose as a diapir which subsequently ballooned at a high level in the crust. This is based upon interpretation of the aureole structures alone and treats the granite largely as a passive body subject to changes in shape permitted by the deformation of the aureole during intrusion. The ballooning process invoked to drive these shape changes during the final stages of emplacement is also dependant upon the evolution of the intruding magma body. In order to obtain a fuller understanding of the ascent and emplacement mechanism of any intrusion it is necessary to make a study of the intrusive body.

CHAPTER 5

THE PETROLOGY OF THE NORTHERN ARRAN COARSE GRANITE

The origin of the acid rocks of the British Tertiary Volcanic Province has largely been resolved in recent years, following a increase in the availability of comprehensive isotope and trace element data for the wide variety of acid and basic magmas and crustal rocks in the province (Dickin et al., 1984). The primary aim of the geochemical work described in this chapter was not to investigate the origin of the acid magma which formed the northern granite, which was covered by Dickin et al. (1981), but to use major and trace element data to deduce the chemical evolution of the magma during its ascent and emplacement and how changes in chemistry might reflect this process. This has been achieved using a combination of petrographic and chemical data.

5.1 General Features of the Coarse Granite.

As previously noted the Northern Arran Granite has a roughly circular outcrop with a diameter of approximately 13 km. The intrusion covers an area of approximately 140 km^2. About one third of the area is of a younger fine grained granite intruded into the coarse (Chapter 7). This chapter will concentrate on the coarse granite which forms the bulk of the intrusion. It has sharp outward dipping contacts against Dalradian rocks to the north, west and south and against ORS to the east (Chapter 4). Interpreted gravity data for North Arran (Tuson, 1959; McLean & Deegan, 1978) suggests that the granite is underlain by a mass of basic magma at about 1.3 km below the present surface. The presence of this basic mass is indicated by the occurrence of basic dykes which cut both the coarse and fine components of the northern granite. Tuson (1959) suggested that the

granite could be modelled as an upright cylinder with a height of approximately 2.5 km on the basis of a data set which was limited by problems of gravity measurement in the mountainous terrain of North Arran. These data suggest the granite has a very low aspect ratio (height : width). However it should be recognised that the basic mass probably post dates the granite and may have intruded its lower levels. Hence the northern granite may have been considerably thicker prior to the intrusion of the basic mass. This was not accounted for in the gravity interpretation.

Considering the size of the granite its thermal aureole is comparatively narrow. Thermal alteration of the country rocks can only be detected within 500 m of the contact. This suggests a high rate of heat conduction away from the margins of the granite. It cannot be explained by a low temperature gradient between the granite and its wall rocks because the granite was emplaced at a shallow level ($\approx$3 km depth), which constrains the wall rock temperature to less than 100^oC (Chapter 2).

Ages for the granite of 60.3 ± 1.6 Ma. and 58.8 ± 1.2 Ma. have been obtained by Dickin et al. (1981) using the $^{87}Rb - ^{87}Sr$ method and by Evans et al. (1973) using the $^{40}Ar - ^{39}Ar$ step heating method respectively. Field evidence indicates that intrusion of the granite was one of the earliest phases of igneous activity in Arran. Some basic dykes are thought to pre-date the granite on the basis of palaeomagnetic evidence (Dagley et al., 1978) although no dykes have been noted which are clearly cut by the northern granite. These early dykes may have fed lava flows, fragments of which occur as remanée masses in the central complex (Chapter 2). The northern granite is thought to pre-date the central complex because the latter cuts updomed ORS to the south of the granite (Tyrrell, 1928; King, 1955).

5.2 Petrography of the Coarse Granite

In general the coarse granite is a mineralogically homogeneous body. Field mapping and hand specimen studies indicate the rock is dominantly composed of quartz and feldspar megacrysts in a groundmass of finer grained quartz, feldspar and biotite. Initial mapping and petrographic work revealed little variation in mineralogy and texture. Typically the granite has a whitish appearance due to weathering and sericitisation of alkali and plagioclase feldspar. When fresh the rock has a deep turquoise blue colour which fades rapidly to a greyish green. Much of the rock collected for petrographic study and geochemical analysis showed some effects of weathering and was typically white (see appendix).

Detailed mapping and petrographic studies of the granite indicated that the body showed some variation in texture. Along its margins it shows evidence of chilling against the country rocks. Where it is observed in contact with the Dalradian or ORS the magma has cooled rapidly to form a quartz feldspar porphyry. The rock coarsens away from the contact over a distance of about 5 m where it attains an appearance corresponding to that of the bulk of the coarse granite. This coarsening occurs by an increase in grain size of the groundmass which results in the phenocrysts becoming less distinct. This indicates the marginal rocks are quenched from a phenocryst bearing magma. This observation also confirms that the granite is younger than the surrounding Dalradian and ORS rocks and that it was intruded into the country rocks while they were at a lower temperature than the magma. The narrow width of the chilled margin suggests a relatively steep temperature gradient existed between the magma and the country rock.

Numerous fine grained or porphyritic sheets were noted within the coarse granite. In many cases these could not be traced for a significant distance due to poor exposure. However in the Garbh Allt (GR 969387), in North Sannox between GR 984468 and GR 976464 and in the Abhainn Tunna (GR 973476 to 966472) a number of fine grained sheets with sharp contacts against the coarse

granite toward the margin of the granite and gradational contacts into coarse granite toward the centre of the intrusion were mapped (Fig 5.1). The internal contact in the Garbh Allt can be traced in a NE direction toward Cnoc Breac for approximately 500 m before it becomes indistinct, passing into coarse granite. Six sheets of this type were mapped in North Sannox burn. Exposure is not good enough to permit correlation of any of these sheets with a further two sheets mapped in the Abhain Tunna. Mapping of the sheets suggests they are laterally discontinuous since they cannot be followed with certainty for distances in excess of 500 m. Other notable sheets were mapped in the south face of Cir Mhor and in Fionn Coire immediately south of this peak, and also in the corrie to the west of A'Chir. The origin of these sheets will be discussed in section 5.5.

The coarse granite is cut by numerous aplites, some of which transgress its margins to intrude the Dalradian. These vary in thickness from approximately 5 to 50cm. Their contacts vary from sharp, on a single crystal scale, to diffuse involving disaggregation of the fabric of the coarse granite. They are generally planar but many are highly irregular. Typically the planar sheets have sharp contacts and the irregular sheets diffuse. They show a variation in texture from strongly porphyritic to fine grained granular. These features, and their origins, will be described further in section 5.5. Petrographically they are dominantly composed of quartz and feldspar, mostly orthoclase but some albite is present, and minor amounts of biotite. Accessory phases are rare. The crystals form a hypidiomorphic granular fabric. When phenocrysts are present they are euhedral to subhedral crystals of quartz and orthoclase up to 1 cm across. Some aplites are enriched in biotite, (due to a high water content in the residual melt), euhedral flakes (up to 2 mm across) of which are commonly aligned parallel to the margins of the sheet against the coarse granite suggesting flow alignment or compression normal to the sheet. Petrographic evidence, of partial enclosure of biotite flakes by granular quartz and orthoclase, suggests the orientation is due to flow alignment.

Figure 5.1. Map showing the distribution of some of the more significant sheets of fine grained rock within the coarse granite in the Abhainn Tunna, North Glen Sannox and Garbh Allt areas. The cross section shows the general form of the sheets and their relationship to the coarse granite.

Fig. 5.1.

Distribution and geometry of chilled internal contacts in coarse granite

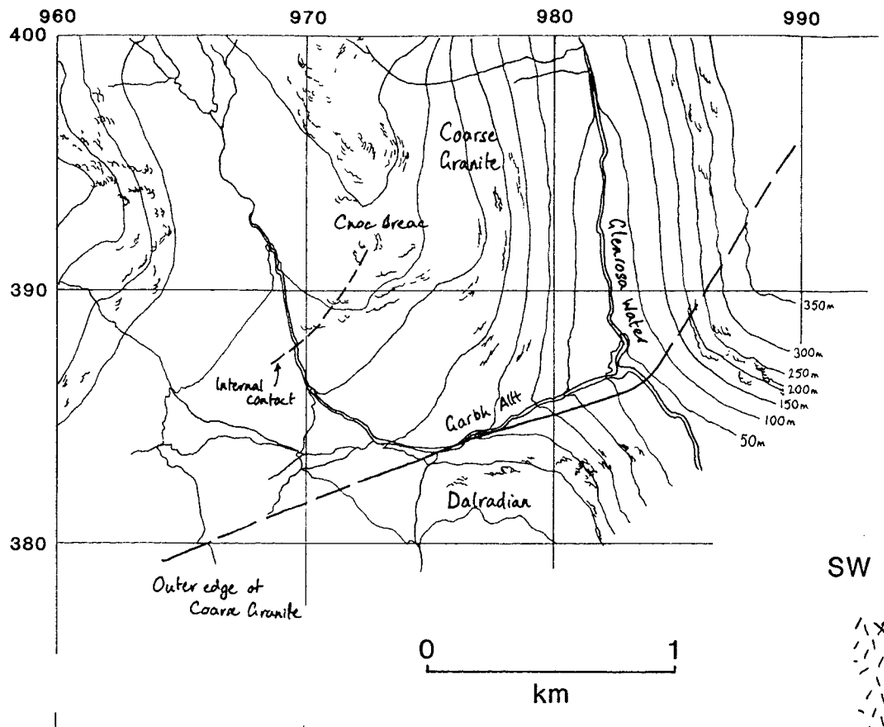

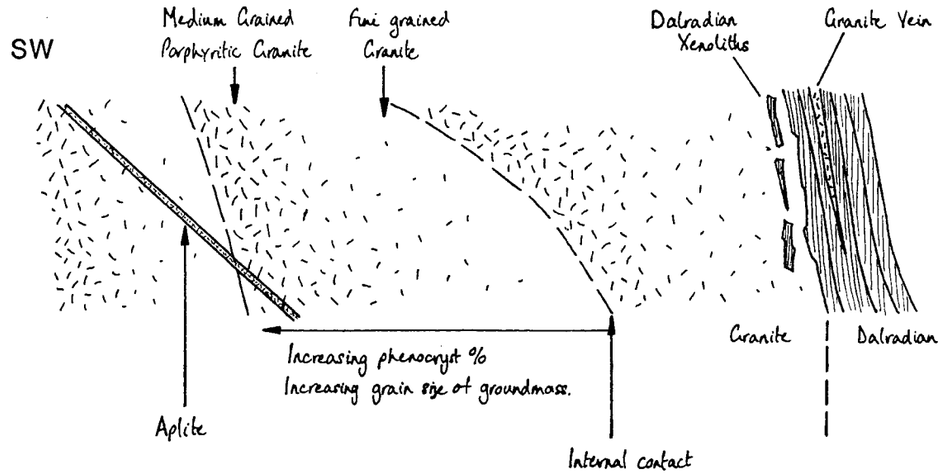

NOT TO SCALE

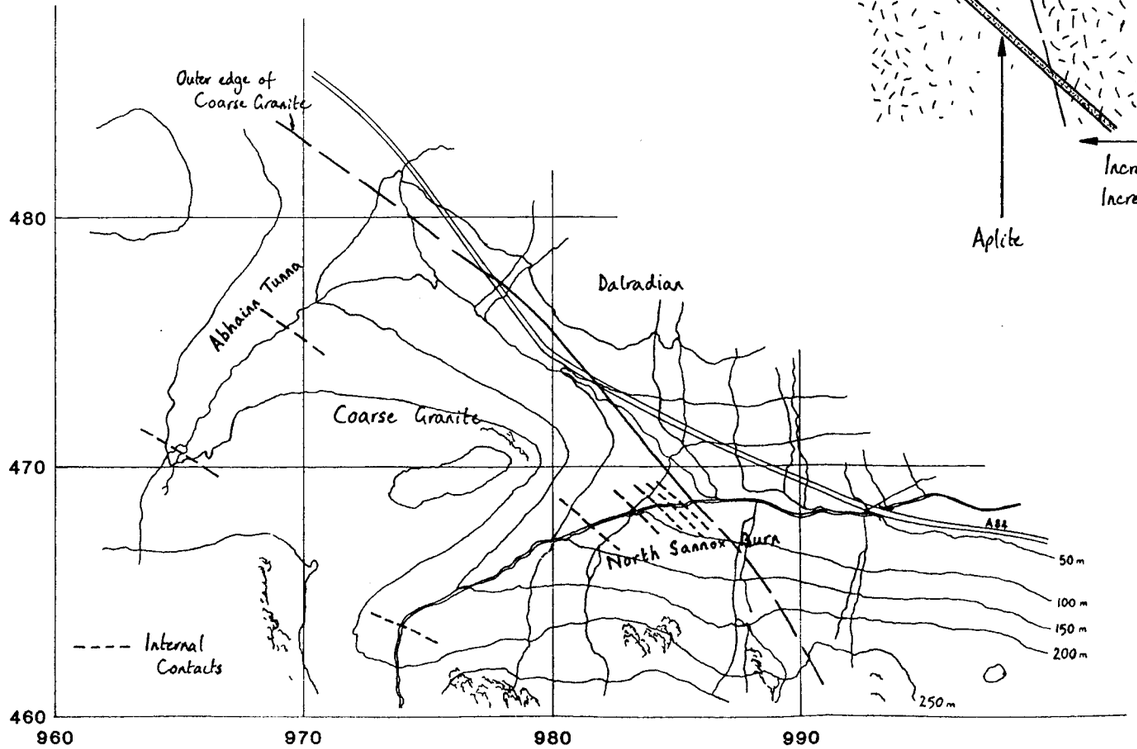

Some of the porphyritic aplites show crystal rich cores and crystal poor margins indicative of flow differentiation. Occasionally examples of multiple injection along the same vein were identified by recognition of internal chilled contacts and multiple flow differentiated units. The geometry of the planar sheets does not indicate any relationship to the present joint set in the granite which is generally the result of unloading of the overburden (i.e. joints are typically parallel or normal to the present surface). Angular junctions between some aplites suggests that they may have exploited early cooling joints within the crystallising magma. Orientation data for 29 planar aplites, measured in Glen Catacol, Glen Easan and the Abhainn Tunna show no clearly indentifiable orientation relative to the margin of the granite (Fig. 5.2). This suggests the aplites exploited features controlled by local stress patterns (thermal or tectonic) rather than a uniform stress field. The origin of the aplites will be discussed in section 5.5.

Detailed mapping and petrographic study of hand specimens revealed differences in the texture of the coarse granite. Excluding the rocks associated with the fine grained sheets described above the coarse granite can be divided into three textural types on the basis of hand specimen characteristics. These variations are distinguishable in the field, although the differences are not immediately obvious. The three textural types will be termed groups 1, 2 and 3. It is not intended that these divisions be used as a new subdivision of the coarse granite as it will be shown (section 5.3) that these variations are the result of in-situ crystallisation of a single magma body.

Group 1 rocks are medium grained (3 - 6 mm) equigranular quartz, two feldspar, biotite granites (Plate 5.1). They are composed of euhedral, equant quartz and feldspar phenocrysts up to 6 mm across surrounded by euhedral to subhedral quartz, subhedral feldspar and occasional flakes of platy subhedral biotite. The latter phases range in size between 1 and 4 mm. Internal variations within the group occurs in the form of slightly more porphyritic variants. The

Figure 5.2. Equal area stereonet showing a compilation of orientation data for the aplites cutting the coarse granite (circles – poles to planes) in relation to the margin of the coarse granite which is set to north (broken line).

Fig. 5.2.

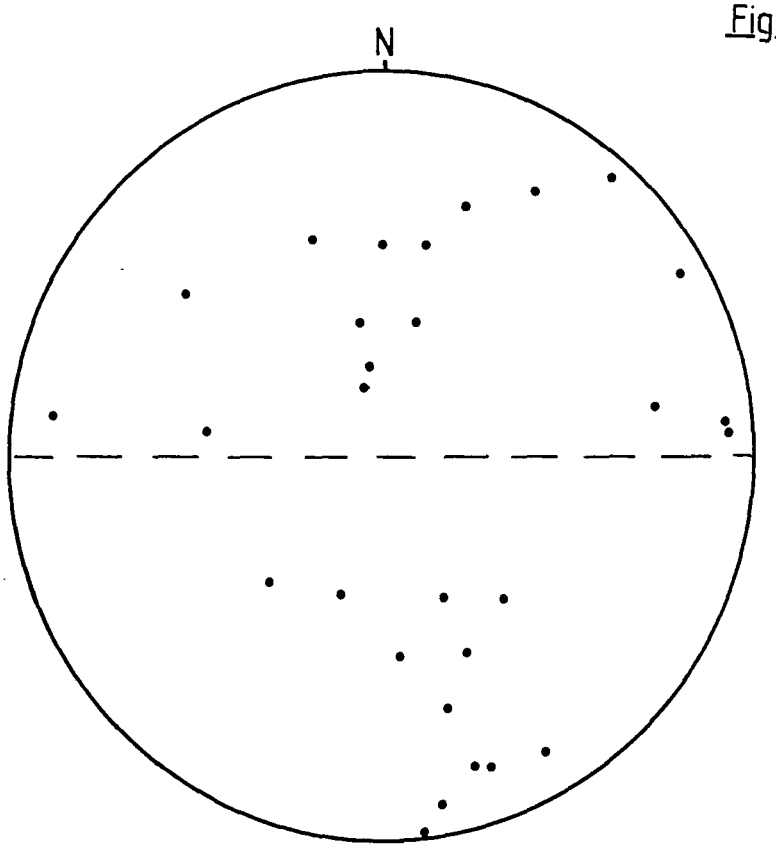

rocks occasionally develop a granophyric texture.

Group 2 rocks are very coarse grained porphyritic granites (Plate 5.2). They have the same mineralogical composition as the group 1 rocks. Their texture is dominated by large tabular to equant euhedral phenocrysts of alkali feldspar up to 12 mm across. These crystals form as much as 50% of the rock. They are surrounded by aggregates of euhedral to subhedral equant crystals of quartz, intersertal feldspar and subhedral biotite. The group can be distinguished from the group 1 rocks by their coarser grain size, inequigranular strongly porphyritic texture and lack of significant amounts of non-porphyritic feldspar.

Group 3 rocks are more variable. Typically they are porphyritic granites with a medium to fine grained matrix (Plate 5.3). Phenocrysts of euhedral, tabular alkali feldspar (up to 10 mm across) and occasional phenocrysts of equant, subhedral quartz are supported by a matrix of granular quartz, feldspar and biotite. However other rocks within the group show a coarsening of the granular texture and a reduction in the percentage of phenocrysts which gives them an appearance similar to the group 1 rocks. However the group 3 rocks are separated in the field from the group 1 rocks by rocks of group 2 (Fig. 5.3). Distinction between rocks of groups 2 and 3 can be made easily on the basis that the former is coarser grained and lacks a granular groundmass.

Rocks of all three groups showed drusiform texture. Vugs were occasionally lined with feldspar, smoky quartz, biotite and unidentified zeolite phases. The actual distribution of the drusiform rocks showed no consistent pattern which is interpreted to indicate variable water content in the magma (section 5.4).

A sample of a biotite rich segregation/enclave was collected from upper Glen Sannox (GR 976435). This was the only xenolith/enclave of either country rock or mafic igneous material found away from the margin of the intrusion (section 4.1).

A small number of samples were collected from the porphyritic margins of

Plate 5.1. (a) Photograph of a typical sample of the group 1 rocks showing the characteristic granular texture. Phenocrysts of feldspar are surrounded by a groundmass of rounded quartz and irregular grains of feldspar and biotite. (mm scale in lower left corner.)

(b) The photomicrograph shows the typical texture of the group 1 rocks. Large phenocrysts of euhedral feldspar and quartz are surrounded by a granular groundmass of subhedral to anhedral quartz, orthoclase, oligoclase and biotite. Group 1 coarse granite, No. 98402b. Width of field = 3.5 mm, crossed polars.

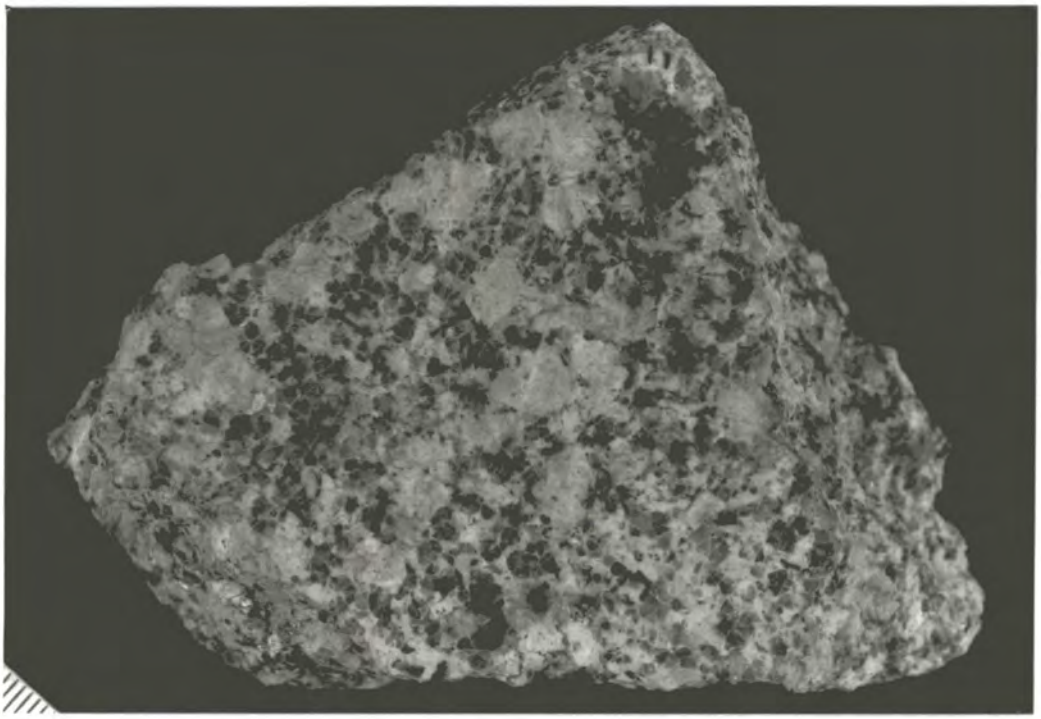

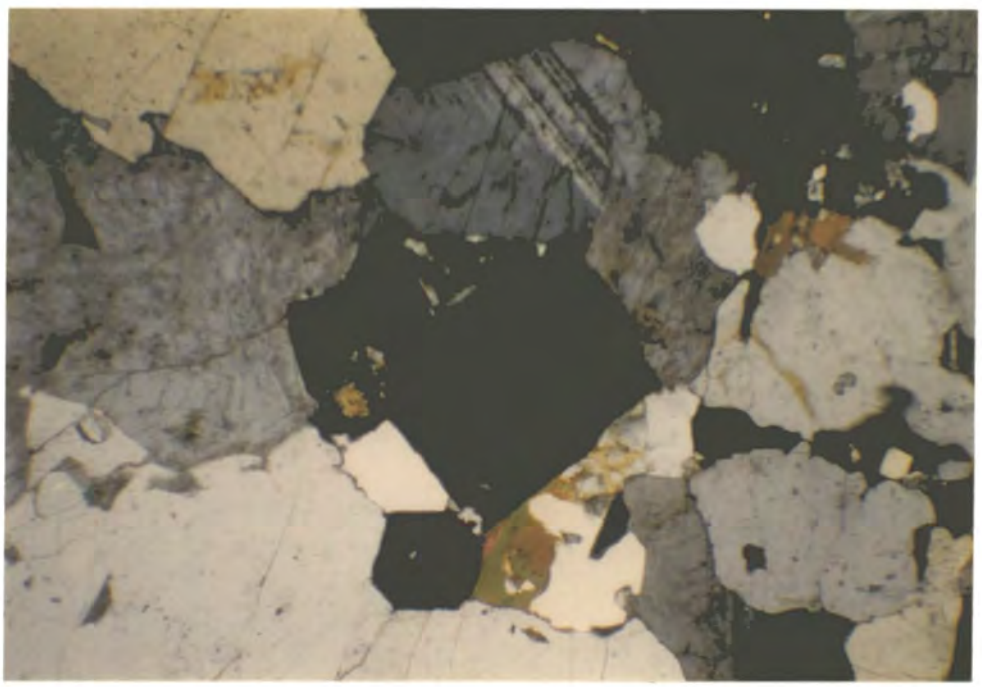

Plate 5.2. (a) Photograph of a typical sample of the group 2 rocks showing very coarse grained porphyritic texture. Large euhedral to subhedral phenocrysts of feldspar are surrounded by aggregates of rounded quartz and intersertal feldspar which forms overgrowths on the phenocrysts. (mm scale in lower left corner.)

(b) This photomicrograph shows the typical texture of the group 2 rocks. Large phenocrysts of feldspar (oligoclase in upper left corner) are surrounded by aggregates of rounded euhedral to subhedral quartz (centre) which is surrounded by intersertal alkali feldspar (in extinction). Group 2 coarse granite, No. 95412c. Width of field = 3.5 mm, crossed polars.

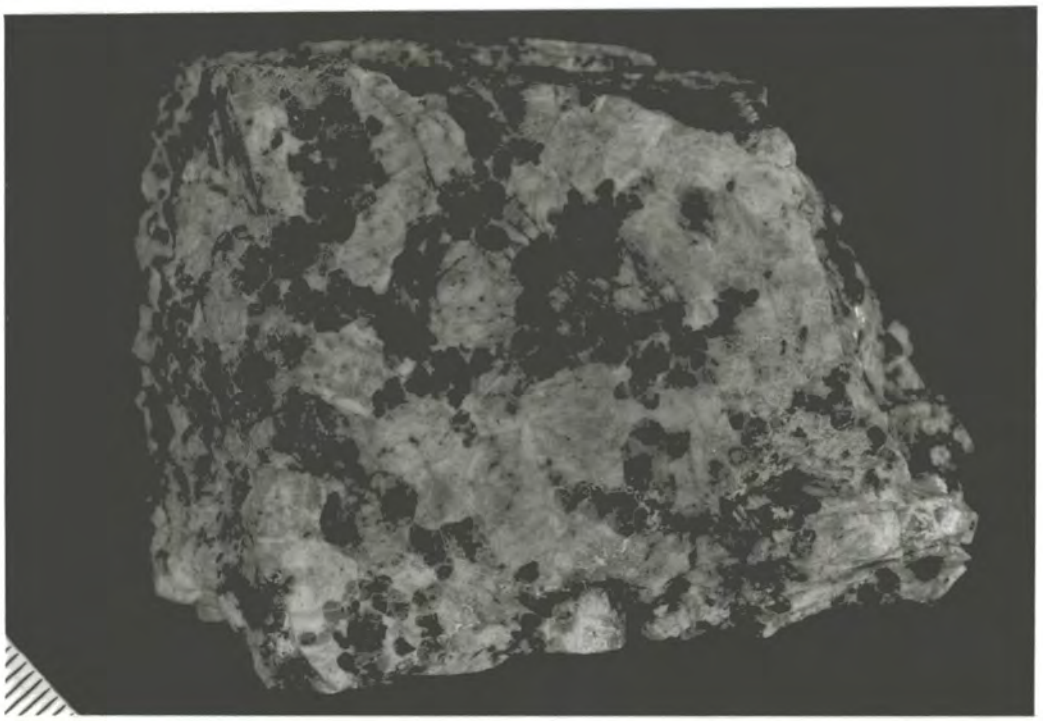

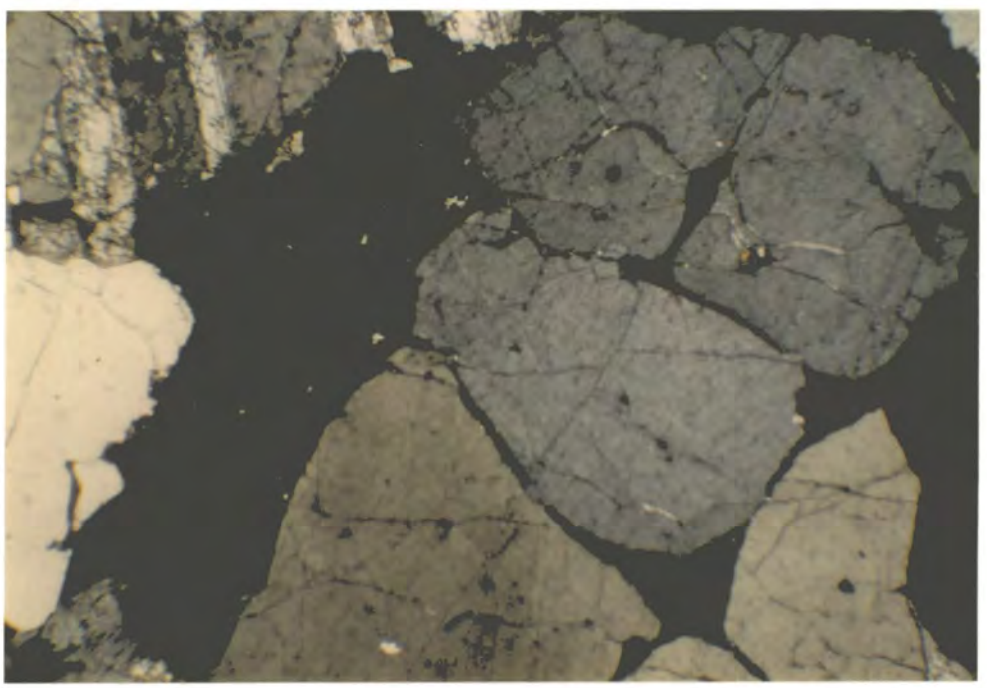

Plate 5.3. (a) Photograph of a typical sample of group 3 granite. The rock shows a well developed texture of porphyritic euhedral quartz and feldspar in a fine grained matrix of quartz, feldspar and finely distributed biotite. This group shows variable texture, the main variation being an increase in the size of the groundmass crystals so that the texture of the rock approaches that of the group 1 rocks (plate 5.1). This particular sample is very drusiform. (mm scale in lower left corner.)

(b) Photomicrograph of a porphyritic fine grained group 3 rock. Euhedral phenocrysts of oligoclase and quartz (centre) are surrounded by a granular, slightly granophyric matrix of quartz, feldspar and biotite. Group 3 coarse granite, No. 96421b. Width of field = 3.5 mm, crossed polars.

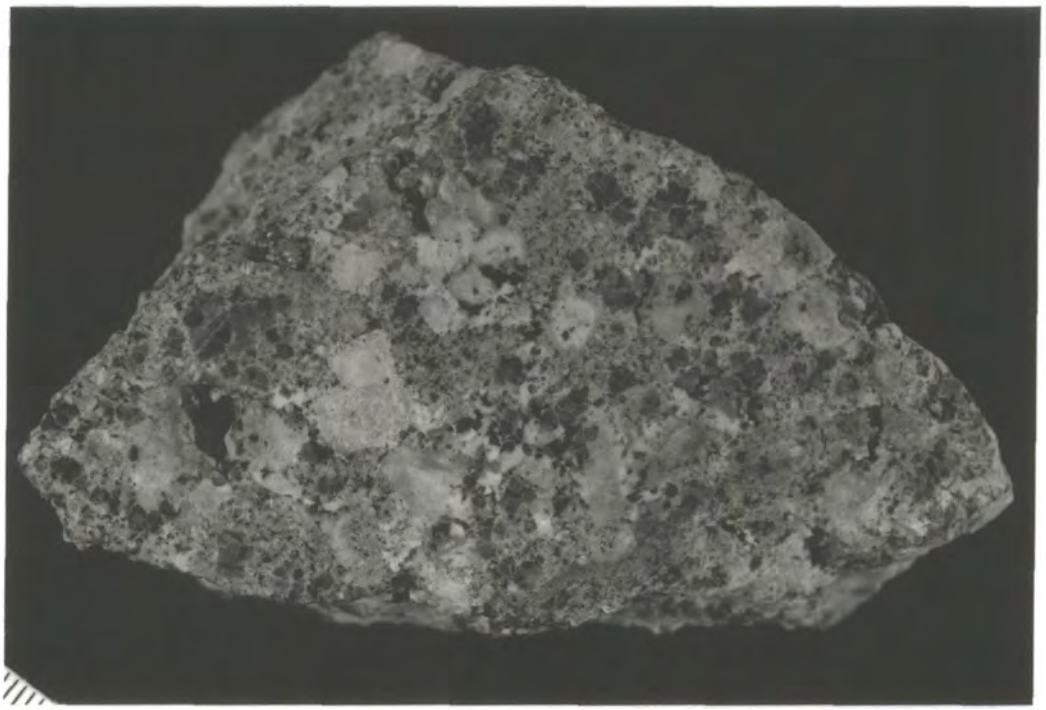

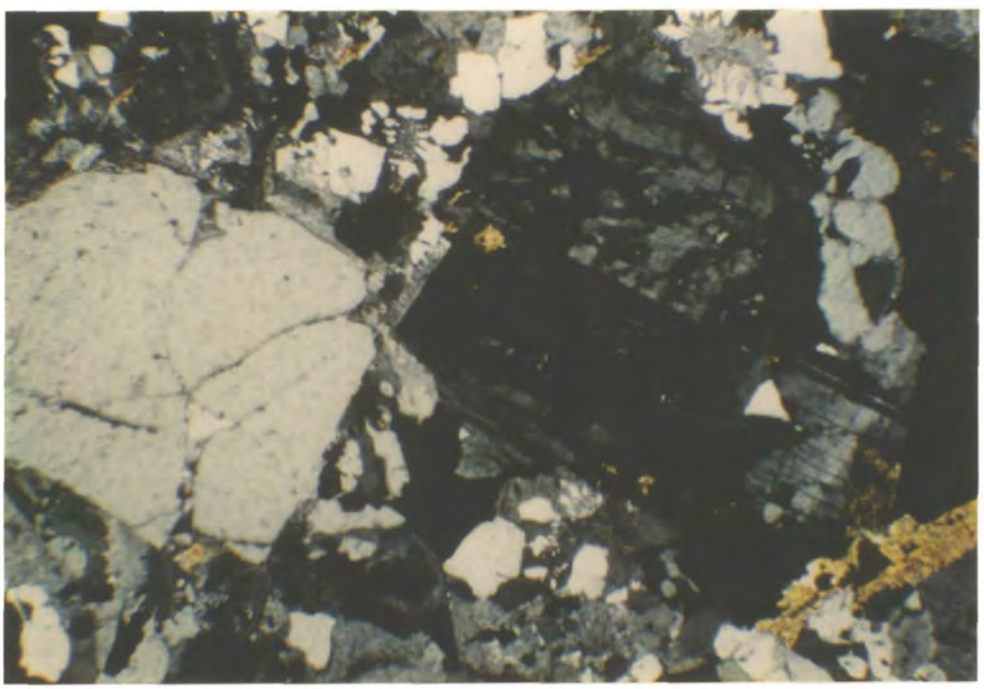

the intrusion. Seven porphyritic rocks adjacent to the coarse grained group 2 rocks contained an average of 23% phenocrysts (point count data, 1000 points per sample) and two porphyritic rocks adjacent to coarse grained group 1 rocks contained an average of 8% phenocrysts. Poor exposure and crushing along the contacts prevented larger sets of samples being examined. However this feature emphasises the more porphyritic nature of the group 2 rocks. Rocks of group 3 do not occur along the margins of the granite.

The distribution of the three groups of rocks is shown in figure 5.3. This map was produced from field mapping and studies of hand specimens collected during mapping. The area of group 1 rocks in the SE corner of the pluton can be clearly mapped. The narrow margins on the north and west sides were defined after petrographic studies of textural variation within the granite. The contact between the group 1 and group 2 rocks is not sharp. It cannot be mapped on the north and west sides of the granite due to poor exposure. However in the SE corner of the granite group 1 rocks are restricted to an area east of Glen Rosa and SE of North Goatfell. A transition from group 1 to group 2 can be traced across the Stacach ridge between Goatfell and North Goatfell and between North Goatfell and Mullach Bhuide. The transition occurs over $\approx$ 50 m. At no point is there a sharp discontinuity between the two groups. The transition is marked by a gradual increase in the size and proportion of feldspar phenocrysts in the rocks passing from group 1 to group 2. Further mapping of the actual position of the contact is prevented by poor or inaccessible exposure. Hence the line drawn on the map (Fig. 5.3) is only approximate and is largely based on the texture of hand specimens collected close to the transition. The topographic control on the position of the contact suggests that it dips steeply toward the SE, toward the margin of the granite.

Rocks of group 2 form most of the coarse granite. They occur in contact with the Dalradian and ORS rocks where there are no group 1 rocks at the margins of

Figure 5.3. Map showing the distribution of the three types of granite distinguishable on the grounds of texture. The boundaries between each group are gradational. The internal contacts dip steeply outwards.

PETROGRAPHIC SUBDIVISION OF THE COARSE GRANITE

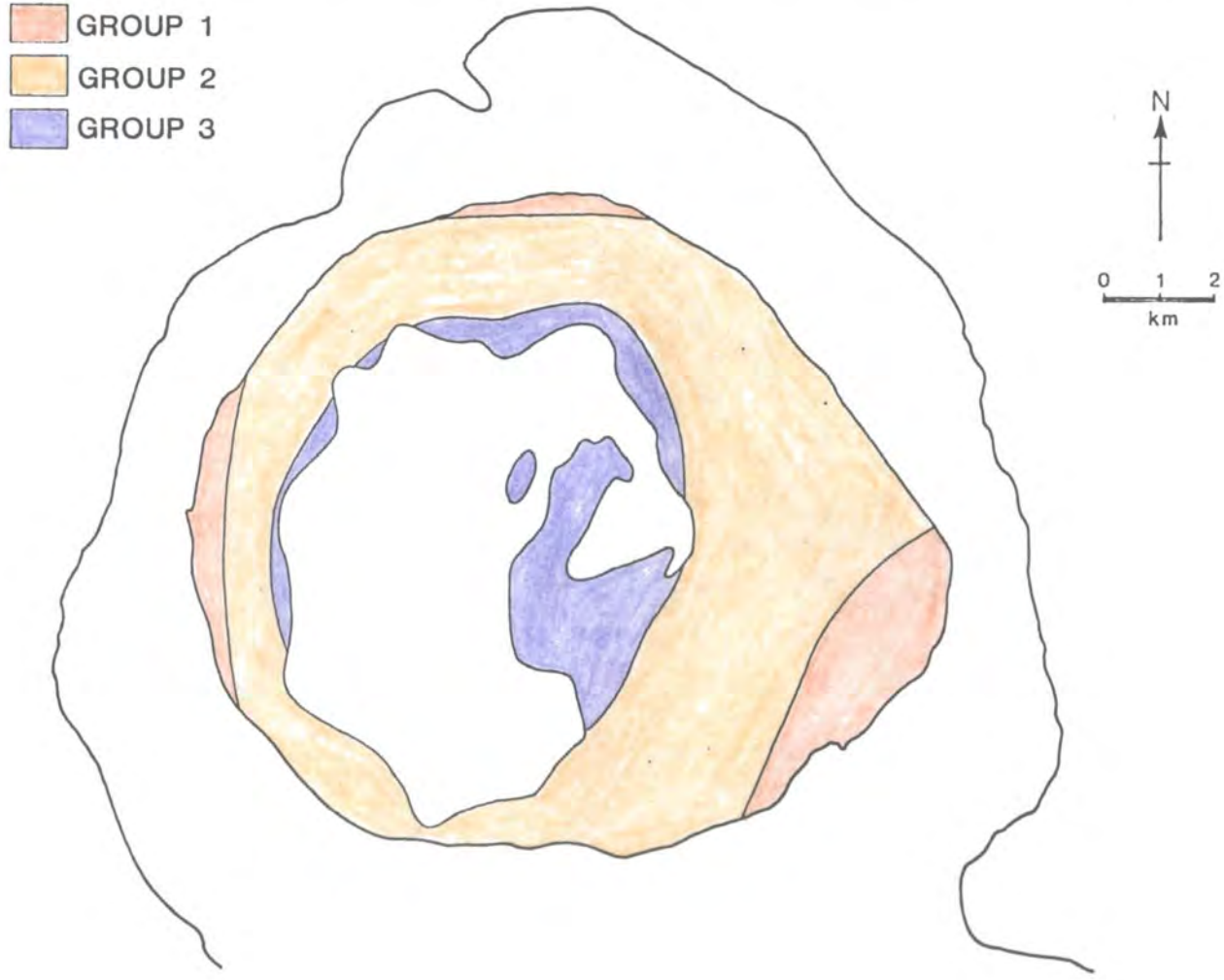

Fig. 5.3.

the intrusion. Group 3 rocks are only found in the centre of the intrusion where their outcrop has been partially obscurred by the emplacement of the younger fine granite. The group 2 rocks completely surround the group 3 rocks. As with the junction between the group 1 and group 2 rocks there is no clear contact between group 2 and group 3. The group 2 rocks become less strongly porphyritic and develop a medium to fine grained groundmass toward the centre of the pluton. This transition can be mapped to within 50 m to the west of A' Chir and Beinn Tarsuinn and across Creag Dubh to the north of Caisteal Abhail.

While it is clear that textural variations can be found within the coarse granite the similar mineralogical content of the three rock types and the lack of sharp contacts between them suggests the intrusion is a single body of magma. Had the coarse granite accumulated from more than one pulse of magma a marked variation in texture and mineralogy between rocks separated by sharp contacts might be expected. These features are not seen in the granite.

Thin section studies of the petrography of the coarse granite confirms the observations made from hand specimens and provides further details about the evolution of the magma. The three textural types described above can be clearly distinguished on the same grounds in thin section (Plates 5.1 – 5.3). All three groups have the mineral assemblage, quartz, orthoclase, sodic plagioclase, biotite and accessory phases. The first three minerals occur as phenocrysts and in the groundmass. Modal analysis by point counting thin sections showed the following variations (Table 5.1):

Table 5.1. Modal analysis of mineralogy.

Group	Quartz	Orthoclase	Plagioclase
1	39 (9.72)	48 (8.70)	10 (5.80)
2	35 (9.48)	48 (12.26)	13 (7.80)
3	38 (8.45)	54 (9.90)	5 (2.5)

Modes given as volume percent, for 16 samples of group 1, 46 samples of group 2 and 12 samples of group 3. Standard deviations are given in brackets. Data determined from 500 point counts per sample. Remainder of rock is composed of minor amounts of biotite and accessory phases.

It is clear from table 5.1 that group 2 rocks are slightly less evolved mineralogically than groups 1 and 3. They show a higher concentration of plagioclase at the expense of quartz. Group 3 rocks appear to be the most evolved. They contain very little plagioclase but have extremely high concentrations of orthoclase. Mafic phases make up betwen 1 and 4% in all three groups which emphasises the extremely evolved nature of the coarse granite.

The major phenocryst phase in all three groups is a euhedral tabular to equant cryptoperthitic orthoclase feldspar. Individual crystals vary in length between 3 and 12 mm. Many of these phenocrysts show euhedral zonation with inclusions of quartz or plagioclase trapped between growth increments (Plate 5.4). The euhedral crystal faces developed during growth indicate that crystallisation progressed without interference from adjacent crystals. Inclusions of quartz and plagioclase suggest that growth was not always continuous. The edges of the crystals are rarely sharp, often having overgrowths of orthoclase which are interpenetrant between adjacent crystals. These overgrowths can be distinguished as being a late stage of crystal growth as they are rarely in optical continuity with their host crystal. From their size and zonation it appears that these crystals had a prolonged growth history in equilibrium with a magma of changing composition. When well formed the crystals typically show Carlsbad twinning. Other crystals are interpenetrant and have coalesced during crystallisation. Some crystals show microperthitic exsolution textures although this is not common. In the groundmass orthoclase forms irregular crystals intergrown with quartz and plagioclase

Plate 5.4. Zonation in orthoclase feldspar. A large phenocryst of orthoclase feldspar showing well developed early euhedral crystal faces. A later overgrowth of more orthoclase (not in optical continuity) has an irregular contact against groundmass orthoclase and quartz. Small inclusions of quartz are visible in the overgrowth which becomes progressively perthitic toward its outer edge. Coarse granite, No. 97441. Width of field = 3.5 mm, crossed polars.

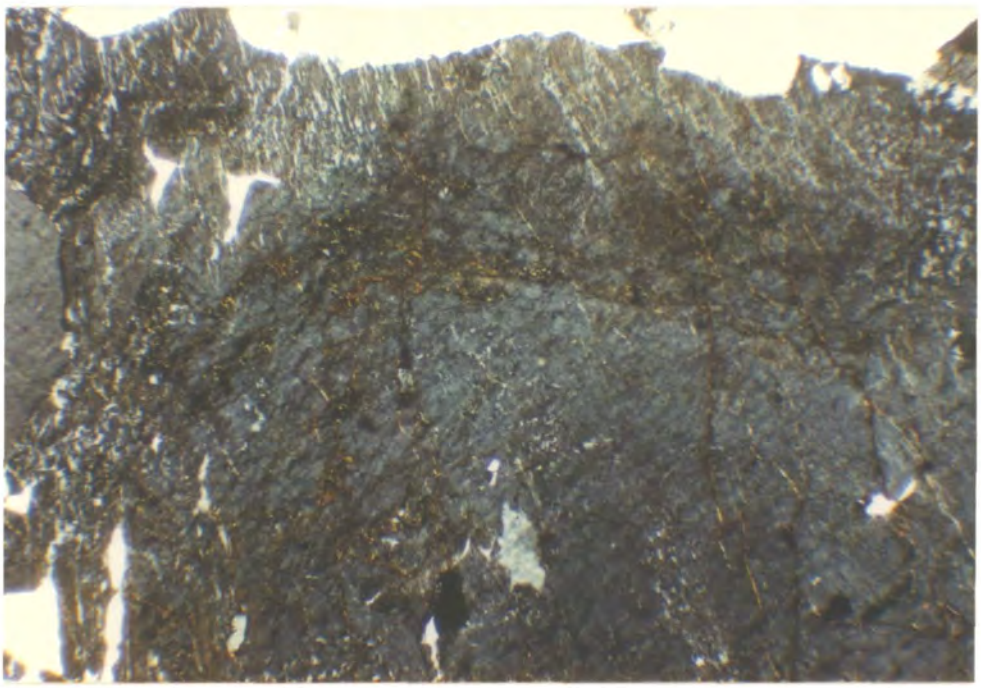

(Plate 5.5). Crystal shapes are generally subhedral to anhedral. Alternatively the orthoclase is intergrown in a radiating granophyric texture with quartz around euhedral phenocrysts of orthoclase or in a graphic intergrowth, again with quartz (Plate 5.6). Intersertal growth of orthoclase between closely packed aggregates of quartz is seen in the group 2 rocks.

Plagioclase forms tabular to equant phenocrysts which vary between 3 and 10 mm in length. Determination of composition by the Michel Levey technique indicated that the majority of crystals had compositions between An_{10} and An_{30}, which is the range for oligoclase. Using the Becke Line test it was possible to establish that the plagioclase had a lower refractive index than quartz which restricts its compositional range to between An_{10} and An_{20}. Some of the phenocrysts were zoned from approximately An_{40} and An_{10}, from core to rim, indicating they had remained in equilibrium with an evolving melt (Plate 5.7). Other crystals show no zoning, either as the result of late crystallisation or re-equilibration with the magma. These crystals are generally free of inclusions and typically have sharp contacts against the groundmass. Phenocrysts occur as both single crystals and glomeroporphyritic aggregates. Albite and carlsbad twinning are very common permitting clear recognition of the plagioclase under crossed polars. Occasionally the twinning is complex. Single crystals contain two sets of albite and carlsbad twins at 90^o. The twinning is occasionally disrupted by zoning of the crystals. This zonation (as described above) is always normal. Some crystals show more complex convolute zonation. Plagioclase also occurs in the groundmass where it forms anhedral crystals intergrown with quartz and orthoclase. The groundmass plagioclase has a composition which ranges between An_{20} and An_5 (determined by a combination of the Michel Levey and Becke Line tests), which is slightly more sodic than the phenocryst plagioclase.

Quartz occurs as equant to prismatic phenocrysts between 2 and 4 mm in length. Crystals have grown in glomeroporphyritic clusters and have euhedral to

Plate 5.5. Groundmass texture of the coarse granite. This photomicrograph shows the typical hypidiomorphic granular intergrowth of quartz, orthoclase, oligoclase and biotite developed in group 1 rocks. Group 1 coarse granite, No. 99413. Width of field = 3.5 mm, crossed polars.

Plate 5.6. Granophyric intergrowth in the coarse granite. This photomicrograph shows a well developed granophyric intergrowth of quartz and orthoclase on phenocrysts of orthoclase which pass into the more common hypidiomorphic granular groundmass (cf Plate 5.5). Group 1 coarse granite, No. 96412. Width of field = 3.5 mm, crossed polars.

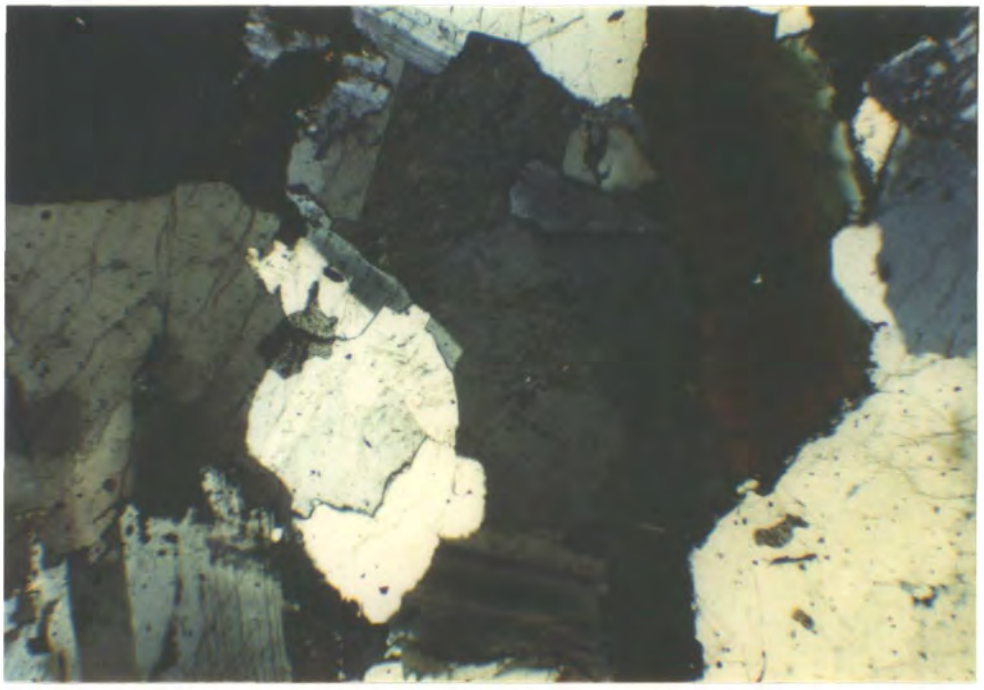

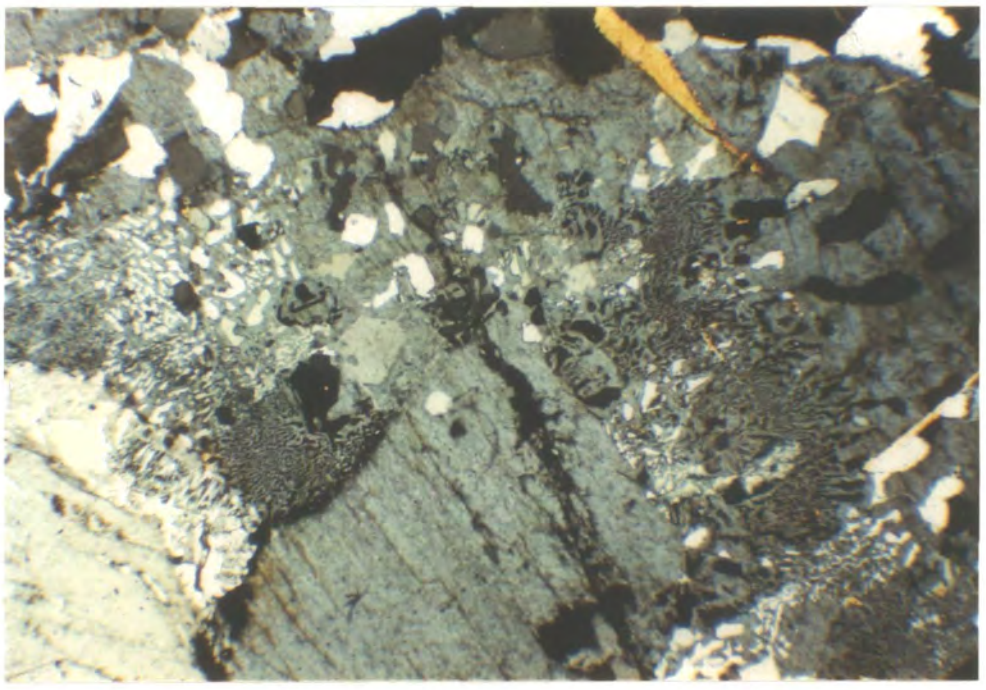

Plate 5.7. Zoned plagioclase. This photomicrograph shows a zoned phenocryst of plagioclase feldspar with euhedral crystal faces developed during early increments of growth which are followed by a later development of an irregular contact with the groundmass. Coarse granite, No. 98402b. Width of field = 3.5 mm, crossed polars.

subhedral shapes. They contain rare inclusions of alkali feldspar. Quartz also occurs as irregularly shaped inclusions in feldspar phenocrysts. Phenocrysts occasionally have overgrowths of later quartz and feldspar developed during the development of the groundmass. In the groundmass quartz occurs in granular intergrowths with feldspar and in granophyric or graphic intergrowths (Plate 5.6). A notable feature of many of the quartz phenocrysts in the coarse granite is undulose extinction and the development of subgrains (Plate 5.8), which is commonly attributed to distortion of the crystal lattice by low strains. Such a distortion may have resulted from stresses created by contraction of the rock during cooling but the development of subgrains, which results from the migration of lattice defects implies higher strains than might be expected from such a process. Many well jointed rocks (which have clearly undergone contraction on cooling) do not even show undulose extinction. The cause of these strain effects will be discussed further in section 5.5. Commonly the quartz occurs as glomeroporphyritic clusters (particularly in group 2 rocks where the clusters surround phenocrysts of feldspar). Within these clusters crystals are frequently seen in optical continuity, suggesting a crystallographic alignment. However in any one thin section no evidence of any crystallographic orientation direction for any of the phenocryst or groundmass phases was recorded. Within the clusters adjacent grains show interpenetrant contacts and subgrain growth along intersecting grain edges. Thin films of intersertal albite and occasionally biotite are visible between crystals where they are not in contact.

Red-brown to green biotite occurs as euhedral to anhedral crystals up to 3 mm across which are restricted to the groundmass. Biotite does not appear to be a phenocryst phase in the sense that it nucleated early in the crystallisation sequence, as it never occurs as inclusions in the plagioclase, orthoclase or quartz phenocrysts. It does however appear to form immediately prior to the crystallisation of the groundmass since euhedral crystals of biotite are commonly observed enclosed in

Plate 5.8. Photomicrograph of coarse granite showing an aggregate of rounded quartz crystals surrounded by thin films of orthoclase feldspar. The quartz crystals show undulose extinction. One crystal at the centre of the view shows a well developed subgrain (in extinction) at its contact with an adjacent quartz crystal. Coarse granite. Width of field = 3.5 mm, crossed polars.

Plate 5.9. This photomicrograph illustrates deformation of biotite in the coarse granite. A large crystal of biotite shows well developed deformation bands resulting from distortion of the crystal lattice. Coarse granite, No. 98401. Width of field = 3.5 mm, crossed polars.

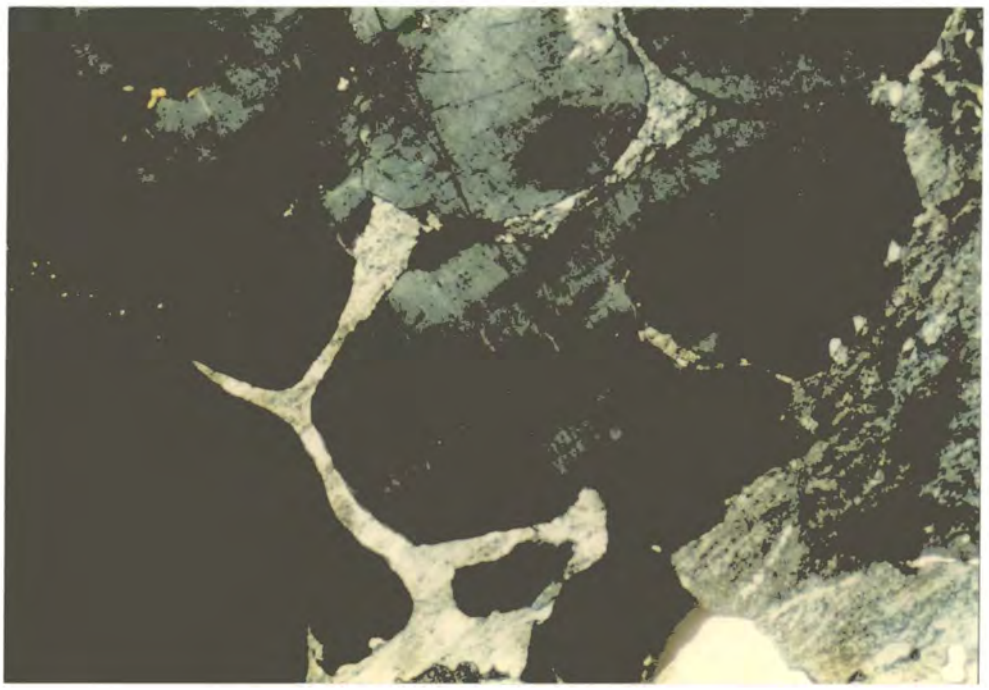

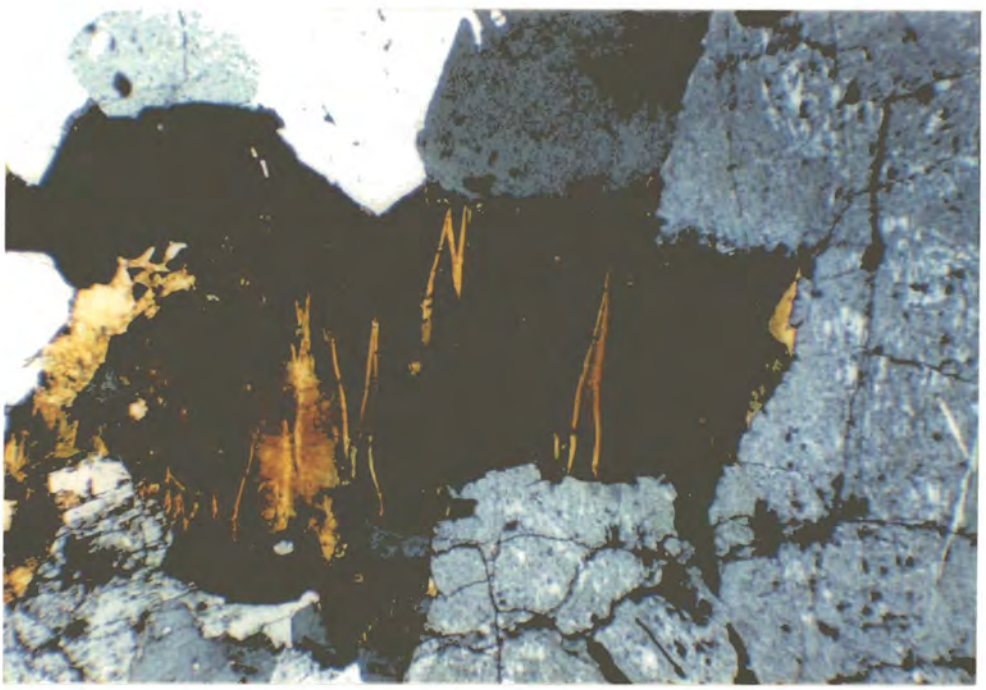

anhedral groundmass quartz and feldspar. It is also found as intersertal growths between aggregates of quartz (described above) which suggests its crystallisation interval extends into that of the groundmass. Within the groundmass it occurs as single crystals or as aggregates of subhedral crystals. Crystals commonly contain inclusions of zircon, allanite, apatite and opaques (magnetite/rutile) which occur as accessory phases. Pleochroic haloes are common around the zircon and allanite crystals due to metamictisation. In addition to the strained quartz crystals distorted biotite crystals also record slight deformation of the coarse granite following crystallisation (Plate 5.9).

The accessory phases recorded in the coarse granite are allanite, zircon, apatite and opaques (in approximate order of crystallisation). These phases generally represent less than 1% of the rock. Strongly pleochroic red-brown allanite forms subhedral to anhedral crystals up to 0.25 mm across. Zircon and apatite generally occur as small (< 0.5 mm) euhedral inclusions in biotite indicating they nucleated prior to the crystallisation of the latter. The opaques form small granular crystals which are always associated with the biotite. Some may be primary but it is also clear that this phase has developed as a result of oxidation and decomposition of biotite. The accessory phases are only seen in association with biotite, with which they form aggregates surrounded by or included in groundmass feldspar (Plate 5.10).

Apart from occasional inclusions of one crystal in another the phenocrysts show no evidence of a definite crystallisation sequence. Quartz tends to be less well crystallised than plagioclase and orthoclase and also tends to cluster around these phases when the phenocryst content of the rock is high. Hence it is thought that the entry of quartz onto the liquidus may slightly post date the other phenocryst phases. The euhedral zonation patterns seen in both the plagioclase and the orthoclase indicates these phases crystallised over a period of time, while completely surrounded by melt, before the crystal content of the magma reached the

Plate 5.10. Accessory minerals in the coarse granite. This photomicrograph shows the typical paragenesis of the accessory phases in the coarse granite. An irregularly shaped biotite crystal encloses or partially encloses opaques (magnetite, Ti-oxide), zircon (identifiable from pleochroic haloes) and deep red-brown high relief allanite. Acicular crystals of apatite are enclosed in groundmass quartz at the centre of the field of view. Coarse granite, No. 97381a. Width of field = 3.5 mm, plane polarised light.

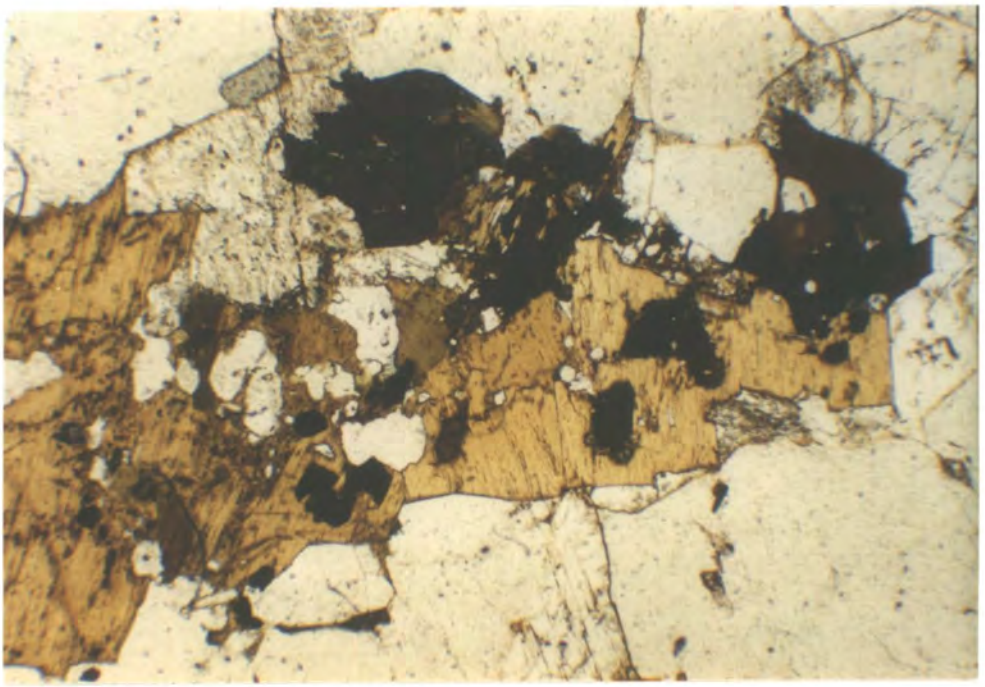

point where crystals began to coalesce. It is clear that by this stage of crystallisation that all three phenocryst minerals were stable liquidus phases. None show embayed margins which would indicate resorption. Hence it is concluded that the assemblage, plagioclase, orthoclase and quartz indicates cotectic (? eutectic) crystallisation, following crystallisation of plagioclase and orthoclase. Early crystallisation of the latter pair of minerals would have increased the silica content of the melt to the point at which it became saturated in quartz. This is discussed further in section 5.4.

As noted above the three phenocryst phases also occur in the groundmass indicating their stability range extends into the later stages of crystallisation of the granite. In addition they are joined by biotite and accessory minerals. Biotite and the accessory phases do not occur as inclusions in the phenocrysts and hence it is concluded that they formed during the early stages of the crystallisation of the groundmass. Biotite commonly forms euhedral to subhedral platy crystals, but is also intersertal to phenocrysts. Euhedral biotite crystals commonly cross cut or are partially enclosed by groundmass quartz or feldspar.

Only the rocks of groups 1 and 3 regularly develop a distinct groundmass (i.e. they show a bimodal distribution of crystal sizes). Rocks of group 2 contain a very high concentration of phenocrysts so that the groundmass is essentially an intersertal fabric. When developed, the groundmass is typically medium to fine grained (0.5 to 2.0 mm) with a hypidiomorphic granular texture (Plate 5.5). In some cases the granular texture has been replaced by a granophyric intergrowth nucleating on the orthoclase phenocrysts or a micrographic intergrowth of quartz and alkali feldspar (Plate 5.6). Biotite and accessory phases are enclosed in these intergrowths. The granular to consertal nature of the groundmass and the local development of granophyric texture suggests it formed by rapid simultaneous crystallisation of quartz and alkali feldspar (Smith, 1974).

Table 5.2 summarises the crystallisation sequence and crystallisation intervals

Table 5.2.

Crystallisation Sequence of the Coarse Granite.

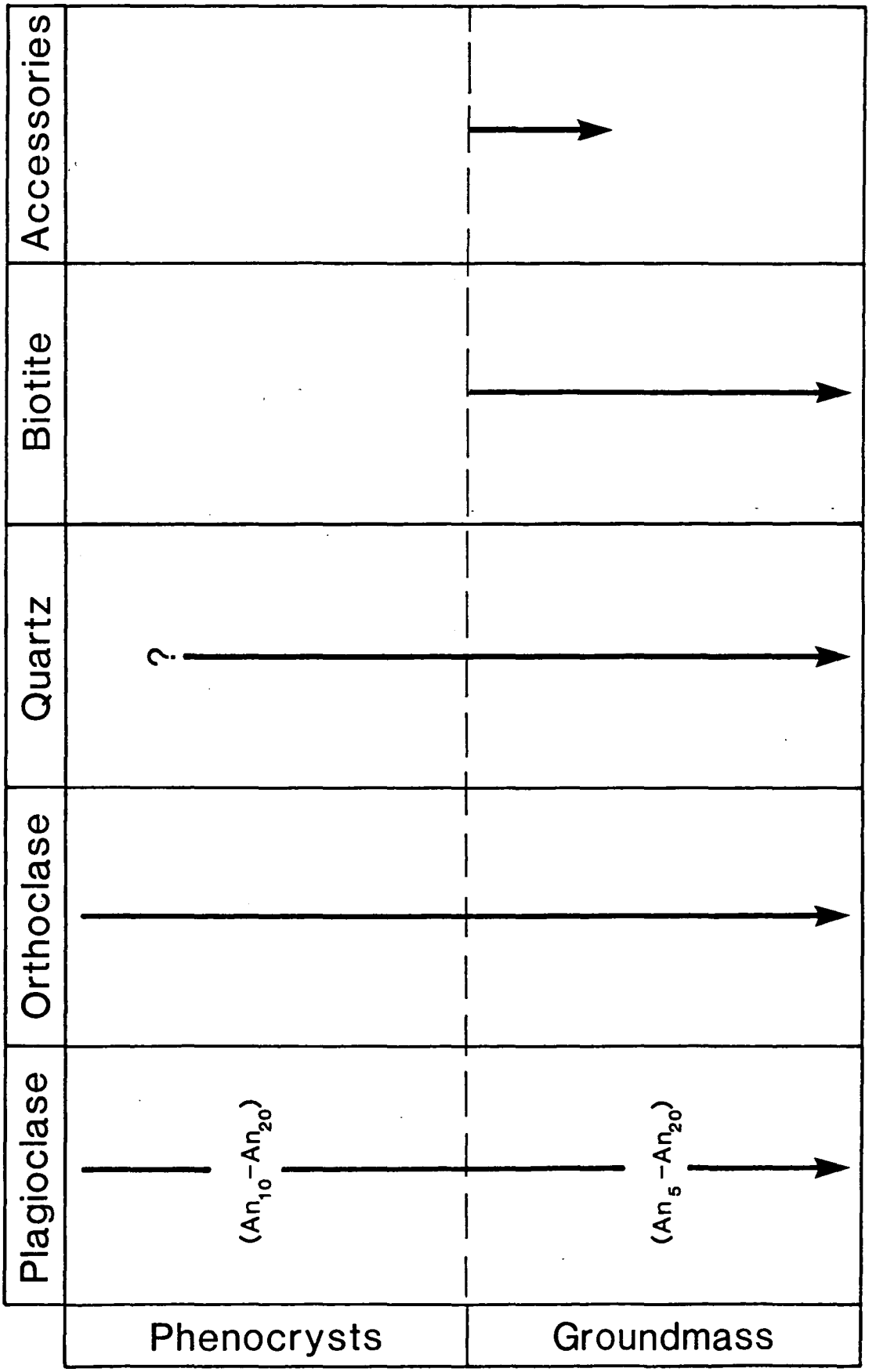

of the mineral phases of the coarse granite as determined from the petrographic observations described above. This table applies to all three textural groups of the coarse granite; the sequence of crystallisation being the same in each group. This further emphasises the similarity between the groups. Crystallisation can be divided, on the basis of the bimodality in crystal sizes of the quartz and feldspars, into a phenocryst interval and a groundmass interval. Plagioclase, orthoclase and quartz remain on the liquidus throughout the crystallisaton of the magma. Biotite and the accessory phases appear to be restricted to the groundmass interval. Textural evidence indicates that groups 1 and 3 have a well developed groundmass. Group 2 rocks can be distinguished from 1 and 3 by the lack of a well developed groundmass. In group 2 rocks the groundmass phases occur as intersertal films around the phenocrysts. If the coarse granite is a single magma body, as the field data suggests, this variation in texture implies that the crystallisation mechanism must be the dominant control on the fabric of the rock. This aspect of the crystallisation and evolution of the composition of the magma from which the coarse granite crystallised will be discussed in the remainder of this chapter.

5.3 Geochemistry of the Coarse Granite.

This section on the geochemistry of the coarse granite is divided into isotope geochemistry and major and trace element geochemistry. The section on isotope geochemistry discusses the origin of the magma from which the coarse granite crystallised, aspects of which are pertinent to understanding the origin and depth of accumulation of the magma prior to its ascent. The second section dealing with the major and trace element geochemistry of the magma concentrates on the evolution of the magma, during its ascent, emplacement and crystallisation.

5.3.1 Isotope Geochemistry.

The major, trace element and isotope geochemistry of a variety of igneous and older crustal rocks from the Isle of Arran was studied in detail by Dickin et al. (1981). These authors showed that the Tertiary igneous rocks could be divided into a silica undersaturated trend and a silica oversaturated trend on the basis of oxide vs differentiation index diagrams. The rocks of the undersaturated trend are characterised by high TiO_2($> 2\%$), total Fe ($> 12\%$), P_2O_5 and Sr ($\approx$ 400 ppm) and low CaO ($\approx 8\%$). Rocks of the oversaturated trend have low TiO_2($\leq 1.5\%$), total Fe ($< 11\%$), P_2O_5 and Sr ($<$ 250 ppm) and CaO ($\approx 9\%$). These characteristics indicate that the more basic members of the two trends could be grouped with the Plateau and the Preshal Mhor magma types respectively, as defined by Thompson (1982). The only oxide/differentiation index plot of Dickin et al. (1981) which makes this distinction clear is of differentiation index against SiO_2, which indicates the oversaturated trend is SiO_2 enriched relative to the undersaturated trend! In both series the acid rocks are separated from the basic by a large Daly gap. Dickin et al. (1981) suggested the acid rocks of the central complex and the northern granite are co-linear with the oversaturated trend and inferred that they were derived from the latter by differentiation with or without crustal contamination. Analyses of the Dalradian, ORS and New Red

Figure 5.4. A plot of $^{87}Sr/^{86}Sr$ corrected to 59 Ma. against Sr concentration measured from the Tertiary igneous and older crustal rocks of Arran (from Dickin et al., 1981). Diamonds – Northern Granite; Squares – Central complex granites; Upright triangles – acid rocks of the oversaturated trend; Inverted triangles – basic rocks of the silica oversaturated trend; Open circles – rocks of the undersaturated trend; Stars – Dalradian; Open squares – ORS; Open diamonds – New red sandstone.

Fig. 5.4.

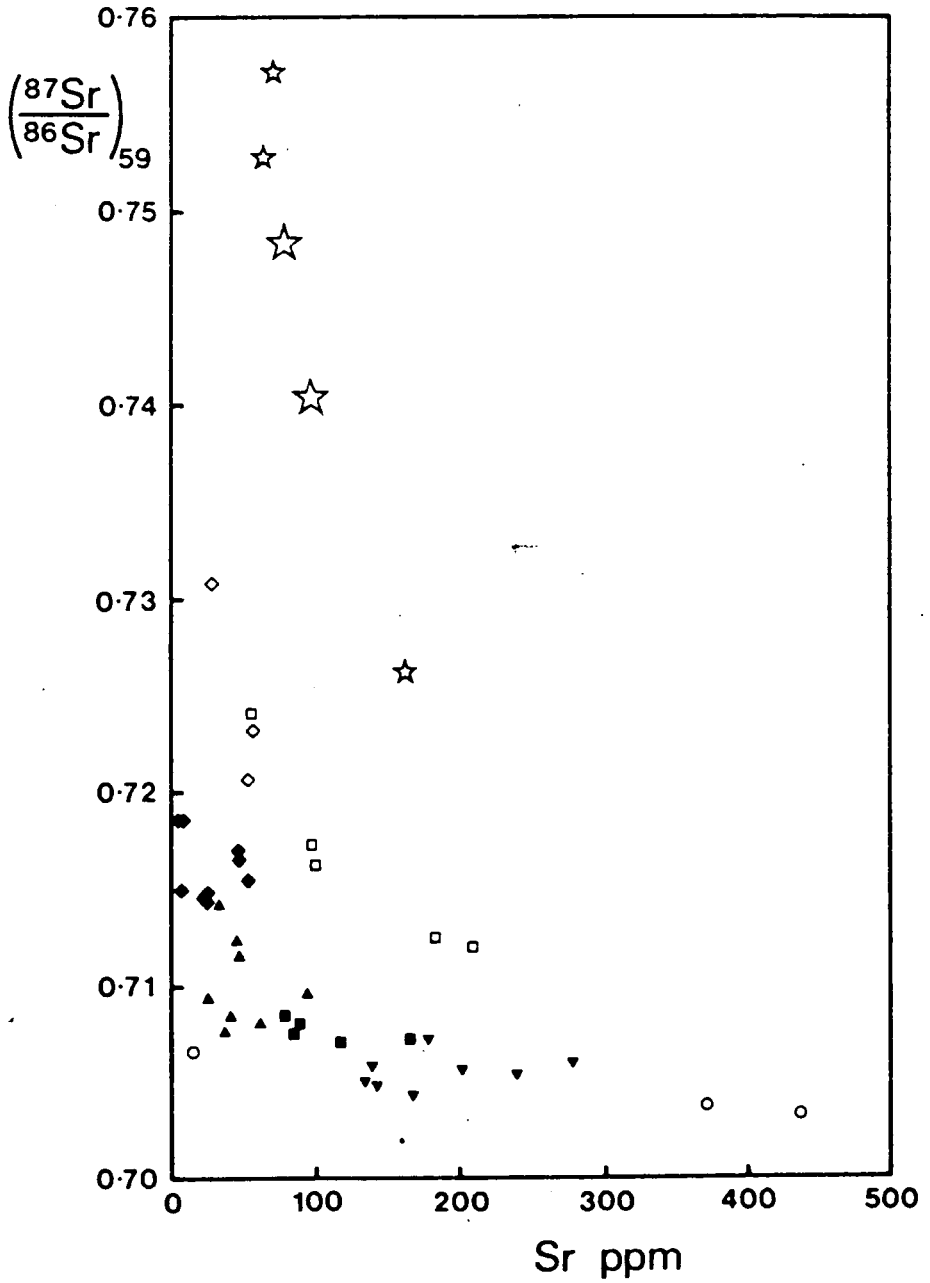
0·76
$\left(\frac{^{87}Sr}{^{86}Sr}\right)_{59}$
0·75
0·74
0·73
0·72
0·71
0·70
0
100
200
300
400
500
Sr ppm

Figure 5.5. A Pb/Pb isochron diagram for the Tertiary igneous and older crustal rocks of Arran (from Dickin et al., 1981). Diamonds – Northern Granite; Squares – Central complex granites; Upright triangles – acid rocks of the oversaturated trend; Inverted triangles – basic rocks of the silica oversaturated trend; Open circles – rocks of the undersaturated trend; Stars – Dalradian; Open squares – ORS; Open diamonds – New red sandstone. L and U define the lower and upper intersection of the best fit line to the range of compositions defined by the Tertiary igneous rocks with the growth curve which gives the rocks an apparent age of 770 Ma. M is the estimated composition of the upper mantle beneath Arran during the Palaeocene.

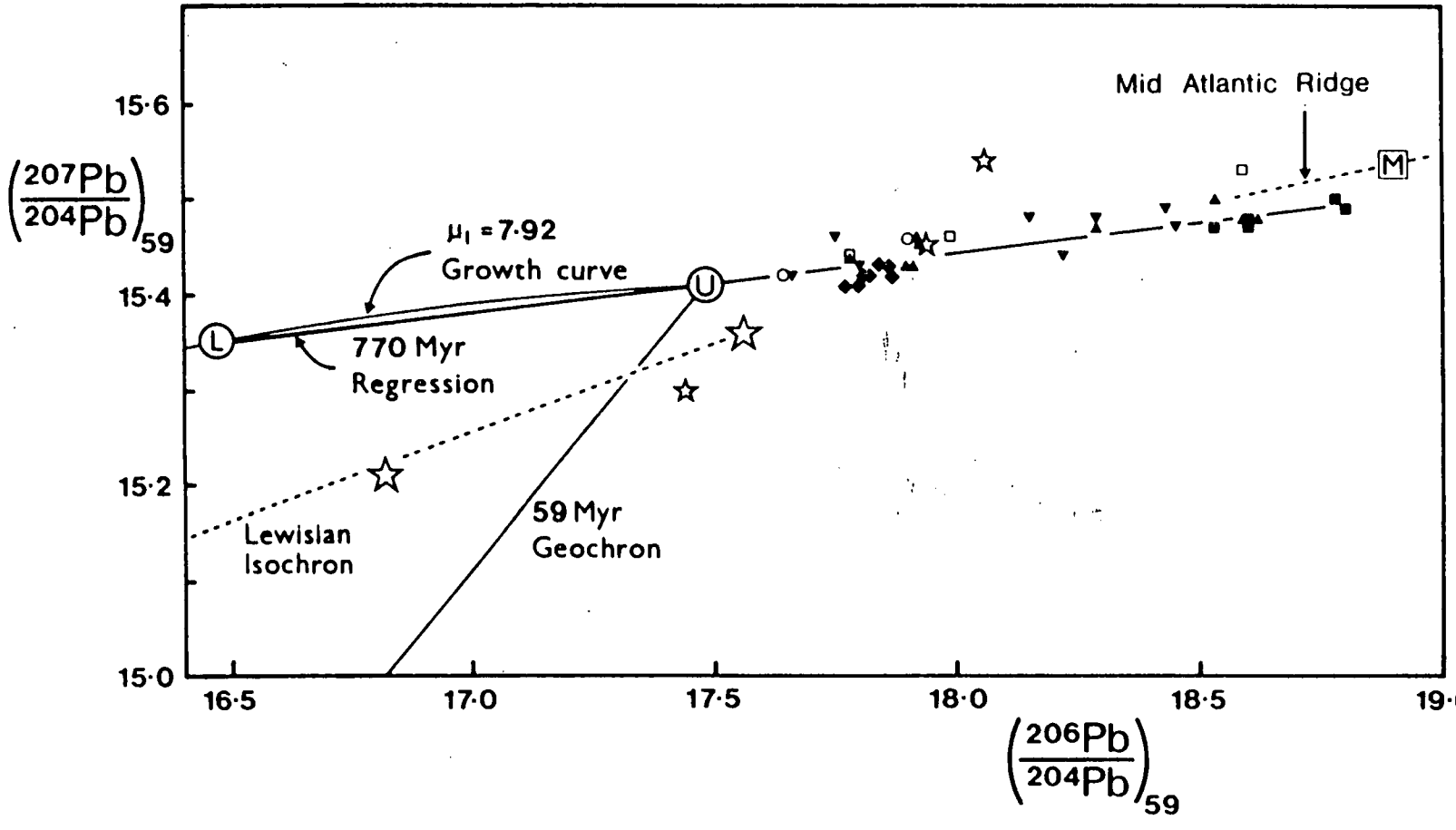
Mid Atlantic Ridge
M
$\mu_1 = 7{\cdot}92$
Growth curve
U
L
770 Myr
Regression
59 Myr
Geochron
Lewisian
Isochron
15·6
15·4
15·2
15·0
16·5
17·0
17·5
18·0
18·5
19·0
$\left(\frac{^{207}Pb}{^{204}Pb}\right)_{59}$
$\left(\frac{^{206}Pb}{^{204}Pb}\right)_{59}$

Fig. 5.5.

Sandstone (NRS) rocks indicate they have compositions which bridge the Daly gap. Consequently it is possible that the acid magmas evolved by partial melting of these units.

The problem of origin by differentiation or crustal melting for the acid rocks of Arran was resolved by Dickin et al. (1981) using Sr and Pb isotope data. All the analysed Dalradian and NRS rocks have higher $^{87}Sr/^{86}Sr$ ratios than the acid igneous rocks. The majority of the acid rocks also have lower $^{87}Sr/^{86}Sr$ ratios than the ORS. Others, including the northern granite ($^{87}Sr/^{86}Sr \approx 0.716$), have similar ratios to the ORS rocks (Fig. 5.4). However since partial melts will always have higher $^{87}Sr/^{86}Sr$ ratios than their parents due to concentration of incompatible Rb in the melt, it appears that the northern granite cannot have been derived solely by partial melting of ORS. Such an origin is also ruled out by the observation that the granite is intruded into Dalradian rocks to the NW of the Highland Boundary Fault (Chapter 4) where the overlying ORS is very thin and of insufficient volume to generate a magma body the size of the northern granite. It is clear that the northern granite cannot have formed solely by partial melting of crustal rocks.

The range Pb isotope compostions of the acid and basic igneous rocks of Arran define an isochron on a $^{206}Pb/^{204}Pb$ vs $^{207}Pb/^{204}Pb$ diagram which indicates an apparent age of 770±180 Ma (Dickin et al., 1981; and Fig. 5.5). This rules out an origin for the granitic rocks or contamination of the basic rocks by partial melting of Lewisian basement, (or Dalradian rocks derived from weathered Lewisian as indicated by the data of Dickin et al. 1981), which would have produced a much steeper pseudo-isochron. This does not rule out partial melting of Proterozoic basement.

Dickin et al. (1981) interpreted the 770 Ma pseudoisochron as representing a mixing line between Pb of Tertiary mantle origin and Pb derived by partial melting of 770 Ma old lower or middle crust. They examined this conclusion by constructing the intersection of the mixing line with a growth curve (μ_1 value of

Figure 5.6. Sample frequency against a). $(^{206}Pb/^{204}Pb)_{59}$ and b). $(^{87}Sr/^{86}Sr)_{59}$ for the Tertiary igneous rocks of Arran. The figures clearly indicate the restricted range of isotope compositions in samples from the coarse granite (C) and the fine granite (F), particularly for $^{206}Pb/^{204}Pb$. Basic rocks are indicated by boxes with diagonal lines. (Data from Dickin et al., 1981.)

Fig. 5.6.

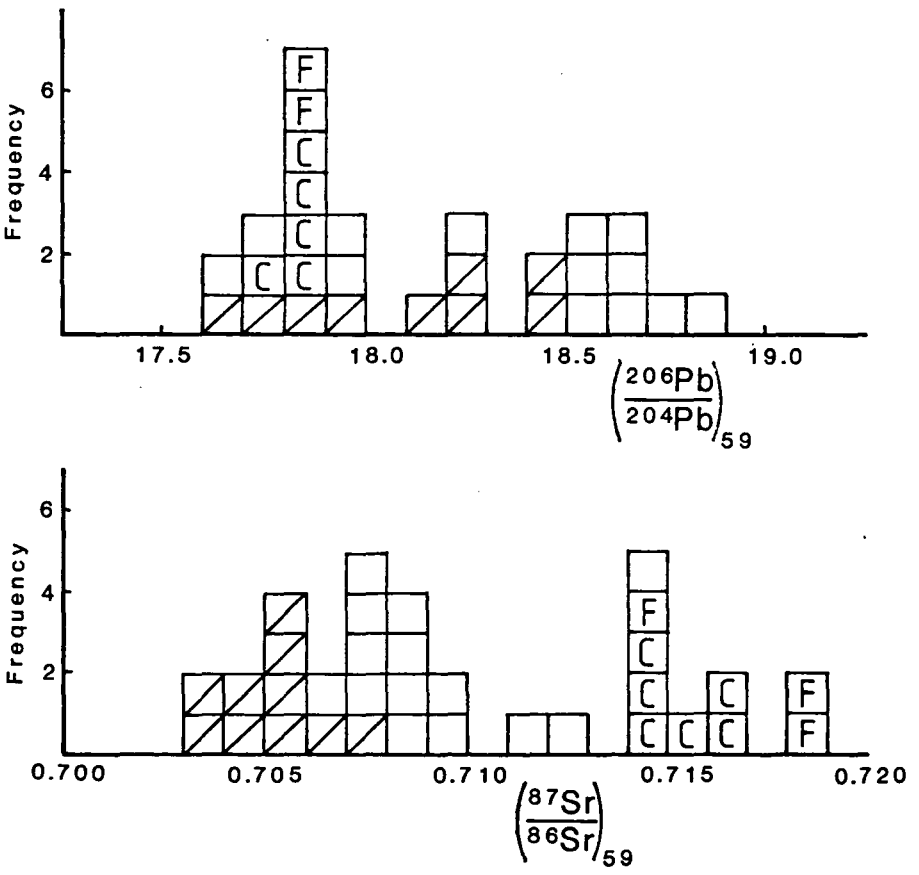
Frequency
6
4
2
F
F
C
C
C
C
C
C
17.5
18.0
18.5
19.0
$\left(\frac{^{206}Pb}{^{204}Pb}\right)_{59}$
Frequency
6
4
2
F
C
C
C
C
C
C
F
F
0.700
0.705
0.710
0.715
0.720
$\left(\frac{^{87}Sr}{^{86}Sr}\right)_{59}$

7.92) assuming that the basement beneath Arran had evolved as a closed system since 4570 Ma (Fig. 5.5). However estimates of the Tertiary mantle composition beneath Arran indicate it had higher $^{207}Pb/^{204}Pb$ and $^{206}Pb/^{204}Pb$ than that predicted by the intersection of the growth curve with the 4570 Ma geochron, but comparable with the least contaminated Arran rocks.

The misfit in the μ_1 growth curve model suggests that the assumption of a closed crust/mantle system beneath Arran is invalid. The assumption is certainly not compatible with the model of Morrison et al. (1980) and Thompson & Morrison (1988) that a Permian mantle melting/extraction event occurred which modified asthenopheric mantle compositions prior to the Tertiary igneous activity. The effect of the inaccuracy in the growth curve model is to introduce greater error into the age and isotope composition of the basement contaminant (Dickin et al. 1981). It is possible that the error in age is sufficiently large to accommodate 1100 Ma Grenvillian crust as a possible contaminant (Dickin et al. 1981). Xenoliths assumed to originate from the basement of the Midland Valley have been dated as Grenvillian by van Breeman & Hawkesworth (1980). Bamford et al. (1977) indicate that this basement may also continue to the north of the HBF (chapter 2) and so it is a possible source of contamination in the northern granite magma.

Dickin et al. (1984) noted that Skye granites have similar Pb isotope compositions to associated basic rocks and hence concluded that they were the differentiation products of crustally contaminated basic magmas. This model can also be applied to Arran, where a similar overlap in isotopic Pb compositions occurs (Fig. 5.6). In the case of Arran it is not possible to determine the degree of contamination by the Proterozoic basement from the isotope data due to a lack of Pb isotope data for the basement rocks. Dickin et al. (1981) showed that there was evidence for crustal contamination of the Arran magmas after they had differentiated from their basic parent. The isotopic composition of magmas with high Sr and Pb concentrations would be hardly affected by the addition of

small volumes of partial melt with isotopically different Sr and Pb. In the case of the Arran acid rocks differentiation from their basaltic parent by plagioclase (and pyroxene) fractionation would have left them depleted in Sr but enriched in Pb. Consequently the addition of partial melts containing isotopically different Pb could have only caused variations in the Pb isotope compostion of the acid magma if the contaminant contained a very high concentrationof Pb or its isotope composition was very different. However in the case of the acid rocks depleted in Sr by fractionation of a Sr bearing phase only a small addition of isotopically different Sr to the melt would cause a significant change in the isotope composition of the rock.

Data from Dickin et al. (1981) indicates that the northern granite has a similar Pb isotope composition to that of the basic rocks of both the undersaturated and the oversaturated trends. However it has a very different Sr isotope composition (Fig. 5.6). This is consistent with post differentiation contamination. This figure also emphasises that the northern granite has a very restricted range of isotope compositions compared with the whole range of Tertiary igneous rocks from Arran. The variations in $^{87}Sr/^{86}Sr$ shown by the samples of the coarse granite lies within the range of analytical error (1% 1σ) quoted by Dickin et al. (1981). This indicates that the granite represents a single magma body and the petrographic variations within it do not represent distinctly different granites. Hence it is assumed on the basis of these data that the coarse granite evolved and remained as a single body of magma during subsequent post differentiation contamination, by Dalradian rocks (discussed below), and ascent. The narrow range of Pb data, compatible with the compositions of the basic rocks, indicates that the granite magma is derived from the same basaltic parent. The remaining acid igneous rocks on Arran have distinctly lower $^{87}Sr/^{86}Sr$ ratios than the northern granite (Fig. 5.6). Dickin et al. (1981) attributed this to the assimilation of Dalradian rocks by the granite. They suggested that this may have also caused the slightly lower $^{207}Pb/^{204}Pb$

ratio of the granite relative to the other acid rocks which are thought to have not come into contact with large volumes of Dalradian rocks. However since Pb is strongly incompatible it is likely to be concentrated in partial melts of Dalradian, as would Sr. Consequently small degree partial melts of Dalradian would be strongly enriched in isotopically different Pb which on mixing with the granite could produce some isotopic variation. Calculations based on the data of Dickin et al. (1981) indicate that the isotopic Pb and Sr composition caused by post differentiation contamination of the northern granite magma is the result of the addition of up to 5% (by weight of the granite) of a very low (< 5%) partial melt of Dalradian (Fig. 5.7), assuming the granite had the same Pb and Sr isotope compositions as its basaltic parent (see above). This minor amount of assimilation of Dalradian rock is consistent with the lack of xenoliths within the granite, which appear to exclude intrusion of the granite by stoping and assimmilation of crustal rock (Chapter 4).

In conclusion, isotope data can be used to show that the northern granite is a differentiate of basaltic magma. The basaltic magma was contaminated with crustal Pb and Sr derived by partial melting of Proterozoic basement beneath Arran prior to differentiation. A lack of significant contamination by partial melts of Dalradian rocks before and following differentiation suggests that the granite accumulated within the Proterozoic basement, which lies 8 km below the present surface. Consequently it is inferred that the granite rose a minimum of 8 km during its ascent. A lack of significant variation in the isotope composition of the coarse granite suggest it accumulated and rose to the surface as a single body.

Figure 5.7. The bulk composition of Sr and Rb in a partial melt change with the degree of partial melting. Mixing of an Sr depleted magma with an Sr enriched partial melt will cause a change in the isotopic compostion of the magma if the two components have different initial isotopic ratios. This graph was constructed by calculating the volume of different percentage partial melts of Dalradian which when mixed with the evolving granite could produce the observed variation in isotopic composition of the granite from its basaltic parent. The graph shows that the variation can only be the result of contamination of the granitic magma by less than 5% (by weight of the granite) of a very low degree partial melt of Dalradian.

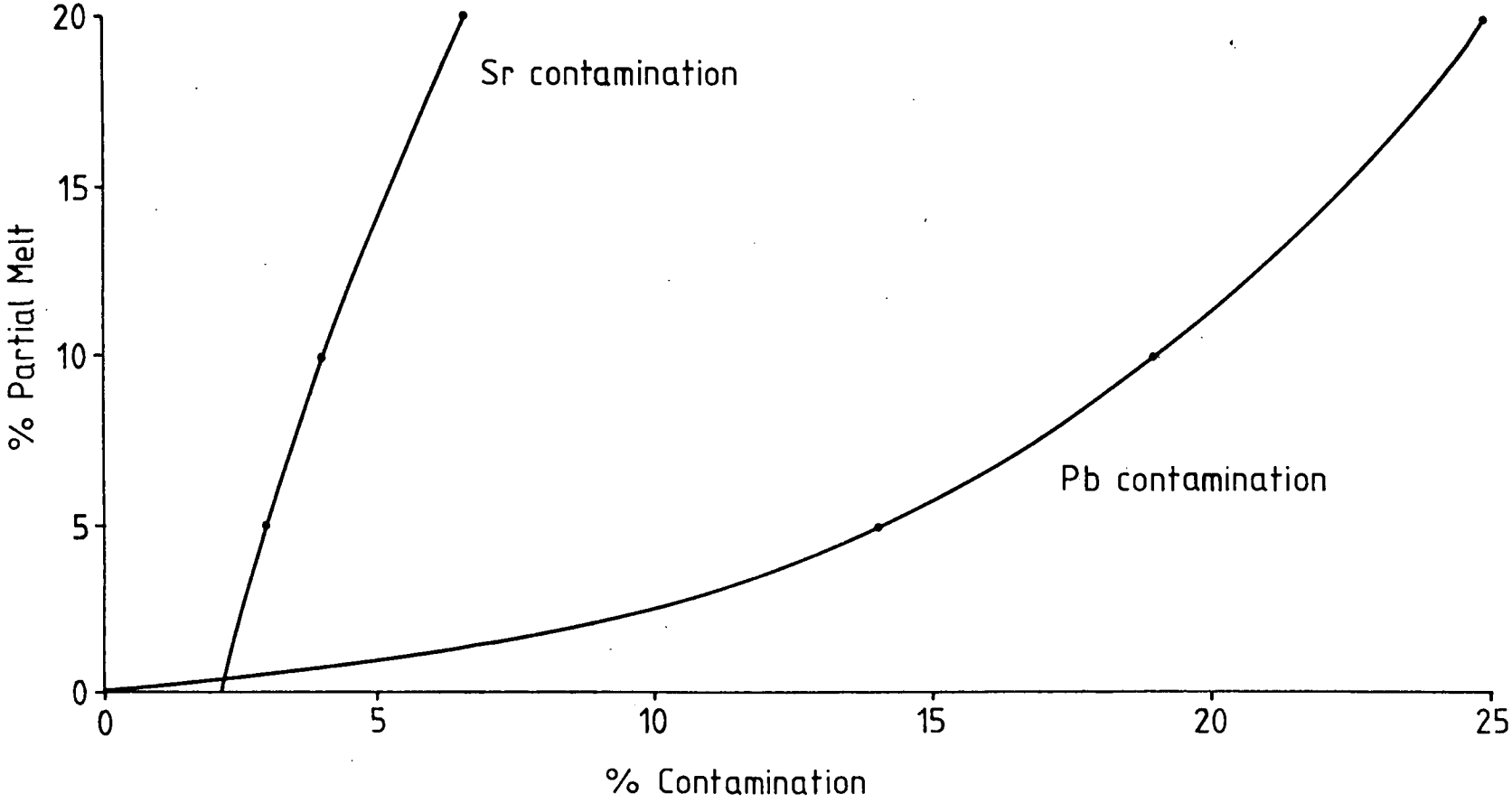
20
15
10
5
0
% Partial Melt
Sr contamination
Pb contamination
0
5
10
15
20
25
% Contamination

Fig. 5.7.

5.3.2 Major and Trace Element Geochemistry.

The major and trace element composition of 191 samples of the coarse granite were determined by XRF spectrometry (see appendix for details). This collection of rocks includes 153 samples of the three textural groups (section 5.2) and samples of the fine sheets within the coarse, which were initially considered uncharacteristic of the groups within which they were collected. A separate collection of the aplites was made.

The range and average major and trace element composition of the collection of rocks (191 samples) is given in Table 5.3. The table clearly shows that the variation in major element chemistry is restricted. The rocks are high in silica, aluminium and alkali metals (Na_2O and K_2O) but are strongly depleted in other major oxides. CIPW norms calculated for each sample (see appendix) plot close to the minimum melting point in the system quartz – albite – orthoclase at 1 kbar $_pH_2O$ (Tuttle & Bowen, 1958; and section 5.4, Fig. 5.40). This indicates that the coarse granite is either the product of extreme fractionation or a partial melt of pre-existing igneous, sedimentary or metamorphic rocks (Thompson, 1983). In this case extreme fractionation is inferred on the basis of the isotope geochemistry of the granite (section 5.3.1).

All the major oxide concentrations decrease with increasing silica. On cartesian co-ordinate plots most oxide compositions lie on parabolic curves indicating they are controlled by crystal fractionation as opposed to mixing (Figs. 5.8 to 5.11). The notable exception to this is aluminium which shows a sharp straight line plot suggestive of mixing of a siliceous melt with an Al rich source. This could be explained by contamination of the granite by a partial melt of pelitic Dalradian. Such contamination may explain why the average composition of the granite is peraluminous:

$$\frac{Al_2O_3}{Na_2O + K_2O + CaO} = 1.073$$

TABLE 5.3

Average and range of major and trace element compositions for the Northern Arran Coarse Granite.

Element	Average	Range
SiO_2	77.29	70.69 - 80.47
TiO_2	0.10	0.00 - 0.50
Al_2O_3	12.49	11.21 - 14.23
Fe_2O_3	1.33	0.03 - 4.61
MgO	0.04	0.00 - 0.17
CaO	0.38	0.10 - 1.73
Na_2O	3.38	2.84 - 4.28
K_2O	4.99	0.51 - 5.88
MnO_2	0.03	0.02 - 0.10
P_2O_5	0.02	0.00 - 0.11
Ba	641	0 - 1365
Nb	31	0 - 59
Zr	147	8 - 635
Y	67	23 - 153
Sr	33	1 - 64
Rb	178	136 - 302
Zn	44	19 - 165
Cu	12	0 - 18
Ni	5	0 - 9
Pb	27	22 - 53
U	2	0 - 4
Th	20	0 - 31
V	5	0 - 24
Cr	10	0 - 40
Nd	48	15 - 151
La	39	3 - 37
Ce	81	0 - 124
K/Rb	233	1 - 308

Total Fe given as Fe_2O_3. Major oxides as wt %, trace elements in ppm. 191 samples.

Figure 5.8. Al_2O_3 (wt %) plotted against SiO_2 (wt %) for the 153 samples representative of the petrographically defined groups of the coarse granite. (Diamonds – group 1; Crosses – group 2; Circles – group 3.)

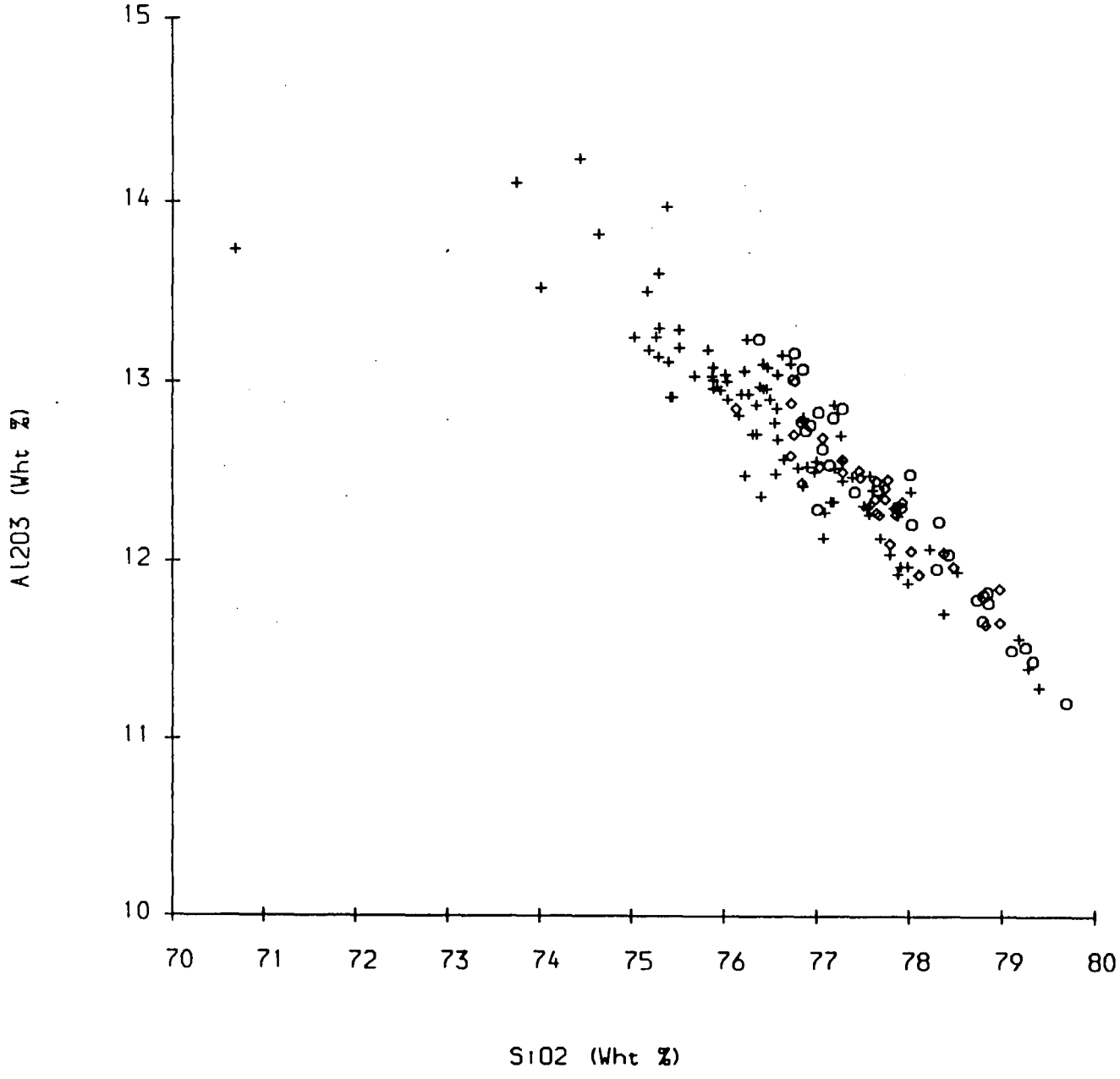

Fig 5.8

Figure 5.9. Na_2O (wt %) plotted against SiO_2 (wt %) for the 153 samples representative of the petrographically defined groups of the coarse granite. (Diamonds – group 1; Crosses – group 2; Circles – group 3.)

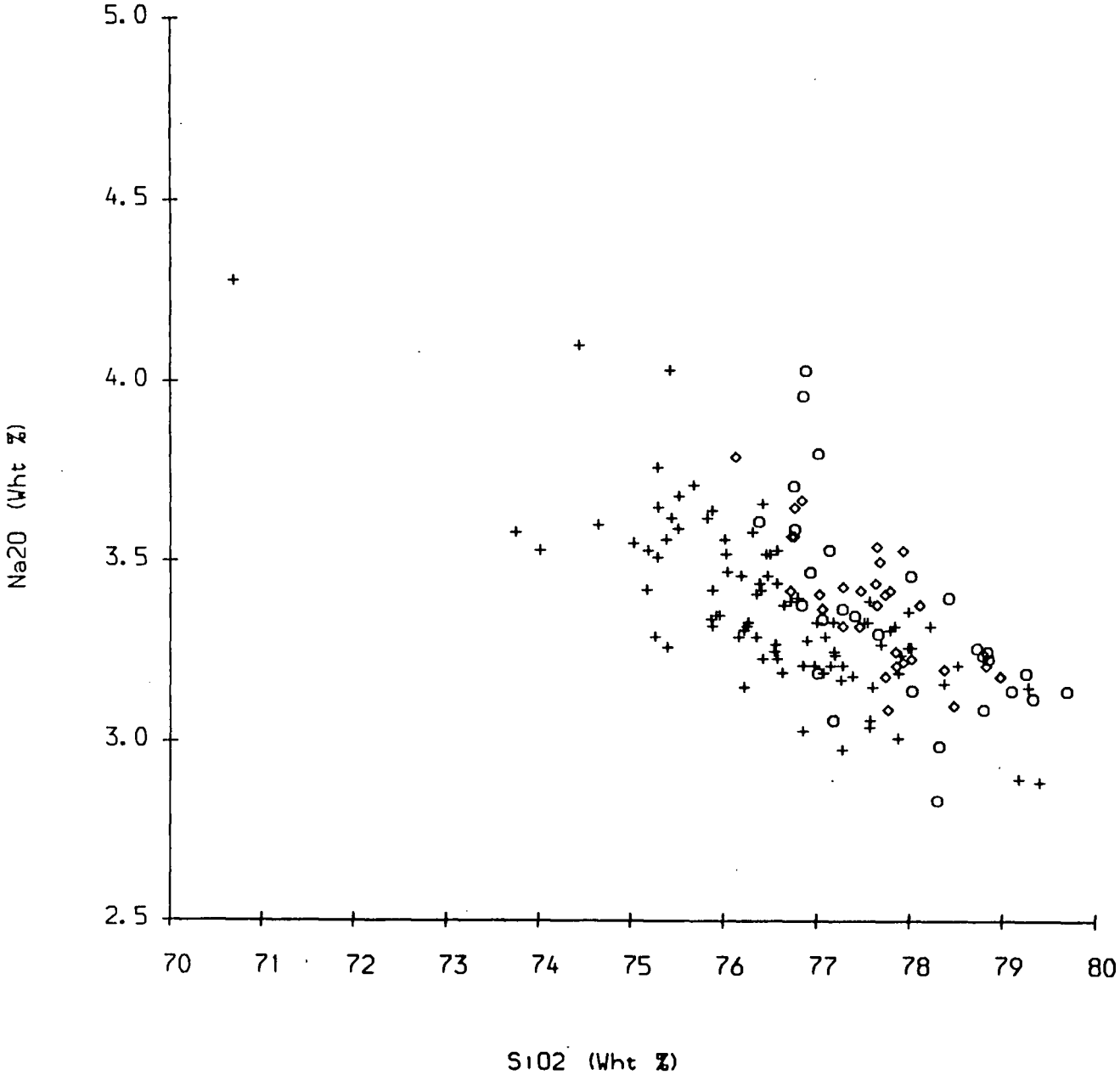

Fig. 5.9.

Figure 5.10. K_2O (wt %) plotted against SiO_2 (wt %) for the 153 samples representative of the petrographically defined groups of the coarse granite. (Diamonds – group 1; Crosses – group 2; Circles – group 3.)

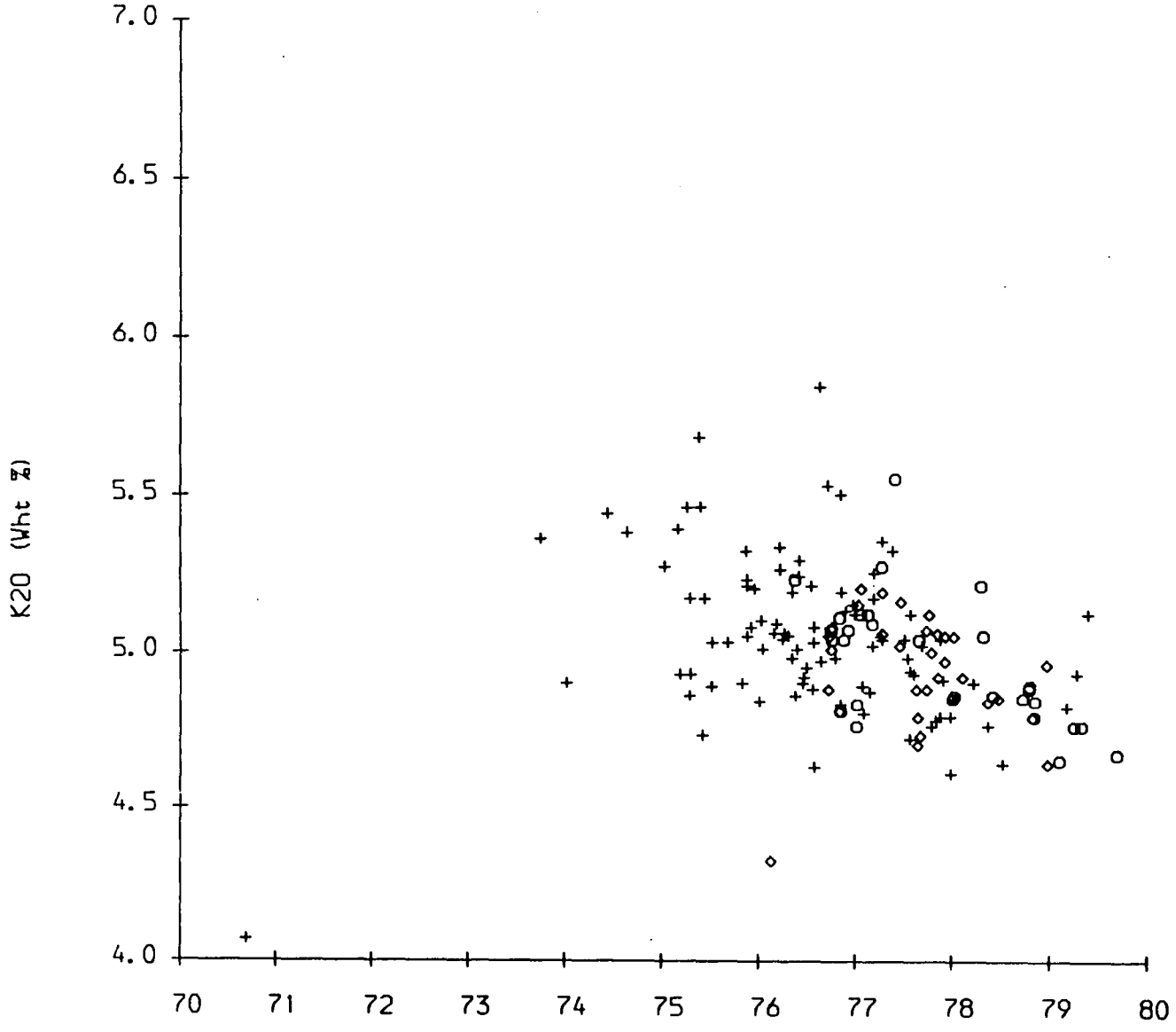

Fig. 5.10.

Figure 5.11. CaO (wt %) plotted against SiO_2 (wt %) for the 153 samples representative of the petrographically defined groups of the coarse granite. (Diamonds – group 1; Crosses – group 2; Circles – group 3.)

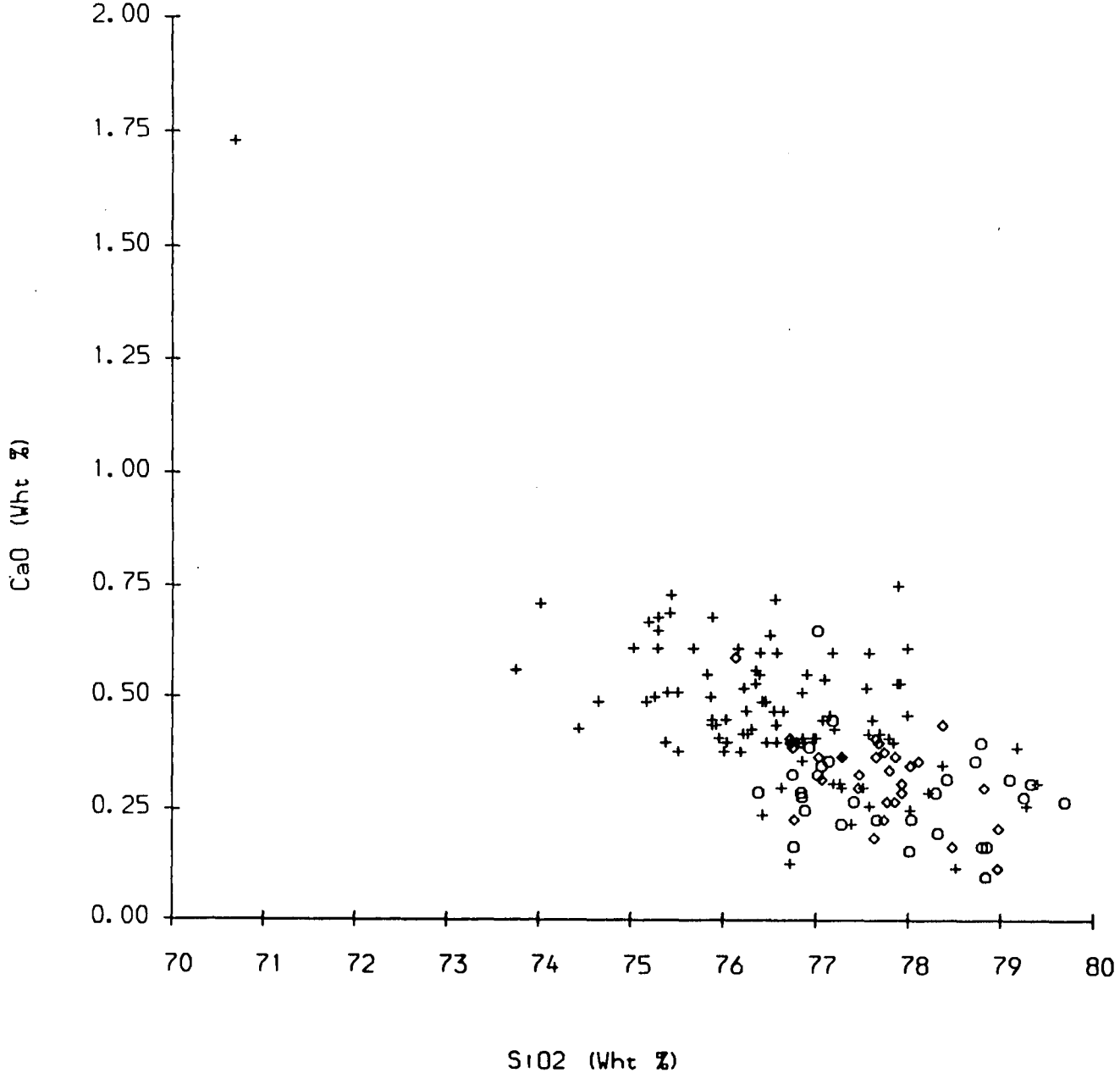
2.00
1.75
1.50
1.25
1.00
0.75
0.50
0.25
0.00
CaO (Wht %)
70
71
72
73
74
75
76
77
78
79
80
SiO2 (Wht %)

Fig 5.11

(Oxides are in molecular proportions.) It is also possible that the aluminiun contentsof the rocks have been enhanced by kaolinisation although there is little evidence for this. Had this contamination been substantial (isotope data indicate that it amounts to less than 5% of the granite, Fig. 5.7) the alkali elements would also be expected to show mixing trends. Since they do no it is concluded that the major control on element variation in the coarse granite is crystal fractionation. The fall in alkalis and aluminium with increasing silica (Figs. 5.8 to 5.11) indicate the fractionating phases could be orthoclase and plagioclase, which is consistent with the presence of these minerals as phenocrysts (section 5.2). Hence chemical variation in the coarse granite due to mixing of a number of pulses of different granitic magmas or crustal contaminants can be ruled out on the basis of major element geochemistry.

Major and trace element data from Table 5.3 and Sm and Tb data from Meighan, (1979) were plotted on a chondrite normalised incompatible element plot (Fig. 5.12). This figure shows a number of prominent troughs corresponding to Ba, Sr, P and Ti, a slight trough at Zr and a prominent peak at Rb, Th and K. The elements La, Ce, Nd, Sm, Tb and Y are generally enriched in granitic systems relative to chondritic bulk earth but are not compatible in many of the common minerals involved in fractionation (e.g. feldspars, micas, apatite and zircon). Consequently these elements do not show the wide variation in concentration shown by the elements compatible in these phases. Hence they may be used to indicate relative enrichment and depletion of the compatible elements which can then be used as indicators of the minerals controlling differentiation.

The distribution of an element between a mineral and a coexisting liquid is controlled by the distribution coefficient of the element. In most cases extraction or enrichment of a particular element is controlled by its bulk distribution coefficient which is the sum of the distribution coefficients for each mineral in equilibrium with the liquid multiplied by the weight proportion of each mineral

Figure 5.12. Chondrite normalised incompatible element pattern showing the average composition and variation in composition (given by 2σ) of selected elements for the coarse granite. (Sm and Tb data from Meighan, 1979; Normalisation factors after Thompson, 1982.)

Fig. 5.12.

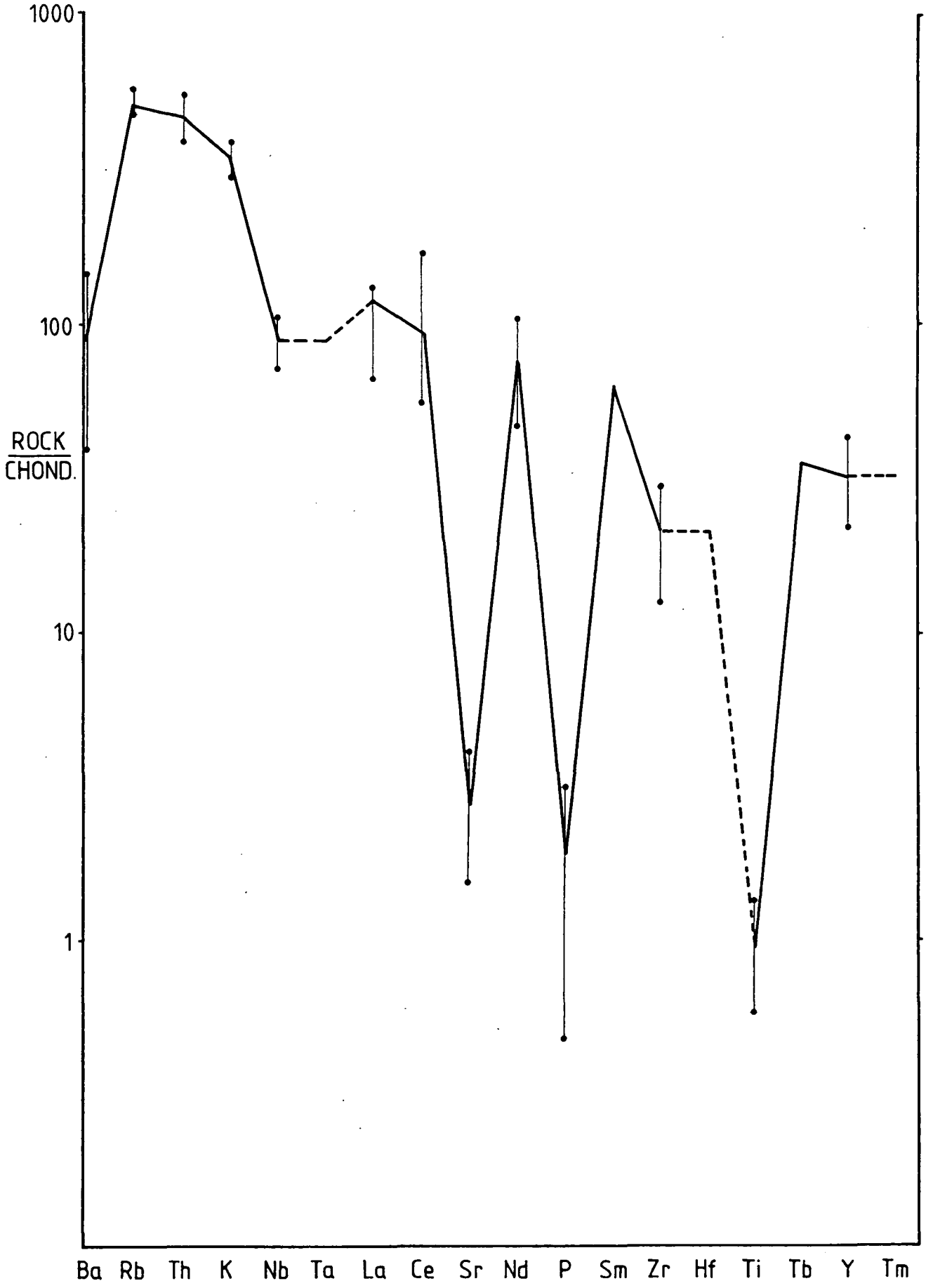
1000
100
ROCK / CHOND.
10
1
Ba Rb Th K Nb Ta La Ce Sr Nd P Sm Zr Hf Ti Tb Y Tm

in the solid assemblage. Distribution coefficients used in this study are given in Table 5.4.

Table 5.4

Selected distribution coefficients for Ba, Rb and Sr.

Mineral	Ba	Rb	Sr
Quartz	0.0001	0.0001	0.0001
Orthoclase	6.60	0.38	4.00
Plagioclase	0.50	0.09	4.40
Biotite	7.55	3.40	0.24

~~narrower~~ Data for quartz, after McCarthy & Hasty (1976), other data from Henderson (1982), average values used, although some variations in values for Rb were made - see text for further details.

The simplest method of producing peaks in the incompatible element diagram is to add more of a particular element to the magma without increasing the concentration of others. Conversly troughs are produced by selectively removing a particular element from the melt. Comparison of the position of the troughs with distribution coefficient data indicate that the troughs at Ba, Sr, P, Zr and Ti can be explained by the removal of these elements from the melt by separating crystallising orthoclase, plagioclase, apatite, zircon, Ti-oxide or Ti rich pyroxene (the absence of a trough at Nb excludes extensive fractionation of spinel group minerals such as magnetite or rutile). The peaks at Rb, Th, and K indicate the addition of an acid partial melt to the magma. The timing of these fractionation and contamination events can be deduced from the petrographic and isotopic data described in sections 5.2 and 5.3.1.

The isotope data records contamination of the basic magma by Proterozoic lower crust. Thompson et al. (1982) showed that Hebredian basalts displayed a range of contamination by large fraction cotectic partial melts of Lewisian leucogneiss. This resulted in the basalt showing enrichment in those elements concentrated in the partial melts. Experimental data of the melting of the gneiss (Thompson, 1981) and theoretical modelling of contamination processes in the lower crust (Patchett, 1981) indicate that partial melting of lower crustal gneisses

selectively removed the leucocratic portion of the rock to leave a refractory restite. The melt would result from the fusion of quartz, alkali feldspar (and muscovite). This would produce a melt enriched in the strongly incompatible elements Ba, Rb, U, Th, Pb, Sr and K and the light rare earth elements (REES), and depleted in Nb, Ta, P, Zr, Hf, Ti, Y and the middle to heavy REES which would remain in the refractory residue. Mixing of this partial melt with the basic magma would cause enrichment of the basic liquid in the incompatible elements relative to the compatible elements, and alter its isotopic composition.

A simple mixing calculation indicates that the observed concentration of Rb and K in an oversaturated basalt with a Pb isotopic composition closely similar to that of the coarse granite (from Dickin et al. 1981) could be produced by mixing 70% primitive Preshal Mhor type magma (SK946 of Thompson, 1982) with 30% of a large fraction partial melt of Grenvillian quartzofeldspathic gneiss (Graham & Upton, 1978) (Fig. 5.13).

This process would explain the relative enrichment of Rb, Th and K shown in the incompatible element plot for the Arran granite. An enrichment of Ba in the granite might also be expected, but instead a trough occurs at this element indicating depletion. This will be discussed below. Sr isotope data for the coarse granite indicate that the contaminated basaltic parent evolved toward a granitic composition by fractionating a Sr bearing phase (or phases), following contamination by Proterozoic basement. The troughs at Sr and Ti suggest this may have been plagioclase and possibly a Ti rich pyroxene. This fractionation episode would have produced a melt with high absolute concentrations of all the incompatible elements. Consequently contamination by a partial melt of crustal rocks (enriched in incompatible elements) would be more difficult to detect. A large volume of partial melt with a significantly different incompatible element composition (i.e. extremely concentrated in incompatible elements) would be required to cause observable changes in the incompatible element pattern. This could only

Figure 5.13. Chondrite normalised incompatible element patterns for Arran basic rock B8 (which has the same $^{206}Pb/^{204}Pb$ isotope composition as the coarse granite) (squares, data from Dickin et al., 1981), Preshal Mhor basalt SK946 (circles, least contaminated Preshal Mhor basalt of Thompson, 1982), Partan Craig Grenvillian Quartzofeldspathic granulite (crosses, data from Graham & Upton, 1978 and van Breeman & Hawkesworth, 1980) and a mixture of 70% SK946 and 30% feldspathic granulite (triangles).

Fig. 5.13.

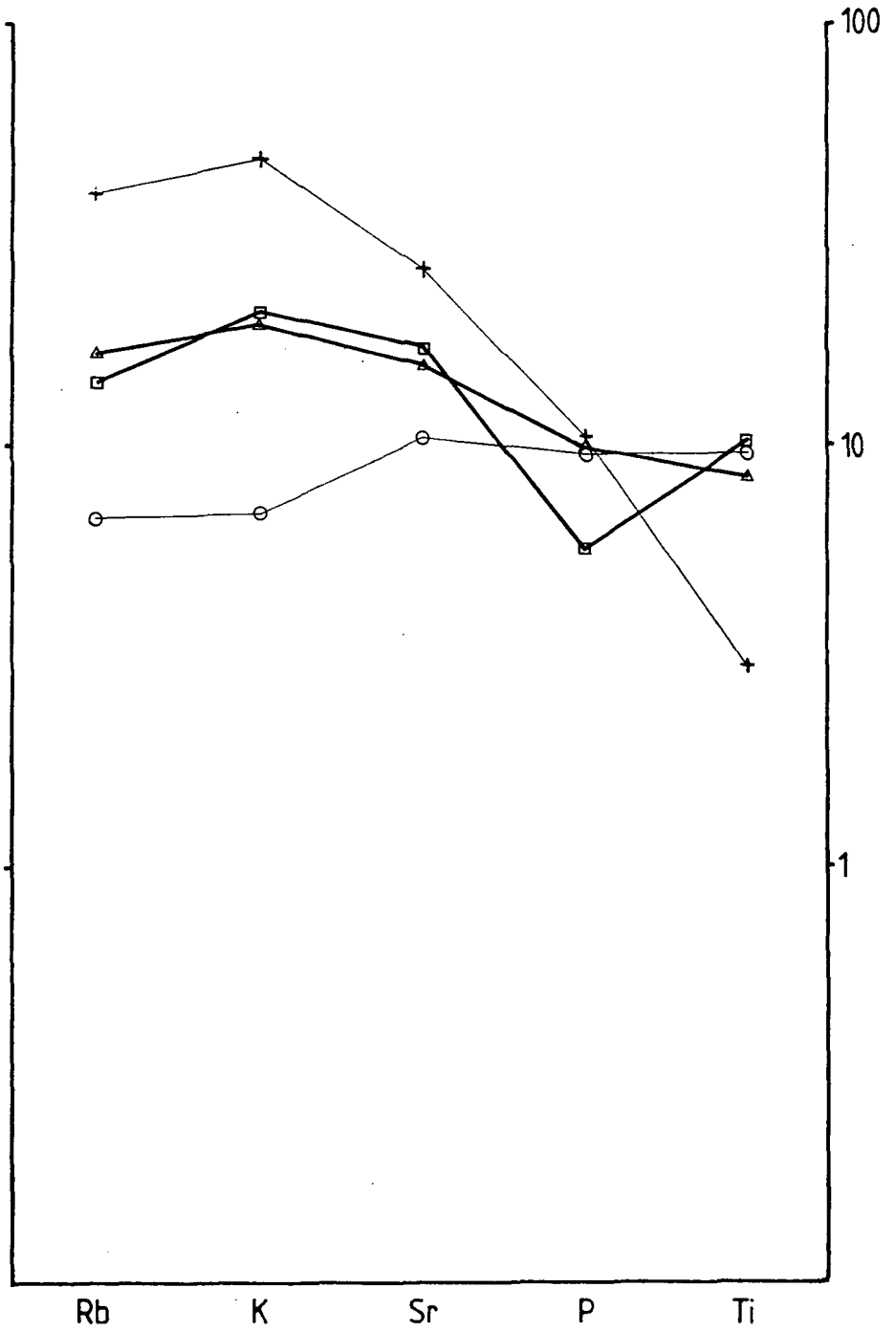

be achieved by contamination by a large volume of low degree partial melts of crustal rocks, which is ruled out by isotope data (Fig. 5.7). Contamination by basic magma can be eliminated on the grounds that the concentrations of MgO and total Fe are very low (Table 5.3).

The depleted Ba concentration can be explained by fractionation of a Ba bearing phase such as alkali feldspar (e.g. Anorthoclase). This fractionation must have occurred after contamination in order to selectively deplete Ba in the melt with respect to Rb, Th, and K. Pre-contamination fractionation is ruled out since a Ba rich phase would not be compatible with a basic magma and hence it would melt, incorporating the Ba in the liquid.

Further contamination during fractionation and ascent of the acid magma could not be detected (unless the contaminant had a very different composition - see discussion above) because the Dalradian rocks through which the granite rose have a very similar element abundance pattern (Fig. 5.14, data from Robertson & Henderson, 1984). Consequently a partial melt of Dalradian would also have a similar abundance pattern to the granite. The effect on the element composition of the granite if these two components were mixed would be negligible. This rules out the use of the incompatible element diagram as a clear indicator of contamination of the granite magma by partial melts of Dalradian.

The petrographic data (section 5.2) indicates that during the last stages of crystallisation of the granite the liquidus phases were orthoclase, sodic plagioclase and quartz. This is consistent with the trace element data which indicates fractionation of orthoclase and plagioclase, which both occur as phenocrysts. The evidence for apatite and Ti-oxide fractionation is contradictory. The incompatible element plot (Fig. 5.12) shows clear depletion of P and Ti indicating fractionation of phases bearing these elements. Ti may have been concentrated in a silicate phase (e.g. pyroxene) causing it to become depleted, although there is no petrographic evidence of fractionation of a mafic silicate phase. P is only concentrated

Figure 5.14. Chondrite normalised incompatible element diagram for Dalradian rocks (data from Robertson & Henderson, 1984) which show a similar pattern to the coarse granite (Fig. 5.12.).

Fig. 5.14.

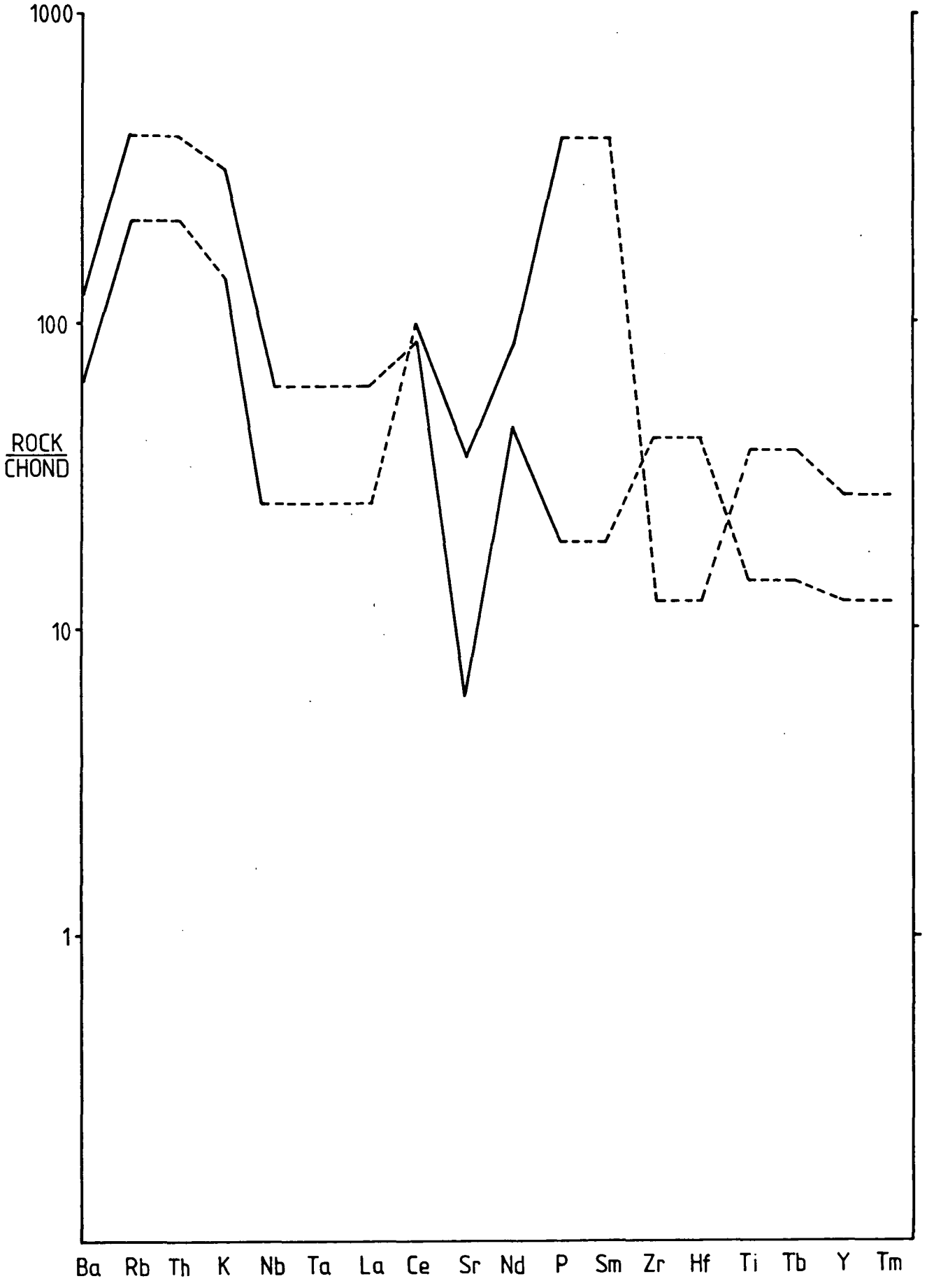
1000
100
10
1
ROCK
CHOND
Ba
Rb
Th
K
Nb
Ta
La
Ce
Sr
Nd
P
Sm
Zr
Hf
Ti
Tb
Y
Tm

in apatite and consequently this phase might be expected to crystallise as a phenocryst phase rather than a groundmass phase as recorded by the petrography. Both apatite and oxides are spatially associated with biotite, zircon and allanite which crystallised as early groundmass phases. There is no evidence of fractionation of biotite (Rb is undepleted) or allanite (La and Ce are also undepleted) and Zr is only slightly depleted indicating limited fractionation of zircon. This anomaly could be explained by rapid separation of these minor phases from the melt before they could become enclosed in growing phenocrysts. An example of this process occurring, to produce layering in the Mourne G1 granite, has been described by Meighan (1979).

It is clear from the incompatible element plot (Fig. 5.12) that certain trace elements show a wider variation in concentration than others. Those elements showing the widest variations correspond to those which are being fractionated by the precipitation and removal orthoclase, plagioclase, apatite, Ti-oxide and to a certain extent zircon, (i.e. Ba, Sr, P, Ti and Zr). The remaining elements which are incompatible in these phases show very little variation in concentration. This lack of variation, together with the field evidence and isotope data provides strong grounds for concluding that the northern granite fractionated from the same basaltic source. If this is correct the observed variation in Ba, Sr, P, Ti and Zr represent variations produced by fractionation of a single body of magma.

Ba and Sr show the widest variation in composition. The concentrations of these elements in the 153 samples selected as representative of the groups from which they were collected were plotted at their localities on a base map of the pluton. These maps of trace element distribution were contoured (by hand) to reveal any spatial (both vertical and horizontal) variation in Ba and Sr concentration. The contouring indicated many local (occasionally extreme) variations in composition across the pluton, but clearly indicated the broad distributions shown in Fig. 5.15 and Fig. 5.16.

Figure 5.15. Map showing the spatial variation in concentration of Ba in the coarse granite. The boundaries separating the region of high and low concentrations of Ba correspond closely to the textural divisions (Fig. 5.3) and with those separating regions of differing Sr concentration (Fig. 5.16).

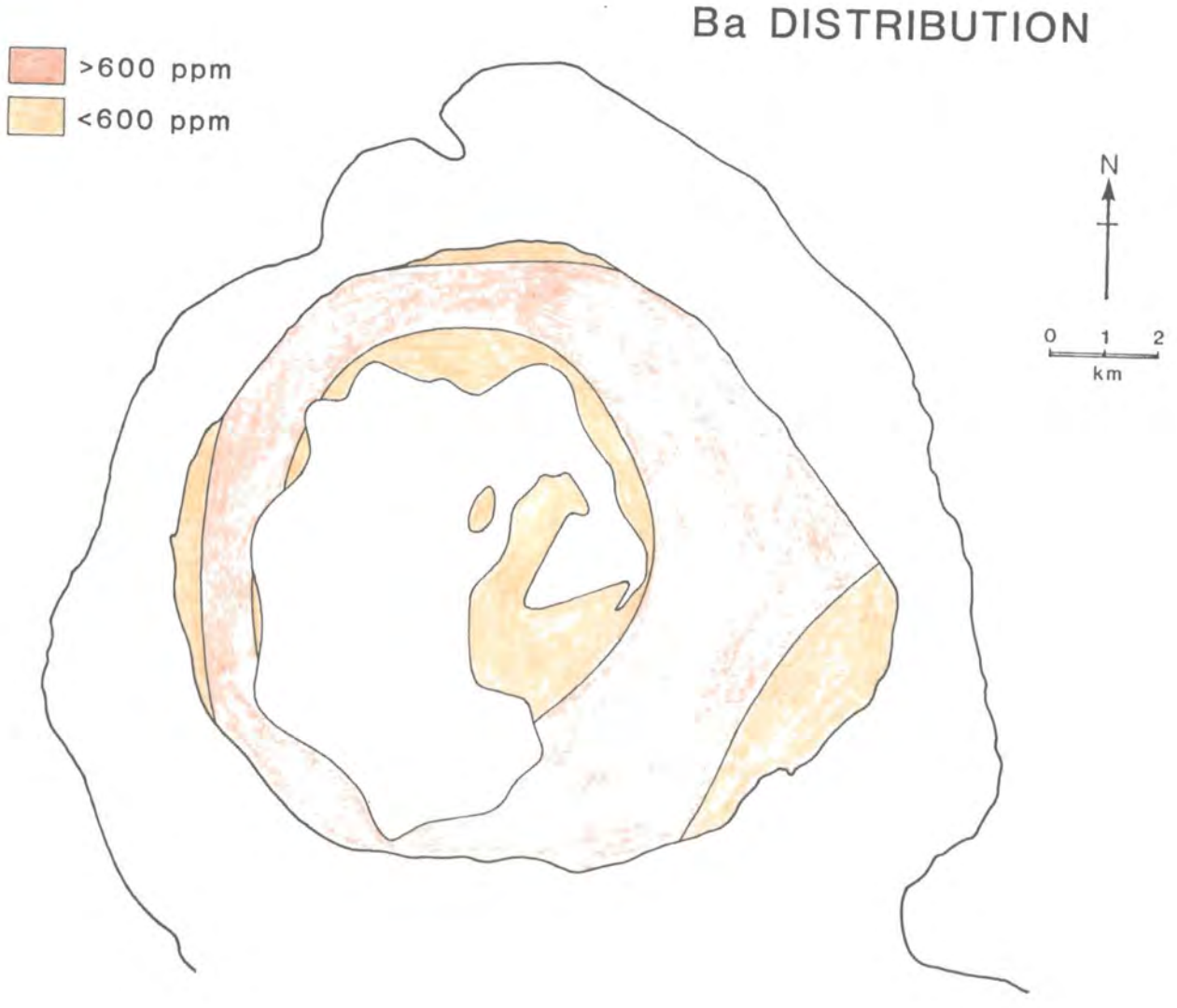

Fig. 5.15.

Figure 5.16. Map showing the spatial variation in concentration of Sr in the coarse granite. The boundaries separating the region of high and low concentrations of Sr correspond closely to the textural divisions (Fig. 5.3) and with those separating regions of differing Ba concentration (Fig. 5.15).

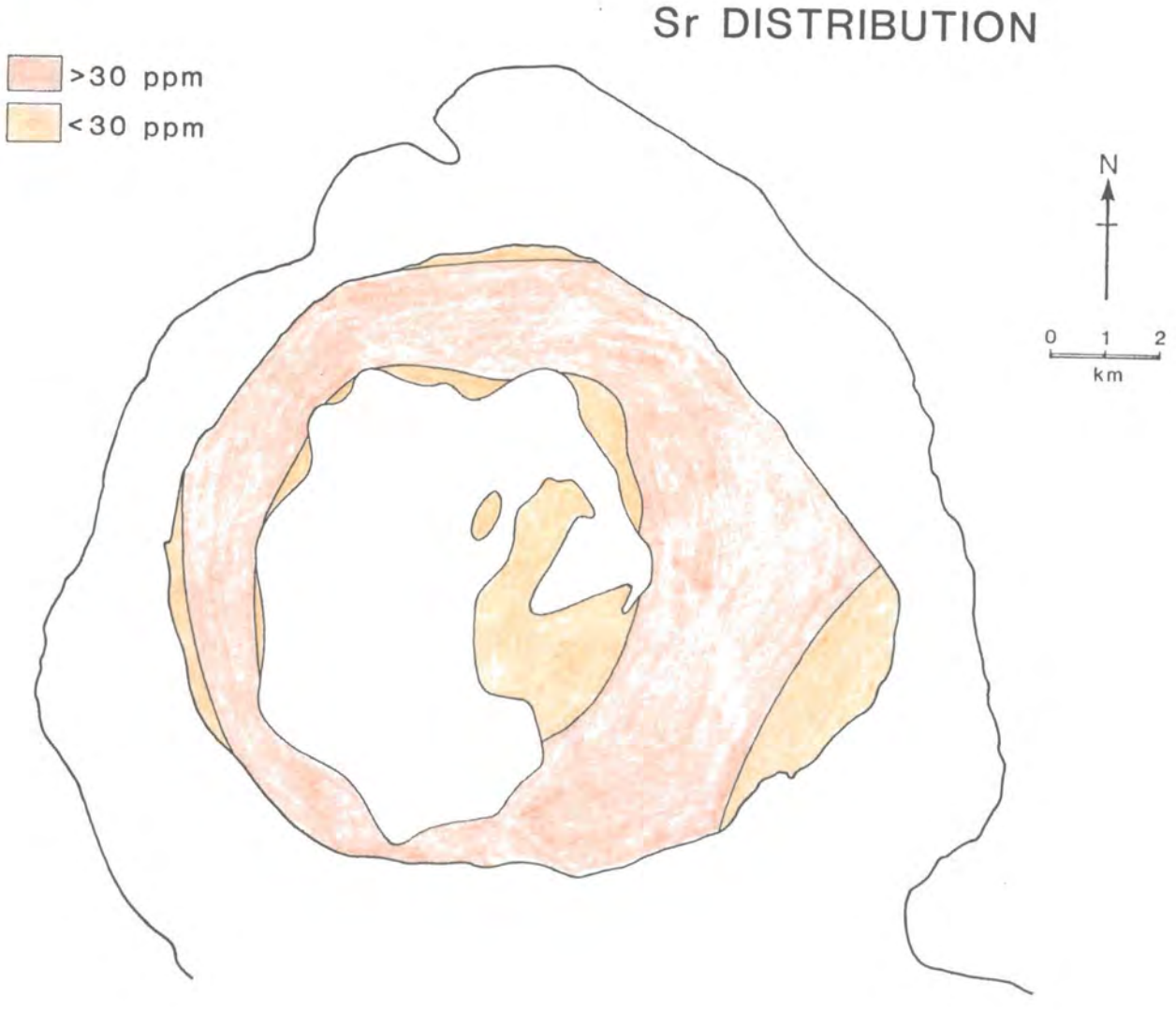

Fig. 5.16.

Comparison of the element distribution plots and the distribution of the three petrographic types (Fig. 5.3) shows that the boundaries between compositionally distinct granites correspond with the boundaries between texturally distinct granites. Ba, which showed the broadest range in composition from 0 to 1400 ppm, revealed the clearest distribution pattern. The 600 ppm contour dividing the three groups is not arbitary. It lies along a sharp discontinuity between the low Ba bearing rocks in the SE of the intrusion and the high Ba rocks which occupy most of the body. The division between the high Ba rocks and the low Ba rocks at the centre of the pluton is less clear as there appears to be a gradual decrease in Ba concentration toward the core of the intrusion. It is recognised that these patterns are strongly dependent upon sample distribution, which although planned on an orthogonal grid (see appendix), was largely controlled by available outcrop. However the variations are assumed to be real because the divisions between rocks with different trace element compositions and petrogaphy are internally consistent, although each of the three groups contain rocks which could equally be assigned to either of the other groups on the grounds of chemical composition. This is illustrated by inter-element plots, described below.

On the basis of textural variation the 153 samples were divided into their respective groups and the range and average major and trace element composition of each group was determined (Table 5.5). It has been argued above that while the coarse granite can be divided into 3 groups on the basis of textural variation it represents a single body of magma. This is also indicated by Table 5.5. Apart from those elements showing variations due to fractionation the composition of each of the three petrographic groups is approximately the same.

The average composition of the three groups were plotted on a chondrite normalised incompatible element diagram (Fig. 5.17). Using this diagram it was possible to exclude crustal contamination as the cause of the compositional variations in selected elements between the three groups. The diagram shows

TABLE 5.5

Average and range of major and trace element compositions for the three groups of the Northern Arran Coarse Granite.

	Group 1		Group 2		Group 3	
Element	Average	Range	Average	Range	Average	Range
SiO_2	77.63	76.13 - 78.98	76.59	70.69 - 80.47	77.84	76.38 - 79.69
TiO_2	0.09	0.05 - 0.15	0.13	0.06 - 0.50	0.08	0.06 - 0.15
Al_2O_3	12.35	11.65 - 13.00	12.75	11.29 - 14.23	12.31	11.21 - 13.24
Fe_2O_3	1.21	0.83 - 2.04	1.57	0.77 - 4.61	1.09	0.83 - 1.84
MgO	0.04	0.00 - 0.08	0.05	0.00 - 0.17	0.03	0.02 - 0.06
CaO	0.33	0.12 - 0.59	0.48	0.12 - 1.73	0.29	0.10 - 0.65
Na_2O	3.37	3.09 - 3.79	3.38	2.89 - 4.28	3.35	2.84 - 4.03
K_2O	4.94	4.33 - 5.20	5.00	0.51 - 5.84	4.97	4.65 - 5.55
MnO_2	0.03	0.02 - 0.04	0.03	0.01 - 0.10	0.02	0.02 - 0.04
P_2O_5	0.01	0.00 - 0.04	0.03	0.01 - 0.11	0.01	0.00 - 0.03
Ba	470	276 - 874	954	528 - 1365	350	0 - 959
Nb	31	27 - 42	30	0 - 58	31	25 - 45
Zr	128	76 - 228	180	8 - 635	112	84 - 175
Y	67	39 - 106	70	4. - 153	66	36 - 143
Sr	26	18 -41	46	28 - 64	20	4 -44
Rb	185	147 - 213	166	136 - 231	184	157 - 240
Zn	44	24 - 113	48	23 -165	36	27 - 48
Cu	12	10 - 17	12	0 -16	12	10 - 14
Ni	5	3 - 8	5	1 - 9	5	0 - 7
Pb	27	24 -33	26	22 - 53	27	23 - 33
U	3	1 - 4	2	1 - 4	2	0 - 4
Th	20	13 - 24	18	0 - 29	21	14 - 27
V	4	0 - 7	7	0 -24	4	0 - 9
Cr	9	5 - 16	10	5 - 40	9	0 - 20
Nd	51	25 - 75	52	18 - 151	44	15 - 80
La	38	21 - 56	46	15 - 137	36	13 -73
Ce	84	42 -125	93	0 - 274	77	42 - 110
K/Rb	228	180 - 273	251	29 - 308	227	166 - 264

Total Fe given as Fe_2O_3. Major oxides as wt %, trace elements in ppm. 153 samples. (31 Group 1; 123 Group 2; 30 Group 3.)

Figure 5.17. Chondrite normalised incompatible element plot showing the average concentrations of selected trace elements for the three petrographically defined groups within the coarse granite. Group 1 diamonds, Group 2 crosses, Group 3 circles.

Fig. 5.17.

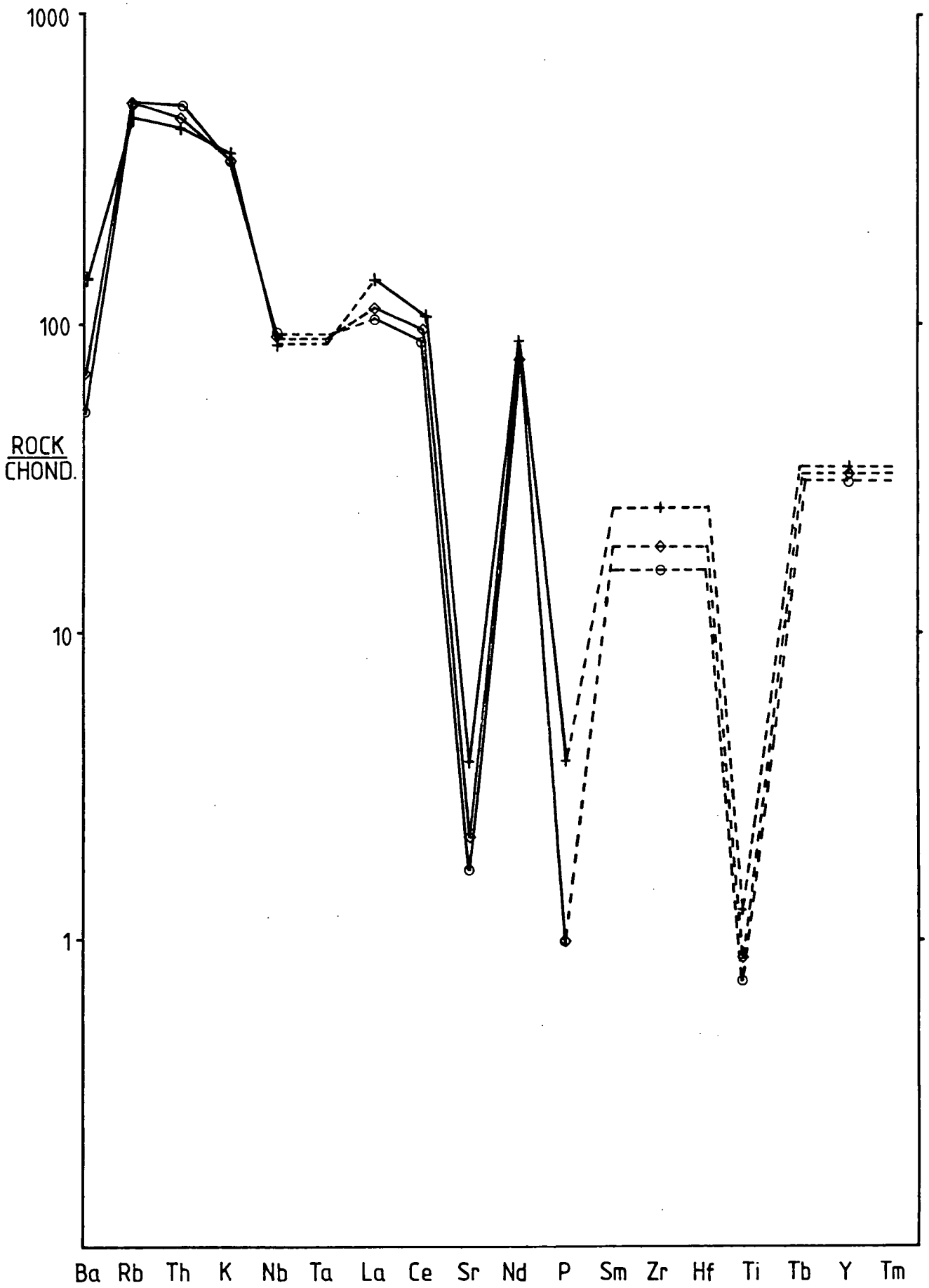
1000
100
ROCK
CHOND.
10
1
Ba
Rb
Th
K
Nb
Ta
La
Ce
Sr
Nd
P
Sm
Zr
Hf
Ti
Tb
Y
Tm

that Ba is depleted as Rb increases in the three groups. Incompatible element diagrams for the Dalradian indicate that significant contamination would produce an increase in both Ba and Rb. Ba would increase more rapidly than Rb with increasing contamination because the Dalradian has a high Ba/Rb ratio ($\approx$ 6.0) than the average for the coarse granite ($\approx$ 3.5). Similarly contamination would cause an increase in K/Rb, while fractionation would produce a fall, as is observed. Hence it is concluded that the textural and chemical variations in the coarse granite are the result of fractionation of a single magma body.

It is clear that the major element chemistry of the magma controlled the assemblage of fractionating phases. Al, Ca, Na and K all fall with increasing silica (Figs. 5.8 to 5.11). This is consistent with crystallisation and removal of orthoclase and plagioclase feldspar. The rocks of groups 1 and 3 are depleted in Al and Ca with respect to rocks of group 2, but generally have higher K. This is consistent with the higher modal plagioclase recorded in the group 2 rocks. Na does not show a clear distribution between the three groups. This must be due to solid solution of this element in orthoclase feldspar (which is confirmed by their cryptoperthitic texture, section 5.2). Hence it appears that the group 2 rocks are the least fractionated. Plagioclase appears, on the basis of this chemical data, to have been the dominant liquidus phase early in the crystallisation sequence followed by orthoclase. This is consistent with theoretical fractionation paths for granitic magmas (Fig. 5.18). The isotope data indicates the granite magma evolved from its basaltic parent by fractionation of an Sr bearing phase (probably plagioclase). Plagioclase would have remained on the liquidus following fractionation to be joined by orthoclase and subsequently quartz as the magma became saturated in these phases. With reference to the system ~~quartz~~ anorthite – albite – orthoclase (Tuttle & Bowen, 1958; Fig. 5.18), plagioclase could be precipitated from the melt until the melt composition reached the boundary curve between the plagioclase solid solution plus liquid field and the orthoclase plus liquid field.

Figure 5.18. Fractional crystallisation of a liquid of initial composition L. Initial fractionation of plagioclase causes the liquid composition to evolve to composition A where it meets the boundary curve between the plagioclase solid solution plus liquid and the orthoclase solid solution plus liquid fields. Between A and B the liquid precipitates plagioclase and increasing amounts of orthoclase. Between B and C plagioclase is resorbed and sodic orthoclase is precipitated. Between C and D a single feldspar is precipitated (after Tuttle & Bowen, 1958).

Fig. 5.18.

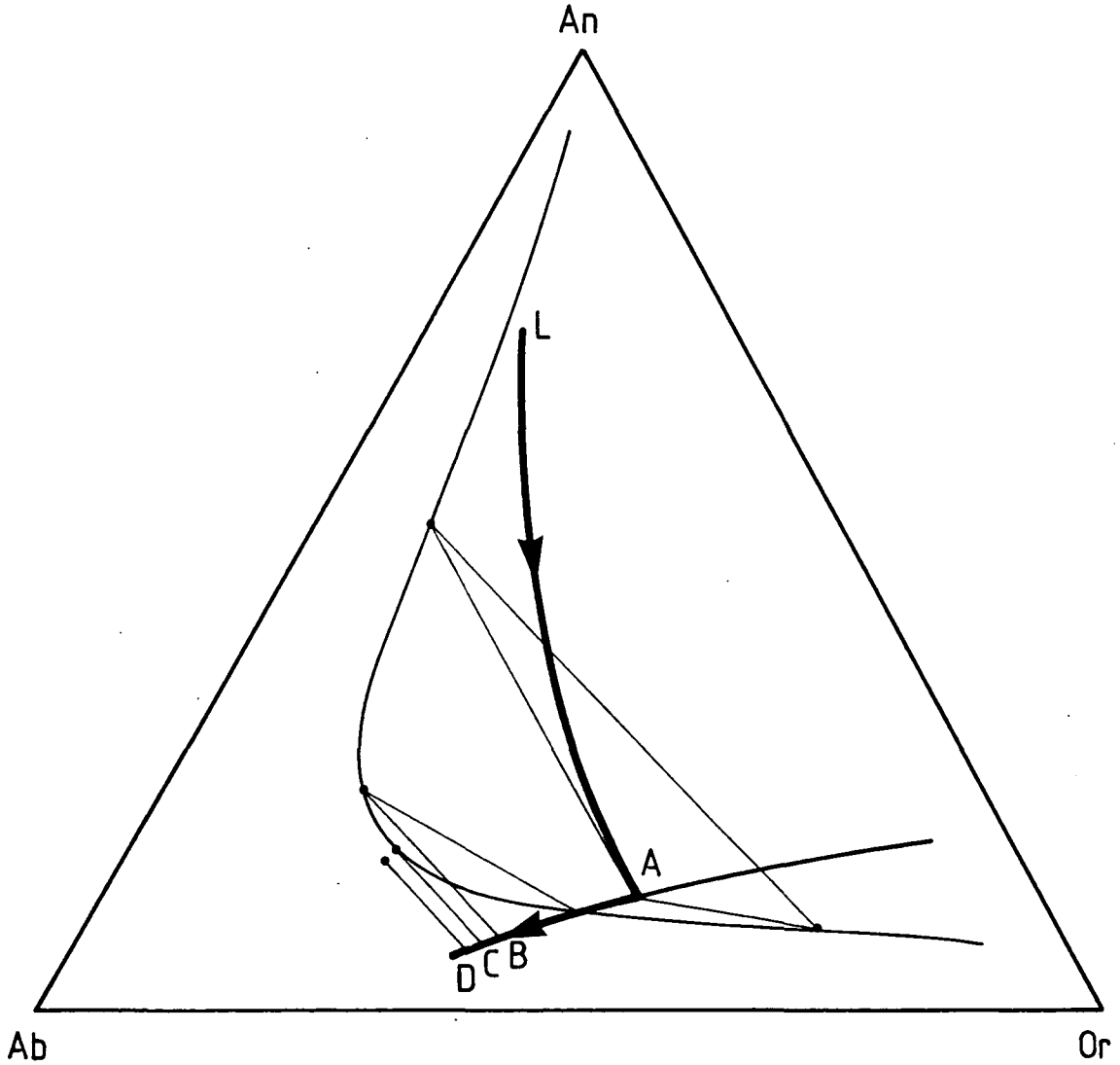

From this point orthoclase would begin to crystallise in increasing proportions with plagioclase. As crystallisation progressed the percentage of orthoclase precipitating from the melt would eventually exceed that of plagioclase. Had the orthoclase component crossed the intersection of the boundary curve at the limit of solid solution plagioclase would have been resorbed. This process has has not been verified for the coarse granite since no microprobe analyses of co-existing feldspars or determination of their relative proportions were carried out as part of this study. There is no evidence of resorption of plagioclase.

Plots of Ba, Sr and Rb against SiO_2 show a number of important features (Figs. 5.19, 5.20 & 5.21). Although the division between the three groups of rocks was made on petrographic grounds the range of variation in Ba and Sr for each of the three groups indicates that the contours at 600 ppm Ba and 30 ppm Sr were appropriate for subdividing the groups on the geochemical variation maps (Figs. 5.15 & 5.16). The bulk of the group 2 rocks contain concentrations of Ba in excess of 600 ppm and Sr concentrations in excess of 30 ppm and the group 1 and 3 rocks have concentrations lower than these values. There is, as noted earlier, some internal variation within the groups which cross this subdivision, but the overall classification of the groups remains consistent.

Those rocks strongly depleted in both Ba and Sr (which belong to group 3) also show a depletion in SiO_2 of the order of 5% with respect to the projected evolution of the granite. This is interpreted as the result of quartz becoming the dominant fractionating phase in the group 3 rocks. This would be consistent with fractionation by gravitational settling since in evolved melts quartz (s.g. 2.65) may have a slightly higher specific gravity (s.g.) than the feldspars (s.g. 2.56–2.63) and hence would sink faster. (Data from Deer et al., 1966). The plot of Rb against SiO_2 (Fig. 5.21) indicates that Rb does not increase with increasing SiO_2, as might be expected when plotting two incompatible elements against each other. This implies that SiO_2 is not strictly incompatible in the coarse granite.

Figure 5.19. Ba (ppm) plotted against SiO_2 (wt %) for the 153 samples representative of the three groups of the coarse granite. (Diamonds – group 1; crosses – group 2; circles – group 3.)

Fig. 5.19.

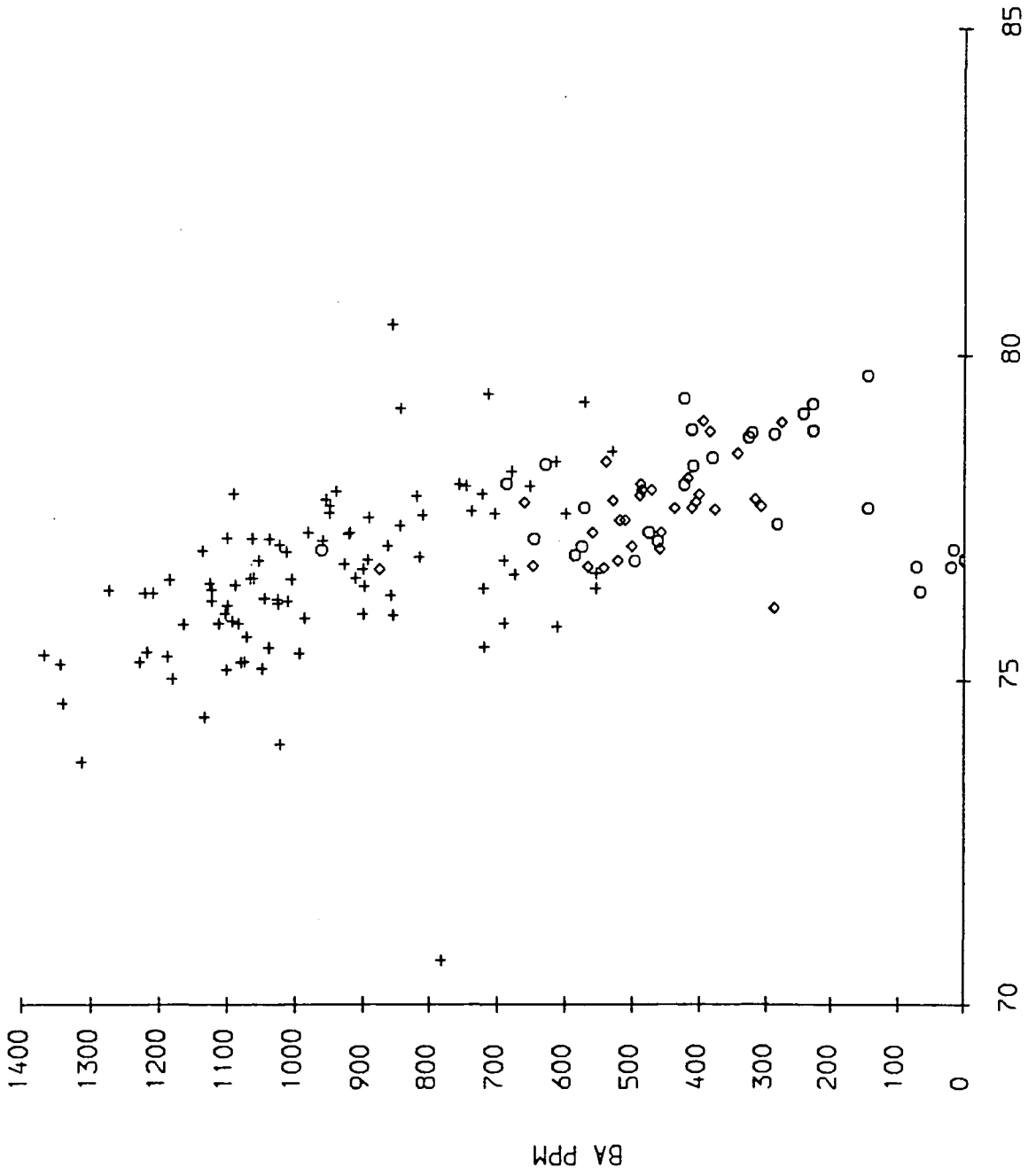
BA ppm
1400
1300
1200
1100
1000
900
800
700
600
500
400
300
200
100
0
70
75
80
85
SIO2 WHT%

Figure 5.20. Sr (ppm) plotted against SiO_2 (wt %) for the 153 samples representative of the three groups of the coarse granite. (Diamonds – group 1; crosses – group 2; circles – group 3.)

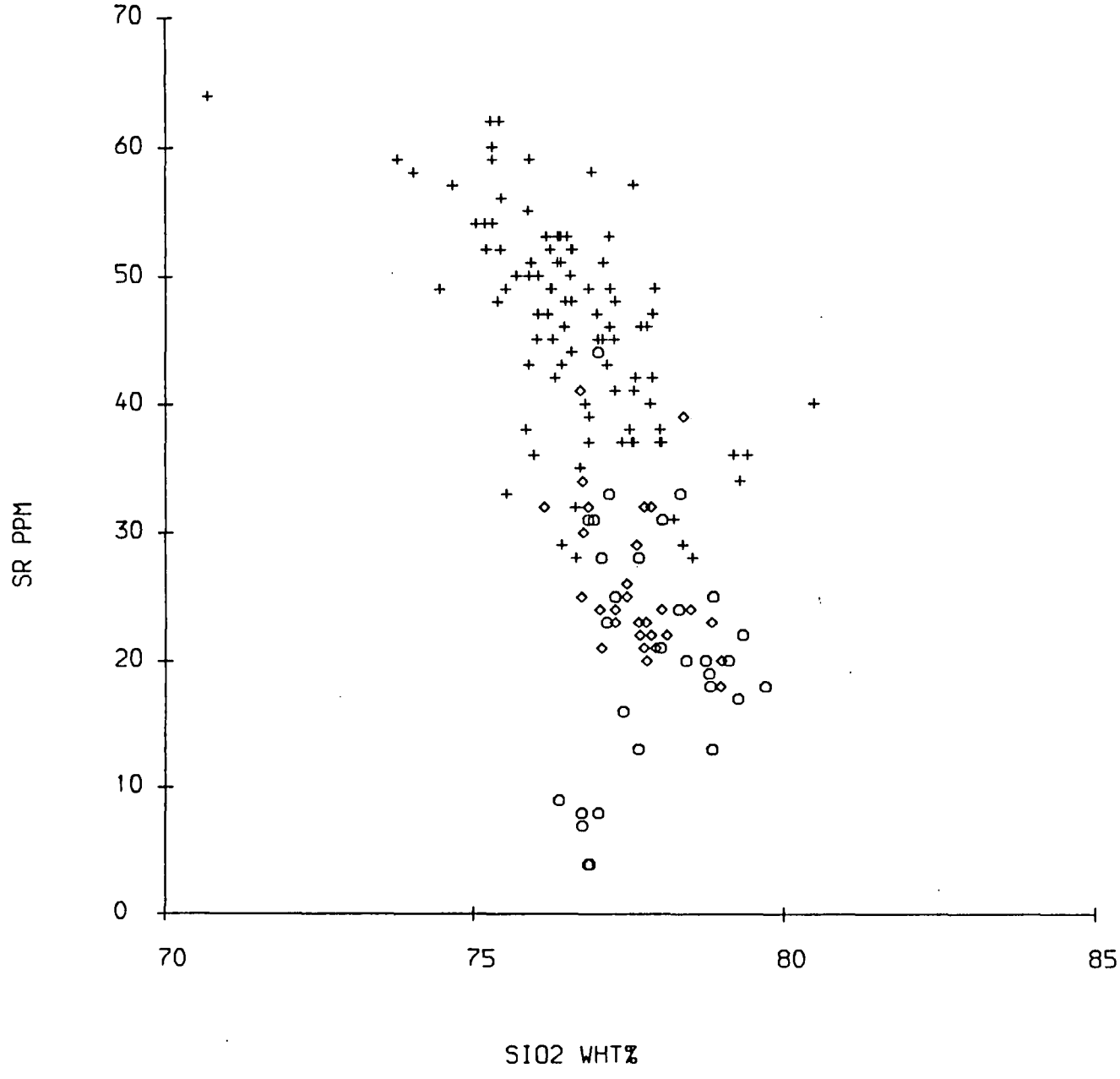

Fig. 5.20.

Figure 5.21. Rb (ppm) plotted against SiO_2 (wt %)for the 153 samples representative of the three groups of the coarse granite. (Diamonds – group 1; crosses – group 2; circles – group 3.)

Fig. 5.21.

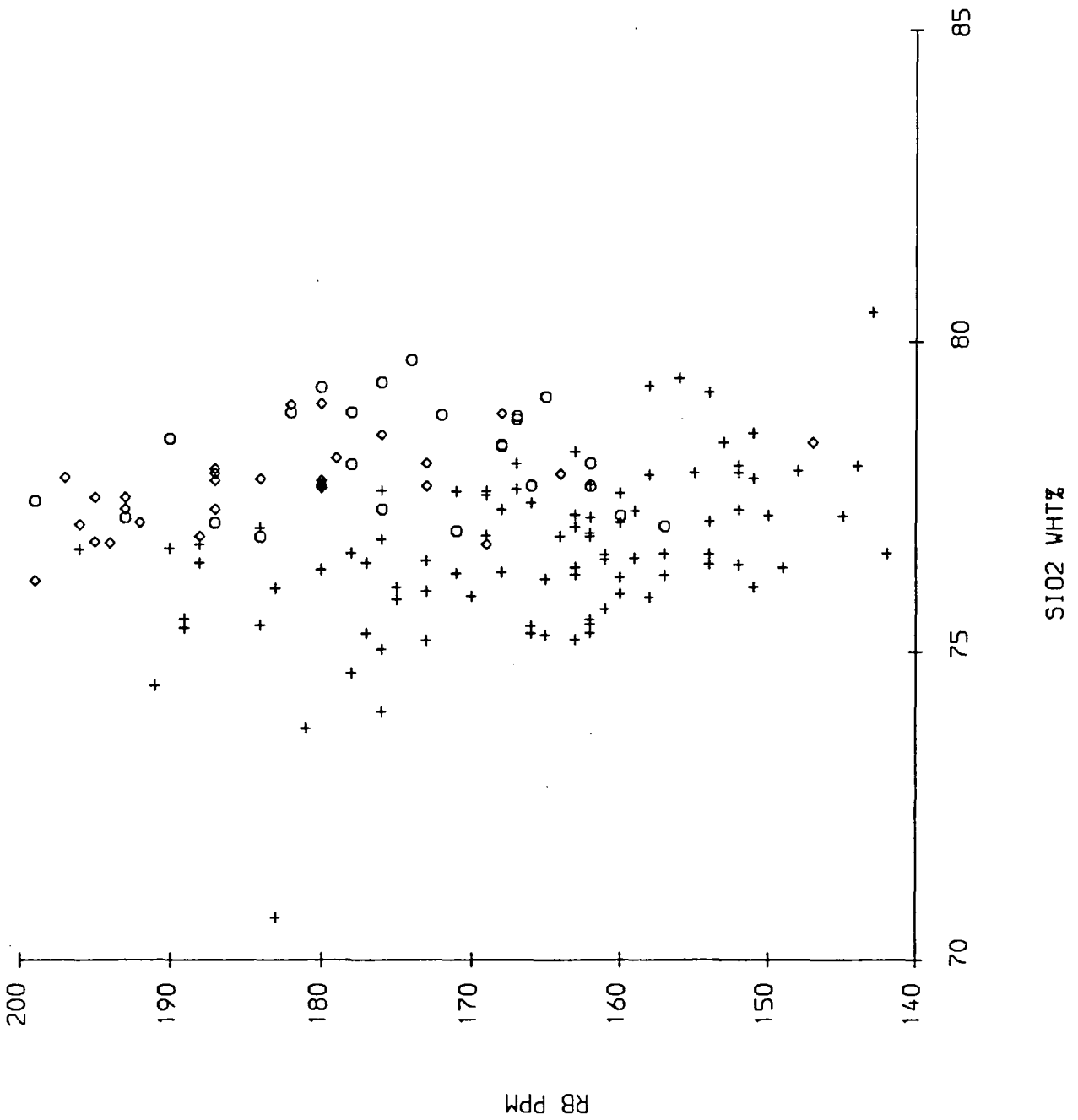

Quartz occurs as a phenocryst phase in addition to orthoclase and plagioclase. This indicates that the northern granite evolved to a minimum melting point composition, which is consistent with a progression of the experimental crystallisation sequence described above. The quartz depleted rocks are known to be strongly evolved because they have the highest Rb concentrations on plots of Ba and Sr against Rb (Figs. 5.22 & 5.23). Rb behaves as an incompatible element in the northern granite as it is not compatible in any of the crystallising phases, with the exception of biotite which only occurs in minor amounts.

Meighan et al. (1984) used a plot of TiO_2, depleted in the coarse granite by some fractionation of Ti-oxide, against K/Rb, which falls with inceasing fractionation due to relative concentration of incompatible Rb in the melt, to distinguish between subtypes of the Mourne G4 and G5 granites. When the Arran data are plotted on this diagram (Fig. 5.24) there is an overlap between the three groups due to the restricted range in TiO_2 composition. Groups 1 and 3 can be separated from 2 at a K/Rb ratio of 225, although there is a great deal of overlap which is ascribed to the extremely evolved nature of the rocks.

The distribution of the three groups of rocks within the pluton indicates that 'evolved' group 1 rocks lie on the outside of the less evolved group 2 rocks which enclose the most evolved group 3 rocks (Figs. 5.15 & 5.16). Well documented examples of horizontally zoned plutons e.g. Tuolumne Intrusive series (Bateman & Chappell, 1979) and Santa Rosa (Peru) (Atherton, 1981) clearly show 'normal' zoning from least evolved to most evolved compositions from the edge of the pluton to their cores. Such patterns can be attributed to fractionation of the original magma body. Where sharp discontinuities occur they have been attributed to bouyant upward movement of evolved, less dense, more felsic magma through the solidifying walls of the chamber. This commonly results in deformation of the crystallising chamber walls which produces a penetrative fabric similar to those seen in gneissic rocks. It is clear that the northern granite is not normally zoned.

Figure 5.22. Ba (ppm) plotted against Rb (ppm) for the 153 samples representative of the three groups of the coarse granite. (Diamonds – group 1; crosses – group 2; circles – group 3.)

Fig. 5.22.

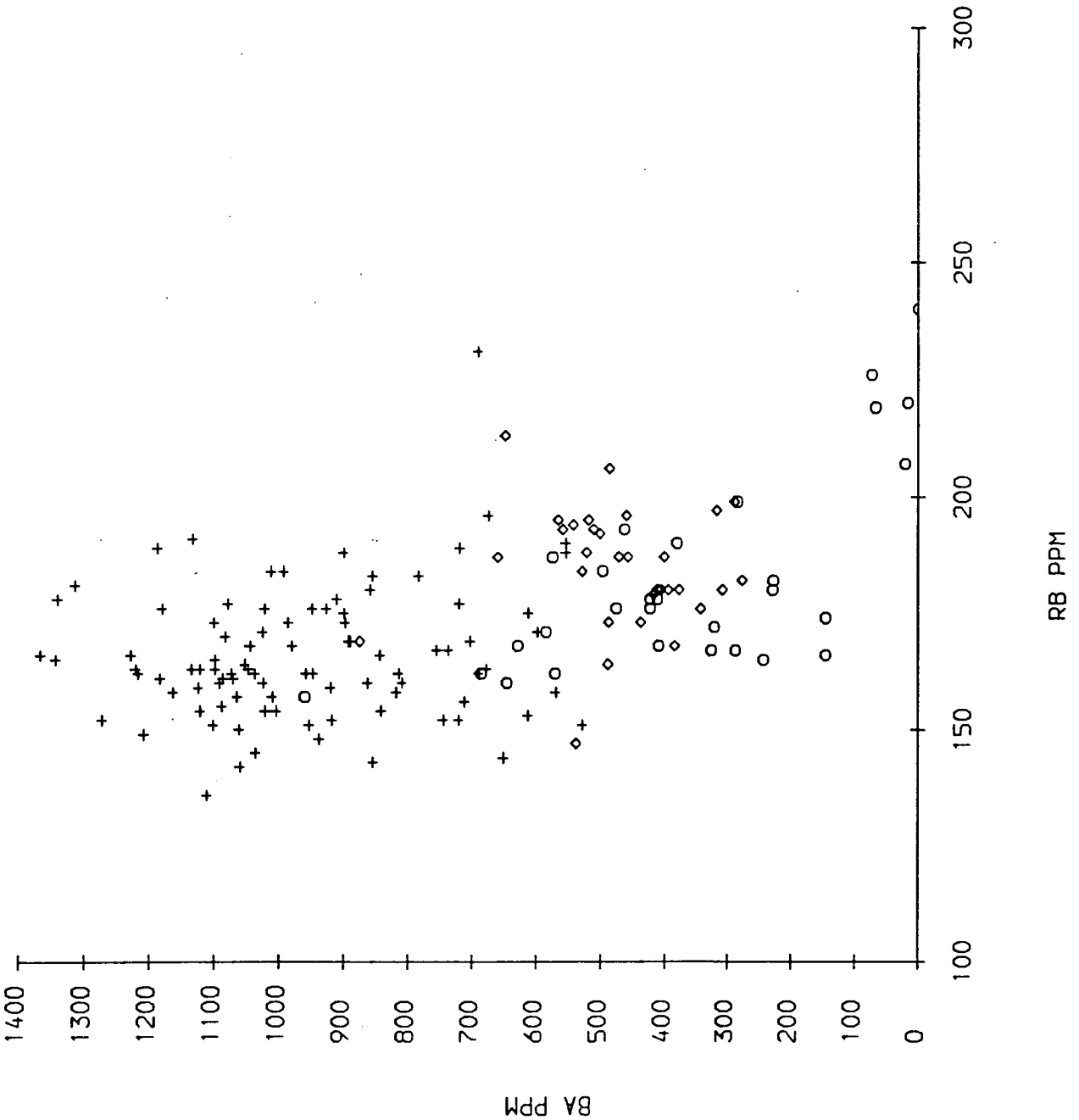
RB PPM
100
150
200
250
300
BA PPM
0
100
200
300
400
500
600
700
800
900
1000
1100
1200
1300
1400

Figure 5.23. Sr (ppm) plotted against Rb (ppm) for the 153 samples representative of the three groups of the coarse granite. (Diamonds – group 1; crosses – group 2; circles – group 3.)

Fig. 5.23.

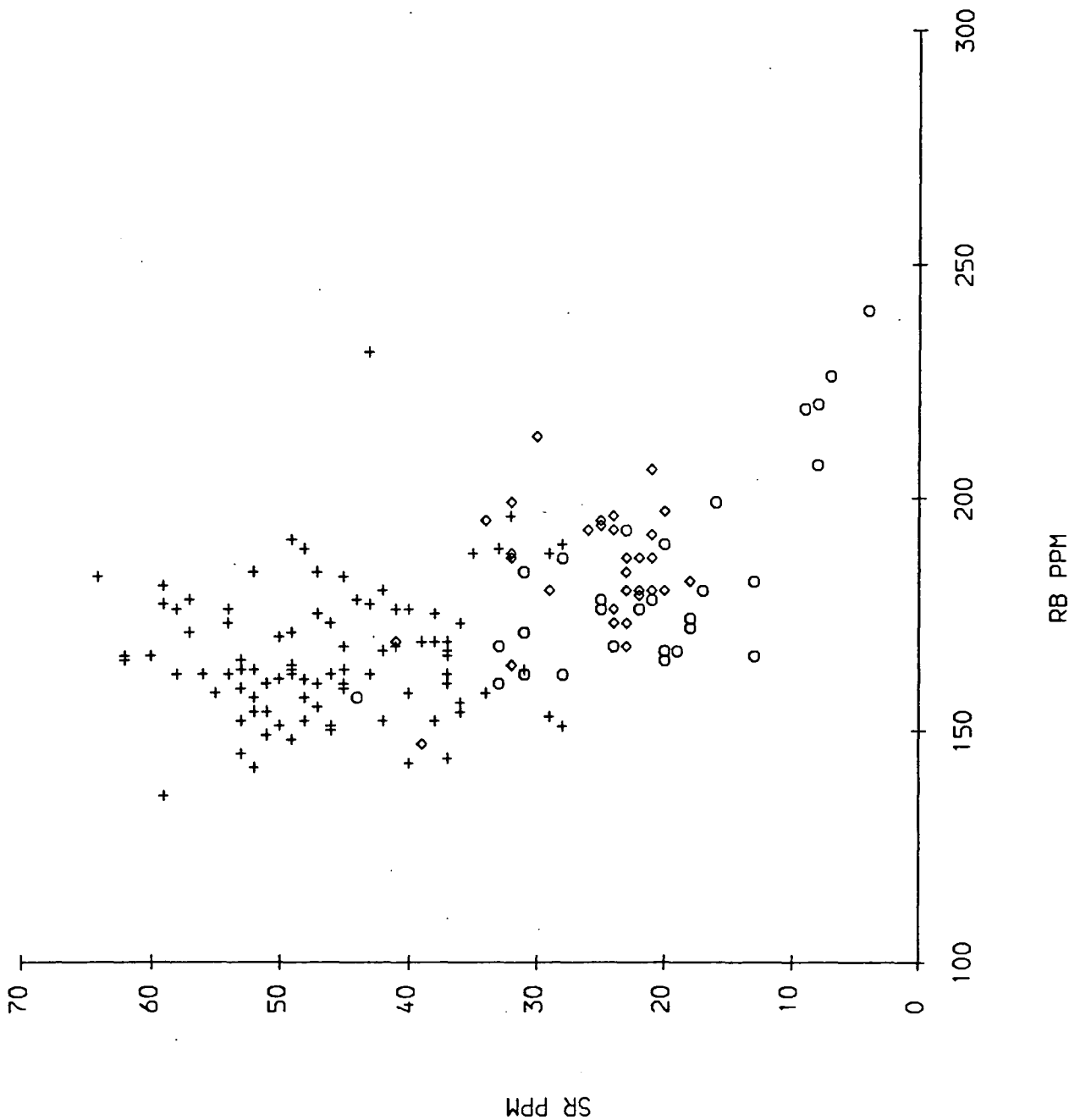

Figure 5.24. TiO_2 (wt %) plotted against K/Rb for the 153 samples representative of the three groups of the coarse granite. (Diamonds – group 1; crosses – group 2; circles – group 3.)

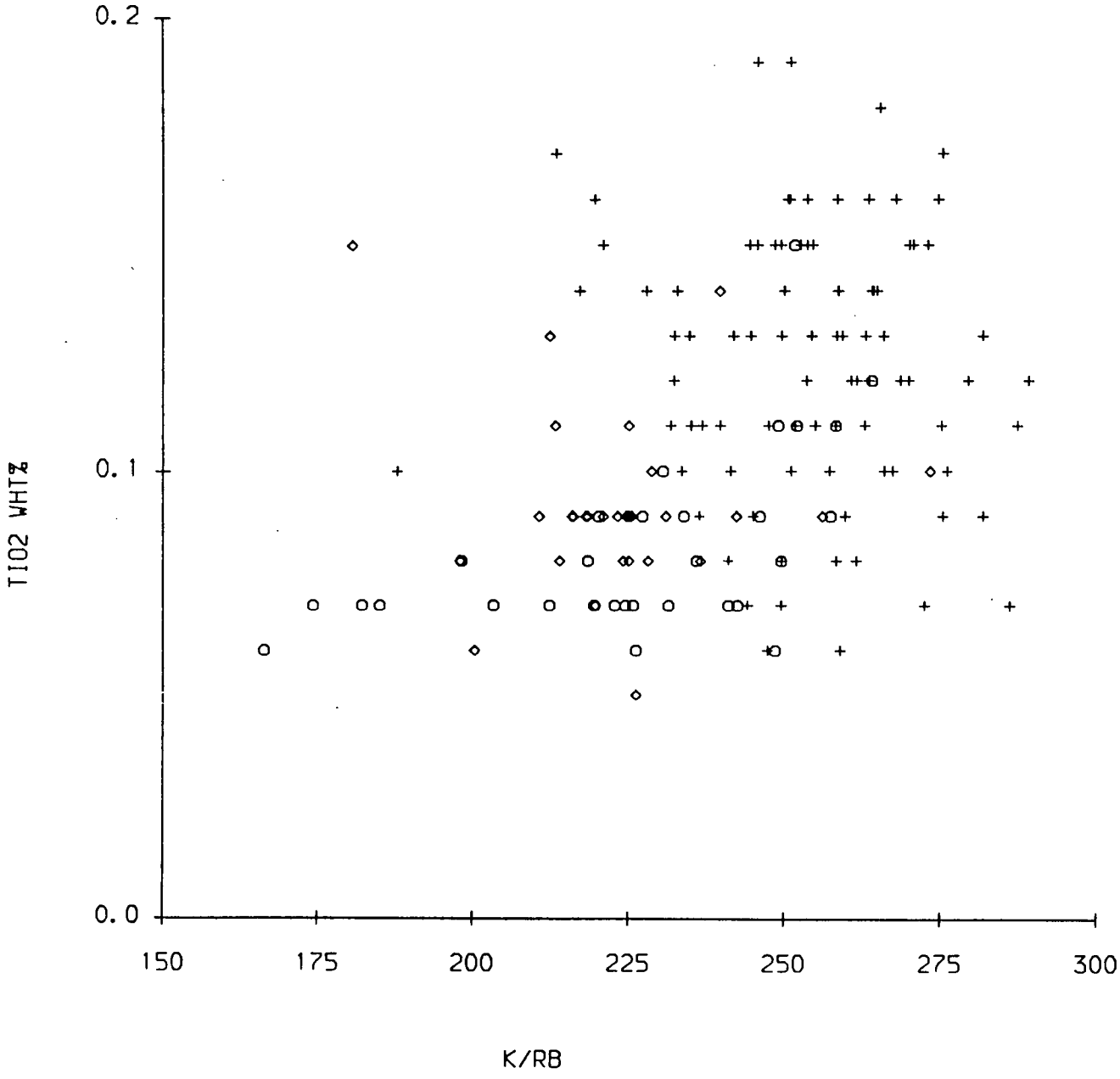

Fig. 5.24.

Bateman & Chappell (1979) argued that the zonation of the Tuolumne intrusive series resulted from either crystal settling or marginal accretion of crystals. They noted that if crystal settling was the only differentiation process operating the different components of the series (which are intrusive into each other and hence represent bouyant liquid) would have the same composition as the liquid from which they solidified. Hence the composition of the marginal granites would represent the composition of the undifferentiated magma as it was intruded, and the granite closer to the core would represent the composition of the evolving liquid. If selective marginal accretion of crystals occurred (with or without some crystal settling) none of the granites within the pluton would be a good representative of the composition of the magma from which they solidified, with the exception of those close to the core. However the average composition of the pluton would represent the bulk composition of the magma before the sequence began to solidify. Both these processes assume that there was no further input of magma into the pluton during crystallisation, which may occur (Hill et al., 1985).

Fractional crystallisation of granitic magmas is considered to be inhibited by the physical properties of the magma (Shaw, 1965). There is little or no density contrast between alkali feldspar and quartz and the melt from which they precipitate, to promote gravitational settling. Recorded examples of layering in granites suggest it is the mafic phases (biotite, allanite, magnetite and sphene) and plagioclase (An_{30}) megacrysts which separate from the liquid (Emeleus, 1963; Meighan, 1979). The higher viscosity of acid magmas may also prevent effective separation of crystals from the melt.

The process of marginal accretion of crystals is generally referred to as sidewall crystallisation. Recent work based on experimental investigations of the fluid dynamics of crystallising magma chambers (Sparks et al., 1984; Baker & McBirney, 1985; Turner & Campbell, 1986) indicated that this process could produce extremely fractionated liquids. Crystallisation on the margins of a magma chamber

would leave the adjacent liquid (or boundary layer) extremely depleted in those elements extracted to form the crystals. Laboratory experiments (McBirney et al., 1985) indicate that these evolved liquids may rise, due to chemical and/or thermal induced bouyancy toward the roof of the chamber where they may accumulate to form a vertically zoned intrusion. Spera et al. (1984) discussed this process in theoretical terms and concluded that while it may operate in basic magma chambers where chemical gradients due to sidewall crystallisation may be high, it is unlikely to occur in magma chambers containing highly evolved acidic melts since chemical gradients produced by fractionation would not be capable of producing the necessary density contrast for the fluid to migrate without the boundary layer breaking down. In rapidly convecting intrusions latent heat released during crystallisation would be convected away from the wall rocks and hence the stability of the boundary layer would depend on the presence of a strong chemical gradient. It seems that vertical layering in acid plutons is unlikely to be caused by transfer of evolved liquids along the walls of the magma chamber. Instead the evolved melt would be incorporated into the liquid reservoir at the core of the pluton. If the mixing process is complete, the effect of the evolved additions to the reservoir will be to deplete it in the elements concentrated in the crystals growing at the walls.

Brandeis & Jaupart (1986) argued that crystallisation would occur predominantly along the walls of silicic magma chambers. The high viscosity of the evolved liquid would mean that the time scales for nucleation and growth of crystals along the walls of the magma chamber would be short compared with the time required to erode the boundary layer by either upward flow or convection. This implies that substantial fractions of evolved melt could be trapped in the crystal mush developing at the chamber walls.

The nucleation of crystals at the sidewalls (sides, roof or floor) of a pluton would be controlled by heat loss through the walls which would result in super-

saturation of the melt. Crystals attached to the wall of the intrusion would grow initially as phenocrysts until they coalesced. Solidification beyond the point of coalescence would involve solidification of an interstitial groundmass. Experimental work by Winkler & Schultes (1982) indicates that phenocryst growth will continue until the rock is 70% crystallised. If crystallisation occurred rapidly the crystals would not equilibrate with the magma and hence they would become zoned.

Fractional crystallisation by complete separation of the precipitating crystals from the liquid appears to be inhibited in acidic melts, and the trapping of intersertal melt between phenocrysts during sidewall crystallisation indicates that the two possible differentiation processes involved in the formation of zoned plutons involve the crystallisation of crystal-liquid mushes. Consequently it may be that no true 'liquid line of descent' (Cox et al., 1979) can be constructed for plutonic granitic rocks. The high concentration of zoned phenocrysts (up to 80% in rocks of group 2) and limited development of a groundmass within the Northern Arran coarse granite indicates that the intrusion probably crystallised from a crystal-liquid mush following or produced during crystal-liquid differentiation.

McCarthy & Hasty (1976) produced a theoretical model for the chemical variation in granitic rocks solidifying from a crystal-liquid mush with variable amounts of crystal liquid separation. These authors based their model on batch equilibrium crystallisation which has as its end members equilibrium crystallisation (no separation of crystals which remain in equilibrium with the melt) and fractional crystallisation (complete separation of crystals which do not remain in equilibrium with the melt) The variation of the liquid composition C^l during batch equilibrium crystallisation is given by the equation:

$$\frac{C_n^l}{C^o} = \prod_{i=1}^{n} \left(\frac{1}{f_i(D_i - 1) + 1}\right) \qquad 5.1$$

and the solid component C^s is given by the equation:

$$\frac{C_n^s}{C^o} = D_n \prod_{i=1}^{n} \left(\frac{1}{f_i(D_i - 1) + 1}\right) \qquad 5.2$$

where

C^o = Initial liquid composition

D = Bulk distribution coefficient

f = Fraction of solid crystallised in equilibriun with the liquid

n = Increment of crystallisation

In the case of equilibrium crystallisation f is equal to 1 and hence all the solid crystallises in equilibrium with the liquid. Perfect fractional crystallisation occurs when f tends toward zero so that the solid is separated from the liquid immediately on crystallisation. Crystallisation of different proportions of solid in equilibrium with the liquid followed by separation of the crystals and liquid can be modelled by varying f between 0 and 1. Using these equations it is possible to plot the evolving compositions of liquids and solids produced by different values of f and for solids with varying proportions of interstitial melt (Fig. 5.25). The shape of the curves produced depends upon the chosen value of f and the respective D values for the compatible and incompatible elements plotted, and are independant of the initial melt composition which only constrains the starting point of the curves on the graph. A change in the liquidus assemblage or proportions of the crystals on the liquidus can be accommodated by changing the D value as appropriate.

A set of curves for Ba vs Rb and Sr vs Rb were plotted for the coarse granite using the distribution coefficients given in Table 5.4 and the phase proportions indicated by the petrography (Table 5.1). Since the proportions of quartz, alkali feldspar and plagioclase remain approximately the same for each group during crystallisation D was kept constant. Experimental data on element partitioning between basic and acid liquids, (Watson, 1976), indicate that the distribution coefficients K_Ds for Ba and Sr should increase in evolved (more acidic) melts as a result of increased polymerisation of the melt. Best fit curves were obtained using the maximum values of K_D^{Rb} given in Henderson (1982). Lower values of K_D^{Rb} produce shallower curves since the evolving liquid is depleted less rapidly

Figure 5.25a. Calculated compositional ranges for Ba vs Rb produced by fractional crystallisation of the coarse granite. Curve A–A' is the compositional trend for the precipitated solid. Curves B–B', C–C', D-D', E–E' and F–F' are for a magma composed of solid with 10, 20, 30, 40 and 50% interstitial evolved liquid. Compositions at intervals of 10% crystallisation of the original liquid (crosses) are shown on each curve.

Figure 5.25b. Calculated compositional ranges for Sr vs Rb produced by fractional crystallisation of the coarse granite. Curve A–A' is the compositional trend for the precipitated solid. Curves B–B', C–C', D-D', E–E' and F–F' are for a magma composed of solid with 10, 20, 30, 40 and 50% interstitial evolved liquid. Compositions at intervals of 10% crystallisation of the original liquid (crosses) are shown on each curve.

Fig. 5.25.a.

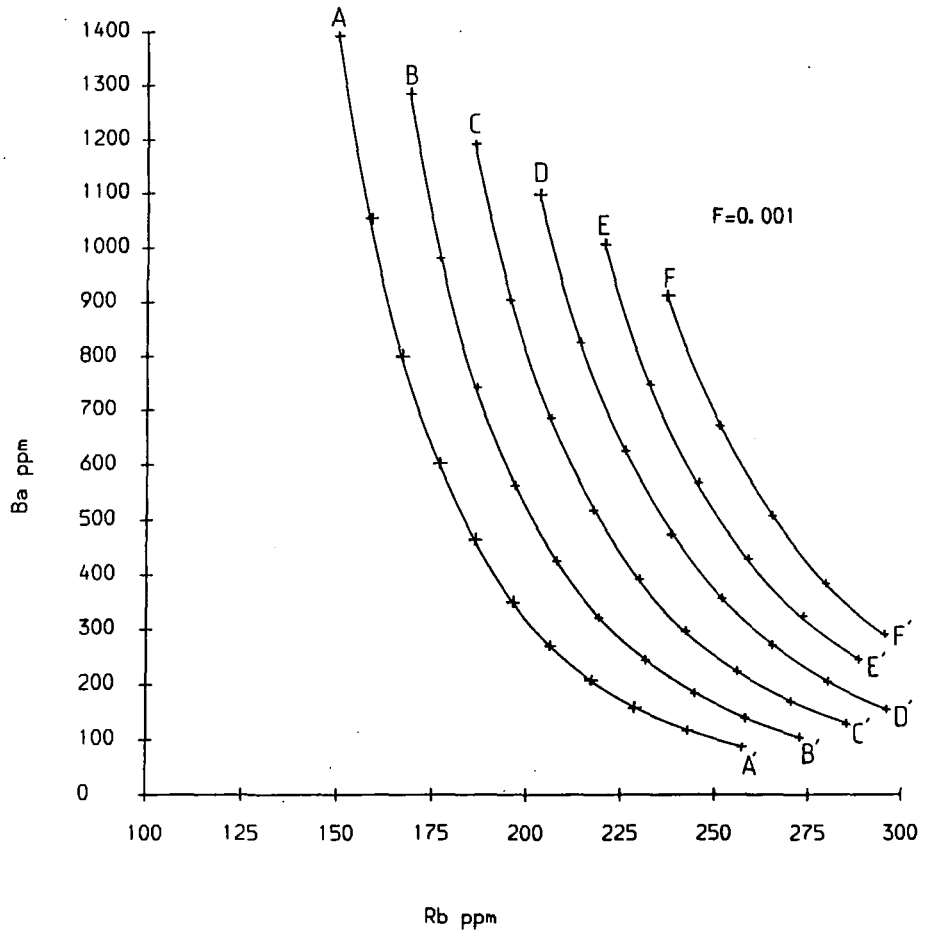

Fig. 5.25.b.

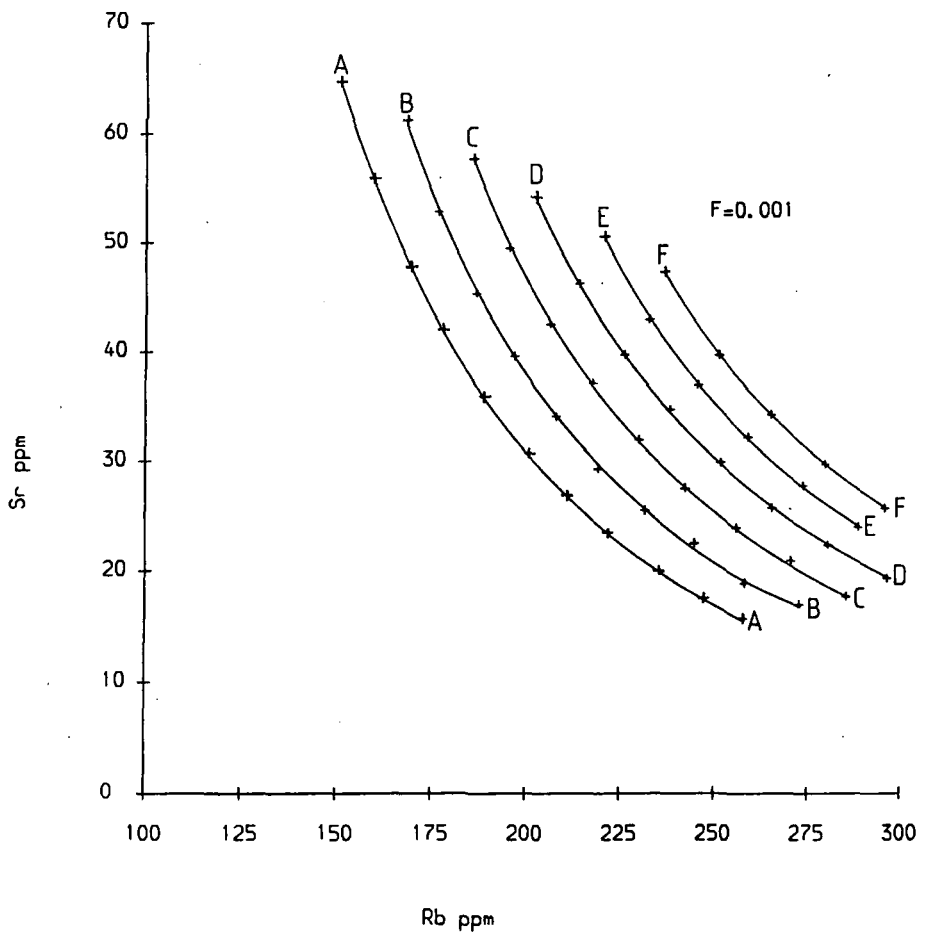

by crystallisation. This would be offset by an increase in K_D^{Ba} and K_D^{Sr} which would produce a steeper curve due to an increased rate of depletion of the liquid. In this case the conclusions of Watson (1976) have little effect in the plots used here to model the fractionation of the coarse granite, although it is recognised that Watson's (1976) results may explain the apparent depletion of Ba and Sr in samples of group 3. It was found that while these curves gave an approximate fit to the observed data for the coarse granite (Figs. 5.26 & 5.27) the petrographic characteristics for the three groups inferred by the modelling were not consistent with the petrographic data or the distribution of the three groups within the pluton.

The best fit curves for the modelled solid composition of the granite (and solid with 0 – 40% interstitial liquid) were produced using f=0.001) which approximates to fractional crystallisation with only minimal equilibrium between solid and liquid before separation. Higher values of f yielded curves with shallower slopes. The value of D also had to be increased to model the steep trend of the observed data. These curves indicated that the group 2 rocks were the least evolved and that groups 1 and 3 crystallised from a differentiated liquid produced by crystallisation of group 2. They also indicate that the group 2 rocks would contain a higher proportion of interstitial liquid than groups 1 and 3 (Fig. 5.25).

Petrographic data (section 5.2) indicates that the group 2 rocks contain the highest proportion of phenocrysts. Where group 2 rocks are chilled against the wall rocks they contain up to 40% phenocrysts, Rocks of group 1 contain up to 8% phenocrysts. The crystallisation sequence indicated by the distribution of the three groups is apparently group 1 and group 2 followed by group 3, assuming that the pluton crystallised from its outer margins toward its core by losing heat to its wall rocks. Crystallisation of group 1 rocks from a liquid depleted by the crystallisation of group 2 rocks would require the latter to be surrounded by liquid which seems unlikely for a magma losing heat through its outer margins. If the

Figure 5.26. Ba (ppm) plotted against Rb (ppm) for the 153 samples representative of the three groups of the coarse granite, (Diamonds – group 1; crosses – group 2; circles – group 3.) showing the best fit line for fractional crystallisation from Fig. 5.25a.

Fig. 5.26.

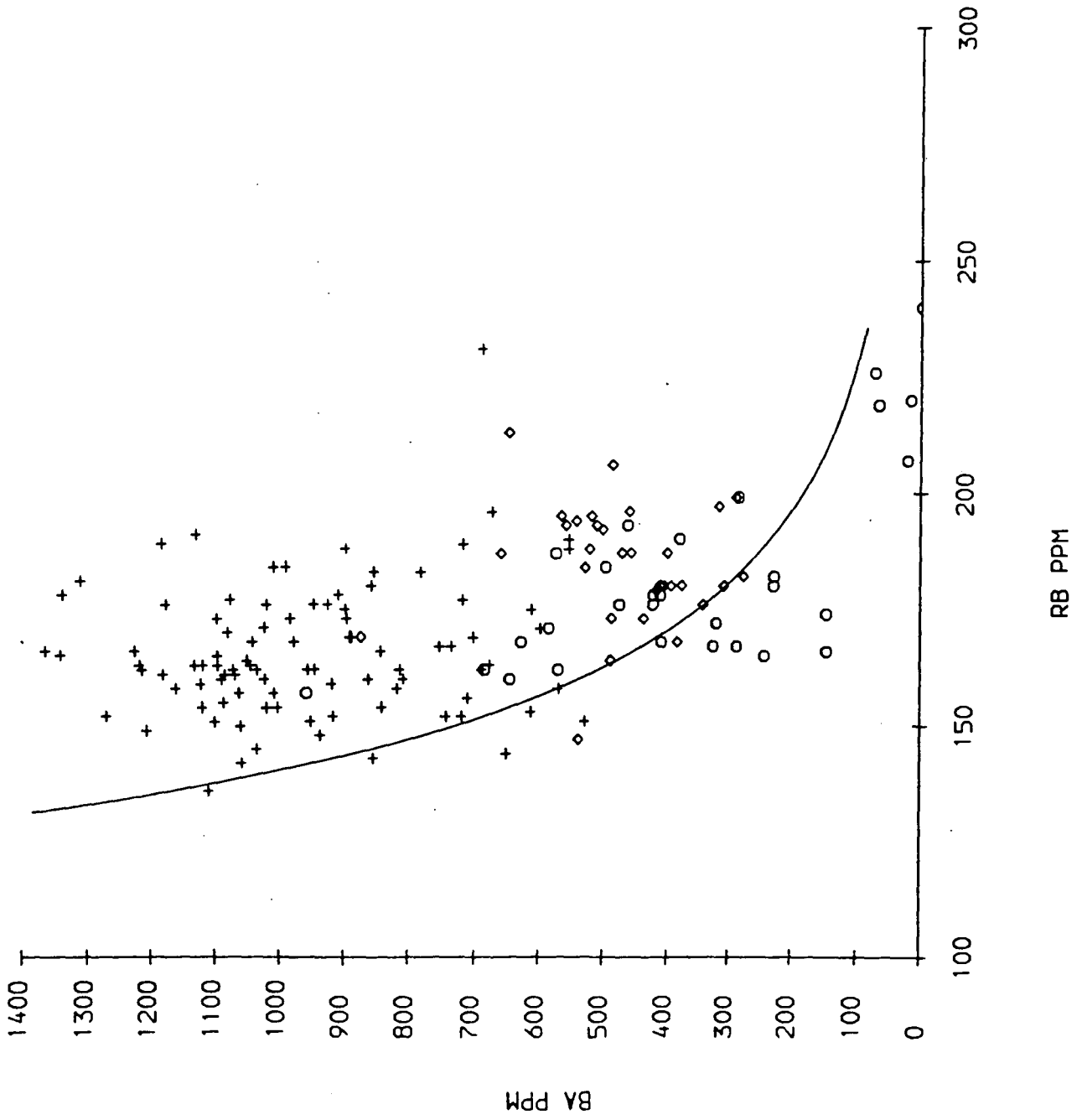
RB PPM
100
150
200
250
300
BA PPM
0
100
200
300
400
500
600
700
800
900
1000
1100
1200
1300
1400

Figure 5.27. Sr (ppm) plotted against Rb (ppm) for the 153 samples representative of the three groups of the coarse granite, (Diamonds – group 1; crosses – group 2; circles – group 3.) showing the best fit line for fractional crystallisation from Fig. 5.25b.

Fig. 5.27.

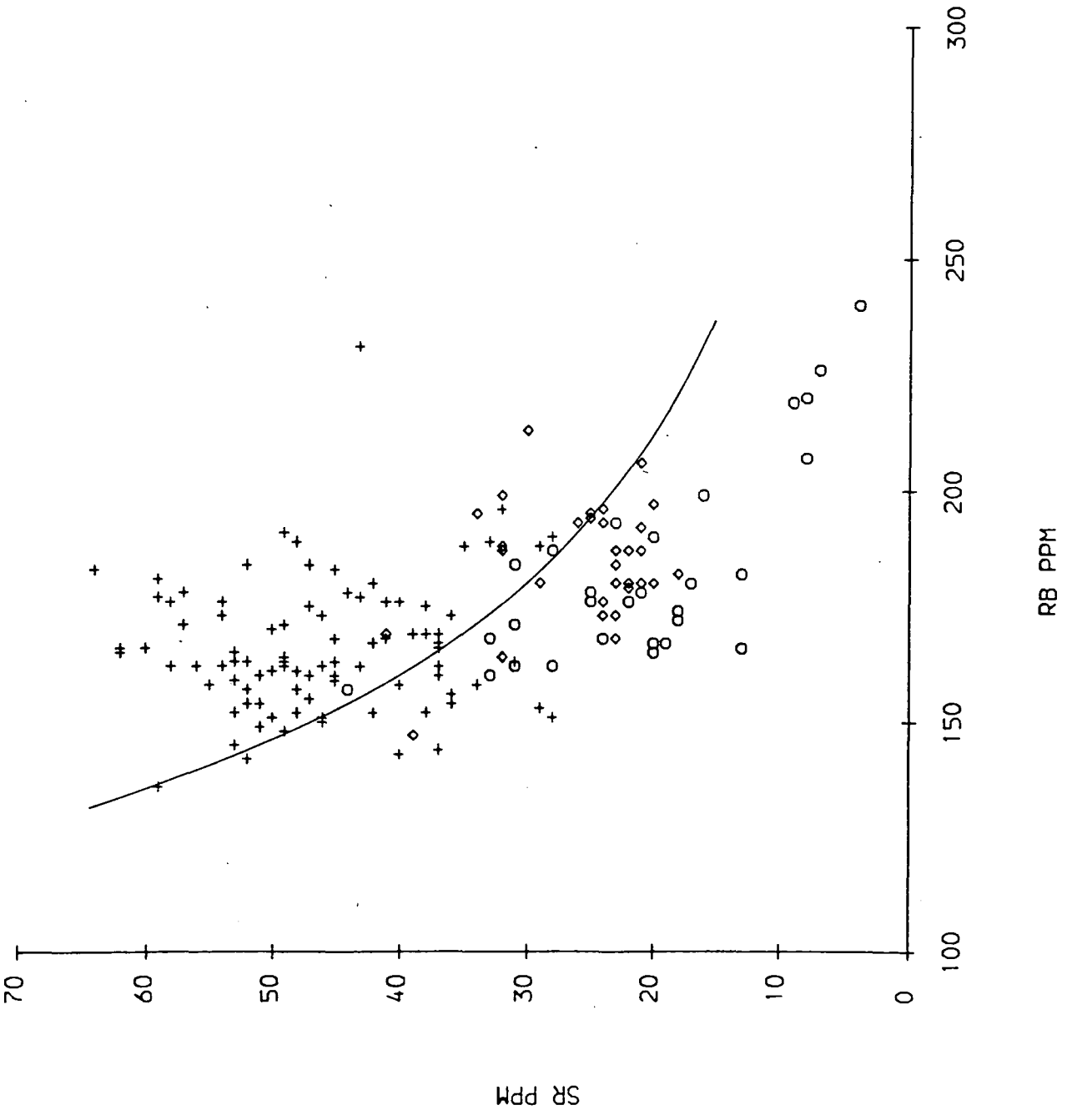

group 1 rocks were liquids Fig. 5.25 predicts that their Rb content should be much higher. On this basis it would appear that the variations in trace element composition in the coarse granite cannot be explained by simple crystal fractionation as the dominant differentiation mechanism.

Sidewall crystallisation was modelled by assuming a spherical body of magma (minimum surface area to volume ratio) and a boundary layer 10 m thick. A spherical body was chosen as the best approximation to the shape of the coarse granite, as deduced from structural data (Chapter 4). The actual thickness of the boundary layer in the Arran granite is not known. This would depend upon the rate of heat loss through the wall and the chemical and thermal diffusivities of the depleted liquid (Spera et al, 1984). A minimum surface area to volume ratio for the pluton was also used to minimise the effects of inaccurate assumptions about the physical properties of the boundary layer. Evolution of the boundary layer was modelled assuming 50% and 30% equilibrium crystallisation to produce a layer of evolved liquid. It was assumed that some of the evolved liquid remained trapped between growing phenocrysts during remixing of the evolved liquid with the undifferentiated reservoir at the core of the pluton. The volume of trapped liquid was set at 30% of the crystal liquid mush formed at the wall of the intrusion. This value is consistent with the 70:30 solid to liquid ratio observed experimentally for the cessation of phenocryst growth (Winkler & Schultes, 1984), and the point at which the mush would attain the rheological properties of a solid (Arzi, 1978). In reality variations in porosity may result in volumes of liquid > 30% of the mush being trapped.

If fractional crystallisation had been used in the modelling, rather than equilibrium crystallisation, this would have implied immediate separation of crystals from the liquid from which they crystallised. This is unrealistic if a boundary layer is to evolve and is not consistent with the theoretical conclusions of Brandeis & Jaupart (1986). Fractional crystallisation would also cause extreme depletion of

the liquid in the boundary layer. This would have a number of effects. Firstly all crystals growing on the wall would be zoned. In the case of the coarse granite not all the phenocrysts show zoning, although some do. There is no evidence of subsolidus recrystallistion which might have obliterated the zoning, hence petrographic evidence is not consistent with fractional crystallisation, but is compatible with equilibrium crystallisation and trapping of phenocrysts derived from the liquid reservoir at the core of the pluton. which is discused below. Secondly when the extremely differentiated liquid is remixed with the reservoir at the core of the pluton the reservoir will also be depleted more rapidly than if equilibrium crystallisation was operating. This would result in steeper chemical gradients across the pluton than would result from equilibrium crystallisation. Equilibrium crystallisation does not produce extremely differentiated liquids. (e.g. 50% and 30% fractional crystallisation of solids with bulk a distribution coefficient of 3.79 from a liquid with an initial composition of 650 ppm, ~~with bulk distribution of 3.79~~ yields liquids with compositions of 93 and 240 ppm respectively. Equilibrium crystallisation of the same proportions of the same solid from the same liquid yields a liquid with 271 and 353 ppm.) Such strongly evolved liquids as those produced by fractional crystallisation are not recorded in the sample of rocks collected from the coarse granite. Initially the distribution coefficients used for modelling fractional crystallisation were used for modelling sidewall crystallisation. These proved to produce too shallow a curve which was a poor fit to the observed data. A good fit was obtained by increasing K_D^{Rb} to 0.8. Variations in D due to polymerisation (Watson, 1976) may not be effective during sidewall crystallisation except during the last increment of crystallisation since the reservoir does not become strongly fractionated until approximately 95% of the pluton has crystallised.

Sidewall crystallisation of the coarse granite was modelled using the conclusion of Bateman & Chappell (1979) that the average composition of the pluton would represent the initial melt composition for a pluton crystallising by marginal

accretion of crystals (with or without crystal settling). If 50% crystallisation of the boundary layer is assumed it is not possible to model the complete range of compositions shown by the coarse granite (Figs. 5.28 & 5.29). However a reduction in crystallisation at the sidewall to 30% results in crystallisation of crystal-liquid mushes at the walls which have significantly higher Ba and Sr compositions, comparable with the range of compositions of group 2 rocks (Figs. 5.30 & 5.31). As with the models for fractional crystallisation the initial composition has no effect on the shape of the calculated evolution curves which are dependant upon the degree of crystallisation in the boundary layer and the bulk distribution coefficients chosen for those elements whose variation is being modelled.

Decreasing the degree of crystallisation in the boundary layer increases the concentration of compatible elements in the solid and decreases the concentration of incompatible elements (cf Figs. 5.28 & 5.29 with 5.30 & 5.31). This results in more rapid depletion and enrichment of compatible and incompatible elements in the reservoir. Figures 5.32, 5.33 & 5.34 show calculated element variation profiles for a spherical pluton of 5 km radius. These show rapid depletion of the compatible elements (particularly Ba) and enrichment of Rb toward the centre of the pluton, which increases rapidly during crystallisation of the last 5% of the liquid.

Comparison of these profiles (Figs. 5.32, 5.33 & 5.34) with Figs. 5.15 and 5.16 shows an approximate correlation between the radius of the pluton and concentrations of Ba and Sr for the modelled and observed data along a cross section through group 2 and group 3 rocks. Figures 5.35 and 5.36 show the observed variation in Ba and Sr against distance from the centre of the pluton for 74 samples plotted against the modelled variation. These plots show there is considerable variation in composition at a given radius contrary to the calculated variation. This is partly the result of the irregular radius of the group 3 rocks, which may reflect different rates of cooling along different radii. The critical feature of these figures is that the bulk of the group 2 rocks plot above the 70% solid / 30% liquid

Figure 5.28. Ba (ppm) plotted against Rb (ppm) for the 153 samples representative of the three groups of the coarse granite. (Diamonds – group 1; crosses – group 2; circles – group 3.) The plot includes curves calculated for sidewall crystallisation involving 50% equilibrium crystallisation of the boundary layer. The curves indicate (from left to right) 100% solid crystallised from the boundary layer; solid crystallised from the boundary layer with 30% interstitial evolved liquid; composition of the reservoir of liquid in the core of the pluton.

Fig. 5.28.

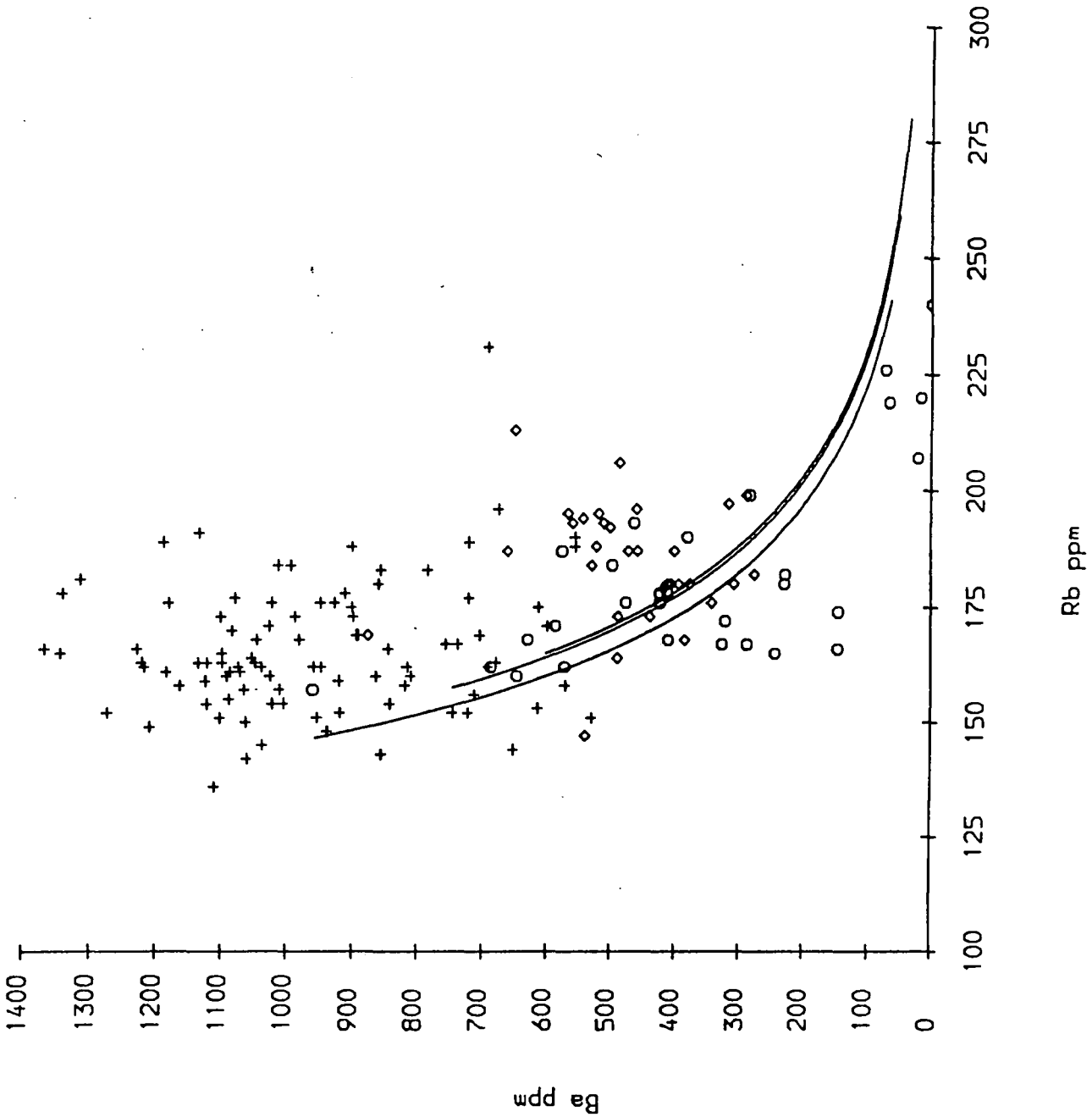
Ba ppm
1400
1300
1200
1100
1000
900
800
700
600
500
400
300
200
100
0
Rb ppm
100
125
150
175
200
225
250
275
300

Figure 5.29. Sr (ppm) plotted against Rb (ppm) for the 153 samples representative of the three groups of the coarse granite. (Diamonds – group 1; crosses – group 2; circles – group 3.) The plot includes curves calculated for sidewall crystallisation involving 50% equilibrium crystallisation of the boundary layer. The curves indicate (from left to right) 100% solid crystallised from the boundary layer; solid crystallised from the boundary layer with 30% interstitial evolved liquid; composition of the reservoir of liquid in the core of the pluton.

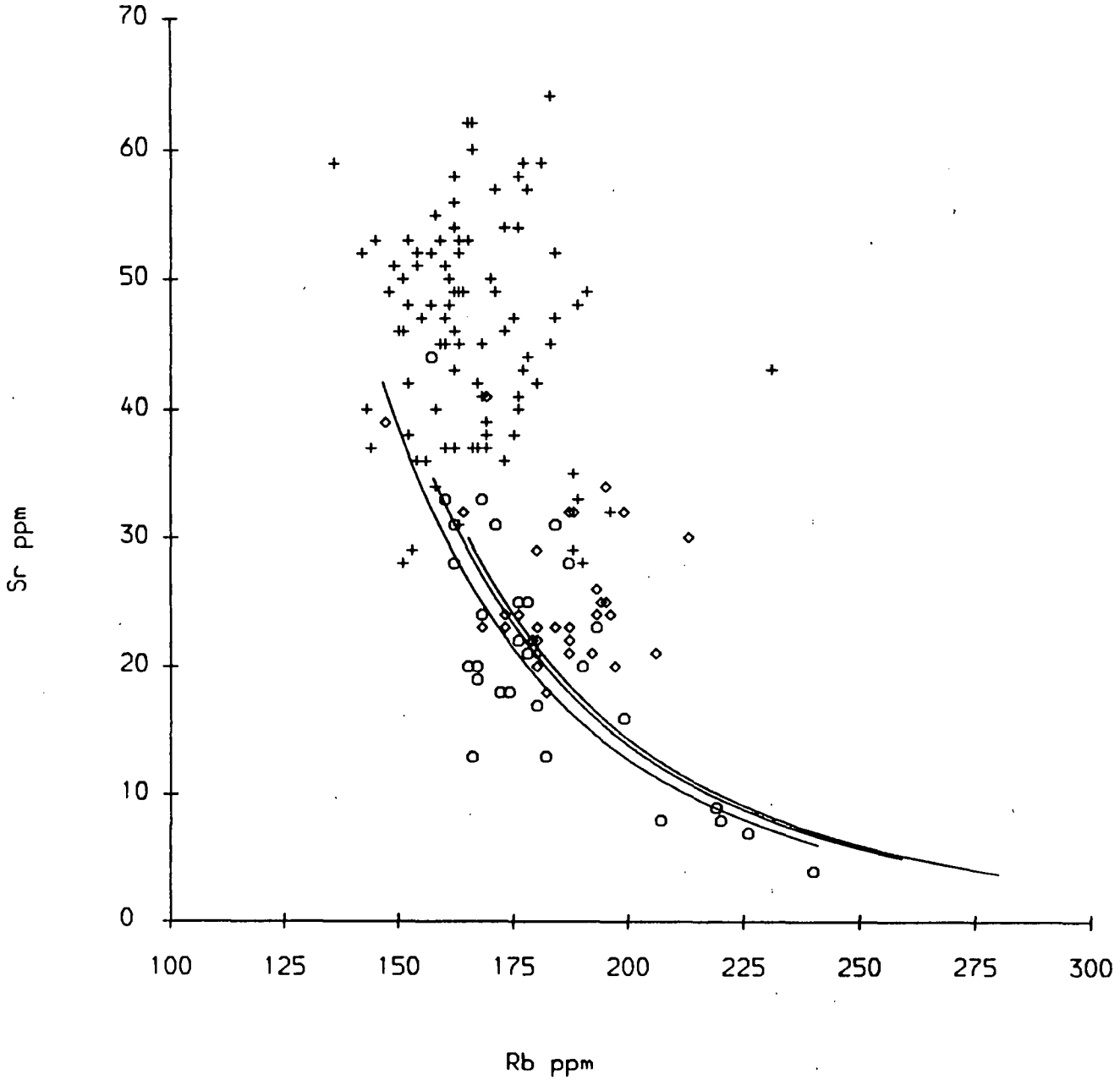
70
60
50
40
30
20
10
0
Sr ppm
100
125
150
175
200
225
250
275
300
Rb ppm

Fig. 5.29.

Figure 5.30. Ba (ppm) plotted against Rb (ppm) for the 153 samples representative of the three groups of the coarse granite. (Diamonds - group 1; crosses - group 2; circles - group 3.) The plot includes curves calculated for sidewall crystallisation involving 30% equilibrium crystallisation of the boundary layer. The curves indicate (from left to right) 100% solid crystallised from the boundary layer; solid crystallised from the boundary layer with 30% interstitial evolved liquid; composition of the reservoir of liquid in the core of the pluton.

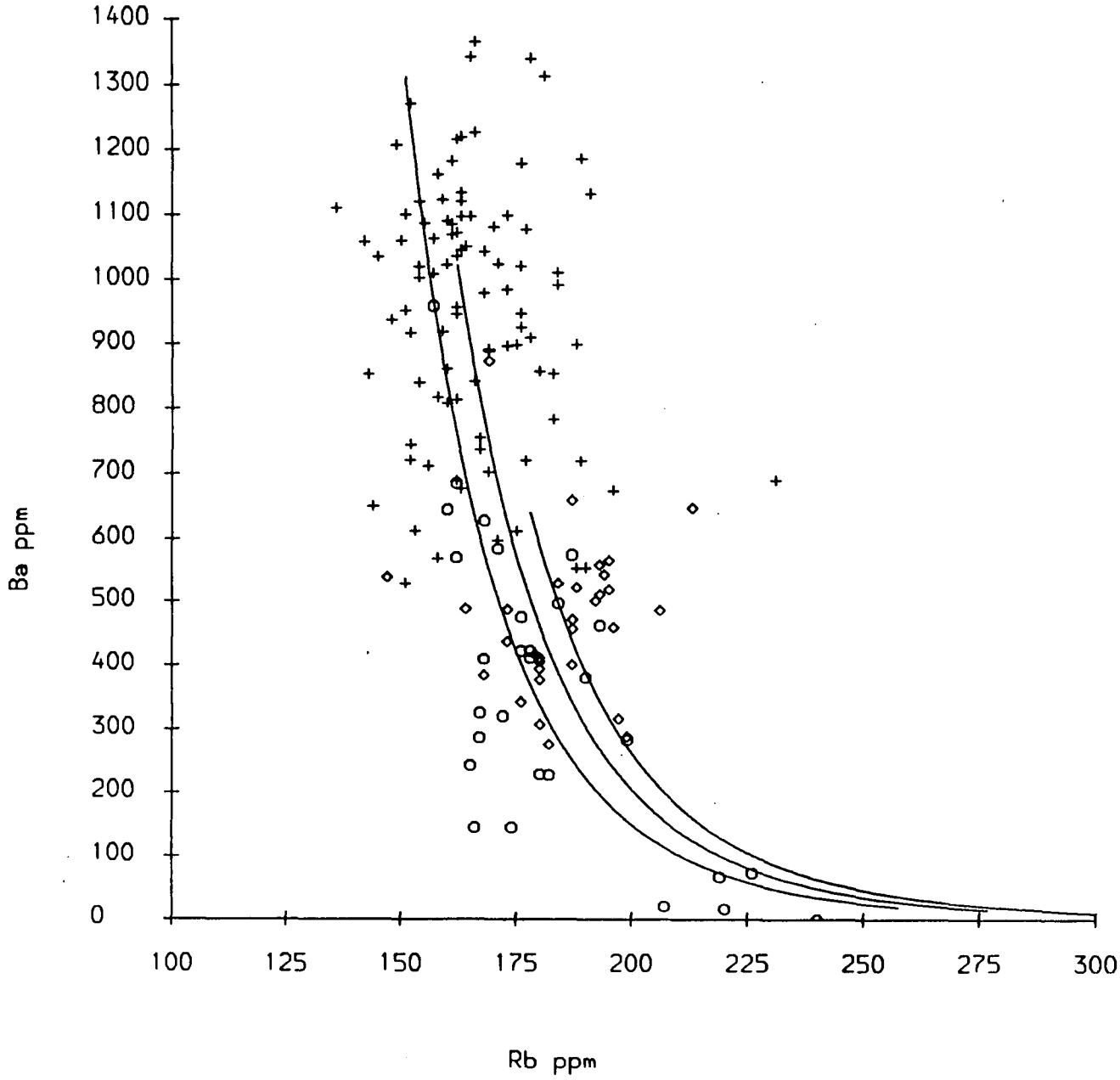
1400
1300
1200
1100
1000
900
800
700
600
500
400
300
200
100
0
Ba ppm
100
125
150
175
200
225
250
275
300
Rb ppm

Fig. 5.30.

Figure 5.31. Sr (ppm) plotted against Rb (ppm) for the 153 samples representative of the three groups of the coarse granite. (Diamonds – group 1; crosses – group 2; circles – group 3.) The plot includes curves calculated for sidewall crystallisation involving 30% equilibrium crystallisation of the boundary layer. The curves indicate (from left to right) 100% solid crystallised from the boundary layer; solid crystallised from the boundary layer with 30% interstitial evolved liquid; composition of the reservoir of liquid in the core of the pluton.

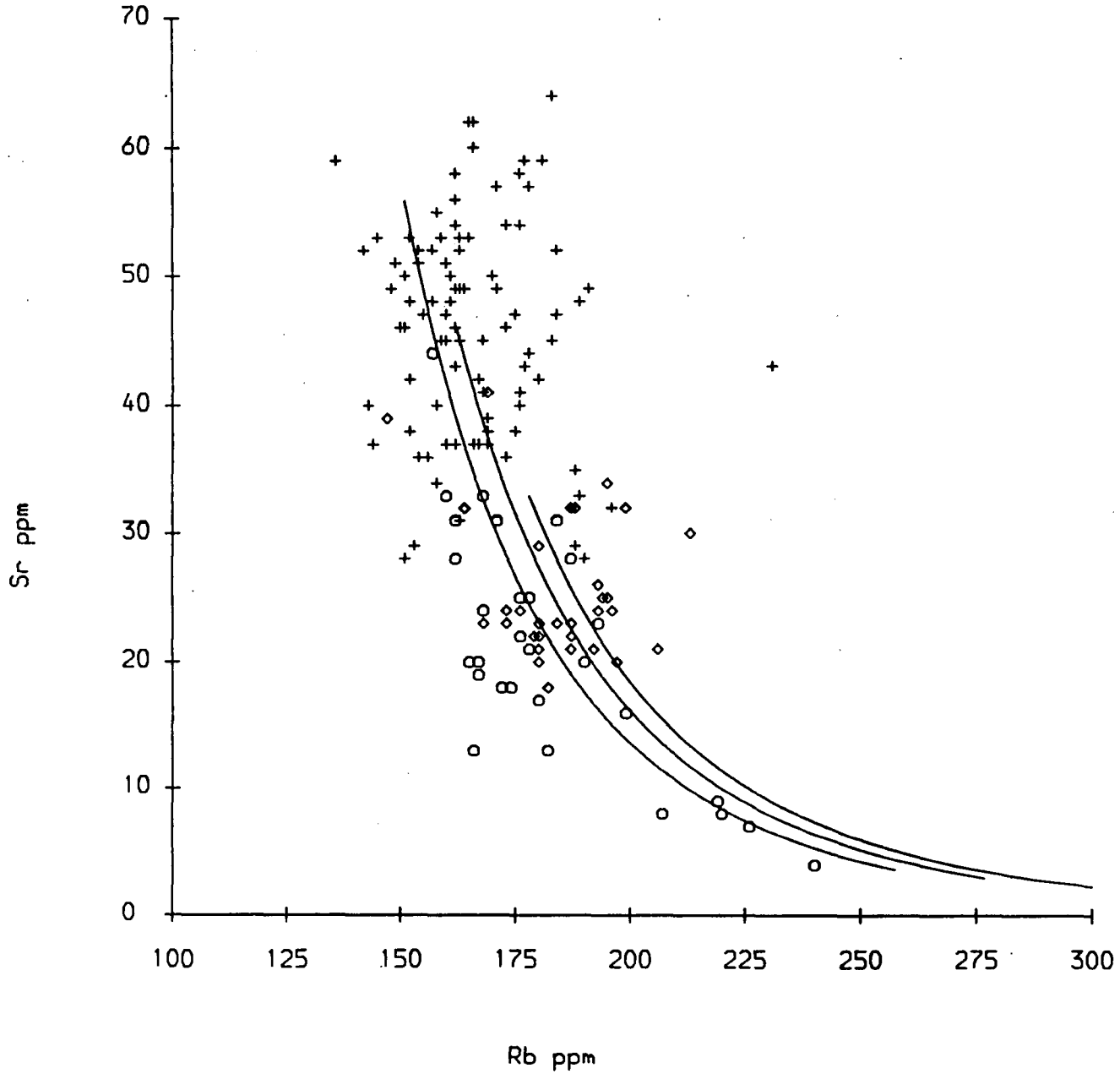
70
60
50
40
30
20
10
0
Sr ppm
100
125
150
175
200
225
250
275
300
Rb ppm

Fig. 5.31.

Figure 5.32. Calculated variation of Ba with distance from the centre of the pluton during sidewall crystallisation. Curves indicate (from top to bottom) 100% solid crystallised from the boundary layer; solid crystallised from the boundary layer with 30% interstitial evolved liquid; composition of the reservoir of liquid in the core of the pluton.

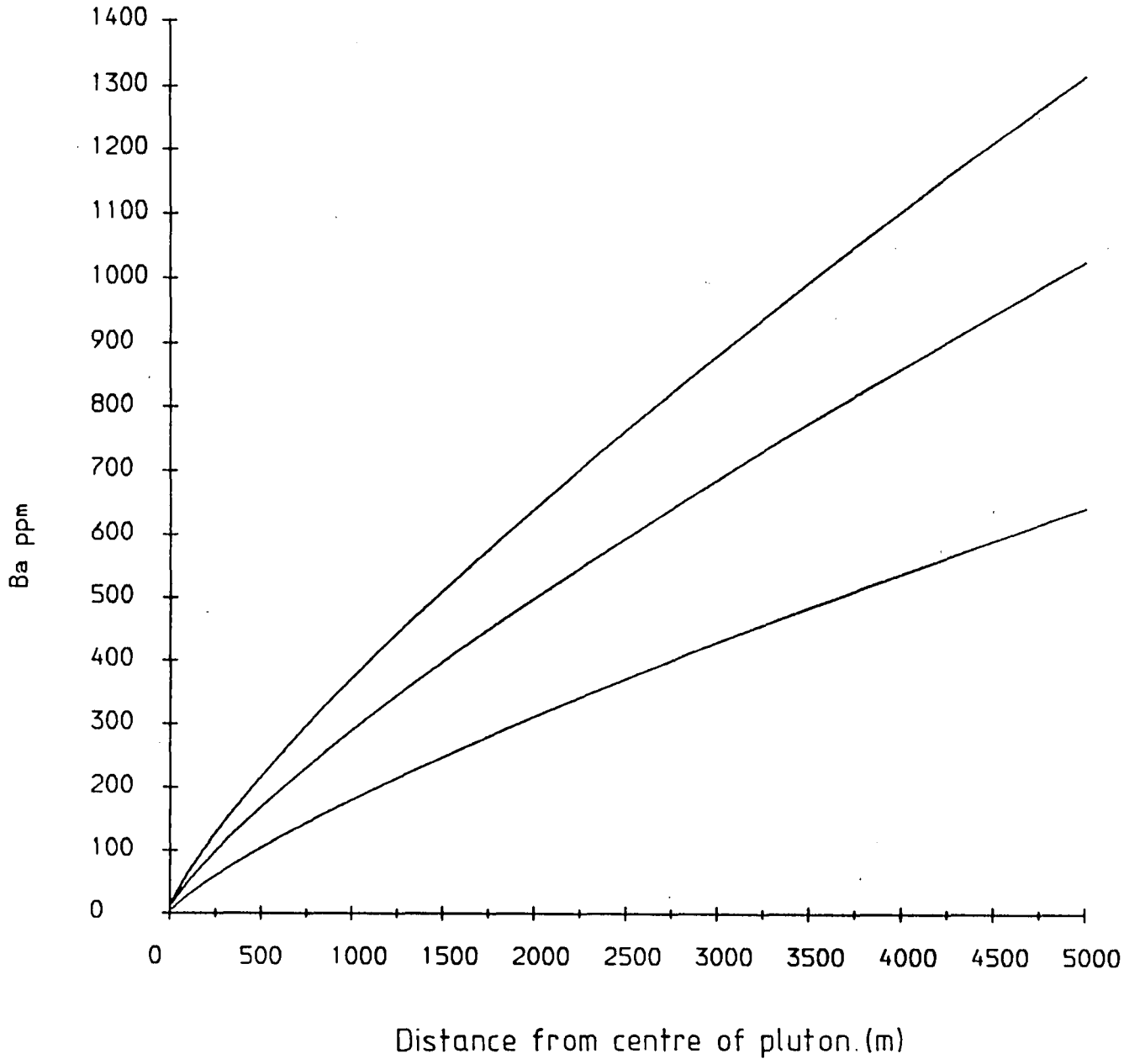
1400
1300
1200
1100
1000
900
800
700
600
500
400
300
200
100
0
Ba ppm
0
500
1000
1500
2000
2500
3000
3500
4000
4500
5000
Distance from centre of pluton.(m)

Fig. 5.32.

Figure 5.33. Calculated variation of Sr with distance from the centre of the pluton during sidewall crystallisation. Curves indicate (from top to bottom) 100% solid crystallised from the boundary layer; solid crystallised from the boundary layer with 30% interstitial evolved liquid; composition of the reservoir of liquid in the core of the pluton.

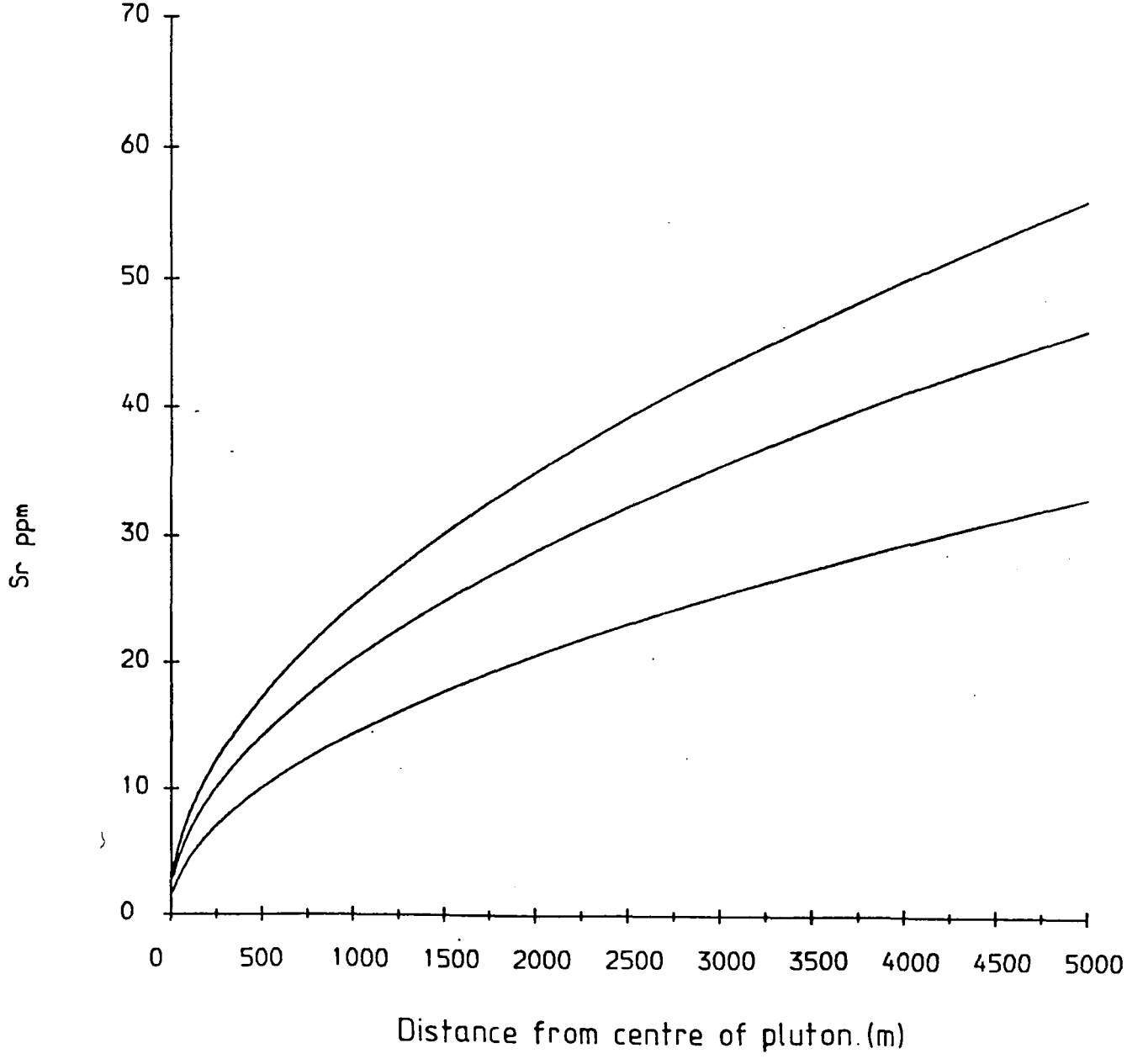
70
60
50
40
30
20
10
0
Sr ppm
0
500
1000
1500
2000
2500
3000
3500
4000
4500
5000
Distance from centre of pluton.(m)

Fig. 5.33.

Figure 5.34. Calculated variation of Rb with distance from the centre of the pluton during sidewall crystallisation. Curves indicate (from top to bottom) 100% solid crystallised from the boundary layer; solid crystallised from the boundary layer with 30% interstitial evolved liquid; composition of the reservoir of liquid in the core of the pluton.

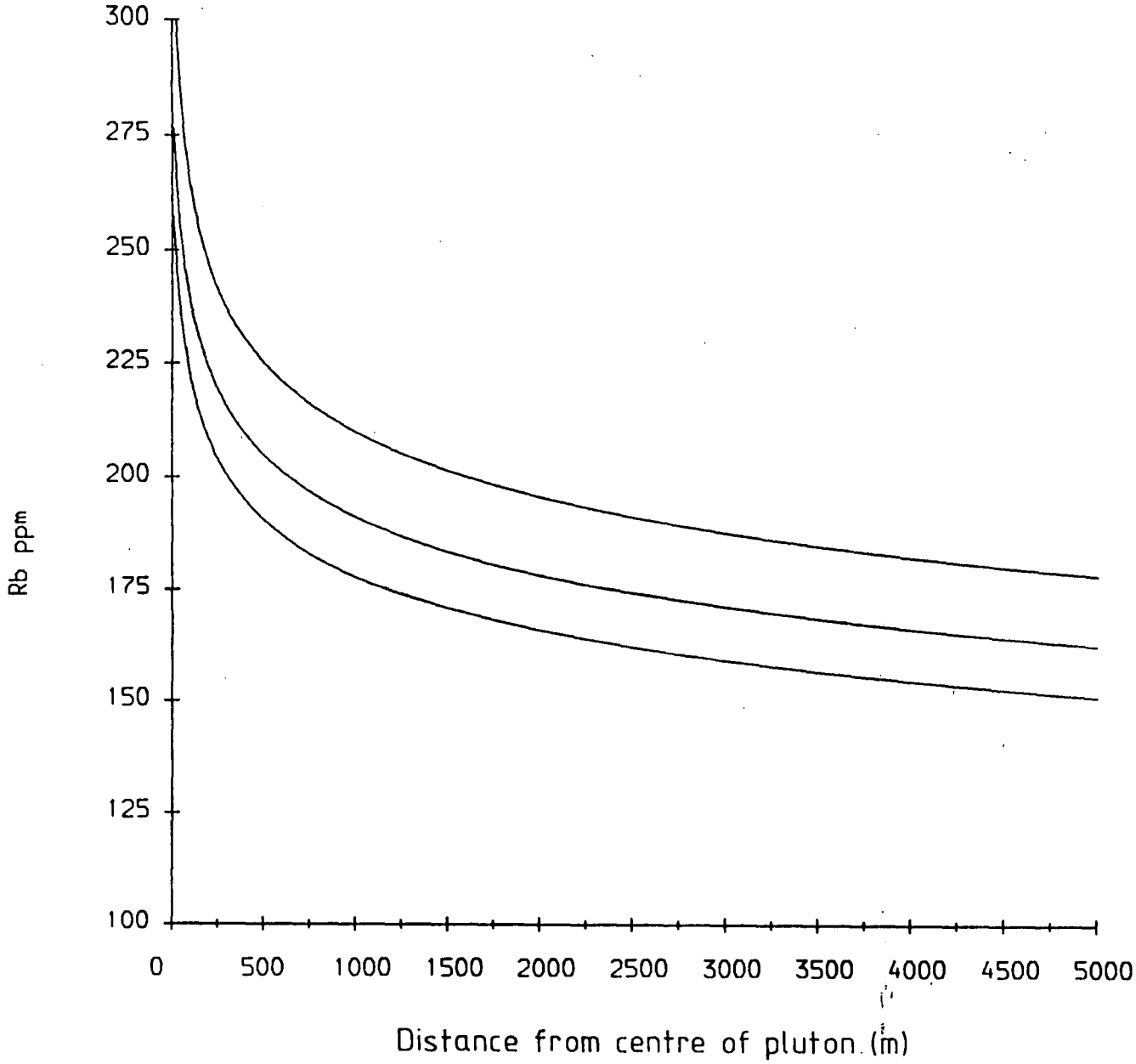
300
275
250
225
200
175
150
125
100
Rb ppm
0
500
1000
1500
2000
2500
3000
3500
4000
4500
5000
Distance from centre of pluton (m)

Fig. 5.34.

Figure 5.35. A comparison of the observed variation in Ba with radius of the pluton (measured from the centre in m) and the calculated variation for sidewall crystallisation.

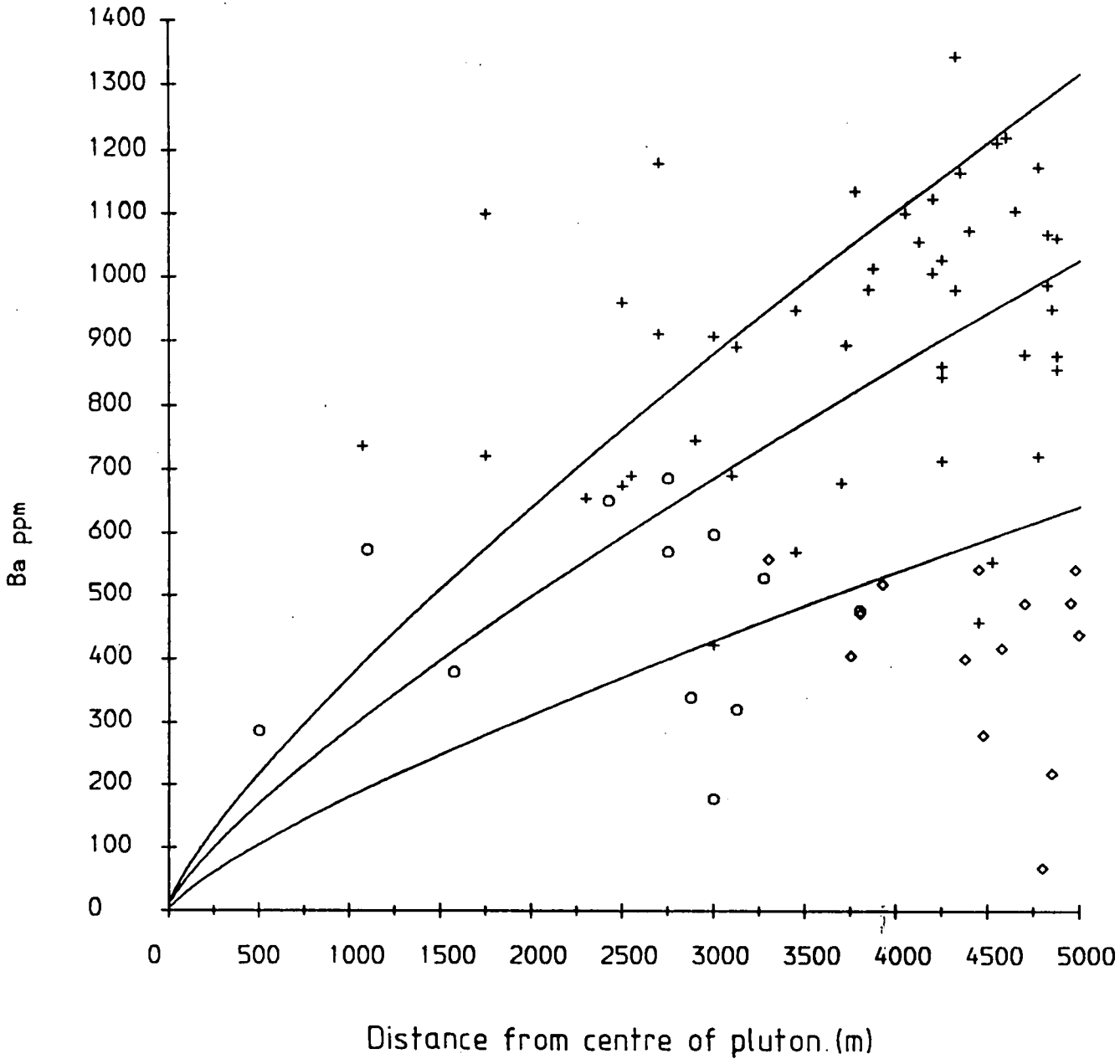
1400
1300
1200
1100
1000
900
800
700
600
500
400
300
200
100
0
Ba ppm
0
500
1000
1500
2000
2500
3000
3500
4000
4500
5000
Distance from centre of pluton (m)

Fig. 5.35.

Figure 5.36. A comparison of the observed variation in Sr with radius of the pluton (measured from the centre in m) and the calculated variation for sidewall crystallisation.

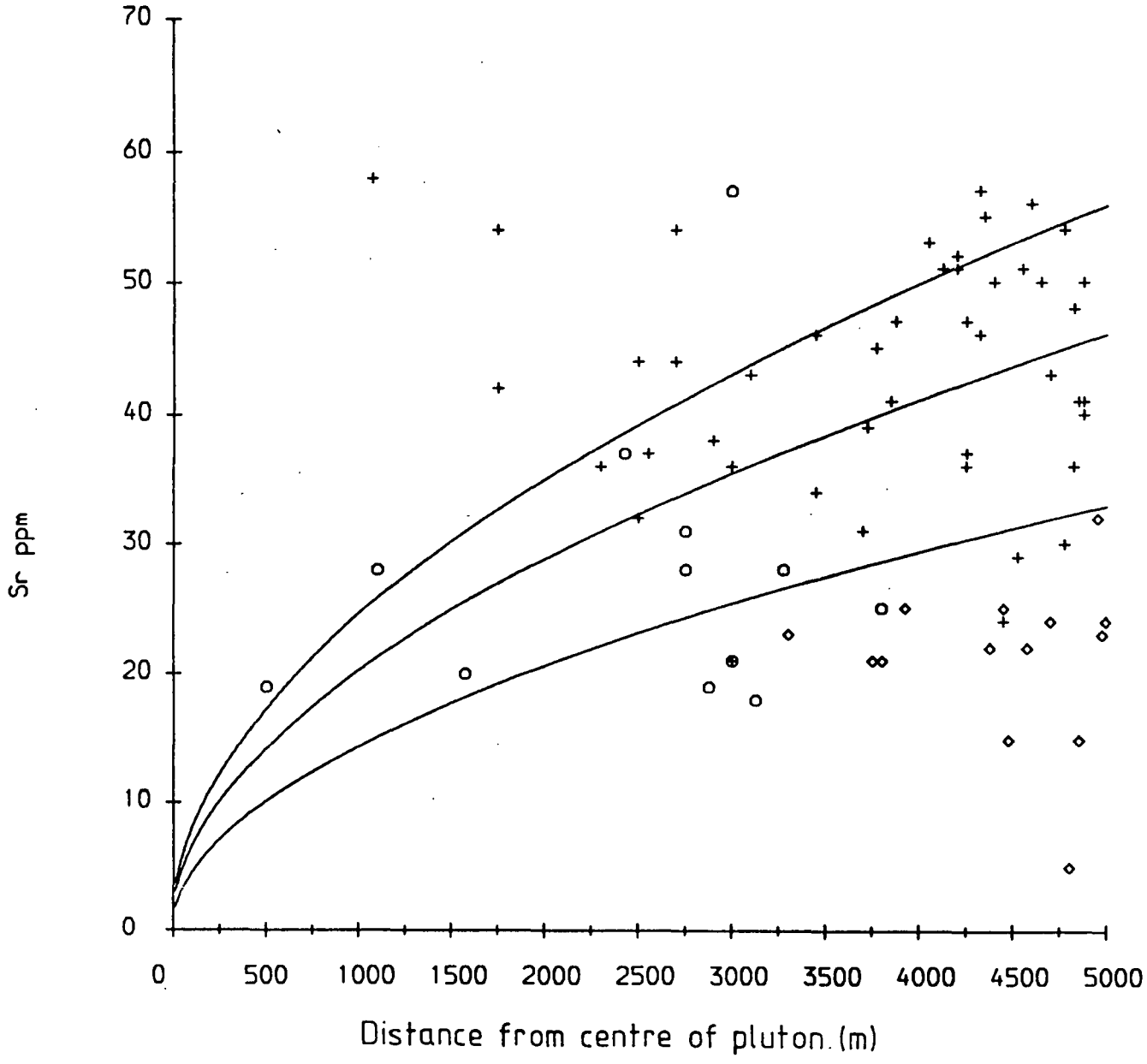
70
60
50
40
30
20
10
0
Sr ppm
0
500
1000
1500
2000
2500
3000
3500
4000
4500
5000
Distance from centre of pluton. (m)

Fig. 5.36.

curve for rocks forming by sidewall crystallisation, and the remainder plot above the curve for the reservoir compostion. Group 1 rocks plot just below the curve for the reservoir composition. Group 3 rocks show no clear trend.

Since the group 1 rocks plot below the reservoir composition curve they cannot be the products of sidewall crystallisation, which have higher compositions than the reservoir curve. On this basis it can be concluded that the group 2 rocks could be the products of sidewall crystallisation. Since there is no evidece that the group 1 rocks crystallised from a separate magma and fractional crystallisation and sidewall crystallisation can be eliminated from the formation of these rocks it is concluded that the group 1 rocks are the products of equilibrium crystallisation of the original magma. This is consistent with these rocks showing the narrowest range in composition in comparison to the other two groups. Equilibrium crystallisation is also required to prevent the composition of the magma becoming so evolved that it could not have crystallised the range of group 2 rocks. If crystallisation of the group 1 rocks had significantly modified the liquid composition assumptions about the initial magma composition may be slightly in error. However the average range of the coarse granite falls within the range of compositions of the group 1 rocks (cf Table 5.3 & Table 5.5). This conclusion is consistent with the distribution of the group 1 rocks along the margin of the granite. It also indicates that initial crystallisation of the coarse granite occurred by equilibrium crystallisation which was then followed by sidewall crystallisation.

The evolution of the group 3 rocks is more difficult to interpret. Figures 5.35 & 5.36 give little indication of their origin. Most of the observed data plot below the calculated solid evolution curve. Petrographic data (visual estimates) indicate the rocks have low phenocryst contents and are markedly different from the group 2 rocks in this respect. On the basis of this evidence it is thought that they may also be the products of equilibrium crystallisation of the reservoir.

As noted above the effects of polymerisation in evolved melts may increase

the distribution coefficients for Ba and Sr (Watson, 1976). This would result in Ba and Sr depletion of the evolving liquids. Many of the group 3 rocks show more pronounced Ba and Sr depletion, and can be distinguished on this basis from group 1 rocks. This is consistent with the crystallisation history described above. Group 1 rocks would crystallise from unevolved liquid but the group 3 rocks would precipitate from liquids depleted by sidewall crystallisation

The spread in the observed data is thought to reflect different ratios of crystals to interstitial evolved liquid preserved in the rocks. Loss of this liquid (section 5.5) would result in an increase in the compatible element concentration in the rock and a fall in the incompatible element concentration relative to the original composition. A similar effect would result from trapping variable quantities of interstitial liquid during crystallisation. Further variations in composition may result from the incorporation of phenocrysts resulting from crystallisation of the reservoir, into the wall during crystallisation. The sidewall crystallisation model assumed that crystallisation only occurs in the boundary layer. However it is likely that convection would cause cooling of the reservoir as heat is lost through the wall rocks. Crystals forming in equilibrium with the evolving liquid in the reservoir would have different compositions to those crystals precipitating in equilibrium with evolved liquid in the boundary layer. These crystals would eventually become trapped as 'xenocrysts' by the inward migrating boundary layer, causing variations in the bulk composition of the solid forming at the wall. Since these phenocrysts would not be in equilibrium with the melt within the boundary layer they may grow zoned margins. The presence of such crystals is implied by the occurrence of zoned phenocrysts, which presumably grew during ascent of the granite (section 5.4), in the chilled marginal rocks of the coarse granite. It may be possible to verify this process by detailed microprobe studies of the variations in feldspar composition within the three groups and within individual rocks.

Prior to analysis of the trace element variations in the coarse granite 38 sam-

ples were removed from the original collection on the grounds that they were uncharacteristic of the groups in which they outcropped. The majority of these rocks were fine grained and similar in appearance to many of the aplites, but differed from the latter in that they have gradational contacts with normal coarse granite. These rocks were notably finer grained than the normal coarse granite in which they occurred, and were interpreted as having crystallised rapidly from liquids coexisting with phenocryst rich magma. The majority of these rocks were collected from group 2.

When these samples are plotted on inter-element diagrams (Figs. 5.37 & 5.38) it is clear that the range of composition of the group 2 rocks is extended into that of groups 1 and 3 and vice versa. The compositions of the rocks remain consistent with the sidewall crystallisation model, but on the basis of the petrographic data which indicates they are liquids their compositions are not compatible with an origin by fractional crystallisation, which would require them to have much higher concentrations of Rb. The general spread of the data make interpretation of these rocks difficult but because of their similarity in composition with the group 1 and group 3 rocks it is thought that they represent fractions of reservoir liquid, trapped by the inward migrating crystallisation front. They do not show any systematic variation in composition with distance from the centre of the pluton but this may be masked by low concentrations of phenocrysts forcing up the compatible element composition of the rocks.

In summary, this section has discussed the variations in the major and trace element geochemistry of the outer coarse granite and their possible causes and implications for the evolution of the granite. The granite crystallised from an extremely evolved (SiO_2) enriched peraluminous magma with a restricted range of major element composition. Parabolic evolution curves on inter-element plots indicate that variations in chemistry are controlled by crystal fractionation processes rather than magma mixing. Depletion of Ba, Sr, P, Zr and Ti on chondrite

Figure 5.37. Ba (ppm) plotted against Rb (ppm) for all the samples collected from the coarse granite including the fine grained rocks considered uncharacteristic of the groups in which they were collected. The evolution curves for sidewall crystallisation are also shown for comparison with Fig. 5.28.

Fig. 5.37.

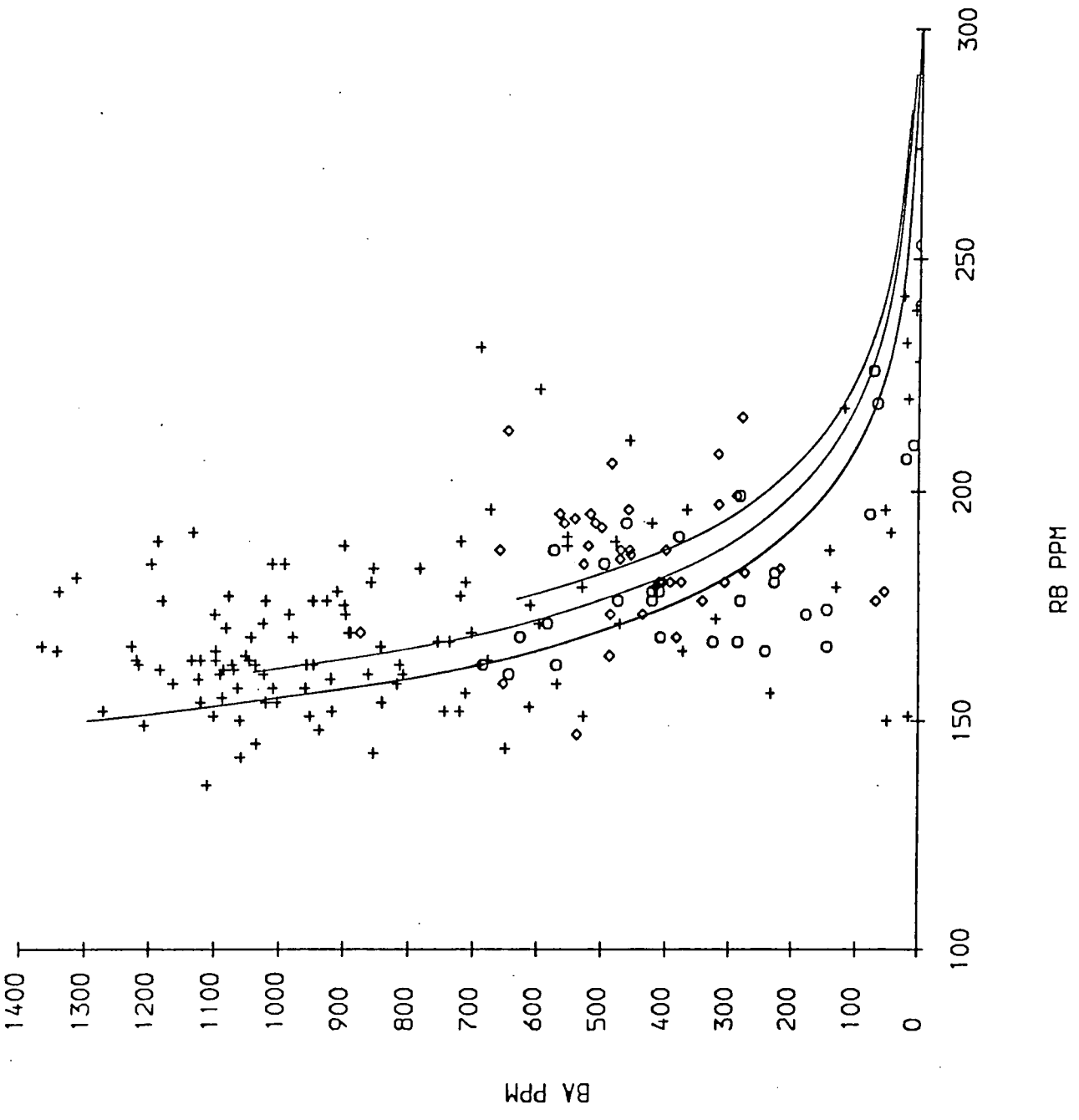
BA PPM
1400
1300
1200
1100
1000
900
800
700
600
500
400
300
200
100
0
RB PPM
100
150
200
250
300

Figure 5.38. Sr (ppm) plotted against Rb (ppm) for all the samples collected from the coarse granite including the fine grained rocks considered uncharacteristic of the groups in which they were collected. The evolution curves for sidewall crystallisation are also shown for comparison with Fig. 5.29.

Fig. 5.38.

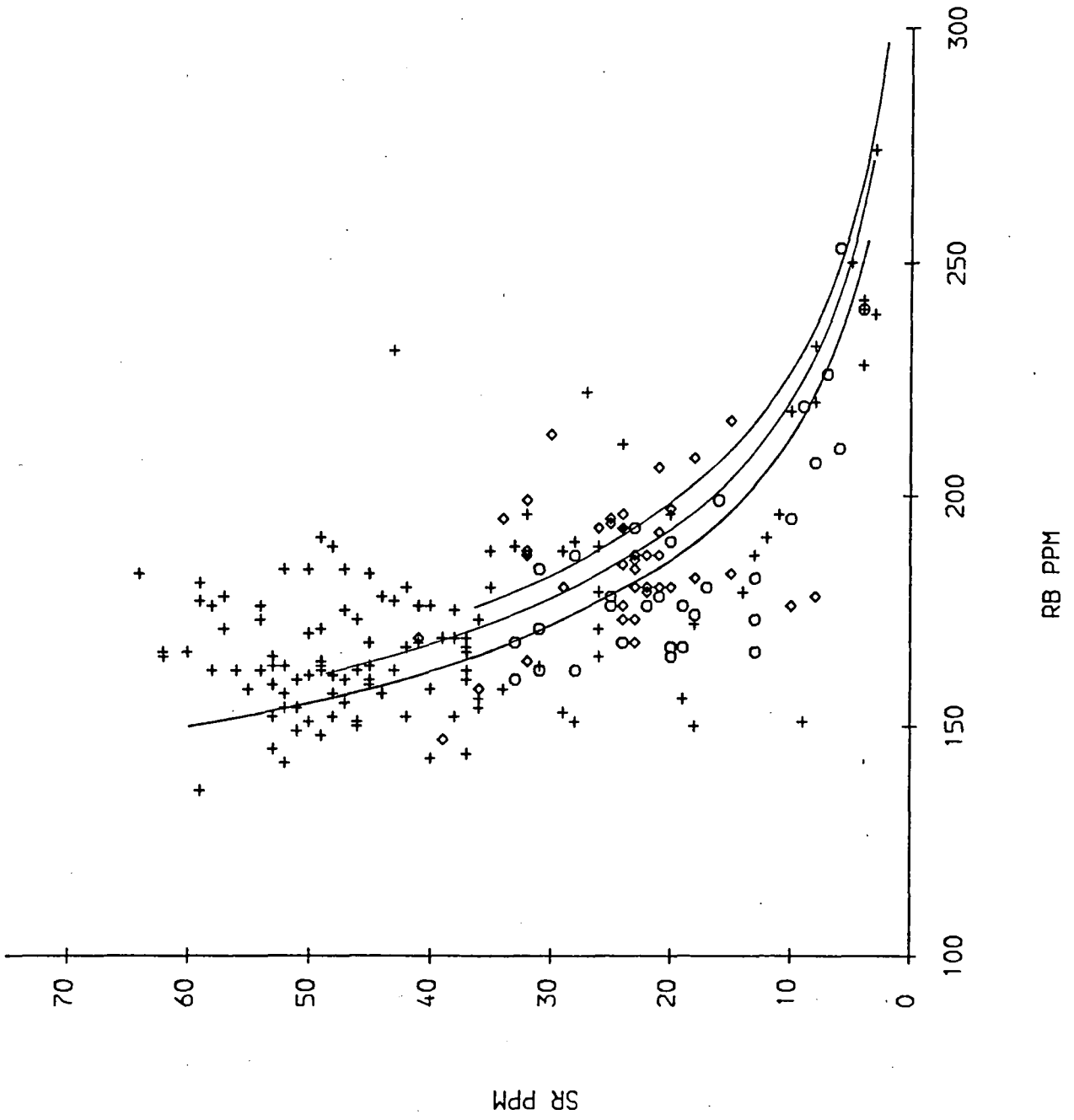

normalised incompatible element diagrams indicate that the magma evolved from its basic parent by fractionation of orthoclase, plagioclase, apatite, zircon and Ti-oxide or pyroxene. Peaks at Rb, Th and K are consistent with contamination of the basaltic parent of the granitic magma by acid partial melts of crustal rocks. The depletion of Ba indicates that fractionation followed contamination. Modification of the trace element composition of the granite by partial melts of Dalradian cannot be completely ruled out on the basis of trace element data because of a similarity in the trace element compositions of the two rock types.

Ba, Sr, P and Ti show a wide range of variation. Other elements show only restricted variations in composition. This is consistent with fractionation of orthoclase, plagioclase, apatite and Ti-oxide during ascent and final crystallisation of the granite. Fractionation of orthoclase and plagioclase is consistent with the petrography which indicates these phases occur as phenocrysts.

Spatial variation in Ba and Sr concentration across the pluton closely matches the petrographic variations on which the granite can be subdivided into three groups. The group 2 rocks are the least fractionated. They contain high concentrations of Ba and Sr and have high K/Rb ratios. Group 3 rocks are the most evolved, having low Ba, Sr and low K/Rb. Depletion of SiO_2 in evolved rocks of group 3 indicates quartz fractionation occurred. This is consistent with the petrography with indicates precipitation of the cotectic assemblage orthoclase – plagioclase – quartz, which dominates major and trace element variations during crystallisation of the pluton.

Trace element variation in the coarse granite was modelled for fractional crystallisation and sidewall crystallisation. The theoretical models showed that sidewall crystallisation could account for the observed variation in element composition caused by differentiation of the magma, and the observed spatial variations in composition. Models for fractional crystallisation were not compatible with the observed spatial and lateral variations in composition.

It is concluded that the granite crystallised in-situ from a single, crystal bearing granitic magma evolved by fractional crystallisation of a contaminated basaltic parent. Initial equilibrium crystallisation producing the marginal group 1 rocks was followed by formation of the group 2 rocks by sidewall crystallisation. Crystallisation of the group 3 rocks appears to have involved equilibrium crystalliastion of the reservoir of evolved liquid produced by sidewall crystallisation.

5.4 Depth of Crystallisation.

Isotope data discussed in section 5.3.1 indicated that the granitic magma accumulated at a depth of $\approx$ 11 km ($\approx$ 3.5 kbar pressure). It has clearly risen toward the surface before fully crystallising. However as the magma rose toward the surface it would have cooled, primarily by losing heat to progressively cooler country rocks. This cooling process would have reduced the temperature of the magma, leading to the crystallisation of plagioclase and orthoclase feldspar as described in section 5.3.2. If cooling occurred throughout the ascent of the magma the resulting mineralogy of the granite may reflect crystallisation over a range of falling temperatures and pressures. This section examines this process.

Tuttle & Bowen (1958) carried out a series of experiments on the melting behavior of the system $NaAlSi_3O_8 - KAlSi_3O_8 - SiO_2 - H_2O$ which is analogous to the composition of granite. These workers determined the variation in water saturation of granitic melts over a range of pressures and temperatures. As noted from petrographic data the coarse granite is drusiform in places suggesting that the magma was just beginning to exsolve water at its depth of emplacement, (i.e. it was just oversaturated at 2 to 3 km depth). At the inferred depth of emplacement (3 km -Chapter 2) or a pressure of 1 kbar, acid melts will absorb up to 4% water. Hence the petrographic data indicates that the coarse granite contained up to 4% water at its depth of emplacement. The origin of this water is unclear. It may be primary magmatic (i.e. derived from its basaltic parent) or inherited in assimilated partial melts (section 5.3.1). The water content of the magma may have been increased slightly during its ascent through increased contamination by wet country rocks or by crystallisation. However this clearly indicates that the granitic magma would have had a water content of less than or equal to 4% at the depth at which it accumulated (11 km). At this depth the granitic magma would have had a liquidus temperature of between 900 and 1000^oC (Fig. 5.39), after Wyllie et al. (1976), assuming it had evolved to the minimum melting

point. Had it not, the temperature of the magma may have been much higher. The liquidus temperature and the crystallisation interval would have decreased during the ascent of the magma (i.e. with falling pressure and water content; Fig. 5.39). Hence the mineral phases in the coarse granite could be expected to have crystallised over a range of falling temperature and pressure.

CIPW norms for the samples of the coarse granite were calculated and normative quartz – albite – orthoclase were plotted on a ternary diagram, together with the position of the minimum melting point in this system and the position of the boundary curve between the quartz plus liquid and feldspar plus liquid fields for a range of pressures (Fig. 5.40). This indicated that the coarse granite represents a minimum melt composition which crystallised at between 1 and 0.5 kbar $_pH_2O$. This is consistent with the estimated overburden thickness for the intrusion of 3 km (Chapter 2) assuming $_pH_2O$ equals $_p$total. The minimum melting temperature for this pressure range is between 700° and 750°C (Fig. 5.39). This clearly indicates the bulk of the coarse granite crystallised over a range of temperatures and pressures.

The petrographic data show the rocks are dominantly composed of phenocrysts of orthoclase (cryptoperthitic texture indicates the presence of Na solid solution), oligoclase and quartz. Such crystallisation behavior is usually associated with sub-solidus two feldspar granites. The experimental work of Tuttle & Bowen (1958) showed that such granites only crystallised at pressures above ≈4 kbar $_pH_2O$. Below this pressure the granite solidus lies above the feldspar solvus and a single feldspar is crystallised from liquids with compositions approaching that of the minimum melt. This group of granites are referred to as hypersolvus granites. Since the coarse granite evolved at a depth of approximately 11 km (3.5 kbar $_pH_2O$) its mineralogy ought to be representative of a hypersolvus (1 feldspar) granite. Experimental work on the phase relations of hypersolvus granites (Tuttle & Bowen, 1958) indicates that early crystallisation of 2 feldspars would be followed

Figure 5.39 Figure illustrating the variation in liquidus and solidus temperature with depth for a granitic magma containing 4% H_2O (after Wyllie et al., 1976).

Fig. 5.39.

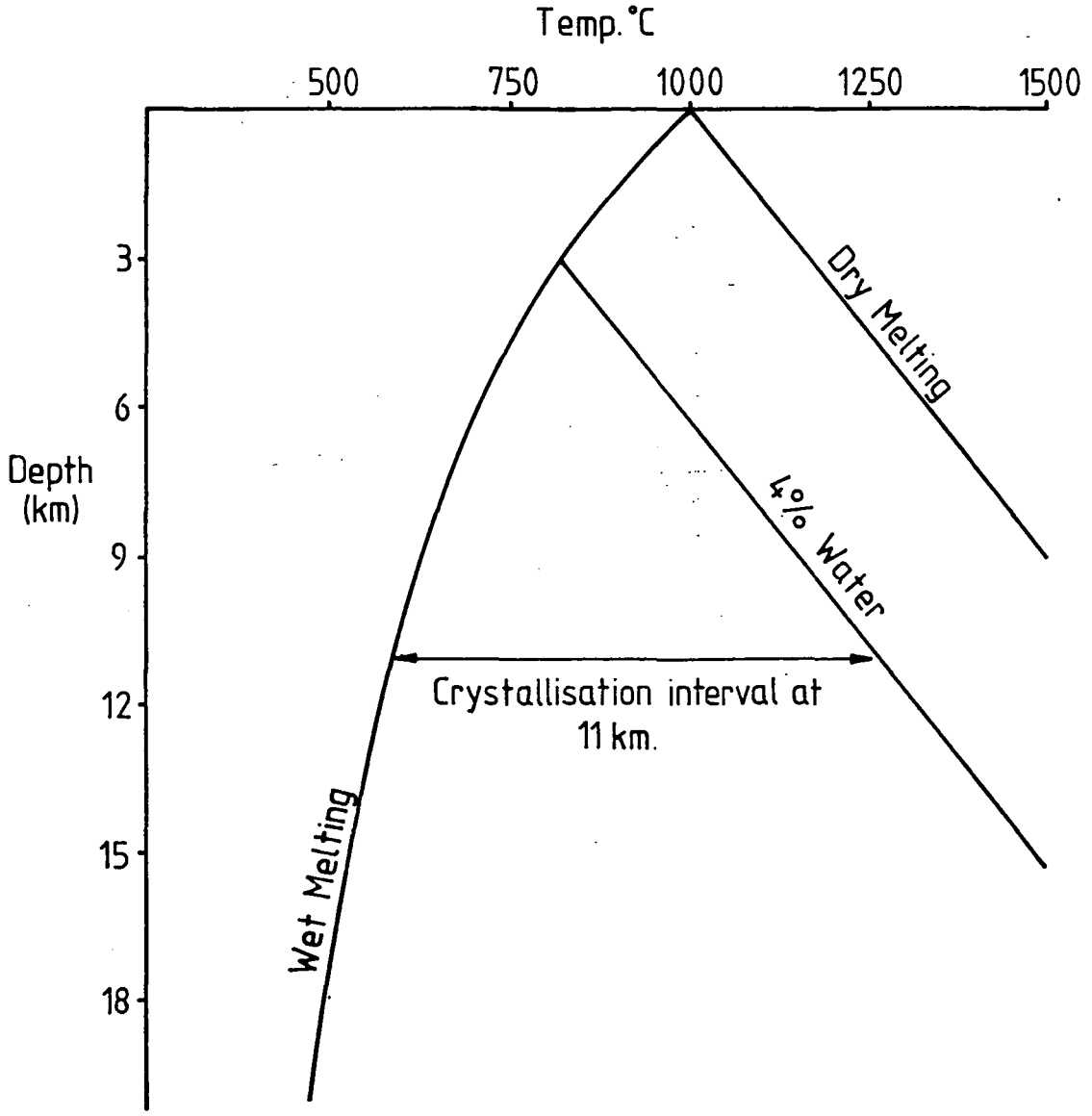
Temp. °C
500
750
1000
1250
1500
Depth (km)
3
6
9
12
15
18
Dry Melting
4% Water
Crystallisation interval at 11 km.
Wet Melting

Figure 5.40 A plot of normative quartz – albite – orthoclase for the Northern Arran coarse granite (shaded), showing the variation in the position of the minimum melting point and the decrease in the stability field of quartz with falling pressure (after Tuttle & Bowen, 1958).

Fig. 5.40.

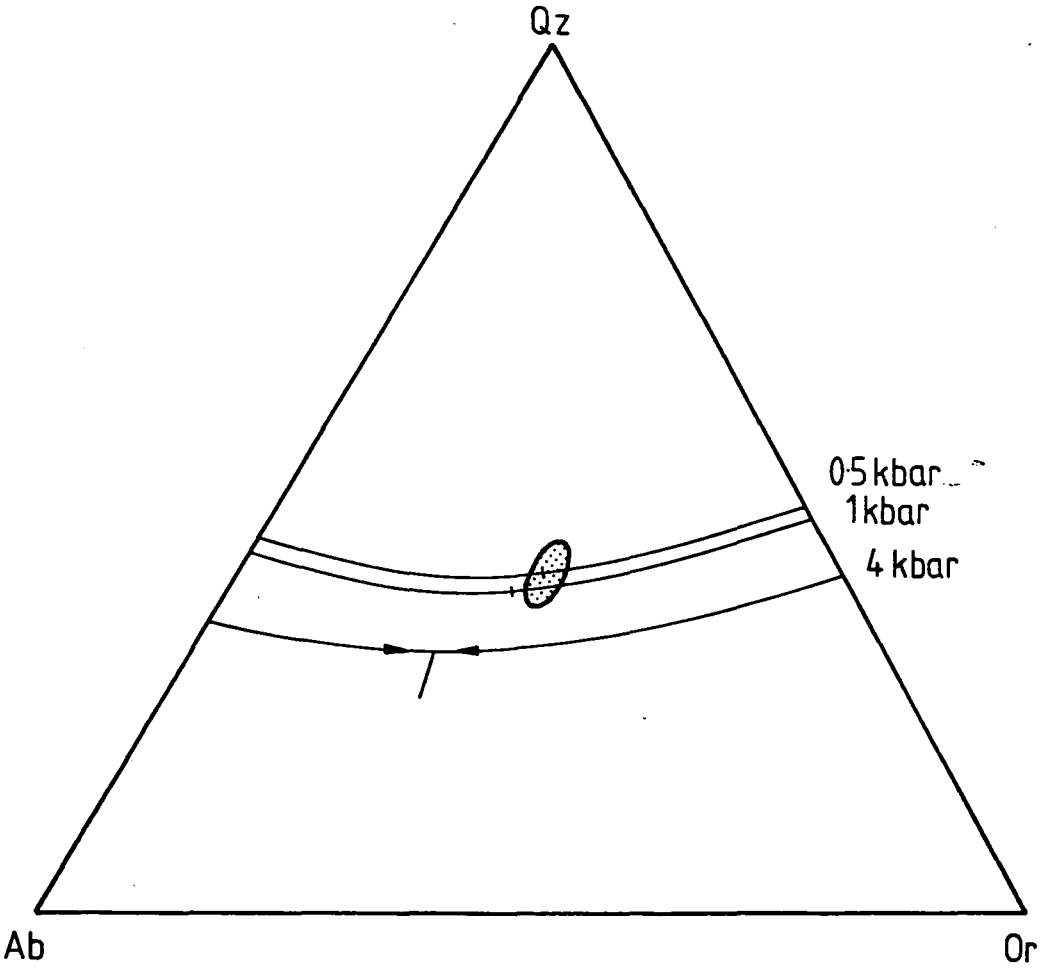

by resorption of plagioclase and the crystallisation of 1 feldspar in equilibrium with the liquid before the minimum melting point is reached (Tuttle & Bowen, 1958) (Fig. 5.18). Petrographic data for the Arran granite indicates that this is clearly not the case. This ambiguity can be explained by further work of Tuttle & Bowen (1958) who also investigated the effect of temperature on solid solution in the system anorthite – albite – orthoclase They showed that the range of solid solution between albite and orthoclase is lowered for melts stable at lower temperatures due to increased solution of silica, water or nepheline (in general phases not taken into solid solution in the feldspars) in the liquid (Fig. 5.41). The coarse granite is quartz saturated so only the solution of silica and water are of interest in this case. Lowering the temperature of the ternary minimum in the system Qz - Ab - Or restricts the amount of solid solution between co-existing feldspars crystallising from liquids evolving to the minimum melt composition. This effectively increases the stability range of two feldspar systems to lower pressures and reduces the range over which one feldspar crystallises in equilibrium with the melt. This problem was investigated further by Yoder et al. (1957) whose studies on the system An - Ab - Or - H_2O showed that small concentrations of Ca feldspar would cause crystallisation of separate Na and K rich feldspars at low pressure.

Hence it can be deduced that the coarse granite magma must have evolved toward a mimimum melting point composition by crystallising phenocryst orthoclase (with Na feldspar in solid solution) and sodic plagioclase. This would have caused an increase in the silica and water dissolved in the melt which would have permitted simultaneous crystallisation of two compositionally different feldspars over an extended range. Some zonation of the plagioclase and orthoclase (section 5.2) points to crystallisation over an extended range of temperature. Optically determined compositions for the plagioclase feldspars (section 5.2) indicates that calcic feldspars which may have formed at high temperatures at deeper levels during differentiation from the basaltic parent have been removed by fractiona-

Figure 5.41. Ternary phase diagram for the system anorthite – albite – orthoclase. The curves show the extent of solid solution between coexisting feldspars at four different temperatures. The decrease in solid solution with falling temperature results from increasing solution of water, silica or nepheline in the melt (after Tuttle & Bowen, 1958).

Fig. 5.41.

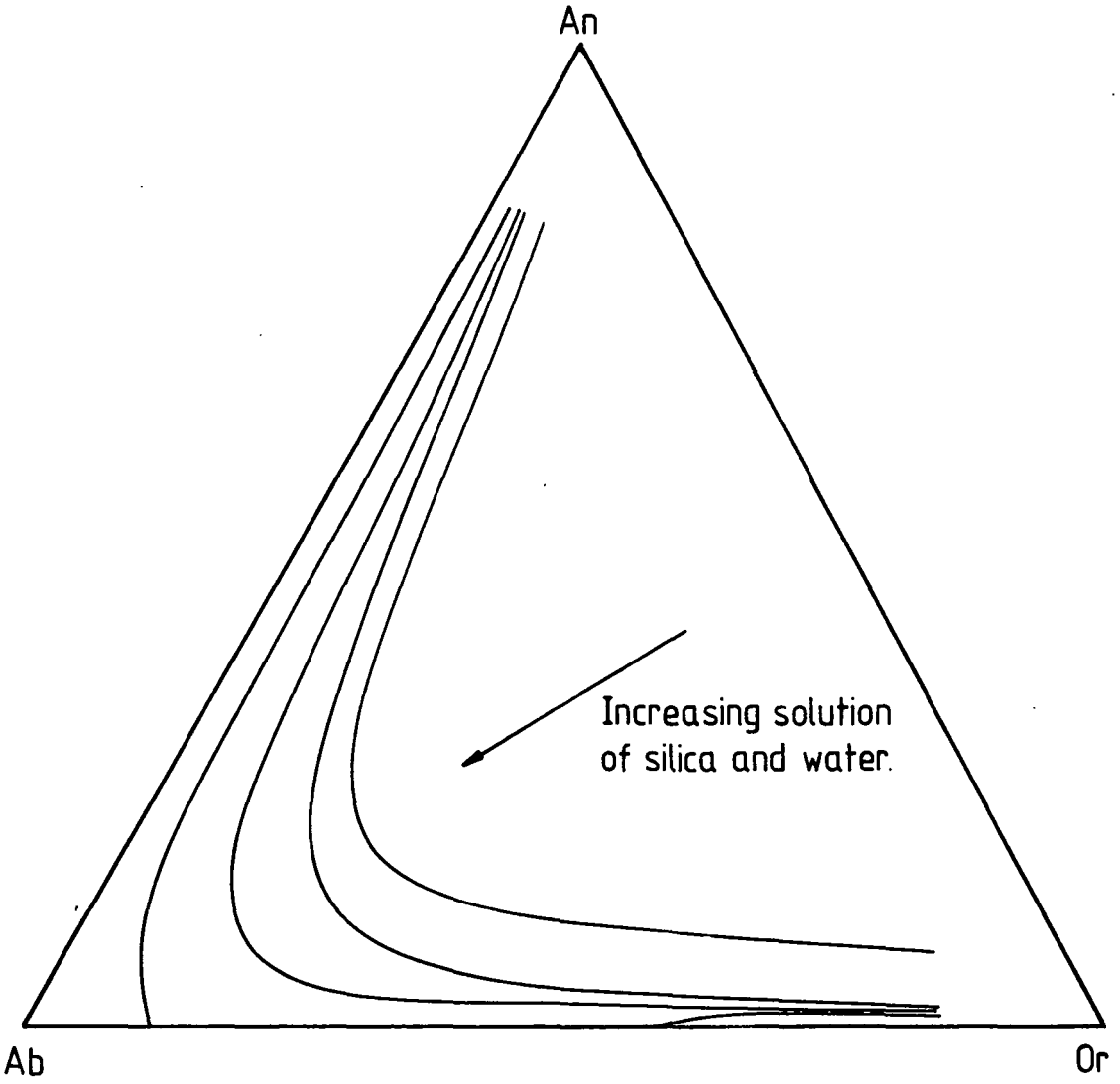

tion, which is consistent with the depletion of Sr in the magma prior to in-situ fractionation (section 5.3.2).

This fractionation process involving a fall in temperature and pressure would have pushed the evolving magma composition toward more quartz rich compositions. At the same time falling pressure during ascent would have caused a shift in the minimum melting point composition toward quartz rich compositions, increasing the solubility of quartz in the melt. The combined effect of these processes would have led to the extreme enrichment of quartz noted in the coarse granite. Quartz enrichment may be the reason that the bulk of the normative quartz – albite – orthoclase data indicate a crystallisation pressure slightly below that indicated by estimates of the thickness of the overburden.

In conclusion, crystallisation of the coarse granite must have occurred throughout its ascent to accommodate a fall in the liquidus temperture caused by falling pressure. Final crystallisation occurred at a pressure of approximately 1 kbar $_pH_2O$ from a liquid of minimum melting point composition, under water saturated conditions. The magma evolved to this composition by crystallising two feldspars throughout its ascent. It was possible for crystallisation of two feldspars to occur at hypersolvus pressures because crystallisation of the feldspars resulted in increasing saturation of the liquid in silica and water, which was buffered by a reduction in the stability field of quartz due to falling pressure. This reduced the range of solid solution between the co-existing feldspars and extended the range of the two feldspar plus liquid field. This model is consistent with the extreme quartz enrichment of the coarse granite magma. The magma which crystallised to form the group 3 rocks fractionated quartz after polybaric fractionation of orthoclase and plagioclase had caused supersaturation of quartz in the melt as it rose toward the surface. It therefore appears that the major element chemistry (and hence trace element chemistry) of the evolving liquid was controlled by crystallisation during its ascent from high to low pressures.

5.5 The Fabric of the Coarse Granite.

The coarse granite can be divided into three petrographic groups which can also be resolved on chemical grounds. This section discusses the textural variation within these groups and the possible causes of the observed variations.

The rocks of group 1 show very little internal variation in texture. As noted in section 5.2 some of the rocks are slightly more porphyritic than the granular rocks which characterise the group. The rocks of group 3 show a wide range in texture, while remaining similar to the rocks of group 1. Group 3 rocks range from medium to coarse grained granular rocks to medium to coarse grained strongly porphyritic rocks with a fine grained groundmass. These variations are not mappable due to poor exposure but do not seem to be bounded by marked textural discontinuities. Variations in texture appear to occur across gradational boundaries. Rocks of group 2 show the most significant textural variations. Internal fine grained sheets were described in section 5.2 (Fig. 5.1), from the Garbh Allt, Abhainn Tunna and North Glen Sannox. Other less well developed sheets were noted in the south face of Cir Mhor, to the west of A' Chir and on Meall Bhig (GR 904464). Trace element data for these fine grained rocks (Figs 5.37 & 5.38) show they are strongly depleted in Ba and Sr, and enriched in Rb, and slightly depleted in SiO_2 relative to the coarse grained group 2 rocks which they grade into. Hence it is apparent that they represent fractionated liquids (i.e. liquid from which quartz and feldspars have crystallised and separated). As the grain size of the rock increases toward the normal coarse granite there is an initial increase in the proportion of phenocrysts in the rock followed by an increase in the grain size of the groundmass. This gradation from liquid to solid dominated texture cannot be explained by sidewall crystallisation processes since this would produce the reverse relationship. It is proposed that the sheets are formed by an inward migrating crystallisation front intersecting flowing magma.

The fluid dynamics of magmas and their changing dynamic properties during

crystallisation has been discussed in theoretical terms by Shaw (1965), Komar (1972), Arzi (1978), McBirney & Murase (1984) and Weinstein et al. (1988) and in experimental terms by Sparks et al. (1984) and Turner & Campbell (1986). In particular Sparks et al. (1984) discussed the effect of increasing crystal content on the type of convective flow in magma chambers and Marsh & Maxey (1985) and Weinstein et al. (1988) showed, by theoretical analysis and experiment, the distribution patterns of crystals within the flow.

Convection in a magma body occurs when the bouyancy forces driving convection overcome the viscous drag forces which oppose fluid flow. The ratio of these forces is given by the dimensionless thermal Rayleigh number Ra_T. When the Rayleigh number exceeds $\approx 10^3$ convection will occur.

$$Ra_T = \frac{g\alpha\Delta T d^3}{\kappa_T \mu} \qquad 5.3$$

where g is the acceleration due to gravity, α is the coefficient of thermal expansion ΔT the temperature difference across a fluid layer of thickness d, κ_T is thermal diffusivity and μ is the viscosity of the magma. Shaw (1965) showed that above $Ra_T \approx 10^6$ the flow of magma is turbulent. Below this value flow would be partially turbulent or completely laminar. Since all the properties of the system will remain approximately constant during the early stages of crystallisation (d will decrease with time during sidewall crystallisation) the major control on flow regime is the viscosity of the magma which is strongly dependent upon crystal content (Arzi, 1978; McBirney & Murase, 1984). The Ra_T for a range of magma viscosities/crystal contents for the Arran granite at low degrees of solidification of the magma body (i.e. d $\approx$ constant) with a minimum thermal gradient of 10^oCkm^{-1} (convective transfer of heat reduces the gradient to a minimum) was calculated and plotted (Fig. 5.42). This shows that the coarse granite was a large enough body to have convected when its crystal content was less than 70%. For crystal contents between 70% and 50% convection would have been laminar and below 50% flow would have been turbulent.

Figure 5.42. The variation in thermal Rayleigh number Ra_T with magma viscosity/crystal content. The graph shows the range of viscosities over which the magma will undergo laminar and turbulent convection.

Fig. 5.42.

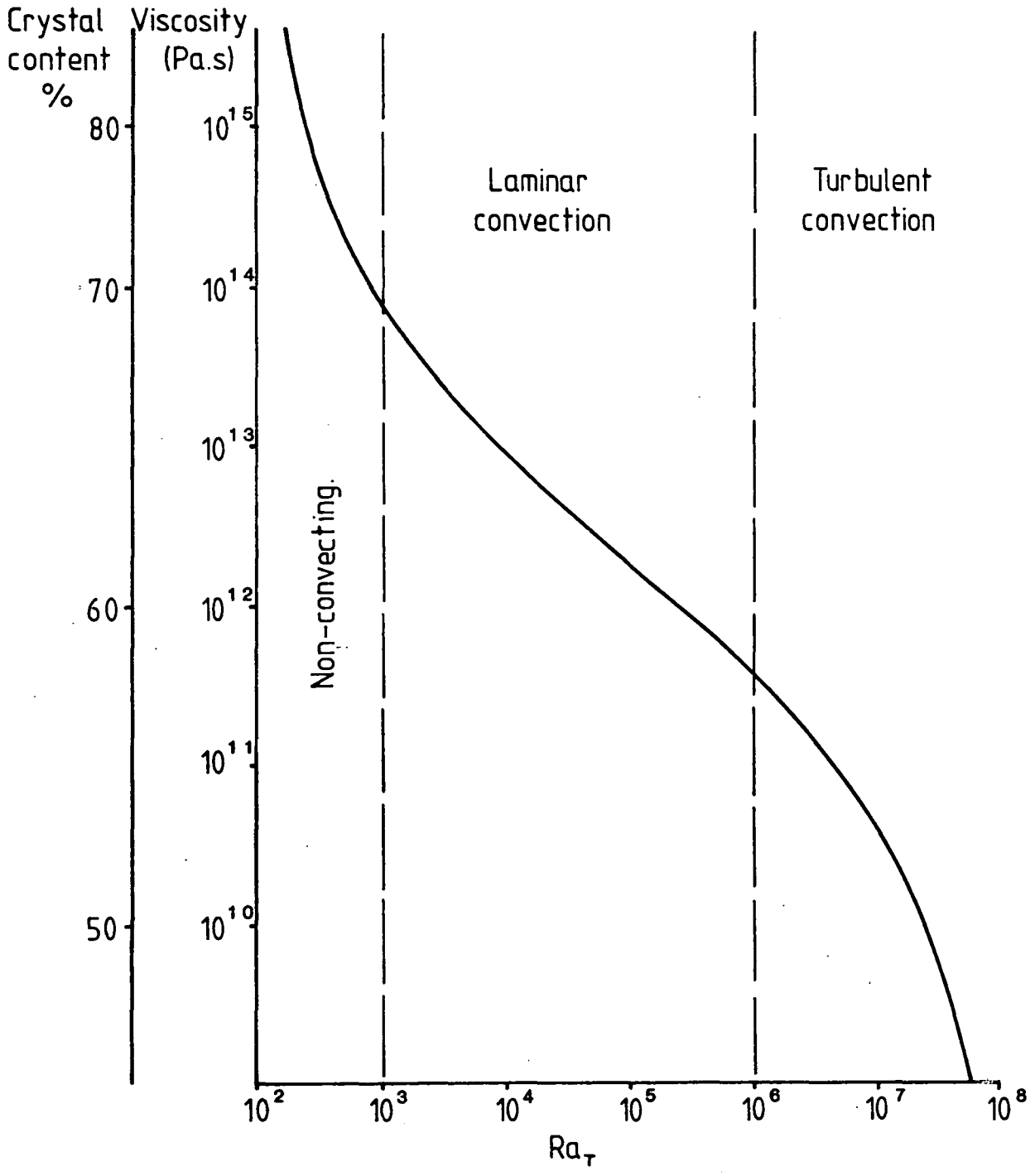
Crystal content %
Viscosity (Pa.s)
80
70
60
50
10^{15}
10^{14}
10^{13}
10^{12}
10^{11}
10^{10}
Laminar convection
Turbulent convection
Non-convecting
10^2
10^3
10^4
10^5
10^6
10^7
10^8
Ra_T

Weinstein et al. (1988) showed by theoretical and experimental analysis that during convective flow crystals were entrained into stream lines separated by comparitively crystal free zones. Crystal free zones would exist at the margins of the magma chamber where shear strains on the flow are highest, due to the Bagnold effect (Komar, 1972 and Thompson & McBirney, 1985) which occurs during laminar flow. Hence the fine grained sheets could be interpreted as having crystallised from a crystal poor zone of convecting magma sweeping across the inward migrating crystallisation front within the magma chamber (Fig. 5.43). These fine grained sheets are discontinuous (section 5.2) which suggests they are only a local phenomena. This could be explained in terms of different crystallisation rates at different times in different parts of the chamber. The governing factor in preservation of the fine sheets would be the rate of inward migration of the crystallisation front away from the contact with the country rock. Where this is rapid it would freeze the convecting flow. If it was slow the convecting flow would scour the inner wall of the chamber and hence remove any crystals beginning to adhere to the crystallisation front (Fig. 5.43). Carrigan (1986) plotted a graph of cooling time against size of magma body for cooling by conduction. From this a crude estimate of $2 \times 10^{-7} ms^{-1}$ for the velocity of the crystallisation front can be determined from the gradient of the graph, assuming a constant rate of crystallisation. This is considerably less than the velocity of convective overturn ω_m determined from:

$$\omega_m = B[(g\alpha\Delta T)^4 \kappa_t^2 \frac{d^2}{\mu}]^{\frac{1}{9}} \qquad 5.4$$

after Sparks et al. (1984), where B is an experimentally determined constant equal to 0.44. Other variables are as given in equation 5.3. For the coarse granite the velocity for convective overturn is $2 \times 10^{-4} ms^{-1}$ for a magma body containing 50% crystals and $1 \times 10^{-4} ms^{-1}$ for a magma containing 70% crystals. (Ignoring the effects of non-uniform viscosities due to entrainment of crystals in stream lines.) Hence in the case of the coarse granite the laminar flow velocity always exceeds

Figure 5.43. Schematic diagram illustrating the proposed mechanism of formation and preservation of the fine grained sheets within the coarse granite.

Fig. 5.43.

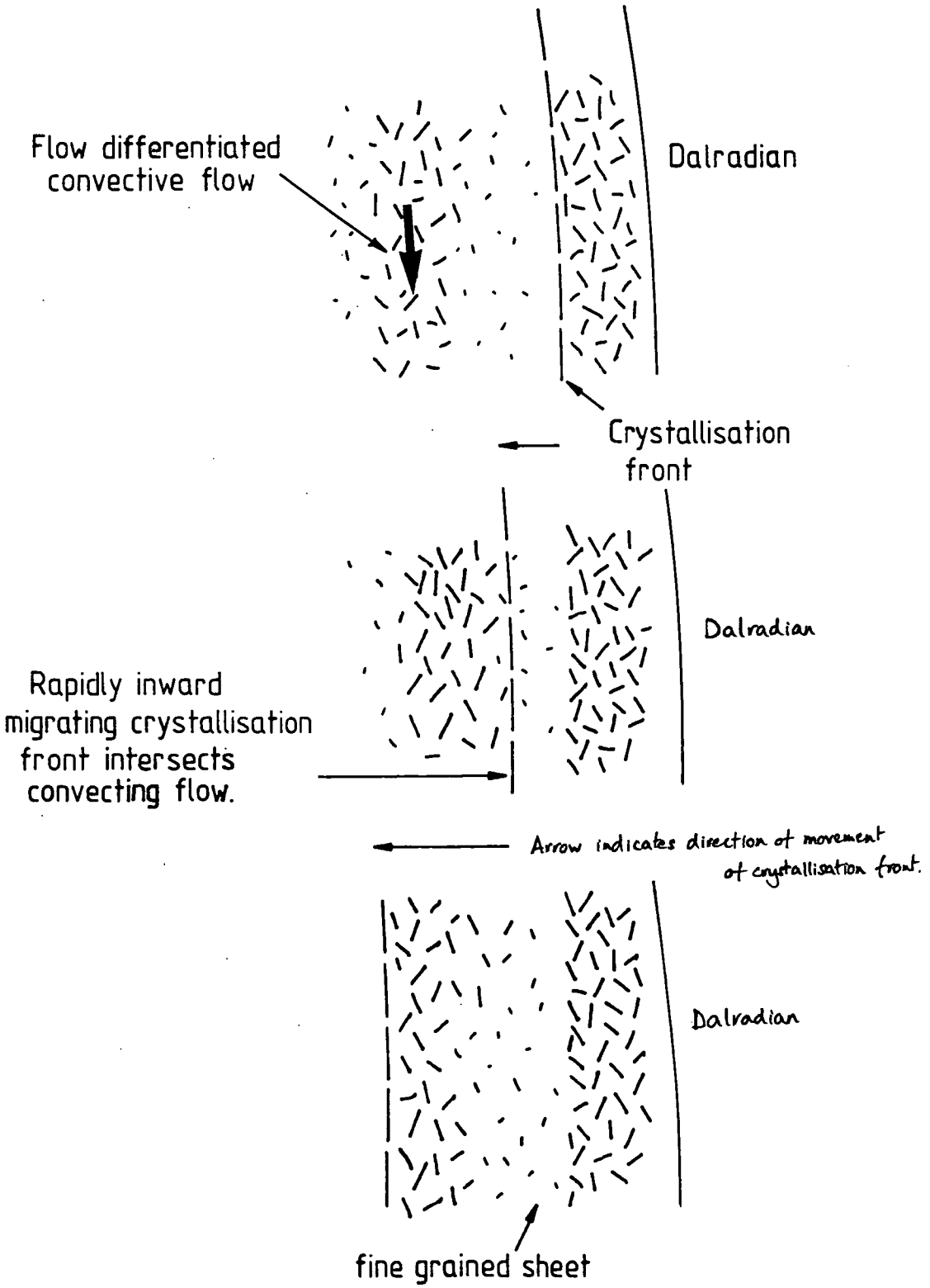
Flow differentiated convective flow
Dalradian
Crystallisation front
Dalradian
Rapidly inward migrating crystallisation front intersects convecting flow.
Arrow indicates direction of movement of crystallisation front.
Dalradian
fine grained sheet

the rate of inward migration of the crystallisation front. Since the relative velocities of the crystallisation front and the convective flow are normal to each other sidewall crystallisation would progress inward, providing that the walls ~~are~~ were not continually scoured by convective flow, but not at a sufficient rate to trap any flows, which would immediately carry away any nucleating cystals within them. Clearly exceptional circumstances, such as a local surge of the crystallisation front are required to trap the flowing magma so that it crystallises sufficiently to prevent it from flowing further. Such areas of rapid cooling (if the interpretation of the fine sheets is correct) have no relation to any exposed structures in the pluton or the aureole which may have caused an enhanced rate of heat loss (e.g. major faults, such as the Goat Fell Fault). Hence it is concluded that the pattern of inhomogeneous crystallisation indicated by the sheets is dependent upon a process occuring within the magma chamber independently of external controls (e.g. transfer of heat by convection) (Plate 5.4).

With the exception of the foliated cataclasites developed along the Goat Fell Fault (section 4.6.3) the coarse granite shows no visible mineral alignment or a foliation. Other well documented plutons which have strongly deformed aureole rocks are always foliated. In this respect the coarse unit of the Northern Arran granite may be unique. Davies (1982) has described a diapiric granite (the Ash Sha'b diapir) from the Ajjaj shear zone in Northern Saudi Arabia in which 'tectonite fabrics are scarce'.

Hutton (1988a) reviewed the development of fabrics in granitic rocks and produced a two fold division based on the rheological boundary referred to as the critical melt percentage at which a magma ceases to be a suspension of crystals with the physical properties of a liquid and becomes a low melt fraction solid, in which crystals form an interconnected network. Hutton (1988a) defined pre-full crystallisation fabrics as those which resulted from alignment of crystals during the flow of magma in response to internal bouyancy forces or tectonic stresses

Plate 5.11. Flow banding in the coarse granite at the north end of the A'Chir ridge. Weathering has enhanced this banding in the coarse granite (not seen elsewhere) which is thought to represent flow banding in the granite as a result of convection. No visible evidence of mineralogical banding of the granite was associated with this feature. Outcrop is approximately 10 m high.

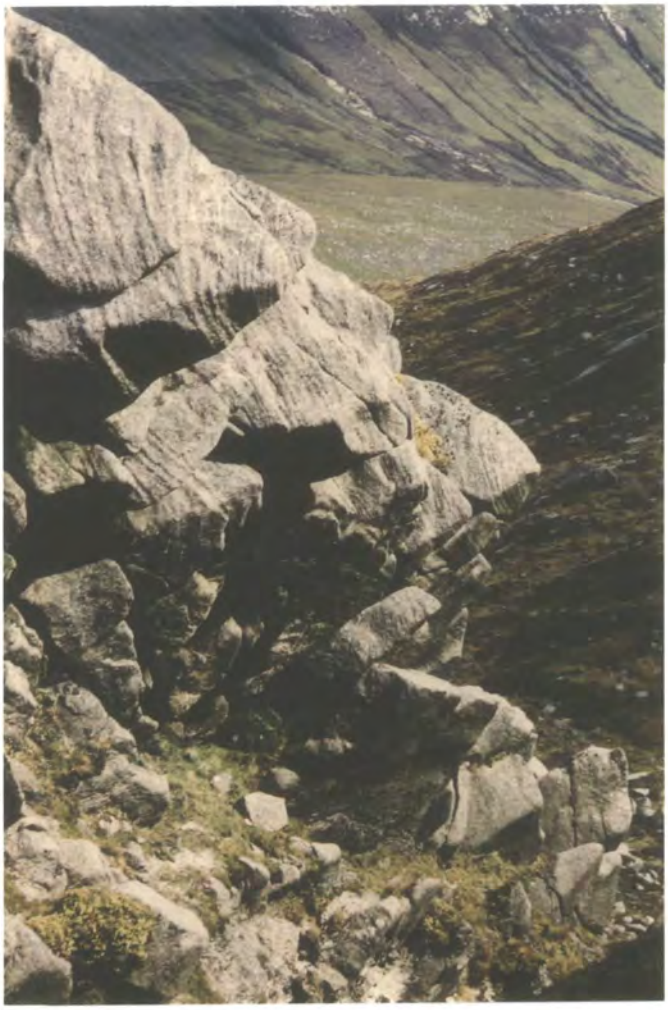

and crystal plastic strain fabrics as resulting from deformation of low melt fraction rocks by crystal plastic strains. The latter rocks are frequently difficult to distinguish from deformed metamorphic rocks. The redistribution of melt during deformation of low melt fraction rocks has been discussed by Hibbard (1987).

The critical melt percentage lies between 50 and 70% crystallisation (Arzi, 1978; Fig. 5.44). Between these melt fractions the magma viscosity increases rapidly as the magma becomes an interconnected network of crystals with interstitial melt. The actual point at which 'lock-up' occurs is probably different for different magmas and is clearly dependent upon crystal size, shape and degree of sorting (Arzi, 1978), melt viscosity and temperature (McBirney & Murase, 1984), ~~and~~ the ability of the magma to wet grain edges and surfaces (Hunter, 1987), and the kinetics of nucleation and crystal growth (Jurewicz & Watson, 1985 and Marsh, 1988). Consequently it should be emphasised that the type of fabric resulting from deformation of a magma is controlled by factors which may alter during or as a result of the deformation and the changing properties of the precipitating crystals.

Petrographic and field evidence indicate that the coarse granite magma was predominantly liquid with a relatively low crystal content when it was chilled against the contact with its present wall rocks. Group 2 rocks collected from the chilled margins contain up to 46% phenocrysts (average 26%). Hence it would appear that conditions for the development of pre-full crystallisation fabrics were satisfied.

However pre-full crystallisation or flow fabrics did not develop in the coarse granite because of the following factors: firstly, although certain marginal rocks contain up to 46% phenocrysts the average for the group 2 rocks is 23% and for the group 1 rocks 8%. Hence the percentage of crystals in the melt was low and therefore modification of the velocity field of the melt around individual crystals is unlikely to effect adjacent crystals since they would be separated by relatively large

Figure 5.44. The variation in magma viscosity with increasing crystal content (CMP - critical melt percentage) (after Arzi, 1978 and van der Molen & Patterson, 1979).

Fig. 5.44.

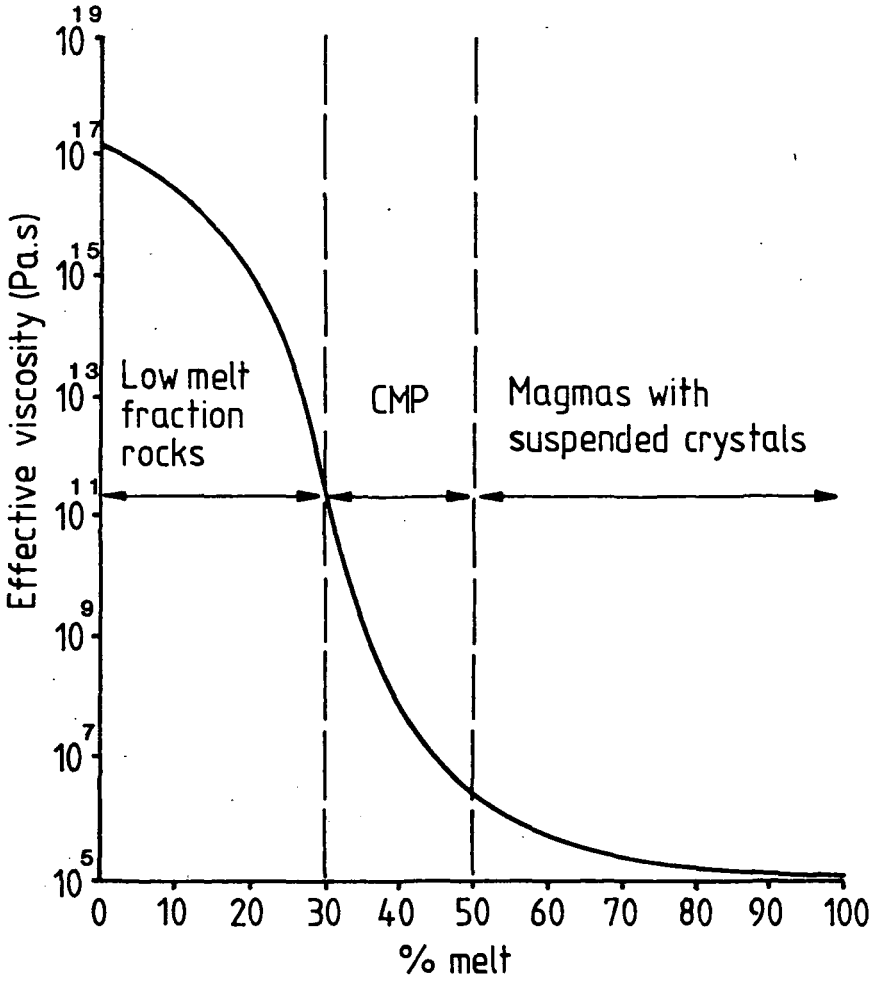
Effective viscosity (Pa.s)
10^19
10^17
10^15
10^13
10^11
10^9
10^7
10^5
Low melt fraction rocks
CMP
Magmas with suspended crystals
0
10
20
30
40
50
60
70
80
90
100
% melt

distances. The variation in velocity (or acceleration) within the melt is responsible for applying stresses to the crystals which cause them to rotate (Komar, 1982). If the crystals were separated to such an extent that their local velocity fields would not interfere no alignment of the crystals would occur. Therefore no fabric would develop. Secondly, for low crystal contents the flow of magma during convection would be turbulent (Fig. 5.42) and hence no constant direction of flow would exist for any distance. Hence the alignment of crystals would be random. Thirdly the phenocrysts described from the coarse granite are typically equant (section 5.2) and consequently would not have a preferred orientation in a flow.

While the existing work on the development of flow fabrics has done much to elucidate the process by which they occur, and the subsequent effects of distribution of crystals within a flow, it is clear that adequate boundary conditions for the development of such fabrics have not been determined. These boundary conditions are probably variable and dependent upon those factors already discussed above e.g. crystal size, shape and sorting, melt viscosity, temperature and crystallisation kinetics. Consequently it is impossible to make accurate inferences about the state of crystalliation of the coarse granite magma purely on the basis that it does not contain a flow fabric.

Holder (1988) and Hutton (1988b) have used deformed mafic xenoliths to measure patterns of strain induced by flow or deformation of the magma. No such xenoliths occur in the northern granite, and hence patterns of strain could not be determined by this technique.

It is also apparent from the petrography of the coarse granite that it does not have a penetrative fabric similar to that observed in gneissic rocks which is associated with deformation of a magma with a low crystal content (Hibbard, 1987). Hence it appears that the granite was not strongly deformed at any stage during or after it crystallised although its aureole was strongly deformed during emplacement (Chapter 4).

This ambiguity can be explained with reference to the physical state of the magma during the final stages of emplacement. The petrographic and isotopic data indicate that the granite was emplaced as a single magma body. Other well documented internally deformed diapiric plutons e.g. Ardara (Holder, 1979) are composed of two or more concentric units. Later pulses of magma intrude and deform earlier pulses. The later pulses are generally less deformed than the earlier units. The latter are typically highly deformed at their contacts with the country rock or immediately preceeding pulses of magma. In simple terms this process represents liquid being injected into a solid. If the solid has a framework e.g. an interconnected crystalline fabric, that framework will deform or flow in reponse to the stresses at the surface of the liquid. However the liquid will have no such fabric (at low crystal contents the crystals will not be close enough to interact - see above). Consequently the stresses in the liquid at its contact with the solid will be distributed hydrostatically (i.e. equally in all directions) throughout the liquid so that the resolved stress at any point within the liquid is zero. Therefore no fabric or crystal alignment will develop in a magma while it is behaving as a liquid (i.e. below the critical melt percentage), or more accurately at the crystal concentration below which the stress fields around individual crystals do not interfere. This occurs at 8% for equidimensional solid suspensions of crystals in liquids (Komar, 1972). In magmas this value may be much higher. In particular an irregular distribution of crystal sizes may increase the value (Arzi, 1978).

This argument implies that while the intruding coarse granite deformed its wall rocks it must have remained liquid (in the sense that its crystal content did not exceed the critical melt percentage). It also indicates that magmas may deform their aureole rocks without recording any internal strain up to the point where they may be as much as 70% crystallised. Hence it appears, if this hypothesis is correct, that the coarse granite passed through the critical melt percentage after it had been emplaced at its present level and attained its present shape by

deformation of its aureole.

There is some evidence for comparatively low stresses acting on the magma during the late stages of crystallisation (i.e. > 70% crystallisation). As noted in section 5.2 many crystals of quartz show undulose extinction and subgrains, and crystals of intersertal biotite are frequently distorted (Plate 5.12). These crystal plastic strain fabrics are found in rocks of all three petrographic groups but are most common in the group 2 rocks which have the highest concentrations of phenocrysts. The phenocrysts are commonly separated by films of intersertal melt. Quartz grains are surrounded by films of feldspar and feldspars are surrounded by films of quartz. Although no chemical data are available for these films it is thought that they represent the remains of an interconnected network of residual melt of initially uniform composition. Feldspars are now surrounded by films of quartz since further crystallisation of feldspar from the adjacent melt film would have left the evolved melt film depleted in feldspar and enriched in quartz, while crystallisation of quartz from the melt film would leave adjacent melt enriched in feldspar. This process relies on the assumption that diffusion rates were low relative to the rate of cooling during the late stages of crystallisation.

Experimental work at 5 kbar pH_2O, by Winkler & Schultes (1982), showed that for three granites of varying modal composition, crystallisation of the last 30% of the melt occurred over a very narrow temperature range ($< 5^oC$) which suggests they had evolved to eutectic compositions, as in the case of the coarse granite (sections 5.3.2 and 5.4). These experimental data also indicated that crystallisation of large phenocrysts is inhibited at melt contents of less than 30%.

Two important conclusions pertinent to the crystallisation of the Northern Arran Coarse granite can be drawn from this work. Firstly that crystallisation of the last 30% of melt in the coarse granite magma probably occurred rapidly, since it would have required only a small decrease in temperature. Hence preservation of un-re-equilibrated melt films may have been possible, and the physical properties

Plate 5.12. This photomicrograph shows well developed undulose extinction and subgrain development in quartz and distortion of the cleavage in a biotite crystal (lower right). These strains are thought to be the result of late stage compaction of partially crystallised magma. (See plates 5.8 & 5.9.) Coarse granite, No. 97391. Width of field = 3.5 mm, crossed polars.

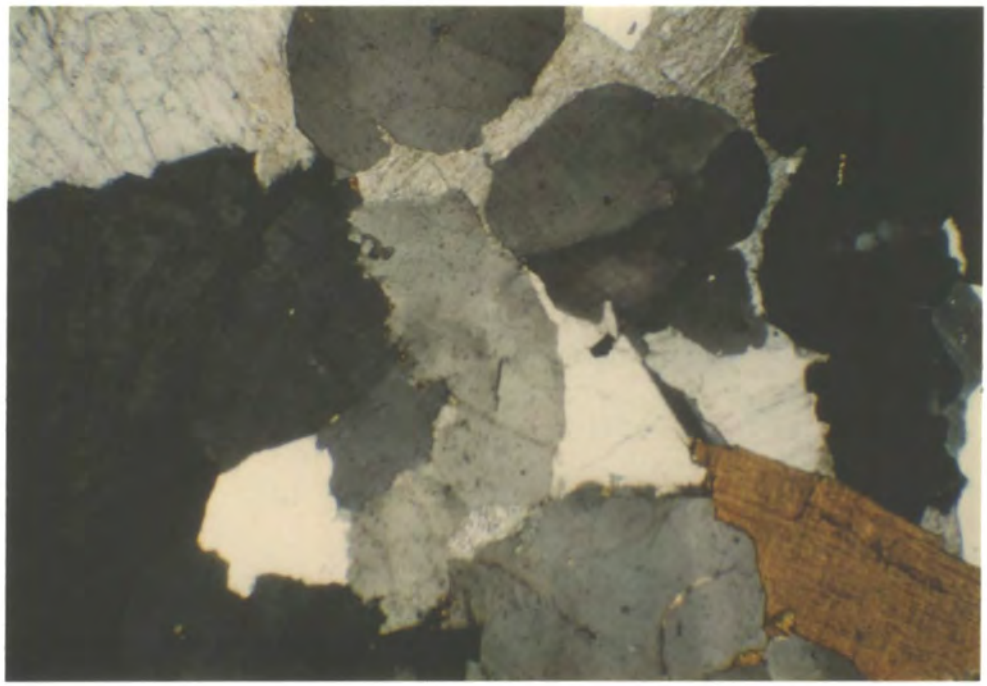

of the magma would have changed from liquid behavior to solid behavior in a very short time interval. This would not be observed for rocks with longer crystallisation intervals or which do not represent eutectic compositions. This aspect of the rate of crystallisation of a magma may have a significant influence on fabric development. Secondly the high phenocryst percentages noted in some of the group 2 rocks (70 - 80%) are not compatible with crystallisation of a magma without some loss of interstitial melt from the evolving crystal-liquid mush.

It is thought that the internal deformation of the quartz and biotite grains is the result of the effect of an applied stress on an almost completely solid magma, although it is equally possible that the deformation occurred at subsolidus temperatures. An enhancement of the perthitic texture in the alkali feldspars might be expected due to exsolution resulting from re-ordering of the crystals under stress (Gates, 1953). The cause of this deformation is not clear (in the absence of strain markers with which to plot the strain field in the pluton) other than stresses related to the emplacement of the magma. These stresses may have resulted from further upward and outward movement of more liquid and hence more bouyant magma at the core of the pluton. The initial phase of this deformation could have caused expulsion of interstitial melt from the crystallised magma at the walls of the intrusion by compaction of the network of crystals. This would account for the anomalous crystal:melt ratio seen in some of the group 2 rocks and also the aggregate texture of the rocks composed largely of phenocrysts of feldspar surrounded by clusters of quartz, with a fine grained or intersertal groundmass, to produce a bimodal grain size distribution (section 5.2). A schematic diagram of the inferred evolution of this texture is given in Figure 5.45. Since this compaction fabric is found in rocks near the margin of the granite and in the core of the intrusion it appears that the compaction process must have occurred throughout the cooling of the pluton. As there is no intensification of strain toward the margin of the pluton it is thought that the compaction process must have occurred in response to

Figure 5.45. Schematic diagram illustrating the development of the 'compaction' texture commonly recorded in the coarse granite, particularly in rocks of group 2.

Fig. 5.45.

Evolution of compaction texture in group 2 rocks.

a

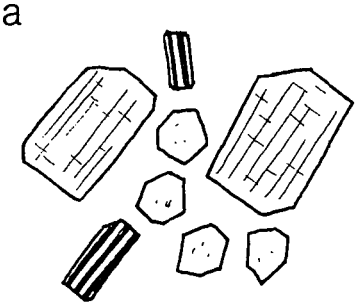

Growth of phenocrysts of quartz, plagioclase and orthoclase.

b

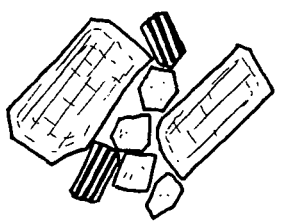

Crystals accumulate at sidewall. Compaction of magma expels melt from between crystals.

c

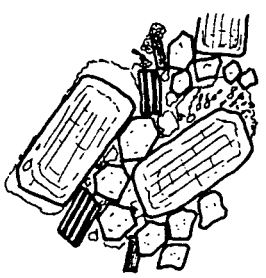

Crystallisation of groundmass. Further compaction produces crystal plastic strains.

1 cm

stresses which were not large enough to deform the granite once it had completely solidified.

Further evidence of expulsion of the interstitial evolved melt from the compacting wall rocks can be obtained from the aplites which cut the coarse granite. These show two types of contact with their host (section 5.2). Some have very sharp straight contacts (Plate 5.13). Others have irregular diffuse contacts. One specimen collected (AR5231) shows progessive disaggregation of the coarse granite toward the aplite, suggesting expulsion of interstitial evolved melt into an opening cavity as described by Hibbard & Watters (1985). This origin for the aplites is to a certain extent confirmed by their trace element compostions which are extremely evolved compared to the range of compositions of the coarse granite (Figs. 5.46 & 5.47). If this interpretation is correct the aplites would have compositions close to that of the evolved melt derived by boundary layer crystallisation and trapped within the crystal mush. Some re-equilibration of this melt with the surrounding crystals and the occurrence of xenocrysts derived by disaggregation of the coarse granite during separation of the liquid could explain the variability in compostion shown by the samples, and hence make their interpretation complex. It is clear that low melt fraction magmas can sustain shear stresses, and hence fracture (Hibbard & Watters, 1985; Wickham, 1987). It has not been determined whether these fractures are uniform and planar or whether they would be irregular. In completely solid rock the fractures would be planar since the completely interconnected fabric of the rock would transmit an approximately uniform stress field. However in the case of a low melt fraction magma where liquid filled pore spaces exist and the fabric of the magma is not strictly coherent an applied stress may not be transmitted uniformly. This could explain why certain aplites injected into partly solidified magma are very irregular. The geometry of the aplites (Fig. 5.2) does not provide any data on the possible orientation of the stresses acting on the magma during their injection, with the exception of those which exploit the

Plate 5.13. Fine grained planar aplites with sharp margins cutting the coarse granite.

Figure 5.46. Ba (ppm) plotted against Rb (ppm) showing the compositional range of the aplites (triangles) in comparison with the three petrographic groups of the coarse granite.

Fig. 5.46.

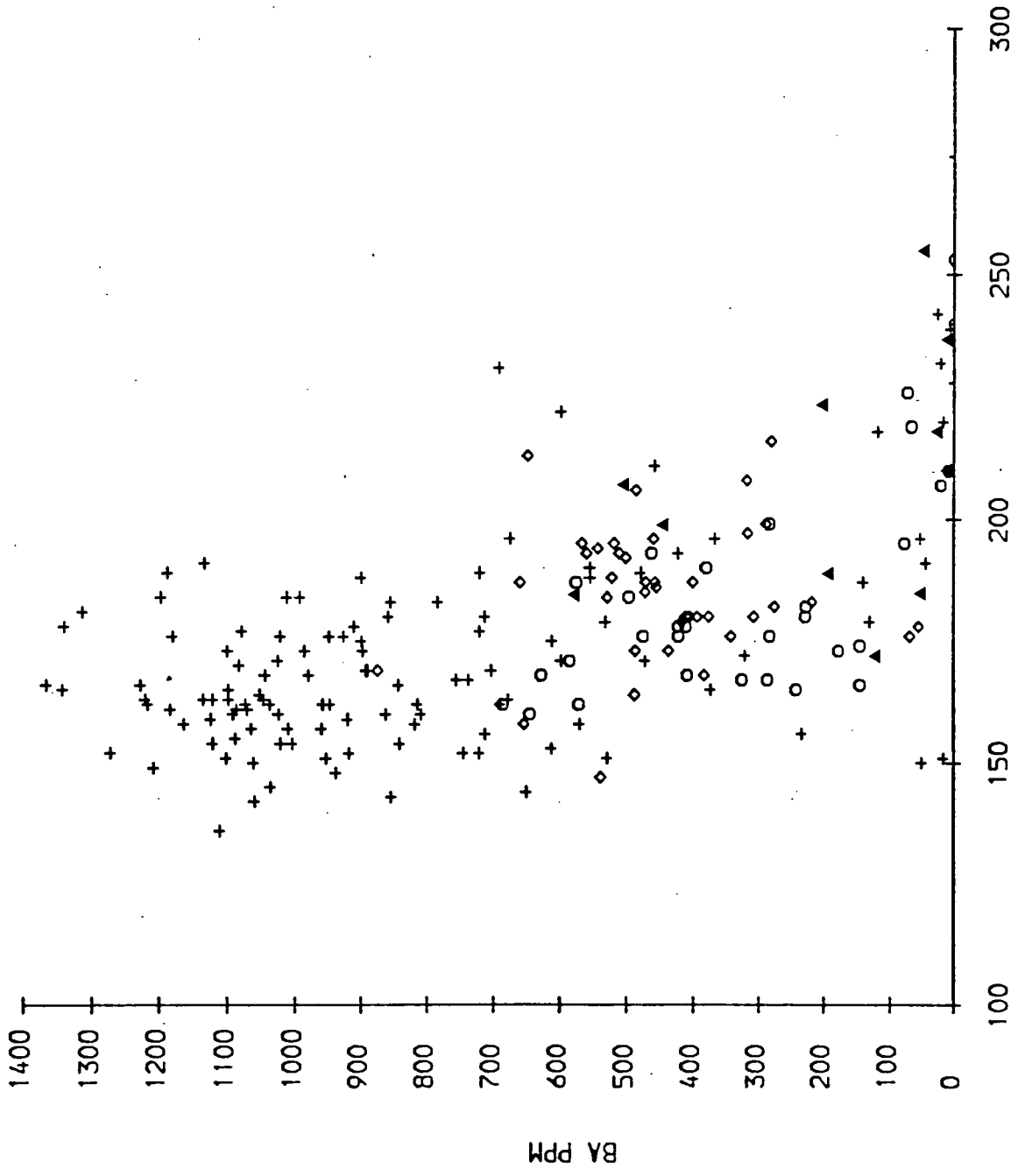
BA PPM
0
100
200
300
400
500
600
700
800
900
1000
1100
1200
1300
1400
RB. PPM
100
150
200
250
300

Figure 5.47. Sr (ppm) plotted against Rb (ppm) showing the compositional range of the aplites (triangles) in comparison with the three petrographic groups of the coarse granite.

Fig. 5.47.

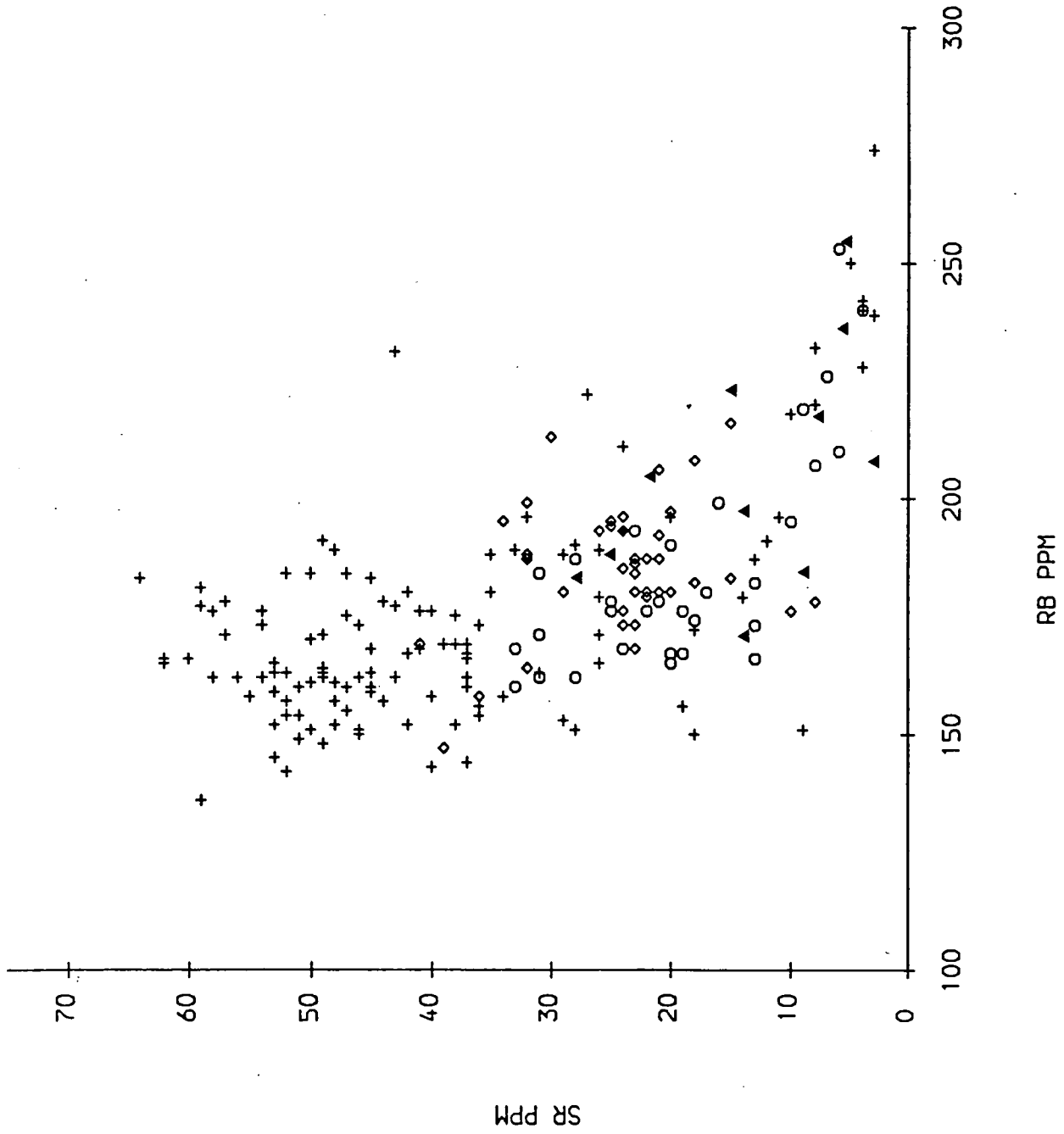

horizontal joints developed in the margin of the intrusion (Chapter 4).

To summarise: The coarse unit of the Northern Arran Granite shows very little textural variation. Simple fluid dynamic analysis of the magma body indicates that it would have convected during the early stages of crystallisation. This process is thought to be reflected in the development of fine grained sheets with sharp contacts toward the margin of the intrusion and gradational contacts with coarse granite toward the core of the pluton which formed by the intersection of a rapidly inward migrating cooling front with a flow differentiated current of magma crossing the inner wall of the pluton. The preservation of these sheets clearly indicates surges in the rate of crystallisation in different areas which bear no relation to structures in the aureole which could enhance heat loss. Consequently it is thought that the pluton cooled inhomogeneously.

The granite shows no foliation or mineral alignment fabric, in contrast to its strongly deformed aureole. It is concluded that the granite could not have deformed its aureole without developing a fabric unless it behaved as a liquid so that stresses at its contact with the country rocks were transmitted as hydrostatic stresses through the magma.

Undulose extinction in quartz grains, distorted crystals of biotite, preservation of interstitial melt as intersertal quartz and feldspar and anomalously high phenocryst concentrations are taken as evidence that the magma suffered compaction at an advanced stage of crystallisation. This is thought to have resulted from the continual upward and outward movement of liquid in the core of the pluton. This compaction is thought to have produced the aplites by expulsion of evolved melts during fracturing of low melt fraction magma.

5.6 A Model for the Evolution of the Northern Arran Coarse Granite.

Isotopic evidence indicates that the magma from which the coarse granite evolved fractionated from a basaltic parent contaminated with partial melts of crustal rocks. This contamination appears to have occurred in an intense lower crustal dyke swarm, heat from which caused partial fusion of crustal rocks along the walls of the dykes. This liquid would have a composition close to the minimum melting point at 11 kbar and hence would be enriched in those elements concentrated in the liquidus phases at the eutectic. When mixed with the basaltic magma the partial melt would have caused enrichment of Ba, Rb, Sr, U, Th, Pb, K and the light REES in the basic magma. Contamination by Rb, Sr, U, Th and Pb caused changes in its isotopic signature. In particular different degrees of Pb contamination cause the Tertiary igneous rocks of Arran to show a range of Pb isotope compositions which define a pseudo-isochron of 770 Ma age. Uncertainties in the determination of this isochron allow for contamination by 1100 Ma old Grenvillian lower crustal granulites which appear to form the floor to the Palaeozoic rocks of the Midland Valley and the Dalradian further north (Chapter 2).

Subsequent fractionation of the basic magma toward a minimum melting point granite by separation of plagioclase, pyroxene and some alkali feldspar resulted in Ba, Sr and Ti depletion of the magma, which remained enriched in Rb, Th and K. Sr depletion of the granite magma made it vulnerable to Sr isotopic contamination by further partial melts of crustal rocks. This does not appear to have occurred. Changes in the Sr isotope composition would be accompanied by variations in Pb isotopes. By using these two isotopic systems it is possible to rule out significant post differentiation contamination of the granitic magma. This eliminates ascent of the magma by significant amounts of stoping and digestion of country rock. The structural data suggests that the granitic magma rose as a diapir. This implies that it must have accumulated at some depth below its present level in the crust.

This depth can be constrained by the isotopic data. The range of Pb isotope variation for the acid and basic Tertiary igneous rocks of Arran indicates they are not contaminated by Dalradian material (which would cause them to show a very different range of isotope compositions) and that contamination is dominantly by partial melts of lower crustal rocks. Hence it is concluded that the granitic magma which rose to form the northern granite must have accumulated and differentiated in the region of the boundary between the Dalradian upper crustal rocks and the mid crustal (? Grenvillian) rocks, which during the Palaeocene would have occurred at a depth of approximately 11 km.

The narrow range of variation in isotope compositions of samples from the coarse granite, coupled with the narrow range of concentrations of trace elements not involved in fractionation, some of which (e.g. Th, Pb and U) were susceptible to contamination, indicate that it rose as a single body of magma. The chondrite normalised incompatible element pattern for the coarse granite indicates that it fractionated plagioclase, orthoclase, apatite, zircon and pyroxene or Ti-oxide prior to its ascent.

Variations in Ba and Sr are considered to be the result of continuing fractionation of orthoclase and plagioclase during the ascent and final emplacement of the magma.

As the granite rose from the depth at which it accumulated the falling pressure would have resulted in a contraction of its crystallisation interval by increasing the solidus temperature and decreasing the liquidus temperature. This would have resulted in crystallisation of orthoclase and plagioclase causing SiO_2 enrichment of the melt, forcing its composition toward that at the minimum melting point in the granitic system. However falling pressure would also reduce the stability field of quartz (i.e. increase its solubility in the melt) which would produce the extreme silica enrichment of the melt. Samples of chilled magma collected from the margins of the pluton contain phenocrysts of quartz, orthoclase and oligoclase

which indicate that the melt had evolved to a minimum melting point composition prior to reaching the level at which it was emplaced. Evolved samples of coarse granite are depleted in quartz which suggests this phase was selectively fractionated from the melt during the last stages of crystallisation. Normative data for the coarse granite plotted in the system quartz – albite – orthoclase indicates that it crystallised at a pressure of between 0.5 and 1 kbar pH_2O which indicates a depth of between 1 and 3 km below the surface.

The absence of a well developed fabric in the coarse granite indicates that it must have behaved as a liquid while it was emplaced into and deformed its aureole. Textural variations in the granite can be related to processes of crystallisation. The intrusion can be divided into three types on the basis of these variations in texture. Group 1 rocks, restricted to the margins of the pluton are porphyritic rocks with a well developed coarse grained groundmass. Group 2 rocks are very coarse grained and lack a well developed groundmass, being largely composed of phenocrysts of quartz and feldspars. Group 3 rocks, which occur in the core of the intrusion are more variable, but are generally porphyritic with a finer grained groundmass. Group 1 and group 3 rocks are considered to have crystallised from liquids with high proportions of phenocrysts. Group 2 rocks are interpreted as the crystallised products of a crystal liquid mush. The three groups are separated by gradational boundaries.

Variations in trace element chemistry reflect these textural variations. Ba and Sr show the widest range in concentrations reflecting fractionation of orthoclase and plagioclase feldspar which is confirmed by the presence of these phases as phenocrysts in all three texturally defined groups. Modelling of the range of compositions by fractional crystallisation indicated that all three textural groups must represent crystal liquid mushes with increasing amounts of phenocrysts in groups 1 and 3. This is not compatible with the petrographic data. It also indicated that group 2 rocks should have crystallised first and groups 1 and 3 crystallised after

from the resulting depleted liquid. Assuming heat loss occurred through the walls of the chamber this would mean the group 2 rocks would have to occur along the walls of the chamber, which is clearly not the case since the group 1 rocks occupy this position.

The crystallisation sequence inferred by the distribution of the three groups within the pluton and their range of chemical compositions can be predicted by sidewall crystallisation involving 30% equilibrium crystallisation of an evolving boundary layer. Initial cooling of the crystal bearing magma, evolved during ascent, adjacent to the margin of the intrusion produced the group 1 rocks. The relatively narrower range of the group 1 rocks suggests equilibrium crystallisation dominated this stage of cooling. This also compatible with the restricted degree to which crystal separation can occur in granitic magmas. This stage was followed by sidewall crystallisation producing the group 2 rocks, which involved the accumulation of crystals and trapped interstitial melt on the inward migrating walls of the chamber and formation of a boundary layer of differentiated liquid. This boundary layer was then separated from the sidewall by convection and the evolved liquid mixed with the 'unevolved' reservoir at the core of the intrusion. The group three rocks crystallised from the magma remaining at the core of the pluton after sidewall crystallisation ceased.

Sidewall crystallisation produces a narrower range of liquid and coexisting solid compositions than fractional crystallisation. This is consistent with the range of compositons of the rocks occurring in the coarse granite and their textural characteristics. Sheets of fine grained granite within the coarse show a wide range of evolved to unevolved compositions consistent with trapping of liquids, derived by boundary layer crystallisation or from the reservoir at the core of the pluton, by inward migration of crystallisation fronts. The irregular distribution of these sheets suggests that crystallisation of the granite following emplacement was inhomogeneous. The range of variability in chemical composition of the sam-

ples from the coarse granite may also be enhanced by incorporation of phenocryst feldspars crystallised during the ascent of the magma and by variable degrees of liquid separation from the crystal liquid mush forming at the walls of the magma chamber.

Many of the rocks, particularly those of group 2, show a well developed compaction texture. Crystals form interlocking aggregates, quartz crystals commonly show undulose extinction and the development of subgrains, and flakes of biotite are distorted. These features are compatible with the granite experiencing low compressive stresses during and after crystallisation. It is thought these stresses are the result of upward and outward movement of the reservoir of liquid at the core of the pluton during crystallisation. Compaction of the crystal mush developed during sidewall crystallisation resulted in the expulsion of interstitial liquid to produce artificial phenocryst enrichment of the rocks, which may be regarded as a form of textural disequilibrium. Later compression after solidification would result in the low crystal plastic strains recorded by the deformed quartz and biotite. Stresses acting on the crystal liquid mush may have caused it to fracture. These fractures would fill with interstitial liquid, aiding the melt expulsion process and producing aplites.

This model for the evolution, ascent and final crystallisation of the coarse granite is derived from a variety of isotopic and trace element data. It demonstrates that the use of such data, interpreted on the basis of our existing understanding of the behavior of chemical elements in magmas, can be used to identify and characterise the various stages in the evolution of a granitic intrusion. Arran is only one specific case. The interpretation of its origin is based largely on techniques and data used to determine the origin of other granites of the British Tertiary igneous province. It does serve to indicate that any granite is an individual with its own evolution controlled partly by the way it interacts with the surrounding crust, which may vary significantly from one intrusion to the next, and by its chemical

evolution over a range of temperature which for granites of similar compositions should be reproducible. By isolating variations in the chemical evolution of the magma controlled by composition it should be possible to identify features which are unique to that particular pluton and which reflect specific features or controls on its evolution. Such specific controls are likely to be the main factors influencing the style of ascent and emplacement of granitic magma.

This work has largely concentrated on the indentification of specific petrographic and chemical features of the Arran coarse granite which are pertinent to deducing its level of accumulation, the degree to which it assimmilated crustal rocks prior to and during ascent, whether it is composed of one pulse of magma or several and how it crystallised. The discussion of the variations in chemistry and what may be inferred from them is intended to illustrate the various processes affecting granites during their ascent and emplacement and on what grounds and to what degree of accuracy they may be identified. One of the major problems in interpreting granitic rocks is our understanding of the final stages of crystallisation of granitic magmas and the chemical variations this can cause which could overprint features of their chemistry which might be used to elucidate their origin. Until a fuller understanding of the physico-chemical properties of crystallising granitic crystal-liquid mushes is available it may not always be possible to eliminate the effects of crystallisation and consequently deduce the composition of the parent magmas or identify features of the chemistry of the magma which relate to its ascent and emplacement. The model presented here for Arran can account for the variations in petrography and chemistry and allows indentification of the parent magma. On these grounds there is clearly scope for more detailed work which may have important implications for our understanding of the crystallisation of granitic plutons which is beyond the scope of the present study.

CHAPTER 6

INTRUSION DYNAMICS AND THERMOMECHANICAL MODELLING OF DIAPIRIC ASCENT

The previous chapters have established that the outer coarse unit of the Northern Arran granite is a diapiric body. This conclusion has been drawn from field and geochemical data which record the rise and expansion of a single body of magma in the upper crust. This chapter discusses the diapiric rise of granitic magma, with particular emphasis on the mechanical and thermal controls on ascent. The intrusion of the Arran granite will be described by a thermomechanical, mathematical model for diapiric ascent based on field observations. The accuracy of this model and its limitations will be discussed in general terms, and in the specific case of Northern Arran.

6.1 The Stokes Equation.

Extensive experimental (e.g. Ramberg, 1967; Soula, 1982) and field based studies (e.g. Braunstein & O'Brien, 1968; Jackson & Talbot, 1986; Talbot & Jackson, 1987) indicate diapiric bodies typically develop a subspherical or elliptical shape, with a tail, during ascent. When the body reaches a level in the crust where it is no longer bouyant, or it cannot penetrate further, its vertical ascent is retarded and it spreads laterally, developing a mushroom shape. The spherical or elliptical form represents a minimum surface area to volume ratio for the body and hence friction between the surface of the body and the material through which it is rising (drag) is reduced to a minimum. On the basis of this evidence diapiric structures are modelled as spherical or elliptical bodies, which represent a good mathematical approximation to their true shape.

Diapirism may occur wherever material of low density lies beneath material of a higher density. The low density material experiences an upward force (F_1):-

$$F_1 = V(\rho_H - \rho_L)g \qquad 6.1$$

where V is the volume of the body, ρ_L is the density of the light material, ρ_H is the density of the heavy material and g is the acceleration due to gravity. If this force is not balanced the low density material will rise through the high density material. However the rise of the low density material is retarded by a viscous drag force (F_2), which for a spherical body is given by:-

$$F_2 = 6\pi\mu a v \qquad 6.2$$

This is the Equation for Stokesian flow of a spherical body of radius a, falling with a velocity v in a fluid of viscosity μ. A body of magma accumulating at depth will rise toward the surface providing F_1 exceeds or is equal to F_2. Setting equation 6.1 equal to 6.2 gives an equation (6.3) for the ascent velocity v:-

$$v = \frac{2a^2}{9\mu}(\rho_H - \rho_L)g \qquad 6.3$$

This equation is adequate for an isoviscous system (i.e. where the viscosity of the fluid is constant). However it has been recognised for some time that magmatic intrusive diapiric bodies are surrounded by a narrow zone of strongly deformed rocks (Grout, 1945; Buddington, 1959; Sanderson & Meneilly, 1981 and this study). This was noted by Marsh (1982) who stated:-

> 'In a medium of constant viscosity , the velocity field extends, for a spherical body, for example, out to about 10 body radii. The usual thin deformation envelope about plutons clearly indicates the wall rock viscosity was not spatially uniform.'

6.2 The Hot Stokes Equation for Diapiric Ascent.

The Stokes equation (6.2) does not account for variations in the viscosity of the wall rocks through which the intrusive body is rising. Marsh & Kantha (1978) recognised the importance of heat transfer from the magma body to its wall rocks in aiding the ascent mechanism. Heating of the wall rocks would result in a reduction in their viscosity. This would cause a reduction in the viscous drag force on the rising diapir. Meissner & Weaver (1986) discussed the variation in viscosity of the crust with temperature, and presented equations describing the relationship between these parameters for different rock types. These show that viscosity is inversly proportional to temperature (Table 6.1). Of interest is the fact that the viscosity of the wall rocks adjacent to the magma body is comparable to that for granitic magma at its solidus temperature (Wickham, 1987; Van der Molen & Patterson, 1979). This appears to rule out Marsh's assumption that, in order to obtain a sufficient reduction in the viscosity of the wall rocks to allow diapiric ascent to occur, the wall rocks would have to be heated to their solidus temperature.

Table 6.1.

The following data for the effective viscosity for steady state creep of wet granite at a given temperature and constant strain rate were calculated from the equation:-

$$\ln\mu = (\frac{1}{n})(\frac{E}{RT} + (1-n)\ln\dot{\eta} - \ln C_n)$$

after Meissner & Weaver (1986). Where n = 1.9, E =1.37×10^3*, $\ln C_n$ = 2.0†, R (the Gas constant) = 8.314 and $\dot{\eta}$ (the strain rate) =$10^{-14}s^{-1}$.

Temperature (T) °C	Viscosity (μ) Pa.s
200	4×10^{22}
250	4×10^{21}
300	7×10^{20}
350	4×10^{19}
400	4×10^{18}
450	5×10^{17}
500	8×10^{16}
550	2×10^{16}
600	4×10^{15}

Viscosity of granitic magma at its solidus has been estimated by Wickham as 1×10^{17} Pa.s. The maximum aureole temperature of the aureole of the Northern Arran Granite is 550°C and

* $E = 1{\cdot}37 \times 10^3$ KJ mol^{-1} (effective activation energy)

† $\ln C_n = 2{\cdot}0$ Q Pa^{-n} s^{-1} (Constant, $n = 1{\cdot}9$)

hence a viscosity $\mu_1 = 2 \times 10^{16}$ Pa.s has been used for the rock adjacent to the granite. A minimum strain rate of $1 \times 10^{-14} s^{-1}$ is taken from Carter & Tsenn (1987).

Hence the variation in viscosity within the wall rocks is directly dependant upon the variation in temperature around the intruding pluton. In a series of papers Jaeger (1957, 1959 & 1964) examined the variation in temperature with time and distance around static bodies of magma. Since a rising body of magma, such as a diapir, is only in contact with a particular area of wall rock for a comparatively short time Jaeger's models are not strictly applicable. More recently this problem was explored by Daly & Raefsky (1985) who modelled the variation in temperature and heat flow around a rising diapir using a finite element method. They showed that the temperature field around a rising body of magma changed with varying ascent velocity. In order to eliminate the effects of variations in the wall rock temperature profile with time only the temperature profile for a thermal aureole a short time after intrusion will be considered in the following discussion. Marsh (1982) and Daly & Raefsky (1985) approximated the temperature gradients around an intrusion to an exponential form, to give an equation for the variation in viscosity (μ) across the aureole:-

$$\mu(y) = \mu_1 e^{(\frac{Ay}{d})} \qquad 6.4$$

Where μ_1 is the viscosity of the wall rock at the contact, y is the distance from the magma body, d is the width of the softened zone and A is a constant (after Marsh, 1982) (see Table 6.2). When this curve is plotted it can be seen that it predicts excessively high wall rock viscosities (Fig. 6.1). A more accurate representation of the viscosity variation across the aureole can be found by plotting the viscosities of the wall rocks at different temperatures, estimated from the aureole of the Northern Arran Granite, from Table 6.1. This produces a profile closer to the temperature curves of Jaeger (1964). The variation in viscosity predicted by this curve is consistent with the structure of the aureole of the Northern Arran Granite,

Figure 6.1. Graph showing variation in wall rock viscosity against distance from the edge of an intrusive body at y = 0. The solid curve indicates the viscosity as calculated from eqn. 6.4. The broken curve indicates viscosities calculated from Table 6.1. The solid curve predicts excessively high wall rock viscosities (e.g. 10^{40} Pa.s). The broken curve indicates a softened zone approximately 200m wide would develop adjacent to a granite body.

Fig. 6.1.

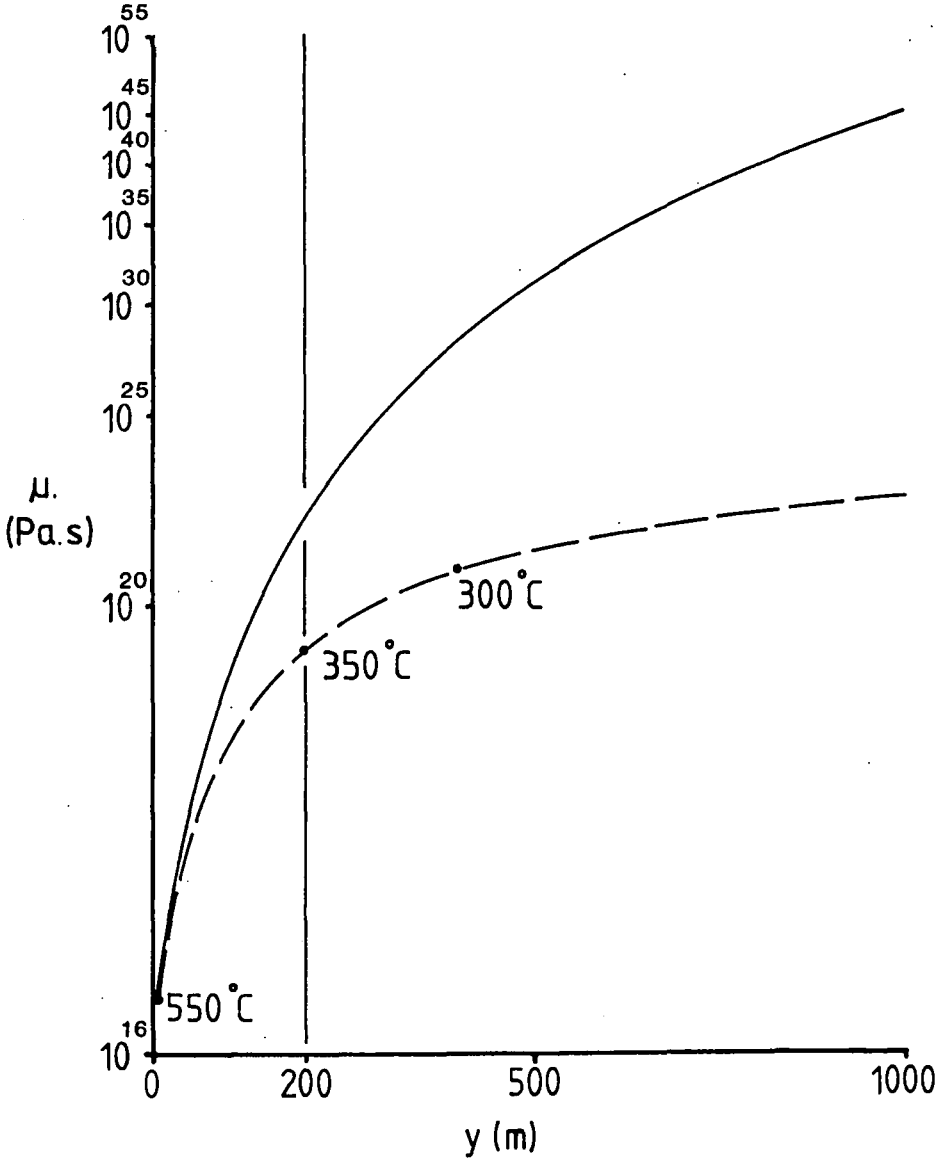
10^{55}
10^{45}
10^{40}
10^{35}
10^{30}
10^{25}
10^{20}
10^{16}
μ.
(Pa.s)
300°C
350°C
550°C
0
200
500
1000
y (m)

in predicting that the intrusion would be surrounded by a narrow zone of softened and strongly deformed rocks. The width of this zone is approximately 20% of the width of the thermal aureole (Chapter 4). The actual width and viscosity of the softened boundary layer would depend upon the mechanism and rate of heat transfer from the magma body to the wall rocks and the thermal properties of the wall rocks. Carrigan (1986) showed that heat transfer through softened rocks with a plastic rheology was predominantly by conduction. Convection, which requires a high rock permeability, would not be particularly important. If convection was important the thermal gradients within the aureole would be shallower since heat transfer to the more distant parts of the aureole would be more rapid (Fig. 6.2). This would result in a wider and more viscous softened zone.

The effect of widening the softened zone would be to make the viscosity field increasingly uniform. This would cause an increase in the drag force on the rising magma body, slowing its ascent. Therefore the ascent velocity is directly related to the mechanism of heat loss from the magma. Marsh (1982) reversed this argument by taking the ascent velocity as the factor controlling heat loss, despite the fact that a magma must lose heat to its overburden, and hence reduce the viscous drag force (F_2, eqn 6.2) before it can rise. A rapid ascent velocity would mean the magma was only in contact with a unit area of wall rock for a short time. Hence the heat transferred across the magma/wall rock interface would be small, even for high rates of heat transfer. This would result in only a limited reduction in the viscosity of the wall rocks which would cause a decrease in the ascent rate. Decreasing the ascent rate would increase the amount of heat lost to a unit area of wall rock. Hence it is apparent that diapiric magma bodies must rise at some equilibrium velocity constrained by the rate of heat transfer to the wall rocks.

The equation derived by Marsh (1982) for the velocity (v) of a body of magma rising within a narrow softened boundary layer of width d in a field of otherwise

Figure 6.2 Temperature profiles for a thermal aureole heated by conduction and by convection. Temperature (T); liquidus temperature of the magma (T_l); distance from contact (y).

Fig. 6.2.

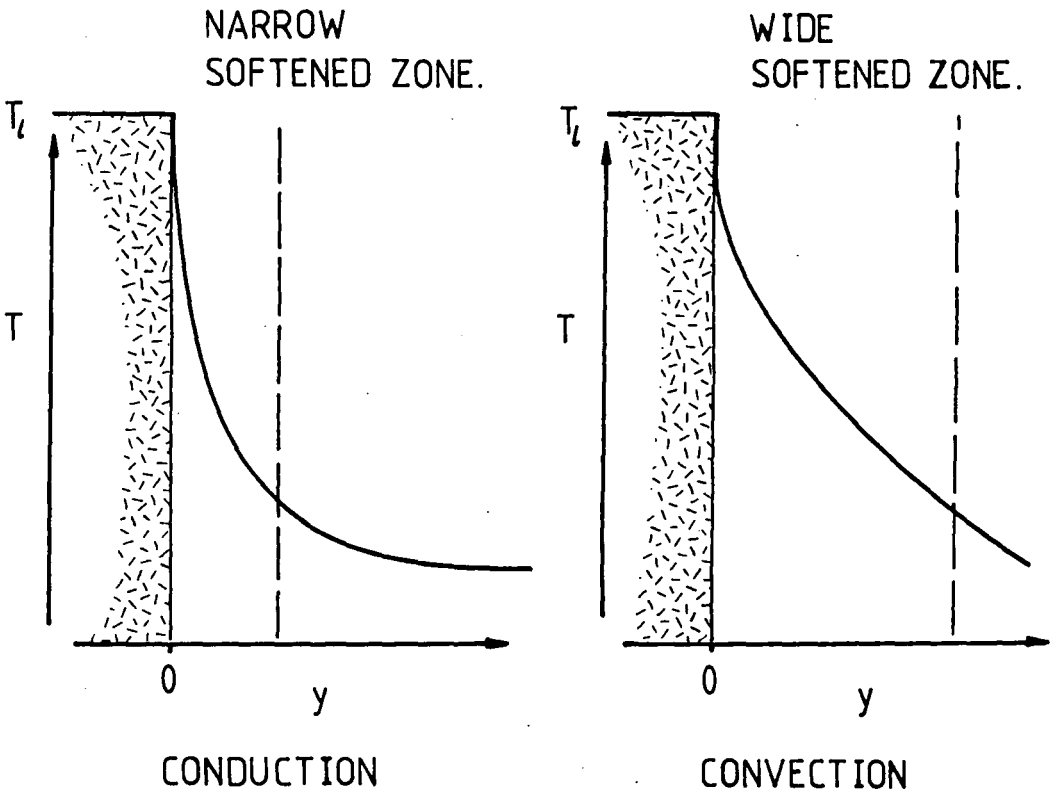
NARROW
SOFTENED ZONE.
T_l
T
0
y
CONDUCTION
WIDE
SOFTENED ZONE.
T_l
T
0
y
CONVECTION

uniform viscosity has the same form as the Stokes equation, i.e.:-

$$v = \frac{2}{3}\frac{\Delta\rho g d^2}{A\mu_1} \qquad 6.5$$

The softened boundary layer is a fraction of the width of the thermal aureole, as noted above. By considering the process of heat transfer from a magma body, of radius a, to the wall rock, the width of the thermal aureole (d') for a particular ascent velocity (v) is given by:-

$$d' = a(1 + 0.5Pe^{\frac{1}{2}})^{-1} \qquad 6.6$$

Where the peclet number $Pe = \frac{va}{\kappa}$, is a dimensionless measurement of the ratio of heat transfer by conduction to that by convection. κ is the thermal diffusivity of the wall rock. Hence the width of the softened boundary layer (d) is given by:-

$$d = f(d') \qquad \text{where } f = 0.2$$

after Marsh (1982). The value of f is determined from field data which indicate the softened zone is approximately 20% of the width of the thermal aureole. Hence the ascent velocity of a magma body rising in a field of non-uniform viscosity can be calculated from:-

$$v = \frac{2}{3}\frac{\Delta\rho g a^2}{A\mu_1} f^2(1 + 0.5Pe^{\frac{1}{2}})^{-2} \qquad 6.7$$

This equation, derived by Marsh (1982), and generally referred to as the Hot Stokes Equation, was used to calculate a possible ascent velocity of the Northern Arran Outer Granite, (see below). In this form the equation has no unique solution since the velocity term is included in both sides of the equation ($Pe = va/\kappa$). To solve this equation a value of v has to be assumed to determine a value for μ_1 (the viscosity of the wall rock adjacent to the magma body). The chosen value of v can then be verified by comparing the value of μ_1 with experimental data for the effective viscosities of rocks at high temperatures.

6.3 Determination of the Peclet Number from Crustal Strain Rates.

A more ideal approach to using the Hot Stokes equation than that proposed by Marsh (1982), would be to determine the effective viscosity of the wall rocks at a temperature appropriate to that of the liquidus temperature of the magma body and calculate Pe by an independent method. The velocity of any rising body of magma is ultimately constrained by the rate at which its aureole will deform. It is apparent from the study of migmatite complexes that for low viscosity, water rich, anatectic melts to separate from an unmelted restite they must migrate at a rate faster than or equal to the rate of deformation of the restite. Hence it is not unreasonable to assume that the movement of magma in the crust is a relatively rapid process involving high crustal strain rates.

A diapir rising through the crust deforms the column of rock around and above it. The radius of this deformed zone is greater than that of the softened zone. The rock above the diapir and outside the softened zone may be considered to have a uniform viscosity. However these rocks must still deform to accommodate the rise of the magma body and its associated thermal aureole from below. Hence these rocks must undergo Stokesian flow (no thermal effects). Marsh (1982) noted that for Stokesian flow the drag effects around the body diminished to zero over a distance no greater than a from the magma body, where a is the radius of the body. So the total width of the deforming zone equals $4a$. This is again consistent with the deformation around the Northern Arran Granite.

Pollard & Johnson (1973) showed that for low strains, the strain produced in the rocks overlying a rising magma body was approximately equal to the initial vertical displacement of the magma body producing the strain. This can be applied to the relatively cold rocks outside the thermal aureole which will deform slowly due to their high viscosities. As the diapir rises these rocks enter the thermal aureole, and higher strain rates and total strains will develop within them. If the vertical movement of an initially horizontal layer B-B, z, is equal

to the strain caused by updoming over the diapir (ϵ_x) in the rocks outside the thermal aureole, $z = \epsilon_x 4a$, (refer to Fig. 6.3). The vertical velocity (v_z) of the rocks is z/t. Since ϵ_x/t is equal to the strain rate $\dot{\epsilon}$, $v_z = 4a\dot{\epsilon}$. Hence the ascent velocity is directly dependent upon the strain rate in the rocks outside the thermal aureole as well as those within it.

This velocity may be used to determine a minimum value for the Peclet number ($Pe = va/\kappa$) based on the minimum strain rate 10^{-14}s^{-1} within the aureole, which is given by:-

$$Pe = \frac{4a^2\dot{\epsilon}}{\kappa} \qquad 6.8$$

This value of Pe can then be substituted into the Hot Stokes equation (6.7). The effect of using a minimum value of Pe in 6.7 is reduced since it is $\sqrt{Pe}$ which appears in the equation rather than Pe.

6.4 The Ascent Velocity of the Northern Arran Granite.

As previously noted field mapping of its contacts and the geometry of its metamorphic aureole suggests the sides of the outer granite are almost vertical at the present surface. There is no evidence to suggest that the body spreads laterally at depth. This indicates that the maximum diameter of the granite may not be much greater than the 13 km now exposed at the surface. This diameter is likely to be a maximum value for the granite, since wall rock deformation records strong radial flattening estimated at 17%, as a result of radial expansion of the pluton during the later stages of its emplacement. Restoration of the aureole of the granite indicated that the original size of the pluton as it came to rest at its present level, prior to radial expansion was 6 km (Chapter 4). This value for the radius of the granite is used in the following calculations.

Very little data on the thermomechanical properties of mixed pelitic and psammitic lithologies are available. Consequently the granite has been assumed to rise in crustal rocks rocks of granitic composition, for which data are available, (Heuze,

Figure 6.3 Geometry of the deforming zone above a rising diapir, radius a, for low strains. A bedding plane (B-B' – solid curve) within the deforming zone (marked by the broken curve) has a new length $\epsilon_x.4a + 4a$, where ϵ_x is the strain induced by the diapir rising a distance z. A-A' represents a bedding plane, to which B-B' was originally parallel, outside the deforming zone.

Fig. 6.3.

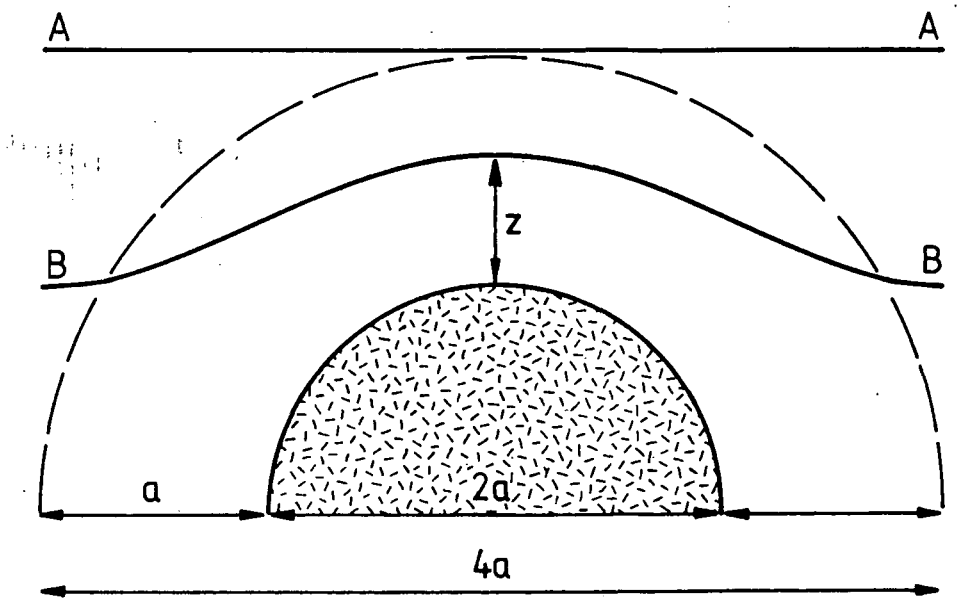

1983; Meissner & Weaver, 1986). The choice was made on the grounds that granite shows more closely comparable melting behavior to pelitic and psammitic rocks than to quartzitic rocks for which data are also available (Heuze, 1983). This can be verified from melting experiments (Thompson, 1981) and from field observations made in the Main Donegal Granite, (Pitcher & Berger, 1972), where rafts of pelitic and psammitic rocks show clear evidence of partial melting while adjacent rafts of quartzite remain unaffected.

The following calculation of the ascent velocity of the Northern Arran Outer Granite used the variables listed in Table 6.2. Data from Meissener & Weaver (1986).

Table 6.2

$a = 6 \times 10^5 \text{cm}$	Radius of granite
$\dot{\epsilon} = 10^{-14}\text{s}^{-1}$	Strain rate
$\kappa = 8 \times 10^{-3}\text{cm}^2\text{s}^{-1}$	Thermal diffusivity of granitic crust
$g = 1000\text{cms}^{-2}$	Gravitational acceleration
$\mu = 2 \times 10^{16}\text{Pa.s}$	Wall rock viscosity
$A = 13.8$	Where $A\mu_1$ is the effective viscosity of the softened layer
$\Delta\rho = 100\text{kgm}^{-3}$	Density contrast

Data from Heuze (1983) and Meissner $ Weaver (1986). Converting to SI units and using equation 6.8:

$$Pe = \frac{4\dot{\epsilon}a^2}{\kappa} = 1.80$$

The ascent velocity of the Northern granite can then be determined by substituting Pe into equation 6.7, and using an estimate of $f = 0.2$ (i.e. approximately 200 m) for the width of the softened zone:

$$v = \frac{2}{3}\frac{\Delta\rho g a^2}{A\mu_1} f^2 (1 + 0.5Pe^{\frac{1}{2}})^{-2} = 1.24 \times 10^{-9}\text{ms}^{-1}$$

Hence the granite had an ascent velocity of approximately 4 cm per year. The data of Dickin et. al. (1981) indicate the granite originated at, and rose from,

a depth of 8 km below the present surface. The calculated velocity indicates that the granite would have taken 0.214 Ma to rise this distance.

6.5 Heat Transfer.

As described above, the process of diapiric ascent is aided by the loss of heat from the magma body to its aureole, thus allowing the the aureole to deform around the magma body. Any single magma body has a finite amount of heat which may be released to the aureole to aid the deformation process. Once this heat source is exhausted upward movement of the diapir will be solely dependent upon Stokesian flow (equations 6.1 & 6.2). Hence the ascent distance (h) of a diapir is strongly controlled by its heat content, and more specifically the rate at which it loses its heat.

The heat content of a magma body is equal to the heat lost in cooling from its initial temperature, which may be above or below its liquidus, to its solidus temperature, plus the latent heat released during crystallisation. The heat capacity of the wall rocks controls the amount of heat required to raise the temperature of a given volume of wall rocks to the temperature at which their viscosity is reduced to a sufficient extent that upward flow of the magma body is possible. This is typically of the same magnitude as the specific heat lost by an equal volume of magma during cooling because the specific heat capacities of magma and wall rock are typically the same (Table 6.3). Hence loss of heat to a given mass of wall rocks by cooling of the magma, without crystallisation, can only produce an increase in temperature of approximately the same magnitude as the fall in temperature in an intrusive magma body of equal mass. Consequently the transfer of specific heat plays only a minor role in aiding the ascent of the pluton. However the latent heat released by a magma body during crystallisation greatly exceeds its specific heat (Table 6.3). Consequently by crystallising during its ascent a magma body can heat a mass of wall rock greatly in excess of its own mass.

Thompson (1983) presented experimental data for fusion of the Southern Porphyritic Epigranite (SK 127) at 1 kbar $_pH_2O$ from the Western Redhills centre of the Tertiary intrusive complex in the Isle of Skye, Scotland. The granite has almost identical major element chemistry and mineralogy to the Northern Arran Granite, allowing a comparison of melting behavior to be made between these two intrusions. This indicates the Northern Arran Granite has a crystallisation interval of 35°C. It has been argued that the granite cannot have been more than 70% crystallised when it reached its final level (section 5.5). However the 70% crystallisation interval is retained at 35°C since experimental data on the crystallisation of three compositionally different granites by Winkler & Schultes (1978) indicates that the last 30% of crystallisation occurs over an interval of < 5°C. This does not account for the fact that the granite would have lost heat as it rose from the top of the middle crust (at 11 km depth) to its depth of emplacement (3 km) as a result of crystallisation caused by a contraction of its crystallisation interval (section 5.4). The amount of heat lost by this process has not been accounted for here because of uncertainties in the initial temperature and composition of the granitic magma and the actual percentage of crystallisation caused by the fall in temperature and pressure during ascent.

In the following calculation of the heat content of the Northern Arran granite the magma body is assumed to be spherical, with a radius of 6 km. In addition the following parameters were taken from Heuze (1983):

Table 6.3.

a = 6000 m	Radius of granite
$d' = 1000$ m	Radius of thermal aureole
$\rho_g = 2.6 \times 10^3 \text{kgm}^{-3}$	Density of granitic magma
$\rho_w = 2.7 \times 10^3 \text{kgm}^{-3}$	Density of wall rock
$L = 80 \times 10^3 \text{cal.kg} - 1$	Latent Heat of crystallisation
$C_P = 0.25 \times 10^3 \text{cal.kg}^{-1\text{o}}\text{C}^{-1}$	Specific Heat Capacity of magma
$C_{PW} = 0.3 \times 10^3 \text{cal.kg}^{-1\text{o}}\text{C}^{-1}$	Specific Heat Capacity of wall rock

Using these data the mass (M) of the body was calculated from:-

$$M = \rho_g.V = 2.35 \times 10^{15}\text{kg}$$

where V is the volume of the granite. Hence the latent heat released during 70% crystallisation (Q_L) was calculated from:-

$$Q_L = 0.7ML = 1.3 \times 10^{20}\text{cal} = 5.51 \times 10^{20}\ \text{J}$$

and the heat released during cooling through the crystallisation interval (Q_S) is given by:-

$$Q_S = 35MC_P = 2.05 \times 10^{19}\text{cal} = 8.61 \times 10^{19}\ \text{J}$$

Hence the total heat released during crystallisation of the granite (Q_T) is:-

$$Q_T = Q_L + Q_S = 6.37 \times 10^{20}\ \text{J}$$

This heat is released in heating a column of country rock. As the magma body rises it displaces its own volume around itself by viscous flow of the overburden. The volume of rock flowing around the body may be considered as a hemisphere of radius $a + d'$ which mantles the upper part of the diapir throughout its ascent (Fig. 6.4). At any instant the volume of this hemisphere surrounding the granite is equal to the volume of the thermal aureole to which heat is being transferred. The rock beneath the granite has a velocity opposite to that of the granite. Therefore this rock moves away from the heat source and heat will no longer be transferred

Figure 6.4 The volume of rocks heated by the ascent of a rising magma body. During ascent of a diapir of radius a, over a distance h it heats and deforms the rocks within a cylinder of height h and radius a + d′. Lines A–A, B–B, C–C and D–D represent bedding planes in rock becoming increasingly heated and deformed (A–A and B–B), and then left to cool as the diapir rises further upwards (C–C and D–D). Line E–E represents cold and as yet undeformed rock.

Fig. 6.4.

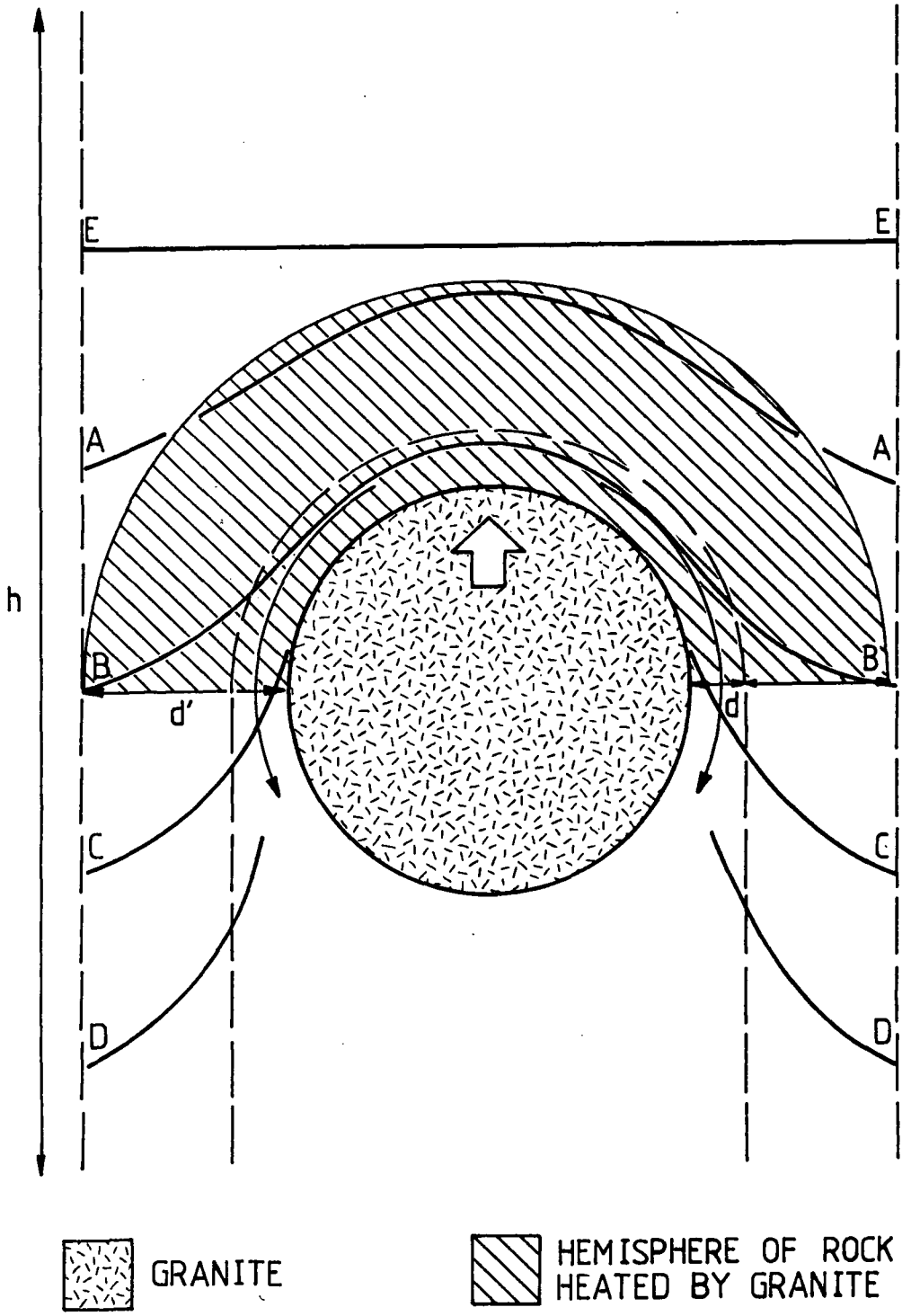
E
E
A
A
h
B
B
d'
d
C
C
D
D
GRANITE
HEMISPHERE OF ROCK
HEATED BY GRANITE

to it. Daly & Raefsky (1985) showed that the maximum heat flux from the diapir to the wall rock occurred through the upper hemisphere and diminished rapidly at angles greater than 90^o to the ascent direction. If the diapir rises vertically the volume of rock to be heated would therefore equal the volume of a cylinder of radius $a + d'$ and height h. At any instant the rocks in the thermal aureole are raised by a temperature (T_a), given by Marsh (1982) as:-

$$T_a = \frac{(T_1 - T_2)}{2} \qquad 6.9$$

where T_1 is the temperature of the rocks in contact with the granite and T_2 is the temperature of the rocks at the edge of the thermal aureole. Assuming a linear geothermal gradient of $25°C.km^{-1}$ and that the granite rose from a depth of 11 km to 3 km (section 5.3.1) the average wall rock temperature at the edge of the thermal aureole during ascent was calculated to be 175°C. The mineral assemblages developed in the thermal aureole indicate a maximum temperature of 550°C adjacent to the granite. Equation 6.9 was used to calculate a value of T_a of 187.5°C. Hence in order to rise the 8 km suggested ascent distance (see above) the granite must release sufficient heat during cooling to raise the temperature of a column of rock of radius 6 km and height 8km by 187.5°C. The amount of heat required (Q) was calculated from:-

$$Q = 187.5MC_{PW} = 7.82 \times 10^{20} \text{ J}$$

Where M is the mass of the cylinder. From this calculation it can be determined that the heat content of the Northern Arran granite is sufficient to enable it to rise 6.51 km. The obvious discrepancy between the heat content of the granite and the heat required to enable it to ascend 8 km may be explained by errors in the modelling, particularly in the estimation of the volume of wall to be heated which is calculated from a very simple model. Neither does it account for additional heat lost by cooling and polybaric crystallisation of the granite during ascent from the

level at which it accumulated. It is clear that the results of the two calculations are of the same order of magnitude, and as such the discrepancy is not large. The main conclusion drawn from this calculation is that the granite potentially released sufficient heat in cooling, from its liquidus to its critical melt percentage, to rise from its source to its present level in the crust.

If the ascent velocity of the granite is taken as $1.24 \times 10^{-9} \mathrm{ms}^{-1}$ it will rise 8 km in 0.214 Ma. Hence for the granite to ascend in the manner described it should cool from its liquidus to ~~its~~ the point at which it is 70% crystallised in 0.214 Ma. Jaeger (1957) presented a series of equations for calculating the variations in temperature with time within a static cooling intrusive body and its metamorphic aureole. The equation:-

$$T_S = \frac{T_1}{(1 + erf\lambda)}\left(1 + erf\frac{x}{2(\kappa t)^{\frac{1}{2}}}\right) \qquad 6.10$$

gives the temperature T_S of solidified magma or wall rock at a distance x from the contact at $x = 0$ (between the country rock, $x > 0$, and the magma, $x < 0$,) at time t. T_1 is the liquidus temperature of the magma. λ is a parameter which is related to the heat loss during cooling between the liquidus and the solidus, (Jaeger, 1957, eqn. 3). Other variables are as given above. By setting T_S equal to T_1 and x equal to the radius of the magma body, the time taken for the magma body to completely crystallise (t) can be determined. For the Northern Arran coarse granite this time is 1.62 Ma. This lies well outside the time of 0.214 Ma estimated for diapiric ascent of the granite.

The discrepancy between these cooling times lies in the fact that eqn. 6.10 relates to a static magma body losing heat to a static thermal aureole, and thus is not strictly applicable to to a rising body of magma which is continually losing heat to comparatively cold wall rock. Daly & Raefsky (1985) analysed the heat flow pattern around a rising hot diapir and showed that steeper thermal gradients would develop around a rapidly ascending body than would develop around a

slowly rising body. Consequently heat flow to the wall rocks would be more rapid in the case of a diapir with a high ascent velocity, and hence it would cool more rapidly than a static body. Consequently the Northern Arran Granite would have cooled in a time which was less than or equal to 1.62 Ma, which is consistent with the calculation above. Marsh (1982) wrote an equation relating the heat lost by a magma body to its ascent velocity. This equation has not been used here since it is based on the assumption that the granite only heats the rocks directly above it, (i.e. no lateral heat loss to the wall rocks occurs). It also assumes that the wall rocks undergo partial melting (see above) and includes a latent heat term to account for this. Hence this equation is clearly not applicable to the Northern Arran granite, where there is no evidence of partial melting in the aureole, (chapter 3).

6.6 The Limits on Ascent of the Northern Arran Granite.

The preceeding sections indicate that, on the basis of a theoretical model consistent with field data, ascent of the Northern Arran granite as a diapir is viable. This model is valid for a magma body rising through rocks of uniform structure and composition, which can be described mathematically as a material of initial constant viscosity. Hence the Hot Stokes model can be applied to the Northern Arran Granite while it is rising through the Dalradian. However when the granite intersected and reactivated the Laggan/Goat Fell Fault system the aureole would effectivly become non–uniform and the Hot Stokes model would no longer hold. In particular the thermal gradients around the granite would have been perturbed in the region of the faults. Brittle deformation along the Goat Fell fault on the eastern side of the granite indicates that aureole temperatures did not reach the same level as those in the Dalradian on its western side. This suggests higher rates of heat transfer along the eastern contact removed heat rapidly from this area. This may have resulted from the flow of water through the

more permeable ORS rocks and the faults (Chapter 3). The faulting may have also brought the granite into contact with rocks of higher heat capacities (e.g. rocks with a higher water content) and consequently a greater amount of heat would have had to be lost to these rocks before they behaved plastically. The enhanced heat loss from the granite may have helped to arrest its ascent. This would be consistent with structural evidence (Chapter 4) which indicates that the granite began to expand radially during reactivation of the Goat Fell fault. Slowing of the granite may also have been caused by it rising into progressively cooler rocks as it approached the surface. This would also have caused an increase in the heat required to cause a sufficient reduction in the viscosity of the wall rocks to allow ascent to continue.

The Hot Stokes model predicts a uniform ascent velocity for a given value of Pe. It is clear that the Peclet number may vary with depth in the crust. Heat transfer by conduction would occur at all levels within the crust. Convective heat transfer may only occur where there is a fluid to transport the heat and a pathway for that fluid to move. Hence convective transfer of heat requires a permeability, which increases toward the surface. So the value of Pe and hence the ascent velocity (eqn 6.7) will increase toward the surface. However it is clear that the ascent velocity decreases toward the surface. There are two probable reasons for this. Firstly the falling amount of heat available to raise the temperature of increasingly cooler wall rocks, as discussed above, and secondly the decrease in density contrast between the magma and the wall rocks. The latter would have the effect of decreasing the bouyancy of the magma body (eqn 6.1).

The remaining variable in the system not accounted for by the Hot Stokes Model, and which may affect the ascent velocity, is the viscosity of the magma body. The work of Arzi (1978) and Van der Molen & Patterson (1979) indicate that the viscosity of a crystallising magma remains approximately constant until it reaches a critical melt percentage (CMP), at which point the viscosity increases

rapidly. In the case of Arran it can be shown that the granite did not cool below the CMP before it came to rest at its present level in the crust. Therefore its viscosity would have remained constant during its ascent, providing the magma cooled homogeneously. Low temperature gradients and hence approximately homogeneous cooling would have been maintained by convection within the magma during ascent (section 5.5).

If the magma adjacent to the wall rocks had cooled more quickly than in the centre of the body a viscosity gradient would have formed between the margins of the body and its core. Hence the less viscous magma in the core of the pluton would flow more rapidly than the margins. Providing the margins of the body remained deformable, the core of the pluton would then rise faster (as it would also be less dense) and the body would become elongate on a vertical axis. This would cause an increase in surface area to volume ratio of the magma body, causing it to cool, particularly where the upper part of the magma body was intruding relatively cooler country rocks. This would increase the viscosity of the upper part of the pluton and hence reduce its ascent velocity. The lower, hotter and now faster rising part of the body would then catch up with the upper part, and the body would regain its spherical configuration. This argument suggests that the viscosity of the magma plays only a minor role in the mechanism of ascent.

Hence it appears that both the ascent velocity and shape of a diapiric magma body are maintained at some equilibrium state which is controlled by a mechanism of thermal feedback.

6.7 Summary.

The structural features of the Northern Arran granite indicate that it rose diapirically, in an incompletely crystallised state, as a subspherical body, within a zone of rock thermally weakened by the loss of heat from the magma. The ascent of this type of intrusion can be described in mathematical terms by the Hot Stokes

model (Marsh, 1982). This model takes into account both the mechanical and thermal controls on ascent and indicates the major factor in controlling ascent is the rate at which the viscosity of the wall rocks is decreased by heat loss from the ascending body.

The level to which a magma body will rise is controlled by its heat content. This governs the volume of wall rock it can heat to a temperature at which its viscosity is reduced to a level at which the drag effects (friction between the magma and the wall rock) over the surface of the rising pluton are reduced to a minimum. Ascent of the granite is largely restricted to the time in which the granite cools through its crystallisation interval, since most of the heat lost to the country rock is in the form of Latent heat.

Ascent of the Northern Arran granite above its present level appears to have been prevented by its diminishing heat content. In addition, an increase in the rate of heat loss from the granite and its aureole due to the proximity of the surface and its intersection with the Goat Fell fault probably caused a rapid decrease in its ascent velocity.

The Hot Stokes Model and the calculations for heat transfer from the Northern Arran Granite and its aureole provide a framework for investigating the factors which need to be taken into account when dealing with the process of diapiric ascent. Conclusions drawn from these models and the solutions obtained from them must be regarded as entirely model dependent. Hence it should be recognised that the results presented here are only as accurate as the models from which they are derived.

CHAPTER 7

THE INNER FINE GRANITE

The preceeding chapters have dealt largely with the structure, geochemistry and intrusion mechanism of the outer coarse unit of the Northern Arran Granite. As noted in chapter 2 the Northern Granite has two components. The inner fine granite is the subject of this chapter.

Gunn (1903) was the first worker to describe the Northern Arran Granite as containing a fine grained mass with the same mineralogical content as the surrounding coarse granite. The extent of this granite and the geometry of its contacts was established after Tyrrell (1928), with alterations by Flett (1942). Flett (1942) remains the most detailed account of the geology to date. Woodcock & Underhill (1987) suggested the inner granite was forcibly emplaced into the outer coarse granite, which resulted in ballooning of the pluton. The evidence for this mechanism of emplacement will be discussed in this chapter.

7.1 The Structure of the Inner Fine Granite.

In a detailed paper, Flett (1942) described the general features of the geology of the fine granite and a detailed study of the contact between the fine and coarse granites. Mapping of the contact between the two granites confirmed the findings of Flett (1942), with some exceptions. Although continuous exposure of the contact between the coarse and fine granites is rare its position can be determined from adjacent outcrops of coarse and fine granite. The geometry of the contact can be deduced from the topographic control on its position at the surface.

In general the contact dips steeply outward (i.e. toward the coarse granite), (Fig. 7.1). This can be clearly demonstrated between Glen Catacol and Glen

Iorsa. Immediately south of Catacol burn a steeply dipping contact can be traced up the NE facing side of Meall nan Damn. Just below the summit of this hill the angle of dip of the contact shallows to about 50°. Then the contact can be traced first south and then west around the steep south facing slopes of Meall nan Damn to the 1000 ft plateau. The next exposures of the contact can be found on the north - south trending ridge to the north of Meall Donn (GR 905450). The contact can then be traced down the SW facing slopes of Meall Donn indicating that the margin of the fine granite dips steeply westward ($\approx$ 70°) in this area. The next good exposures of the contact occur in Glas Chorein, NNW of Beinn Bharrainn, from which a steeply west to southwest dipping contact can be followed for approximately 3 km in a southerly direction across the NE ridge of Beinn Bharrainn toward Glen Scaftigill. The contact is not exposed in Glen Scaftigill but can be located just south of the summit of Sail Charmadale (GR 913397) where it dips steeply to the SW.

In Glen Iorsa (Fig. 7.1) the contact cannot be traced accurately due to poor exposure. Its position is determined from the general extent of outcrops of coarse and fine granite. The original geometry of the contacts on either side of Glen Iorsa were established by Gunn (1903) and later corrected by Flett (1942). Mapping of the contacts revealed a general agreement with Flett (1942) although the actual shape of the fine granite and the orientation of its contact in this area is open to interpretation since the only available exposure occurs in a few stream sections. The 'tongue' of coarse granite forming the floor of Glen Iorsa described by Flett (1942) can be clearly mapped. Its northern termination, 600 m south of Loch na Davie, can be located in the bed of the stream which flows south from the loch at GR 950450 (Fig. 7.2). Although the actual contact between the coarse and fine granites was not exposed, outcrops in the steep banks of the stream indicate that the fine granite dips at approximately 60° beneath the coarse. Flett (1942) suggested the tongue of coarse granite formed the roof to the fine granite in this

Figure 7.1. Map of the outcrop of the fine granite showing the position of the localities described in the text.

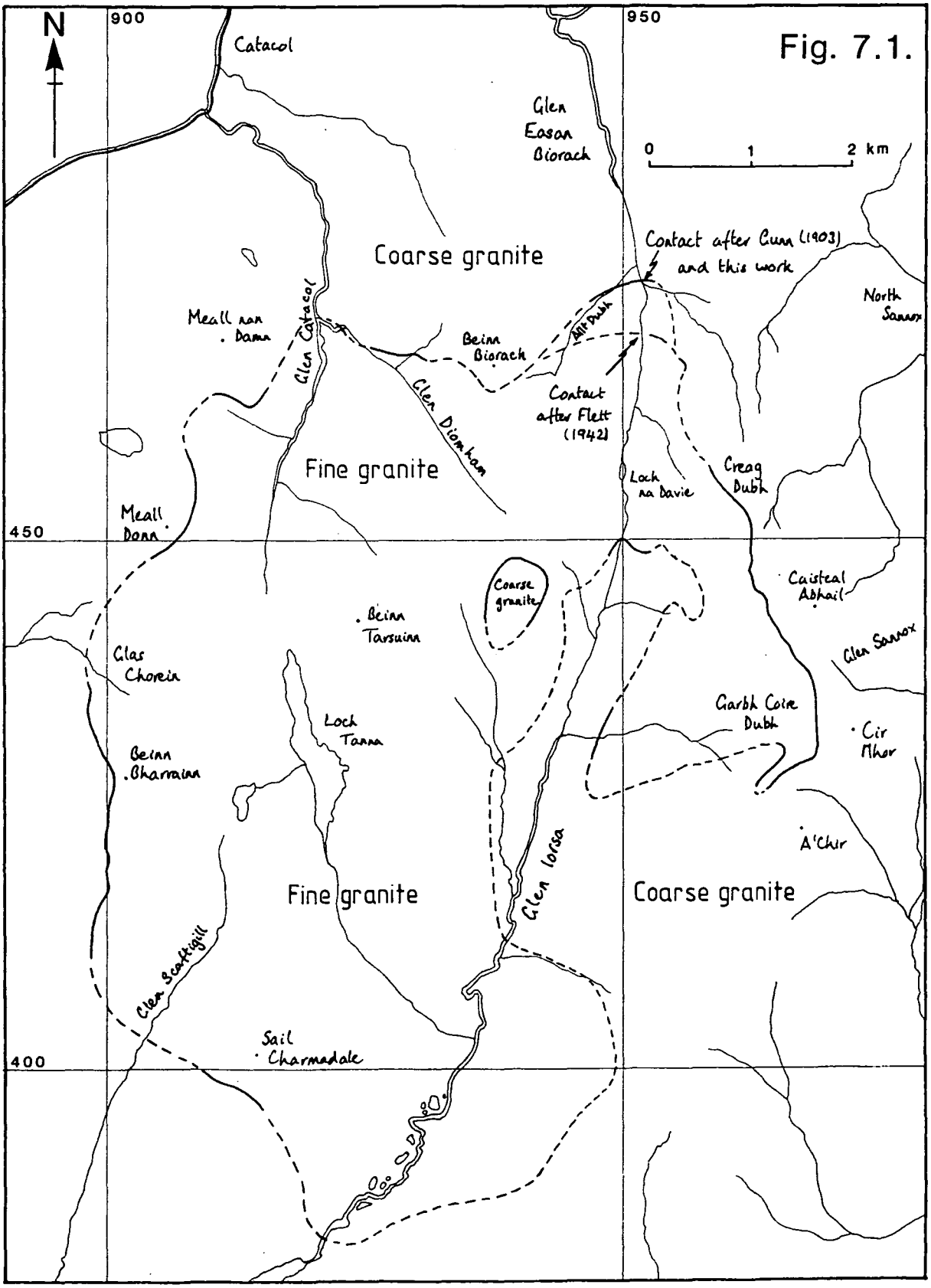
N
900
950
Fig. 7.1.
Catacol
Glen Easan Biorach
0 1 2 km
Coarse granite
Contact after Cunn (1903) and this work
North Sannox
Meall nan Damh
Glen Catacol
Beinn Biorach
Allt Dubh
Glen Diomhan
Contact after Flett (1942)
Fine granite
Loch na Davie
Creag Dubh
Meall Donn
450
Coarse granite
Caisteal Abhail
Beinn Tarsuinn
Glen Sannox
Clas Chorein
Garbh Coire Dubh
Loch Tanna
Cir Mhor
Beinn Bharrain
A'Chir
Fine granite
Glen Iorsa
Coarse granite
Glen Scaftigill
Sail Charmadale
400

Figure 7.2. A map and cross section across upper Glen Iorsa, illustrating the relation of the 'tongue' of coarse granite to the fine granite.

Fig. 7.2.

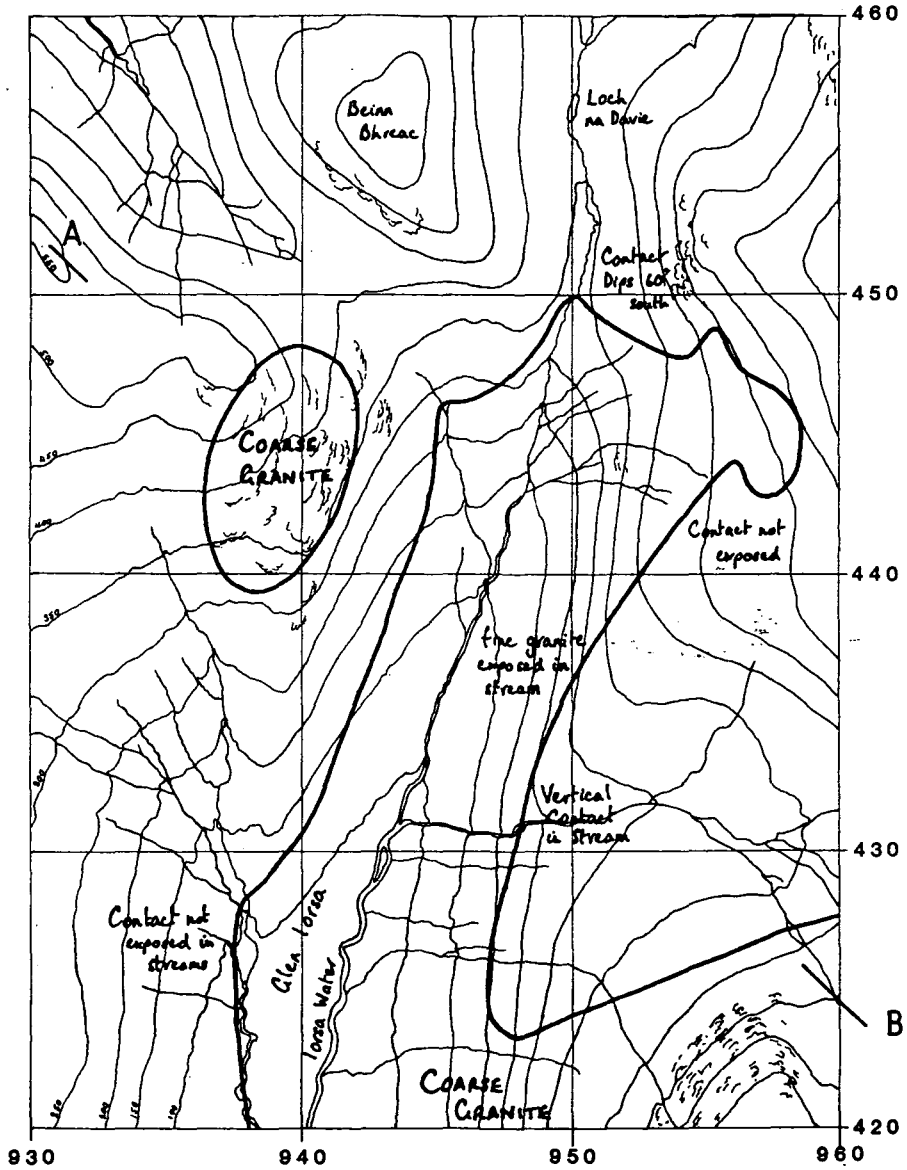
Beinn Bhreac
Loch na Dàvie
A
Contact Dips 60° south
COARSE GRANITE
Contact not exposed
fine granite exposed in stream
Vertical Contact in Stream
Contact not exposed in streams
Glen Torra
Torra Water
B
COARSE GRANITE
460
450
440
430
420
930
940
950
960

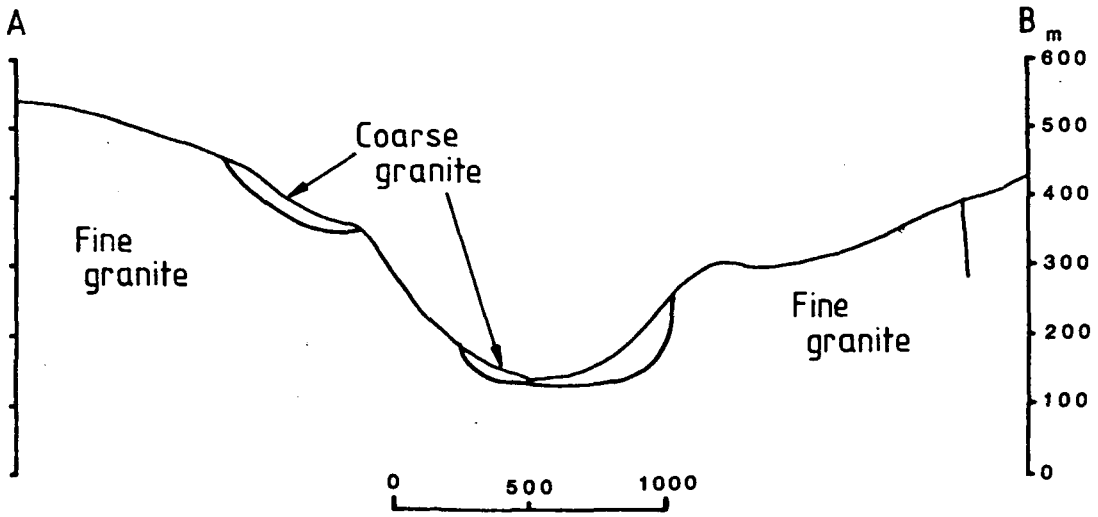
A
B
m
Coarse granite
Fine granite
Fine granite
600
500
400
300
200
100
0
0
500
1000

area (Flett, 1942, Fig. 5. & Fig. 7.2). Evidence supporting this interpretation was found at GR 947439 where fine grained granite, strongly depleted in Ba and Sr (Table 7.1) outcrops in the bed of the Iorsa water beneath coarse granite. This fine grained granite is interpreted as being fine granite *sensu - stricto* rather than a fine grained sheet in the coarse granite because it is strongly depleted in Ba and Sr but enriched in Rb relative to the coarse granite, which is a distinguishing feature of the fine granite (section 7.3).

Table 7.1.

Analyses of coarse and fine granite collected from Glen Iorsa at GR 947349.

Granite	No.	Ba	Sr	Rb
Coarse granite	4220	269	20	171
Fine granite	4210	n.d.	4	251

(n.d. not detected, analyses in ppm.)

The contact between the coarse and fine granites on either side of the tongue of coarse is rarely exposed. Its position, determined from isolated outcrops of fine and coarse granite, does not appear to be controlled by the topography, which suggests the contact is steeply dipping. On the east side of the glen a vertical contact between coarse (to the west) and fine (to the east) is exposed at GR 948431 where it is eroded by a waterfall (Fig. 7.2). Approximately 500 m south of this point the contact appears to swing sharply eastward toward Garbh Coire Dubh. The contact is well exposed in the upper part of this corrie on the east side of the north ridge of A' Chir where it dips steeply toward the coarse granite. It can then be followed northeastwards across the col between A' Chir and Cir Mhor and then north and northwestward across the head of Glen Sannox toward Caisteal Abhail (Fig. 7.3). Approximately 100 m west of the north ridge of A' Chir fine granite is seen to overly coarse granite. This contact dips shallowly eastward indicating that the fine granite forms an intrusive sheet in the coarse at

Figure 7.3. A map and cross section showing the geometry of the contact between the coarse and fine granites east of A' Chir.

Fig. 7.3.

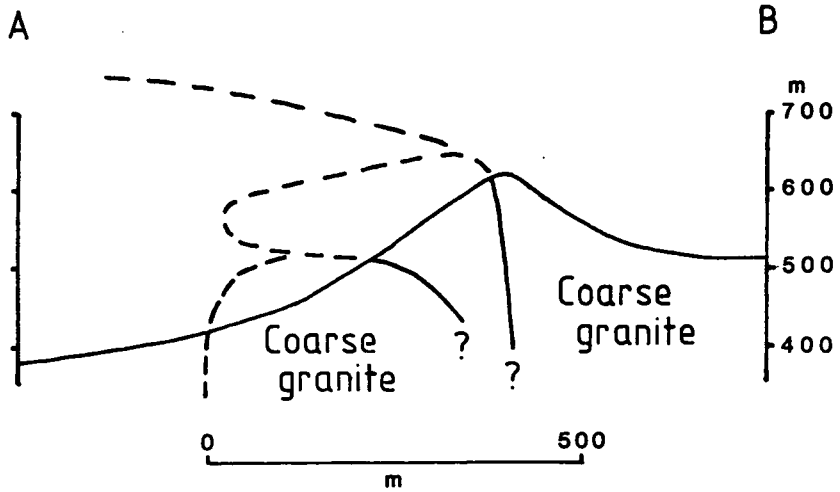
A
B
m
700
600
500
400
Coarse granite
?
?
Coarse granite
0
500
m

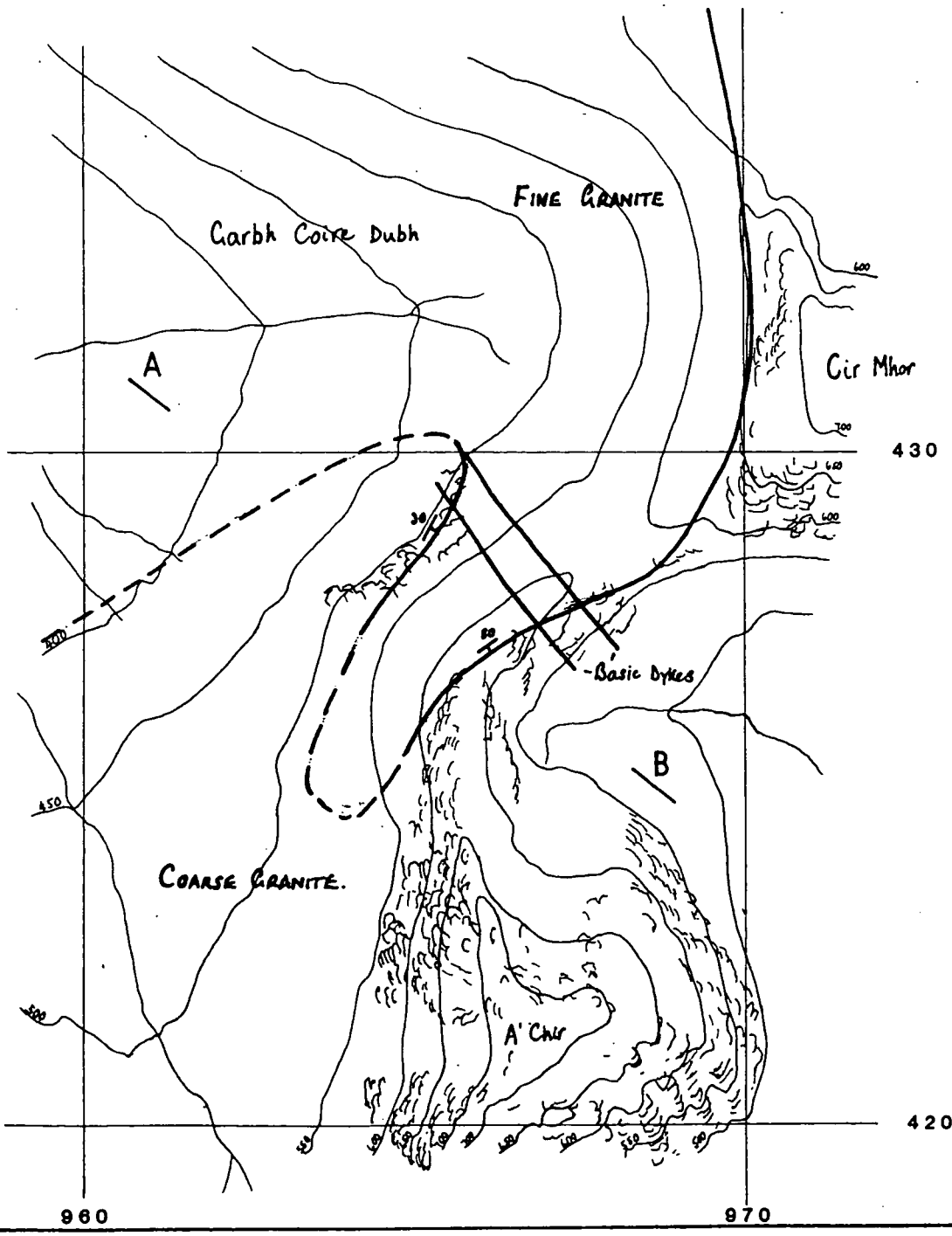
Fine Granite
Carbh Coire Dubh
A
Cir Mhor
430
Basic Dykes
B
Coarse Granite.
A' Chir
420
960
970

this point. The edge of the sheet can be traced north and south for about 500 m before it is lost in boulders and scree (Fig. 7.3).

The contact is clearly exposed between Cir Mhor and Caisteal Abhail in the back wall of the corrie at the head of Glen Sannox. The steeply eastward dipping orientation of the contact is discernable from an abrupt change in weathering properties across it. The coarse granite with its widely spaced orthogonal joints has resisted erosion but the fine granite, with its more closely spaced joints, has been frost shattered and forms a steep scree slope.

The contact crosses the ridge of Caisteal Abhail to the west of the summit. It then runs down the north face of this hill and northwestward across the back wall of the Garbh Coire from which it rises to the col between Caisteal Abhail and Creag Dubh. The course of the contact again emphasises its near vertical orientation. The exact position of the contact to the west of the col is difficult to determine. With the exception of a few isolated outcrops of coarse and fine granite which indicate its general position, it is obscured by peat.

A sharp vertical contact between coarse granite (to the north) and fine granite (to the south) occurs at GR 953474 in Glen Easan Biorach. This junction was mapped as the contact between the coarse and fine granites by Gunn (1903) but this was disputed by Flett (1942) and the geological survey map was subsequently revised. The source of this confusion appears to be that the fine granite becomes porphyritic and medium grained to the south of the contact. There is a further contact of fine grained granite against the medium grained granite 4 m upstream from the first (Fig. 7.4). This fine granite becomes medium grained and then gradually passes into normal fine granite approximately 200 m south of the first contact. Similar contacts between fine and medium grained granite can be found in a tributary stream (the Allt Dubh) to the west of the Easan Biorach. Flett (1942) interpreted the medium grained granite as belonging to the coarse and hence placed the coarse/fine contact immediately south of the last outcrops of the

Figure 7.4. A map and cross section showing the distribution and geometry of the internal sheets within the granite in Glen Easan. The contact between the coarse and fine granites has been restored to its original position (after Gunn, 1903). Localities of samples listed in Table 7.2 are shown on the cross section.

Fig. 7.4.

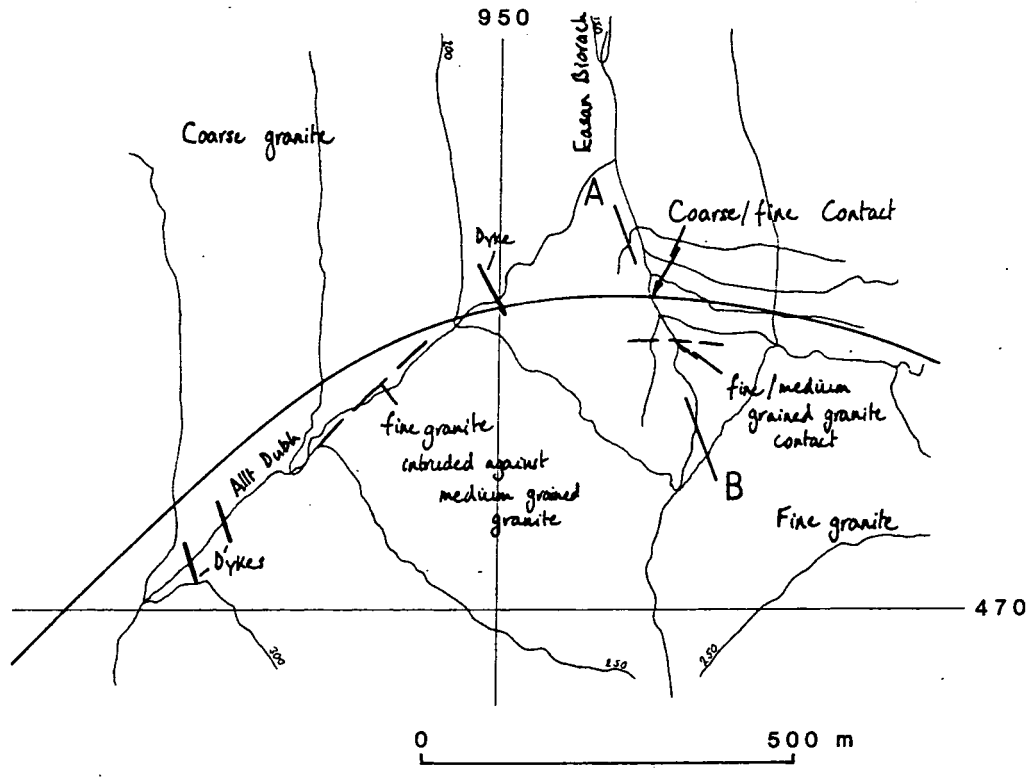
950
Easan Biorach
Coarse granite
A
Coarse/fine Contact
Dyke
fine/medium grained granite contact
fine granite cabruded against medium grained granite
Allt Dubh
Dykes
B
Fine granite
470
0
500 m

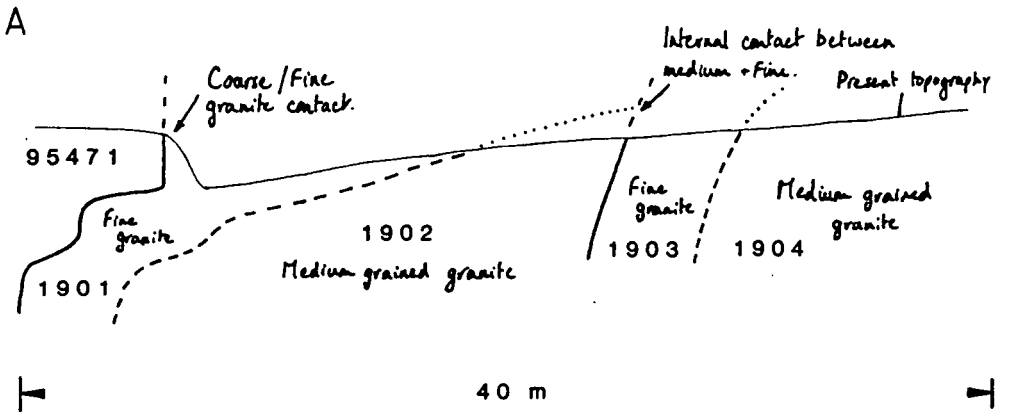
A
B
Internal contact between medium + Fine.
Present topography
Coarse/Fine granite contact.
95471
Fine granite
1902
Medium grained granite
Fine granite
Medium grained granite
1901
1903
1904
40 m

medium grained granite, where there is no observable contact in either the Easan Biorach or the Allt Dubh. Comparison of chemical analyses of the medium and fine grained granites with the coarse granite at GR 953474, Table 7.2, indicates that the former are depleted in Ba and Sr and enriched in Rb relative to the coarse granite, which is a characteristic of rocks of the fine granite (section 7.3). Hence it is concluded that the contact between the coarse and fine granites in Glen Easan lies at GR 953474, where it was originally placed by Gunn (1903).

Table 7.2.

Analyses of coarse, medium and fine granite collected from Glen Easan Biorach at GR 953474.

Granite	No.	Ba	Sr	Rb
Coarse granite	95471	528	28	151
Fine granite	1901	30	5	222
Medium granite	1902	347	20	179
Fine granite	1903	19	3	258
Medum granite	1904	183	11	176

(Analyses in ppm.)

The vertical contact seen in Glen Easan is not exposed further west. There are outcrops of coarse granite on the summit of Beinn Biorach. The contact is therefore mapped as skirting the lower slopes of this hill. This requires a shallowing of the angle of dip of the contact toward the north which suggests the roof of the fine granite may lie at a elevation below that of the summit of Beinn Biorach in this area. The next exposure of the contact at GR 930467 is in a gulley at the head of an unnamed tributary stream draining into Glen Diomhan. The contact is almost vertical at this locality, and it is cut by two basalt dykes. The contact can then be traced in a westerly direction toward Glen Diomhan where it is exposed at GR 922469.

The last two exposures are partially obscured by crushing of the fine and coarse granites. A zone of crushed granite is shown in Tyrrell (1928), after the work of Smith (1896). Although crushing of the fine granite is locally extensive, e.g. at

the contacts in Glen Diomham and at one locality in Glen Catacol (GR 918462) there is no evidence for the continuous zone of crushed rock indicated by Tyrrell (1928). Where it is well developed the crushing occurs on numerous irregular joint surfaces formed by cataclasis (Plate 7.1), which suggest the deformation occurred when the granite was relatively cool.

The fine granite shows well developed closely spaced joints which, other than those associated with the crushing, are normal or parallel to the present topography, which suggests they are the result of unloading. However there is clear evidence that some of the joints normal to the surface formed shortly after crystallisation of the granite. In Glen Catacol at GR 916454, in a stream to the north of Loch na Davie and adjacent to the contact to the west of the summit of Caisteal Abhail conspicuous green griesen veins (Flett, 1942) follow parallel sets of joints, normal to the surface. The veins occur over an area of no more than a few 100 m^2. They are between 1 and 2 cm wide and are composed of a 1 - 2 mm wide core of quartz and kaolinite with 0.5 to 1 cm wide margins of chloritised fine granite with sericitised feldspar. There is no mineralisation associated with these veins and their origin is unclear. They do provide evidence that the fine granite was locally affected by fluid/rock interaction.

Detailed study of the contact relationships of the coarse and fine granites confirmed the interpretations of Tyrrell (1928) and Flett (1942) that the fine granite is intruded into, and therefore younger, than the coarse. Where the contact is well exposed, on Meall Donn, to the northwest and southeast of Beinn Bharrainn and to the west of A' Chir the fine granite is finer grained against the coarse, indicating chilling. Veins of fine granite can be traced from the fine into the coarse. Occasional xenoliths of coarse granite in the fine were also noted along the contact to the southeast of Beinn Bharrainn. These xenoliths are restricted to the margins of the fine granite and are not seen elsewhere. The contact is always very sharp (on a grain size scale) and approximately planar. There is no evidence

Plate 7.1. This fine grained granular to micrographic textured granite is cut by closely spaced joints along which cataclastic (grain reduction) deformation has occurred. Incipient joints or fractures can be seen cutting some of the crystals in the lower part of the photomicrograph. Fine granite, No. 2600a, Glen Catacol. Width of field = 3.5 mm, crossed polars.

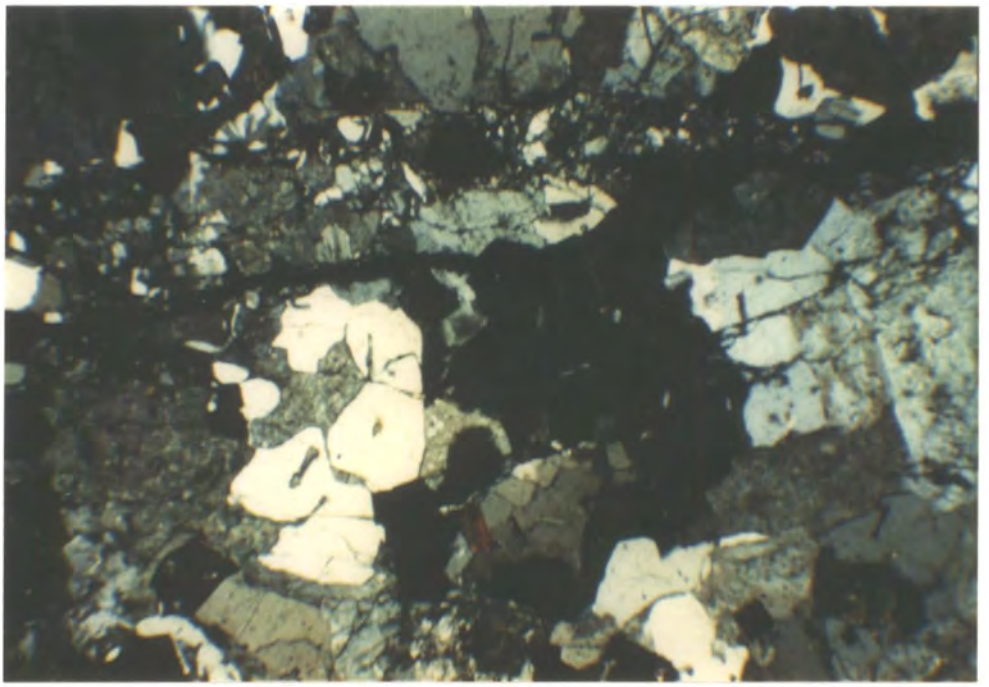

of any deformation of the coarse and fine granites adjacent to the contact (with the exception of crushed contacts in Glen Diomhan) which might indicate forceful emplacement of the fine granite into the coarse, and would imply that the granite 'ballooned' as suggested by Woodcock & Underhill (1987). Neither the coarse nor the fine granites show a foliation, although the fine granite often contains bands of un-orientated biotite parallel and adjacent to the contact. The sharp planar nature of the contact and the veining of the coarse granite by the fine granite suggests the coarse granite was solid, or had the rheological properties of a solid during intrusion of the fine granite. The veins of fine granite cutting the coarse granite show no evidence of later deformation, e.g. they are not folded or faulted. On the basis of these observations, which are consistent along the contact, it is concluded that the fine granite was passively emplaced into the coarse granite. The actual mode of emplacement of the fine granite will be discussed in section 7.4 after examination of its petrographic and geochemical features

7.2 The Petrography of the Fine Granite.

Over most of its outcrop the fine granite is a texturally homogeneous uniformly fine grained slightly drusy biotite granite, which is locally porphyritic. However in Glen Catacol and Glen Diomhan and on the north and west sides of Beinn Tarsuinn a series of continuous sheets within the fine granite can be clearly mapped (Fig. 7.5). With the exception of a sheet parallel to the coarse/fine contact in Glen Diomhan, these sheets are of fine granite which becomes drusiform toward the base of the overlying sheet ~~above~~ (Fig. 7.6), and are typically 30 to 50 m thick. The contacts between individual sheets are gradational. No clear discontinuity could be found at the top of any of the drusy horizons, which suggests the earlier sheets were still unconsolidated at the time the following sheet was intruded. The sheet parallel to the coarse/fine contact in Glen Diomhan differs from the others in that it is porphyritic. In hand specimen it is indentical to the porphyritic medium

Figure 7.5. A detailed map showing the distribution of the drusiform sheets in the fine granite in Glen Catacol and Glen Diomhan. Ba and Sr concentrations measured in samples collected from the sheets are shown adjacent to sample numbers (upper figure - Ba, lower figure - Sr).

Fig. 7.5.

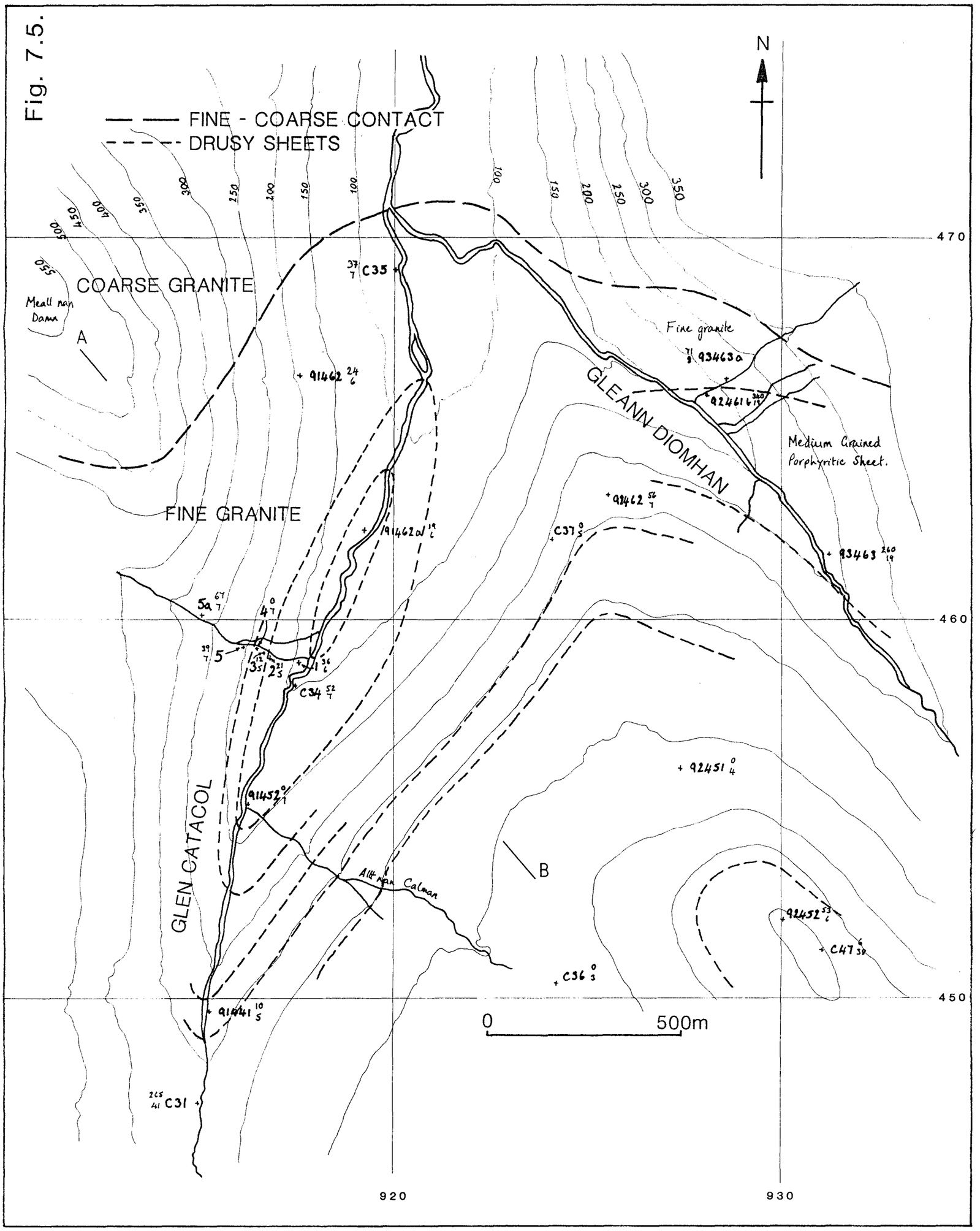
FINE - COARSE CONTACT
DRUSY SHEETS
N
COARSE GRANITE
FINE GRANITE
Meall nan Dama
A
B
GLEANN DIOMHAN
GLEN CATACOL
Allt nam Calman
Fine granite
Medium Grained Porphyritic Sheet.
C35
C34
C31
C37
C36
C47
5a
5
4
3
2
1
+ 91462 24/6
+ 91462 54/7
+ 91462 19/6
+ 93463a 71/8
+ 92461 340/19
+ 93463 260/19
+ 92451 0/4
+ 91452 0/7
+ 92452 53/6
+ 91441 10/5
0
500m
470
460
450
920
930

Figure 7.6. A cross section through Glen Catacol (marked A-B in Fig. 7.5) showing the inferred roof structure of the fine granite determined from the geometry of the drusiform horizons.

Fig. 7.6.

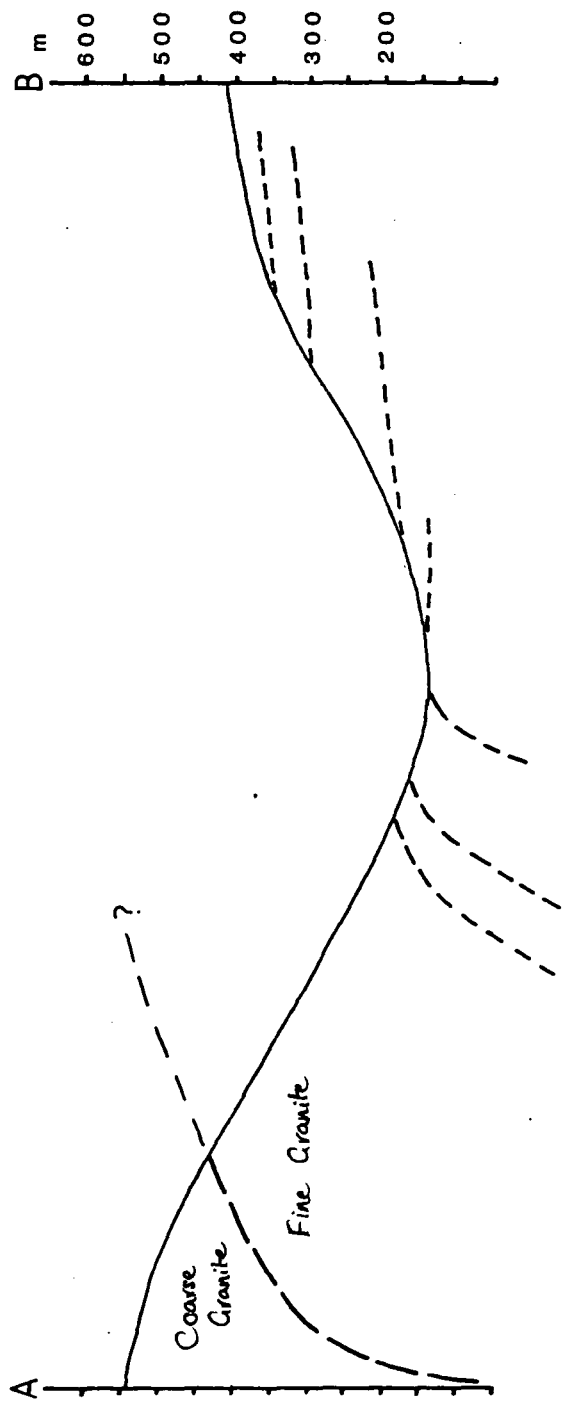

grained rock that can be mapped adjacent to the coarse granite in Glen Easan (section 7.1 & Fig. 7.4). It is not possible to deduce whether the two rocks form a continuous sheet along the inner margin of the contact, due to poor exposure. In Glen Diomhan the porphyritic medium grained sheet is clearly part of the fine granite since a sheet of fine granite lies between it and the contact between it and the ~~fine~~ coarse granite (Fig. 7.5). On the basis of this evidence it would appear that the medium grained granites in Glen Easan could also be a facies of the fine granite, rather than the coarse as suggested by Flett (1942). This would confirm that the coarse/fine contact in Glen Easan does occur at GR 953474, where it was originally placed by Tyrrell (1928).

Mapping of the orientation of the drusiform sheets and their distribution (Fig. 7.5) indicates that they are steeply dipping and approximately parallel to the coarse/fine contact on the west side of Glen Catacol and the north side of Glen Diomhan. To the south of Glen Diomhan, east of Catacol burn and on the slopes of Beinn Tarsuinn the sheets ~~dip~~ either dip shallowly toward the coarse granite or they are approximately horizontal. In Glen Catacol drusiform horizons can be mapped with steep contacts against non-drusiform fine granite, which are continuous with shallowly dipping sheets exposed on the lower slopes of Beinn Tarsuinn. These sheets parallel the contact between the coarse and fine granites which implies that the fine granite had an originally flat roof in the Beinn Tarsuinn area at a level only a few hundred metres above the present surface (Fig. 7.6). The continuation of some of the sheets could clearly be verified from detailed field mapping. However it is clear that more sheets are exposed on the east side of Glen Catacol than on the west, where exposure is equally as good. This makes attempts to extrapolate individual sheets difficult, and hence it is concluded that some of the sheets are laterally impersistent (Fig. 7.5).

In hand specimen the granite is a pale grey colour when fresh, which weathers to a powdery white or pink. It is uniformly fine grained, (grain size varies between

1 and 3 mm), and granular, and is composed dominantly of quartz and feldspar in a ratio of approximately 2:3. Biotite content is very low. When Biotite occurs it usually forms platy crystals up to 1 mm across. Occasionally the rock is porphyritic (few samples were completely devoid of phenocrysts). The phenocrysts, dominantly of quartz with subsidiary feldspar are euhedral and vary in size between 2 and 6 mm. With the exception of the porphyritic sheet in Glen Diomhan field relationships between porphyritic and non-porphyritic granite were difficult to determine due to poor exposure.

Thin section examination of the rocks revealed that the fine granite is generally composed of a hypidiomorphic granular intergrowth of quartz, orthoclase and albite with minor amounts of biotite and accessory zircon and magnetite. Its grain size varies between 0.5 and 4 mm, with an average of about 1 mm. Phenocrysts of quartz, orthoclase and occasionally albite occur as euhedral to subhedral crystals between 2 and 6 mm across. Orthoclase phenocrysts commonly have granophyric overgrowths of quartz and orthoclase, and contain inclusions of quartz. The phenocrysts are rarely zoned. The groundmass of the granite is usually a granular intergrowth of anhedral quartz and feldspar (Plate 7.2) but micrographic and granophyric intergrowths of quartz and feldspar are common (Plate 7.3). Some rocks clearly show a gradation between these textures with patches of granophyric granite surrounded by granular granite. Platy crystals of biotite, which occurs as an early groundmass phase, are usually partially enclosed by groundmass quartz and feldspar. The groundmass orthoclase is commonly perthitic, and forms anhedral crystals between quartz and plagioclase. Groundmass plagioclase is albitic in composition (from optical determinations) and forms subhedral tabular crystals. Rare accessory zircon and magnetite are only found in association with biotite. Magnetite may have formed by oxidation of the biotite, as in the coarse granite. Zircons are contained within the biotite and can usually be identified by pleochroic haloes.

Plate 7.2. This photomicrograph illustrates the typical hypidiomorphic granular texture of the fine granite. The rock is largely composed of subhedral to anhedral crystals of quartz, orthoclase and albite (together with minor amounts of biotite, not present in this view). In common with much of the fine granite this sample is slightly granophyric. Fine granite, No. 92461. Width of field = 3.5 mm, crossed polars.

Plate 7.3. Well developed granophyric to micrographic texture in the fine granite. This sample was collected from a drusy horizon which is thought to have crystallised rapidly following volatile exsolution. Fine granite, No. 93463. Width of field = 3.5 mm, crossed polars.

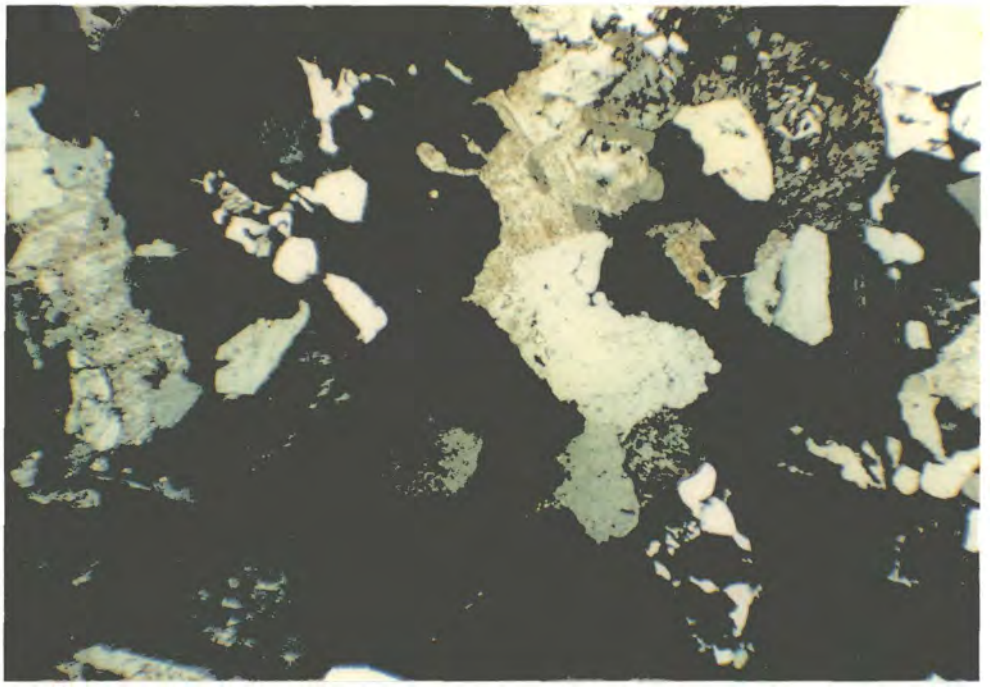

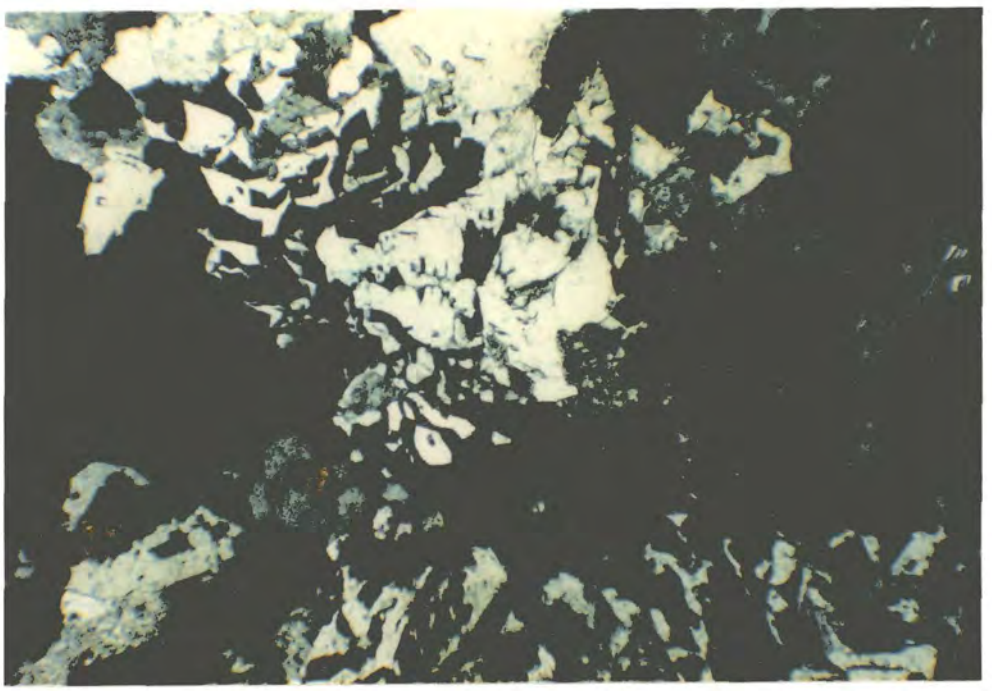

This general description confirms the conclusions of previous workers (Tyrrell, 1928; Flett, 1942) that the fine granite is a mineralogically fine grained equivalent of the coarse granite. Visual estimations of the modal composition of the fine granite suggest it is composed of approximately 40% quartz and 60% feldspar with minor amounts of biotite. Some of the more porphyritic facies of the fine granite are superficially similar to some of the rocks of group 3 of the coarse granite, but the fine granite can be identified on the basis that its groundmass is finer grained and commonly granophyric. The group 3 rocks have a medium to fine grained groundmass with a granular texture.

The drusiform sheets have a number of petrographic features which distinguish them from the normal fine granite (as described above) into which they grade. Apart from being conspicuously drusiform, some cavities lined with smoky quartz, feldspar, biotite and unidentified zeolites are up to 2 cm across, these rocks are usually granophyres. The well developed granophyric texture is interpreted as the result of rapid cooling of the magma by volatile exsolution which promoted rapid simultaneous crystallisation of quartz and orthoclase (Smith, 1974). Some of the rocks are notably porphyritic (e.g. the sheet parallel to the coarse/fine contact in Glen Diomhan). The groundmass becomes increasingly granular across the transition from drusiform to non-drusiform rock suggesting the granular texture developed during slower cooling. The drusiform rocks also contain a lower modal fraction of mafic phases than the non-drusy rocks which are richer in biotite (visual determination). This would be consistent with the crystallisation of biotite being controlled by the concentration of dissolved water in the magma.

The fine granite shows no evidence of deformation apart from the cataclastic crush rocks in Glen Catacol and Glen Diomhan. Neither the phenocrysts nor the groundmass quartz show undulose extinction which would indicate they have been stressed. Occasional distorted flakes of biotite were recorded but there was no other ~~other~~ evidence of strain in the rocks in which they occur. Clusters of

quartz and feldspar separated by thin films of feldspar and quartz similar to those described from the compacted rocks of the coarse granite were also noted but there is no evidence of widespread compaction of the fine granite.

To summarise. The fine granite has the same mineralogical composition as the surrounding coarse granite. It is a fine grained, occasionally porphyritic rock, composed of quartz and orthoclase, albitic plagioclase and minor amounts of biotite. Phenocrysts of quartz, orthoclase and rarely albite indicate that these phases may have been involved in fractionation of the magma. No systematic variations in texture across the intrusion are seen, apart from a series of sheets of fine granite passing upward into drusiform fine granite which mirror the contact between the fine and coarse granite in Glen Catacol and Glen Diomhan.

7.3 Major and Trace Element Geochemistry of the Fine Granite.

Chemically the fine granite is very similar to the coarse granite (described in section 5.3). The average and range of major and trace element compositions of the fine granite are given in table 7.3. Like the coarse granite the fine granite is extremely silica enriched and has a high aluminium content. In general the range of major element compositions of the two granites is very similar. The fine granite may be considered to be slightly more evolved on the basis of lower average CaO and higher average Na_2O (Fig. 7.7), and SiO_2. The higher Al_2O_3 content of the fine granite suggests it may be more contaminated than the coarse granite. In this case the high Al_2O_3 content cannot be the result of kaolinisation since all the samples analysed were fresh. The trace element composition of the fine granite is very similar to the coarse granite with the noteable exceptions of Ba, Sr, and Rb. Ba and Sr are depleted and Rb enriched in the fine granite relative to the coarse granite. This suggests the fine is more strongly fractionated than the coarse. These differences and similarities between the two granites are illustrated on an incompatible element plot (Fig. 7.8). This figure shows there

TABLE 7.3

Average and range of major and trace element compositions for the Northern Arran Fine Granite.

Element	Average	Range
SiO_2	77.26	74.70 - 81.12
TiO_2	0.07	0.04 - 0.32
Al_2O_3	12.74	11.52- 14.01
Fe_2O_3	1.08	0.81 - 3.61
MgO	0.03	0.00 - 0.13
CaO	0.27	0.02 - 1.26
Na_2O	3.63	2.97 - 4.50
K_2O	4.88	3.69 - 5.39
MnO_2	0.03	0.00 - 0.07
P_2O_5	0.01	0.00 - 0.07
Ba	81	0 - 843
Nb	38	24 - 48
Zr	131	90 - 406
Y	69	4 - 176
Sr	9	3 - 41
Rb	219	147 - 297
Zn	42	23 - 102
Cu	12	10 - 17
Ni	5	1 - 8
Pb	28	24 - 34
U	3	1 - 4
Th	23	15 - 30
V	3	0 - 14
Cr	10	5 - 31
Nd	46	14 - 118
La	35	13 - 89
Ce	76	30 - 207
K/Rb	187	27 - 283

Total Fe given as Fe_2O_3. Major oxides as wt %, trace elements in ppm. 74 samples.

Figure 7.7. Na_2O (wt %) plotted against CaO (wt %) for the coarse and fine granites. (Coarse granite - squares, fine granite - triangles.)

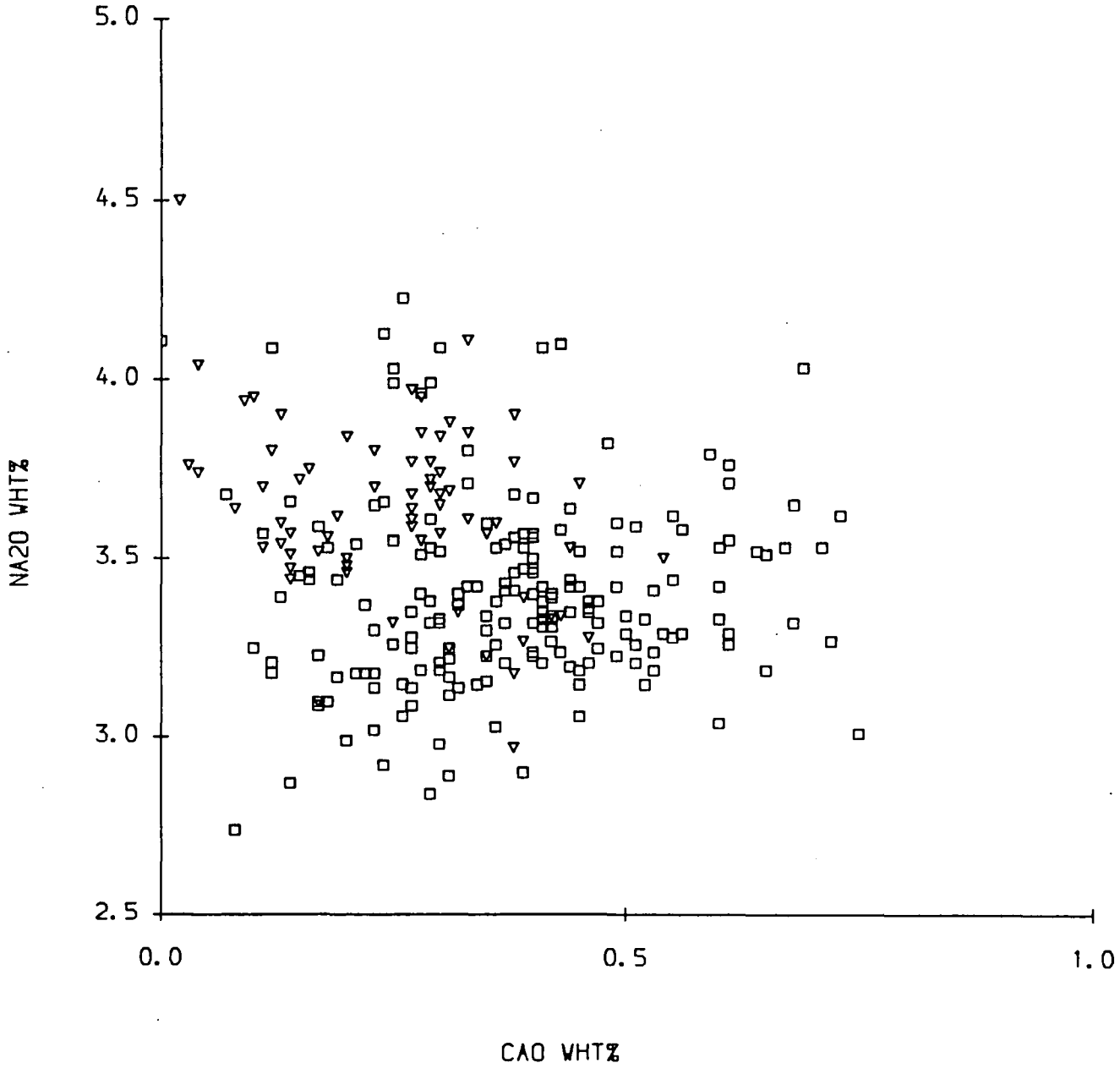

Fig. 7.7

Figure 7.8. Chondrite normalised incompatible element diagram showing the average concentrations of selected major and trace elements from the fine and coarse granites. (Coarse granite - squares, fine granite - triangles.) Normalisation factors from Thompson (1982).

Fig. 7.8.

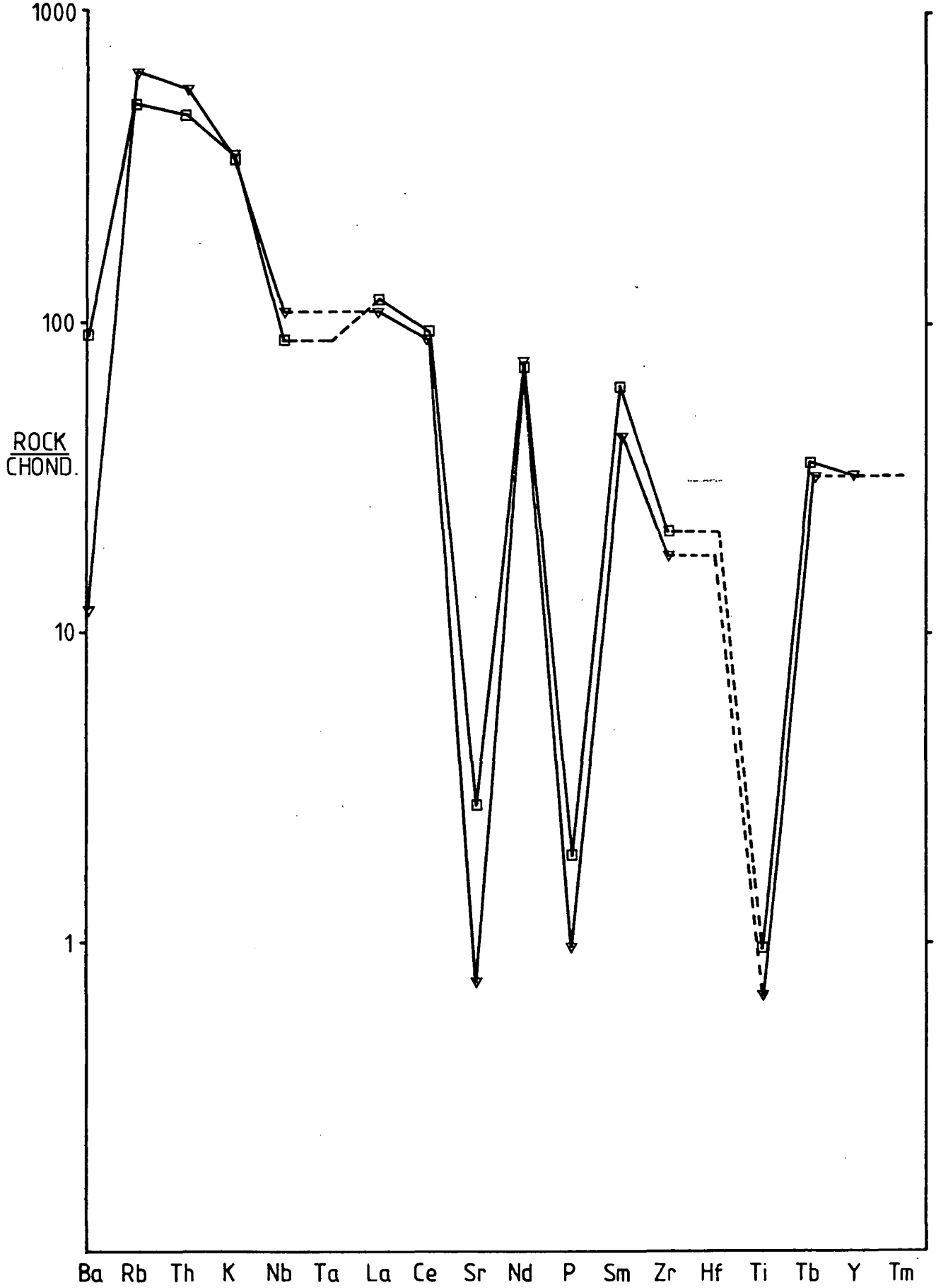
1000
100
ROCK
CHOND.
10
1
Ba
Rb
Th
K
Nb
Ta
La
Ce
Sr
Nd
P
Sm
Zr
Hf
Ti
Tb
Y
Tm

is little variation in the concentration of elements not involved in fractionation in either of the granites, but considerable variation in the elements partitioned into phenocryst orthoclase and plagioclase or enriched in the melt. It was argued in section 5.3.2 that the variation in chemistry of the granites is due to crystallisation and then separation of phenocrysts from the magma. Increased fractionation of plagioclase in the fine granite (and hence increased depletion of Sr) is confirmed by REE data (Meighan, 1979) which indicates that it has a larger Eu anomaly ($Eu/Eu^* = 0.06$) than the coarse granite ($Eu/Eu^* = 0.37$), (Fig. 7.9).

These data all indicate that the fine granite could be a more fractionated portion of the same magma body that rose to form the coarse granite. The fine granite is clearly a separate body to the coarse since it intrudes it, but it is possible that it represents acid magma which remained at depth as the bulk of the coarse granite began its ascent. Resolution of this question is difficult because essentially the two granites have the same history. They are both evolved from the same mantle derived basaltic source which would potentially have been contaminated by partial melts of the same crustal rocks before and after differentiation.

The isotope data of Dickin et al. (1981) does not provide a solution to this problem (as might be expected for two granites with the same evolution). Age dating by Dickin et al. (1981) using the Rb/Sr method showed that isotope data for the two granites plotted on the same isochron and hence any difference in age cannot be resolved by this method. The same workers analysed samples of the coarse and fine granites for $^{206}Pb/^{204}Pb$ and $^{87}Sr/^{86}Sr$ (section 5.3.1). These data showed that the two granites have almost identical Pb isotope compositions (Fig. 5.6) which Dickin et al. (1981) attributed to post differentiation contamination of the acid magma. The slightly higher average $^{87}Sr/^{86}Sr$ ratio of the fine granite (0.71733) compared with the coarse granite (0.71547) is compatible with the fine granite being slightly more fractionated (Sr depleted) when it was contaminated. This implies that the granites were separate bodies at the time this contamination

Figure 7.9. Chondrite normalised Rare Earth element plots for the fine and coarse granites. (Coarse granite - squares, fine granite - triangles.) Normalisation factors from Nakamura (1982), data from Meighan (1979).

Fig. 7.9.

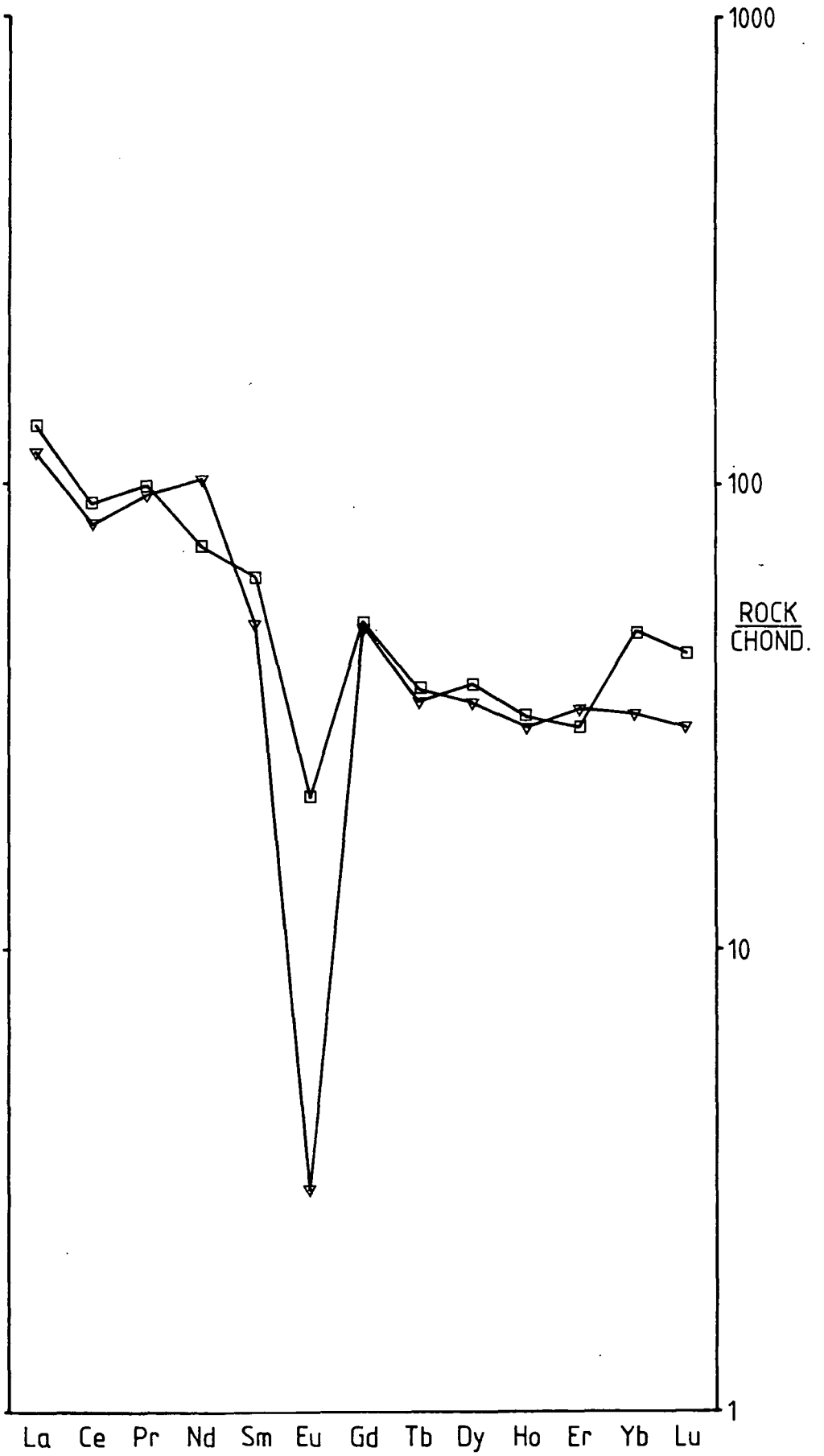

occurred. However there is an overlap in the $^{87}Sr/^{86}Sr$ composition of the two granites, and the fact that their $^{206}Pb/^{204}Pb$ ratios are the same does not rule out that they may originate from the same granitic source. It is clear from the isotope data that the fine granite did fractionate a substantial amount of plagioclase (or another Sr bearing phase) after contamination. Had the fine granite become strongly fractionated (Sr depleted) before contamination its $^{87}Sr/^{86}Sr$ isotope ratio would have been significantly affected by the addition of partial melts of isotopicaly different Sr. Therefore if the fine granite had been contaminated by partial melts of any of the crustal rocks in the Midland Valley following differentiation it would have a significantly different isotope composition to the coarse granite, which it does not.

On the basis of the field data, the coarse and fine granites will be treated as having risen separately. It is not possible to determine on the basis of the available trace element and isotope data whether they originated from the same or separate bodies of magma.

The fine granite has the same Rb, Th and K enriched incompatible element pattern as the coarse granite (Fig. 7.8). This enrichment pattern was used to show that the coarse granite was derived from a basaltic parent contaminated by partial melts of crustal rocks (section 5.3.2). The further enhanced concentration of Rb in the fine granite, relative to the coarse, is clearly resolvable on a plot of Rb against SiO_2 (Fig. 7.10). This is interpreted as the result of concentration of these elements in the melt during extreme fractionation, which is indicated by the very low Ba and Sr contents and low K/Rb of the fine granite relative to the coarse granite (Figs. 7.11, 7.12 & 7.13). The plots of Ba and Sr against SiO_2 indicate that the fine granite has fractionated a significant amount of quartz. This can be confirmed from plots of Ba and Sr against Rb. Rb in the fine granite increases rapidly with falling Ba and Sr (Figs. 7.14 & 7.15) but silica falls with falling Ba and Sr. This indicates that quartz is being depleted more rapidly than the

Figure 7.10. Rb (ppm) plotted against SiO_2 (wt %) for the coarse and fine granites. (Coarse granite - squares, fine granite - triangles.)

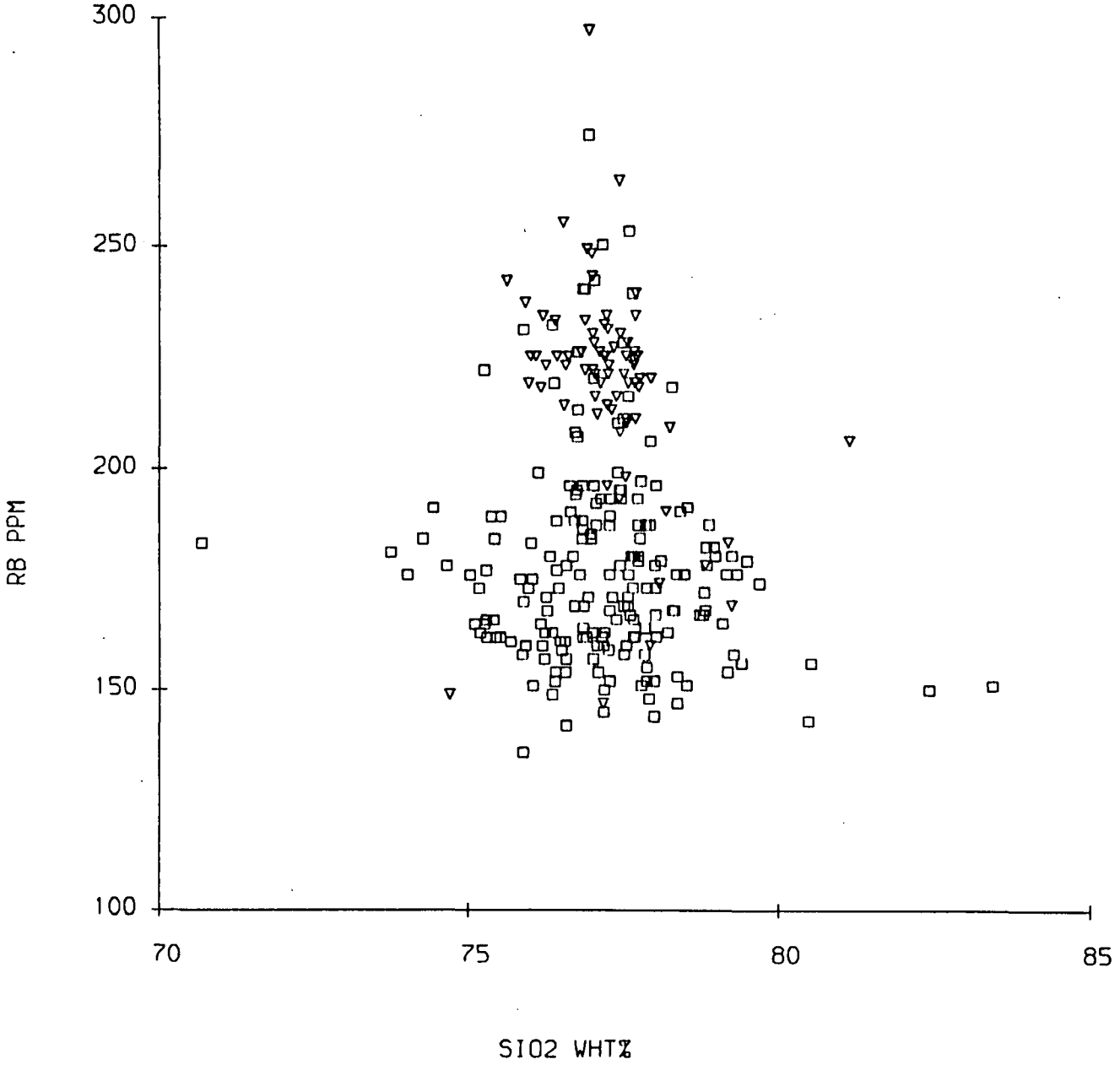

Fig. 7.10.

Figure 7.11. Ba (ppm) plotted against SiO_2 (wt %) for the coarse and fine granites. (Coarse granite - squares, fine granite - triangles.)

Fig. 7.11.

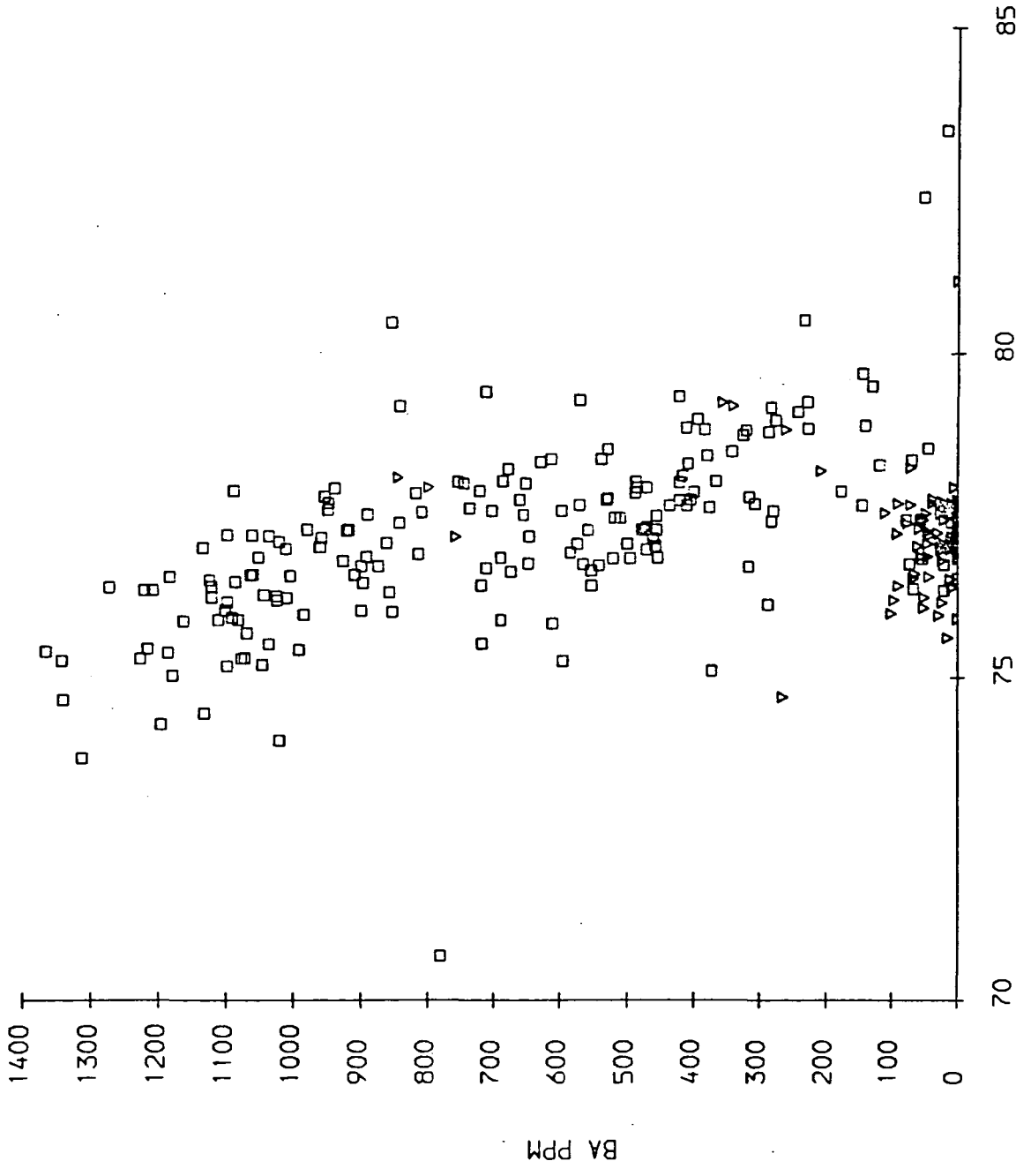
BA PPM
1400
1300
1200
1100
1000
900
800
700
600
500
400
300
200
100
0
SIO2 WHT%
85
80
75
70

Figure 7.12. Sr (ppm) plotted against SiO_2 (wt %) for the coarse and fine granites. (Coarse granite - squares, fine granite - triangles.)

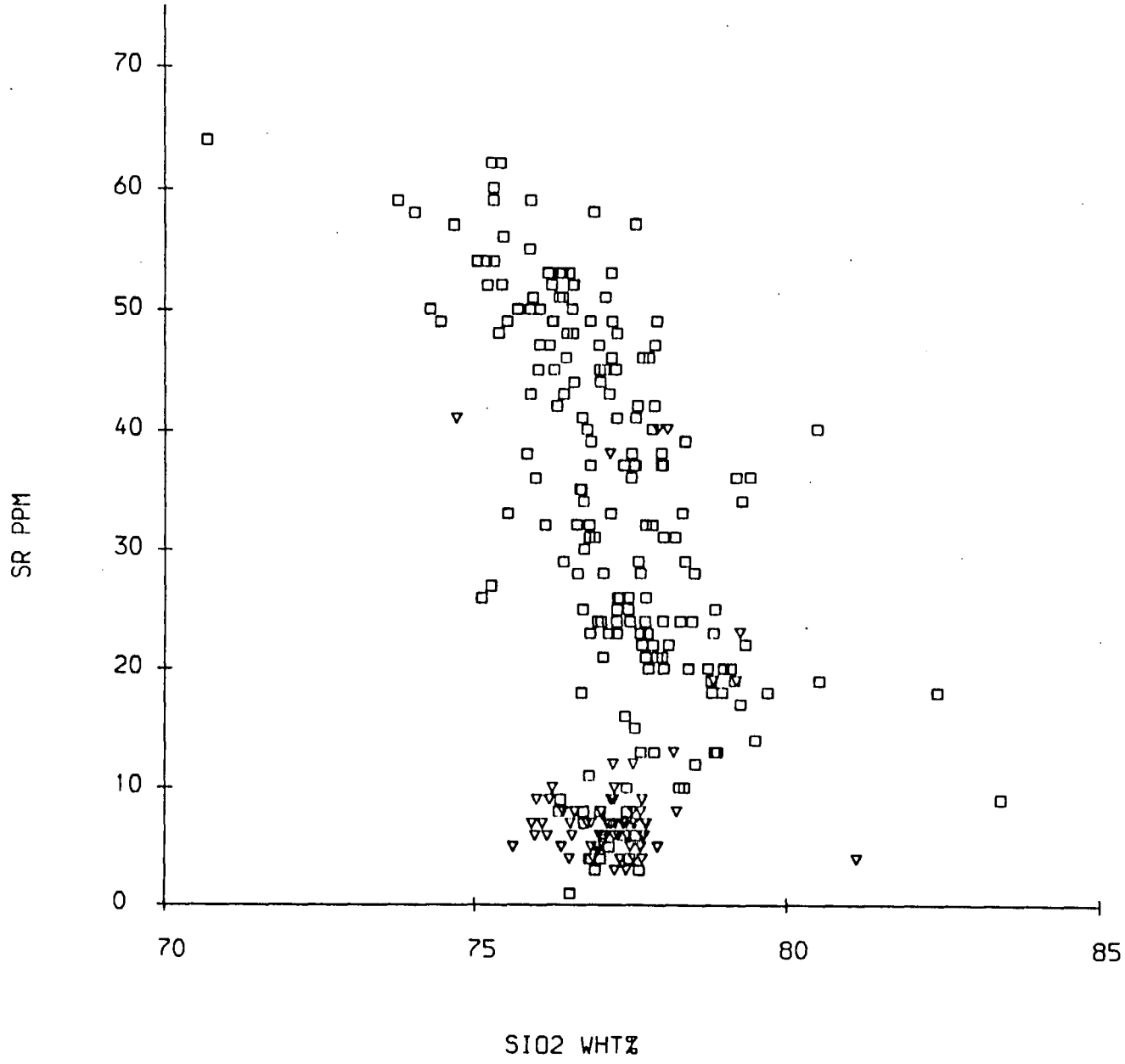

Fig. 7.12.

Figure 7.13. TiO_2 (wt %) plotted against K/Rb for the coarse and fine granites. (Coarse granite - squares, fine granite - triangles.)

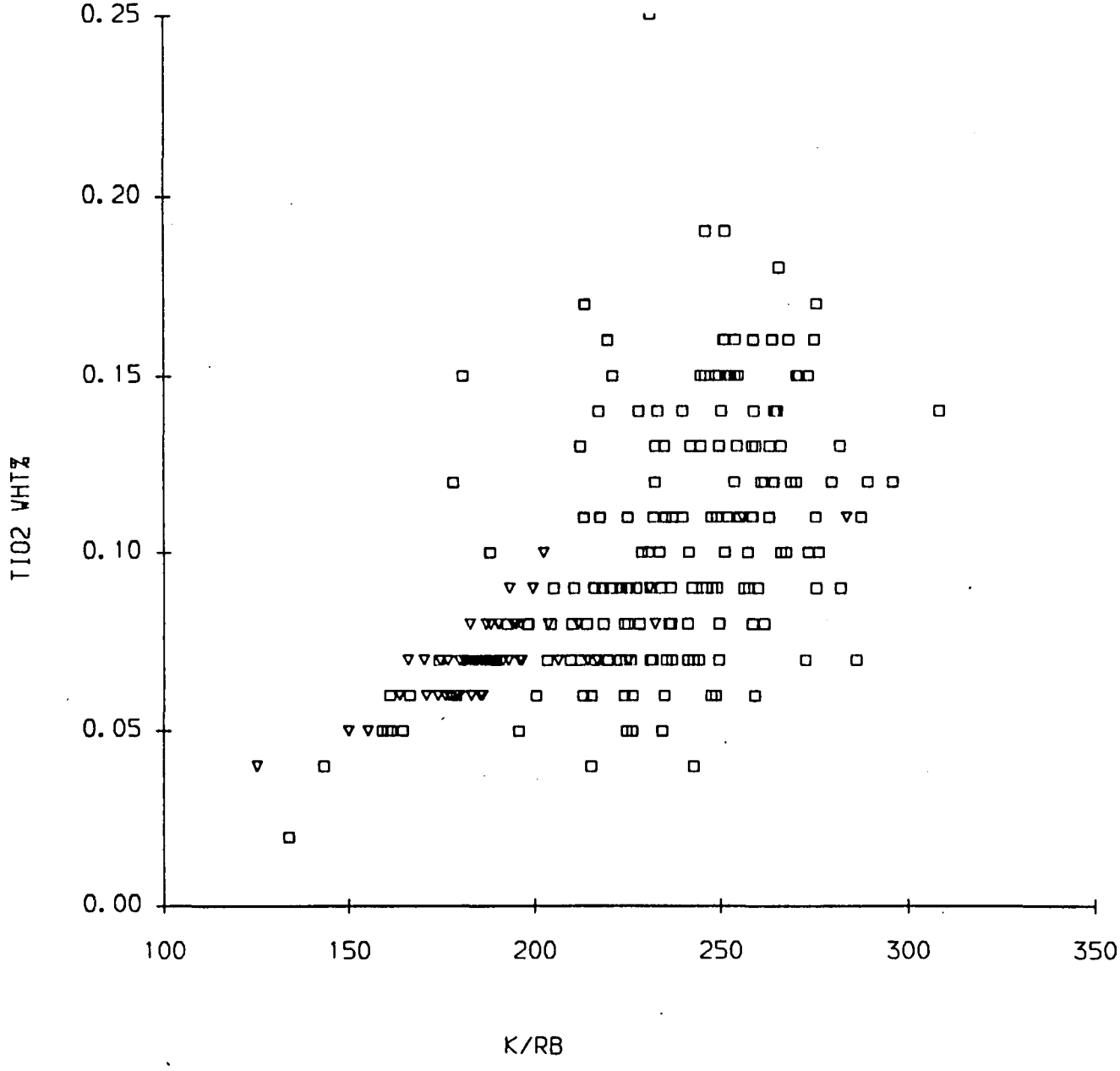

Fig. 7.13.

Figure 7.14. Ba (ppm) plotted against Rb (ppm) for the coarse and fine granites. (Coarse granite - squares, fine granite - triangles.)

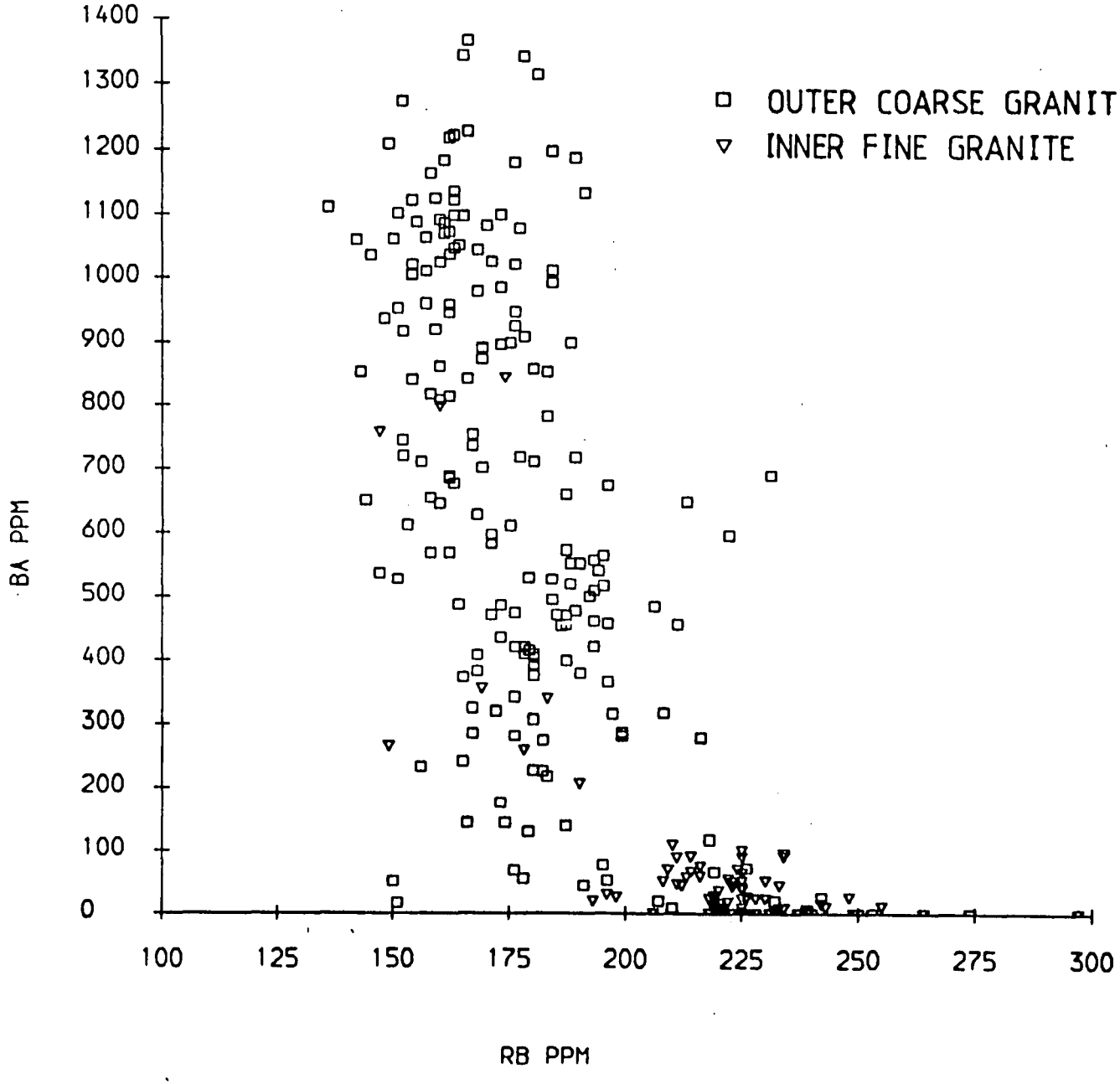
OUTER COARSE GRANITE
INNER FINE GRANITE
BA PPM
RB PPM
1400
1300
1200
1100
1000
900
800
700
600
500
400
300
200
100
0
100
125
150
175
200
225
250
275
300

Fig. 7.14.

Figure 7.15. Sr (ppm) plotted against Rb (ppm) for the coarse and fine granites. (Coarse granite - squares, fine granite - triangles.)

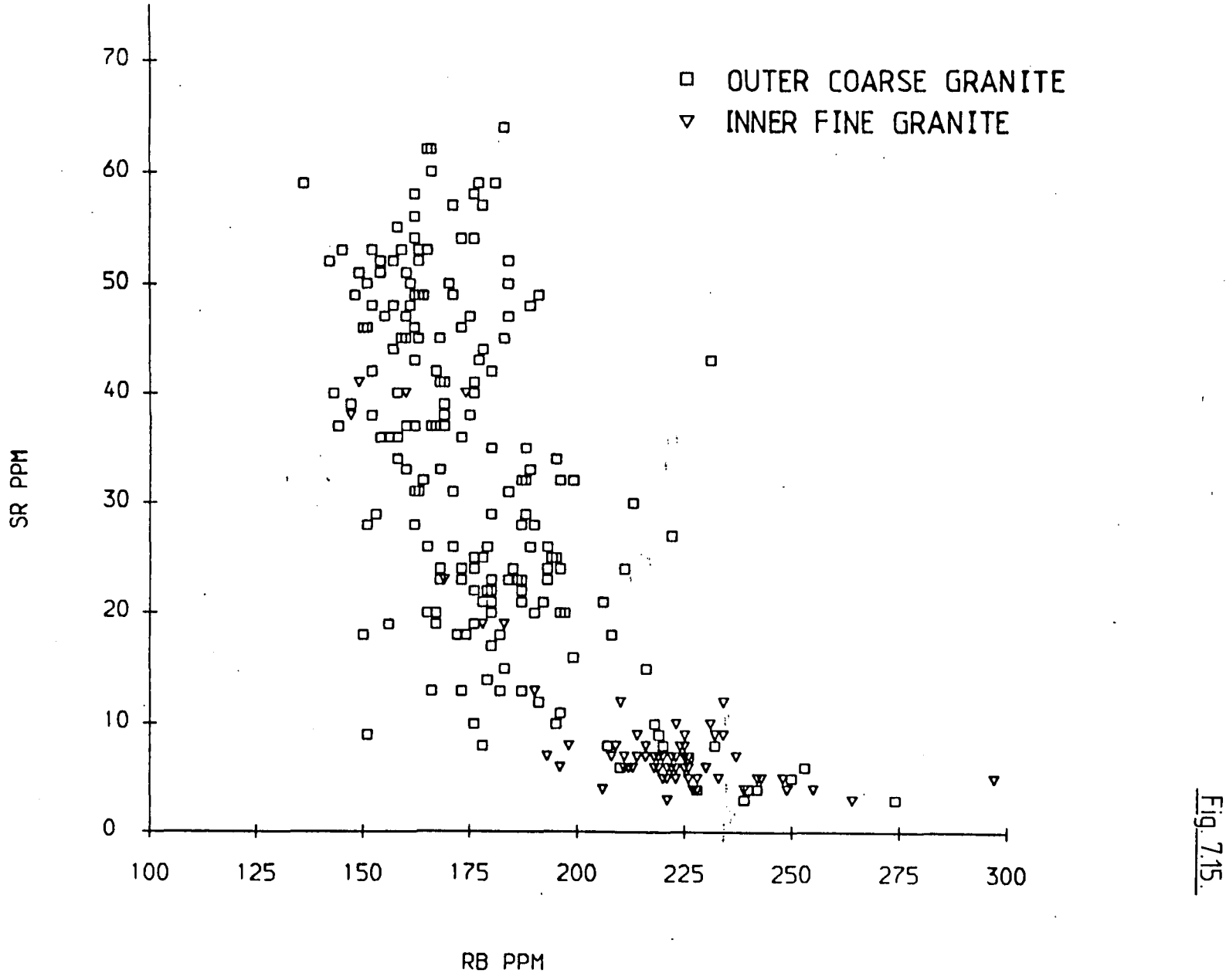
OUTER COARSE GRANITE
INNER FINE GRANITE
SR PPM
RB PPM
0
10
20
30
40
50
60
70
100
125
150
175
200
225
250
275
300

Fig. 7.15.

feldspars, which could be accounted for by the difference in the specific gravities of the fractionating phases (section 5.3.2). The plots of Ba and Sr against Rb indicate that the fine granite has approximately the same evolution trend as the coarse granite.

The range of falling Ba and Sr concentrations against increasing Rb in the fine granite is narrow but does clearly show a parabolic trend which is consistent with crystal fractionation. Petrographic data indicates that the chemical variation in the rocks is controlled by separation of phenocrysts of feldspar and quartz, which is consistent with the variations in major and trace element composition (Figs. 7.11 to 7.15). Furthermore the porphyritic to fine grained texture of the coarse granite indicates that it crystallised from a crystal bearing liquid. This is clearly not compatible with evolution by sidewall crystallisation (section 5.3.2) and hence it is concluded that the fine granite crystallised from a liquid evolved by fractional crystallisation. Figure 7.16 indicates that if this is the case the coarse and fine granites must have had different initial Ba, Sr and Rb compositions and the apparent continuation of the fine granite on the evolution trend of the coarse granite is purely coincidental. The evolution curve for a liquid fractionating orthoclase and plagioclase (with complete separation of crystals from the liquid) lies to the right of the evolution trend of the fine granite (which contains some phenocrysts, and hence represents liquid plus a small volume of trapped solid) (Fig. 7.16). This curve predicts a different initial liquid composition for the fine granite to the initial composition used to derive evolution curves for sidewall crystallisation of the coarse granite (section 5.3.2). Hence it can be concluded that the coarse and fine granites are derived from compositionally different liquids, on the basis of the theoretical models which predict their chemical evolution. This conclusion cannot be verified by the other data discussed above and consequently will be treated with caution.

The narrow range of variation in those elements concentrated in the fraction-

Figure 7.16. Figure showing the modelled fractional crystallisation path for the fine granite compared with the sidewall crystallisation path of the coarse granite. The two models predict different initial trace element compositions for the liquids crystallising the coarse and fine granites. (IC - initial composition of the coarse granite, IF - calculated initial composition of the fine granite.)

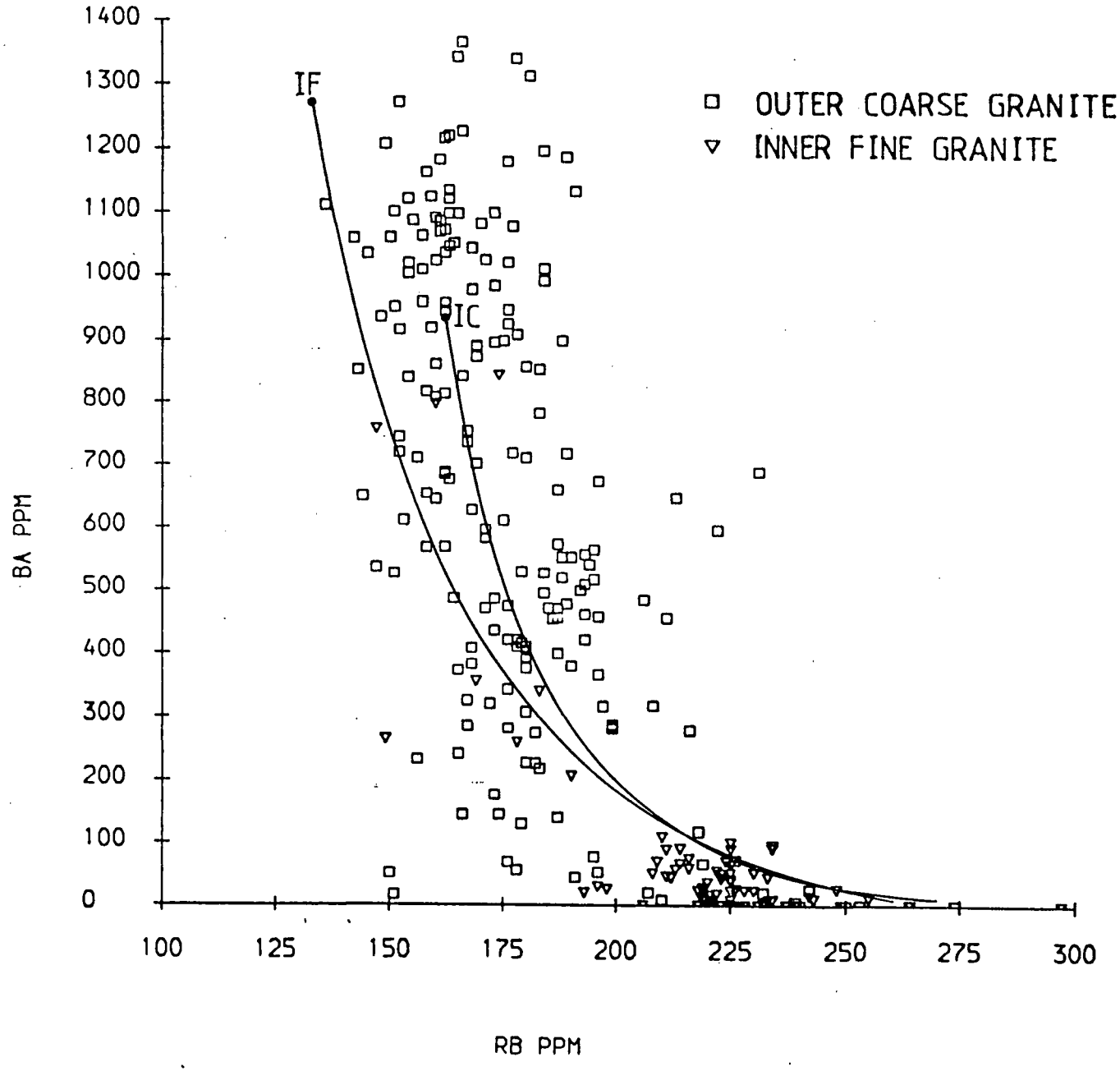
1400
1300
1200
1100
1000
900
800
700
600
500
400
300
200
100
0
BA PPM
100
125
150
175
200
225
250
275
300
RB PPM
IF
IC
OUTER COARSE GRANITE
INNER FINE GRANITE

Fig. 7.16.

ating phases (i.e. Ba and Sr in orthoclase and plagioclase respectively) indicates that the fine granite crystallised from a liquid with a low phenocryst content. This is consistent with the observation that the fine granite is generally non-porphyritic. It was shown for the coarse granite that the compositional range of a pluton is considerably extended during crystallisation of magmas which evolve by in-situ crystal fractionation (section 5.3.2). The retention of phenocrysts to produce porphyritic species of the fine granite indicates that the rate of crystallisation, or rate of migration of the crystallisation front, exceeded the rate at which crystals were separating from the melt. This implies that complete separation of phenocrysts had occurred in the non-porphyritic rocks, or that the non-porphyritic rocks never contained phenocrysts. The latter case is favoured since separation of crystals from granitic melts is inhibited by the low differences in density between the crystals and the melt (section 5.3.2). Hence it is thought that the fine granite solidified by equilibrium crystallisation, in the sense that only limited separation of crystals and liquid occurred during the final stages of crystallisation. Consequently variations in the composition of the fine granite are thought to reflect the magma composition immediately before final crystallisation but following fractionation of plagioclase, orthoclase and quartz. This is indicated by analyses of the sheets of magma in Glen Catacol and Glen Diomhan (Fig. 7.5) which have a range of compositions which show no clear trend with the interpreted order of emplacement. This is thought to indicate that these sheets were derived by tapping of a predominantly liquid body of magma in which variations in composition occurred due to irregular distributions of phenocrysts. The remainder of the fine granite shows no spatial variation in texture or chemistry and hence it is interpreted as a homogeneous body.

CIPW norms for the fine granite plotted on a diagram of normative quartz - albite - orthoclase indicate a crystallisation pressure of between 1 and 2 kbar (i.e. at a depth of 3 - 6 km) (Fig. 7.17). This pressure is clearly higher than that

Figure 7.17. A plot of normative quartz - albite - orthoclase for the Northern Arran fine granite (shaded), showing the variation in the position of the minimum melting point composition with falling pressure (after Tuttle & Bowen, 1958).

Fig. 7.17.

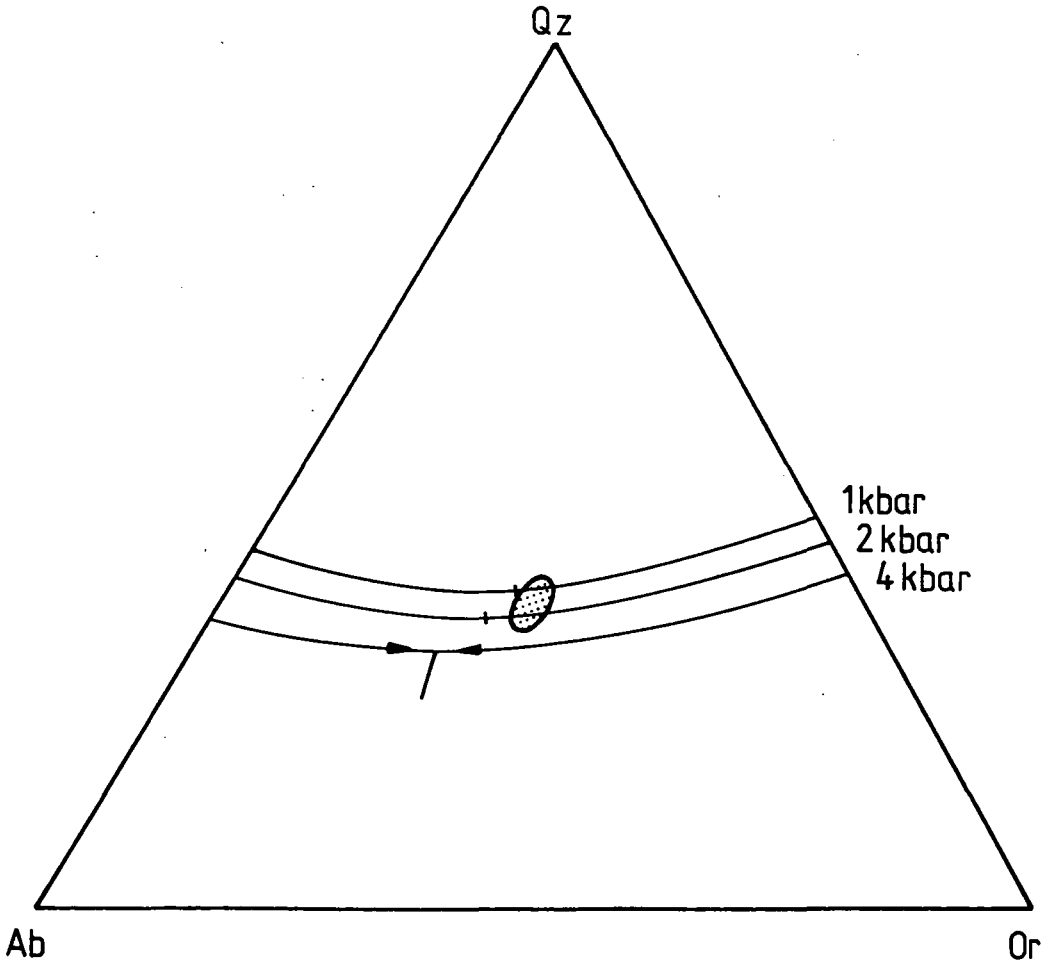

for the coarse granite, (0.5 - 1 kbar) although it is clear that the fine granite was intruded at the same structural level. However the crystallisation pressure may be anomalous. As noted above the fine granite has fractionated quartz, and as a result would be enriched in normative and modal feldspar, which would account for the higher Al_2O_3 content of the fine granite. This would cause normative analyses of the fine granite to plot below the minimum melting point, within the feldspar plus liquid field of the system quartz - albite - orthoclase, and hence indicate anomalous crystallisation pressures. The silica enrichment of the fine granite indicated by its high SiO_2 composition and fractionation of phenocryst quartz is thought to have resulted from the same polybaric fractionation mechanism invoked to cause silica enrichment in the coarse granite. However in the case of the coarse granite the less extensive fractionation of feldspars caused the evolving liquid to reach the minimum melting point composition at a shallower depth (and lower pressure) than that at which the fine granite is now intruded. This would account for the increased fractionation of quartz in the fine granite relative to the coarse granite.

The similarity in major element, trace element and isotope composition of the fine granite to the coarse granite indicates that the fine granite evolved by the same process of differentiation of a crustally contaminated basaltic magma as the coarse granite. Because of this similarity it is not possible to resolve whether the coarse and fine granites are derived from the same or different bodies of granitic magma. The fine granite is clearly intruded into the coarse granite which indicates that it rose as a separate body after emplacement of the coarse granite. Variations in Ba, Sr, Rb and Eu between the two granites indicate that the fine granite had a separate post differentiation history to the coarse granite. Low concentrations of Sr and Eu in the fine granite indicate that it fractionated substantial amounts of plagioclase following differentiation and contamination. The depletion of Ba indicates extensive fractionation of orthoclase following contamination. Fractional crystallisation of the fine granite magma would have caused the observed Rb

enrichment.

The petrographic and trace element data is consistent in indicating that the fine granite crystallised from a liquid precipitating plagioclase, orthoclase and quartz. If the composition of the fine granite represents a liquid evolved by fractional crystallisation the composition of its parental magma would have a different initial trace element composition to the parent magma of the coarse granite. The narrow range of compositions shown by the fine granite indicates that it solidified by equilibrium crystallisation after it was intruded into the coarse granite. A lack of a systematic variation in the composition of the intrusive sheets in Glen Catacol with their sequence of emplacement suggests the fine granite was initially emplaced by repeated tapping of a body of magma containing inhomogeneous concentrations of fractionating orthoclase, plagioclase and quartz crystals.

The fine granite shows a trend of falling silica with increasing fractionation. This is interpreted as the result of fractionation of quartz after polybaric fractionation during ascent had caused supersaturation of silica in the magma. This results in an anomalous crystallisation pressure for the fine granite.

7.4 The Emplacement of the Fine Granite.

Field mapping, petrographic and chemical data indicate that the fine granite magma was passively emplaced into the coarse in a predominantly liquid form. Sheets of drusiform granite parallel the walls and the roof of the intrusion in Glen Catacol and Glen Diomhan. The emplacement of these sheets suggests initial intrusion of the fine granite magma was sporadic and occurred in response to intermittent opening of the space into which it rose. These sheets appear to pass gradually into homogeneous fine granite which suggests that the final stage of emplacement of the granite was short and involved movement of the fine granite magma into a rapidly opening space.

The emplacement of the fine granite does not appear to have been permitted

by stoping of the coarse granite since the fine granite only contains xenoliths of coarse granite along its margins, neither does its intrusion appear to have been permitted by upward movement of a block of coarse granite as there is no evidence of faulting along the contact between the two granites. The junction between the coarse and fine granites is always continuous where it shallows to form the roof to the fine. Consequently it is concluded that the fine granite is intruded into the space resulting from the subsidence of a large block of coarse granite.

Intrusions formed by the rise of magma into a space created by the subsidnce of a block of pre-existing igneous or crustal rock are generally referred to as ring dykes. The concept of ring dykes was first described by Clough et al. (1909) to explain the structure of the Glen Coe complex, and was later applied to many of the British Tertiary intrusive complexes (Richey, 1932), notably in Mull (Bailey et al., 1924), Ardnamurchan (Richey & Thomas, 1930) and the Mourne mountains (Richey, 1928), and was examined mathematically by Anderson (1936). The concept of a subsiding block forming the space for intruding magma is not entirely valid. The subsiding block is rarely identified in many central complexes, e.g. Ardnamurchan and the eastern Mournes, although some examples are known, e.g. Loch Ba (Isle of Mull). Furthermore the subsidence of a central block does not create new space for the magma. It only redistributes the volume of magma in the crust. The subsiding block must fill the space left by the magma upwelling around it. Space for the magma prior to subsidence must be created by other means. In the case of the Northern Arran granite it is proposed that the space was created by crustal extension and initial diapiric ascent of the coarse granite, which is discussed in chapter 8.

The fine granite magma appears to have risen beneath the coarse granite after the latter had solidified. It is envisaged that a combination of contraction of the coarse granite during cooling, extensional regional stresses and a low magmatic pressure in the liquid fine granite would result in the base of the coarse gran-

ite becoming unsupported from below, which would allow it to begin to subside. Once initial subsidence began fine granite magma would flow up the initial fracture in order to accommodate the downward movement of the block of coarse granite into the reservoir of fine granite below (Fig. 7.18). The presence of the fine grained sheets in Glen Catacol and Glen Diomhan suggest that the initial fracturing occurred along the north and northwest margins of the fine granite and propagated east and south respectively. Intermittent extension of the fracture caused intermittent upwelling of fine granite magma into the fracture and across the top of the subsiding block of coarse granite against the lower and inner walls of previously injected, but unconsolidated, sheets of fine granite. Rapid cooling of the magma would have resulted in exsolution of water and subsequent chilling of the magma to produce drusiform granophyric fine granite. As the thermal gradient decreased the inner parts of the sheet would cool more slowly to produce fine grained non-drusiform granite.

Initial subsidence of the coarse granite block at its NW corner would require it to rotate toward the SE. This would only permit a small amount of subsidence, before the block would have to move vertically, because there would be no space for it to rotate into. Rotation of the block would result in tensional stresses and fracturing above the point about which it hinged. This would cause the developing ring fracture to propagate toward the SE corner of the coarse granite in order to release the stresses and allow vertical collapse of the block (Fig. 7.18). The fine granite magma would flow rapidly into the space created by the collapse of the block to maintain the volume of the crust, and the block would occupy the space originally filled by the magma. Intermittent collapse of the block at this stage could lead to the development of additional sheets of drusiform granite. Field evidence (section 7.1) indicates that the roof of the granite is irregular. The tongue of coarse granite in Glen Iorsa, which overlies the fine granite (section 7.1) may have subsided during collapse of the central block, but there is no evidence

Figure 7.18. Diagram illustrating the envisaged mechanism of emplacement of the fine granite as a ring dyke.

Fig. 7.18.

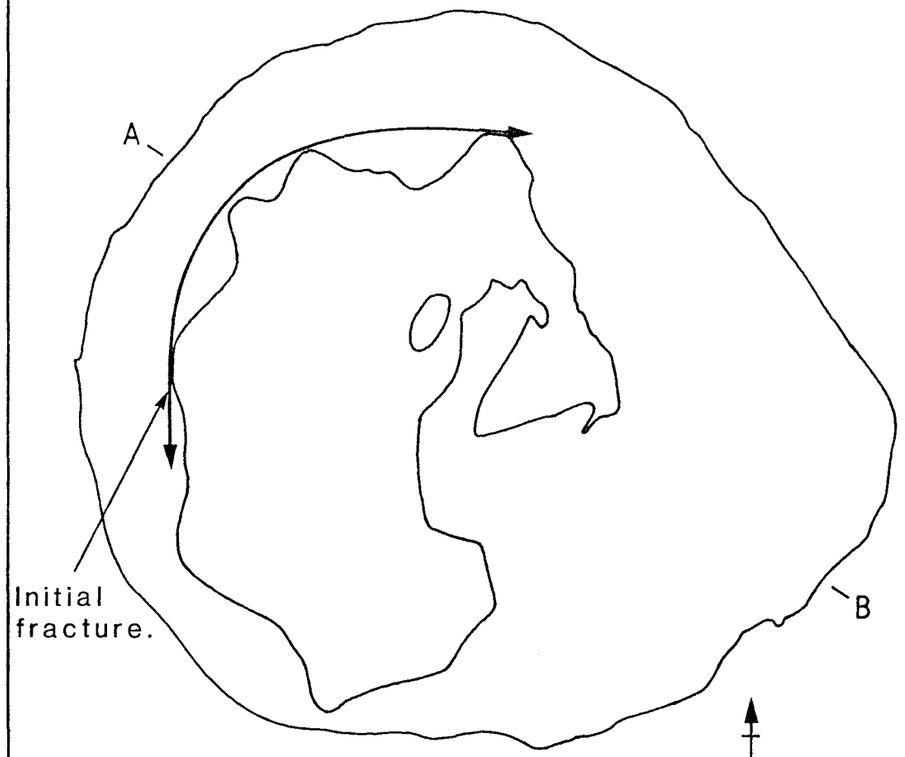

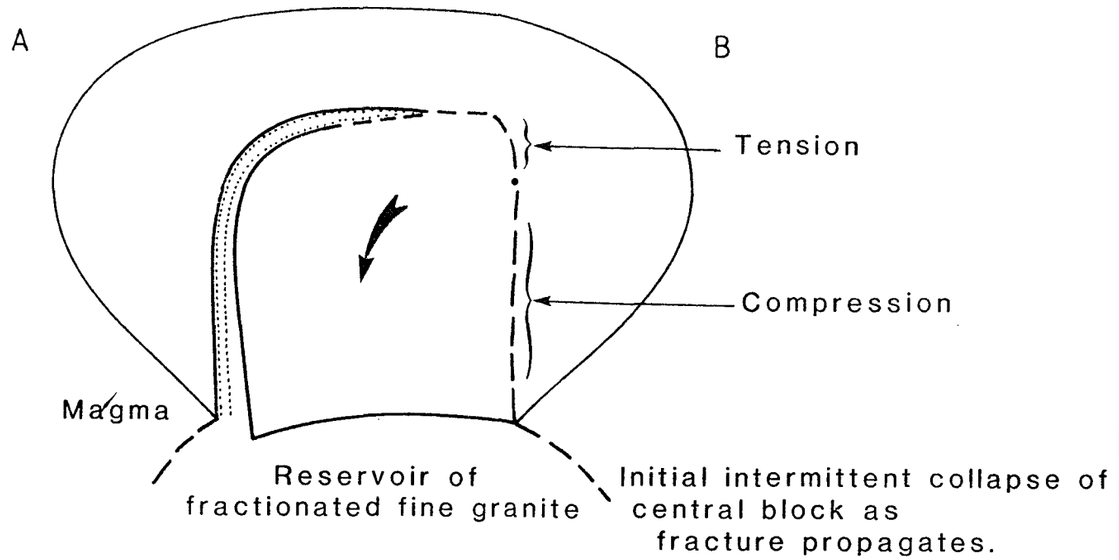

Not to scale

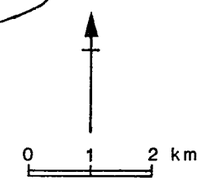

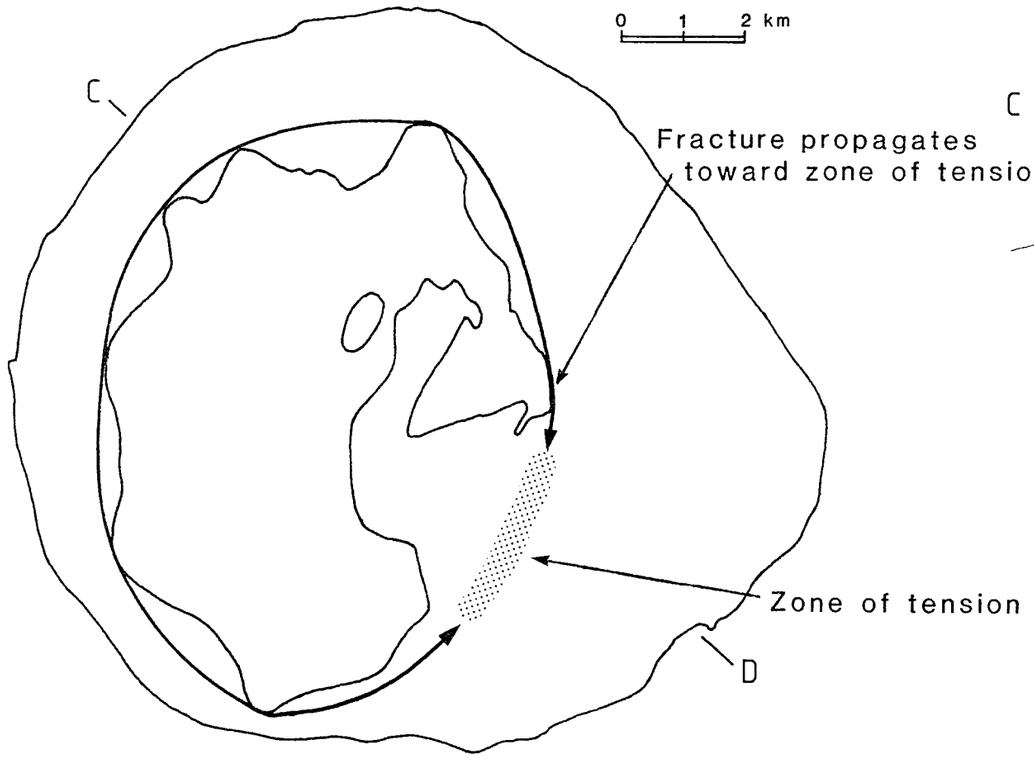

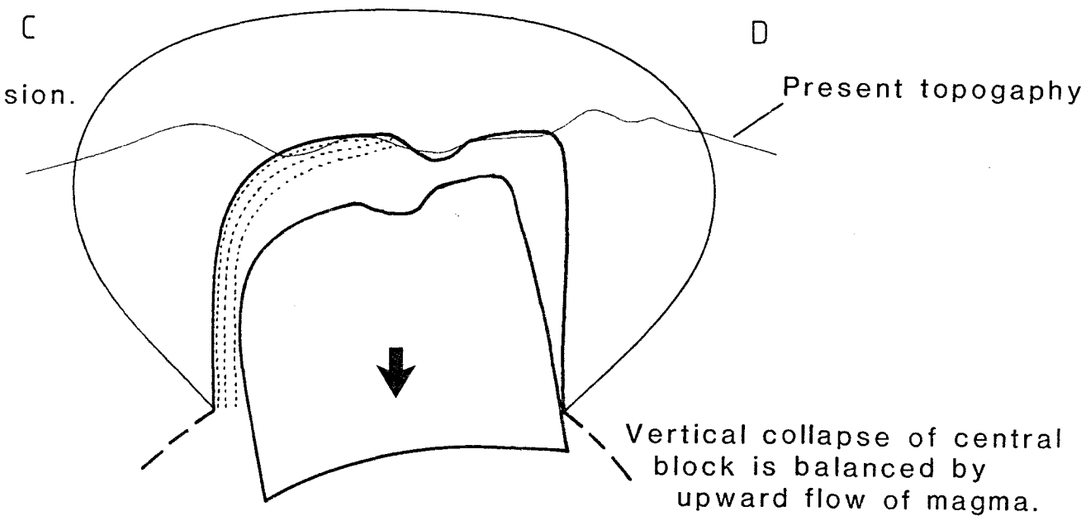

Not to scale

to support this view. The horizontal sheet of fine granite cutting, and overlying the coarse granite to the west of A' Chir is interpreted as a failed extension of the roof of the granite.

7.5 Conclusions.

The fine granite is chemically very similar to the coarse granite, but has a strongly contrasting structure, texture and style of emplacement.

The fine granite evolved by differentiation of a basaltic parent contaminated with partial melts of lower crustal rocks. Following differentiation the magma was contaminated by small volumes of low percentage partial melts of Dalradian. Subsequently it fractionated large volumes of orthoclase and plagioclase during ascent which resulted in supersaturation of quartz, which then joined the feldspars on the liquidus. Hence the chemical characteristics of the fine granite evolved as a result of its origin and ascent through and interaction with the crust in a similar way to the coarse granite.

In contrast to the coarse granite, the fine granite is passively emplaced. Initial intermittent collapse of an unsupported block of coarse granite into an underlying reservoir of fine granite magma was followed by rapid vertical movement of the block once it had become completely detached, from the rest of the coarse granite, resulted firstly in sheets of fine granite being emplaced into the coarse followed by passive injection of a large generally homogeneous body of magma. Petrographic data indicates that the magma was emplaced in a dominantly liquid state and that it cooled rapidly. Local variations in chemistry are considered to be due to inhomogeneous concentrations of phenocrysts in the liquid trapped during post emplacement equilibrium crystallisation of the magma.

It is clear form these conclusions that the contrast in granite types seen in Northern Arran is entirely the result of contrasting mechanisms of emplacement. This confirms the conclusions of chapter 5 that magmas originating from the same

source and ascending through and interacting with the same column of crust will have the same chemical features. These characteristics are then overprinted by aspects of their evolution related to their emplacement and final crystallisation. In this case the variations in texture are due to different mechanisms of crystallisation. The coarse granite is a much larger body than the fine and hence would have a lower surface area to volume ratio. Consequently its capacity to lose heat to its wall rocks would be lower than the smaller body of fine granite. This would reduce the rate of cooling of the coarse granite magma which controls crystal size and nucleation rates and sites and hence the texture of the crystallising granite.

The reason why the coarse and fine granites of North Arran have different emplecement mechanisms will be discussed in the next chapter. The similarity in chemical composition of the two granites suggests their mechanism of ascent was the same, since their chemistry indicates they have interacted with the crust in an identical way. Consequently the variation between the two granites appears to be related to processes acting during the final stages of emplacement rather than at the source or ascent stage of their evolution.

CHAPTER 8

THE ASCENT AND EMPLACEMENT OF GRANITIC MAGMA: IMPLICATIONS FROM A STUDY OF THE NORTHERN ARRAN GRANITE

This chapter combines the conclusions drawn from the preceding chapters and integrates them to produce a model for the ascent and emplacement of the Northern Arran Granite. The remainder of this chapter discusses the implications of some of these conclusions and the model derived from them for present and future studies of granitic magmas.

8.1 An Integrated Structural and Petrological Model for the Ascent of the Northern Arran Granite.

A diagrammatic summary of the ascent and emplacement of the Northern Arran Granite is given in Fig. 8.1. The emplacement of the fine granite is illustrated in Fig. 7.18.

The granitic magma from which the Northern Arran granite is derived was evolved at a depth of approximately 11 km by differentiation of basaltic magma contaminated by partial melts of granulite facies (?Grenvillian) middle crust (sections 5.3.1 & 5.3.2 and Fig. 8.1a & 8.1b). Emplacement of the basic magma into the lower crust was permitted by crustal extension which is recorded by the presence of Early Tertiary basic dykes at the surface (Chapter 2 and Fig. 8.1a).

The chemistry of the coarse granite indicates that it suffered only slight contamination during its ascent through the Dalradian rocks overlying the middle crust (sections 5.3.1 & 5.3.2 and Fig. 8.1c). This indicates that the granite behaved as a closed system and was essentially isolated from its wall rocks during its ascent. This eliminates ascent of the granite by stoping and/or assimmilation

Figure 8.1 A schematic diagram summarising the ascent and emplacement of the Northern Arran coarse granite. The emplacement of the fine granite is illustrated in figure 7.18.

Fig. 8.1.

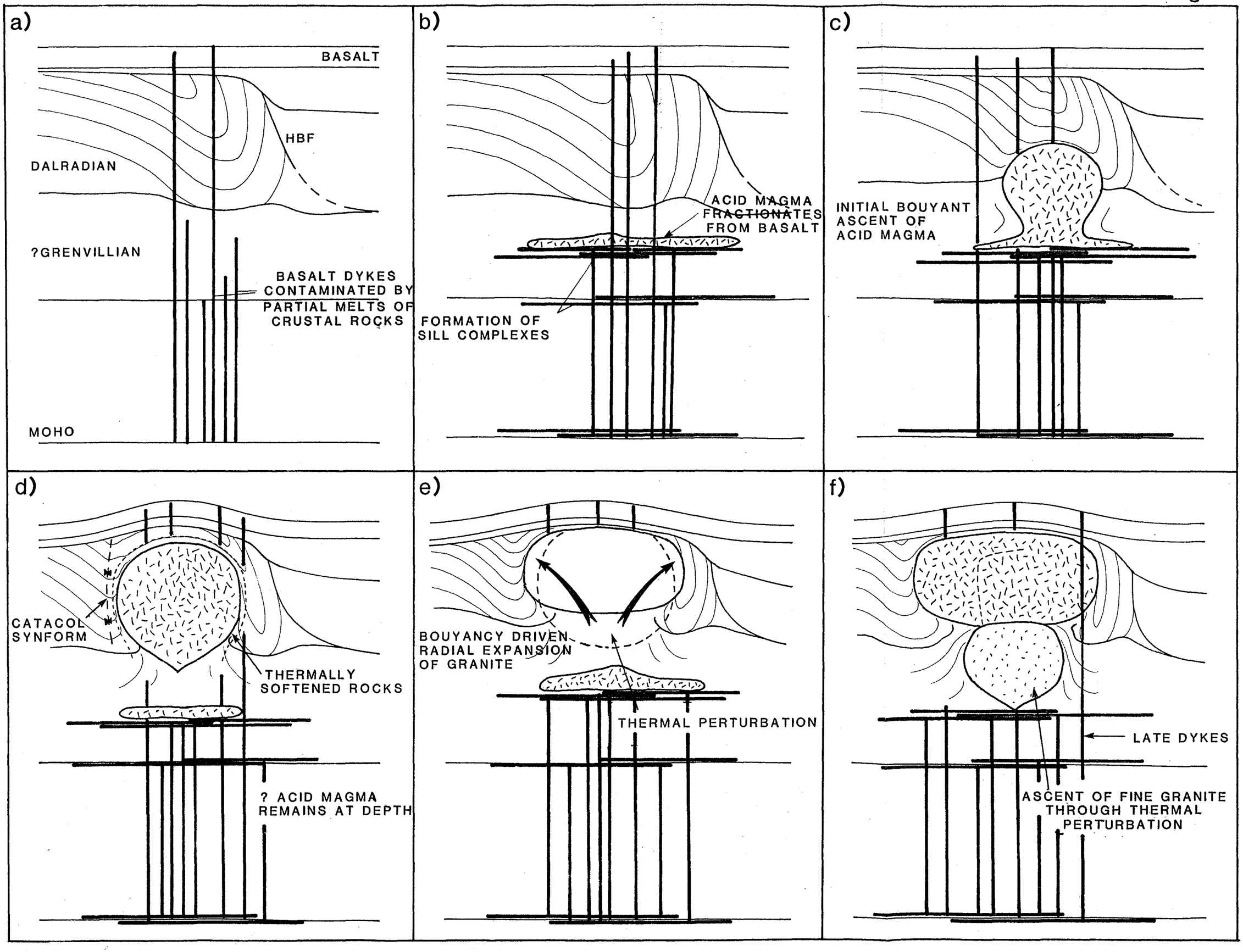
a)
BASALT
HBF
DALRADIAN
?GRENVILLIAN
BASALT DYKES CONTAMINATED BY PARTIAL MELTS OF CRUSTAL ROCKS
MOHO
b)
ACID MAGMA FRACTIONATES FROM BASALT
FORMATION OF SILL COMPLEXES
c)
INITIAL BOUYANT ASCENT OF ACID MAGMA
d)
CATACOL SYNFORM
THERMALLY SOFTENED ROCKS
? ACID MAGMA REMAINS AT DEPTH
e)
BOUYANCY DRIVEN RADIAL EXPANSION OF GRANITE
THERMAL PERTURBATION
f)
LATE DYKES
ASCENT OF FINE GRANITE THROUGH THERMAL PERTURBATION

of country rock. Minimal stoping is consistent with the lack of xenoliths found in the granite at the present level of exposure.

Data collected at the present level of exposure of the granite indicates that it rose through the crust surrounded by a narrow thermal aureole in which rocks adjacent to the granite were heated to the point at which they attained a plastic rheology (Chapters 3 & 4). This is consistent with the ascent of the granite as a diapiric body of magma driven by bouyancy forces (Fig. 8.1c & 8.1d) (Chapter 6). The rate of ascent was controlled by the rate of heat loss from the granite (due to cooling and the release of latent heat of crystallisation) which controlled the rate at which the viscosity of the wall rock, and hence drag over the surface of the body, was reduced (Chapter 6). Crystallisation during ascent (releasing latent heat) is confirmed by chemical evidence which indicates that the magma became saturated in silica as a result of polybaric crystallisation (section 5.4). This process controlled the subsequent crystallisation of the magma, which will be discussed further below. This model for the early evolution and ascent of the Northern Arran granite is constrained by geochemical and geophysical data, and theoretical modelling.

Structural data can be used to demonstrate that the granite intersected the hinge of the Aberfoyle synform during its ascent, deflecting the SW limb of the fold outwards toward the south and east parallel to the surface of the magma body. The granite intersected the SE dipping NW limb of the Aberfoyle synform at approximately 90^o. Upward deflection of this limb around around a hinge parallel to the margin of the granite produced a monoformal structure which is referred to as the Catacol synform (Chapter 4 and Fig. 8.1d). The interpretation of this phase of ascent of the coarse granite and the deformation of its aureole is restricted to the interpretation of the strains recorded in those structures which have well constrained pre-intrusion geometries which project across the axis of ascent of the granite at depth.

Deformation of the aureole of the Northern Arran granite by ballooning (in-situ expansion) can be eliminated because the ballooning process could not produce the observed uplift of the NW limb of the Aberfoyle Synform without some vertical movement. Structures in the NW limb of the Aberfoyle synform do not record a combination of contractional and extensional strains consistent with it rotating through a flattening strain field normal to the surface of the granite (Chapter 4).

The Catacol synform and the zone of softened rocks adjacent to the granite are cut by a system of linked thrust and normal faults and extensional shears respectively. Principal stress orientations determined from these structures and kink bands in the opposing limbs of the Catacol synform indicate that these structures represent pure flattening strains without further concentric folding (Chapter 4). A set of dextral strike slip faults to the south of the granite and a major component of sinistral displacement on the reactivated Goat Fell fault, forming the eastern margin of the northern granite, record radial and tangential expansion of the granite which reflects a change in the shape of the pluton after it came to rest. This is contemporaneous with the radial flattening across the Catacol synform to the north and west of the granite (Chapter 4 and Fig. 8.1e).

The granite does not contain a fabric resulting from strong deformation of a crystal-liquid mush which indicates that the magma behaved rheologically as a liquid (i.e. it was <70% crystallised) during ascent and emplacement, so that stresses within it were hydrostatic (section 5.5). Consequently the radial expansion of the intrusion following ascent must be explained by the flow of a liquid body of magma. It would appear that the ascent of the body ceased because the upper parts of the body reached a level at which their density was equal to that of the surrounding rocks and hence the bouyancy forces on this region of the body fell to zero or because the aureole of the granite suffered rapid cooling, and therefore a rapid increase in viscosity, possibly through heat loss along the

Goat Fell fault. In either case the liquid in the lower portion of the pluton would continue to rise bouyantly until it reached equilibrium. In order to accommodate this upward flow it would be necessary for the granite to spread laterally, if it could not rise vertically. Lateral expansion would result in the observed radial shortening and concentric expansion of the aureole. Evidence that this process may have continued during crystallisation of the coarse granite can be found in the form of undulose extinction in quartz and distortion of biotite crystals (sections 5.2 & 5.5).

Hence it can be seen that it is possible to constrain the mechanism of emplacement of the Northern Arran coarse granite from structural data, combined with an evaluation of the rheological and physical properties of the intruding magma.

The conclusions derived from the structural data require that the crystallisation and solidification of the coarse granite occurred after it was emplaced. Modelling of the crystallisation of granitic magmas (section 5.3.2) indicated that the variations in trace elements, due to fractionation of orthoclase and oligoclase feldspars, biotite and quartz, could be accounted for by both fractional crystallisation, involving separation of crystals from liquid, and by sidewall crystallisation, involving separation of evolved liquids from crystals. However the petrographic/textural variations within the granite could only be explained by sidewall crystallisation following early equilibrium crystallisation. This theory is also substantiated by consideration of the physical constraints which inhibit the separation of felsic crystals from a convecting granitic magma (section 5.5).

Details of the early evolution of the fine granite (Fig. 8.1e & 8.1f) can only be deduced from geochemical (isotope and trace element) data since there are no structures exposed at the surface which could be used to elucidate its mechanism of ascent. The geochemistry of the fine granite is very similar to the coarse granite (Chapter 7) consequently it is thought that the derivation and ascent mechanism of this body of magma was the same as that of the coarse granite.

The emplacement of the fine granite emphasises the roles of pre-existing structure and regional tectonics in influencing mechanisms of ascent and emplacement, and the lack of a control on emplacement by crustal level. It is envisaged that the fine granite rose diapirically beneath the coarse granite, after the coarse granite had crystallised, to form a magma chamber in which fractionation of quartz and feldspars occurred. A combination of regional tensional stresses, contraction of the coarse granite during cooling and the upward directed bouyant stress exerted by the rising fine granite magma caused an arcuate fracture to develop in the coarse granite (Fig. 7.18) which was exploited by the fine granite. As the tips of the ring fracture converged a central block of coarse granite collapsed into the reservoir of fine granite forcing the fine granite magma up and around it.

Restoration of the aureole of the coarse granite using structural data indicates that much of the volume occupied by the coarse granite was created by displacement and deformation of the crust during ascent of the coarse granite magma. Estimations of regional extension (from dyke swarms, Knapp, 1973) indicate that 5% of this volume could be accommodated by crustal extension at the level at which the granite was emplaced. It is recognised that the granite only represents dilation of the crust at its present level. The actual dilation of the crust required to permit the ascent and emplacement of a body of magma, would depend upon the ability of the crustal rocks to flow around the rising magma body, which is enhanced by diapiric ascent (Chapter 6). Consequently it must be appreciated that the emplacement of a body of magma with a diameter of 12 km at a depth of 3 km does not require an increase in the volume of the crust which corresponds to a cylinder 12 km in diameter and a height equal to the thickness of the crust below 3 km. In this case the actual volume increase in the crust (or 'space problem') represented by the coarse granite may be comparatively small. The fine granite represents less of a 'space problem' because it presumably rose through rocks already stretched by the ascent of the coarse granite. Its final emplacement does

not constitute a space problem since the collapse of a central block and upflow of magma maintains crustal volume (Chapter 7).

In conclusion: This analysis of the ascent and emplacement of the Northern Arran granite is based on the intergration of a wide variety of geological data. Different data are used to constrain different aspects of the ascent and emplacement process, which may be verified by other data. Certain aspects of the ascent and emplacement mechanism may have implications for the subsequent evolution of the granite which should be consistent with the observed data. If this is not the case the intial interpretation may be wrong. By eliminating inconsistences in the model by methodical 'cross checking' for internal consistency and by hypothesis testing this study shows that it is possible to determine all the stages of the ascent and emplacement of a body of granitic magma.

Petrological data has been used to constrain the origin, early stages of ascent and the crystallisation of the Northern Arran granite. Structural data has been used to determine the late stages of ascent and the mechanism of emplacement of the granite. The structural data provide more accurate information on the actual process of ascent than the petrological data, which may only be used to eliminate certain processes e.g. stoping and assimilation. Models derived from the structural and petrological data can both be cross checked by considering the mechanism of ascent of the granite by theoretical modelling. By this approach it is possible to overcome and extend the limitations of each data set. Most of the data obtained from the exposed level of a pluton record processes of emplacement and crystallisation. It is important to fully understand these aspects of the evolution of the magma body and identify their effects before the pre-emplcement history of the pluton is examined.

8.2 Implications for the Ascent of Granitic Magma.

This study of the Northern Arran granite indicates that it is possible to model

the early stages of the ascent of a granitic magma body using geochemical data and by applying a theoretical model for the ascent of granitic magma and determining if they are internally consistent. However the accuracy of this approach is not good. The geochemical data, in this case, can only be used to eliminate ascent by stoping and assimilation but does not provide positive indications of the actual ascent process. While the Hot Stokes model predicts that diapiric ascent of a granitic magma body over a distance of approximately one body radii is possible the conclusions drawn from this theory are strongly model dependant (Chapter 6). However these data can be used to constrain the ascent of magma through levels of the crust to which we do not have direct access. The model is based on field data collected at the level of emplacement which is necessarily extrapolated. This may induce further errors. The main implications of the theoretical model are: The shape of the magma body is maintained at some equilibrium configuration (spherical, minimum drag) by a mechanism of thermal feedback. The ascent distance of a magma body is dependent upon its size which controls the amount of heat it may release as a result of cooling and in the form of latent heat evolved by cooling induced crystallisation. Consequently if a magma body rises as a diapir for any distance, within the constraints of the Hot Stokes model, it will inevitably be partially crystallised when it comes to rest. Although actual ascent of the magma is driven by bouyancy forces its ability to rise is controlled by the reduction in the viscosity of its wall rocks. Hence it can be seen that the thermal evolution of a magma body is a critical factor in determining its mechanism and distance of ascent, and its physical state as it comes to rest. However a great deal of error exists in this area since we do not yet fully understand the thermo-mechanical properties of the wall rocks which will be inhomogeneous and therefore beyond the constraints of the Hot Stokes model. Neither do we know what volume of country rocks are heated, and to what temperature they are heated during ascent. Further work is required in this area. The work presented in this thesis (Chapter

6) indicates that it is possible to parameterise the Peclet number in terms of the strain rate associated with the ascent of a body of magma and that the assumption of Marsh (1982) that the wall rocks have to be heated to their solidus before their viscosity is reduced sufficiently to permit ascent of the magma body is invalid.

Structural data collected from the aureole of the Northern Arran granite provide better constraints on the later stages of ascent of the magma body. These largely confirm the conclusion that it rose as a diapir. The formation of the Catacol synform clearly indicates that the ascent of a hemispherical/?spherical body of magma occurred in North Arran. Fabrics developed parallel to the surface of the granite overprint porphyroblasts which grew during thermal metamorphism of the aureole rocks. The metamorphism reduced the viscosity of the aureole rocks to a level at which they would deform in a ductile manner to permit ascent of the magma, as predicted by the Hot Stokes model. Subsequent deformation of these thermally softened rocks to accommodate the magma body as it rose would produce the observed overprinting fabrics in the rocks. Any granitic body which rises as a diapir would show this relationship which should be added to the list compiled by Coward (1981) and Bateman (1984) as an additional diagnostic feature of igneous diapirs. It is concluded that diapiric ascent of granitic magma by a mechanism similar to that predicted by the Hot Stokes model is viable and consistent with the observable features of some granitic intrusions.

A further important implication derived from this study is that the chemistry of granitic magmas can be influenced by their ascent mechanism. If a granite rises by a mechanism which results in crystallisation certain mineral phases may be fractionated to such an extent that the composition of the magma is significantly altered and leaves the stability field of that phase so that it is no longer precipiated, or, as in the case of the Northern Arran coarse and fine granites polybaric crystallisation resulted in silica satuation of the magmas which in turn resulted in eutectic crystallisation. These changes in magma chemistry may have

significant effects on our interpretation of the origin of granitic magmas and on the rheology of the granitic magma during emplacement, deformation and final crystallisation, which are the subjects of current research (Hutton, 1988a and section 8.4).

8.3 Implications for the Emplacement of Granitic Magma.

The Northern Arran granite provides a great deal of information about the transition from the ascent of a magma body to its final emplacement. The lack of a regional tectonic control on the development of fabrics within the aureole of the granite indicates that the bouyant forces acting on the magma dominated the process of emplacement (Brun & Pons, 1981; Soula, 1982; Hutton, 1988a). Restoration of aureole strains (Chapter 4) indicated that most of the volume occupied by the coarse granite was created by diapiric ascent and associated ductile deformation. Semi-brittle to brittle structures overprinting the earlier ductile deformation record a shape change in the pluton, by radial expansion, caused by the dissipation of bouyancy forces. It is clear from this observation that the final shape of a pluton, following emplacement, may not be the same as its shape during ascent, which was modified by the emplacement process.

Chemical data indicate that the coarse granite is formed from a single body of magma rather than the result of the accumulation and mixing of a number of chemically distinct batches of magma. This indicates that the folding and flattening strains in the aureole of the northern granite are the result of the ascent and emplacement of a single body of magma and not the in-situ expansion of a pluton by multiple injection of pulses of magma. This implies that the coarse granite is not a ballooning diapir and that the term ballooning diapir should only be applied to plutons where it can be demonstrated that the space occupied by the pluton was created by forceful expansion of the wall rocks resulting from an increase in the volume of magma by multiple intrusion at the level of emplacement,

described by Bateman (1984). In the case of the coarse granite (a single pulse diapiric body) radial expansion is a consequence of the dissipation of bouyancy forces as typified by the 'montgolfiere' type diapir illustrated by Brun & Pons (1981) (Fig. 8.1e). Patterns of strain around the Northern Arran granite may prove useful in determining and restoring sequential deformation histories recorded in plutons which have ballooned as a result of multiple emplacement of diapiric bodies of magma into the same intrusion. The coarse granite also illustrates the the types of structure which might be used to recognise and distinguish between diapiric ascent and radial expansion, which is not possible from the classifications of Coward (1981) and Bateman (1984). These classifications (Chapter 1) would include both true diapirs and ballooning diapirs as diapiric bodies. The division between diapirism as a mechanism of ascent and as a mechanism of emplacement should be made clear in future as it is obvious from the work of Bateman (1984) that the two processes are not mutually inclusive. In particular, evidence of post thermal metamorphism deformation of the aureole and direct evidence of updoming would characterise an ascending diapir. A ballooning diapir would show syn-metamorphism flattening strains within its aureole.

The role of the reactivation of the Goat Fell fault in influencing the final emplacement geometry of the coarse granite, and in particular its influence during the transition from ascent to radial expansion of the granite illustrates the importance of pre-existing structure in influencing the emplacement mechanism of granitic intrusions. This factor may have to be considered as of equal importance as the interaction between tectonic and bouyancy forces in controlling the ascent and emplacement geometry of granitic bodies.

8.4 Implications for Crystallisation and Fabric Development in Granitic magmas.

Trace element variations and detailed petrographic studies were used to de-

termine the crystallisation history of the Northern Arran granites. Bateman & Chappell, (1979) discussed the relative importance of fractional crystallisation and sidewall crystallisation in the solidification of intrusive granites. Modelling of the crystallisation of the coarse granite indicated that it solidified by sidewall crystallisation. The work presented in this thesis (Chapter 5) describes how this was done and establishes the petrographic and chemical criteria employed to distinguish this process from fractional crystallisation. However it is recognised that while this modelling produces results consistent with laboratory models (Baker & McBirney, 1985) it should be appreciated that the accuracy of these results, and interpretations based upon them, are dependant upon the accuracy of the model in simulating the actual processes occurring in a granitic magma during crystallisation.

As noted above changes in the chemistry of the magma caused by its ascent can also have a significant effect on the combinations of phases preciptated during crystallisation and on the fabric and crystallisation history of the magma. Arzi (1978), van der Molen & Patterson (1979) and Marsh (1988) investigated the effect of crystal content, crystal sizes and size distribution and the rates of nucleation and crystallisation on the rheology of crystallising magmas. The fundamental control on all these parameters is the chemistry of the magma itself. It appears from this conclusion that there is the need for an increase in our knowledge of how magmas crystallise, before we can fully understand the development of fabrics in granitic rocks which result from deformation. Time scales may be critical in fabric development. The coarse granite may have retained the properties of a liquid while it deformed its wall rocks because nucleation rates in the magma were low and so few crystals formed until the magma became strongly supercooled. Conversely a magma with a different chemistry may have developed a fabric under the same circumstances because a higher nucleation rate would have caused the magma to cross the critical melt percentage at an earlier stage of the emplacement process.

Further research is clearly required in this field if we are to understand why fabrics develop in certain granitic rocks but not in others.

The group 2 rocks of the coarse granite (Chapter 5) contain unrealistically high proportions of phenocrysts, interpreted as the result of compaction and melt expulsion following sidewall crystallisation. This represents non-constant volume deformation of the magma and consequently coexisting proportions of solid and liquid will not be in equilibrium. Detailed microprobe studies of this chemical disequilibrium may be employed to determine the volume of liquid lost from the system and consequently the amount of deformation of the magma. The problems and uncertainties involved in testing this hypothesis are numerous but may be overcome by collecting large data sets. There is clearly scope for studies of this type to determine the amount of deformation in apparently undeformed granites such as the Northern Arran coarse granite.

8.5 The Contribution of an Integrated Approach to the Study of Granitic Magmas.

Much of the work described in this thesis has employed a semi-quantitative approach to the study of the ascent and emplacement of the Northern Arran granite. Particularly in the investigation of its mechanisms of ascent and crystallisation. The equations used have been derived or chosen because they are based on direct field or petrographic observations which can be derived from a study of the northern granite. Placing mathematical constraints on the processes of ascent and crystallisation has required or prompted an increased understanding of the role and affect of, for example, rates of heat loss, or the affect of different degrees of solid/liquid separation on final rock composition. This has lead to an increased need for internal consistency between the models for emplacement of the granite derived from structural data and petrological data. This clearly justifies an integrated structural and petrological approach to understanding the ascent

and emplacement of granitic magmas.

REFERENCES.

ABBEY, S. 1983. Studies in 'standard samples' of silicate rocks and minerals. Canadian Geological Survey Paper 83 - 15.

ANDERSON, E. M. 1936. Dynamics of formation of cone sheets, ring dykes and cauldron subsidences. Proceedings of the Geological Society of Edinburgh, 56, 128–157.

ANDERSON, J. G. C. 1944. The Dalradian rocks of Arran. Transactions of the Geological Society of Glasgow, 20, 264–86.

ANDERSON, T. B. 1974. The relationship between kink-bands and shear fractures in the experimental deformation of slate. Journal of the Geological Society, London, 130, 367–82.

ARZI, A. A. 1978. Critical phenomena in the rheology of partially melted rocks. Tectonophysics, 44, 173–84.

ASTIN, T. R. & MacDONALD. D. I. M. 1983. Syn-depositional faulting and valley fill breccias in the Permo-Triassic of Arran. Scottish Journal of Geology, 19, 47–58.

ATHERTON, M. P. 1981. Horizontal and vertical zoning in the Peruvian coastal batholith. Journal of the Geological Society, London, 138, 343–49.

BAILEY, E. B. 1926. Domes in Scotland and South Africa: Arran and Vredfort. Geological Magazine, 63, 481–95.

BAILEY, E. B., CLOUGH, C. T., WRIGHT, W. B., RICHEY, J. E. & WILSON, G. V. 1924. The Tertiary and Post Tertiary geology of Mull, Loch Aline and Oban. Memoir of the Geological Survey of Scotland, HMSO.

BAKER, B.H. & McBIRNEY, A. R. (eds). 1985. Processes in Magma Chambers. Journal of Volcanolgy and Geothermal Research, 24, 1–204.

BALK, R. 1937. Structural Behavior of Igneous Rocks. Geological Society of America Memoir No. 5.

BAMFORD, D., NUNN, K., PRODEHL, C. & JACOB, B. 1977. LISPB–III upper crustal structure of northern Britain. Journal of the Geological Society, London, 133, 481–88.

BAMFORD, D., NUNN, K., PRODEHL, C. & JACOB, B. 1978. LISPB–IV crustal structure of northern Britain. Geophysical Journal of the Royal Astronomical Society, 54, 43–60.

BARRIERE, M. 1974. Deformation associated with the Ploumanac'h intrusive complex, Brittany. Journal of the Geological Society, London, 134, 311–24.

BATEMAN, P. & CHAPPELL, B. W. 1979. Crystallisation, fractionation and solidification of the Tuolumne intrusive series, Yosemite National Park, California. Bulletin of the Geological Society of America, 90, 465–82.

BATEMAN, R. J. 1984. On the role of diapirism in the segregation, ascent and final emplacement of granitoid magmas. Tectonophysics, 110, 211–31.

BATEMAN, R. J. 1985a. Aureole deformation around a diapir during in-situ ballooning: the Cannibal Creek granite. Journal of Geology, 93, 293–310.

BATEMAN, R. J. 1985b. Progressive crystallisation of a granitoid diapir and its relationship to stages of emplacement. Journal of Geology, 93, 645–62.

BLUCK, B. J. 1984. Pre–Carboniferous history of the Midland Valley of Scotland. Transactions of the Royal Society of Edinburgh, 75, 275–96.

BONIN, B. 1986. Ring complex granites and Anorogenic Magmatism. North Oxford Academic.

BRANDEIS, G. & JAUPART, C. 1986. On the interaction between convection and crystallisation in cooling magma chambers. Earth and Planetary Science Letters, 77, 345–61.

BRAUNSTEIN, J. & O'BRIEN, G. D. (eds). 1968. Diapirism and Diapirs. American Association of Petroleum Geologists, Memoir No. 8.

BRUN, J. P. & PONS, J. 1981. Strain patterns of pluton emplacement in a crust undergoing non-coaxial deformation, Sierra Morena, Southern Spain. Journal of Structural Geology, 3, 219–29.

BUDDINGTON, A. F. 1959. Granite emplacement with special reference to North America. Bulletin of the Geological Society of America, 70, 671–747.

CARRIGAN, C. R. 1986. A two–phase hydrothermal cooling model for shallow intrusions. Journal of Volcanology and Geothermal Research, 28, 175–192.

CARTER, N. L. & TSENN, M. C. 1987. Flow properties of the continental lithosphere. Tectonophysics, 136, 27–63.

CLOUGH, C. T., MAUFE, H. B. & BAILEY, E. B. 1909. The cauldron subsidence of Glen Coe and associated igneous phenomena. Quarterly Journal of the Geological Society of London, 65, 611–676.

CHAPPELL, B. W., WHITE, A. J. R. & WYBORN, D. 1987. The importance of residual source material (restite) in granite petrogenesis. Journal of Petrology, 28, 1111–38.

CHESTER, F. M., FRIEDMAN, M. & LOGAN,J. M. 1985. Foliated cataclasites. Tectonophysics, 111, 139–46.

CLOOS, H. 1923. Das Batholiten Problem. Fortschritte der Geologie und Palaeontologie, Berlin, 1, 1–80.

COMPTON, R. R. 1955. Trondhjemite batholith near Bidwell Bar. Bulletin of the Geological Society of America, 66, 9–44.

COSGROVE, J. W. 1976. The formation of crenulation cleavage. Journal of the Geological Society, London, 132, 155–78.1

COWARD, M. P. 1981. Diapirism and gravity tectonics: report of a TSG conference held at Leeds University, 25–26th March, 1980. Journal of Structural Geology, 3, 89–95.

COX, K. G., BELL, J. D. & PANKHURST, R. J. 1979. The Interpretation of Igneous Rocks. George Allen & Unwin.

CURRY, G. B., BLUCK, B. J., BURTON, C. J., INGHAM, J. K., SIVETER, D. J. & WILLIAMS, A. 1984. Age, evolution and tectonic history of the Highland Border Complex, Scotland. Transactions of the Royal Society of Edinburgh, 75, 113–34.

DAGLEY, P., MUSSETT, A. E., WILSON, R. L. & HALL, J. M. 1978. The British Tertiary Igneous Province: palaeomagnetism of the Arran dykes. Geophysical Journal of the Royal Astronomical Society, 54, 75–91.

DALY, R. A. 1933. Igneous rocks and the depths of the earth. McGraw-Hill, New York.

DALY, S. F. & RAEFSKY, A. 1985. On the penetration of a hot diapir through a strongly temperature dependent viscosity medium. Geophysical Journal of the Royal Astronomical Society, 83, 657–81.

DAVIES, F. B. 1982. Pan-African granite intrusion in response to tectonic volume change in a ductile shear zone from Northern Saudi Arabia. Journal of Geology, 90, 467–83.

DEER, W. A., HOWIE, R. A. & ZUSSMAN, J. 1966. An introduction to the rock forming minerals. Longman, London.

DEWEY, J. F. 1965. Nature and origin of kink bands. Tectonophysics, 1, 459–94.

DEWEY, J. F. 1969. The origin and development of kink bands in a foliated body. Geological Journal, 6, 193–216.

DICKIN, A. P., MOORBATH, S. & WELKE, H. J. 1981. Isotope, trace element and major element geochemistry of Tertiary igneous rocks, Isle of Arran, Scotland. Transactions of the Royal Society of Edinburgh, 72, 159–70.

DICKIN, A. P., BROWN, J. L., THOMPSON, R. N., HALLIDAY, A. N. & MORRISON, M. A. 1984. Crustal contamination and the granite problem in the British Tertiary Volcanic Province. Philosophical Transactions of the Royal Society of London, A310, 755–80.

DIXON, J. M. 1975. Finite strain and progressive deformation in models of diapiric structures. Tectonophysics, 28, 89–124.

DIXON, J. M. & SIMPSON, D. G. 1987. Centrifuge modelling of laccolith intrusion. Journal of Structural Geology, 9, 87–104.

DONATH, F. A. 1969. Experimental deformation of kink band development in strongly anisotropic rock. Geological Survey of Canada Paper 68–52, 255–93.

EMELEUS, C. H. 1963. Structural and petrographic observations on layered granites from southern Greenland. Special Paper of the Mineralogical Socety of America, 1, 22–9.

ESKOLA, P. 1932. On the origin of granitic magmas. Tschermaks Mineralalogische und Petrographische Mitteilungen, 52, 455–81

EVANS, A. L., FITCH, F. J. & MILLER, J. A. 1973. Potassium – argon age determinations on some British Tertiary igneous rocks. Journal of the Geological Society, London, 129, 419–43.

FLETT, W. R. 1942. The contact between the granites of North Arran. Transactions of the Geological Society of Glasgow, 20, 180–205.

FRIEND, P. F., HARLAND, W. B. & HUDSON, J. D. 1963. The Old Red Sandstone and the Highland Boundary in Arran, Scotland. Transactions of the Geological Society of Edinburgh, 19, 363–425.

FRIEND, P. F., HARLAND, W. B. & SMITH, A. G. 1970. Reddening and fissuring associated with the Caledonian unconformity in Northwest Arran. Proceedings of the Geologists Association, 81, 75–85.

GATES, R. M. 1953. Petrogenetic significance of perthite. In Emmons, R. C. (ed). Selected petrogenic relationships of plagioclase. Geological Society of America Memoir No. 52, 55–69.

GEORGE, T. N. 1966. Geomorphic evolution of Scotland. Scottish Journal of Geology, 2, 1–34.

GILBERT, G. K. 1877. Report on the geology of the Henry Mountains. U. S. Geographical and Geological Survey, Rocky Mountains Region.

GILL, R. C. O. 1972 b. The geochemistry of the Gronnedal Ika alkaline complex, South Greenland. Unpublished Ph.D Thesis, University of Durham.

GRAHAM, C. M. & UPTON, B. G. J. 1984. Gneisses in diatremes, Scottish Midland Valley: Petrology and tectonic implications. Journal of the Geological Society, London, 135, 219–28.

GROUT, F. F. 1945. Scale models of structures related to batholiths. Amer-

ican Journal of Science, 243-A (Daly Volume), 260–84.

GUNN, W. 1903. The Geology of North Arran, South Bute and the Cumbraes, with parts of Aryshire and Kintyre. Memoir of the Geological Survey of Scotland, HMSO.

HALL, J. 1978. In McLean, A. C. & Deegan, C. E. (eds). 1978. The Solid Geology of the Clyde Sheet, (55N/6W). Report of the Institute of Geological Sciences, 78/9, HMSO.

HARRIS, A. L., SHACKLETON, R. M., WATSON, J., DOWNIE, C., HARLAND, W. B. & MOORBATH, S. 1975. A Correlation of the Precambrian rocks in the British Isles. Geological Society Special Report, No. 6.

HARRIS, A. L., BRADBURY, H. J. & McGONIGAL, M. H. 1976. The evolution and transport of the Tay Nappe. Scottish Journal of Geology, 12, 103–13.

HARRY, W. T. & RICHEY, J. E. 1963. Magmatic pulses in the emplacement of plutons. Liverpool and Manchester Geological Journal, 3, 254–68.

HEINRICH, K. F. J. 1967. Second national conference on electron probe microanalysis, Boston, USA. Paper No. 7.

HENDERSON, P. 1982. Inorganic Geochemistry. Pergamon Press.

HENDERSON, W. G. & ROBERTSON, A. H. F. 1982. The Highland Border rocks and their relation to marginal basin development in the Scottish Caledonides. Journal of the Geological Society, London, 139, 433–50.

HEUZE, F. E. 1983. High–temperature mechanical, physical and thermal properties of granitic rocks, – A review. International Journal of Rock Mechanics, Mining Science and Geomechanics Abstracts, 20, 3–10.

HIBBARD, M. J. 1987. Deformation of incompletely crystallised magma systems: Granitic gneisses and their tectonic implications. Journal of Geology, 95, 543–61.

HIBBARD, M. J. & WATTERS, R. J. 1985. Fracturing and dyking in incompletely crystallised granitic plutons. Lithos, 18, 1–12.

HILL, R. I., SILVER, L. T., CHAPPELL, B. W. & TAYLOR Jr, H. P. 1985. Solidification and recharge of SiO_2 rich plutonic magma chambers. Nature, 313, 643–46.

HOBBS, B. E., MEANS, W. D. & WILLIAMS, P. F. 1976. An Outline of Structural Geology. Wiley.

HOLDER, M. T. 1979. An emplacement mechanism for post–tectonic granites and its implications for their geochemical features. In: Atherton, M. P. & Tarney, J. (eds). Origin of Granite Batholiths, Geochemical Evidence, 116–128.

HUNTER, R. H. 1987. Textural equilibrium in layered igneous rocks. In Parson, I. (ed). Origins of Igneous Layering, 473–503, Reidel Publishing Company.

HUNTER, R. H., UPTON, B. G. J. & ASPEN P. 1984. Meta-igneous granulite and ultramafic xenoliths from basalts of the Midland Valley of Scotland:

Petrology and mineralogy of the lower crust and upper mantle. Transactions of the Royal Society of Edinburgh, 75, 75–84.

HUTTON, D. H. W. 1982. A tectonic model for the emplacement of the Main Donegal Granite, NW Ireland. Journal of the Geological Society, London, 139, 615–631.

HUTTON, D. H. W. 1988a. Granite emplacement mechanisms and tectonic controls: inferences from deformation studies. Transactions of the Royal Society of Edinburgh, 79, in press.

HUTTON, D. H. W. 1988b. Igneous emplacement in a shear zone termination: the biotite granite at Strontian, Scotland. Bulletin of the Geological Society of America, in press.

HUTTON, J. 1795. Theory of the earth, with proofs and illustrations. Edinburgh.

JACKSON, M. D. & POLLARD, D. D. 1988. The laccolith – stock controversy: New results from the southern Henry Mountains, Utah. Bulletin of the Geological Society of America, 100, 117–39.

JACKSON, M. P. A. & TALBOT, C. J. 1986. External shapes, strain rates and dynamics of salt structures. Bulletin of the Geological Society of America, 97, 305–23.

JAEGER, J. C. 1957. The temperature in the neighbourhood of a cooling intrusive sheet. American Journal of Science, 255, 306–318.

JAEGER, J. C. 1959. Temperatures outside a cooling intrsive sheet. American Journal of Science, 257, 44–54.

JAEGER, J. C. 1964. Thermal effects of intrusions. Reviews of Geophysics, 2, 443–60.

JOHNSON, A. M. & POLLARD, D.D. 1973. Mechanisms of growth of some laccolithic intrusions in the Henry Mountains, Utah, 1. (Field observations, Gilberts model, physical properties and flow of magma.) Tectonophysics, 18, 261–99.

JOHNSON, T. P. & MEIGHAN, I. G. 1975. The Northern Granite Complex, Isle of Arran. Journal of the Geological Society, London, 131, 331.

JUREWICZ, S. R. & WATSON, E. B. 1985. The distribution of partial melt in a granitic system; The application of liquid phase sintering theory. Geochemica et Cosmochemica Acta, 49, 1109–21.

KING, B. C. 1955. The Ard Bheinn area of the Central Igneous Complex of Arran. Quarterly Journal of the Geological Society of London, 110, 323–56.

KNAPP, R. J. 1973. The form and structure of the Islay, Jura and Arran Tertiary basic dyke swarms. Unpublished Ph.D. Thesis, University of London.

KOMAR, P. D. 1972. Mechanical interactions of phenocrysts and flow differentiation of igneous dykes and sills. Bulletin of the Geological Society of America, 83, 973–88.

LEAKE, B. E. 1978. Granite emplacement: The granites of Ireland and

their origin. In Bowes, D. R. & Leake, B. E. (eds), Crustal evolution in Northwestern Britain and adjacent regions. Special Issue of the Geological Journal, 10, 221–48.

LEFORT, P., CUNEY, M., DANIEL, C., FRANCE-LANORD, C., SHEPPARD, S. M. F., UPRETI, B. N. & VIDAL, P. 1987. Crustal generation of Himalayan leucoganites. Tectonophysics, 134, 39–57.

LOVERING, T. S. 1936. Heat conduction in dissimilar rocks and the use of thermal models. Bulletin of the Geological Society of America, 47, 87–100.

MARSH, B. D. 1982. On the mechanics of igneous diapirism, stoping and zone melting. American Journal of Science, 282, 808–55.

MARSH, B. D. 1988. Crystal size distribution (CSD) in rocks and the kinetics and dynamics of crystallisation. Contributions to Mineralogy and Petrology, 99, 277–91.

MARSH, B. D. & KANTHA, L. H. 1978. On the heat and mass transfer from ascending magma. Earth and Planetary Science Letters, 39, 435–43.

MARSH, B. D. & MAXEY, M. R. 1985. On the distribution and separation of crystals in convectng magma. Journal of Volcanology and Geothermal Research, 24, 95–150.

MARTIN. M. R. 1953. The structure of the granite massif in Flamanville, Manche, North West France. Quarterly Journal of the Geological Society of London, 108, 311–42.

McBIRNEY, A. R., BAKER, B. H. & NILSON, R. H. 1985. Liquid fractionation. Part 1. Basic principles and experimental simulations. Journal of Volcanology and Geothermal Research, 24, 1–24.

McBIRNEY, A. R. & MURASE, T. 1984. Rheological properties of magmas. Annual Reviews in Earth and Planetary Sciences, 12, 337–57.

McCARTHY, T. S. & HASTY, R. A. 1976. Trace element distribution patterns and their relationship to the crystallisation of granitic melts. Geochimica et Cosmochimica Acta, 40, 1351–58.

McLEAN, A. C. & DEEGAN, C. E. (eds). 1978. The solid geology of the Clyde sheet (55N/6W). Report of the Institute of Geological Sciences, 78/9, HMSO.

MEIGHAN, I. G. 1979. The acid igneous rocks of the British Tertiary province. Bulletin of the Geological Survey of Great Britain, 70, 10–22.

MEIGHAN, I. G., GIBSON, D. & HOOD, D. N. 1984. Some aspects of Tertiary acid magmatism in NE Ireland. Mineralogical Magazine, 48, 351–63.

MEISSNER, R. & WEAVER, T. 1986. Intracontinental seismicity, strength of crustal units, and the seismic signature of fault zones. Philosophical Transactions of the Royal Society of London, A317, 45–61.

MORRISON, M. A., THOMPSON, R. N., GIBSON, I. L. & MARRINER, G. F. 1980. Lateral chemical heterogeneity in the Palaeocene upper mantle beneath the Scottish Hebrides. Philosophical Transactions of the Royal Society of London, A297, 229–44.

MURPHY, F. C. 1984. Fluidised breccias: A record of brittle transitions during ductile deformation. Tectonophysics, 104, 325–349.

NAKAMURA, N. 1974. Determination of REE, Ba, Fe, Mg, Na and K in carbonaceous and ordinary chondrites. Geochimica et Cosmochimica Acta, 38, 757–75.

PATCHETT, P. J. 1981. Thermal effects of basalts on continental crust and crustal contamination of magmas. Nature, 283, 559–61.

PATTISON, D. & HARTE, B. 1985. A petrogenetic grid for pelites in the Ballachulish and other Scottish Thermal Aureoles. Journal of the Geological Society, London, 142, 7–28.

PEARCE, N. J. G. 1988. The petrology and geochemistry of the Igaliko dyke swarm, South Greenland, Vols. 1 & 2. Unpublished Ph.D. thesis, University of Durham.

PITCHER, W. S. 1979. The Nature, ascent and emplacement of granitic magmas. Journal of the Geological Society, London, 136, 627–62.

PITCHER, W. S. & BERGER, A. R. 1972. The geology of Donegal: A study of granite emplacement and unroofing. Wiley Interscience, New York.

POLLARD, D. D. & JOHNSON, A. M. 1973. Mechanics of growth of some laccolithic intrusions in the Henry Mountains, Utah, 2. (Bending and failure of overburden layer and sill formation.) Tectonophysics, 18, 311–54.

PRINGLE, J. 1940. The discovery of Cambrian Trilobites in the Highland

Border rocks near Callander, Perthshire. Advancement of Science, London, 1, 252.

RAMBERG, H. 1967. Gravity, deformation and the earth's crust as studied by centrifuged models. Academic Press, London & New York.

RAMSAY, J. G. 1960. The deformation of early linear structures in areas of repeated folding. Journal of Geology, 68, 75–93.

RAMSAY, J. G. & HUBER, M. I. 1987. The Techniques of Modern Structural Geology Volume 2. Folds and Fractures. Academic Press, London.

READ, H. H. 1957. The Granite Controversy, Thomas Murby & Co., London.

RICHEY, J. E. 1928. The structural relations of the Mourne granites, (Northern Ireland). Quarterly Journal of the Geological Society of London, 83, 653–88.

RICHEY, J. E. 1932. Tertiary ring structures in Britain. Transactions of the Geological Society of Glasgow, 19, 42–140.

RICHEY, J. E. 1939. The dykes of Scotland. Transactions of the Geological Society of Edinburgh, 13, 393–435.

RICHEY, J. E. & THOMAS, H. H. 1930. The geology of Arnamurchan, North - West Mull and Coll. Memoir of the Geological Survey of Scotland, HMSO.

ROBERTSON, A. H. F. & HENDERSON, W. G. 1984. Geochemical evidence for the origins of igneous and sedimentary rocks of the Highland Border, Scot-

land. Transactions of the Royal Society of Edinburgh, 75, 135–50.

SANDERSON, D. J. & MENEILLY, A. W. 1981. Strain modified uniform distributions: Andalusite from a granite aureole. Journal of Structural Geology, 3, 109–16.

SCHMELING, H., CRUDEN, A. R. & MARQUART, G. 1988. Finite deformation in and around a fluid sphere moving through a viscous medium: Implications for diapiric ascent. Tectonophysics, 149, 17–34.

SEDERHOLM, J. 1907. On granite and gneiss (English Summary). Bulletin, Commission Geologique de la Finlande, 23, 1–90.

SHACKLETON, R. M. 1958. Downward-facing structures of the Highland Border. Quarterly Journal of the Geological Society of London, 113, 361–92.

SHAW, H. R. 1965. Comments on viscosity, crystal settling and convection in granitic magmas. American Journal of Science, 263, 120–52.

SIBSON, R. H., MOORE, J. McM. & RANKIN, A. H. 1975. Seismic pumping – A hydrothermal fluid transport mechanism. Journal of the Geological Society, London, 131, 653–59.

SMITH, J. 1896. A new view of the Arran granite mountains. Transactions of the Geological Society of Glasgow, 10, 216.

SMITH, J. V. 1974. Feldspar Minerals. Volume 2, Chemical and textural properties. Springer–Verlag.

SOPER, N. J. 1963. The structure of the Rogart igneous complex. Quarterly Journal of the Geological Society of London, 119, 445–78.

SOPER, N. J. 1986. Geometry of transecting, anastomosing solution cleavage in transpression zones. Journal of Structural Geology, 8, 937–940.

SOULA, J-C. 1982. Characteristics and mode of emplacement of gneiss domes and plutonic domes in central–eastern Pyrenees. Journal of Structural Geology, 4, 313–42.

SPARKS, R. S. J., HUPPERT, H. E. & TURNER, J. S. 1984. The fluid dynamics of evolving magma chambers. Philosophical Transactions of the Royal Society of London, A310, 511–34.

SPERA, F. J., YUEN, D. A. & KEMP, D. V. 1984. Mass transfer rates along vertical walls in magma chambers and marginal upwelling. Nature, 310, 764–7.

SYLVESTER, A. C., OERTEL, G., NELSON, C. A. & CHRISTIE, J. M. 1978. Papoose Flat pluton: A granitic blister in the Inyo Mountains, California, Bulletin of the Geological Society of America, 89, 1025–219.

TALBOT, C.J. & JACKSON, M. P. A. 1987. Internal kinematics of salt diapirs. Bulletin of the American Association of Petroleum Geologists, 71, 1068–93.

THOMPSON, M. E. & McBIRNEY, A. R. 1985. Redistribution of phenocrysts by convective flow in a viscous boundary layer. Journal of Volcanology and Geothermal Research, 24, 83–94.

THOMPSON, R. N. 1981. Thermal aspects of the origin of hebridean Tertiary acid magmas I. An experimental study of partial fusion of Lewisian gneisses and Torridonian sediments. Mineralogical Magazine, 44, 161–170.

THOMPSON, R. N. 1982. Magmatism of the British Tertiary Igneous Province. Scottish Journal of Geology, 18, 49–107.

THOMPSON, R. N. 1983. Thermal aspects of the origin of Hebridean Tertiary acid magmas II. Experimental melting behavior of the granites at 1kbar P_{H_2O}. Mineralogical Magazine, 47, 111–21.

THOMPSON, R. N., DICKIN, A. P., GIBSON, I. L. & MORRISON, M. A. 1982. Elemeentalfingerprints of isotopic contamination of Hebridean Palaeocene mantle derived magmas by Archean sial. Contributions to Mineralogy and Petrology, 79, 159–68.

THOMPSON, R. N. & MORRISON, M. A. 1988. Asthenosphere and lower lithospheric mantle contributions to continental extensional magmatism: an example from the British Tertiary province. Chemical Geology, 68, 1–15.

TINDALE, A. G., McGARVIE, D. W. & WEBB, P. C. 1988. The role of hybridisation and crystal fractionation in the evolution of the Cairnsmore of Carsphain intrusion, Southern Uplands of Scotland. Journal of the Geological Society, London, 145, 11–22.

TURNER, F. J. 1981. Metamorphic Petrology – Mineralogical, field and tectonic aspects. 2nd Edition, McGraw-Hill.

TURNER, J. S. & CAMPBELL, I. H. 1986. Convection and mixing in magma

chambers. Earth Science Reviews, 23, 255–352.

TUSON, J. 1959. A geophysical investigation of the Tertiary volcanic districts of western Scotland. Unpublished Ph.D. thesis, University of Durham.

TUTTLE, O. F. & BOWEN, N. L. 1958. Origin of granite in the light of experimental studies. Geological Society of America Memoir No. 74.

TYRRELL, G. W. 1928. The Geology of Arran. Memoir of the Geological Survey of Scotland, HMSO.

van BREEMAN, O, & HAWKSWORTH, C. J. 1980. Sm–Nd isotope study of garnets and their metamorphic host rocks. Transactions of the Royal Society of Edinburgh, 71, 97–102.

UNDERHILL, J. R. & WOODCOCK, N. H. 1987. Faulting mechanisms in high porosity sandstones, Arran, Scotland. In: Jones, M. E. & Preston, R. M. F. (eds). Deformation of Sediments and Sedimentary Rocks. Geological Society Publication No. 29, 91–105.

van der MOLEN, I. & PATTERSON, M. S. 1979. Experimental deformation of partially melted granite. Contributions to Mineralogy and Petrology, 70, 299–318.

WALKER, G. P. L. 1975. A new concept in the evolution of British Tertiary intrusive centres. Journal of the Geological Society, London, 131, 121–41.

WATSON, E. B. 1976. Two liquid partition coefficients: experimental data and geochemical applications. Contributions to Mineralogy and Petrology, 56,

119–34.

WEINSTEIN, S. A., YUEN, D. A. & OLSON, P. L. 1988. Evolution of crystal settling in magma chamber convection. Earth and Planetary Science Letters, 87, 237–48.

WHITE, S. H. 1977. Geological significance of recovery and recrystallisation processes in quartz. Tectonophysics, 39, 143–170.

WICKHAM, S. M. 1987. The segregation and ascent of granitic magmas. Journal of the Geological Society, London, 144, 281–287.

WINKLER, H. G. F. & SCHULTES, H. 1982. On the problem of alkali feldspar phenocrysts in granitic rocks. Neus Jahrbuch für Mineralogie, 12, 558–64.

WOODCOCK, N. H. & UNDERHILL, J. R. 1987. Emplacement related fault patterns around the Northern Granite, Arran, Scotland. Bulletin of the Geological Society of America, 98, 515–27.

WYLLIE, P. J., HUANG WUU-LIANG, STERN, C. R. & MAALOE, S. 1976. Granitic magmas: possible and impossible sources, water contents, and crystallisation sequences. Canadian Journal of Earth Sciences, 13, 1007–19.

YODER, H. S., STEWART, D. B. & SMITH, J. R. 1957. Ternary Feldspars. Carnegie Institute, Washington, Yearbook, 56, 206–214.

APPENDIX

MAJOR AND TRACE ELEMENT ANALYSES OF SAMPLES OF THE NORTHERN ARRAN GRANITE

A.1 Sample Collection and Identification.

Whole rock major and trace element analyses from three sets of samples were used in this study of the Northern Arran granite. The bulk of the samples were collected on a grid sample basis in order to determine whether there was any horizontal or vertical variation in element concentration within the intrusion. The grid map on which the sample collection was based was produced by dividing the granite into 1 km square blocks using the national grid. Each km square was then subdivided at contour intervals of 200 m, starting at 50 m, to produce a vertical subdivision. If a sample had been collected from each horizontally and vertically defined grid unit a set of approximately 240 samples would have been collected. In practice this was not possible due to poor exposure or the heavily weathered nature of the rock. Consequently a total of 187 samples were collected. 136 of these were of coarse granite and 51 were of fine granite. These rocks are identified by five figure numbers. Generally the first four numbers refer to the coordinates of the national grid square from which the sample was collected. The fifth number refers to the subdivision of the grid. Six figure grid references of for the sample localities are given in the following tables. In some cases the five figure number is followed by a letter, a, b and c which refer to samples collected from the same grid unit. F refers to a particularly fresh sample of rock, W refers to a particularly weathered sample. Other annotations are explained in the tables.

The rocks collected to examine the granite for spatial variations in chemistry were supplemented with a set of 78 samples (splits of powders) ground from rocks collected by Mr. T. P. Johnson, formerly of Queen's University, Belfast, which were given to the author by Dr. I. G. Meighan. Of these, 53 samples were of the coarse granite and 23 were of the fine granite. These samples are identified by the prefix 'C'. No thin sections or hand specimens of these rocks were available.

An additional collection of 65 samples which were not used in the spatial analysis of the chemistry of the granite were also analysed for major and trace elements. These rocks are samples of aplite veins and sheets of fine grained granite within the coarse granite. These can be identified by four figure numbers. This collection also includes some samples collected by Mr. T. P. Johnson, identifiable by the prefix 'C'.

A.2 Sample Quality and Size.

The Northern Arran coarse granite is often severely weathered, particularly on exposed peaks and ridges. This hampered the collection of fresh samples for analysis. Fresh unweathered coarse granite is a bright turquoise blue, which rapidly fades to a grey green colour as a result of oxidation. Surface weathering of the granite extends to a depth in excess of 20 cm into the rock (even in eroded stream beds). Hence the freshest rock obtainable was collected. At the surface the coarse granite has a deep brown discolouration (rust) due to oxidation of biotite. The oxidation decreases over a few cm and the rock has a white or grey colour, due to sericitisation of feldspars, with minor discolouration due to oxidation. This rock passes into blue rock. Most of the samples collected and analysed were white or grey with some minor oxidation. Thin section examination showed that these rocks were fairly fresh, with only minor sericitisation of the feldspars and local development of oxidation rims around biotite. The degree of weathering shown by all the analysed samples was generally even and the internal consistency in the observed spatial variation in trace element concentration suggests that its effects are not great. Analysis of fresh rock and weathered crusts of some rocks showed no variation in composition in excess of analytical errors between weathered and unweathered rock.

The fine granite shows signs of weathering at the surface but this was usually superficial and samples of fresh grey rock with unaltered feldspars and biotite were easy to obtain.

Sample sites were chosen to aviod aplites, strongly drusiform rock and griesen veins.

The weight of the samples collected for analysis varied between 1 and 2 kg. Larger samples were collected from the coarse granite in an attempt to reduce compositional inhomogeneity introduced by irregular distributions of large crystals. Weathered crusts were usually removed in the field by hammering.

A.3 Sample Preparation.

After slices for thin sections had been taken any remaining weathered material was removed from the samples using a hydraulic rock splitter. Large samples were also reduced in size by splitting before being fed into a jaw crusher. All samples of the coarse and fine granite were reduced to chips (0.5 to 1.5 cm across) by jaw crushing. At this stage any remaining weathered material was removed by hand picking. The chips were then quartered and approximately 50 g of chips were removed from one quarter and ground to fine powder in a swing mill with a tungsten carbide barrel. The chips were ground for 1 to 3 mins. and as a result the existing powders are not suitable for anlysis of FeO/Fe_2O_3 ratios.

No facilities for making fused beads were available in Durham while this work was carried out. As a result all samples for major and trace element analysis were made up as pressed powder briquettes. These were produced by mixing approximately 5 g of powdered sample with 0.5 ml of a 4% solution of Moviol (organic adhesive). This mixture was then placed in a mould

and compressed in a hydraulic press at 8 tons psi. The briquettes were removed from the mould and dried for 12 hours at $80°C$.

The rocks were not analysed for FeO/Fe_2O_3 ratios and loss on ignition (LOI). In the first case because of the generally oxidised nature of the samples would have resulted in meaningless results (section A.2) and in the second case because no suitable furnace was available for fusion during the period in which the analyses were completed.

A.4 XRF Analysis.

All the samples were analysed on a Phillips PW1400 X-ray fluorescence spectrometer with the assistance of Mr. R. G. Hardy (the department's Senior Experimental Officer). Previous analyses of the Northern Arran granite (Dickin et al., 1981) and thin section examination of the samples indicated that the range of composition of the granite was restricted. The samples were run with pressed powder briquettes of international standards appropriate to the known range of compostion of the granite. Additional standards were used to improve the range of calibration of the trace elements.

The samples and unknowns were analysed using the operating conditions given in Table A.1, and peak and background counts were recorded. Machine drift, indicated by variation in count rates for the standards, was negligible.

A.4.1 Major Elements.

The raw peak and background counts for the major elements were processed using the computer program XRF.CBI written by Colin Watson, formerly of the Department of Engineering Geology, University of Durham. This program reads the raw counts for the measured standards and compares them with the known compositions of the standards (from Abbey, 1983) to produce a linear regression equation. This linear regression is used to calculate an approximate measured composition of the standard from the raw counts. This approximate composition is used to calculate and apply mass absorption coefficients (MAC) (from Heinrich, 1973) to the raw counts. The corrected raw counts are then compared with the known composition of the standards and a cubic regression is calculated from which a second approximation to the measured composition of the standard can be determined. This second approximation is used to recalculate and apply MAC corrections. This process is repeated until the measured composition of the standards is the same as that produced by the previous iteration. This reiteration procees generates a cubic equation for the composition of the standards given the counts corrected for mass absorption effects.

The composition of the unknowns are determined by calculating an approximate compostion for the unknowns from the cubic equation derived by calibration of the standards. These compositions are used to calculate MAC corrections for the raw counts for each unknown. The

TABLE A1

Operating Conditions for XRF Analysis.

Element	Line	Crystal	Angle (2θ)	+bkg	-bkg	Peak time	Bkg time
Si	K_α	3	109.175	3.80	2.00	20	10
Ti	K_α	2	86.270	5.00	2.00	20	10
Al	K_α	6	19.620	2.10	0.00	20	10
Fe	K_α	2	57.570	2.30	2.00	20	10
Mg	K_α	6	23.315	1.92	2.40	80	20
Ca	K_α	2	113.265	4.30	2.00	20	10
Na	K_α	6	28.140	2.00	1.30	80	20
K	K_α	2	136.930	3.00	1.80	20	10
Mn	K_α	1	95.375	4.60	2.00	20	10
P	K_α	5	141.040	4.00	3.50	40	10
Ba	K_α	1	15.550	1.38	0.78	40	20
Nb	K_α	1	30.400	0.60	0.60	80	20
Zr	K_α	1	32.055	0.96	0.90	80	20
Y	K_α	1	33.870	1.00	0.90	80	20
Sr	K_α	1	35.815	1.10	1.00	80	20
Rb	K_α	1	37.945	0.70	1.16	80	20
Zn	K_α	1	60.560	1.00	1.00	80	20
Cu	K_α	1	65.540	1.10	0.50	80	20
Ni	K_α	1	71.265	2.00	1.30	80	20
Pb	K_α	1	40.345	2.20	1.80	80	20
U	L_α	1	37.295	1.40	0.60	80	20
Th	L_α	1	39.215	0.60	0.76	80	20
V	K_α	1	123.485	2.00	2.00	80	40
Cr	K_α	1	107.320	2.00	2.00	80	20
Nd	L_α	1	112.930	1.40	2.00	80	20
La	L_α	1	139.085	3.90	2.00	80	20
Ce	L_β	1	111.840	2.60	1.50	80	20

+background and -background in degrees (2θ). Crystal 1 = LiF220, crystal 2 = LiF200, crystal 3 = PE, crystal 4 = THAP, crystal 5 = GE, crystal 6 = PX1. All analyses run at 80 kv, 35 mA. Count times for peaks and backgrounds are given in seconds.

corrected counts are used to calculate a second approximation to the unknown composition using the cubic calibration curve. This process is repeated until the composition calculated from one iteration is equal to that calculated by the previous iteration.

Calculation of the compostion of the unknowns by this iteration process was monitored by using standards as unknowns. This showed that compositions of the standards run as unknowns compared very favourably with the known compositions of the standards. Analyses were generally within ±0.2%. A necessary part of this iteration process is that all analyses are calculated to 100% if loss on ignition determinations are not included in the file containing the raw counts for the standards and unknowns, or to 100% less loss on ignition if LOI data are included. The linear correlation between the counts and the standard composition after calibration and the range of calibration are given in Table A.2.

Table A.2.

Correlation between standard compositions determined from corrected analyses and known compositions of standards and the range of calibration used in analysis of major element compositions of samples collected from the Northern Arran granite.

Element	Correlation	Calibration
SiO_2	0.902	66.64 - 99.00
TiO_2	0.999	0.00 - 0.28
Al_2O_3	0.991	1.00 - 15.53
Fe_2O_3	0.995	0.00 - 4.33
MgO	0.988	0.00 - 2.43
CaO	0.999	0.00 - 2.54
Na_2O	0.988	0.00 - 4.09
K_2O	0.999	0.00 - 5.55
MnO_2	0.995	0.00 - 0.09
P_2O_5	0.997	0.00 - 0.28

Linear regression after calibration of the standards.

A.4.2 Trace Elements.

The raw peak and background counts for the trace elements were processed using the trace element analysis programs written by Dr. N. J. G. Pearce (Pearce, 1988). These programs are based on a technique used by the Greenland Geological Survey. The program determines the concentrations of trace elements in a sample in ppm from the equation:

$$\text{ppm(sample)} = \text{cps} \times \text{MAC} \times \text{K} \qquad A.1$$

cps is the net count rate per second ((peak - background) - blank), MAC is the mass absorption coefficient for the element (calculated from the the major element composition of the sample) and

K is a constant. Counts per second for the blanks was determined by solution of simultaneous equations (by hand calculation) after determining an initial K value from a number of standards. After determining a K value and the blank correction for each element, which gave the best fit for the determined composition of the standards compared with their known compostions, the compositions of the unknowns were calculated using equation *A*.1.

The error in the trace element analyses was determined from standards run as unknowns. The analytical errors determined (Table A.3) were calculated following determination of the concentration of the element in each sample and hence represent compounded errors due to machine instability and calculation of compositions.

Errors were calculated by the following method: For each element the mean and standard deviation (2σ) were calculated for each standard (analysed as an unkown at least six times) which had a concentration within the calibration range of the element. The ranges for each standard as a percentage of the mean composition of the standard were determined by dividing 2σ by the mean of the analyses for each standard. The range of accuracy for a particular element for the range over which it was calibrated was determined by taking the average of the range of variability for the standards used to calibrate that element.

Table A.3.

Analytical errors (2σ) calculated for trace elements as a percentage of calculated composition.

Element	Error (%)
Ba	±9
Nb	±9
Zr	±12
Y	±10
Sr	±7
Rb	±7
Zn	±4
Cu	±18
Ni	±40
Pb	±8
U	±43
Th	±18
V	±30
Cr	±18
Nd	±28
La	±17
Ce	±14

A.4.3 CIPW Norms.

The CIPW norms of each of the samples of coarse and fine granite were determined using the

program NORMCAL written by Dr. R. C. O. Gill (Formerly of the Department of Geological Sciences, Durham University) (Gill, 1972 b). FeO/Fe_2O_3 ratios for the coarse and fine granites were taken from Dickin et al. (1981).

A.5 Note on the organisation of the sample listings.

The samples are divided into the following groups: Coarse granite, fine granite and miscellaneous rocks. The three groups contain samples collected by the author and by Mr. T. P. Johnson. Notations are as described in section A.1.

In each case the the sample number is followed by the grid reference of the locality from which it was collected, and a short description of the sample. In the case of the coarse granite the number of the petrographic group to which the sample belongs is included, and an asterisk indicates that it was not included in the compilation of the maps showing the distribution of Ba and Sr across the pluton (section 5.3.2). No thin sections or hand specimens of the rocks collected by Mr. T. P. Johnson were available. Therefore they have been allocated to the group in which they spatially belong. The last number refers to the page of the appendix on which an analysis of the rock may be found.

The analyses of the rocks are listed in a different order to that in which they appear in the list of samples. Major oxides are given as weight %, trace elements in ppm. Total Fe is given as Fe_2O_3. No norms are supplied for the collection of miscellaneous samples of aplites etc. Abbreviations used in the norm tables are as follows: Qz - quartz, Cor - corundum, Or - orthoclase, Ab - albite, An - anorthite, Hy - hypersthene, Mgtte - magnetite, Ilm - ilmenite, Aptte - apatite, DI - differentiation index.

COARSE GRANITE SAMPLES

91481	NR914483	Coarse granite	2	3
92481	NR922487	Coarse granite	1*	1,19
92482	NR927486	Coarse granite	2	2,19
93482	NR935484	Coarse granite	2	2
94481	NR946487	Coarse granite	2	4
95481	NR952489	Coarse granite	1*	4
95482	NR956491	Coarse granite	1	4,18
90472	NR909476	Coarse granite	2	1,19
91471	NR916469	Coarse granite	2	2
91472	NR916476	Coarse granite	2	5
92471	NR921477	Coarse granite	2	6,18
93471	NR936477	Coarse granite	2	1
94471	NR947472	Coarse granite	3	3
94472	NR948473	Coarse granite	2	1,8
95471	NR952474	Coarse granite	2	2
96472	NR965471	Coarse granite	2	1
97471	NR974477	Coarse granite	2	2,19
89461	NR896464	Coarse granite	2	6
90461	NR904463	Coarse granite	2	7
90461a	NR904463	Coarse granite	2	5
90461b	NR904463	Coarse granite	2	6,17
93461	NR937468	Coarse granite	3	3
93462	NR937467	Coarse granite	3	4
95462	NR956468	Coarse granite	3	17
95462a	NR956468	Coarse granite	3*	3
95462b	NR956468	Coarse granite	3*	6
97462	NR975465	Coarse granite	2	3
98461	NR985468	Coarse granite	2*	5
98462	NR985460	Coarse granite	2	5
89451	NR897457	Coarse granite	2	2,18
90451	NR906459	Coarse granite	2	6
90452	NR907455	Coarse granite	3	4,18
96451	NR964458	Coarse granite	3	5,8
96452	NR965452	Coarse granite	2	24
96452a	NR965452	Coarse granite	2*	34
96453	NR968459	Coarse granite	2	8
96453a	NR968456	Coarse granite	2	32
97451	NR974451	Coarse granite	2	24
98451	NR984454	Coarse granite	2*	30
99451	NR992457	Coarse granite	2	7
99452	NR994454	Coarse granite	2	5
88441	NR883441	Coarse granite	2	24

93442	NR940446	Coarse granite	3	31
93443	NR941445	Coarse granite	3	31
94443	NR949449	Coarse granite	3	4
94443a	NR952444	Coarse granite	3	31
94444	NR947442	Coarse granite	3	24
96443	NR966448	Coarse granite	3	26
96444	NR965445	Coarse granite	3	8
96444b	NR965445	Coarse granite	*	8
97441	NR976447	Coarse granite	2	31
97442	NR977444	Coarse granite	2*	26
99441	NR997449	Coarse granite	2	18
99441a	NR994448	Coarse granite	2	1,27
99442	NR002442	Coarse granite	2	8
88431	NR888439	Coarse granite	1	9
89431	NR896434	Coarse granite	2	7
94432a	NR946431	Coarse granite	3	23
94432b	NR946431	Coarse granite	3	27
94432c	NR944434	Coarse granite	3	26
97431	NR974436	Coarse granite	2	25
97432	NR977435	Coarse granite	2	28
97433	NR976431	Coarse granite	2*	28,29
97434	NR972431	Coarse granite	2	31
98431F	NR983435	Coarse granite	2	22,57
98432F	NR984430	Coarse granite	2	21,57
99435	NR998432	Coarse granite	1	28
00431	NR005438	Coarse granite	2	7
00432	NR004435	Coarse granite	1*	21
89421	NR898430	Coarse granite	3	7
89422	NR892426	Coarse granite	1	7
89423	NR897423	Coarse granite	2	6,18
96421a	NR965425	Coarse granite	3	24
96421b	NR961421	Coarse granite	3	26
96421c	NR691421	Coarse granite	3	26
96423	NR966425	Coarse granite	2	34
97434	NR972431	Coarse granite	2	31
97421	NR973428	Coarse granite	2*	25
97422c	NR974424	Coarse granite	*	30
98421	NR979425	Coarse granite	2*	21
98422	NR984426	Coarse granite	2*	25
98423	NR986427	Coarse granite	2*	29
98424	NR989424	Coarse granite	*	22
99421	NR995427	Coarse granite	1	27
99422	NR999424	Coarse granite	1	30
00422	NS006425	Coarse granite	1	34

00423	NS010423	Coarse granite	1	29
88411	NR898416	Coarse granite	2	32
95411a	NR960420	Coarse granite	3*	23
95411b	NR960420	Coarse granite	3	25
95412	NR962414	Coarse granite	2	34
95412a	NR962414	Coarse granite	2*	23
95412c	NR959412	Coarse granite	2*	34
96411	NR964417	Coarse granite	3	26
96411c	NR964417	Coarse granite	3	24
96412	NR965412	Coarse granite	2	20
96413	NR969416	Coarse granite	2	34
97411	NR980417	Coarse granite	2	19
99411	NR995416	Coarse granite	1	22
99412	NR992416	Coarse granite	1	27
99413	NR995418	Coarse granite	1	27
99414	NR996415	Coarse granite	1	30
00411	NS003420	Coarse granite	1	20
00412	NS003413	Coarse granite	1	28
00413a	NS007417	Coarse granite	1	28
00413b	NS010417	Coarse granite	1	21
95404	NR957401	Coarse granite	2	29
96402	NR968405	Coarse granite	2	23
96404a	NR970407	Coarse granite	2	20
96404b	NR970407	Coarse granite	*	21
96404c	NR970407	Coarse granite	*	20
97403	NR980403	Coarse granite	2	20
98401	NR987402	Coarse granite	2	21
98402a	NR997408	Coarse granite	1	28
98402b	NR991407	Coarse granite	1	25
99401	NR998404	Coarse granite	1	30
00401	NS001408	Coarse granite	1	22
90391	NR901398	Coarse granite	2	32
91393	NR913397	Coarse granite	2	33
91395	NR910392	Coarse granite	2	25
95391	NR952399	Coarse granite	3	23,32
95392	NR953398	Coarse granite	3	32
95394	NR959394	Coarse granite	2	31,32
96391	NR968391	Coarse granite	2	33
97391	NR974391	Coarse granite	2	22
97392	NR982395	Coarse granite	2	19
98391	NR989397	Coarse granite	1	29,32
91381	NR917388	Coarse granite	2	23
95382	NR953380	Coarse granite	*	27
96381	NR967384	Coarse granite	2	29

97381a	NR970387	Coarse granite	2	30
97382	NR972385	Coarse granite	1*	22
97382b	NR972385	Coarse granite	*	20
C2	NR940420	Coarse granite	3	9
C3	NR979471	Coarse granite	2	9
C4	NR968461	Coarse granite	2	9
C6	NS011418	Coarse granite	1	9
C7	NS010418	Coarse granite	1	33
C9	NR983463	Coarse granite	2	9
C14	NR986428	Coarse granite	2*	10
C19	NR954402	Coarse granite	3*	10
C42	NR930468	Coarse granite	3*	10
C43	NR913398	Coarse granite	2*	10
C45	NR913398	Coarse granite	2*	10
C73	NR976387	Coarse granite	2	10
C74	NR970387	Coarse granite	2*	11
C77	NR949473	Coarse granite	3*	11
C78	NR949473	Coarse granite	3	11
C89	NR948488	Coarse granite	2	11
C92	NR910481	Coarse granite	2	11
C93	NR964394	Coarse granite	2	11
C94	NR948488	Coarse granite	2	12
C95	NR970408	Coarse granite	2	12
C98	NR895464	Coarse granite	1	12
C99	NR951476	Coarse granite	2	12
C108	NR940420	Coarse granite	3	12
C114	NR885439	Coarse granite	1	12
C118	NR895451	Coarse granite	2	13
C120	NR995399	Coarse granite	1	13
C121	NR925478	Coarse granite	2	13
C122	NR925487	Coarse granite	2	13
C123	NR930468	Coarse granite	3	13
C124	NR951476	Coarse granite	2*	13
C125	NR947493	Coarse granite	1	13
C127	NR948484	Coarse granite	2	14
C132	NR898424	Coarse granite	2	14
C133	NR893441	Coarse granite	2*	14
C134	NR962411	Coarse granite	2	14
C135	NR996450	Coarse granite	2	14
C136	NR977432	Coarse granite	2	14
C137	NR979433	Coarse granite	2*	15
C138	NR993409	Coarse granite	1	15
C139	NR979436	Coarse granite	2	33
C140	?	Coarse granite	*	15

C141	NR891429	Coarse granite	2	15
C143	NR918484	Coarse granite	2	15
C144	NR002442	Coarse granite	2*	15
C145	NR974453	Coarse granite	2	16
C146	NR997433	Coarse granite	2	16
C147	NR955399	Coarse granite	3	16
C148	NR981448	Coarse granite	2*	16
C149	NR971398	Coarse granite	2	16
C151	NR962457	Coarse granite	3	16
C153	NR973432	Coarse granite	2	17
C154	NR984452	Coarse granite	2	17
C155	NR976383	Coarse granite	2*	33
C158	NR992415	Coarse granite	2	17
C159	NR985468	Coarse granite	2	17

FINE GRANITE SAMPLES

90462	NR914463	Fine granite	42
91461	NR914465	Fine granite	42
91462	NR917466	Fine granite	36
91462a	NR919463	Fine granite	35
92461	NR923470	Fine granite	35,41
92461b	NR929467	Fine granite	43
92462	NR925464	Fine granite	37
93463	NR931462	Fine granite	42
93463a	NR929467	Fine granite	46
94461	NR944466	Fine granite	35
95461	NR952464	Fine granite	37
91451	NR908459	Fine granite	37
90453	NR988452	Fine granite	36
91452	NR916455	Fine granite	35
92451	NR924456	Fine granite	36
92452	NR930453	Fine granite	36
93451a	NR933458	Fine granite	46
93451b	NR937453	Fine granite	44
94451	NR943453	Fine granite	42
94452	NR947454	Fine granite	36
95451	NR954458	Fine granite	37
95452	NR955453	Fine granite	35
90441	NR902442	Fine granite	45
90442	NR906447	Fine granite	36
90444	NR907444	Fine granite	38
91441	NR915447	Fine granite	35
92442	NR926444	Fine granite	38
93441	NR933447	Fine granite	42
94441	NR945446	Fine granite	45
95441	NR962442	Fine granite	45
96441	NR963447	Fine granite	37
96442	NR961454	Fine granite	37
90431	NR898435	Fine granite	43
90432	NR910438	Fine granite	41
93433	NR935432	Fine granite	43
95431	NR953432	Fine granite	47
95433	NR962430	Fine granite	45
96431	NR969429	Fine granite	44
90421	NR903427	Fine granite	42
91421	NR916427	Fine granite	45
92421	NR926424	Fine granite	43
95421	NR949421	Fine granite	44

95424	NR958429	Fine granite	46
90411	NR902417	Fine granite	46
91411	NR913419	Fine granite	45
90403	NR907408	Fine granite	42
91401	NR918407	Fine granite	43
91401a	NR910401	Fine granite	43
91392	NR914399	Fine granite	44
91394	NR918399	Fine granite	46
92391	NR919389	Fine granite	44
C1	NR949431	Fine granite	38
C5	NR961453	Fine granite	38
C8	NR962447	Fine granite	38
C29	NR915420	Fine granite	38
C30	NR923443	Fine granite	39
C31	NR915446	Fine granite	39
C32	NR915446	Fine granite	39
C34	NR917458	Fine granite	39
C35	NR920469	Fine granite	39
C36	NR925450	Fine granite	39
C37	NR924463	Fine granite	40
C44	NR930447	Fine granite	40
C47	NR931452	Fine granite	46
C48	NR921468	Fine granite	40
C82	NR945460	Fine granite	40
C96	NR906445	Fine granite	40
C102	NR911463	Fine granite	40
C103	NR916467	Fine granite	41
C109	NR950431	Fine granite	41
C116	NR909431	Fine granite	41
C150	NR966443	Fine granite	41

MISCELLANEOUS SAMPLES COLLECTED FROM THE NORTHERN ARRAN GRANITE

907	NR930489	Aplite	49
909	NR930489	Aplite	49
1107	NR921486	Aplite	49
1108	NR922487	Aplite	50
1400	NR974481	Microgranite	49
1401	NR968475	Porphyritic granite	52
1403	NR975465	Fine granite sheet	50
1602	NR911484	Marginal granite	50
1700a	NR904464	Fine granite sheet	52
1701a	NR904464	Fine granite sheet	51
1703	NR982474	Marginal granite	51
1901	NR953474	Fine granite sheet	48
1902	NR953474	Medium grained sheet	48
1903	NR953474	Fine grained sheet	52
1904	NR953474	Medium grained sheet	50
1909	NR952470	Medium grained sheet	48
1912	NR952467	Coarse granite	48
1914	NR950449	Coarse granite	51
1915	NR950449	Aplite	51
2200	NR977477	Marginal granite	51
2500	NR904464	Fine granite sheet	51
96412F	NR966411	Fine granite sheet	58
96401Q	NR965409	Qtz rich granite	58
96453aCG	NR968456	Granite next to 96453a	59
96453aA	NR968456	Aplite	59
97422F	NR974424	Fine granite sheet	58
96421F	NR966411	Fine granite sheet	
97381bF	NR970387	Fine granite sheet	58
98431W	NR984430	Weathered 98432F	57
98432W	NR983435	Weathered 98431F	57
4100	NR941492	Aplite	59
4210	NR947439	Fine granite	58
4220	NR947439	Coarse granite	59
5000CC	NR965425	Coarse granite	58
5000FC	NR965425	Coarse granite	57
5010	NR965425	Fine granite	59
C10	NR966472	Porphyritic granite	53
C11	NR951492	?	53
C17	NR972386	Fine granite sheet	53
C24	NR972417	Aplite	53
C25	NR974417	Quartz rich granite	53

C46	NR920481	Porphyritic granite	54
C49	NR913398	Porphyritic granite	54
C50	NR913398	Quartz rich granite	54
C75	NR951480	Aplite	54
C76	NR950479	Porphyritic sheet	54
C84	NR947488	Aplite	54
C86	NR950481	Aplite	55
C91	NR913478	Fine granite	55
C97	NR945490	Porphyritic aplite	55
C100	NR948487	Aplite	55
C126	NR925487	Porphyritic aplite	55
C129	NR978433	Coarse granite	55
C130	NR898424	Coarse granite	
C150	NR948487	Porphyritic aplite	56
C156	NR919483	Porphyritic aplite	
1	NR917459	Fine granite	48, 56
2	NR917459	Drusy fine granite	52, 56
3	NR916459	Fine granite	49, 56
4	NR916459	Drusy fine granite	50, 57
5	NR916459	Fine granite	50, 52, 56
5a	NR915460	Fine granite	48, 56
2302	NR915446	Drusy fine granite	49
4410	NR898435	Fine granite sheet	59
C39	NR925450	Aplite	52
C79	NR943457	Fine granite	53

ANALYSES OF SAMPLES OF NORTHERN ARRAN COARSE GRANITE

	92481	90472	94472	99441	93471	96472
SiO_2	76.85	76.31	78.80	75.42	78.22	77.28
TiO_2	0.04	0.14	0.08	0.17	0.08	0.14
Al_2O_3	13.16	12.71	11.81	12.91	12.07	12.45
Fe_2O_3	0.76	1.64	1.10	1.88	1.05	1.41
MgO	0.03	0.07	0.03	0.07	0.03	0.04
CaO	0.11	0.43	0.17	0.69	0.29	0.30
Na_2O	3.57	3.58	3.09	4.03	3.32	2.98
K_2O	5.44	5.05	4.89	4.73	4.90	5.35
MnO_2	0.02	0.04	0.02	0.04	0.01	0.03
P_2O_5	0.01	0.04	0.02	0.04	0.02	0.03
Ba	455.	857.	321.	991.	677.	978.
Nb	28.	38.	28.	37.	24.	23.
Zr	68.	227.	101.	290.	92.	151.
Y	61.	71.	57.	68.	52.	53.
Sr	23.	42.	18.	52.	31.	41.
Rb	186.	180.	172.	184.	163.	168.
Zn	27.	56.	31.	93.	29.	34.
Cu	13.	14.	14.	13.	13.	12.
Ni	6.	3.	6.	5.	3.	5.
Pb	30.	33.	27.	24.	28.	27.
U	2.	2.	2.	1.	2.	1.
Th	16.	24.	22.	24.	18.	16.
V	2.	8.	5.	9.	5.	8.
Cr	7.	10.	7.	8.	8.	15.
Nd	20.	41.	32.	60.	31.	30.
La	6.	40.	29.	55.	23.	29.
Ce	36.	83.	64.	113.	58.	0.
Qz	34.7	34.6	41.3	31.7	39.1	38.3
Cor	1.2	0.7	1.2	0.0	0.8	1.3
Or	32.2	29.9	28.9	28.0	29.0	31.6
Ab	30.2	30.3	26.2	34.2	28.1	25.2
An	0.5	1.9	0.7	3.2	1.3	1.3
Hy	0.8	1.7	1.1	1.9	1.0	1.4
Mgtte	0.3	0.6	0.4	0.7	0.4	0.5
Ilm	0.1	0.3	0.2	0.3	0.2	0.3
Aptte	0.0	0.1	0.0	0.1	0.0	0.1
DI	97.1	94.8	96.4	93.8	96.2	95.2

	92482	95471	91471	97471	93482	89451
SiO_2	76.39	78.52	77.00	76.47	74.65	76.65
TiO_2	0.18	0.11	0.12	0.15	0.16	0.14
Al_2O_3	12.97	11.94	12.56	13.08	13.82	12.57
Fe_2O_3	1.47	1.37	1.37	1.40	1.78	1.70
MgO	0.06	0.04	0.04	0.05	0.05	0.05
CaO	0.55	0.12	0.41	0.40	0.49	0.47
Na_2O	3.44	3.21	3.33	3.46	3.60	3.38
K_2O	4.86	4.64	5.12	4.92	5.38	4.97
MnO_2	0.04	0.03	0.03	0.03	0.03	0.04
P_2O_5	0.04	0.02	0.03	0.04	0.03	0.04
Ba	1271.	528.	1133.	1085.	1339.	553.
Nb	34.	30.	34.	34.	32.	35.
Zr	249.	143.	151.	205.	213.	228.
Y	69.	61.	68.	69.	68.	103.
Sr	53.	28.	45.	48.	57.	28.
Rb	152.	151.	163.	161.	178.	190.
Zn	47.	45.	35.	40.	48.	53.
Cu	13.	15.	13.	13.	13.	14.
Ni	3.	3.	4.	7.	3.	2.
Pb	28.	26.	34.	28.	24.	28.
U	2.	2.	2.	2.	1.	1.
Th	22.	19.	21.	20.	16.	22.
V	10.	5.	6.	7.	8.	10.
Cr	6.	10.	7.	20.	11.	13.
Nd	40.	47.	29.	46.	38.	40.
La	42.	40.	37.	45.	38.	34.
Ce	88.	92.	85.	84.	81.	67.
Qz	36.1	41.3	36.6	36.2	31.4	36.3
Cor	1.1	1.5	0.9	1.4	1.3	0.9
Or	28.8	27.4	30.3	29.1	31.8	29.4
Ab	29.1	27.2	28.2	29.3	30.5	28.6
An	2.5	0.5	1.8	1.7	2.2	2.1
Hy	1.4	1.4	1.4	1.4	1.8	1.7
Mgtte	0.5	0.5	0.5	0.5	0.6	0.6
Ilm	0.3	0.2	0.2	0.3	0.3	0.3
Aptte	0.1	0.0	0.1	0.1	0.1	0.1
DI	94.0	95.9	95.1	94.6	93.7	94.4

	93461	90473	94471	91481	97462	95462A
SiO_2	78.02	76.86	77.57	75.96	77.26	78.01
TiO_2	0.08	0.11	0.11	0.15	0.12	0.06
Al_2O_3	12.39	12.80	12.26	12.95	12.70	12.49
Fe_2O_3	1.07	1.33	1.39	1.83	1.29	0.91
MgO	0.03	0.04	0.04	0.06	0.05	0.02
CaO	0.25	0.41	0.60	0.41	0.31	0.16
Na_2O	3.26	3.21	3.04	3.35	3.17	3.46
K_2O	4.85	5.19	4.94	5.20	5.05	4.85
MnO_2	0.02	0.03	0.03	0.04	0.02	0.02
P_2O_5	0.02	0.02	0.01	0.04	0.03	0.01
Ba	754.	891.	597.	984.	919.	422.
Nb	29.	27.	26.	35.	27.	28.
Zr	131.	134.	141.	219.	263.	108.
Y	58.	63.	68.	57.	54.	60.
Sr	37.	39.	57.	36.	45.	21.
Rb	167.	169.	171.	173.	159.	178.
Zn	40.	37.	39.	42.	39.	42.
Cu	14.	13.	13.	13.	13.	13.
Ni	2.	6.	6.	5.	1.	6.
Pb	27.	26.	26.	26.	25.	27.
U	2.	2.	2.	1.	1.	1.
Th	20.	20.	20.	23.	19.	19.
V	6.	8.	5.	6.	6.	3.
Cr	11.	7.	8.	10.	7.	6.
Nd	33.	41.	46.	46.	33.	35.
La	34.	41.	44.	53.	34.	35.
Ce	78.	74.	87.	91.	72.	83.
Qz	39.5	36.9	39.1	35.0	38.3	38.6
Cor	1.4	1.2	0.8	1.2	1.5	1.3
Or	28.7	30.7	29.2	30.8	29.9	28.7
Ab	27.6	27.2	25.8	28.4	26.9	29.3
An	1.1	1.9	2.9	1.8	1.3	0.7
Hy	1.1	1.3	1.4	1.9	1.3	0.9
Mgtte	0.4	0.5	0.5	0.7	0.5	0.3
Ilm	0.2	0.2	0.2	0.3	0.2	0.1
Aptte	0.0	0.0	0.0	0.1	0.1	0.0
DI	95.8	94.8	94.1	94.1	95.1	96.6

	93462	94481	90452	95481	94443	95482
SiO_2	78.03	76.04	76.93	77.45	78.30	77.77
TiO_2	0.11	0.17	0.09	0.05	0.09	0.09
Al_2O_3	12.21	12.90	12.76	12.91	11.96	12.46
Fe_2O_3	1.35	1.86	1.22	0.90	1.20	1.13
MgO	0.03	0.07	0.03	0.04	0.05	0.03
CaO	0.23	0.40	0.39	0.14	0.29	0.27
Na_2O	3.14	3.47	3.47	3.66	2.84	3.09
K_2O	4.86	5.01	5.07	4.82	5.21	5.12
MnO_2	0.02	0.04	0.02	0.01	0.03	0.03
P_2O_5	0.02	0.04	0.02	0.02	0.02	0.02
Ba	685.	1100.	584.	57.	409.	528.
Nb	31.	34.	29.	36.	29.	34.
Zr	138.	215.	125.	99.	114.	116.
Y	69.	74.	79.	56.	78.	48.
Sr	31.	50.	31.	8.	24.	23.
Rb	162.	151.	171.	178.	168.	184.
Zn	48.	59.	40.	36.	35.	45.
Cu	14.	14.	13.	13.	13.	14.
Ni	2.	2.	0.	2.	1.	6.
Pb	29.	25.	27.	30.	25.	32.
U	1.	2.	2.	2.	2.	1.
Th	17.	21.	23.	24.	20.	20.
V	9.	6.	8.	5.	3.	6.
Cr	0.	6.	8.	11.	12.	7.
Nd	58.	44.	41.	28.	40.	37.
La	48.	39.	37.	21.	37.	27.
Ce	100.	72.	63.	34.	74.	67.
Qz	40.2	35.1	36.0	37.0	40.7	39.2
Cor	1.4	1.1	0.9	1.5	1.2	1.4
Or	28.8	29.6	30.0	28.5	30.8	30.3
Ab	26.6	29.4	29.4	31.0	24.1	26.2
An	1.0	1.7	1.8	0.6	1.3	1.2
Hy	1.3	1.9	1.2	1.0	1.3	1.2
Mgtte	0.5	0.7	0.4	0.3	0.4	0.4
Ilm	0.2	0.3	0.2	0.1	0.2	0.2
Aptte	0.0	0.1	0.0	0.0	0.0	0.0
DI	95.5	94.2	95.4	96.5	95.6	95.6

	99452	96451	98461	91472	98462	90461A
SiO_2	77.58	77.66	76.97	77.39	77.57	76.19
TiO_2	0.10	0.11	0.11	0.10	0.11	0.14
Al_2O_3	12.48	12.40	12.81	12.47	12.31	12.93
Fe_2O_3	1.30	1.19	1.38	1.23	1.36	1.67
MgO	0.04	0.02	0.05	0.04	0.05	0.05
CaO	0.26	0.23	0.25	0.22	0.42	0.38
Na_2O	3.06	3.30	3.55	3.18	3.39	3.46
K_2O	5.12	5.04	4.85	5.32	4.72	5.09
MnO_2	0.02	0.02	0.02	0.03	0.03	0.04
P_2O_5	0.02	0.03	0.02	0.03	0.03	0.03
Ba	947.	570.	472.	842.	702.	1023.
Nb	32.	25.	39.	26.	31.	34.
Zr	140.	93.	177.	131.	150.	246.
Y	48.	67.	104.	64.	56.	72.
Sr	41.	28.	24.	37.	37.	47.
Rb	176.	162.	185.	166.	169.	160.
Zn	35.	39.	44.	34.	41.	57.
Cu	14.	14.	13.	13.	13.	13.
Ni	9.	2.	7.	7.	1.	3.
Pb	28.	26.	30.	27.	26.	26.
U	1.	1.	2.	2.	2.	2.
Th	20.	18.	24.	19.	18.	20.
V	6.	6.	5.	6.	7.	12.
Cr	15.	15.	8.	13.	9.	11.
Nd	26.	42.	57.	43.	32.	52.
La	24.	40.	49.	33.	21.	43.
Ce	41.	75.	86.	60.	49.	99.
Qz	39.1	38.3	36.7	37.6	38.4	35.1
Cor	1.5	1.2	1.3	1.2	0.9	1.1
Or	30.3	29.8	28.7	31.5	27.9	30.1
Ab	25.2	27.9	30.1	26.9	28.7	29.3
An	1.2	0.9	1.1	0.9	1.9	1.7
Hy	1.3	1.1	1.4	1.3	1.4	1.7
Mgtte	0.5	0.4	0.5	0.4	0.5	0.6
Ilm	0.2	0.2	0.2	0.2	0.2	0.3
Aptte	0.0	0.1	0.0	0.1	0.1	0.1
DI	95.3	96.0	95.4	96.0	95.0	94.6

	89461	89423	90461B	95462B	90451	92471
SiO_2	80.47	75.83	76.01	78.84	76.72	77.19
TiO_2	0.11	0.13	0.16	0.08	0.07	0.07
Al_2O_3	13.04	13.18	13.04	11.83	13.10	12.87
Fe_2O_3	1.46	1.67	1.87	1.04	0.98	1.06
MgO	0.06	0.06	0.06	0.02	0.03	0.03
CaO	0.29	0.55	0.38	0.10	0.13	0.31
Na_2O	3.99	3.62	3.56	3.25	3.39	3.25
K_2O	0.51	4.90	4.84	4.79	5.53	5.17
MnO_2	0.03	0.04	0.04	0.02	0.02	0.03
P_2O_5	0.02	0.03	0.05	0.02	0.03	0.01
Ba	853.	611.	853.	228.	898.	1060.
Nb	26.	32.	34.	37.	34.	34.
Zr	177.	177.	213.	140.	127.	250.
Y	76.	104.	93.	93.	72.	89.
Sr	40.	38.	45.	13.	35.	46.
Rb	143.	175.	183.	182.	188.	150.
Zn	42.	44.	46.	34.	30.	54.
Cu	11.	13.	13.	13.	13.	12.
Ni	6.	5.	4.	4.	2.	3.
Pb	24.	27.	30.	26.	27.	25.
U	2.	2.	2.	2.	2.	2.
Th	16.	21.	21.	25.	23.	19.
V	8.	5.	7.	3.	3.	10.
Cr	5.	9.	6.	10.	8.	10.
Nd	49.	51.	48.	51.	23.	47.
La	37.	58.	49.	29.	22.	52.
Ce	76.	110.	90.	75.	30.	99.
Qz	54.1	34.2	35.3	41.0	35.2	37.4
Cor	5.5	1.0	1.4	1.2	1.4	1.4
Or	3.0	29.0	28.6	28.3	32.7	30.6
Ab	33.8	30.7	30.2	27.5	28.7	27.5
An	1.3	2.5	1.6	0.4	0.4	1.5
Hy	1.5	1.7	1.9	1.0	1.0	1.1
Mgtte	0.5	0.6	0.7	0.4	0.4	0.4
Ilm	0.2	0.2	0.3	0.2	0.1	0.1
Aptte	0.0	0.1	0.1	0.0	0.1	0.0
DI	90.9	93.8	94.1	96.9	96.6	95.5

	00431	99451	89431	90461	89421	89422
SiO_2	76.72	76.57	76.16	75.51	77.28	76.42
TiO_2	0.14	0.13	0.15	0.16	0.06	0.10
Al_2O_3	12.59	12.85	12.81	13.29	12.85	12.96
Fe_2O_3	1.71	1.45	1.78	1.92	0.92	1.24
MgO	0.05	0.05	0.07	0.06	0.02	0.04
CaO	0.41	0.44	0.61	0.51	0.22	0.24
Na_2O	3.42	3.44	3.29	3.59	3.37	3.66
K_2O	4.88	5.03	5.06	4.89	5.27	5.29
MnO_2	0.04	0.03	0.03	0.03	0.02	0.03
P_2O_5	0.04	0.02	0.04	0.04	0.0	0.02
Ba	874.	1063.	1097.	1036.	475.	553.
Nb	36.	30.	30.	32.	25.	31.
Zr	228.	189.	218.	230.	93.	93.
Y	89.	57.	74.	75.	63.	50.
Sr	41.	48.	53.	49.	25.	29.
Rb	169.	157.	165.	162.	176.	188.
Zn	56.	44.	46.	52.	27.	42.
Cu	17.	14.	13.	15.	13.	13.
Ni	3.	4.	6.	2.	4.	5.
Pb	26.	26.	25.	24.	29.	30.
U	2.	2.	1.	1.	2.	1.
Th	21.	19.	22.	20.	19.	18.
V	5.	5.	10.	10.	5.	5.
Cr	10.	10.	7.	9.	9.	9.
Nd	43.	45.	61.	42.	21.	19.
La	40.	35.	62.	39.	18.	15.
Ce	90.	78.	138.	90.	52.	37.
Qz	36.6	35.8	35.7	34.1	36.6	33.9
Cor	1.0	1.0	0.9	1.3	1.2	0.8
Or	28.9	29.8	29.9	28.9	31.2	31.3
Ab	29.0	29.1	27.9	30.4	28.5	31.0
An	1.8	2.1	2.8	2.3	1.1	1.1
Hy	1.7	1.5	1.8	1.9	0.9	1.3
Mgtte	0.6	0.5	0.6	0.7	0.3	0.4
Ilm	0.3	0.2	0.3	0.3	0.1	0.2
Aptte	0.1	0.0	0.1	0.1	0.0	0.0
DI	95.5	94.7	93.5	93.4	96.3	96.2

	96444A	99442	96451	96444B	94472	96453
SiO_2	77.18	76.58	77.66	76.76	77.03	77.51
TiO_2	0.12	0.15	0.11	0.07	0.05	0.11
Al_2O_3	12.80	12.68	12.40	13.16	12.83	12.31
Fe_2O_3	1.20	1.69	1.19	1.14	1.01	1.33
MgO	0.04	0.06	0.02	0.03	0.02	0.04
CaO	0.45	0.60	0.23	0.17	0.24	0.30
Na_2O	3.06	3.53	3.30	3.59	4.13	3.33
K_2O	5.09	4.63	5.04	5.04	4.64	5.04
MnO_2	0.04	0.04	0.02	0.03	0.02	0.03
P_2O_5	0.02	0.04	0.03	0.01	0.01	0.02
Ba	645.	1059.	146.	74.	26.	889.
Nb	29.	32.	34.	45.	45.	29.
Zr	114.	221.	116.	141.	150.	148.
Y	87.	83.	102.	42.	86.	74.
Sr	33.	52.	13.	7.	4.	38.
Rb	160.	142.	166.	226.	242.	169.
Zn	39.	50.	46.	46.	35.	42.
Cu	14.	14.	14.	13.	13.	0.
Ni	5.	4.	3.	7.	4.	4.
Pb	25.	26.	24.	33.	32.	28.
U	2.	2.	2.	1.	3.	2.
Th	23.	19.	23.	27.	27.	21.
V	6.	7.	7.	6.	6.	5.
Cr	10.	8.	9.	7.	12.	10.
Nd	62.	54.	44.	15.	36.	52.
La	56.	50.	32.	15.	32.	44.
Ce	110.	86.	87.	42.	79.	84.
Qz	38.5	36.4	38.3	35.7	34.3	37.7
Cor	1.5	0.9	1.2	1.5	0.6	0.9
Or	30.1	27.4	29.8	29.8	27.4	29.8
Ab	25.9	29.9	27.9	30.4	35.0	28.2
An	2.1	2.7	0.9	0.8	1.1	1.4
Hy	1.2	1.7	1.1	1.2	1.0	1.3
Mgtte	0.4	0.6	0.4	0.4	0.4	0.5
Ilm	0.2	0.3	0.2	0.1	0.1	0.2
Aptte	0.0	0.1	0.1	0.0	0.0	0.0
DI	94.5	93.7	96.0	95.9	96.7	95.7

	88431	C2	C3	C4	C6	C9
SiO_2	75.52	77.40	77.28	77.84	77.63	75.92
TiO_2	0.15	0.07	0.11	0.10	0.11	0.16
Al_2O_3	13.19	12.61	12.56	12.30	12.35	12.97
Fe_2O_3	1.91	1.05	1.33	1.17	1.31	1.94
MgO	0.07	0.02	0.04	0.04	0.03	0.05
CaO	0.38	0.12	0.37	0.40	0.19	0.44
Na_2O	3.68	4.09	3.21	3.32	3.44	3.35
K_2O	5.03	4.60	5.04	4.78	4.88	5.08
MnO_2	0.03	0.02	0.03	0.03	0.03	0.04
P_2O_5	0.04	0.01	0.03	0.03	0.02	0.04
Ba	718.	9.	917.	817.	377.	1090.
Nb	35.	35.	25.	30.	33.	31.
Zr	241.	109.	158.	124.	135.	232.
Y	87.	75.	44.	62.	88.	66.
Sr	33.	6.	48.	40.	29.	51.
Rb	189.	210.	152.	158.	180.	160.
Zn	53.	36.	46.	47.	55.	51.
Cu	13.	11.	11.	12.	12.	11.
Ni	2.	6.	5.	5.	6.	5.
Pb	28.	28.	25.	29.	26.	26.
U	2.	4.	1.	2.	3.	2.
Th	20.	23.	15.	19.	18.	21.
V	9.	2.	5.	7.	5.	12.
Cr	7.	5.	6.	7.	7.	7.
Nd	45.	50.	42.	41.	67.	60.
La	33.	40.	38.	38.	56.	53.
Ce	77.	76.	75.	86.	102.	118.
Qz	33.3	35.3	38.0	38.9	38.0	35.3
Cor	1.1	0.7	1.2	1.0	1.1	1.3
Or	29.8	27.2	29.8	28.3	28.9	30.1
Ab	31.2	34.6	27.2	28.1	29.1	28.4
An	1.6	0.5	1.6	1.8	0.8	1.9
Hy	2.0	1.1	1.3	1.2	1.3	1.9
Mgtte	0.7	0.4	0.5	0.4	0.5	0.7
Ilm	0.3	0.1	0.2	0.2	0.2	0.3
Aptte	0.1	0.0	0.1	0.1	0.0	0.1
DI	94.2	97.2	95.0	95.3	96.0	93.8

	C14	C19	C42	C43	C45	C73
SiO_2	77.73	76.54	77.59	78.28	77.16	77.15
TiO_2	0.09	0.02	0.06	0.06	0.05	0.13
Al_2O_3	12.39	13.46	12.55	12.21	13.02	12.33
Fe_2O_3	1.23	0.95	1.00	1.07	1.07	1.73
MgO	0.03	0.0	0.04	0.02	0.03	0.06
CaO	0.18	0.0	0.46	0.15	0.07	0.46
Na_2O	3.53	4.11	3.35	3.45	3.68	3.21
K_2O	4.77	4.87	4.91	4.70	4.86	4.87
MnO_2	0.03	0.02	0.03	0.03	0.03	0.03
P_2O_5	0.02	0.01	0.01	0.02	0.01	0.03
Ba	422.	0.	0.	119.	0.	957.
Nb	33.	59.	40.	38.	42.	31.
Zr	132.	107.	128.	111.	122.	179.
Y	60.	23.	90.	41.	29.	73.
Sr	24.	1.	6.	10.	5.	43.
Rb	193.	302.	253.	218.	250.	162.
Zn	45.	42.	42.	115.	154.	42.
Cu	11.	14.	12.	16.	18.	11.
Ni	4.	4.	8.	3.	3.	6.
Pb	26.	31.	29.	31.	31.	24.
U	3.	3.	3.	3.	4.	2.
Th	22.	25.	22.	23.	25.	19.
V	3.	0.	2.	5.	2.	9.
Cr	8.	6.	7.	11.	6.	7.
Nd	33.	15.	58.	29.	33.	55.
La	19.	15.	39.	15.	13.	39.
Ce	56.	12.	86.	43.	42.	77.
Qz	38.1	33.6	37.9	39.5	36.5	38.2
Cor	1.1	1.4	0.9	1.2	1.6	1.0
Or	28.2	28.8	29.0	27.8	28.7	28.8
Ab	29.9	34.8	28.4	29.2	31.2	27.2
An	0.8	0.0	2.2	0.6	0.3	2.1
Hy	1.2	1.0	1.1	1.1	1.1	1.8
Mgtte	0.5	0.4	0.4	0.4	0.4	0.6
Ilm	0.2	0.0	0.1	0.1	0.1	0.2
Aptte	0.0	0.0	0.0	0.0	0.0	0.1
DI	96.2	98.2	95.3	96.5	96.5	94.2

	C74	C77	C78	C89	C92	C93
SiO_2	83.42	79.16	77.49	75.40	76.84	73.75
TiO_2	0.05	0.07	0.05	0.15	0.13	0.19
Al_2O_3	9.32	11.59	12.50	13.11	12.44	14.10
Fe_2O_3	0.77	0.97	1.00	1.88	1.61	2.31
MgO	0.02	0.03	0.02	0.15	0.04	0.06
CaO	0.08	0.24	0.30	0.51	0.40	0.56
Na_2O	2.74	2.92	4.09	3.26	3.67	3.58
K_2O	3.56	4.99	4.52	5.46	4.81	5.36
MnO_2	0.02	0.02	0.02	0.04	0.04	0.04
P_2O_5	0.01	0.01	0.01	0.04	0.03	0.04
Ba	17.	283.	0.	1365.	521.	1312.
Nb	26.	29.	44.	30.	29.	35.
Zr	72.	92.	129.	187.	177.	245.
Y	49.	76.	108.	66.	69.	52.
Sr	9.	19.	4.	62.	32.	59.
Rb	151.	176.	228.	166.	188.	181.
Zn	26.	30.	34.	72.	51.	60.
Cu	11.	12.	11.	11.	11.	11.
Ni	4.	3.	8.	6.	5.	6.
Pb	23.	24.	31.	31.	26.	27.
U	3.	2.	3.	3.	2.	3.
Th	17.	20.	23.	16.	19.	19.
V	2.	2.	0.	7.	5.	10.
Cr	6.	7.	6.	7.	6.	7.
Nd	29.	43.	39.	57.	50.	36.
La	16.	34.	24.	51.	45.	36.
Ce	36.	72.	69.	98.	94.	102.
Qz	53.4	42.2	35.3	33.6	35.6	30.3
Cor	0.8	1.0	0.4	1.0	0.5	1.5
Or	21.1	29.5	26.7	32.3	28.5	31.7
Ab	23.2	24.7	34.6	27.6	31.1	30.3
An	0.3	1.1	1.4	2.3	1.8	2.5
Hy	0.8	1.0	1.0	2.1	1.6	2.3
Mgtte	0.3	0.4	0.4	0.7	0.6	0.9
Ilm	0.1	0.1	0.1	0.3	0.2	0.4
Aptte	0.0	0.0	0.0	0.1	0.1	0.1
DI	97.6	96.4	96.7	93.5	95.1	92.4

	C94	C95	C98	C99	C108	C114
SiO_2	75.26	76.46	74.44	78.37	78.85	76.76
TiO_2	0.16	0.11	0.09	0.11	0.07	0.08
Al_2O_3	13.25	12.96	14.23	11.71	11.77	13.00
Fe_2O_3	1.86	1.46	1.18	1.44	1.00	1.14
MgO	0.14	0.05	0.03	0.05	0.02	0.02
CaO	0.50	0.49	0.43	0.35	0.17	0.23
Na_2O	3.29	3.52	4.10	3.16	3.23	3.65
K_2O	5.46	4.90	5.44	4.76	4.84	5.08
MnO_2	0.04	0.03	0.03	0.03	0.02	0.02
P_2O_5	0.04	0.02	0.03	0.02	0.02	0.02
Ba	1342.	896.	1131.	612.	411.	647.
Nb	30.	30.	33.	26.	28.	28.
Zr	198.	154.	130.	152.	102.	109.
Y	64.	66.	74.	76.	51.	56.
Sr	62.	46.	49.	29.	25.	30.
Rb	165.	173.	191.	153.	178.	213.
Zn	75.	43.	34.	36.	32.	35.
Cu	11.	11.	11.	11.	11.	11.
Ni	6.	5.	6.	6.	4.	5.
Pb	30.	25.	26.	26.	25.	30.
U	2.	3.	3.	3.	3.	3.
Th	16.	19.	18.	22.	18.	21.
V	7.	7.	7.	5.	2.	2.
Cr	7.	6.	6.	6.	6.	7.
Nd	41.	32.	45.	79.	30.	37.
La	41.	31.	30.	67.	30.	30.
Ce	73.	55.	68.	125.	53.	42.
Qz	33.3	35.6	28.4	40.4	40.8	35.2
Cor	1.1	1.0	0.9	0.8	1.0	1.1
Or	32.3	29.0	32.2	28.2	28.6	30.0
Ab	27.9	29.8	34.7	26.8	27.4	30.9
An	2.2	2.3	1.9	1.6	0.7	1.0
Hy	2.1	1.5	1.2	1.5	1.0	1.1
Mgtte	0.7	0.5	0.4	0.5	0.4	0.4
Ilm	0.3	0.2	0.2	0.2	0.1	0.2
Aptte	0.1	0.0	0.1	0.0	0.0	0.0
DI	93.5	94.4	95.3	95.4	96.8	96.1

	C118	C120	C121	C122	C124	C125
SiO_2	75.88	77.46	77.07	78.37	78.89	76.75
TiO_2	0.13	0.09	0.16	0.10	0.07	0.11
Al_2O_3	13.08	12.51	12.13	12.05	11.71	12.71
Fe_2O_3	1.74	1.22	1.96	0.94	0.95	1.33
MgO	0.04	0.03	0.06	0.04	0.02	0.08
CaO	0.45	0.30	0.45	0.44	0.16	0.39
Na_2O	3.42	3.32	3.19	3.20	3.44	3.57
K_2O	5.21	5.02	4.89	4.84	4.72	5.01
MnO_2	0.03	0.03	0.03	0.02	0.02	0.03
P_2O_5	0.03	0.02	0.04	0.01	0.02	0.03
Ba	1081.	510.	861.	538.	141.	565.
Nb	30.	33.	32.	27.	29.	36.
Zr	176.	132.	203.	131.	106.	147.
Y	54.	62.	63.	57.	61.	91.
Sr	50.	26.	45.	39.	13.	34.
Rb	170.	193.	160.	147.	187.	195.
Zn	42.	39.	42.	24.	26.	37.
Cu	11.	11.	11.	11.	11.	11.
Ni	7.	6.	7.	5.	5.	5.
Pb	26.	27.	24.	28.	27.	28.
U	3.	3.	3.	4.	3.	3.
Th	18.	21.	19.	13.	17.	23.
V	7.	2.	7.	3.	0.	3.
Cr	6.	5.	7.	14.	6.	6.
Nd	55.	52.	68.	34.	43.	65.
La	39.	46.	55.	26.	35.	48.
Ce	79.	107.	108.	58.	74.	90.
Qz	34.4	37.8	38.1	39.9	40.1	35.4
Cor	1.1	1.1	0.9	0.8	0.7	0.8
Or	30.8	29.7	28.9	28.6	27.9	29.6
Ab	29.0	28.1	27.0	27.1	29.1	30.2
An	2.0	1.4	2.0	2.1	0.7	1.7
Hy	1.7	1.2	1.9	0.9	0.9	1.4
Mgtte	0.6	0.5	0.7	0.3	0.4	0.5
Ilm	0.2	0.2	0.3	0.2	0.1	0.2
Aptte	0.1	0.0	0.1	0.0	0.0	0.1
DI	94.2	95.6	94.1	95.6	97.2	95.3

	C127	C132	C133	C134	C135	C136
SiO_2	76.22	76.85	79.49	76.25	75.29	76.23
TiO_2	0.13	0.15	0.06	0.13	0.16	0.16
Al_2O_3	13.06	12.42	11.45	13.24	13.14	12.48
Fe_2O_3	1.44	1.90	0.94	1.43	1.95	2.05
MgO	0.04	0.05	0.02	0.04	0.05	0.07
CaO	0.42	0.51	0.19	0.47	0.65	0.52
Na_2O	3.31	3.21	3.17	3.32	3.51	3.15
K_2O	5.33	4.83	4.64	5.04	5.17	5.26
MnO_2	0.03	0.03	0.02	0.05	0.04	0.04
P_2O_5	0.03	0.04	0.02	0.04	0.04	0.05
Ba	1009.	1051.	131.	1024.	1226.	1120.
Nb	24.	32.	26.	30.	34.	34.
Zr	164.	192.	67.	178.	229.	198.
Y	49.	95.	56.	61.	81.	102.
Sr	52.	49.	14.	49.	60.	49.
Rb	157.	164.	179.	171.	166.	163.
Zn	38.	99.	25.	38.	53.	49.
Cu	10.	13.	11.	12.	10.	11.
Ni	5.	7.	4.	5.	5.	7.
Pb	26.	27.	28.	25.	26.	25.
U	2.	3.	3.	3.	2.	3.
Th	15.	17.	21.	17.	21.	19.
V	10.	7.	0.	10.	7.	7.
Cr	8.	6.	6.	7.	10.	10.
Nd	41.	82.	42.	56.	66.	75.
La	42.	63.	25.	47.	55.	62.
Ce	80.	123.	68.	94.	123.	120.
Qz	35.1	37.9	42.5	36.1	33.0	35.9
Cor	1.2	1.1	0.9	1.6	0.7	0.8
Or	31.5	28.6	27.4	29.8	30.6	31.1
Ab	28.0	27.2	26.8	28.1	29.7	26.7
An	1.9	2.3	0.8	2.1	3.0	2.3
Hy	1.4	1.9	0.9	1.4	1.9	2.1
Mgtte	0.5	0.7	0.3	0.5	0.7	0.8
Ilm	0.2	0.3	0.1	0.2	0.3	0.3
Aptte	0.1	0.1	0.0	0.1	0.1	0.1
DI	94.7	93.7	96.8	94.1	93.3	93.7

	C137	C138	C140	C141	C143	C144
SiO_2	82.40	78.97	74.02	75.19	77.79	78.03
TiO_2	0.04	0.05	0.25	0.19	0.12	0.08
Al_2O_3	9.93	11.85	13.52	13.18	12.04	12.10
Fe_2O_3	0.67	0.83	2.90	2.17	1.46	1.02
MgO	0.02	0.0	0.08	0.07	0.06	0.02
CaO	0.14	0.12	0.71	0.67	0.41	0.21
Na_2O	2.87	3.18	3.53	3.53	3.31	3.54
K_2O	3.89	4.96	4.90	4.93	4.76	4.96
MnO_2	0.02	0.02	0.05	0.04	0.03	0.02
P_2O_5	0.02	0.01	0.04	0.04	0.02	0.02
Ba	52.	276.	1020.	1046.	952.	367.
Nb	25.	28.	40.	32.	31.	33.
Zr	88.	76.	352.	238.	165.	127.
Y	47.	42.	78.	60.	68.	40.
Sr	18.	18.	58.	52.	46.	20.
Rb	150.	182.	176.	163.	151.	196.
Zn	19.	31.	85.	63.	31.	34.
Cu	11.	10.	11.	12.	11.	11.
Ni	4.	3.	7.	4.	6.	5.
Pb	24.	27.	27.	27.	26.	27.
U	2.	2.	3.	3.	3.	3.
Th	19.	19.	20.	19.	16.	24.
V	0.	2.	10.	12.	3.	3.
Cr	5.	10.	8.	5.	7.	7.
Nd	26.	34.	89.	53.	45.	41.
La	16.	22.	84.	47.	35.	26.
Ce	41.	62.	184.	90.	72.	58.
Qz	50.3	40.9	32.1	33.5	38.8	37.6
Cor	0.8	1.1	1.2	0.9	0.7	0.6
Or	23.0	29.3	29.0	29.2	28.2	29.3
Ab	24.3	26.9	29.9	29.9	28.0	30.0
An	0.6	0.5	3.3	3.1	1.9	0.9
Hy	0.7	0.8	2.8	2.2	1.5	1.0
Mgtte	0.2	0.3	1.1	0.8	0.5	0.4
Ilm	0.1	0.1	0.5	0.4	0.2	0.2
Aptte	0.0	0.0	0.1	0.1	0.0	0.0
DI	97.6	97.2	91.0	92.6	95.0	96.9

	C145	C146	C147	C148	C149	C151
SiO_2	77.09	77.74	76.58	80.51	76.80	76.84
TiO_2	0.14	0.09	0.11	0.07	0.13	0.10
Al_2O_3	12.27	12.41	13.04	10.84	12.52	12.78
Fe_2O_3	1.76	1.21	1.46	0.92	1.65	1.40
MgO	0.05	0.03	0.04	0.02	0.05	0.04
CaO	0.54	0.23	0.40	0.23	0.40	0.29
Na_2O	3.29	3.18	3.23	3.02	3.40	3.38
K_2O	4.80	5.07	5.08	4.34	4.98	5.11
MnO_2	0.03	0.03	0.02	0.02	0.04	0.03
P_2O_5	0.03	0.02	0.03	0.02	0.03	0.02
Ba	1020.	659.	909.	234.	925.	496.
Nb	31.	32.	27.	24.	32.	36.
Zr	167.	118.	151.	89.	185.	122.
Y	68.	75.	68.	50.	53.	143.
Sr	51.	32.	44.	19.	40.	31.
Rb	154.	187.	178.	156.	176.	184.
Zn	49.	45.	102.	29.	46.	42.
Cu	11.	15.	14.	11.	11.	11.
Ni	4.	6.	6.	5.	4.	7.
Pb	26.	26.	25.	24.	26.	26.
U	3.	3.	3.	2.	4.	4.
Th	22.	21.	14.	17.	20.	21.
V	5.	2.	7.	2.	9.	3.
Cr	14.	6.	13.	7.	8.	10.
Nd	63.	59.	42.	41.	30.	80.
La	44.	41.	39.	25.	34.	64.
Ce	90.	86.	73.	32.	67.	96.
Qz	37.7	38.9	36.9	45.5	36.5	36.4
Cor	0.8	1.3	1.6	0.8	0.9	1.2
Or	28.4	30.0	30.1	25.7	29.5	30.2
Ab	27.9	26.9	27.4	25.6	28.8	28.6
An	2.5	1.0	1.8	1.0	1.8	1.3
Hy	1.7	1.2	1.4	0.9	1.7	1.4
Mgtte	0.7	0.4	0.5	0.3	0.6	0.5
Ilm	0.3	0.2	0.2	0.1	0.2	0.2
Aptte	0.1	0.0	0.1	0.0	0.1	0.0
DI	94.0	95.8	94.4	96.8	94.7	95.3

	C153	C154	C158	C159	95462	90461B
SiO_2	75.30	76.27	78.98	76.13	77.88	76.03
TiO_2	0.15	0.14	0.08	0.15	0.06	0.13
Al_2O_3	13.30	12.93	11.66	12.85	12.41	13.00
Fe_2O_3	1.84	1.73	1.18	2.04	0.88	1.66
MgO	0.05	0.04	0.03	0.04	0.04	0.05
CaO	0.68	0.42	0.21	0.59	0.30	0.45
Na_2O	3.65	3.33	3.18	3.79	3.52	3.52
K_2O	4.93	5.06	4.64	4.33	4.89	5.10
MnO_2	0.05	0.03	0.03	0.04	0.02	0.04
P_2O_5	0.04	0.04	0.02	0.02	0.01	0.02
Ba	1072.	1043.	394.	288.	178.	898.
Nb	31.	30.	30.	42.	34.	31.
Zr	217.	190.	123.	171.	121.	186.
Y	92.	57.	48.	92.	84.	83.
Sr	54.	45.	20.	32.	13.	47.
Rb	162.	168.	180.	199.	173.	175.
Zn	52.	78.	40.	47.	34.	46.
Cu	12.	14.	11.	11.	11.	11.
Ni	6.	6.	5.	8.	7.	7.
Pb	25.	28.	24.	26.	25.	27.
U	3.	3.	3.	2.	3.	2.
Th	18.	20.	20.	24.	20.	17.
V	7.	5.	3.	5.	3.	7.
Cr	5.	9.	5.	10.	11.	6.
Nd	84.	50.	39.	67.	54.	59.
La	61.	43.	32.	55.	38.	49.
Ce	174.	107.	103.	125.	73.	96.
Qz	33.0	36.0	41.8	35.4	37.7	34.4
Cor	0.8	1.3	1.1	0.9	0.8	0.9
Or	29.2	29.9	27.4	25.6	28.9	30.2
Ab	30.9	28.2	26.9	32.1	29.8	29.8
An	3.1	1.8	0.9	2.8	1.4	2.1
Hy	1.9	1.7	1.2	2.0	0.9	1.7
Mgtte	0.7	0.6	0.4	0.8	0.3	0.6
Ilm	0.3	0.3	0.2	0.3	0.1	0.2
Aptte	0.1	0.1	0.0	0.0	0.0	0.0
DI	93.2	94.2	96.2	93.2	96.4	94.4

	92471	89423	90452	89451	95482	99441
SiO_2	76.04	76.04	77.00	76.54	77.33	75.30
TiO_2	0.17	0.12	0.08	0.13	0.08	0.16
Al_2O_3	12.58	13.04	12.63	12.62	12.48	12.99
Fe_2O_3	2.11	1.65	1.18	1.68	1.03	1.92
MgO	0.07	0.05	0.04	0.06	0.04	0.06
CaO	0.55	0.58	0.45	0.52	0.35	0.70
Na_2O	3.43	3.58	3.52	3.42	3.62	4.04
K_2O	4.98	4.90	5.06	4.99	5.04	4.76
MnO_2	0.04	0.03	0.02	0.04	0.03	0.04
P_2O_5	0.03	0.01	0.01	0.01	0.0	0.02
Ba	1060.	611.	584.	553.	528.	991.
Nb	34.	32.	29.	35.	34.	37.
Zr	250.	177.	125.	228.	116.	290.
Y	89.	104.	79.	103.	48.	68.
Sr	46.	38.	31.	28.	23.	52.
Rb	150.	175.	171.	190.	184.	184.
Zn	54.	44.	40.	53.	45.	93.
Cu	12.	13.	13.	14.	14.	13.
Ni	3.	5.	0.	2.	6.	5.
Pb	25.	27.	27.	28.	32.	24.
U	2.	2.	2.	1.	1.	1.
Th	19.	21.	23.	22.	20.	24.
V	10.	5.	8.	10.	6.	9.
Cr	10.	9.	8.	13.	7.	8.
Nd	47.	51.	41.	40.	37.	60.
La	52.	58.	37.	34.	27.	55.
Ce	99.	110.	63.	67.	67.	113.
Qz	37.4	34.2	36.0	36.3	39.2	31.7
Cor	1.4	1.0	0.9	0.9	1.4	0.0
Or	30.6	29.0	30.0	29.4	30.3	28.0
Ab	27.5	30.7	29.4	28.6	26.2	34.2
An	1.5	2.5	1.8	2.1	1.2	3.2
Hy	1.1	1.7	1.2	1.7	1.2	1.9
Mgtte	0.4	0.6	0.4	0.6	0.4	0.7
Ilm	0.1	0.2	0.2	0.3	0.2	0.3
Aptte	0.0	0.1	0.0	0.1	0.0	0.1
DI	95.5	93.8	95.4	94.4	95.6	93.8

	92482	97471	90472	92481	97392	97411
SiO_2	76.49	76.69	76.19	76.84	76.56	76.63
TiO_2	0.16	0.13	0.13	0.05	0.13	0.06
Al_2O_3	12.85	12.91	12.83	13.05	12.49	13.15
Fe_2O_3	1.43	1.34	1.61	0.71	1.84	0.77
MgO	0.06	0.05	0.07	0.04	0.07	0.03
CaO	0.58	0.46	0.47	0.27	0.72	0.30
Na_2O	3.44	3.46	3.63	3.58	3.27	3.19
K_2O	4.92	4.91	5.02	5.43	4.88	5.84
MnO_2	0.04	0.02	0.04	0.02	0.03	0.01
P_2O_5	0.03	0.02	0.01	0.0	0.01	0.01
Ba	1271.	1085.	857.	455.	1003.	673.
Nb	34.	34.	38.	28.	30.	24.
Zr	249.	205.	227.	68.	184.	62.
Y	69.	69.	71.	61.	87.	42.
Sr	53.	48.	42.	23.	52.	32.
Rb	152.	161.	180.	186.	154.	196.
Zn	47.	40.	56.	27.	48.	23.
Cu	13.	13.	14.	13.	11.	10.
Ni	3.	7.	3.	6.	6.	4.
Pb	28.	28.	33.	30.	24.	28.
U	2.	2.	2.	2.	2.	3.
Th	22.	20.	24.	16.	17.	15.
V	10.	7.	8.	2.	9.	2.
Cr	6.	20.	10.	7.	13.	16.
Nd	40.	46.	41.	20.	60.	18.
La	42.	45.	40.	6.	55.	22.
Ce	88.	84.	83.	36.	104.	30.
Qz	36.1	36.2	34.6	34.7	36.5	34.8
Cor	1.1	1.4	0.7	1.2	0.5	1.1
Or	28.8	29.1	29.9	32.2	28.9	34.5
Ab	29.1	29.3	30.3	30.2	27.7	27.0
An	2.5	1.7	1.9	0.5	3.5	1.4
Hy	1.4	1.4	1.7	0.8	1.9	0.8
Mgtte	0.5	0.5	0.6	0.3	0.7	0.3
Ilm	0.3	0.3	0.3	0.1	0.2	0.1
Aptte	0.1	0.1	0.1	0.0	0.0	0.0
DI	94.0	94.6	94.8	97.1	93.1	96.3

	00411	96404A	96404C	97382B	97403	96412
SiO_2	77.06	76.85	76.94	76.72	77.88	75.38
TiO_2	0.09	0.09	0.04	0.08	0.12	0.07
Al_2O_3	12.69	12.78	12.92	13.03	11.93	13.97
Fe_2O_3	1.21	1.31	0.83	1.19	1.23	0.88
MgO	0.04	0.05	0.03	0.04	0.05	0.04
CaO	0.32	0.36	0.26	0.28	0.53	0.40
Na_2O	3.37	3.03	4.23	3.51	3.19	3.56
K_2O	5.20	5.50	4.73	5.12	5.04	5.68
MnO_2	0.02	0.03	0.03	0.02	0.02	0.02
P_2O_5	0.01	0.01	0.01	0.01	0.02	0.01
Ba	500.	689.	0.	318.	1087.	1185.
Nb	32.	27.	41.	34.	28.	26.
Zr	105.	134.	151.	118.	156.	103.
Y	62.	49.	64.	44.	68.	40.
Sr	21.	37.	3.	18.	47.	48.
Rb	192.	162.	274.	208.	155.	189.
Zn	42.	39.	40.	38.	36.	35.
Cu	12.	11.	10.	11.	12.	11.
Ni	5.	7.	7.	6.	5.	3.
Pb	27.	25.	31.	29.	25.	29.
U	3.	1.	4.	2.	3.	3.
Th	17.	19.	31.	24.	14.	16.
V	5.	5.	2.	3.	9.	2.
Cr	13.	24.	8.	11.	7.	14.
Nd	40.	35.	19.	34.	69.	34.
La	27.	32.	13.	21.	62.	15.
Ce	71.	57.	41.	76.	116.	64.
Qz	36.4	36.8	33.3	35.6	38.4	31.7
Cor	1.0	1.2	0.4	1.2	0.3	1.3
Or	30.8	32.5	28.0	30.3	29.8	33.6
Ab	28.5	25.7	35.8	29.7	27.0	30.1
An	1.5	1.7	1.2	1.3	2.5	1.9
Hy	1.2	1.4	0.9	1.2	1.2	0.9
Mgtte	0.4	0.5	0.3	0.4	0.5	0.3
Ilm	0.2	0.2	0.1	0.2	0.2	0.1
Aptte	0.0	0.0	0.0	0.0	0.0	0.0
DI	95.6	95.0	97.1	95.6	95.2	95.4

	98401	96404B	98421	00432	00413B	98432F
SiO_2	76.55	75.10	76.69	77.57	77.85	70.69
TiO_2	0.12	0.12	0.09	0.07	0.09	0.50
Al_2O_3	12.77	13.67	12.84	12.52	12.30	13.74
Fe_2O_3	1.55	1.33	1.27	1.14	1.09	4.61
MgO	0.05	0.05	0.05	0.04	0.05	0.17
CaO	0.47	0.42	0.35	0.30	0.27	1.73
Na_2O	3.25	3.40	3.30	3.52	3.25	4.28
K_2O	5.21	5.88	5.37	4.83	5.06	4.07
MnO_2	0.02	0.03	0.03	0.02	0.03	0.10
P_2O_5	0.02	0.01	0.01	0.0	0.01	0.11
Ba	1182.	374.	711.	280.	488.	782.
Nb	27.	29.	28.	37.	31.	58.
Zr	165.	90.	111.	147.	129.	635.
Y	62.	52.	67.	52.	76.	153.
Sr	50.	26.	35.	15.	32.	64.
Rb	161.	165.	180.	216.	164.	183.
Zn	47.	38.	36.	115.	41.	165.
Cu	11.	12.	11.	17.	12.	12.
Ni	7.	6.	5.	5.	6.	7.
Pb	26.	26.	26.	29.	25.	22.
U	3.	3.	4.	3.	2.	4.
Th	15.	18.	16.	21.	21.	29.
V	3.	9.	3.	2.	3.	24.
Cr	7.	12.	24.	11.	15.	6.
Nd	58.	30.	52.	24.	59.	151.
La	42.	27.	38.	26.	49.	137.
Ce	86.	53.	66.	47.	88.	274.
Qz	36.1	31.3	35.6	37.4	38.5	25.1
Cor	1.0	1.0	1.0	1.0	1.0	0.0
Or	30.8	34.8	31.8	28.6	29.9	24.1
Ab	27.5	28.8	28.0	29.8	27.5	36.3
An	2.2	2.0	1.7	1.5	1.3	6.3
Hy	1.5	1.3	1.3	1.2	1.1	3.8
Mgtte	0.6	0.5	0.5	0.4	0.4	1.7
Ilm	0.2	0.2	0.2	0.1	0.2	1.0
Aptte	0.0	0.0	0.0	0.0	0.0	0.3
DI	94.4	94.9	95.3	95.8	96.0	85.6

	98431F	98424	99411	97382	97391	00401
SiO_2	77.18	78.36	77.28	99.69	76.40	76.73
TiO_2	0.11	0.06	0.09	0.0	0.15	0.09
Al_2O_3	12.33	11.99	12.50	0.24	12.36	12.88
Fe_2O_3	1.33	0.87	1.17	0.03	1.93	1.21
MgO	0.05	0.04	0.05	0.0	0.06	0.04
CaO	0.60	0.37	0.37	0.02	0.60	0.40
Na_2O	3.33	3.54	3.32	0.0	3.42	3.57
K_2O	5.02	4.75	5.19	0.02	5.01	5.05
MnO_2	0.03	0.02	0.03	0.0	0.03	0.02
P_2O_5	0.01	0.0	0.0	0.0	0.03	0.0
Ba	1035.	70.	558.	219.	1120.	542.
Nb	22.	25.	30.	29.	32.	34.
Zr	146.	71.	107.	68.	203.	146.
Y	52.	48.	59.	78.	49.	57.
Sr	53.	10.	24.	15.	51.	25.
Rb	145.	176.	193.	183.	154.	194.
Zn	40.	29.	42.	29.	44.	38.
Cu	12.	11.	11.	11.	11.	11.
Ni	6.	5.	5.	4.	4.	6.
Pb	25.	26.	27.	25.	25.	28.
U	3.	3.	3.	3.	3.	4.
Th	16.	20.	17.	17.	18.	20.
V	5.	2.	3.	1.	9.	2.
Cr	8.	8.	5.	6.	8.	12.
Nd	65.	37.	50.	45.	51.	50.
La	57.	24.	35.	20.	49.	40.
Ce	124.	50.	115.	43.	108.	99.
Qz	36.7	38.4	36.8	99.6	35.3	35.2
Cor	0.4	0.4	0.7	0.2	0.3	0.8
Or	29.7	28.1	30.7	0.1	29.7	29.9
Ab	28.2	30.0	28.1	0.0	29.0	30.2
An	2.9	1.8	1.8	0.1	2.8	2.0
Hy	1.4	0.9	1.2	0.0	1.9	1.2
Mgtte	0.5	0.3	0.4	0.0	0.7	0.4
Ilm	0.2	0.1	0.2	0.0	0.3	0.2
Aptte	0.0	0.0	0.0	0.0	0.1	0.0
DI	94.7	96.4	95.6	99.7	93.9	95.4

	96402	95411A	95391	95412A	94432A	91381
SiO_2	75.03	77.44	79.18	76.35	79.33	75.88
TiO_2	0.15	0.06	0.09	0.12	0.07	0.14
Al_2O_3	13.25	12.65	11.57	12.87	11.44	13.01
Fe_2O_3	2.01	0.96	0.99	1.66	0.91	1.79
MgO	0.06	0.04	0.05	0.05	0.04	0.07
CaO	0.61	0.27	0.39	0.53	0.31	0.68
Na_2O	3.55	3.28	2.90	3.41	3.12	3.32
K_2O	5.27	5.26	4.82	4.98	4.76	5.05
MnO_2	0.03	0.02	0.02	0.03	0.02	0.04
P_2O_5	0.02	0.01	0.01	0.02	0.01	0.02
Ba	1178.	78.	840.	1219.	422.	1110.
Nb	30.	33.	0.	31.	28.	26.
Zr	211.	100.	8.	209.	104.	198.
Y	74.	53.	93.	51.	51.	103.
Sr	54.	10.	36.	53.	22.	59.
Rb	176.	195.	154.	163.	176.	136.
Zn	48.	30.	35.	49.	28.	50.
Cu	11.	11.	11.	11.	11.	11.
Ni	5.	4.	5.	7.	6.	6.
Pb	27.	28.	24.	25.	25.	25.
U	3.	2.	2.	3.	2.	2.
Th	17.	24.	0.	17.	22.	19.
V	7.	2.	3.	5.	3.	3.
Cr	7.	6.	6.	15.	7.	9.
Nd	58.	35.	61.	36.	48.	117.
La	61.	25.	50.	38.	37.	120.
Ce	111.	91.	92.	81.	95.	169.
Qz	32.1	37.2	42.6	35.6	41.9	35.0
Cor	0.6	1.1	0.9	1.0	0.6	0.9
Or	31.2	31.1	28.5	29.5	28.1	29.9
Ab	30.1	27.8	24.6	28.9	26.4	28.1
An	2.9	1.3	1.9	2.5	1.5	3.2
Hy	2.0	1.0	1.0	1.7	1.0	1.8
Mgtte	0.7	0.4	0.4	0.6	0.3	0.7
Ilm	0.3	0.1	0.2	0.2	0.1	0.3
Aptte	0.0	0.0	0.0	0.0	0.0	0.0
DI	93.4	96.1	95.6	94.0	96.5	93.0

	94444	96411C	96452	97451	88441	96421
SiO_2	78.79	78.42	77.99	77.69	79.40	77.61
TiO_2	0.07	0.07	0.10	0.10	0.07	0.09
Al_2O_3	11.67	12.04	11.97	12.13	11.29	12.40
Fe_2O_3	0.87	0.83	1.21	1.29	0.85	1.29
MgO	0.04	0.04	0.05	0.05	0.04	0.04
CaO	0.40	0.32	0.61	0.42	0.31	0.45
Na_2O	3.24	3.40	3.26	3.27	2.89	3.15
K_2O	4.88	4.86	4.79	5.02	5.12	4.93
MnO_2	0.02	0.03	0.03	0.02	0.02	0.02
P_2O_5	0.01	0.0	0.01	0.01	0.01	0.01
Ba	287.	380.	650.	946.	711.	736.
Nb	26.	27.	25.	25.	23.	29.
Zr	103.	97.	150.	109.	81.	138.
Y	67.	48.	67.	62.	56.	49.
Sr	19.	20.	37.	46.	36.	42.
Rb	167.	190.	144.	162.	156.	167.
Zn	28.	34.	34.	35.	24.	39.
Cu	11.	12.	11.	11.	11.	11.
Ni	3.	5.	5.	5.	7.	3.
Pb	26.	27.	24.	23.	25.	25.
U	2.	3.	3.	2.	2.	3.
Th	18.	18.	20.	16.	15.	19.
V	5.	2.	0.	5.	3.	5.
Cr	6.	9.	7.	8.	17.	19.
Nd	42.	34.	52.	52.	35.	33.
La	34.	28.	49.	37.	24.	34.
Ce	77.	59.	95.	90.	58.	68.
Qz	40.0	39.0	38.9	38.0	42.0	38.9
Cor	0.4	0.6	0.3	0.6	0.5	1.1
Or	28.9	28.7	28.3	29.7	30.3	29.2
Ab	27.4	28.8	27.6	27.7	24.5	26.7
An	1.9	1.6	3.0	2.0	1.5	2.2
Hy	0.9	0.9	1.3	1.3	0.9	1.3
Mgtte	0.3	0.3	0.4	0.5	0.3	0.5
Ilm	0.1	0.1	0.2	0.2	0.1	0.2
Aptte	0.0	0.0	0.0	0.0	0.0	0.0
DI	96.3	96.5	94.8	95.4	96.7	94.8

	95411B	97431	98402B	97421	98422	91395
SiO_2	77.14	77.91	77.47	77.29	74.27	75.68
TiO_2	0.09	0.09	0.07	0.07	0.10	0.13
Al_2O_3	12.54	11.97	12.47	12.61	14.18	13.03
Fe_2O_3	1.16	1.25	1.02	1.11	1.38	1.71
MgO	0.04	0.05	0.04	0.04	0.05	0.06
CaO	0.36	0.53	0.33	0.39	0.48	0.61
Na_2O	3.53	3.24	3.42	3.53	3.82	3.71
K_2O	5.12	4.91	5.16	4.92	5.70	5.03
MnO_2	0.02	0.03	0.02	0.03	0.03	0.03
P_2O_5	0.01	0.02	0.01	0.01	0.01	0.01
Ba	462.	937.	518.	478.	1195.	1069.
Nb	33.	25.	31.	32.	27.	32.
Zr	133.	117.	110.	122.	144.	167.
Y	47.	57.	68.	74.	47.	56.
Sr	23.	49.	25.	26.	50.	50.
Rb	193.	148.	195.	189.	184.	161.
Zn	38.	35.	33.	44.	35.	41.
Cu	12.	11.	11.	11.	11.	10.
Ni	6.	4.	4.	6.	5.	5.
Pb	28.	24.	27.	27.	28.	25.
U	3.	2.	2.	3.	2.	2.
Th	23.	20.	20.	18.	19.	20.
V	2.	3.	5.	2.	7.	5.
Cr	7.	17.	11.	10.	10.	6.
Nd	46.	60.	60.	45.	44.	52.
La	28.	47.	34.	35.	29.	37.
Ce	70.	103.	82.	72.	69.	67.
Qz	35.7	38.6	36.7	36.6	28.6	32.8
Cor	0.6	0.4	0.7	0.8	0.9	0.4
Or	30.3	29.0	30.5	29.1	33.7	29.8
Ab	29.9	27.4	29.0	29.9	32.4	31.4
An	1.7	2.5	1.6	1.9	2.3	3.0
Hy	1.2	1.3	1.1	1.2	1.4	1.7
Mgtte	0.4	0.5	0.4	0.4	0.5	0.6
Ilm	0.2	0.2	0.1	0.1	0.2	0.2
Aptte	0.0	0.0	0.0	0.0	0.0	0.0
DI	95.9	95.1	96.1	95.6	94.7	94.0

	97442	96443	94432C	96411	96421C	96421B
SiO_2	77.74	77.41	78.73	76.75	76.38	77.06
TiO_2	0.05	0.07	0.07	0.07	0.08	0.09
Al_2O_3	12.70	12.39	11.79	13.01	13.24	12.63
Fe_2O_3	0.71	0.89	0.88	1.00	1.12	1.34
MgO	0.04	0.04	0.04	0.04	0.04	0.04
CaO	0.28	0.27	0.36	0.33	0.29	0.35
Na_2O	3.40	3.35	3.26	3.71	3.61	3.34
K_2O	5.05	5.55	4.85	5.07	5.23	5.12
MnO_2	0.01	0.02	0.02	0.02	0.03	0.02
P_2O_5	0.01	0.01	0.0	0.01	0.0	0.01
Ba	530.	283.	326.	21.	68.	574.
Nb	24.	29.	29.	30.	37.	31.
Zr	82.	111.	104.	84.	93.	120.
Y	51.	63.	58.	54.	36.	61.
Sr	26.	16.	20.	8.	9.	28.
Rb	179.	199.	167.	207.	219.	187.
Zn	27.	29.	29.	34.	39.	35.
Cu	11.	10.	11.	12.	11.	11.
Ni	6.	7.	5.	7.	4.	5.
Pb	26.	26.	25.	30.	31.	26.
U	2.	3.	4.	3.	3.	3.
Th	15.	21.	18.	22.	25.	21.
V	0.	3.	2.	2.	3.	5.
Cr	6.	7.	5.	9.	12.	7.
Nd	43.	50.	43.	55.	26.	40.
La	29.	33.	39.	37.	20.	38.
Ce	3.	75.	75.	79.	91.	73.
Qz	37.7	35.7	40.0	34.6	34.2	36.7
Cor	1.2	0.4	0.5	0.8	1.1	1.0
Or	29.9	32.8	28.7	30.0	30.9	30.3
Ab	28.8	28.4	27.6	31.4	30.6	28.3
An	1.3	1.3	1.8	1.6	1.4	1.7
Hy	0.8	0.9	0.9	1.0	1.2	1.4
Mgtte	0.3	0.3	0.3	0.4	0.4	0.5
Ilm	0.1	0.1	0.1	0.1	0.2	0.2
Aptte	0.0	0.0	0.0	0.0	0.0	0.0
DI	96.4	96.9	96.3	96.0	95.7	95.3

	99441A	94432B	99421	99412	95382	99413
SiO_2	75.44	76.88	77.93	77.28	77.64	77.65
TiO_2	0.14	0.07	0.06	0.09	0.05	0.09
Al_2O_3	12.91	12.73	12.33	12.57	12.50	12.27
Fe_2O_3	1.86	0.94	0.83	1.14	0.89	1.21
MgO	0.06	0.03	0.04	0.04	0.03	0.04
CaO	0.73	0.25	0.29	0.37	0.25	0.37
Na_2O	3.62	4.03	3.53	3.43	3.99	3.54
K_2O	5.17	5.04	4.97	5.06	4.62	4.79
MnO_2	0.03	0.02	0.02	0.02	0.03	0.03
P_2O_5	0.03	0.0	0.0	0.0	0.01	0.01
Ba	1215.	0.	485.	457.	6.	411.
Nb	30.	38.	29.	30.	45.	32.
Zr	191.	102.	77.	116.	123.	138.
Y	80.	52.	39.	54.	83.	70.
Sr	56.	4.	21.	23.	3.	23.
Rb	162.	240.	206.	187.	239.	180.
Zn	46.	38.	31.	113.	38.	46.
Cu	11.	10.	11.	11.	11.	11.
Ni	3.	4.	4.	5.	6.	5.
Pb	26.	28.	28.	28.	30.	26.
U	4.	2.	3.	3.	3.	3.
Th	17.	21.	19.	17.	23.	21.
V	9.	3.	3.	3.	0.	5.
Cr	9.	7.	9.	7.	15.	7.
Nd	58.	39.	25.	33.	28.	50.
La	46.	37.	21.	27.	14.	36.
Ce	97.	80.	63.	51.	32.	84.
Qz	32.3	33.2	37.4	36.7	35.8	37.4
Cor	0.1	0.2	0.6	0.8	0.5	0.6
Or	30.6	29.8	29.4	29.9	27.3	28.3
Ab	30.7	34.1	29.9	29.0	33.8	30.0
An	3.4	1.2	1.4	1.8	1.2	1.8
Hy	1.9	1.0	0.9	1.2	1.0	1.2
Mgtte	0.7	0.3	0.3	0.4	0.3	0.4
Ilm	0.3	0.1	0.1	0.2	0.1	0.2
Aptte	0.1	0.0	0.0	0.0	0.0	0.0
DI	93.6	97.1	96.6	95.6	96.9	95.7

	00413A	97433	99435	97432	98402A	00412
SiO_2	78.02	75.25	77.65	77.01	77.68	77.03
TiO_2	0.09	0.08	0.09	0.15	0.09	0.09
Al_2O_3	12.06	13.68	12.45	12.29	12.26	12.53
Fe_2O_3	1.12	1.27	1.24	1.84	1.27	1.34
MgO	0.04	0.04	0.05	0.06	0.04	0.04
CaO	0.35	0.41	0.41	0.65	0.40	0.37
Na_2O	3.23	4.09	3.38	3.19	3.50	3.41
K_2O	5.05	5.15	4.70	4.76	4.73	5.15
MnO_2	0.03	0.03	0.02	0.03	0.03	0.02
P_2O_5	0.01	0.0	0.02	0.01	0.0	0.01
Ba	487.	596.	437.	959.	308.	459.
Nb	29.	36.	29.	33.	34.	32.
Zr	123.	152.	127.	175.	144.	149.
Y	63.	59.	106.	77.	93.	51.
Sr	24.	27.	23.	44.	22.	24.
Rb	173.	222.	173.	157.	180.	196.
Zn	37.	39.	57.	43.	38.	52.
Cu	12.	11.	13.	11.	11.	11.
Ni	6.	4.	6.	5.	5.	6.
Pb	25.	29.	33.	25.	26.	27.
U	2.	2.	1.	3.	2.	3.
Th	17.	23.	20.	21.	20.	22.
V	5.	2.	3.	5.	3.	0.
Cr	7.	6.	12.	12.	9.	7.
Nd	55.	32.	74.	65.	75.	33.
La	36.	30.	46.	55.	48.	31.
Ce	78.	61.	69.	107.	105.	66.
Qz	38.7	30.3	38.6	38.1	37.8	36.1
Cor	0.7	0.6	1.1	0.7	0.7	0.7
Or	29.9	30.5	27.8	28.2	28.0	30.5
Ab	27.4	34.6	28.6	27.0	29.6	28.9
An	1.7	2.0	1.9	3.2	2.0	1.8
Hy	1.2	1.3	1.3	1.8	1.3	1.4
Mgtte	0.4	0.5	0.5	0.7	0.5	0.5
Ilm	0.2	0.2	0.2	0.3	0.2	0.2
Aptte	0.0	0.0	0.0	0.0	0.0	0.0
DI	95.9	95.4	95.0	93.3	95.4	95.5

	98391	96381	95404	98423	00423	98451
SiO_2	78.11	76.35	77.02	77.51	78.82	77.49
TiO_2	0.08	0.12	0.07	0.11	0.08	0.07
Al_2O_3	11.93	12.71	12.83	12.05	11.65	12.63
Fe_2O_3	1.13	1.67	1.04	1.47	1.09	0.97
MgO	0.04	0.06	0.04	0.05	0.04	0.04
CaO	0.36	0.56	0.33	0.46	0.30	0.35
Na_2O	3.38	3.29	3.80	3.38	3.21	3.60
K_2O	4.92	5.19	4.83	4.92	4.79	4.82
MnO_2	0.03	0.03	0.02	0.03	0.03	0.02
P_2O_5	0.01	0.02	0.01	0.02	0.0	0.01
Ba	417.	1207.	17.	654.	384.	457.
Nb	30.	27.	31.	27.	30.	30.
Zr	112.	163.	107.	164.	107.	99.
Y	50.	60.	60.	81.	82.	50.
Sr	22.	51.	8.	36.	23.	24.
Rb	179.	149.	220.	158.	168.	211.
Zn	38.	42.	40.	44.	41.	37.
Cu	11.	11.	10.	11.	11.	10.
Ni	5.	5.	5.	6.	6.	6.
Pb	26.	24.	28.	24.	24.	27.
U	3.	2.	3.	3.	2.	3.
Th	22.	15.	25.	18.	17.	18.
V	2.	5.	2.	7.	7.	7.
Cr	10.	10.	10.	21.	16.	12.
Nd	61.	54.	56.	51.	47.	30.
La	40.	46.	32.	31.	35.	26.
Ce	106.	86.	55.	65.	81.	58.
Qz	38.4	35.4	35.3	37.4	40.7	36.9
Cor	0.4	0.7	0.8	0.4	0.6	0.9
Or	29.1	30.7	28.6	29.1	28.3	28.5
Ab	28.6	27.9	32.2	28.6	27.2	30.5
An	1.7	2.7	1.6	2.2	1.5	1.7
Hy	1.2	1.7	1.1	1.5	1.1	1.0
Mgtte	0.4	0.6	0.4	0.5	0.4	0.4
Ilm	0.2	0.2	0.1	0.2	0.2	0.1
Aptte	0.0	0.0	0.0	0.0	0.0	0.0
DI	96.1	94.0	96.0	95.2	96.2	95.9

	99414	99422	97381A	97422C	99401	97441
SiO_2	77.93	77.74	75.87	77.32	77.79	75.88
TiO_2	0.08	0.08	0.12	0.09	0.09	0.10
Al_2O_3	12.30	12.35	13.03	12.33	12.10	12.96
Fe_2O_3	1.06	1.09	1.70	1.19	1.20	1.63
MgO	0.04	0.04	0.06	0.04	0.03	0.06
CaO	0.31	0.38	0.50	0.44	0.34	0.44
Na_2O	3.22	3.41	3.34	3.42	3.42	3.64
K_2O	5.05	4.88	5.32	5.13	5.00	5.23
MnO_2	0.02	0.02	0.03	0.02	0.02	0.04
P_2O_5	0.0	0.0	0.03	0.01	0.01	0.02
Ba	471.	405.	1162.	472.	317.	689.
Nb	32.	28.	29.	24.	32.	34.
Zr	109.	122.	189.	113.	142.	164.
Y	53.	57.	60.	55.	86.	65.
Sr	21.	21.	55.	26.	20.	43.
Rb	187.	180.	158.	171.	197.	231.
Zn	33.	35.	47.	33.	50.	44.
Cu	11.	11.	10.	11.	13.	11.
Ni	5.	6.	6.	3.	6.	6.
Pb	26.	26.	24.	26.	28.	28.
U	2.	2.	1.	2.	3.	3.
Th	18.	20.	19.	18.	22.	20.
V	5.	5.	9.	0.	2.	3.
Cr	15.	7.	8.	9.	11.	40.
Nd	43.	43.	55.	28.	63.	40.
La	26.	33.	39.	29.	46.	34.
Ce	46.	64.	94.	84.	103.	78.
Qz	38.7	37.9	34.3	36.4	37.5	33.0
Cor	1.0	0.8	0.9	0.4	0.5	0.6
Or	29.9	28.9	31.5	30.3	29.6	30.9
Ab	27.3	28.9	28.3	29.0	29.0	30.8
An	1.5	1.9	2.3	2.1	1.6	2.1
Hy	1.1	1.1	1.7	1.2	1.2	1.7
Mgtte	0.4	0.4	0.6	0.4	0.4	0.6
Ilm	0.2	0.2	0.2	0.2	0.2	0.2
Aptte	0.0	0.0	0.1	0.0	0.0	0.0
DI	95.9	95.7	94.1	95.7	96.1	94.8

	93442	94443A	93443A	97434	95394	90391
SiO_2	79.25	79.10	79.69	75.17	79.28	76.42
TiO_2	0.07	0.09	0.07	0.14	0.06	0.15
Al_2O_3	11.52	11.50	11.21	13.50	11.40	13.10
Fe_2O_3	0.88	1.13	0.90	1.79	0.84	1.27
MgO	0.04	0.05	0.04	0.06	0.05	0.06
CaO	0.28	0.32	0.27	0.49	0.26	0.49
Na_2O	3.19	3.14	3.14	3.42	3.15	3.23
K_2O	4.76	4.65	4.67	5.39	4.93	5.24
MnO_2	0.02	0.02	0.02	0.03	0.02	0.02
P_2O_5	0.01	0.01	0.0	0.02	0.01	0.02
Ba	229.	243.	146.	1098.	569.	719.
Nb	28.	32.	30.	29.	22.	38.
Zr	98.	114.	101.	199.	102.	190.
Y	48.	89.	77.	88.	71.	118.
Sr	17.	20.	18.	54.	34.	43.
Rb	180.	165.	174.	173.	158.	177.
Zn	32.	34.	33.	46.	36.	42.
Cu	11.	10.	11.	12.	11.	11.
Ni	6.	7.	6.	6.	5.	7.
Pb	24.	23.	25.	25.	28.	25.
U	2.	0.	3.	3.	3.	3.
Th	18.	22.	23.	16.	11.	21.
V	2.	3.	0.	5.	3.	3.
Cr	10.	20.	17.	16.	21.	25.
Nd	37.	75.	55.	90.	46.	137.
La	30.	73.	44.	68.	38.	128.
Ce	75.	108.	89.	110.	55.	270.
Qz	41.5	41.9	42.6	32.9	41.1	36.0
Cor	0.6	0.7	0.5	1.2	0.4	1.3
Or	28.1	27.5	27.6	31.9	29.2	31.0
Ab	27.0	26.6	26.6	29.0	26.7	27.4
An	1.3	1.5	1.3	2.3	1.2	2.3
Hy	0.9	1.2	0.9	1.8	0.9	1.2
Mgtte	0.3	0.4	0.3	0.7	0.3	0.5
Ilm	0.1	0.2	0.1	0.3	0.1	0.3
Aptte	0.0	0.0	0.0	0.0	0.0	0.0
DI	96.6	96.0	96.8	93.7	97.0	94.4

	95392	88411	96453A	91393	C7	C123
SiO_2	76.85	76.98	77.99	75.29	78.48	78.32
TiO_2	0.06	0.12	0.11	0.14	0.10	0.08
Al_2O_3	13.07	12.50	11.88	13.60	11.97	12.22
Fe_2O_3	0.91	1.54	1.50	1.62	1.25	1.08
MgO	0.03	0.05	0.05	0.06	0.03	0.03
CaO	0.28	0.41	0.46	0.61	0.17	0.20
Na_2O	3.96	3.21	3.36	3.76	3.10	2.99
K_2O	4.81	5.15	4.61	4.86	4.85	5.05
MnO_2	0.02	0.02	0.03	0.04	0.04	0.03
P_2O_5	0.0	0.03	0.01	0.02	0.01	0.01
Ba	0.	1010.	744.	1077.	343.	628.
Nb	38.	30.	27.	29.	31.	26.
Zr	105.	177.	143.	199.	128.	103.
Y	42.	97.	73.	90.	63.	49.
Sr	4.	47.	38.	59.	24.	33.
Rb	240.	184.	152.	177.	176.	168.
Zn	40.	44.	41.	134.	39.	31.
Cu	12.	12.	11.	16.	14.	11.
Ni	5.	4.	3.	7.	3.	4.
Pb	30.	26.	24.	53.	31.	26.
U	3.	3.	2.	1.	2.	2.
Th	25.	18.	17.	15.	20.	14.
V	0.	3.	7.	9.	2.	2.
Cr	17.	17.	12.	17.	11.	6.
Nd	33.	66.	67.	74.	64.	32.
La	13.	53.	57.	68.	42.	37.
Ce	74.	105.	114.	117.	91.	67.
Qz	34.4	37.1	39.2	32.8	41.0	40.7
Cor	0.8	1.0	0.6	1.1	1.3	1.5
Or	28.4	30.5	27.3	28.8	28.7	29.9
Ab	33.5	27.2	28.5	31.9	26.3	25.3
An	1.4	1.8	2.2	2.9	0.8	0.9
Hy	0.9	1.5	1.5	1.6	1.3	1.1
Mgtte	0.3	0.6	0.6	0.6	0.5	0.4
Ilm	0.1	0.2	0.2	0.3	0.2	0.2
Aptte	0.0	0.1	0.0	0.0	0.0	0.0
DI	96.4	94.8	94.9	93.4	95.9	95.9

	C139	C155	96391	96413	95412	96452A
SiO_2	77.20	78.54	77.55	76.50	76.35	76.84
TiO_2	0.10	0.06	0.08	0.13	0.12	0.07
Al_2O_3	12.52	12.10	12.30	12.90	12.87	13.04
Fe_2O_3	1.19	1.06	1.15	1.25	1.66	0.90
MgO	0.0	0.03	0.05	0.06	0.05	0.06
CaO	0.43	0.18	0.52	0.64	0.53	0.34
Na_2O	3.24	3.10	3.33	3.52	3.41	3.15
K_2O	5.25	4.90	4.98	4.95	4.98	5.59
MnO_2	0.02	0.02	0.03	0.02	0.03	0.02
P_2O_5	0.03	0.01	0.01	0.03	0.02	0.0
Ba	1097.	45.	808.	1123.	21.	54.
Nb	27.	31.	26.	30.	30.	28.
Zr	140.	95.	106.	181.	80.	86.
Y	66.	51.	62.	103.	28.	106.
Sr	49.	12.	37.	53.	8.	11.
Rb	163.	191.	160.	159.	232.	196.
Zn	31.	30.	36.	50.	33.	27.
Cu	11.	11.	12.	12.	12.	11.
Ni	6.	5.	4.	5.	5.	7.
Pb	26.	27.	25.	25.	29.	28.
U	4.	2.	2.	2.	3.	3.
Th	18.	21.	19.	18.	20.	24.
V	3.	0.	3.	7.	2.	3.
Cr	9.	12.	12.	8.	6.	7.
Nd	53.	36.	50.	99.	22.	53.
La	43.	30.	33.	83.	3.	34.
Ce	93.	55.	70.	173.	24.	55.
Qz	37.0	40.9	37.5	35.2	35.6	35.9
Cor	0.8	1.4	0.5	0.7	1.0	1.2
Or	31.1	29.0	29.5	29.3	29.5	33.1
Ab	27.4	26.3	28.2	29.8	28.9	26.7
An	1.9	0.8	2.5	3.0	2.5	1.7
Hy	1.1	1.1	1.2	1.2	1.7	1.0
Mgtte	0.4	0.4	0.4	0.5	0.6	0.3
Ilm	0.2	0.1	0.2	0.2	0.2	0.1
Aptte	0.1	0.0	0.0	0.1	0.0	0.0
DI	95.5	96.2	95.1	94.3	94.0	95.7

	00422	96423	95412C	96413	95412	96452A
SiO_2	77.86	76.90	77.88	76.50	76.35	76.84
TiO_2	0.09	0.11	0.08	0.13	0.12	0.07
Al_2O_3	12.26	12.53	12.25	12.90	12.87	13.04
Fe_2O_3	1.21	1.42	1.16	1.25	1.66	0.90
MgO	0.04	0.06	0.06	0.06	0.05	0.06
CaO	0.37	0.55	0.75	0.64	0.53	0.34
Na_2O	3.21	3.28	3.01	3.52	3.41	3.15
K_2O	4.92	5.13	4.79	4.95	4.98	5.59
MnO_2	0.02	0.02	0.02	0.02	0.03	0.02
P_2O_5	0.01	0.01	0.01	0.03	0.02	0.0
Ba	400.	813.	720.	1123.	21.	54.
Nb	33.	26.	23.	30.	30.	28.
Zr	131.	150.	136.	181.	80.	86.
Y	73.	46.	62.	103.	28.	106.
Sr	22.	58.	42.	53.	8.	11.
Rb	187.	162.	152.	159.	232.	196.
Zn	38.	33.	31.	50.	33.	27.
Cu	12.	11.	11.	12.	12.	11.
Ni	5.	4.	4.	5.	5.	7.
Pb	28.	25.	24.	25.	29.	28.
U	4.	3.	3.	2.	3.	3.
Th	18.	16.	15.	18.	20.	24.
V	5.	9.	3.	7.	2.	3.
Cr	15.	12.	17.	8.	6.	7.
Nd	57.	46.	48.	99.	22.	53.
La	53.	33.	39.	83.	3.	34.
Ce	111.	67.	61.	173.	24.	55.
Qz	39.1	36.4	39.9	35.2	35.6	35.9
Cor	1.0	0.6	0.8	0.7	1.0	1.2
Or	29.1	30.3	28.3	29.3	29.5	33.1
Ab	27.2	27.8	25.5	29.8	28.9	26.7
An	1.8	2.7	3.7	3.0	2.5	1.7
Hy	1.2	1.5	1.2	1.2	1.7	1.0
Mgtte	0.4	0.5	0.4	0.5	0.6	0.3
Ilm	0.2	0.2	0.2	0.2	0.2	0.1
Aptte	0.0	0.0	0.0	0.1	0.0	0.0
DI	95.4	94.5	93.7	94.3	94.0	95.7

ANALYSES OF NORTHERN ARRAN FINE GRANITE

	94461	95452	91441	92461	91452	91462A
SiO_2	77.69	77.02	76.99	77.19	75.91	77.00
TiO_2	0.07	0.07	0.06	0.07	0.07	0.07
Al_2O_3	12.64	12.80	12.99	12.87	13.58	13.03
Fe_2O_3	1.01	1.12	1.03	1.06	1.03	1.07
MgO	0.02	0.02	0.03	0.03	0.02	0.03
CaO	0.03	0.12	0.27	0.31	0.44	0.17
Na_2O	3.76	3.80	3.59	3.25	3.53	3.52
K_2O	4.74	5.01	5.00	5.17	5.39	5.08
MnO_2	0.02	0.03	0.03	0.03	0.03	0.03
P_2O_5	0.02	0.01	0.01	0.01	0.01	0.01
Ba	90.	24.	10.	2.	0.	19.
Nb	35.	43.	44.	38.	43.	43.
Zr	120.	130.	132.	131.	139.	143.
Y	54.	37.	138.	98.	104.	105.
Sr	6.	5.	5.	9.	7.	6.
Rb	211.	228.	243.	232.	237.	222.
Zn	33.	36.	44.	57.	37.	34.
Cu	13.	13.	12.	15.	13.	13.
Ni	1.	6.	4.	5.	5.	5.
Pb	29.	32.	32.	33.	32.	29.
U	2.	3.	2.	1.	2.	1.
Th	20.	23.	25.	22.	28.	26.
V	5.	6.	3.	3.	3.	5.
Cr	15.	16.	11.	12.	22.	31.
Nd	37.	19.	50.	49.	48.	51.
La	24.	13.	40.	41.	29.	44.
Ce	63.	43.	71.	82.	79.	86.
Qz	37.3	35.1	36.0	37.4	33.4	36.3
Cor	1.3	0.9	1.2	1.4	1.2	1.5
Or	28.0	29.6	29.6	30.6	31.9	30.0
Ab	31.8	32.2	30.4	27.5	29.9	29.8
An	0.0	0.5	1.3	1.5	2.1	0.8
Hy	0.9	1.0	1.0	1.0	0.9	1.0
Mgtte	0.4	0.5	0.4	0.5	0.4	0.5
Ilm	0.1	0.1	0.1	0.1	0.1	0.1
Aptte	0.0	0.0	0.0	0.0	0.0	0.0
DI	97.2	96.9	96.0	95.5	95.2	96.2

	94452	91462	92451	90453	92452	90442A
SiO_2	77.44	77.00	76.91	77.04	77.45	75.97
TiO_2	0.08	0.07	0.06	0.08	0.08	0.09
Al_2O_3	12.65	12.75	13.03	13.06	12.47	13.39
Fe_2O_3	1.14	1.13	0.98	1.20	1.13	1.18
MgO	0.03	0.03	0.03	0.03	0.03	0.03
CaO	0.20	0.33	0.10	0.14	0.14	0.20
Na_2O	3.50	3.61	3.95	3.44	3.47	3.84
K_2O	4.92	5.04	4.91	4.95	5.18	5.26
MnO_2	0.03	0.03	0.03	0.03	0.03	0.03
P_2O_5	0.01	0.01	0.01	0.02	0.02	0.01
Ba	20.	24.	0.	60.	53.	28.
Nb	36.	41.	43.	40.	37.	42.
Zr	139.	141.	140.	152.	133.	118.
Y	102.	64.	74.	69.	47.	70.
Sr	7.	6.	4.	8.	6.	6.
Rb	193.	230.	249.	216.	230.	219.
Zn	54.	40.	43.	43.	41.	45.
Cu	17.	13.	13.	13.	12.	13.
Ni	6.	7.	2.	7.	1.	2.
Pb	33.	32.	30.	29.	32.	31.
U	2.	1.	2.	2.	2.	2.
Th	23.	23.	28.	29.	23.	25.
V	5.	5.	3.	6.	6.	3.
Cr	18.	15.	14.	12.	15.	7.
Nd	67.	37.	50.	37.	19.	52.
La	64.	25.	31.	21.	20.	37.
Ce	127.	70.	76.	70.	60.	74.
Qz	37.4	35.6	34.5	37.4	36.7	32.6
Cor	1.2	0.8	1.1	1.8	0.9	1.0
Or	29.1	29.8	29.0	29.3	30.6	31.1
Ab	29.6	30.6	33.4	29.1	29.4	32.5
An	0.9	1.6	0.4	0.6	0.6	0.9
Hy	1.0	1.1	0.9	1.1	1.0	1.1
Mgtte	0.5	0.5	0.4	0.5	0.5	0.5
Ilm	0.2	0.1	0.1	0.2	0.2	0.2
Aptte	0.0	0.0	0.0	0.0	0.0	0.0
DI	96.1	96.0	97.0	95.8	96.8	96.3

	95461	95451	96441	91451	96442	92462
SiO_2	77.07	77.54	76.54	77.24	75.62	76.88
TiO_2	0.08	0.07	0.08	0.10	0.07	0.07
Al_2O_3	12.57	12.43	13.05	12.57	14.01	13.00
Fe_2O_3	1.11	1.04	1.20	1.23	1.07	1.04
MgO	0.03	0.03	0.03	0.01	0.02	0.06
CaO	0.28	0.23	0.19	0.23	0.04	0.20
Na_2O	3.85	3.70	3.62	3.80	4.04	3.48
K_2O	4.98	4.92	5.25	4.78	5.09	5.24
MnO_2	0.02	0.03	0.03	0.03	0.03	0.03
P_2O_5	0.01	0.02	0.02	0.02	0.01	0.01
Ba	45.	26.	68.	30.	15.	56.
Nb	37.	36.	39.	31.	40.	41.
Zr	139.	136.	140.	106.	134.	107.
Y	88.	100.	47.	86.	60.	4.
Sr	6.	8.	7.	6.	5.	7.
Rb	212.	198.	214.	196.	242.	222.
Zn	23.	35.	49.	41.	35.	30.
Cu	13.	15.	14.	13.	13.	13.
Ni	3.	4.	4.	5.	2.	5.
Pb	31.	29.	33.	29.	29.	31.
U	3.	2.	1.	2.	2.	2.
Th	26.	24.	24.	23.	27.	22.
V	5.	6.	5.	3.	3.	6.
Cr	9.	7.	13.	9.	7.	27.
Nd	44.	44.	29.	55.	24.	35.
La	33.	35.	21.	48.	21.	30.
Ce	65.	72.	56.	94.	55.	69.
Qz	34.6	36.3	34.6	36.0	32.2	35.7
Cor	0.4	0.6	1.1	0.8	1.8	1.3
Or	29.5	29.1	31.0	28.3	30.1	31.0
Ab	32.6	31.3	30.7	32.2	34.2	29.5
An	1.3	1.0	0.8	1.0	0.1	0.9
Hy	1.0	1.0	1.1	1.0	1.0	1.0
Mgtte	0.5	0.4	0.5	0.5	0.5	0.4
Ilm	0.2	0.1	0.2	0.2	0.1	0.1
Aptte	0.0	0.0	0.0	0.0	0.0	0.0
DI	96.7	96.7	96.3	96.4	96.5	96.2

	92442	90444	C1	C5	C8	C29
SiO_2	76.88	76.81	77.66	77.34	77.67	77.67
TiO_2	0.07	0.07	0.06	0.06	0.06	0.07
Al_2O_3	13.00	13.08	12.62	12.93	12.66	12.55
Fe_2O_3	1.04	1.08	0.97	1.05	1.03	1.05
MgO	0.06	0.02	0.02	0.02	0.03	0.02
CaO	0.20	0.16	0.15	0.08	0.11	0.13
Na_2O	3.48	3.75	3.72	3.64	3.53	3.54
K_2O	5.24	4.99	4.76	4.84	4.87	4.93
MnO_2	0.03	0.03	0.02	0.02	0.03	0.03
P_2O_5	0.01	0.01	0.01	0.02	0.01	0.02
Ba	45.	23.	0.	0.	26.	71.
Nb	42.	42.	35.	42.	46.	37.
Zr	144.	133.	120.	131.	135.	131.
Y	59.	74.	57.	52.	47.	74.
Sr	5.	7.	5.	4.	5.	8.
Rb	233.	226.	223.	227.	226.	224.
Zn	46.	44.	46.	39.	47.	43.
Cu	13.	13.	11.	11.	11.	11.
Ni	4.	1.	6.	6.	7.	6.
Pb	34.	33.	28.	27.	29.	28.
U	2.	2.	3.	4.	3.	4.
Th	27.	26.	21.	24.	25.	22.
V	5.	3.	2.	0.	0.	2.
Cr	8.	9.	7.	7.	5.	7.
Nd	48.	50.	48.	41.	34.	69.
La	33.	38.	39.	21.	26.	47.
Ce	71.	62.	90.	62.	93.	96.
Qz	35.7	35.2	37.1	37.1	37.9	37.6
Cor	1.3	1.2	1.1	1.6	1.4	1.2
Or	31.0	29.5	28.2	28.6	28.8	29.2
Ab	29.5	31.8	31.5	30.8	29.9	30.0
An	0.9	0.7	0.7	0.3	0.5	0.5
Hy	1.0	1.0	0.9	1.0	1.0	1.0
Mgtte	0.4	0.5	0.4	0.5	0.4	0.5
Ilm	0.1	0.1	0.1	0.1	0.1	0.1
Aptte	0.0	0.0	0.0	0.0	0.0	0.0
DI	96.2	96.4	96.8	96.6	96.6	96.7

	C30	C31	C32	C34	C35	C36
SiO_2	77.72	74.70	77.50	77.44	77.76	77.44
TiO_2	0.07	0.32	0.06	0.07	0.07	0.05
Al_2O_3	12.58	12.28	12.67	12.56	12.35	12.70
Fe_2O_3	1.00	3.61	1.03	1.04	1.11	0.98
MgO	0.02	0.13	0.02	0.02	0.02	0.0
CaO	0.20	1.26	0.18	0.35	0.18	0.09
Na_2O	3.46	3.88	3.56	3.57	3.56	3.94
K_2O	4.91	3.69	4.94	4.91	4.91	4.77
MnO_2	0.02	0.07	0.03	0.03	0.03	0.03
P_2O_5	0.02	0.07	0.01	0.02	0.02	0.01
Ba	23.	265.	8.	52.	37.	0.
Nb	38.	48.	39.	36.	32.	45.
Zr	126.	406.	105.	122.	129.	149.
Y	25.	139.	63.	105.	44.	49.
Sr	6.	41.	5.	7.	7.	3.
Rb	225.	149.	221.	208.	220.	264.
Zn	36.	102.	36.	36.	33.	39.
Cu	10.	11.	11.	11.	11.	11.
Ni	6.	8.	4.	5.	4.	6.
Pb	28.	25.	28.	27.	27.	30.
U	3.	2.	3.	3.	3.	3.
Th	22.	25.	22.	22.	21.	24.
V	0.	14.	2.	2.	3.	2.
Cr	6.	9.	6.	8.	6.	7.
Nd	23.	118.	56.	52.	53.	37.
La	14.	89.	46.	46.	47.	23.
Ce	40.	207.	70.	91.	117.	47.
Qz	38.0	34.2	37.1	36.8	37.5	35.7
Cor	1.3	0.0	1.2	0.8	0.9	0.9
Or	29.0	21.9	29.2	29.0	29.0	28.2
Ab	29.3	32.9	30.1	30.2	30.1	33.4
An	0.9	5.2	0.8	1.6	0.8	0.4
Hy	0.9	3.0	1.0	0.9	1.0	0.9
Mgtte	0.4	1.6	0.4	0.4	0.5	0.4
Ilm	0.1	0.6	0.1	0.1	0.1	0.1
Aptte	0.0	0.2	0.0	0.0	0.0	0.0
DI	96.4	89.0	96.5	96.0	96.7	97.3

	C37	C44	C48	C82	C96	C102
SiO_2	76.96	76.98	77.17	77.54	76.56	77.57
TiO_2	0.04	0.07	0.11	0.08	0.07	0.06
Al_2O_3	12.93	13.05	12.49	12.54	13.23	12.68
Fe_2O_3	1.03	1.07	1.34	1.15	1.11	1.02
MgO	0.0	0.02	0.03	0.03	0.02	0.02
CaO	0.02	0.11	0.43	0.04	0.13	0.13
Na_2O	4.50	3.70	3.34	3.74	3.90	3.60
K_2O	4.48	4.96	5.02	4.84	4.94	4.89
MnO_2	0.02	0.03	0.03	0.03	0.03	0.02
P_2O_5	0.01	0.01	0.03	0.01	0.01	0.01
Ba	0.	26.	757.	48.	43.	13.
Nb	48.	41.	25.	34.	37.	39.
Zr	153.	115.	151.	136.	125.	123.
Y	66.	30.	57.	56.	47.	72.
Sr	5.	5.	38.	7.	6.	7.
Rb	297.	248.	147.	211.	223.	219.
Zn	31.	42.	39.	44.	37.	35.
Cu	11.	10.	11.	12.	11.	10.
Ni	5.	5.	4.	4.	6.	6.
Pb	29.	30.	25.	28.	29.	28.
U	3.	2.	2.	4.	3.	3.
Th	28.	22.	21.	23.	23.	22.
V	2.	0.	3.	3.	0.	3.
Cr	6.	6.	6.	6.	6.	6.
Nd	26.	42.	46.	49.	25.	38.
La	19.	32.	36.	37.	19.	20.
Ce	36.	57.	74.	87.	40.	54.
Qz	33.2	35.8	37.2	36.7	34.3	37.3
Cor	0.7	1.4	0.9	1.1	1.3	1.3
Or	26.5	29.3	29.7	28.6	29.2	28.9
Ab	38.1	31.3	28.3	31.7	33.0	30.5
An	0.0	0.5	1.9	0.1	0.6	0.6
Hy	0.9	1.0	1.2	1.1	1.0	0.9
Mgtte	0.4	0.5	0.6	0.5	0.5	0.4
Ilm	0.1	0.1	0.2	0.2	0.1	0.1
Aptte	0.0	0.0	0.1	0.0	0.0	0.0
DI	97.8	96.5	95.2	97.0	96.5	96.7

	C103	C109	C116	C150	92461	90432
SiO_2	77.93	79.24	77.26	78.08	77.24	76.08
TiO_2	0.11	0.08	0.07	0.09	0.07	0.08
Al_2O_3	12.11	11.52	12.78	12.07	12.81	13.50
Fe_2O_3	1.48	1.08	1.10	1.26	1.00	1.01
MgO	0.03	0.04	0.01	0.04	0.05	0.03
CaO	0.38	0.17	0.14	0.35	0.39	0.29
Na_2O	2.97	3.10	3.57	3.23	3.27	3.72
K_2O	4.93	4.73	5.03	4.84	5.15	5.26
MnO_2	0.03	0.03	0.02	0.03	0.03	0.02
P_2O_5	0.03	0.02	0.02	0.03	0.01	0.01
Ba	797.	356.	45.	843.	0.	52.
Nb	24.	27.	31.	31.	34.	36.
Zr	131.	114.	131.	133.	117.	126.
Y	66.	58.	36.	61.	99.	49.
Sr	40.	23.	7.	40.	10.	7.
Rb	160.	169.	223.	174.	231.	225.
Zn	49.	34.	36.	37.	57.	40.
Cu	11.	11.	11.	11.	12.	12.
Ni	4.	4.	5.	6.	5.	3.
Pb	25.	24.	28.	27.	29.	27.
U	4.	2.	3.	2.	2.	3.
Th	17.	21.	20.	21.	18.	22.
V	5.	2.	3.	3.	5.	3.
Cr	7.	9.	8.	7.	9.	6.
Nd	54.	59.	28.	45.	51.	33.
La	46.	38.	14.	36.	43.	21.
Ce	88.	80.	48.	67.	88.	61.
Qz	40.5	42.3	36.6	39.6	37.3	33.3
Cor	1.3	1.0	1.3	1.0	1.2	1.2
Or	29.2	28.0	29.7	28.6	30.5	31.1
Ab	25.2	26.2	30.2	27.4	27.7	31.5
An	1.7	0.7	0.6	1.5	1.9	1.4
Hy	1.3	1.0	1.0	1.2	1.0	0.9
Mgtte	0.6	0.5	0.5	0.5	0.4	0.4
Ilm	0.2	0.2	0.1	0.2	0.1	0.2
Aptte	0.1	0.0	0.0	0.1	0.0	0.0
DI	94.8	96.6	96.6	95.6	95.4	95.9

	91461	94451	90421	93441	93463	90403
SiO_2	77.04	77.25	76.20	76.39	78.82	76.24
TiO_2	0.08	0.06	0.07	0.07	0.07	0.09
Al_2O_3	12.80	12.83	13.36	13.32	11.74	13.18
Fe_2O_3	1.12	1.01	1.05	0.95	0.91	1.17
MgO	0.04	0.04	0.04	0.04	0.04	0.05
CaO	0.27	0.27	0.31	0.28	0.38	0.54
Na_2O	3.61	3.64	3.88	3.95	3.18	3.50
K_2O	5.01	4.87	5.07	4.96	4.83	5.19
MnO_2	0.03	0.02	0.03	0.03	0.02	0.03
P_2O_5	0.01	0.0	0.0	0.0	0.0	0.01
Ba	0.	0.	97.	8.	260.	51.
Nb	39.	36.	36.	38.	30.	40.
Zr	130.	125.	126.	113.	109.	129.
Y	69.	31.	34.	77.	71.	152.
Sr	6.	3.	9.	5.	19.	10.
Rb	221.	221.	234.	233.	178.	223.
Zn	62.	40.	43.	42.	33.	37.
Cu	11.	12.	11.	11.	11.	11.
Ni	4.	5.	5.	6.	6.	6.
Pb	28.	29.	31.	28.	26.	29.
U	3.	3.	3.	2.	2.	3.
Th	23.	24.	27.	23.	21.	26.
V	2.	3.	2.	2.	0.	3.
Cr	12.	7.	8.	6.	10.	7.
Nd	78.	18.	14.	60.	43.	81.
La	49.	16.	15.	49.	41.	61.
Ce	96.	48.	40.	78.	86.	119.
Qz	35.8	36.4	33.1	33.4	40.6	34.4
Cor	1.0	1.1	0.9	0.9	0.6	0.8
Or	29.6	28.8	30.0	29.3	28.6	30.7
Ab	30.6	30.8	32.9	33.5	26.9	29.6
An	1.3	1.3	1.5	1.4	1.9	2.6
Hy	1.0	1.0	1.0	0.9	0.9	1.1
Mgtte	0.5	0.4	0.5	0.4	0.4	0.5
Ilm	0.2	0.1	0.1	0.1	0.1	0.2
Aptte	0.0	0.0	0.0	0.0	0.0	0.0
DI	96.0	96.1	95.9	96.2	96.1	94.7

	93433	91401	90413	91401A	92461B	92421
SiO_2	76.16	76.61	76.42	77.39	79.19	77.13
TiO_2	0.08	0.07	0.08	0.07	0.07	0.07
Al_2O_3	13.28	13.15	13.06	12.56	11.53	12.93
Fe_2O_3	1.09	1.01	1.03	1.03	0.86	0.92
MgO	0.06	0.04	0.04	0.04	0.04	0.06
CaO	0.45	0.29	0.33	0.29	0.25	0.39
Na_2O	3.71	3.77	3.85	3.70	3.32	3.39
K_2O	5.15	5.03	5.15	4.89	4.72	5.09
MnO_2	0.02	0.03	0.03	0.02	0.02	0.02
P_2O_5	0.0	0.0	0.0	0.01	0.0	0.0
Ba	23.	65.	90.	76.	340.	10.
Nb	46.	38.	36.	37.	32.	41.
Zr	149.	126.	117.	115.	120.	108.
Y	109.	39.	45.	39.	49.	176.
Sr	6.	8.	8.	7.	19.	7.
Rb	218.	225.	225.	216.	183.	219.
Zn	44.	65.	44.	42.	29.	33.
Cu	11.	11.	11.	11.	11.	11.
Ni	5.	5.	4.	4.	6.	8.
Pb	29.	29.	29.	28.	26.	28.
U	4.	3.	3.	3.	3.	3.
Th	25.	22.	24.	21.	20.	25.
V	3.	2.	5.	3.	3.	3.
Cr	5.	6.	7.	14.	10.	5.
Nd	54.	26.	36.	31.	42.	104.
La	49.	21.	31.	19.	34.	80.
Ce	80.	30.	78.	44.	87.	178.
Qz	33.4	34.4	33.2	36.1	40.9	36.7
Cor	0.8	1.0	0.6	0.7	0.5	1.1
Or	30.5	29.7	30.5	28.9	27.9	30.1
Ab	31.4	31.9	32.6	31.3	28.1	28.7
An	2.2	1.4	1.6	1.4	1.2	1.9
Hy	1.1	1.0	1.0	1.0	0.8	0.9
Mgtte	0.5	0.4	0.4	0.4	0.4	0.4
Ilm	0.2	0.1	0.2	0.1	0.1	0.1
Aptte	0.0	0.0	0.0	0.0	0.0	0.0
DI	95.3	96.0	96.2	96.4	96.9	95.5

	91392	92391	95421	93451B	96431	95432
SiO_2	77.69	77.22	81.12	78.19	75.99	77.11
TiO_2	0.07	0.06	0.06	0.07	0.07	0.07
Al_2O_3	12.37	12.77	13.02	12.16	13.54	12.89
Fe_2O_3	1.06	0.97	0.83	0.88	1.00	0.98
MgO	0.04	0.04	0.03	0.06	0.04	0.04
CaO	0.27	0.32	0.27	0.32	0.30	0.30
Na_2O	3.68	3.35	3.97	3.35	3.84	3.57
K_2O	4.80	5.24	0.68	4.96	5.19	5.00
MnO_2	0.02	0.02	0.02	0.02	0.02	0.02
P_2O_5	0.0	0.0	0.01	0.01	0.0	0.01
Ba	8.	92.	0.	208.	101.	27.
Nb	43.	35.	40.	30.	39.	39.
Zr	126.	116.	114.	94.	131.	132.
Y	61.	73.	52.	40.	60.	35.
Sr	9.	12.	4.	13.	9.	6.
Rb	234.	234.	206.	190.	225.	226.
Zn	50.	51.	46.	28.	45.	41.
Cu	12.	11.	10.	11.	11.	12.
Ni	6.	6.	5.	6.	5.	5.
Pb	29.	29.	28.	26.	30.	28.
U	3.	4.	3.	3.	3.	4.
Th	26.	21.	23.	15.	25.	22.
V	2.	2.	3.	2.	2.	5.
Cr	13.	10.	8.	12.	7.	6.
Nd	36.	48.	38.	45.	50.	41.
La	26.	30.	28.	26.	38.	29.
Ce	54.	75.	92.	59.	92.	58.
Qz	36.9	36.6	54.5	38.7	32.7	36.2
Cor	0.6	1.0	5.3	0.7	1.1	1.1
Or	28.4	31.0	4.0	29.3	30.7	29.6
Ab	31.2	28.4	33.6	28.4	32.5	30.2
An	1.3	1.6	1.3	1.5	1.5	1.4
Hy	1.0	0.9	0.8	0.9	0.9	0.9
Mgtte	0.5	0.4	0.4	0.4	0.4	0.4
Ilm	0.1	0.1	0.1	0.1	0.1	0.1
Aptte	0.0	0.0	0.0	0.0	0.0	0.0
DI	96.4	95.9	92.2	96.3	95.9	96.0

	94441	95441	90441	91421	91411	95433
SiO_2	77.21	77.68	77.18	77.54	77.30	77.56
TiO_2	0.07	0.06	0.06	0.08	0.07	0.06
Al_2O_3	12.61	12.43	12.68	12.47	12.55	12.65
Fe_2O_3	1.05	0.98	0.97	1.07	1.07	0.93
MgO	0.05	0.04	0.04	0.04	0.04	0.04
CaO	0.30	0.27	0.38	0.28	0.38	0.30
Na_2O	3.68	3.77	3.90	3.55	3.77	3.65
K_2O	5.01	4.74	4.77	4.95	4.80	4.78
MnO_2	0.02	0.02	0.03	0.02	0.02	0.02
P_2O_5	0.0	0.0	0.0	0.0	0.0	0.0
Ba	42.	24.	8.	0.	59.	0.
Nb	35.	38.	40.	38.	42.	40.
Zr	126.	126.	107.	136.	146.	90.
Y	96.	43.	127.	114.	128.	78.
Sr	7.	6.	7.	8.	6.	4.
Rb	225.	219.	225.	225.	213.	228.
Zn	44.	33.	36.	38.	40.	37.
Cu	11.	11.	11.	12.	11.	11.
Ni	7.	5.	7.	7.	7.	5.
Pb	30.	27.	28.	26.	28.	30.
U	3.	2.	3.	2.	3.	3.
Th	19.	24.	24.	24.	22.	24.
V	3.	2.	0.	3.	2.	0.
Cr	8.	7.	15.	11.	21.	12.
Nd	70.	25.	73.	83.	86.	51.
La	54.	16.	58.	59.	67.	34.
Ce	111.	54.	98.	95.	149.	71.
Qz	35.5	36.6	35.0	36.9	35.7	37.0
Cor	0.6	0.6	0.4	0.8	0.5	0.9
Or	29.6	28.0	28.2	29.3	28.4	28.3
Ab	31.2	31.9	33.0	30.1	31.9	30.9
An	1.5	1.3	1.9	1.4	1.9	1.5
Hy	1.0	0.9	0.9	1.0	1.0	0.9
Mgtte	0.5	0.4	0.4	0.5	0.5	0.4
Ilm	0.1	0.1	0.1	0.2	0.1	0.1
Aptte	0.0	0.0	0.0	0.0	0.0	0.0
DI	96.3	96.6	96.2	96.2	96.1	96.2

	90411	91394	93451A	93463A	95424	C47
SiO_2	77.23	77.55	77.74	78.24	76.53	77.70
TiO_2	0.08	0.07	0.07	0.07	0.05	0.06
Al_2O_3	12.66	12.40	12.49	12.11	13.34	12.67
Fe_2O_3	1.07	0.98	0.99	1.01	0.81	1.01
MgO	0.04	0.04	0.06	0.05	0.03	0.02
CaO	0.31	0.36	0.42	0.46	0.33	0.14
Na_2O	3.69	3.60	3.34	3.28	4.11	3.51
K_2O	4.90	4.97	4.88	4.77	4.77	4.84
MnO_2	0.02	0.02	0.02	0.02	0.02	0.03
P_2O_5	0.0	0.01	0.01	0.0	0.0	0.01
Ba	92.	110.	0.	71.	11.	38.
Nb	33.	35.	35.	36.	48.	37.
Zr	123.	118.	117.	125.	144.	114.
Y	43.	73.	89.	89.	41.	33.
Sr	9.	12.	7.	8.	4.	6.
Rb	214.	210.	218.	209.	255.	225.
Zn	40.	43.	35.	39.	46.	44.
Cu	11.	11.	11.	13.	11.	11.
Ni	6.	5.	5.	6.	5.	6.
Pb	27.	28.	27.	27.	28.	30.
U	3.	2.	2.	2.	4.	2.
Th	18.	23.	24.	20.	30.	24.
V	2.	2.	0.	2.	2.	0.
Cr	17.	9.	10.	14.	13.	6.
Nd	16.	49.	61.	51.	29.	39.
La	16.	37.	51.	38.	22.	28.
Ce	49.	72.	91.	74.	49.	64.
Qz	35.9	36.4	38.3	39.5	33.3	38.1
Cor	0.7	0.5	1.0	0.7	0.8	1.4
Or	29.0	29.4	28.9	28.2	28.2	28.6
Ab	31.2	30.5	28.3	27.8	34.8	29.7
An	1.5	1.7	2.0	2.3	1.6	0.6
Hy	1.0	0.9	1.0	1.0	0.8	0.9
Mgtte	0.5	0.4	0.4	0.4	0.3	0.4
Ilm	0.2	0.1	0.1	0.1	0.1	0.1
Aptte	0.0	0.0	0.0	0.0	0.0	0.0
DI	96.1	96.3	95.4	95.5	96.3	96.4

	93431	95431	93451A	93463A	95424	C47
SiO_2	77.94	77.70	77.74	78.24	76.53	77.70
TiO_2	0.06	0.06	0.07	0.07	0.05	0.06
Al_2O_3	12.23	12.48	12.49	12.11	13.34	12.67
Fe_2O_3	0.93	0.98	0.99	1.01	0.81	1.01
MgO	0.04	0.04	0.06	0.05	0.03	0.02
CaO	0.30	0.29	0.42	0.46	0.33	0.14
Na_2O	3.74	3.72	3.34	3.28	4.11	3.51
K_2O	4.75	4.71	4.88	4.77	4.77	4.84
MnO_2	0.02	0.02	0.02	0.02	0.02	0.03
P_2O_5	0.0	0.0	0.01	0.0	0.0	0.01
Ba	5.	0.	0.	71.	11.	38.
Nb	37.	38.	35.	36.	48.	37.
Zr	115.	133.	117.	125.	144.	114.
Y	60.	32.	89.	89.	41.	33.
Sr	5.	4.	7.	8.	4.	6.
Rb	220.	239.	218.	209.	255.	225.
Zn	33.	49.	35.	39.	46.	44.
Cu	10.	11.	11.	13.	11.	11.
Ni	6.	5.	5.	6.	5.	6.
Pb	27.	31.	27.	27.	28.	30.
U	2.	3.	2.	2.	4.	2.
Th	23.	20.	24.	20.	30.	24.
V	2.	2.	0.	2.	2.	0.
Cr	11.	15.	10.	14.	13.	6.
Nd	48.	28.	61.	51.	29.	39.
La	36.	27.	51.	38.	22.	28.
Ce	69.	46.	91.	74.	49.	64.
Qz	37.0	37.0	38.3	39.5	33.3	38.1
Cor	0.4	0.7	1.0	0.7	0.8	1.4
Or	28.1	27.9	28.9	28.2	28.2	28.6
Ab	31.7	31.5	28.3	27.8	34.8	29.7
An	1.5	1.4	2.0	2.3	1.6	0.6
Hy	0.9	0.9	1.0	1.0	0.8	0.9
Mgtte	0.4	0.4	0.4	0.4	0.3	0.4
Ilm	0.1	0.1	0.1	0.1	0.1	0.1
Aptte	0.0	0.0	0.0	0.0	0.0	0.0
DI	96.7	96.4	95.4	95.5	96.3	96.4

ANALYSES OF MISCELLANEOUS ROCKS FROM THE NORTHERN ARRAN GRANITE

	1	5a	1909	1902	1912	1901
SiO_2	77.08	76.99	77.88	78.25	77.15	76.22
TiO_2	0.06	0.08	0.07	0.09	0.08	0.08
Al_2O_3	12.90	12.89	12.22	11.98	12.56	12.83
Fe_2O_3	1.04	1.13	0.99	1.22	1.06	1.41
MgO	0.02	0.03	0.05	0.03	0.07	0.03
CaO	0.33	0.33	0.40	0.21	0.32	0.40
Na_2O	3.59	3.35	3.32	3.18	3.68	3.81
K_2O	4.94	5.17	5.02	4.98	5.04	5.16
MnO_2	0.03	0.03	0.02	0.03	0.03	0.04
P_2O_5	0.02	0.01	0.02	0.02	0.01	0.01
Ba	36.	67.	131.	347.	83.	30.
Nb	41.	37.	32.	33.	35.	48.
Zr	140.	121.	108.	112.	113.	195.
Y	89.	62.	87.	84.	92.	127.
Sr	6.	7.	12.	20.	8.	5.
Rb	217.	205.	183.	179.	211.	222.
Zn	35.	41.	31.	32.	30.	38.
Cu	13.	14.	13.	13.	12.	13.
Ni	1.	3.	4.	5.	3.	4.
Pb	30.	30.	27.	26.	29.	31.
U	3.	2.	2.	2.	3.	3.
Th	22.	24.	23.	21.	22.	29.
V	5.	3.	3.	6.	3.	3.
Cr	18.	17.	13.	7.	8.	8.
Nd	42.	30.	39.	43.	42.	54.
La	37.	18.	32.	34.	38.	46.
Ce	80.	61.	69.	70.	78.	105.

	2302	909	907	1107	1400	3
SiO_2	76.87	76.48	77.62	77.04	77.28	76.20
TiO_2	0.07	0.07	0.08	0.07	0.08	0.06
Al_2O_3	12.99	13.08	12.32	12.65	12.59	13.51
Fe_2O_3	1.00	1.04	1.04	1.13	1.18	1.07
MgO	0.03	0.03	0.02	0.02	0.04	0.03
CaO	0.20	0.16	0.28	0.34	0.34	0.31
Na_2O	3.65	4.03	3.58	3.89	3.42	3.62
K_2O	5.16	5.06	5.01	4.81	5.03	5.17
MnO_2	0.02	0.03	0.03	0.02	0.03	0.03
P_2O_5	0.01	0.02	0.02	0.01	0.01	0.01
Ba	29.	46.	290.	49.	326.	12.
Nb	39.	37.	36.	44.	32.	41.
Zr	130.	115.	135.	154.	116.	137.
Y	56.	28.	42.	69.	87.	44.
Sr	5.	5.	16.	8.	21.	5.
Rb	215.	255.	198.	186.	174.	226.
Zn	35.	42.	35.	36.	41.	38.
Cu	13.	12.	13.	14.	13.	14.
Ni	3.	2.	2.	8.	2.	2.
Pb	33.	30.	31.	34.	29.	31.
U	2.	2.	1.	3.	1.	3.
Th	22.	24.	22.	29.	20.	26.
V	3.	5.	6.	6.	7.	6.
Cr	7.	7.	9.	7.	10.	6.
Nd	33.	17.	29.	22.	52.	27.
La	25.	6.	14.	16.	34.	15.
Ce	85.	27.	51.	54.	67.	50.

	5	4	1904	1108	1602	1403
SiO_2	76.58	76.50	78.74	76.73	76.76	76.50
TiO_2	0.07	0.07	0.07	0.02	0.11	0.08
Al_2O_3	13.31	13.32	11.73	12.98	12.63	13.12
Fe_2O_3	1.07	1.12	1.05	0.93	1.31	1.08
MgO	0.03	0.02	0.04	0.0	0.04	0.03
CaO	0.31	0.39	0.21	0.0	0.40	0.33
Na_2O	3.42	3.22	3.21	4.66	3.86	3.24
K_2O	5.16	5.31	4.89	4.64	4.84	5.59
MnO_2	0.03	0.03	0.03	0.03	0.03	0.02
P_2O_5	0.01	0.01	0.01	0.02	0.02	0.01
Ba	257.	0.	183.	143.	250.	70.
Nb	41.	44.	33.	61.	35.	34.
Zr	137.	131.	116.	179.	167.	120.
Y	109.	124.	92.	47.	83.	96.
Sr	7.	7.	11.	7.	17.	13.
Rb	219.	234.	176.	390.	179.	185.
Zn	39.	45.	36.	38.	41.	28.
Cu	13.	13.	13.	14.	13.	13.
Ni	3.	2.	3.	4.	4.	1.
Pb	30.	32.	27.	42.	28.	28.
U	2.	2.	1.	3.	2.	2.
Th	25.	24.	22.	34.	22.	24.
V	3.	8.	6.	6.	5.	5.
Cr	7.	8.	14.	6.	7.	9.
Nd	50.	51.	34.	14.	39.	41.
La	35.	46.	30.	1.	36.	37.
Ce	76.	54.	71.	22.	77.	78.

	1703	1914	1915	2500	2200	1701a
SiO_2	75.87	76.83	78.28	76.37	75.33	76.70
TiO_2	0.17	0.09	0.07	0.07	0.15	0.08
Al_2O_3	13.09	13.29	12.33	13.24	13.40	12.90
Fe_2O_3	1.83	1.16	0.97	1.07	1.63	1.24
MgO	0.12	0.04	0.08	0.02	0.07	0.03
CaO	0.30	0.15	0.15	0.11	0.44	0.23
Na_2O	3.30	3.12	3.04	3.89	3.62	3.87
K_2O	5.24	5.28	5.05	5.21	5.29	4.89
MnO_2	0.04	0.02	0.01	0.03	0.03	0.03
P_2O_5	0.03	0.01	0.02	0.01	0.04	0.02
Ba	979.	304.	331.	296.	828.	459.
Nb	32.	32.	32.	43.	33.	37.
Zr	185.	111.	93.	110.	188.	138.
Y	85.	69.	66.	97.	93.	70.
Sr	47.	15.	17.	13.	42.	22.
Rb	161.	186.	182.	239.	176.	207.
Zn	44.	35.	30.	36.	41.	39.
Cu	13.	13.	12.	14.	13.	13.
Ni	2.	0.	9.	6.	9.	4.
Pb	25.	27.	27.	31.	27.	30.
U	2.	1.	1.	1.	2.	2.
Th	21.	19.	20.	28.	21.	22.
V	9.	5.	6.	5.	8.	7.
Cr	17.	8.	17.	13.	17.	8.
Nd	70.	49.	38.	48.	68.	25.
La	77.	47.	38.	37.	62.	19.
Ce	125.	70.	58.	63.	115.	46.

	1700a	1401	1903	2	5	C39
SiO_2	76.86	75.94	76.71	76.36	76.58	76.79
TiO_2	0.06	0.11	0.05	0.06	0.07	0.03
Al_2O_3	12.97	13.25	12.94	13.41	13.31	12.95
Fe_2O_3	0.89	1.41	1.04	0.99	1.07	0.98
MgO	0.02	0.04	0.02	0.02	0.03	0.0
CaO	0.30	0.32	0.36	0.24	0.31	0.0
Na_2O	3.98	3.80	4.08	3.76	3.42	4.65
K_2O	4.89	5.07	4.75	5.12	5.16	4.57
MnO_2	0.02	0.03	0.03	0.02	0.03	0.03
P_2O_5	0.01	0.03	0.02	0.01	0.01	0.02
Ba	10.	571.	19.	21.	39.	0.
Nb	0.	34.	49.	38.	41.	75.
Zr	35.	161.	145.	125.	134.	293.
Y	61.	98.	124.	43.	109.	58.
Sr	9.	28.	3.	5.	7.	1.
Rb	182.	185.	258.	216.	217.	354.
Zn	29.	39.	34.	37.	40.	40.
Cu	12.	13.	13.	13.	13.	11.
Ni	5.	4.	10.	8.	1.	6.
Pb	29.	30.	32.	31.	31.	33.
U	2.	2.	3.	3.	3.	4.
Th	21.	21.	26.	25.	23.	36.
V	5.	7.	5.	2.	5.	0.
Cr	8.	10.	19.	9.	6.	6.
Nd	29.	34.	47.	28.	52.	25.
La	15.	33.	31.	16.	38.	14.
Ce	21.	60.	58.	43.	71.	27.

	C79	C10	C11	C17	C24	C25
SiO_2	78.31	76.91	77.15	77.75	76.85	77.93
TiO_2	0.07	0.05	0.10	0.03	0.04	0.04
Al_2O_3	12.22	12.86	12.66	12.60	13.03	12.36
Fe_2O_3	0.99	1.04	1.23	0.76	0.89	0.87
MgO	0.02	0.0	0.03	0.04	0.02	0.0
CaO	0.10	0.23	0.35	0.12	0.18	0.18
Na_2O	3.38	4.33	3.71	3.78	4.34	3.99
K_2O	4.87	4.52	4.72	4.86	4.61	4.59
MnO_2	0.02	0.02	0.03	0.03	0.02	0.02
P_2O_5	0.01	0.02	0.03	0.01	0.01	0.02
Ba	43.	75.	528.	0.	2.	0.
Nb	30.	37.	32.	38.	41.	34.
Zr	99.	103.	133.	65.	123.	102.
Y	126.	83.	87.	76.	72.	59.
Sr	7.	11.	28.	6.	3.	5.
Rb	191.	187.	182.	250.	211.	238.
Zn	30.	31.	45.	35.	28.	35.
Cu	11.	11.	12.	11.	11.	11.
Ni	6.	5.	6.	4.	4.	5.
Pb	26.	30.	28.	29.	29.	29.
U	2.	4.	4.	2.	3.	3.
Th	19.	25.	21.	23.	29.	25.
V	2.	2.	3.	3.	0.	0.
Cr	6.	6.	11.	6.	7.	19.
Nd	69.	33.	41.	32.	32.	34.
La	49.	19.	30.	19.	14.	25.
Ce	90.	29.	55.	32.	30.	49.

	C46	C49	C50	C75	C76	C84
SiO_2	76.89	78.05	74.16	76.98	77.24	77.60
TiO_2	0.09	0.09	0.15	0.01	0.11	0.05
Al_2O_3	12.64	12.24	14.39	12.62	12.21	12.39
Fe_2O_3	1.23	1.14	1.65	0.88	1.55	1.04
MgO	0.03	0.03	0.06	0.0	0.05	0.02
CaO	0.44	0.27	0.44	0.18	0.57	0.27
Na_2O	3.61	3.13	3.62	5.03	3.75	4.15
K_2O	5.02	5.01	5.46	4.26	4.46	4.44
MnO_2	0.03	0.03	0.04	0.03	0.04	0.03
P_2O_5	0.03	0.02	0.03	0.02	0.03	0.01
Ba	665.	283.	1016.	0.	417.	33.
Nb	29.	26.	29.	74.	33.	37.
Zr	143.	141.	192.	129.	168.	99.
Y	73.	72.	96.	159.	88.	113.
Sr	36.	19.	55.	2.	28.	7.
Rb	182.	160.	187.	358.	184.	238.
Zn	36.	111.	276.	36.	49.	45.
Cu	11.	20.	23.	11.	11.	11.
Ni	5.	5.	6.	7.	4.	8.
Pb	27.	26.	32.	39.	23.	31.
U	3.	2.	3.	3.	2.	3.
Th	21.	21.	17.	43.	22.	23.
V	3.	2.	7.	0.	7.	2.
Cr	5.	7.	7.	8.	7.	6.
Nd	34.	62.	76.	31.	65.	32.
La	26.	40.	62.	13.	45.	21.
Ce	63.	77.	169.	38.	97.	35.

	C86	C91	C97	C100	C126	C129
SiO_2	77.16	78.35	77.97	96.98	78.10	78.12
TiO_2	0.05	0.04	0.05	0.0	0.05	0.09
Al_2O_3	12.50	12.26	12.31	1.68	12.20	11.94
Fe_2O_3	1.07	0.96	1.02	0.03	1.00	1.10
MgO	0.02	0.02	0.03	0.0	0.02	0.13
CaO	0.36	0.09	0.12	0.0	0.17	0.27
Na_2O	4.33	3.74	4.12	0.67	3.91	2.88
K_2O	4.46	4.50	4.34	0.64	4.52	5.44
MnO_2	0.03	0.02	0.03	0.0	0.02	0.02
P_2O_5	0.02	0.02	0.01	0.01	0.02	0.02
Ba	181.	13.	212.	121.	27.	1100.
Nb	39.	36.	49.	33.	37.	25.
Zr	109.	91.	107.	86.	96.	112.
Y	105.	56.	105.	60.	82.	58.
Sr	15.	6.	14.	13.	7.	45.
Rb	222.	219.	224.	172.	219.	155.
Zn	38.	41.	40.	39.	34.	43.
Cu	11.	11.	11.	10.	10.	12.
Ni	7.	5.	6.	5.	6.	5.
Pb	30.	30.	31.	23.	30.	26.
U	3.	4.	4.	4.	3.	2.
Th	23.	22.	30.	19.	24.	17.
V	2.	2.	2.	1.	3.	3.
Cr	6.	6.	6.	6.	7.	9.
Nd	43.	34.	35.	22.	35.	49.
La	26.	15.	21.	18.	19.	50.
Ce	55.	17.	38.	27.	41.	68.

	C152	2	1	5	5a	3
SiO_2	77.82	76.36	77.08	76.58	76.99	76.20
TiO_2	0.06	0.06	0.06	0.07	0.08	0.06
Al_2O_3	12.39	13.41	12.90	13.31	12.89	13.51
Fe_2O_3	0.99	0.99	1.04	1.07	1.13	1.07
MgO	0.06	0.02	0.02	0.03	0.03	0.03
CaO	0.20	0.24	0.33	0.31	0.33	0.31
Na_2O	3.74	3.76	3.59	3.42	3.35	3.62
K_2O	4.70	5.12	4.94	5.16	5.17	5.17
MnO_2	0.01	0.02	0.03	0.03	0.03	0.03
P_2O_5	0.02	0.01	0.02	0.01	0.01	0.01
Ba	194.	0.	54.	18.	43.	0.
Nb	35.	35.	38.	39.	35.	38.
Zr	103.	111.	123.	117.	105.	122.
Y	64.	39.	78.	100.	53.	39.
Sr	15.	6.	7.	7.	7.	5.
Rb	194.	218.	225.	219.	217.	224.
Zn	32.	34.	34.	38.	40.	37.
Cu	11.	11.	11.	11.	12.	12.
Ni	4.	6.	6.	6.	5.	4.
Pb	27.	30.	29.	28.	29.	30.
U	3.	2.	3.	3.	4.	4.
Th	24.	23.	26.	26.	21.	24.
V	0.	0.	0.	0.	0.	3.
Cr	6.	8.	18.	6.	17.	7.
Nd	34.	41.	56.	60.	32.	28.
La	17.	23.	44.	46.	19.	21.
Ce	41.	58.	86.	90.	57.	51.

	4	98432F	98432W	98431F	98431W	5000FC
SiO_2	76.50	70.69	71.52	77.18	75.49	77.01
TiO_2	0.07	0.50	0.41	0.11	0.14	0.10
Al_2O_3	13.32	13.74	13.71	12.33	12.89	12.69
Fe_2O_3	1.12	4.61	4.09	1.33	2.13	1.39
MgO	0.02	0.17	0.13	0.05	0.06	0.05
CaO	0.39	1.73	1.50	0.60	0.58	0.44
Na_2O	3.22	4.28	4.36	3.33	3.38	3.44
K_2O	5.31	4.07	4.14	5.02	5.29	4.84
MnO_2	0.03	0.10	0.08	0.03	0.02	0.02
P_2O_5	0.01	0.11	0.07	0.01	0.01	0.01
Ba	0.	782.	732.	1035.	1233.	748.
Nb	40.	58.	55.	22.	26.	33.
Zr	114.	635.	530.	146.	176.	167.
Y	111.	153.	144.	52.	49.	73.
Sr	7.	64.	63.	53.	55.	36.
Rb	231.	183.	181.	145.	159.	177.
Zn	46.	165.	152.	40.	42.	40.
Cu	11.	12.	12.	12.	11.	11.
Ni	6.	7.	7.	6.	5.	5.
Pb	30.	22.	23.	25.	25.	27.
U	4.	4.	4.	3.	2.	2.
Th	19.	29.	32.	16.	17.	20.
V	3.	24.	17.	5.	7.	7.
Cr	9.	6.	16.	8.	7.	5.
Nd	61.	151.	147.	65.	55.	50.
La	45.	137.	124.	57.	50.	37.
Ce	55.	274.	273.	124.	110.	93.

	5000CC	96401Q	96412F	97381BF	97422F	4210
SiO_2	76.71	81.53	77.14	77.41	76.75	77.63
TiO_2	0.09	0.05	0.05	0.05	0.07	0.07
Al_2O_3	12.88	10.22	13.05	12.60	12.96	12.48
Fe_2O_3	1.38	0.74	0.77	0.89	1.01	0.99
MgO	0.05	0.04	0.04	0.04	0.04	0.04
CaO	0.43	0.28	0.31	0.27	0.33	0.24
Na_2O	3.43	2.94	3.52	3.97	3.75	3.73
K_2O	5.00	4.18	5.10	4.74	5.07	4.79
MnO_2	0.02	0.01	0.02	0.03	0.02	0.03
P_2O_5	0.01	0.01	0.01	0.0	0.01	0.01
Ba	708.	14.	9.	0.	16.	0.
Nb	31.	25.	30.	42.	34.	40.
Zr	153.	75.	73.	99.	124.	133.
Y	70.	38.	39.	61.	57.	53.
Sr	36.	10.	8.	5.	6.	4.
Rb	176.	161.	209.	261.	209.	251.
Zn	40.	28.	33.	40.	35.	42.
Cu	11.	11.	10.	11.	10.	13.
Ni	5.	6.	5.	6.	6.	5.
Pb	26.	26.	31.	29.	28.	28.
U	2.	3.	2.	4.	3.	2.
Th	20.	19.	19.	25.	23.	26.
V	3.	2.	0.	2.	2.	3.
Cr	19.	25.	12.	19.	13.	19.
Nd	52.	28.	19.	33.	20.	48.
La	46.	19.	15.	18.	12.	28.
Ce	95.	45.	46.	41.	42.	74.

	4220	4410	96453AA	96453AC	4100	5010
SiO_2	79.14	76.64	77.78	77.65	77.38	77.53
TiO_2	0.06	0.04	0.12	0.07	0.04	0.07
Al_2O_3	11.67	12.87	12.02	12.41	12.62	12.57
Fe_2O_3	0.88	0.85	1.26	0.90	0.80	0.97
MgO	0.05	0.03	0.04	0.04	0.03	0.04
CaO	0.31	0.07	0.31	0.26	0.30	0.31
Na_2O	3.01	4.95	3.42	3.40	4.37	3.65
K_2O	4.85	4.52	5.02	5.24	4.43	4.84
MnO_2	0.02	0.03	0.02	0.02	0.03	0.02
P_2O_5	0.01	0.0	0.01	0.01	0.0	0.0
Ba	269.	3.	170.	457.	0.	0.
Nb	24.	84.	30.	26.	79.	36.
Zr	98.	190.	125.	90.	99.	118.
Y	44.	32.	67.	48.	50.	43.
Sr	20.	1.	16.	24.	12.	9.
Rb	171.	476.	200.	196.	308.	208.
Zn	31.	39.	37.	28.	29.	37.
Cu	11.	11.	11.	10.	11.	11.
Ni	5.	6.	5.	5.	6.	4.
Pb	25.	35.	28.	27.	36.	27.
U	4.	4.	2.	2.	4.	3.
Th	15.	32.	22.	17.	25.	18.
V	3.	0.	3.	2.	2.	5.
Cr	9.	13.	14.	11.	14.	13.
Nd	54.	10.	61.	49.	19.	30.
La	38.	12.	39.	37.	13.	22.
Ce	74.	5.	93.	71.	19.	68.